Sat. Jun 5, 2021

[J] Poster | U (Union)：Union

5:15 PM - 6:30 PM JST | 8:15 AM - 9:30 AM UTC | Ch.01_2

[U-14] Current status and issues of the earth education necessary for living on the changing earth

convener:Hiroshi Ichikawa, Saori Nakai(kyoto koka womens university department of child education), Hidenori Kumagai(Japan Agency for Marine-Earth Science and Technology), Hiroshi Nishi(The Center for Academic Resources and Archives, The Tohoku Museum Tohoku University)

[U14-P01] WG for Studying on Teacher Training System in JpGU

*Hidenori Kumagai[1], Saori Nakai[2], Teacher's training WG JpGU Education Comittee (1.Japan Agency for Marine-Earth Science and Technology, 2.Kyoto Koka Women's University)

[U14-P02] Current state of Geoscience education in primary school teacher training courses to obtain a Type II teacher’s license

*Hiroo Nemoto[1] (1.Ritsumeikan University)

[J] Poster | P (Space and Planetary Sciences)：P-PS Planetary Sciences

5:15 PM - 6:30 PM JST | 8:15 AM - 9:30 AM UTC | Ch.02_2

[P-PS07] Formation and evolution of planetary materials in the Solar System

convener:Megumi Matsumoto(Graduate School of Science, Tohoku University), Shin Ozawa(Department of Earth Science, Graduate School of Science, Tohoku University), Yuki Hibiya(Submarine Resources Research Center, Japan Agency for Marine-Earth Science and Technology), Noriyuki Kawasaki(Department of Earth and Planetary Sciences, Graduate School of Science, Hokkaido University)

[PPS07-P01] Study of porosity change of simulated chondrite materials by impact experiments

*Akiko Nakamura[1], Yuki Hanzawa[2], Tomomi Omura[3], Sunao Hasegawa[4] (1.Graduate School of Science, Kobe University, 2.Faculty of Science, Kobe University, 3.Osaka Sangyo University, 4.Japan Aerospace Exploration Agency)

[PPS07-P02] Formation process of a multi-layered chondrule rim and relationship of fine-grained rim and matrix in two LL chondrites

Yukina Hashimoto[1], *Tomoki Nakamura[1], Megumi Matsumoto[1] (1.Department of Earth and Planetary Materials Sciences, Faculty of Science, Tohoku University)

[PPS07-P03] Mineralogical variations of CM chondrites revealed from X-ray diffraction method: Application to the parent body evolution

*Naoya Imae[1,2], Makoto Kimura[1], Akira Yamaguchi[1,2] (1.Antarctic Meteorite Research Center, National Institute of Polar Research, 2.The Graduate University for Advanced Studies (SOKENDAI))

[PPS07-P04] **Combined XRD-XCT-FIB-TEM analysis of experimentally heated Murchison CM chondrite**

*Megumi Matsumoto[1], Junya Matsuno[2], Akira Tsuchiyama[2,3], Yuri Fujioka[1], Tomoki Nakamura[1], Akira Miyake[4], Masahiro YASUTAKE[5], Shota Okumura[4], Kentaro Uesugi[5], Akihisa Takeuchi[5] (1.Graduate School of Science, Tohoku University, 2.Research Organization of Science and Technology, Ritsumeikan University, 3.Guangzhou Institute of Geochemistry, Chinese Academy of Science GIG, CAS , 4.Graduate School of Science, Kyoto University, 5.Japan Synchrotron Radiation Research Institute/SPring-8)

[PPS07-P05] Variations in initial 26Al/27Al ratios among condensate CAIs from CV chondrites

*Noriyuki Kawasaki[1], Naoya Sakamoto[2], Hisayoshi Yurimoto[2] (1.Department of Earth and Planetary Sciences, Graduate School of Science, Hokkaido University, 2.Hokkaido University)

[PPS07-P06] Petrology and mineralogy of a coarse-grained CAI “TTA01” from Allende

*Tadakatsu Yamasaki[1], Noriyuki Kawasaki[1], Hisayoshi Yurimoto[1] (1.Hokkaido University)

[PPS07-P07] **Development of a chemical separation procedure for determining the initial niobium-92 abundance of chondritic components**

*Yuki Hibiya[1] (1.Submarine Resources Research Center, Japan Agency for Marine-Earth Science and Technology)

[PPS07-P08] Motion of silicate particles in protoplanetary disk

*Tamami Okamoto[1], Shigeru Ida[1] (1.Earth-Life Science Institute, Tokyo Institute of Technology)

[PPS07-P09] Thermal history of andesitic achondrite Erg Chech 002

*Akira Yamaguchi[1], Atsushi Takenouchi[1], Jean-Alix Barrat[2] (1.National Institute of Polar Research, 2.UBO-IUEM)

[PPS07-P10] Excess silica in plagioclase in some mesosiderites

*naoji sugiura[1], tomoko Arai[1] (1.Chiba Institute of Technology)

[PPS07-P11] The petrological and mineralogical descriptions of nakhlites NWA 6148 and NWA 10153

*Kakeru Kukihara[1], Masaaki Miyahara[1], Akira Yamaguchi[2], Yoshio Takahashi[3], Yasuo Takeichi[4], Naotaka Tomioka[5], Eiji Ohtani[6] (1.hiroshima university , 2.National Institute of Polar Research, 3.Tokyo university, 4.Institute of Materials Structure Science, High-Energy Accelerator Research Organization (KEK), 5.Kochi Institute for Core Sample Research, Japan Agency for Marine-Earth Science and Technology (JAMSTEC), 6.Tohoku university)

[J] Poster | P (Space and Planetary Sciences)：P-EM Solar-Terrestrial Sciences, Space Electromagnetism & Space Environment

5:15 PM - 6:30 PM JST | 8:15 AM - 9:30 AM UTC | Ch.03_2

[P-EM14] Heliosphere and Interplanetary Space

convener:Kazumasa Iwai(Institute for Space–Earth Environmental Research (ISEE), Nagoya University), Yasuhiro Nariyuki(Faculty of Education, University of Toyama), Ken Tsubouchi(University of Electro-Communications), N Masaki Nishino(Japan Aerospace Exploration Agency, Institute of Space and Astronautical Science)

[PEM14-P01] Relationship between solar type III radio bursts and electron energy spectra in solar impulsive electron events

Tatsuya Fujimoto[1], *Hiroaki Misawa[1], Fuminori Tsuchiya[1], Takahiro Obara[1] (1.Planetary Plasma and Atmospheric Research Center, Graduate School of Science, Tohoku University)

[PEM14-P02] Occurrence dependence on solar activity cycle for ordinary type III bursts and micro-type III bursts

*Yuichiro Seki[1], Hiroaki Misawa[1], Takahiro Obara[1], Fuminori Tsuchiya[1] (1.Tohoku University)

[PEM14-P03] Simple Estimation of the Global Solar Wind Structure

*Ken'ichi Fujiki[1], Munetoshi Tokumaru[1], Kazumasa Iwai[1] (1.Institute for Space-Earth Environmental Research)

[J] Poster | A (Atmospheric and Hydrospheric Sciences)：A-OS Ocean Sciences & Ocean Environment

5:15 PM - 6:30 PM JST | 8:15 AM - 9:30 AM UTC | Ch.06_1

[A-OS14] Coastal physical processes associated with mixing, eddies, internal waves

convener:Eisuke Tsutsumi(Atmosphere and Ocean Research Institute, The University of Tokyo), Eiji Masunaga(Ibaraki University), Taira Nagai(Graduate School of Science, The University of Tokyo)

[AOS14-P01] Material transport and diffusion around Sagami Bay and Suruga Bay using a particle tracking model

*Takayoshi Inoue[1], Eiji Masunaga[1], Taichi Kosako[2], Yusuke Uchiyama[3] (1.Ibaraki University, 2.Port and Airport Research Institute, 3.Kobe University)

[AOS14-P02] Physical structure and mixing processes in the inner part of Tokyo Bay

*Haruki Itozu[1], Eiji Masunaga[1] (1.Ibaraki University)

[AOS14-P03] Secular variations of M_2 tide, its resonant amplification, and the associated energy dissipation in a semi-enclosed sea connected to the East China Sea (Ariake Sea, Japan), 1980–2019.

*Eisuke Tsutsumi[1], Matsuno Takeshi[2], Sachihiko Itoh[1] (1.Atmosphere and Ocean Research Institute, The University of Tokyo, 2.Research Institute for Applied Mechanics, Kyushu University)

[J] Poster | A (Atmospheric and Hydrospheric Sciences)：A-OS Ocean Sciences & Ocean Environment

5:15 PM - 6:30 PM JST | 8:15 AM - 9:30 AM UTC | Ch.06_2

[A-OS16] Global ocean observing systems, their status, research results and future perspective

convener:Shigeki Hosoda(Japan Marine-Earth Science and Technology), Shuhei Masuda(Japan Agency for Marine-Earth Science and Technology), Yosuke Fujii(Meteorological Research Institute, Japan Meteorological Agency), Fujiki Tetsuichi(Japan Agency for Marine-Earth Science and Technology)

[AOS16-P01] Spatiotemporal variability of vertical structures of temperature and salinity in the mid-latitude northwest Pacific Ocean based on unsupervised clustering

★Invited Papers

*Fumika Sambe[1], Toshio Suga[1,2] (1.Graduate School of Science, Tohoku University, 2.JAMSTEC)

[AOS16-P02] Temporal variations of Kuroshio transport based on a repeated hydrographic section along 137E

*Yuma Kawakami[1], Toshiya NAKANO[1], Atsushi Kojima[1], Kiyoshio Murakami[1], Shusaku Sugimoto[2] (1.Japan Meteorological Agency, 2.Tohoku University)

[AOS16-P03] Global distribution of 10-day differences of temperature and salinity around 2000 m depth observed with Argo floats

*Yoshimi Kawai[1] (1.Research Institute for Global Change, Japan Agency for Marine-Earth Science and Technology)

[AOS16-P04] GO-SHIP Easy Ocean: formatted and gridded ship-based hydrographic section data

*Katsuro Katsumata[1], Sarah Purkey[2], Rebecca Cowley[3], Bernadette Sloyan[3], Stephen Diggs[4], Thomas Moore, II[3], Lynne Talley[2], James Swift[4] (1.JAMSTEC, 2.Scripps Institution of Oceanography, 3.Oceans and Atmosphere, CSIRO, 4.CLIVAR and Carbon Hydrographic Data Office, Scripps Institution of Ocenaography)

[AOS16-P05] Salinity bias with negative pressure dependency caused by anisotropic deformation of CTD measuring cell under pressure examined with a dual-cylinder cell model

*Taiyo Kobayashi[1] (1.Japan Agency for Marine-Earth Science and Technology)

[AOS16-P06] pH measurement in the ocean

*Hajime Kayanne[1], Toshimasa Miyawaki[1], Nori Fujita[1], Kenta Suzuki[2], Hizuru Nakajima[2], Kazuhiro Morioka[3], Akihide Hemmi[4] (1.the University of Tokyo, 2.Tokyo Metropolitan Univ., 3.Tokyo Univ. Pharmacy Life Sci., 4.Möbius Advanced Tech.)

[AOS16-P07] Advances in the estimation of global surface net heat flux based on satellite observation: J-OFURO3 V1.1

*Hiroyuki Tomita[1], Kunio Kutsuwada[2], Masahisa Kubota[3], Tsutomu Hihara[4] (1.Institute for Space-Earth Environmental , Nagoya University, 2.School of Marine Science and Technology, Tokai University, 3.Institute of Ocean Research and Development, 4.Japan Fisheries Information Service Center)

[AOS16-P08] Keeping the PACE with the NASA Plankton, Aerosol, Cloud, ocean Ecosystem (PACE) mission

*Lachlan McKinna[1], Ivona Cetinić[2,3], Jeremy Werdell[3] (1.Go2Q Pty Ltd, 2.USRA, 3.NASA GSFC)

[J] Poster | A (Atmospheric and Hydrospheric Sciences)：A-OS Ocean Sciences & Ocean Environment

5:15 PM - 6:30 PM JST | 8:15 AM - 9:30 AM UTC | Ch.06_3

[A-OS19] Physical Oceanography (General)

convener:Yoshimi Kawai(Research Institute for Global Change, Japan Agency for Marine-Earth Science and Technology), Kitade Yujiro(Tokyo University of Marine Science and Technology)

[AOS19-P01] Long-term variability of summertime convective activity over the tropical northwestern Pacific and its influence on large-scale atmospheric circulation

*Shota Sera[1], Shusaku Sugimoto[1] (1.Graduate School of Science, Tohoku University)

[AOS19-P02] **Temporal variation of heat content within surface mixed layer in the western Arctic from Iridium-based autonomous thermistor strings**

*EunYae Son[1], Yusuke Kawaguchi[1] (1.University of Tokyo)

[AOS19-P03] Data and Sample Management for Marine Observation Cruises: Complaint can be Awareness

*Takayuki Tomiyama[1], Takako Sato[1], Kazuyo Fukuda[1], Hajime Kawakami[1], Makoto Ito[1], Chizuru Saito[1] (1.Japan Agency for Marine-Earth Science and Technology)

[AOS19-P04] Meridional heat transport in the North Pacific subtropical gyre -Analysis by ARMOR 3D-

*Yukina Fukaumi[1], Kazuyuki Uehara[1] (1.The Graduate School of Marine Science and Technology of Tokai University)

[J] Poster | A (Atmospheric and Hydrospheric Sciences)：A-HW Hydrology & Water Environment

5:15 PM - 6:30 PM JST | 8:15 AM - 9:30 AM UTC | Ch.07_3

[A-HW24] Water Environment and Geology in Urban Areas

convener:Takeshi Hayashi(Faculty of Education and Human Studies, Akita University), Akinobu Miyakoshi(Geological Survey of Japan, AIST)

[AHW24-P01] Variability of land-use in the catchments of spring water in the western marginal area of Kanto Plain

*Takeshi Hayashi[1], Masaya Yasuhara[2], Takashi Nakamura[3] (1.Faculty of Education and Human Studies, Akita University, 2.Department of Environment Systems, Rissho University, 3.ICRE, University of Yamanashi)

[AHW24-P02] Evaluation of subsurface warming in the Tokyo metropolitan area, Japan: Effective application of groundwater observation wells for subsurface temperature monitoring

*Akinobu Miyakoshi[1], Takeshi Hayashi[2], Hideki Hamamoto[3], Shoichi Hachinohe[3] (1.Geological Survey of Japan, AIST, 2.Faculty of Education and Human Studies, Akita University, 3.Center for Environmental Science in Saitama)

[AHW24-P03] Demonstration of Ground Source Heat Pump systems and variations of the subsurface temperatures in Saitama Prefecture

*Hideki Hamamoto[1], Hidetaka Shiraishi[1], Masaki Nakayama[2], Shingo Uchiyama[2], Shuhei Ishiguro[3], Junya Takeshima[3] (1.Center for Environmental Science in Saitama, 2.Environmental Energy Division, Environment Department, Saitama Prefecture, 3.OYO Corporation)

[AHW24-P04] Examination of groundwater level measurement method by microtremor array exploration

*Yuji Miyashita[1], Hideki Hamamoto[2], Shigeki Senna[3] (1.Hot Springs Research Institute of Kanagawa Prefecture, 2.Center for Environmental Science in Saitama, 3.National Research Institute for Earth Science and Disaster Resilience)

[J] Poster | A (Atmospheric and Hydrospheric Sciences)：A-CG Complex & General

5:15 PM - 6:30 PM JST | 8:15 AM - 9:30 AM UTC | Ch.08_3

[A-CG37] Biogeochemical cycles in Land Ecosystem

convener:Tomomichi Kato(Research Faculty of Agriculture, Hokkaido University), Kazuhito Ichii(Chiba University), Takeshi Ise(FSERC, Kyoto University), Munemasa Teramoto(Arid Land Research Center, Tottori University)

[ACG37-P01] Change in soil respiration rate and soil organic matter for three years after clear-cutting in a *Cryptomeria japonica* plantation

*Yukiko Abe[1], Naishen Liang[2], Munemasa Teramoto[3], Takeshi Tange[1] (1.The University of Tokyo, 2.National Institute for Environmental Studies, 3.Tottori University)

[ACG37-P02] Continuous measurement of atmospheric methane mixing ratio at a cool-temperate deciduous forest site, Takayama, Japan

*Shohei Murayama[1], Shigeyuki Ishidoya[1], Tomoyuki Hori[1], Shinpei YOSHITAKE[2], Takahisa Maeda[1] (1.National Institute of Advanced Industrial Science and Technology, 2.Waseda University)

[ACG37-P03] Seasonal variation and controlling factors of stem methane emissions from *Alnus japonica* revealed by continuous measurements

*Ayaka Sakabe[1], Kenshi Takahashi[1], Wakana Azuma[2], Masayuki Itoh[3], Makiko Tateishi[1], Yoshiko Kosugi[1] (1.Kyoto University, 2.Kobe University, 3.University of Hyogo)

[ACG37-P04] **Spatio-temporal variation of soil respiration in coastal sand dunes and the mechanisms**

*Munemasa Teramoto[1], Toru Hamamoto[1], Naishen Liang[2], Takeshi Taniguchi[1], Takehiko Y. Ito[3], Richa Hu[4], Norikazu Yamanaka[1] (1.Arid Land Research Center, Tottori University, 2.Center for Global Environmental Research, National Institute for Environmental Studies, 3.International Platform for Dryland Research and Education, Tottori University, 4.The United Graduate School of Agricultural Sciences, Tottori University)

[ACG37-P05] Validation of Two Vegetation Indices: NDVI and PRI Derived from GCOM-C/SGLI

*Sasagawa Taiga[1], Tomoko Kawaguchi Akitsu[2], Kenlo Nishida Nasahara[2] (1.Graduate School of Science and Technology, University of Tsukuba, 2.Faculty of Life and Environmental Sciences, University of Tsukuba)

[ACG37-P06] **Seasonal variation in Solar Induced chlorophyll Fluorescence detected by multi-vertical layer spectroscopy in a canopy of cool-temperate deciduous broadleaf forest in Takayama, Gifu**

*Tomoki Morozumi[1], Tomomichi Kato[1], Katsuto Tsujimoto[2], KANOKRAT BUAREAL[3], Naohisa Nakashima[1], Yuma Sakai[4], Hideki Kobayashi[4], Kenlo Nasahara[5], Tomoko Akitsu[5], Shohei Murayama[6], Hibiki M Noda[7], Hiroyuki Muraoka[8] (1.Research Faculty of Agriculture, Hokkaido University, 2.Graduate School of Life Sciences, Tohoku University, 3.Graduate School of Global Food Resources, Hokkaido University, 4.Institute of Arctic Climate and Environment Research, Japan Agency for Marine-Earth Science and Technology, 5.Faculty of Life and Environmental Sciences, University of Tsukuba, 6.Environmental Management Research Institute, National Institute of Advanced Industrial Science and Technology, 7.Center for Global Environmental Research, National Institute for Environmental Studies, 8.River Basin Research Center, Gifu University)

[ACG37-P07] On the factors affecting reproducibility of GPP estimated by the Earth System Model MIROC-ES2L

*Akira Kurisu[1], Toru Nozawa[2], Manabu Abe[3], Tomohiro Hajima[3] (1.Faculty of Science, Okayama University, 2.Graduate School of Natural Science and Technology, Okayama University, 3.Japan Agency for Marine-Earth Science and Technology)

[ACG37-P08] Estimation of forest above ground biomass from PALSAR Data

*Hantao Li[1], Tomomichi Kato[2], Lan Wu[3], Masato Hayashi[4] (1.Graduate School of Agriculture, Hokkaido University, 2.Research Faculty of Agriculture, Hokkaido University, 3.College of Ecology and Environment, Hainan University, China, 4.Earth Observation Research Center, Japan Aerospace Exploration Agency)

[ACG37-P09] Development of process-based model for estimating wheat production MATCRO-Wheat

*Maki Nakaguki[1], Tomomichi Kato[2], Yuji Masutomi[3], Leilei Liu[4], Seiji Shimoda[5] (1.Hokkaido University, 2.Research Faculty of Agriculture, Hokkaido University, 3.National Institute for Environmental Studies, 4.National Engineering and Technology Center for Information Agriculture, Nanjing Agricultural University, 5.Hokkaido Agricultural Research Center, National Agriculture and Food Research Organization)

[J] Poster | H (Human Geosciences)：H-QR Quaternary research

5:15 PM - 6:30 PM JST | 8:15 AM - 9:30 AM UTC | Ch.09_1

[H-QR04] Quaternary, Diachronic dynamics of human-environment interactions

convener:Mamoru Koarai(Earth Science course, College of Science, Ibaraki University), Yusuke Yokoyama(Atmosphere and Ocean Research Institute, University of Tokyo), Koji Okumura(Graduate School of Letters, Hiroshima University), Yasufumi Satoguchi(Lake Biwa Museum)

[HQR04-P01] Formation age of mire on marine terraces in Nemuro Peninsula, Hokkaido, Japan

*Reisuke Kondo[1], Minoru Yokochi[2], Takashi Inoue[5], Kazuhiro Kaneko[4], Hiroko Fujita[3], Mari Sumita[6], Yosuke Miyairi[1], Yusuke Yokoyama[1] (1.Atmosphere and Ocean Research Institute, The University of Tokyo, 2.Graduate School of Global Food Resources, Hokkaido University, 3.The Field Science Center for Northern Biosphere, Hokkaido University, 4.Graduate School of Agriculture, Hokkaido University, 5.Research Faculty of Agriculture, Hokkaido University, 6.GEOMAR Helmholtz Centre for Ocean Research Kiel)

[HQR04-P02] **Changes in sedimentary environment during the Holocene in a wetland in Chanai area on Konsen plateau, eastern Hokkaido**

*Ren Tsuneoka[1], Yusuke Yokoyama[1], Reisuke Kondo[1], Kosuke Ota[1], Minoru Yokochi[2], Kazuhiro Kaneko[3], Hiroko Fujita[4], Takashi Inoue[5], Norio Kito[6], Mari Sumita[7], Kyota Uemura[8], Yosuke Miyairi[1], Arata Momohara[9] (1.Atmosphere and Ocean Research Institute, The University of Tokyo, 2.Graduate School of Global Food Resources, Hokkaido University, 3.Graduate School of Agriculture, Hokkaido University, 4.The Field Science Center for Northern Biosphere, Hokkaido University, 5.Research Faculty of Agriculture, Hokkaido University, 6.International and Regional Studies, Hokkaido University of Education, 7.GEOMAR Helmholtz Centre for Ocean Research Kiel, 8.College of Humanities and Sciences, Nihon University, 9.Faculty of Horticulture, Chiba University)

[HQR04-P03] Holocene coastal evolution and vertical deformation in the Hachinohe plain, NE Japan, inferred from sedimentary analyses

*Yuichi Niwa[1], Toshihiko Sugai[2] (1.Faculty of Science and Engineering, Chuo University, 2.Department of Natural Environmental Studies, Graduate School of Frontier Sciences, The University of Tokyo)

[HQR04-P04] Landform evolution and estimation of crustal movement since MIS 12 in the central-northern part of the Kanto Plain

*Tatsuki Miyamoto[1], Toshihiko Sugai[1], Yuichi Niwa[2], Toshimichi Nakanishi[3], Tetsuya Komatsu[4], Yuki Hiura[4] (1.Department of Natural Environmental Studies, Institute of Environmental Studies,Graduate School of Frontier Science, The University of Tokyo, 2.Chuo Univ., 3.Museum of Natural and Environmental History, Shizuoka, 4.JAEA)

[HQR04-P05] Rock surface dating of granodiorite cobbles obtained from fluvial terrace deposits in the Chichibu Basin, central Japan

*Yuji Ishii[1], Takayuki Takahashi[2], Kazumi Ito[1] (1.National Institute of Advanced Industrial Science and Technology, 2.Tohoku Univ.)

[HQR04-P06] Identification of reworked volcaniclastic deposits composing the upper Alluvium along the Moto-arakawa River, east part of the Saitama Prefecture, Central Japan

*Masanori Murata[1], Takayuki Takahashi[2], Kaori Aoki[1], Fumikatsu NISHIZAWA[3], Makoto Kobayashi[4], Takehiko Suzuki[1,5] (1.Research Center for Volcanic Hazards and Their Mitigation, Tokyo Metropolitan University, 2.International Research Institute of Disaster Science, Tohoku University, 3.Kanagawa Prefectural Museum of Natural History, 4.Mt. Fuji World Heritage Centre, Shizuoka, 5.Department of Geography, Tokyo Metropolitan University)

[HQR04-P07] Tephrostratigraphy during the past 30,000 years in the Jaishi Oike Moor, southern Izu Peninsula, Japan.

*Tatsuki Watanabe[1], Takehiko Suzuki[1], Daisuke Ishimura[1] (1.Department of Geography, Tokyo Metropolitan University)

[HQR04-P08] Landform evolution since the Middle Pleistocene estimated at the lower reaches of the Himekawa River, central Japan

*Jun Matsukaze[1], Masaaki Shirai[1] (1.Tokyo Metropolitan University)

[HQR04-P09] Radiocarbon dating using pollen fossils and its potential in Quaternary studies

*Keitaro Yamada[1], Takayuki Omori[2], Ikuko Kitaba[3], Takeshi Nakagawa[3] (1.Research Organization of Science and Technology, Ritsumeikan University, 2.The University Museum, The University of Tokyo, 3.Research Centre for

Palaeoclimatology, Ritsumeikan University)

[HQR04-P10] Identification of middle to late Pleistocene marine sediments inferred from electric conductivity analysis of the Bando observation well core in Tokushima Plain, western Japan

*Yoshiki Sato[1], Kiyohide Mizuno[1], Yuki Haneda[1], Koretaka Nakatani[1], Rei Nakashima[1] (1.Advanced Industrial Science and Technology, Geological Survey of Japan)

[J] Poster | H (Human Geosciences)：H-DS Disaster geosciences

5:15 PM - 6:30 PM JST | 8:15 AM - 9:30 AM UTC | Ch.10_2

[H-DS07] Seismic hazards on subduction earthquakes and active faults in the Central Japan

convener:Takashi Azuma(National Institute of Advanced Industrial Science and Technology), Yasuhiro Suzuki(Nagoya University)

[HDS07-P01] Issues for long-term evaluation of Byobu-yama/Ena-san fault zone

*Yasuhiro Suzuki[1] (1.Nagoya University)

[HDS07-P02] Paleoseismological trenching surveys on the Enasan-Sanageyamakita fault zone, Central Japan

*Takashi Azuma[1], Norio Shigematsu[1], Rei Nakashima[1], Ken-ichi Yasue[2], Ryo Tateishi[2], Daisuke Hirouchi[3] (1.National Institute of Advanced Industrial Science and Technology, 2.Toyama University, 3.Shinshu University)

[HDS07-P03] Questionnaire survey for experts on long-term evaluation of active faults and evaluation of ground motion (Part 1)

*Noa Mitsui[1], Takeshi Sagiya[1] (1.Disaster Mitigation Research Center, Nagoya University)

[J] Poster | H (Human Geosciences)：H-DS Disaster geosciences

5:15 PM - 6:30 PM JST | 8:15 AM - 9:30 AM UTC | Ch.10_3

[H-DS10] Geohazards in humid, tectonically active countries and their precursors

convener:Satoru Kojima(Department of Civil Engineering, Gifu University), Taro Uchida(University of Tsukuba), Yoshihiko Kariya(Department of Environmental Geography, Senshu University)

[HDS10-P01] Large-scale collapse of permafrost waste dump at Kumtor gold mine in Kyrgyz republic

*Ayano Aoki[1], Chiyuki Narama[1], Tsutomu Yamanokuchi[2], Murataly Duishonakunov[3] (1.Niigata university, 2.Remote Sensing Technology Center of Japan, 3.Kyrgyz National University)

[HDS10-P02] Relationship between landslide distribution and topographic feature and subsurface structure for the case of the 2018 Hokkaido Eastern Iburi Earthquake

*Junichiro Furuyama[1], Issei Doi[1], Toshitaka Kamai[1], Yuki Matsushi[1] (1.Kyoto University)

[HDS10-P03] Sediment movement on landslide slopes and river channel after the 2018 Hokkaido Eastern Iburi Earthquake

*Takashi Koi[1], Yasutaka Tanaka[1], Shin'ya Katsura[2], Norifumi Hotta[3] (1.Center for Natural Hazards Research, Hokkaido University, 2.Research Faculty of Agriculture, Hokkaido University, 3.Graduate School of Agricultural and Life Sciences, The University of Tokyo)

[HDS10-P04] Surface changes of Ganpei landslide in Joetsu region

*Yutaka Inoue[1], Chiyuki Narama[2], Chunxiang WANG[3], Eiji Takita[3] (1.Graduate Student,Niigata University, 2.Niigata University, 3.KITAK Corporation)

[HDS10-P05] **Surface changes of rock slopes in the Hakuba-Daisekkei Valley, northern Japanese Alps**

*Hirotaka Sugiyama[1], Chiyuki Narama[1], Hiroshi Inoue[2] (1.Niigata University, 2.NIED)

[HDS10-P06] Revisiting stratigraphy and age of so-called Otsukigawa debris avalanche deposits in the upper Otsukigawa and Yukawa Rivers on the eastern side of Yatsugatake Volcano in central Japan

*Takahiro Kurimoto[1], Yoshihiko Kariya[2] (1.Graduate School of Humanities, Senshu Univ., 2.Senshu Univ.)

[HDS10-P07] Relationship between a natural dam at the Yomogisawa River in the headwater area of the Abe River and the Oya-Kuzure rockslide with reference to new chronological information

*Keiju Kimura[1], Yoshihiko Kariya[2] (1.Graduate, Senshu Univ., 2.Senshu Univ.)

[HDS10-P08] Activities of landslides and their precursors: Case studies in Okutabora, Gujo, Gifu Prefecture and in Kuchisakamoto, Shizuoka Prefecture, central Japan

*Satoru Kojima[1], Kazuhide Sawada[1], Mizuki Tatekawa[1] (1.Department of Civil Engineering, Gifu University)

[J] Poster | H (Human Geosciences)：H-TT Technology & Techniques

5:15 PM - 6:30 PM JST | 8:15 AM - 9:30 AM UTC | Ch.11_3

[H-TT18] Environmental Remote Sensing

convener:Naoko Saitoh(Center for Environmental Remote Sensing), Hitoshi Irie(Center for Environmental Remote Sensing, Chiba University), Hiroto Shimazaki(National Institute of Technology, Kisarazu College), Teppei Ishiuchi(Miyagi University)

[HTT18-P01] Feasibility of observations of middle and upper tropospheric and lower stratospheric ozone concentrations by GOSAT/TANSO-FTS

*Eito Seki[1], Naoko Saitoh[1] (1.Center for Environmental Remote Sensing, Chiba University)

[HTT18-P02] Data quality of GOSAT-2/TANSO-FTS-2 GHG profile data retrieved from the V102.102 radiance spectra

*Naoko Saitoh[1], Ryoichi Imasu[2], kei Shiomi[3] (1.Center for Environmental Remote Sensing, Chiba University, 2.Atmosphere and Ocean Research Institute, The University of Tokyo, 3.Japan Aerospace Exploration Agency)

[HTT18-P03] Land use and land cover change of illegal settlements by landless peasants in the Brazilian Amazon

*Sayaka Yoshikawa[1,3], Kanae Ishimaru[2] (1.Ibaraki university , 2.Fukui Prefectural University, 3.Tokyo institute of technology)

[HTT18-P04] Evaluation of heterogeneity in growth of black pines planted for artificial coastal forests in the Sendai Plain

*Takuto Kajiwara[1], Masayuki Kawahigashi[2] (1.Graduate Student of Tokyo Metropolitan University, 2.Tokyo Metropolitan University)

[HTT18-P05] Accounting for atmospheric factors to estimate photosynthetically active radiation from surface solar irradiance

*YAJIE DAI[1], Hitoshi Irie[1], Alessandro Damiani[1] (1.chiba university)

[HTT18-P06] Data-assimilation-based Estimation of Infectivity Parameter of COVID-19 Epidemic Model and its Relation to NO2 satellite observation.

*Osamu Kabayama[1], Okazaki Atsushi[2], Shunji Kotsuki[1] (1.Centre for Environment Remote Sensing, Chiba University, 2.The Pennsylvania State University)

[HTT18-P07] Changes in the NO2 weekly cycle under COVID-19 pandemic

*Alessandro Damiani[1], Hitoshi Irie[1], Saito Hikaru[1], Ying Cai[1], Dmitry Belikov[1], Raul R. Cordero[2] (1.CEReS, Chiba University, 2.Santiago de Chile University)

[J] Poster | H (Human Geosciences)：H-CG Complex & General

5:15 PM - 6:30 PM JST | 8:15 AM - 9:30 AM UTC | Ch.12_2

[H-CG23] Nuclear Energy and Geoscience

convener:Eiji Sasao(Tono Geoscience Center, Japan Atomic Energy Agency), Shinji Takeuchi(Department of Earth and Environmental Sciences, College of Humanities & Sciences, Nihon University), Takuma HASEGAWA(Central Research Institute of Electric Power Industry)

[HCG23-P01] Modeling of Radial Dikes by Topographical Analysis using GIS for Quaternary Volcanoes

Yuki Hiura[1], *Makoto Kawamura[1], Umeda Koji[2], Masakazu Niwa[1] (1.Japan Atomic Energy Agency, 2.Hirosaki Univ.)

[HCG23-P02] Three-dimensional resistivity distribution by magnetotelluric survey to evaluate the distribution of fossil seawater

*Naomi Satoh[1], Akira Hayano[1], Minoru Teshima[2], Tateyuki Negi[2], Terumasa Yamane[3], Shinji Kawasaki[3] (1.Japan Atomic Energy Agency, 2.Nittetsu Mining Consultants Co., Ltd., 3.JGI, Inc.)

[HCG23-P03] Microbial community analysis of deep-seated fluids: Do microbes live in slab-derived fluid?

*Ayumi Sugiyama[1,2], Yuichi Tomioka[1], Shin-ichi Hirano[1], Tokihiro Kurita[1] (1.Central Research Institute of Electric Power Industry, 2.Asano Taiseikiso Engineering Co., Ltd.)

[HCG23-P04] Constructions of hydrogeological structure and mass transport model around hydraulic conductive fractures

*Ai Hamada[1], Kimio Miyakawa[1], Yasuharu Tanaka[1] (1.Central Research Institute of Electric Power Industry)

[HCG23-P05] Development of multi-scale modeling for estimation of inflow volume into tunnels of the geological disposal facility

*Naoki Katsumata[1], Satoru Suzuki[1], Hiromitsu Saegusa[1], Tatsuya Tanaka[2], Yoshito Kitagawa[1] (1.Nuclear Waste Management Organization of Japan, 2.OBAYASHI CORPORATION)

[HCG23-P06] Introduction of the “KiNa” international project of natural analogue studies of the long-term stability of bentonite

*Satoru Suzuki[1], Tsutomu Sato[2], Tsubasa Otake[2], Kikuchi Ryosuke[2], Fujimura Tatsuya[2], Takahiro Goto[1], Yusuke Ogawa[1], Patrik Sellin[3], Daniel Svensson[3], Albert H. Gilg[4], Ulf B. Andersson[5], Elizaveta Klein[6], Olivier X. Leupin[6], Simon Norris[9], Russell W. Alexander[10], Mehran Behazin[7], Nicolas Michau[8] (1.Nuclear Waste Management Organization of Japan , 2.Hokkaido University, 3.SKB, 4.TU Munich, 5.Luossavaara-Kiirunavaara AB, 6.Nagra, 7.NWMO, 8.ANDRA, 9.RWM, 10.Bedrock Geosciences)

[HCG23-P07] Interaction at the interface between compacted bentonite and carbon steel plate in artificial seawater

*Tatsuya Fujimura [1], Tsutomu Sato[2], Tsubasa Otake[2], Kikuchi Ryosuke[2], Satoru Suzuki[3], Takahiro Goto[3] (1.Graduate School of Engineering, Hokkaido University, 2.Faculty of Engineering, Hokkaido University, 3.Nuclear Waste Management Organization of Japan)

[J] Poster | H (Human Geosciences)：H-CG Complex & General

5:15 PM - 6:30 PM JST | 8:15 AM - 9:30 AM UTC | Ch.12_3

[H-CG24] Coastal wetlands: geomorphologic, biologic and anthropogenic processes

convener:Kiyoshi Fujimoto(Nanzan University)

[HCG24-P01] Mapping of mangrove species and communities using UAV photography and high-resolution satellite data to evaluate surface erosion induced by sea-level rise on Pohnpei Island, Micronesia

*Kiyoshi Fujimoto[1], Takeki Yaguchi[1], Yasumasa HIrata[2], Shin Watanabe[3], Kodai Hasada[4], Kenji Ono[2], Shingo Taniguchi[3], Keita Furukawa[5], Saimon Lihpai[6] (1.Nanzan University, 2.Forestry and Forest Products Research Institute, 3.University of the Ryukyus, 4.Hosei University, 5.Association for Shore Environment Creation , 6.Pohnpei State Government, FSM)

[HCG24-P02] **Consideration of sea level rise effect on sediment transport process in mangrove forest - preliminary attempt for long-term analysis-**

*Keita Furukawa[1,2], Kiyoshi Fujimoto[3], Kenji Ono[4], Shin Watanabe[5], Shingo Taniguchi[5], Yasumasa Hirata[4], Kodai Hasada[6], Renpei Suwa[7], Saimon Lihpai[8] (1.Association for Shore Environment Creation, 2.Ocean Policy Research Institute, Sasakawa Peace Foundation, 3.Nanzan University, 4.Forestry and Forest Products Research Institute, 5.Ryukyu University, 6.Hosei University, 7.Japan International Research Center for Agricultural Sciences, 8.Pohnpei State Government)

[HCG24-P03] Comparison of Fine Root Production among Several Types of Tropical Mangrove Stands in the Federated States of Micronesia using the Continuous Inflow Estimation Method

*Kenji Ono[1], Kiyoshi Fujimoto[2], Yasumasa Hirata[3], Ryuuichi Tabuchi[3], Shingo Taniguchi[4], Shin Watanabe[4], Keita Furukawa[5], Rempei Suwa[6], Saimon Lihpai[7] (1.Tohoku research center, Forestry and Forest Products Research Institute, 2.Nanzan Univ., 3.Forestry and Forest Products Research Institute, 4.Univ. of Ryukyu, 5.Association for Shore Enviromnent Creation, 6.Japan International Research Center for Agricultural Science, 7.Phonpei State Gov. FSM)

[J] Poster | H (Human Geosciences)：H-CG Complex & General

5:15 PM - 6:30 PM JST | 8:15 AM - 9:30 AM UTC | Ch.12_4

[H-CG27] Nuclear Power and Geoscience in Japan: 10 years after the 3.11 complex disaster

convener:Daisuke Suetsugu(institute for Marine Geodynamics, Japan Agency for Marine-Earth Science and Technology), Kohta Juraku(Department of Humanities, Social and Health Sciences, School of Engineering, Tokyo Denki University), Satoshi Kaneshima(Department of Earth and Planetary Sciences, Kyushu University), Takeshi Sagiya(Disaster Mitigation Research Center, Nagoya University)

[HCG27-P01] Nuclear Power and Geoscience in Japan

*Daisuke Suetsugu[1], Satoshi Kaneshima[2], Takeshi Sagiya[4], Kohta Juraku[3] (1.institute for Marine Geodynamics, Japan Agency for Marine-Earth Science and Technology, 2.Department of Earth and Planetary Sciences, Kyushu University, 3.Department of Humanities, Social and Health Sciences, School of Engineering, Tokyo Denki University, 4.Disaster Mitigation Research Center, Nagoya University)

[HCG27-P02] Model and “Unexpected”

*Manabu Hashimoto[1] (1.Disaster Prevention Research Institute, Kyoto University)

[HCG27-P03] Does science give us THE answer? (2)
Issues centering on scientific advice

*Kohta Juraku[1] (1.Department of Humanities, Social and Health Sciences, School of Engineering, Tokyo Denki University)

[HCG27-P04] A personal summary of JPGU sessions about earth science and nuclear power plants in Japan

*Satoshi Kaneshima[1] (1.Department of Earth and Planetary Sciences, Kyushu University)

[HCG27-P05] Has the situation surrounding nuclear power generation and earth science changed during the last decade?

*Takeshi Sagiya[1] (1.Disaster Mitigation Research Center, Nagoya University)

[J] Poster | S (Solid Earth Sciences)：S-SS Seismology

5:15 PM - 6:30 PM JST | 8:15 AM - 9:30 AM UTC | Ch.13_2

[S-SS09] Seismic wave propagation: Theory and Application

convener:Kaoru Sawazaki(National Research Institute for Earth Science and Disaster Resilience), Kiwamu Nishida(Earthquake Research Institute, University of Tokyo), Takao Nibe(JAPEX), Kyosuke Okamoto(National Institute of Advanced Industrial Science and Technology)

[SSS09-P01] Temporal variation in seismic velocity at the shallow part of the overriding plate in the Japan Trench

*Takashi Tonegawa[1], Ryota Takagi[2], Kaoru Sawazaki[3], Katsuhiko Shiomi[3] (1.Japan Agency for Marine-Earth Science and Technology, 2.Tohoku University, 3.National Research Institute for Earth Science and Disaster Resilience)

[SSS09-P02] Estimation of instrumental clock errors at 46 active volcanoes in Japan based on seismic interferometry

*Takashi Hirose[1] (1.National Research Institute for Earth Science and Disaster Resilience)

[SSS09-P03] On the factors influencing ambient-noise passive seismic imaging

*Xin Guo[1], Zhihui Zou[1,2], Yongjun Rui[3], Qinghui Cui[3], Xinmin Shang[3] (1.College of Marine Geosciences, Key Lab of Submarine Geosciences and Prospecting Techniques. MOE, Ocean University of China, Qingdao 266100, China, 2.Evaluation and Detection Technology Laboratory of Marine Mineral Resources, Qingdao National Laboratory for Marine Science and Technology, Qingdao 266061, China, 3.Geophysical Research Institute of Shengli Oilfield, Sinopec, Dongying, China 257022)

[SSS09-P04] **Migration of fluid during oil recovery revealed by Reverse Time Imaging**

*Runbi Yuan[1], Zhihui Zou[2,1], Cui Qinghui[3], Rui Yongjun[3], Shang Xinmin[3] (1.College of Marine Geosciences, Key Lab of Submarine Geosciences and Prospecting Techniques. MOE, Ocean University of China, Qingdao 266100, China, 2.Evaluation and Detection Technology Laboratory of Marine Mineral Resources, Qingdao National Laboratory for Marine Science and Technology, Qingdao 266061, China, 3.Geophysical Research Institute of Shengli Oilfield, Sinopec, Dongying, China 257022)

[SSS09-P05] Effects of fine-scale heterogeneity distribution in the Pacific slab on the generation of anomalously large intensities from deep-focus earthquakes

*Takashi Furumura[1], Brian LN Kennett[2] (1.Earthquake Research Institute The University of Tokyo, 2.Research School of Earth Sciences The Australian National University)

[SSS09-P06] Scattering properties in Japanese volcanoes as inferred from the peak ratio analysis of teleseismic P waves using the JMA seismometer network data

*Gugi Aucklandi Ganefianto[1], Hisashi Nakahara[1], Takeshi Nishimura[1] (1.Tohoku University)

[SSS09-P07] Crack source and volcanic structural heterogeneity inferred from oscillatory waveforms of long-period seismic events: Application at Kusatsu-Shirane Volcano

*Nakano Masayuki[1], Hiroyuki Kumagai[1] (1.Nagoya University)

[SSS09-P08] Applying the shortest path method to anisotropic media in order to calculate ray paths

*Shoji Sekiguchi[1] (1.National Research Institute for Earth Science and Disaster Resilience)

[SSS09-P09] Numerical simulations of weak localization of scalar waves based on the finite difference method (2)

*Jun Kawahara[1], Masanobu Sato[1] (1.Graduate School of Science and Engineering, Ibaraki University)

[SSS09-P10] Observability of seismic radial anisotropy parameters by the analysis of surface waves and receiver functions based on the MCMC analysis

*Jumpei Maruyama[1], Hitoshi Kawakatsu[1], Nozomu Takeuchi[1] (1.University of Tokyo, Earthquake Research Institute)

[J] Poster | S (Solid Earth Sciences)：S-GL Geology

5:15 PM - 6:30 PM JST | 8:15 AM - 9:30 AM UTC | Ch.15_1

[S-GL23] Geologic structure and tectonic history of East Asia and Japanese Islands

convener:Makoto Otsubo(Geological Survey of Japan, Research Institute of Earthquake and Volcano Geology), Jun Hosoi(Geological Survey of Japan, Institute of Geology and Geoinformation, AIST)

[SGL23-P01] Estimation of fluid migration along the Out of Sequence Thrust from quartz vein geometric information
-Estuimation of permeability at Nobeoka Thrust in Kyushu, southwest Japan-

*Hinako Hosono[1], Takato Takemura[1], Makoto Otsubo[2] (1.Nihon University Colledge of Humanities and Sciences, 2.Geological Survey of Japan, Research Institute of Earthquake and Volcano Geology)

[SGL23-P02] Detrital zircon geochemistry in the Shimanto Accretionary Complex: Tectonic constraints on formations of the Jurassic to Cretaceous batholiths in the eastern Asian margin

*Shogo Aoki[1], Kazumasa Aoki[2], Mayuko Fukuyama[3], Masatsugu Ogasawara[4] (1.Graduate School of International Resource Sciences, Akita University, 2.Center For Fundamental Education, Okayama Univerisity of Science, 3.Graduate School of Engeneering Science, Akita University, 4.Institute of Geology and Geoinformation, Geological Survey of Japan, National Institute of Advanced Industrial Science and Technology)

[SGL23-P03] Itayama Nappe, meta-chert and gabbro in the Ryoke Belt of the Takato-Itayama area, central Japan

*Akira Ono

[SGL23-P04] Publication of the 1:50,000 geological map of the Ikeda District

*Atsushi Noda[1], Kazuhiro Miyazaki[1], Kiyohide Mizuno[1], Mitsuhiro Nagata[2] (1.National Institute of Advanced Industrial Science and Technology, 2.Japan Atomic Energy Agency)

[SGL23-P05] Tectonic slices at the Anko outcrop of Median Tectonic Line, Oshika Village, Nagano Prefecture, Japan

*RYOSUKE ISAJI[1], HIDEO TAKAGI[1] (1.Waseda University)

[SGL23-P06] Zircon U–Pb age of Paleoproterozoic granite gneiss from the Ogcheon Belt, Geumsan area and Paleoproterozoic leucogranite and quartzite from the Yeongnam Massif, Seolcheon area, South Korea

*Kenichiro Iwamizu[1,2], Yasutaka Hayasaka[1], Ji-Hoon Kang[3], Kosuke Kimura[1,4], Tomoyuki Shibata[1] (1.Hiroshima Univ., 2.The Univ. of Tokyo, 3.Andong National Univ., 4.National Inst. of Tech., Kure College)

[J] Poster | S (Solid Earth Sciences)：S-VC Volcanology

5:15 PM - 6:30 PM JST | 8:15 AM - 9:30 AM UTC | Ch.16_1

[S-VC28] Active Volcanism

convener:Yuta Maeda(Nagoya University), Takahiro Miwa(National research institute for earth science and disaster prevention), Takeshi Matsushima(Institute of Seismology and Volcanology, Faculty of Science, Kyushu University)

[SVC28-P01] Local deformation at Mt.Tokachi detected by TS-InSAR

*Satoshi Okuyama[1], Shinobu Ando[1] (1.Meteorological Research Institute)

[SVC28-P02] Volcanic tremor source location at Tokachidake volcano from cross-correlation analysis of 2018-2020 seismic data

*Theodorus Permana[1], Hiroshi Aoyama[1] (1.Institute of Seismology and Volcanology, Faculty of Science, Hokkaido University.)

[SVC28-P03] Time-series of crustal deformation on Azuma volcano revealed by PALSAR-2 data

*Yuji Himematsu[1], Taku Ozawa[1] (1.National Research Institute for Earth Science and Disaster Resilience)

[SVC28-P04] Existence of deep pressure sources and its behaviors during recent volcanic activity at Azumayama, NE Japan

*Jun Okada[1], Yu Nihara[2], Yuji Miyagawa[3], Susumu Seki[3], Takuya Yamamura[2], Shin Chikasawa[3] (1.Volcanology Research Department, Meteorological Research Institute - Japan Meteorological Agency, 2.Regional Volcanic Observation and Warning Center, Sendai Regional Headquarters - Japan Meteorological Agency, 3.Seismology and Volcanology Division, Sendai Regional Headquarters - Japan Meteorological Agency)

[SVC28-P05] Amorphous silica coating on flank deposits of the 1783 CE (Tenmei) eruption at Asama volcano

*Takayuki Nakatani[1], Sarina Sugaya[2], Maya Yasui[3], Satoshi Okumura[2], Michihiko Nakamura[2] (1.Geological Survey of Japan, National Institute of Advanced Industrial Science and Technology, 2.Department of Earth Science, Graduate School of Science, Tohoku University, 3.Department of Earth and Environmental Sciences, College of Humanities and Sciences, Nihon University,)

[SVC28-P06] **Monitoring of underground temperature in Jigokudani, Midagahara volcano using LPWA devices**

*Tohru Watanabe[1] (1.Faculty of Sustainable Design, University of Toyama)

[SVC28-P07] Formation of N_3 member from the younger Ō-shima group distributed around the Habu area, southeastern part of Izu-Ō-shima Island.

*Ryota Uchiyama[1], Izumi Sakamoto[1] (1.School of Marine and Technology, Tokai University)

[SVC28-P08] Banded Tremors Activity at Miyakejima Volcano

*Yoshihiro Otsuka[1], Shinya Nagato[1] (1.Japan Meteorological Agency)

[SVC28-P09] Estimating the underground pressure source of Miyakejima volcano by integrated processing of GNSS and leveling data

*Haruna Watanabe[1], Takeshi Matsushima[2], Miyo Fukui, Atsushi Watanabe[3], Jun Oikawa[3], Takashi OKUDA[4], Taku Ozawa[5], Yosuke Miyagi[5] (1.Department of Earth and Planetary Sciences, Graduate School of Science, Kyushu University, 2.Institute of Seismology and Volcanology, Faculty of Sciences, Kyushu University, 3.Earthquake Research Institute, University of Tokyo, 4.Earthquake and Volcanology Research Center, 5.National Research Institute for Earth Science and Disaster Resilience)

[SVC28-P10] Three-Dimensional Crustal Structure beneath Hachijojima Island using dense seismic observation data

*Shotaro Kanke[1], Hiroyuki Azuma[1], Yoshiya Oda[1] (1.Tokyo Metropolitan Univ.)

[SVC28-P11] Ground deformation between eruptions at Nishinoshima Island using InSAR time series analysis

*Shinobu Ando[1], Satoshi Okuyama[1] (1.Volcanology Research Department, Meteorological Research Institute)

[SVC28-P12] Abrupt change in eruption style during the 2019-2020 eruption of Nishinoshima, Ogasawara

*Fukashi Maeno[1], Takayuki Kaneko[1], Natsumi Hokanishi[1], ATSUSHI YASUDA[1], Yoshihiko Tamura[2] (1.Earthquake Research Institute, University of Tokyo, 2.Japan Agency for Marine-Earth Science and Technology)

[SVC28-P13] The depth of the air-magma interface and the sound velocity in the shallow conduit of Aso volcano inferred from seismic and infrasound signals

*Kyoka Ishii[1], Akihiko Yokoo[1] (1.Graduate School of Science, Kyoto University)

[SVC28-P14] Estimation of source location of high-frequency tremor at Aso volcano by array analysis

*hirotaka tanaka[1], Takahiro Ohkura[2], Hiroyuki Inoue[2], Shin Yoshikawa[2] (1.kyoto university, 2.Aso Volcanological Laboratory)

[SVC28-P15] Debris avalanche deposits and the stratigraphy on the outcrop to north east from Mt.Unzen

*Daisuke Nagai[1] (1.Mt.Unzen disaster memorial hall)

[SVC28-P16] Vault-housed extensometers and tiltmeters recorded continuous crustal movement during the eruption of Kirishima Shinmoe-dake in 2018

*Koki Yoshinaga[1], Takeshi Matsushima[2], Hiroshi Shimizu[2], Yusuke Yamashita[3], Shintaro Komatsu[3], Ken'ichi Yamazaki[3] (1.Department of Earth and Planetary Sciences, Graduate School of Science, Kyushu University, 2.Institute of Seismology and Volcanology, Faculty of Sciences, Kyushu University, 3.Miyazaki Observatory, Disaster Prevention Research Institute, Kyoto University)

[SVC28-P17] Two experiments using a small-aperture infrasonic array at Kirishima

*Kazuya Yamakawa[1], Mie Ichihara[1], Dan Muramatsu[2], Takeshi Matsushima[2], Ruka Wada[3], Hideki Takahashi[3], Isao Shimoyama[4] (1.Earthquake Research Institute, University of Tokyo, 2.Institute of Seismology and Volcanology, Faculty of Science, Kyushu University, 3.Department of Mechanical Engineering, Faculty of Science and Technology, Keio University, 4.Department of Intelligent Robotics, Toyama Prefectural University)

[SVC28-P18] Estimating the source of volcanic earthquakes during eruption events at Kirishima Volcanos, in 2018, using spatial distribution of earthquake amplitude.

*Daiki Goshima[1], Satoshi Matsumoto[2], Ayaho Mitsuoka[1], Yuhei Yuasa[4], Yuta Kawamura[1], Mie Ichihara[3] (1.Department of Earth and Planetary Sciences, Graduate School of Science, Kyushu University, 2.Institute of Seismology and Volcanology, Faculty of Sciences, Kyushu University, 3.Earthquake Research Institute, University of Tokyo, 4.Osaka Regional Headquarters, Japan Meteorological Agency)

[SVC28-P19] S-wave attenuation structure of Mt.Kirishima estimated using coda of S-wave

*Takuji Watanabe[1], Ayaho Mitsuoka[1], Yuhei Yuasa[1], Yuta Kawamura[1], Daiki Goshima[1], Satoshi Matsumoto[2], Mie Ichihara[3] (1.Department of Earth and Planetary Sciences, Graduate School of Science, Kyushu University, 2.Institute of seismology and Volcanology, Faculty of Sciences, Kyushu University, 3.Earthquake Research Institute, University of Tokyo)

[SVC28-P20] Estimate of magma supply beneath Aira caldera during the last 10 years based on ground deformation observation and amount of volcanic ejecta

*Daisuke Miki[1], Tomoki Tsutsui[1], Masato Iguchi[1] (1.Sakurajima Volcano Research Center, Disaster Prevention Research Institute, Kyoto University)

[SVC28-P21] Temporal changes of seismic velocities and scattering properties at Suwanosejima volcano inferred from seismic interferometry

*Takashi Hirose[1], Hideki Ueda[1], Eisuke Fujita[1] (1.National Research Institute for Earth Science and Disaster Resilience)

[SVC28-P22] Development of volcano deformation calculation system using boundary element method (2)

*Ryohei Kawaguchi[1] (1.Meteorological Research Institute)

[SVC28-P23] Estimation of seismic scattering coefficients at active volcanoes

*Mare Yamamoto[1] (1.Research Center for Prediction of Earthquakes and Volcanic Eruptions, Graduate School of Science, Tohoku University)

[SVC28-P24] Temporal Change in Coda-Q at the upper East Rift Zone of Kīlauea volcano, Island of Hawai‘i

*Takuji Yamada[1], Paul G Okubo[2] (1.Faculty of Science, Graduate School of Science and Technology, Ibaraki University, 2.University of Hawai‘i at Mānoa)

[SVC28-P25] A prototype of advanced Multi-GAS for unmanned aircraft systems

*Masaaki Morita[1], Toshiya Mori[2] (1.Geological Survey of Japan, AIST, 2.Graduate School of Science, The University of Tokyo)

[J] Poster | S (Solid Earth Sciences)：S-VC Volcanology

5:15 PM - 6:30 PM JST | 8:15 AM - 9:30 AM UTC | Ch.16_2

[S-VC31] Dynamics of volcanic eruptions and their physical and chemical processes

convener:Yujiro Suzuki(Earthquake Research Institute, The University of Tokyo), Atsuko Namiki(Graduate School of Environmental Studies, Nagoya University), Masatoshi Ohashi(Earthquake Research Institute, the University of Tokyo)

[SVC31-P01] **PHENO-BUBBLE NUMBER DENSITY (PBND) AS INDICATOR OF OVERPRESSURE IN PRE-ERUPTIVE MAGMA CHAMBER**

*Indranova Suhendro[1], Atsushi Toramaru[1] (1.Department of Earth and Planetary Sciences, Graduate School of Sciences, Kyushu University)

[SVC31-P02] **Crystal Fracture in the Youngest Toba Tuff (74 ka) Pumices**

*Gabriela Nogo Retnaningtyas Bunga Naen[1], Atsushi Toramaru[1], Haryo Edi Wibowo[2] (1.Department of Earth and Planetary Science, Kyushu University, Fukuoka, Japan, 2.Geological Engineering Department, Universitas Gadjah Mada, Yogyakarta, Indonesia)

[SVC31-P03] **Textural study of the 7.3 ka caldera-forming eruption of Kikai Caldera: Correlating bulk density to bubble-size observations**

*Selvia Novianty[1], Masatoshi Ohashi[1], Atsushi Toramaru[1] (1.Department of Earth and Planetary Sciences, Graduate School of Science, Kyushu University)

[SVC31-P04] Factors controlling bulk density of pumice in explosive eruption deposits

*Atsushi Toramaru[1], Miki Ogata[1], Haruka Ino[1], Indranova Suhendro[1], Gabriela Bunga Naen[1] (1.Department of Earth and Planetary Sciences, Faculty of Sciences, Kyushu University)

[SVC31-P05] Eruptive style and sequence of the 1235 eruption of Ohachi volcano, Kirishima, Japan - constraints from distribution, shape, and texture of pyroclasts-

*Sayaka Shohata[1], Fukashi Maeno[2], Natsumi Hokanishi[2], ATSUSHI YASUDA[2] (1.Department of Earth and Planetary Science, School of Science, The University of Tokyo, 2.Earthquake Research Institute, The University of Tokyo)

[SVC31-P06] Conduit ascent process of mafic subplinian eruption: Constraints from plagioclase microlites in the 1235 scoria of Kirishima-Ohachi volcano, Japan.

*Yoshiharu Iwaki[1], Hidemi Ishibashi[1], Natsumi Hokanishi[2], ATSUSHI YASUDA[2], Toru Ishikawa[3], Taketo Shimano[4] (1.Shizuoka University Graduate School of Integrated Science and Technology, 2.Earthquake Research Institute, University of Tokyo, 3.Kirishima Geopark Council, 4.Graduate School of Environment and Disaster Reserch, Tokoha University)

[SVC31-P07] Texture of ejecta of summit eruptions in Izu-Oshima

*Yuya Ikenaga[1], Fukashi Maeno[1], ATSUSHI YASUDA[1] (1.Earthquake Research Institute, The University of Tokyo)

[SVC31-P08] Shallow conduit process of Strombolian eruption: A case study of Izu-Omuroyama monogenetic volcano, Japan

*Hidemi Ishibashi[1], Risako Hatakeyama[1], Ryuta Sakamoto[1], Natsumi Hokanishi[2], ATSUSHI YASUDA[2] (1.Faculty of Science, Shizuoka University, 2.Earthquake Research Institute, The University of Tokyo)

[SVC31-P09] **Parameters to control bubble - crystal interaction styles**

*Kyoko Ikeda[1], Atsushi Toramaru[2] (1.Department of Earth and Planetary Sciences, Graduate School of Science, Kyushu University, 2.Department of Earth and Planetary Sciences, Faculty of Science, Kyushu University)

[SVC31-P10] 3D crystal size distributions of pyroxene nanolites plotted against short-axis length reflect magma ascent dynamics

*Shota Okumura[1], Mayumi Mujin[2], Akira Tsuchiyama[3,4], Akira Miyake[1] (1.Department of Geology and Mineralogy, Graduate School of Science, Kyoto University, 2.Division of Earth and Planetary Materials Science, Department of Earth Science, Tohoku University, 3.Research Organization of Science and Technology, Ritsumeikan University, 4.Guangzhou Institute of Geochemistry, Chinese Academy of Sciences)

[SVC31-P11] Petrological characteristics of the Kawago-daira rhyolite lava, Izu Peninsula, Japan

*Hiroshi Oka[1], Motohiro Tsuboi[1], Kuniyuki Furukawa[2] (1.Kwansei Gakuin University, 2.Aichi University)

[SVC31-P12] Determination of water solubility in the rhyolitic melt at 650°C and its interpretation by "hydrogen bonding model"

*Mizuki Nishiwaki[1], Takahiro Miwa[2] (1.Department of Earth and Planetary Sciences, Graduate School of Sciences, Kyushu University, 2.National Research Institute for Earth Science and Disaster Resilience)

[SVC31-P13] Flowage of the 1991 Unzen lava: Discussion to Goto et al.(2020) Rigid migration of Unzen lava rather than flow. JVGR

*Hiroaki Sato[1], Shigeru Suto[2], Tadahide Ui[3], Toshitsugu Fujii[4], Takahiro Yamamoto[2], Shinji Takarada[2], Keiichi Sakaguchi[2] (1.Kobe Univ., 2.Geological Survey of Japan, 3.Hokkaido Univ., 4.Mount Fuji Research Institute)

[J] Poster | S (Solid Earth Sciences)：S-GC Geochemistry

5:15 PM - 6:30 PM JST | 8:15 AM - 9:30 AM UTC | Ch.17_2

[S-GC33] Solid Earth Geochemistry, Cosmochemistry

convener:Gen Shimoda(Geological Survey of Japan, AIST), Katsuhiko Suzuki(Submarine Resources Research Center, Japan Agency for Marine-Earth Science and Technology), Katsuyuki Yamashita(Graduate School of Natural Science and Technology, Okayama University), Akira Ishikawa(Department of Earth and Planetary Sciences, Tokyo Institute of Technology)

[SGC33-P01] Origin of intra-plate magmatism in Kamchatka constrained by noble gas isotopes

*Masao Fukagawa[1], Hirochika Sumino[2], Anna O Volynets[3], Yuri Taran[3] (1.Department of Integrated Science, College of Arts and Science, the University of Tokyo, 2.Department of General Systems Studies Graduate School of Arts and Sciences, The University of Tokyo, 3.Russian Academy of Sciences)

[SGC33-P02] **Rare earth elements composition of carbonate concretion in the Miocene Morozaki Group, southwestern Japan**

*Ryosuke Kitanaka[1], Motohiro Tsuboi[1] (1.Kwansei Gakuin University)

[SGC33-P03] Investigation of Validity for Evaluation Particle numbers on Characterization of Soil Particle Morphology Using Automated Particle Image Analysis and Computed Simulations.

*Daisuke Sasakura[1] (1.Malvern Japan ,Div of Spectris Co.Ltd,.)

[SGC33-P04] Role of fluid rock reaction for the production of FOZO isotopic composition

*Gen Shimoda[1], Tetsu Kogiso[2], Katsuhiko Suzuki[3], Akira Ishikawa[4], Norikatsu Akizawa[5] (1.Geological Survey of Japan, AIST, 2.Kyoto University, 3.Japan Agency for Marine-Earth Science and Technology, 4.Tokyo Institute of Technology, 5.University of Tokyo)

[J] Poster | S (Solid Earth Sciences)：S-TT Technology & Techniques

5:15 PM - 6:30 PM JST | 8:15 AM - 9:30 AM UTC | Ch.18_1

[S-TT36] Synthetic Aperture Radar and its application

convener:Yohei Kinoshita(University of Tsukuba), Takahiro Abe(Graduate School of Bioresources, Mie University), Shoko Kobayashi(Tamagawa University), Yuji Himematsu(National Research Institute for Earth Science and Disaster Resilience)

[STT36-P01] Long-term crustal deformation of domestic volcanoes detected by InSAR time series analysis

*Kano Mikihara[1], Takaaki Inukai[1], Nobuhiro Ishikura[1], Kumi Shimazaki[1], Masayoshi Ishimoto[1], Tomokazu Kobayashi[1] (1.GSI of Japan)

[STT36-P02] Surface displacement in Hachijojima Island since 2014 by InSAR analysis and GNSS

*yusei Hamamura[1], HIROYUKI AZUMA[1], Yoshiya Oda[1] (1.Tokyo Metropolitan University)

[STT36-P03] Observing Crustal Deformation Using Interferometric Synthesis Aperture Rader and Estimating Magma Chamber Associating with the 2018 Eruption of Shinmoedake of Kirishima Volcanoes, Japan.

*Takahisa Tashiro[1], Koichi Suzuki[2] (1.Cooperative Program for Resources Engineering, Graduate School of Engineering, Hokkaido University, 2.Research Group of Geoenvironmental Engineering, Division of Sustainable Resource Engineering, Faculty of Engineering, Hokkaido University)

[STT36-P04] **Using InSAR for evaluating the accuracy of earthquake location determination, Comparison of Iranian and Japanese cases**

*Nematollah Ghayournajarkar[1], Yo Fukushima[2] (1.Graduate School of Science, Tohoku University, 2.International Research Institute of Disaster Science, Tohuku University)

[STT36-P05] Progress on developing a GNSS-based InSAR atmospheric delay correction model

*Yohei Kinoshita[1] (1.University of Tsukuba)

[STT36-P06] **Ship Detection Using Synthetic Aperture Radar**

*Kengo Iwata[1], Masanobu Shimada[1] (1.Tokyo Denki University)

[J] Poster | S (Solid Earth Sciences)：S-TT Technology & Techniques

5:15 PM - 6:30 PM JST | 8:15 AM - 9:30 AM UTC | Ch.13_3

[S-TT38] Creating future of solid Earth science with high performance computing (HPC)

convener:Takane Hori(R&D Center for Earthquake and Tsunami, Japan Agency for Marine-Earth Science and Technology), Yuji Yagi(Graduate School of Life and Environmental Sciences, University of Tsukuba, Tsukuba), Katsuhiko Shiomi(National Research Institute for Earth Science and Disaster Resilience), Ryoichiro Agata(Japan Agency for Marine-Earth Science and Technology)

[STT38-P01] CMT catalog based on a local 3D structure model for simulations of long-period ground motions in the Kanto region, Japan

*Kazuo Yoshimoto[1], Kosuke Minamihama[1], Shunsuke Takemura[2], Katsuhiko Shiomi[3] (1.Yokohama City University, 2.Earthquake Research Institute, The University of Tokyo, 3.NIED)

[STT38-P02] Coordinate Independent Visualization Method for Stress Tensor Field by Using Principal Axis Line

*Sayako Hirobe[1], Kenji Oguni[1], Muneo Hori[1] (1.Japan Agency for Marine-Earth Science and Technology)

[J] Poster | S (Solid Earth Sciences)：S-CG Complex & General

5:15 PM - 6:30 PM JST | 8:15 AM - 9:30 AM UTC | Ch.19_1

[S-CG45] Ocean Floor Geoscience

convener:Kyoko Okino(Atmosphere and Ocean Research Institute, The University of Tokyo)

[SCG45-P01] **Temporal variation of crustal accretion along the Vulcan Transform, the Southern Ocean: Preliminary results of KH-19-6 cruise**

*Kyoko Okino[1], Kenichiro Tani[2], Osamu Ishizuka[3], Hiroaki Koge[3], JINYU ZHOU[1] (1.Atmosphere and Ocean Research Institute, The University of Tokyo, 2.National Museum of Nature and Science, 3.National Institute of Advanced Industrial Science and Technology)

[SCG45-P02] S wave velocity structure at the Kairei Hydrothermal Vent Field near the Rodriguez Triple Junction in the Indian Ocean

*Ayato Morii[1], Toshinori Sato[1], Hiroyoshi Takata[1], Tomoaki Yamada[2], Masanao Shinohara[3] (1.Chiba Unv., 2.JMA, 3.ERI, Unv. Tokyo)

[SCG45-P03] **Deep-tow magnetics for 29–33 Myr seafloor of the Southeast Indian Ridge**

*Masakazu Fujii[1,2], Kyoko Okino[3], Chiori Tamura[3] (1.National Institute of Polar Research, 2.SOKENDAI (The Graduate University for Advanced Studies), 3.AORI, UTokyo)

[SCG45-P04] **Magnetic and gravity constraints on crustal structure of the Nosappu Fracture Zone, Northwestern Pacific**

*Mai Kintsu[1], Nobukazu Seama[1], Masakazu Fujii[2,3], Tomoko Hanyu[4] (1.Department of Planetology, Graduate School of Science, Kobe University, 2.National Institute of Polar Research, 3.SOKENDAI (The Graduate University for Advanced Studies), 4.Kobe Ocean-Bottom Exploration Center)

[SCG45-P05] Multibeam bathymetric and single-channel seismic surveys of the Mid-Slope Terrace off Sanriku in the northern Japan Trench

*Toshiya Fujiwara[1], Toshiya Kanamatsu[1], KanHsi Hsiung[1] (1.Research Institute for Marine Geodynamics, Japan Agency for Marine-Earth Science and Technology)

[SCG45-P06] Deformation of the upper plate within the Tohoku Region Pacific Coast analyzed by the top surface structure

*Hiroaki Koge[1], Ayanori Misawa[1], Toshiya Fujiwara[2], Yoshiaki Suzuki[1], Yusuke Sato[3], Ryosuke Komatsu[5], Chiori Tamura[4], Katsura Kameo[4] (1.AIST, 2.JAMSTEC, 3.Tokai Univ., 4.AORI. UTokyo, 5.MOL Marine Co., Ltd)

[SCG45-P07] Classification and estimation of petit-spot volcanos by multibeam backscatter data

*Matamura Yuki[1], Naoto Hirano[2], Masakazu Fujii[3,4] (1.Tohoku University, 2.Center for Northeast Asian Studies, Tohoku University, 3.National Institute of Polar Research, 4.SOKENDAI)

[SCG45-P08] Origin of Philippine Sea basins -Tectonic setting leading to subduction initiation of Izu-Bonin-Mariana arc-

*Osamu Ishizuka[1,2], Kenichiro Tani[3], Gen Shimoda[1], Yumiko Harigane[1], Taichi Sato[1], Rex Taylor[4], Susumu Umino[5], Tian Yu Ping[5], Izumi Sakamoto[6], Yuka Yokoyama[6], Sho Yatsuka[6], Ryota Uchiyama[6], Tomoaki Wakayama[6], Aimi Suzuki[6], Kana Narita[7], Chinatsu Ogawa[7], Yasuhiko Ohara[8,2,9], Chris Conway[1] (1.Geological Survey of Japan, AIST, 2.JAMSTEC, 3.NMNS, 4.University of Southampton, 5.Kanazawa University, 6.Tokai University, 7.Ehime University, 8.Japan Coast Guard, 9.Nagoya University)

[SCG45-P09] What happened to the seafloor around Nishinoshima volcano during deployment of OBEMs between September 2018 and December 2020?

*Noriko Tada[1], Kiyoshi Baba[2], Toshiya Fujiwara[1], Yoshihiko Tamura[1], Toshiya Kanamatsu[1], Kenta Yoshida[1], Akimichi Takagi[3], Fukashi Maeno[2] (1.Research Institute for Marine Geodynamics, Japan Agency for Marine-Earth Science and Technology, 2.Earthquake Research Institute, The University of Tokyo, 3.Japan Meteorological Agency)

[SCG45-P10] Estimation of the Active Faults from BSR-derived heat flow by Automated Velocity Analysis in the Nankai Trough, Japan

*Shuto Takenouchi[1], Kota Mukumoto[1], Takeshi Tsuji[1], Shuichi Kodaira[2], Gou Fujie[2], Yasuyuki Nakamura[2], Kazuya Shiraishi[2] (1.Kyushu-university, 2.Japan Agency for Marine-Earth Science and Technology)

[SCG45-P11] Precipitation process and early diagenesis after deposition of iron hydroxide in Nagahama Bay, Satsuma Iwo-Jima Island, Kagoshima, Japan.

*Koki Hori[1], Shoichi Kiyokawa[2], Minoru Ikehara[3] (1.Department of Earth and Planetary Sciences, Graduate School of Sciences, Kyushu University, 2.Department of Earth and Planetary Sciences Faculty of sciences, Kyuushu University, 3.Center for Advanced Marine Core Research, Kochi University)

[SCG45-P12] Geological structures in the southern part of the Okinawa Trough north off Ishigaki Island: Preliminary results of the KH-21-3 cruise

*Ayanori Misawa[1], Ryuta Arai[2], Masahiko Sato[3], Saki Ishino[1], Misaki Horiuchi[4], Keita Suzuki[4], Chiori Tamura[5], Katsura Kameo[5], Satoshi Okumura[6], Makoto Otsubo[1], KH-21-3 Shipboard Scientists (1.Geological Survey of Japan, National Institute of Advanced Industrial Science and Technology(AIST), 2.Research Institute for Marine Geodynamics, Japan Agency for Marine-Earth Science and Technology (JAMSTEC), 3.Department of Earth and Planetary Science, The University of Tokyo, 4.Nippon Marine Enterprises, Ltd., 5.Atmosphere and Ocean Research Institute, The University of Tokyo, 6.MOL Marine Co. Ltd.)

[SCG45-P13] **The link between volcanism and tectonics at back-arc rifting stage: analysis of three volcanic areas in the southern Okinawa Trough**

*JINYU ZHOU[1], Kyoko Okino[1], Masakazu Fujii[2,3] (1. Atmosphere and Ocean Research Institute, The University of Tokyo, 2.National Institute of Polar Research, 3.The Graduate University for Advanced Studies)

[SCG45-P14] Mineralogical and geochemical study of sediment cores collected from the Ieyama hydrothermal field in the Okinawa Trough

*Jun-ichiro Ishibashi[1], Takashi Miyamoto[1,3], Shuhei Totsuka[1,2], Kazuhiko Shimada[1], Toru Yamasaki[2], Ken Ikehara[2], Toshiro Nagase[4], Yutaro Takaya[5], Hideaki Machiyama[6], Koichi Iijima[6], Hirofumi Yamamoto[6], Hidenori Kumagai[6] (1.Department of Earth and Planetary Sciences, School of Science, Kyushu University, 2.National Institute of Advanced Industrial Science and Technology, 3.School of science, University of Tokyo, 4.Tohoku University Museum, 5.Waseda Research Institute for Science and Engineering, 6.Japan Agency for Marine-Earth Science and Technology)

[SCG45-P15] Geochemical and geochronological study of barite in sediment cores obtained from Higashi Izena hydrothermal field, Okinawa Trough

Yushi Itatani[1], *Jun-ichiro Ishibashi[1], Makiko Tomita[2], Shin Toyoda[2], Ryuichi Shinjo[3], Kazuno Arai[4], Taisei Fujiwara[5] (1.Department of Earth and Planetary Sciences, Graduate School of Science, Kyushu University, 2.Okayama University of Science, 3.Faculty of Science, University of Ryukyus, 4.Center for Advanced Marine Core Research, Kochi University, 5.Institute for Geology and Geochronology)

[SCG45-P16] Fin whale signals recorded by S-net

*Masashi Mochizuki[1], Takeshi Nakamura[2], Ryoichi Iwase[3], Kenji Uehira[1] (1.National Research Institute for Earth Science and Disaster Resilience, 2.Central Research Institute of Electric Power Industry, 3.Japan Agency for Marine-Earth Science and Technology)

[SCG45-P17] Effective removal of oceanic variation from ocean bottom pressure gauge data using the MSSA

*Kenta Shimizu[1], Toshinori Sato[1], Koichi Murata[1], Norihisa Usui[2], Hajime Shiobara[3], Tomoaki Yamada[4], Masanao Shinohara[3] (1.Chiba Univ., 2.MRI, 3.ERI. Univ. Tokyo, 4.JMA)

[SCG45-P18] Sampling process of seafloor sediments as a source of information on their rheology

*Nikita Dubinya[1,2], Sergey Tikhotskiy[1,2], Victor Nachev[1,3] (1.Moscow Institute of Physics and Technology, 2.Schmidt Institute of Physics of the Earth of the Russian Academy of Sciences, 3.Sadovsky Institute of Geosphere Dynamics of the Russian Academy of Sciences)

[SCG45-P19] Technical protocol for deep-sea environmental monitoring by the portable seafloor observation platform Edokko Mark 1

*Hiroyuki Yamamoto[1], Tetsuya Miwa[1], Shinsuke Kawagucci[1], Sangkyun Lee[2], Atsuo Oono[3], Kousuke Tsutsumi[3], Hideki Sugishima[3] (1.Japan Agency for Marine-Earth Science and Technology, 2.J-MARES/JGI, 3.J-MARES/idea)

[J] Poster | S (Solid Earth Sciences)：S-CG Complex & General

5:15 PM - 6:30 PM JST | 8:15 AM - 9:30 AM UTC | Ch.18_2

[S-CG46] Rheology, fracture and friction in Earth and planetary sciences

convener:Shintaro Azuma(Department of Earth and Planetary Sciences, School of Science, Tokyo Institute of Technology), Ichiko Shimizu(Division of Earth and Planetary Sciences, Graduate School of Science, Kyoto University), Osamu Kuwano(Japan Agency for Marine-Earth Science and Technology), Miki Tasaka(Shizuoka University)

[SCG46-P01] Experimental investigation of the pyroxene-garnet and olivine-spinel transformations under shear deformation using synchrotron radiation and acoustic emission techniques

*Yuki Mori[1], Tomoaki Kubo[1], Rikuto Honda[1], Takuya Iwasato[2], Yuji Higo[3], Yoshinori Tange[3] (1.Kyushu Univ., 2.Shin-Nippon Nondestructive Inspection Co.,Ltd., 3.JASRI)

[SCG46-P02] Creep behavior during the post-spinel transformation in $(Mg, Fe)_2SiO_4$

*Yuta Goto[1], Tomoaki Kubo[1], Rikuto Honda[1], Yumiko Tsubokawa[1], Yuichiro Mori[2] (1.Kyushu Univ., 2.The University of Tokyo)

[SCG46-P03] SOR and AE study on the olivine-spinel transformation in $(Mg,Fe)_2SiO_4$ under uniaxial deformation with D111-type apparatus

*Rikuto Honda[1], Tomoaki Kubo[1], Yuichiro Mori[2], Goto Yuta[1], Yumiko Tsubokawa[1], Takuya Iwasato[3], Yuji Higo[4] (1.Kyushu University, 2.The University of Tokyo, 3.Shin-Nippon Nondestructive Inspection Co., Ltd., 4.JASRI)

[SCG46-P04] Frequency characteristics of acoustic emission in the fracture process of thermally cracked granite

*Sueyoshi Kazumasa[1], Manami Kitamura[2], Xinglin Lei[2], Ikuo Katayama[1] (1.Department of Earth and Planetary Systems Science, Hiroshima University, 2.National Institute of Advanced Industrial Science and Technology)

[SCG46-P05] Flow-to-fracture transition of linear Maxwell-type fluid by air injection

*Claudia Sanchez[1], Osamu Kuwano[2], Mie Ichihara[1] (1.Earthquake Research Institute, Tokyo University , 2.JAMSTEC)

[SCG46-P06] Role of lithology in deformation mechanisms of shallow-crustal active faults: Evidence from the Nahan thrust of Himalayas

*Dyuti Prakash Sarkar[1], Jun-ichi Ando[1], Kaushik Das[1], Gautam Ghosh[2], Prabir Dasgupta[3] (1.Hiroshima University, 2.Presidency University, 3.Durgapur Govt. College)

[SCG46-P07] Study of the mobile granular layer in bedload transport by laminar shearing flow in a tilted channel

*Chong-Wei Hong[1], Franco Tapia[2], Pascale Aussillous[3], Élisabeth Guazzelli[4], Chi-Yao Hung[1] (1.Department of Soil and Water Conservation, National Chung Hsing University, Taichung, Taiwan, 2.Department of Mechanical Engineering, Tokyo University of Agriculture and Technology, Tokyo, Japan, 3.Aix-Marseille Université, CNRS, IUSTI, Marseille, France, 4.Université de Paris, CNRS, Matière et Systèmes Complexes (MSC) UMR 7057, Paris, France)

[SCG46-P08] Fracture behavior of silicate network phase-separating from aqueous fluid

*Takehito Koyama[1] (1.Institute of Industrial Science, the University of Tokyo)

[SCG46-P09] Evolution of patterns of hydraulically conductive natural fractures during inelastic deformation of rocks

*Nikita Dubinya[1,2] (1.Moscow Institute of Physics and Technology, 2.Schmidt Institute of Physics of the Earth of the Russian Academy of Sciences)

[SCG46-P10] Theoretical study on rock anelasticity;
Extension of a grain-boundary sliding model to two dimensions

*Mitsuyoshi Kunugihara[1], Yasuko Takei[1] (1.Earthquake Research Institute,The University of Tokyo)

[SCG46-P11] A DEM model of uniaxial and triaxial compression test of rocks

*Mikito Furuichi[1], Daisuke Nishiura[1], Yuzuru Yamamoto[2] (1.Japan Agency for Marine-Earth Science and Technology, 2.Kobe University)

[SCG46-P12] Relaxation of the frictional force in a statistical mechanical model of magnetic friction

*Komatsu Hisato[1] (1.National Institute for Materials Science)

[J] Poster | M (Multidisciplinary and Interdisciplinary)：M-IS Intersection

5:15 PM - 6:30 PM JST | 8:15 AM - 9:30 AM UTC | Ch.21_3

[M-IS12] Planetary Volcanology

convener:Rina Noguchi(Faculty of Science, Niigata University), Nobuo Geshi(Geological Survey of Japan, The National Institute of Advanced Industrial Science and Technology), Tomokatsu Morota(Department of Earth and Planetary Science, The University of Tokyo)

[MIS12-P01] Review of duration and spatial heterogeneity of mare volcanism on the Moon

*Tomokatsu Morota[1] (1.Department of Earth and Planetary Science, The University of Tokyo)

[MIS12-P02] **Possible existence of lava tube cave and pit/fissure cave in the Moon and Mars**

*Tsutomu Honda[1] (1.Vulcano-speleological Society)

[MIS12-P03] Geomorphological and geological study of the summit caldera of Olympus Mons on Mars.

*Mayuko Nakamura[1], Tomohiro Tsuji[1] (1.Division of Earth Science The Graduate School of Sciences and Technology for Innovation , Yamaguchi University)

[MIS12-P04] The extent of shallow underground water-ice in the Amazonian period on Mars inferred from the distribution of rootless cones

*Rina Noguchi[1] (1.Institute of Space and Astronautical Science, Japan Aerospace Exploration Agency)

[J] Poster | M (Multidisciplinary and Interdisciplinary)：M-IS Intersection

5:15 PM - 6:30 PM JST | 8:15 AM - 9:30 AM UTC | Ch.22_1

[M-IS14] Aqua planetology

convener:Yasuhito Sekine(Earth-Life Science Insitute, Tokyo Institute of Technology), Takazo Shibuya(Japan Agency for Marine-Earth Science and Technology), Hidenori Genda(Earth-Life Science Institute, Tokyo Institute of Technology), Keisuke Fukushi(Institute of Nature & Environmental Technology, Kanazawa University)

[MIS14-P01] Experimental study of hypervelocity impact penetration of asteroids into the Ocean and benthic cratering

*Manabu Nishizawa[1] (1.Japan Agency for Marine-Earth Science and Technology)

[MIS14-P02] Experimental study on the growth process of iron rind in Fe-oxide concretions

*Hiroyuki Okamura[1], Sin-iti Sirono[1] (1.Department of Earth and Planetary Sciences, Nagoya University)

[MIS14-P03] **Redox change by coseismic water-rock reactions in the interior of planets**

*Takehiro Hirose[1], Ryoichi Nakada[1], Keishi Okazaki[1], Takazo Shibuya[1] (1.Japan Agency for Marine-Earth Science and Technology)

[MIS14-P04] Characterizations of mineralogy and infrared spectra of serpentinized samples in Oman ophiolite along with redox gradients in subsurface: Toward identification of redox gradients in Martian subsurface

*Takumi Sato[1], Yasuhito Sekine[1], Ikuo Katayama[2] (1.Tokyo Institute of Technology , 2.Hiroshima University)

[MIS14-P05] Experimental study of element dissolution to liquid CO_2 from artificial seawater and hydrothermal vent chimney

*Kaito Seo[1,2], Takazo Shibuya[2], Kosuke Fujishima[3], Ken Takai[2], Masaru Tomita[1,4] (1.Graduate School of Media and Governance, Keio Univ., 2.JAMSTEC, 3.ELSI, 4.IAB, Keio Univ.)

[MIS14-P06] Rocognition and classification of Martian chaos terrains using imagery marchine learning: Implications for groundwater distribution and hydrological cycles

Hiroki Shozaki[2], *Yasuhito Sekine[1], Nicholas Guttenberg[1] (1.Earth-Life Science Insitute, Tokyo Institute of Technology, 2.Dept. Earth Planetary Sci., Tokyo Institute of Technology)

[MIS14-P07] No effective oxychloride formations on Europa's surface inferred from UV/electron irradiation experiments onto salt-ice mixtures

*Shuya Tan[1], Yasuhito Sekine[1], Takashi Kikuchi[2], Hisayuki Suematsu[2], Tetsuya Hama[3], Yoshio Takahashi[4] (1.Earth-Life Science Institute, Tokyo Institute of Technology, 2.Nagaoka University of Technology, 3.Komaba Institute for Science, The University of Tokyo, 4.Department of Earth and Planetary Science, Graduate School of Science, The University of Tokyo)

[MIS14-P08] An experimental study on evaporite formation around the north pole of Titan

*Eito Hirai[1,2], Yasuhito Sekine[2], ZHANG NAIZHONG[2] (1.Department of Earth and Planetary Sciences, School of Science, Tokyo Institute of Technology, 2.Earth-Life Science Institute, Tokyo Institute of Technology)

[MIS14-P09] **Prediction of the composition of the primordial ocean just after its formation**

*Hisahiro Ueda[1], Takazo Shibuya[1] (1.JAMSTEC)

[MIS14-P10] **Formation conditions of magnetite and hematite in Sheepbed mudstone and bioavailable energies in lake water-groundwater mixing zone in Gale crater, Mars**

*Sakiko Kikuchi[1], Takazo Shibuya[1] (1.Japan Agency for Marine-Earth Science and Technology)

[MIS14-P11] Measurements of elastic wave velocity of mafic and ultramafic rocks below the freezing point: Consideration about reflectivity due to ice-water phase transition in Mars

*Haruna Wakabayashi[1], Ikuo Katayama[1] (1.Hiroshima University)

[MIS14-P12] Viscosity of aqueous MgSO4 solutions at high-pressure and low-temperature: implications for icy satellites

*Shunsuke Nozaki[1], Seiji Kamada[2,3], Akio Suzuki[2] (1.Division of Earth and Planetary Materials Science, Faculty of Science, Tohoku University , 2.Department of Earth Science, Graduate School of Science, Tohoku University,

3.Frontier Research Institute for Interdisciplinary Sciences, Tohoku University)

[MIS14-P13] Formation mechanism of spherical concretions in Tatsukushi area: Possible analogy with spherical nodule in Gale crater, Mars

*Saki Asai[1], Hitoshi Hasegawa[1], Hidekazu Yoshida[2], Minoru Ikehara[1], Nagayoshi Katsuta[3], Masakazu Nara[1], Yui Tomonao[1], Satoru Imai[4] (1.Kochi University, 2.Nagoya University, 3.Gifu University, 4.Tosashimizu GeoPark)

[MIS14-P14] Synthesis and reversible redox properties of iron-saponite

*Hiroshi Sakuma[1], Koki Morida[2], Keisuke Fukushi[2], Yoshio Takahashi[3], Natsumi Noda[3,4], Yasuhito Sekine[4], Kenji Tamura[1] (1.National Institute for Materials Science, 2.Kanazawa University, 3.University of Tokyo, 4.Tokyo Institute of Technology)

[MIS14-P15] Physical dependence of stable carbon and hydrogen isotopic ratio of methane gas in gas hydrate

*Kushi Kudo[1], Atsushi Tani[1], Keita Yamada[2], Naohiro Yoshida[3] (1.Graduate School of Human Development and Environment, Kobe University, 2.Department of Chemical Science and Engineering, School of Materials and Chemical Technology, Tokyo Institute of Technology, 3.Earth–Life Science Institute)

[MIS14-P16] **Clumped isotope signatures of abiotic methane formed via Fischer-Tropsch catalysis and their implications**

*ZHANG NAIZHONG[1], Yasuhito Sekine[1], Mayuko Nakagawa[1], Naohiro Yoshida[1] (1.Tokyo Institute of Technology)

[MIS14-P17] Possibilities of the rubidium stable isotope ratio as geochemical tools

*Rimi Konagaya[1], Hiroyuki Tsuboi[1], Takaaki Itai[1], Yoshio Takahashi[1] (1.The University of Tokyo)

[MIS14-P18] **Determination method of ^{13}C-labeled isotopomer ratio of dissolved organic acids by GC-MS analysis**

*Konomi Suda[1] (1.National Institute of Advanced Industrial Science and Technology)

[MIS14-P19] **Selectivity coefficient of Na^+-NH_4^+ exchange in saponite interlayer: Reconstruction of ammonium concentration in early ocean on Ceres**

*Hiroto Tokumon[1], Keisuke Fukushi[2], Yasuhito Sekine[3], Kosuke Inoue[1], Koki Morida[1] (1.Kanazawa University , 2.Institute of Nature and Environmental Technology Kanazawa University, 3.Tokyo institute of technology)

[J] Poster | M (Multidisciplinary and Interdisciplinary) : M-IS Intersection

5:15 PM - 6:30 PM JST | 8:15 AM - 9:30 AM UTC | Ch.23

[M-IS16] Paleoclimatology and paleoceanography

convener:Yusuke Okazaki(Department of Earth and Planetary Sciences, Graduate School of Science, Kyushu University), Hitoshi Hasegawa(Faculty of Science and Technology, Kochi University), Atsuko Yamazaki(Faculty of Science, Kyushu University), Akitomo Yamamoto(Japan Agency for Marine-Earth Science and TechnologyAtmosphere and Ocean Research Institute)

[MIS16-P01] Temperature effect on Japanese stalagmite $\delta^{18}O$ records from Hiroshima and Gifu

*Hirokazu Kato[1], Taiki Mori[2], Shota Amekawa[1], Akihiro Kano[1] (1.Department of Earth and Planetary Science, The University of Tokyo, 2.Chuo Kaihatsu Corporation)

[MIS16-P02] **Oxygen isotope equilibrium of the shallow-water benthic foraminifer *Hanzawaia nipponica* (Asano) in Tosa Bay, southwest Japan**

*Minoru Ikehara[1,2], Shigetaka Kita[2], SHUNGO KAWAGATA[3] (1.Center for Advanced Marine Core Research, Kochi University, 2.Graduate School of Integrated Arts and Sciences, Kochi University, 3.Faculty of Education, Yokohama National University)

[MIS16-P03] **Variations in shell morphology of the planktonic foraminifer *Globigerina bulloides* in the sediment off Kashima**

*Yuya Hashimoto[1], Takuya Sagawa[2] (1.Kanazawa University College of Science and Engineering, 2.Institute of Science and Engineering, Kanazawa University)

[MIS16-P04] Climate characteristics of Amami , Kagoshima , Japan over the past 200 years inferred from tree-ring cellulose oxygen isotope ratio data

*Akihiro Masuoka[1], Kenjiro Sho[1], Masafumi Ohata[2], Zhen Li[3], Takeshi Nakatsuka[3] (1.Nagoya Institute of Technology, 2.Taisei Corporation, 3.Nagoya University)

[MIS16-P05] Coral skeletal records reveal the relationship between Kuroshio variability and North Pacific climate

*Atsuko Yamazaki[1,2], Tsuyoshi Watanabe[2,3] (1.Kyushu University, 2.KIKAI institute for Coral Reef Sciences, 3.Hokkaido University)

[MIS16-P06] Reconstruction of environmental and flooding histories since AD1250 at Lake Kortta, an annually laminated lake at the Central Finland presumed by Diatom and Chrysophyceae assemblages

*Kaoru Kashima[1], Yu Fukumoto[2], Timo Saarinen[3] (1.Department of Earth and Planetary Sciences, Kyushu University, 2.Osaka City University, 3.University of Turku)

[MIS16-P07] **Sphagnum and grass cellulose oxygen isotopes in peat cores reveal climate changes in northern Japan over the past 4400 years and close relationship with human histories**

*Masanobu Yamamoto[1], Osamu Seki[2] (1.Faculty of Environmental Earth Science, Hokkaido University, 2.Insititute of Low Temperature Science)

[MIS16-P08] Can Sedimentary fish DNA track decadal to centennial scale fish abundance?

*Michinobu Kuwae[1], Hiromichi Tamai[1], Hideyuki Doi[2], Masayuki Sakata[3], Toshifumi Minamoto[3], Yoshiaki Suzuki[4] (1.Center for Marine Environmental Studies, 2.Graduate School of Simulation Studies, University of Hyogo, 3.Graduate School of Human Development and Environment, Kobe University, 4.Research Institute of Geology and Geoinformation, Geological Survey of Japan, National Institute of Advanced Industrial Science and Technology)

[MIS16-P09] Paleoenvironmental variations reconstructed by algal biomarker analysis of a sediment core from Lake Nakaumi, Japan

*Akiko Taneichi[1], Yuki Hattori[1], Ken Sawada[1], Takuto Ando[2], Hideto Nakamura[3], Kotaro Hirose[4] (1.Hokkaido Univ., 2.Shimane Univ., 3.Osaka City Univ., 4.Waseda Univ.)

[MIS16-P10] Paleoceanographic changes in the western part of the Arctic Sea based on ostracods

*Katsura Yamada[1], Kosuke Yamaguchi[1], Masao Uchida[2], Takuya Itaki[3], Kanako Mantoku[2] (1.Department of Geology, Faculty of Science, 2.National Institute for Environmental Studies, 3.National Institute of Advanced Industrial Science and Technology)

[MIS16-P11] **Mid- to late Holocene variability of the Aleutian Low Atmospheric Pressure Cell: Forcing by the Western Jet**

*Kana Nagashima[1], Jason Addison[2], Tomohisa Irino[3], Takayuki Omori[4], Kei Yoshimura[5], Naomi Harada[1] (1.Research Institute for Global Change, Japan Agency for Marine-Earth Science and Technology, 2.U.S. Geological Survey, 3.Faculty of Environmental Earth Science, Hokkaido University, 4.The University Museum, The University of Tokyo, 5.Institute of Industrial Science, The University of Tokyo)

[MIS16-P12] Sedimentary characteristics, age and event of a marine core collected from Uranouchi Bay, Kochi, Japan

*Masafumi MURAYAMA[1,3], Wataru Tanikawa[2], Akira Ijiri[2], Tatsuhiko Hoshino[2], Takehiro Hirose[2], Katsuya Nejigaki[3], Kazuno Arai[3], Go-Ichiro Uramoto[3], Kondo Yasuo[4], Hiromasa Ozaki[5], Minoru Yoneda[5] (1.Faculty of Agriculture and Marine Science, Kochi University, 2. Institute for Extra-cutting-edge Science and Technology Avant-garde Research, Kochi Institute for Core Sample Research, JAMSTEC, 3.Center for Advanced Marine Core Research, Kochi University, 4.Faculty of Science and Technology, Kochi University, 5.The University Museum,The University of Tokyo)

[MIS16-P13] Estimation of amount of meltwater discharge from the Laurentide to the Arctic Ocean during the MWP1a event

★Invited Papers

*Kenta Suzuki[1], Masanobu Yamamoto[1], Leonid Polyak[2], Tomohisa Irino[1] (1.Faculty of Environmental Earth Science, Hokkaido Univ., 2.Byrd Polar and Climate Research Center, The Ohio State Univ.)

[MIS16-P14] Millennial variability in precipitation in Papua New Guinea during the last deglaciation

*Gaku Sudo[1], Masanobu Yamamoto[1], Samantha Bova[2], Yair Rosenthal[2] (1.Faculty of Environmental Earth Science, Hokkaido Univ., 2.Rutgers Univ.)

[MIS16-P15] A paleoclimatic reconstruction of the southeastern Pacific last deglacial using geochemical proxies obtained from offshore Chile

*Karin Nemoto[1,2], Yusuke Yokoyama[1,2], Adam David Sproson[2], Yosuke Miyairi[2], Takahiro AZE[2], Hiroyuki Matsuzaki[3,4], Yair Rosentha[5], Samantha Bova[5] (1.Department of Earth and Planetary Science, The University of Tokyo, 2.Atmosphere and Ocean Research Institute, The University of Tokyo, 3.The University Museum,The University of Tokyo, 4.School of Engineering, The University of Tokyo, 5.Department of Marine and Coastal Sciences, School of Environmental and Biological Sciences, Rutgers University)

[MIS16-P16] Paleovegetation changes in the northern Mongolia since the last glacial

*Ryosuke Imaoka[1], Koji Shichi[2], Hitoshi Hasegawa[1], Niiden Ichinnorov[3], Nagayoshi Katsuta[4], Davaasuren Davaadorj[5], Masafumi MURAYAMA[1], Masao Iwai[1], masami izuho[6] (1.Kochi University, 2.Forestry and Forest Products Research Institute, 3.Paleontological Center of Mongolia, 4.Gifu University, 5.National University of Mongolia, 6.Tokyo Metropolitan University)

[MIS16-P17] Glacial–interglacial variations in the Leeuwin Current for the last 50,000 years based on Nd isotope records of benthic foraminifers

*Ryota Wako[1], Hideko Takayanagi[1], Shigeyuki Wakaki[2], Takeshige Ishiwa[4], Yusuke Yokoyama[5], Hitomi Uchimura Wakaki[3], Tsuyoshi Ishikawa[2], Yasufumi Iryu[1] (1.Department of earth science, Tohoku university , 2.Kochi Institute for Core Sample Research, JAMSTEC, 3.Center for Advanced Marine Core Research, Kochi University, 4.National Institute of Polar Research, 5.Atmosphere and Ocean Research Institute, University of Tokyo)

[MIS16-P18] Changes in carbonate dissolution and preservation in Southern Ocean sediment off Chilean margin during the last 140 kyrs based on fragmentation and size-normalized weight of planktic foraminiferal tests.

*Takuto Kasuya[1], Yusuke Okazaki[2], Shinya Iwasaki[3], IODP Expedition 383 Scientific Party (1.Department of Earth and Planetary Sciences, School of Science, Kyushu University , 2.Department of Earth and Planetary Sciences, Faculty of Science, Kyushu University, 3.MARUM Center for Marine Environmental Sciences and Department of Geosciences, University of Bremen)

[MIS16-P19] Examining MIS 5e Sea-Levels around Japan: 60+ Years of Sea-Level Proxy Analysis and Applied Dating Techniques

*Evan Tam[1,2], Yusuke Yokoyama[1,2] (1.University of Tokyo, Atmosphere and Ocean Research Institute, 2.University of Tokyo, Graduate Program on Environmental Science)

[MIS16-P20] Integrated stratigraphy of the sediment core retrieved from the Manihiki Plateau in the central Pacific and the paleotemperature change for the last 800 kyr

*MISAKI URAKAMI[1], Takuya Sagawa[2], Yoshimi Kubota[3] (1.College of Science and Engineering, Kanazawa University, 2.Institute of Science and Engineering, Kanazawa University, 3.National Museum of Nature and Science)

[MIS16-P21] Preliminary results of oxygen isotopic, paleomagnetic, and pollen analyses from a mid-Piacenzian marine succession in the Boso Peninsula, central Japan.

*Yuki Haneda[1] (1.Geological Survey of Japan, AIST)

[MIS16-P22] The mid-Pliocene Warm Period: climate sensitivity to atmospheric CO_2 levels and inclusion of dynamic vegetation in the MIROC4m model

*Wing-Le Chan[1], Ayako Abe-Ouchi[1,2] (1.Atmosphere and Ocean Research Institute, The University of Tokyo, 2.National Institute of Polar Research)

[MIS16-P23] Chemical weathering feedback during the early Paleogene hyperthermals based on osmium isotope analysis

*Kakeru Ikegami[1], Kazutaka Yasukawa[1,2], Erika Tanaka[1], Junichiro Ohta[1,2], Yusuke Kuwahara[1], Moei Yano[2,1], Koichiro Fujinaga[2,1], Yasuhiro Kato[1,2] (1.School of Engineering, The University of Tokyo, 2.ORCeNG, Chiba Institute of Technology)

[MIS16-P24] High latitude paleoenvironments in Southern Hemisphere during mid-Cretaceous

*Hiromichi Komiya[1], Takashi Hasegawa[1] (1.Kanazawa University)

[MIS16-P25] A study on the responses of the climate field in the Cretaceous to orbital parameter changes

★Invited Papers

*Taro Higuchi[1], Ayako Abe-Ouchi[1], Wing-Le Chan[1] (1.Atmospheric and Ocean Research Institute, the University of Tokyo)

[MIS16-P26] **Eccentricity paced increase in the continental weathering in the latest Hauterivian, Early Cretaceous**

★Invited Papers

*Hironao Matsumoto[1], Rodolfo Coccioni[2], Fabrizio Frontalini[2], Kotaro Shirai[1], Junichiro Kuroda[1] (1.Atmosphere and Ocean Research Institute, the University of Tokyo, 2.University of Urbino)

[MIS16-P27] Millennial-scale cyclicities recorded in the Cretaceous lacustrine core using Monte Carlo approach

*Hitoshi Hasegawa[1], Hirofumi Asahi[2] (1.Faculty of Science and Technology, Kochi University, 2.Center for Advanced Marine Core Research, Kochi University)

[J] Poster | M (Multidisciplinary and Interdisciplinary)：M-IS Intersection

5:15 PM - 6:30 PM JST | 8:15 AM - 9:30 AM UTC | Ch.21_4

[M-IS17] Interface- and nano-phenomena on crystal growth and dissolution

convener:Yuki Kimura(Institute of Low Temperature Science, Hokkaido University), Hitoshi Miura(Graduate School of Science, Department of Information and Basic Science, Nagoya City University), Hisao Satoh(Low-Level Radioactive Waste Disposal Center, Japan Nuclear Fuel Limited)

[MIS17-P01] Toward for the developing the thermal storage materials utilizing the Electrostatic Levitation Furnace in "Kibo" in space

*Hidekazu Kobatake[1], Kazuki Tonooka[2], Shumpei Ozawa[2], Ken'ichi Sugioka[3], Suguru Shiratori[4], Ken Nagashima[5], Hirohisa Oda[6], Hideki Saruwatari [6], Chihiro Koyama[6], Takehiko Ishikawa[6] (1.Hirosaki University, 2.Chiba Institute of Technology, 3.Toyama Prefectural University, 4.Tokyo City University, 5.Hokkaido University, 6.JAXA)

[MIS17-P02] Heteroepitaxial growth mechanism in colloidal crystallization

*Jun Nozawa[1], Hiromasa Niinomi[1], Junpei Okada[1], Satoshi uda[1] (1.Tohoku University)

[MIS17-P03] Fabrication of evaluation model for adgesion mechanism between bone mineral and soft tissue

*Yuki Sugiura[1], Masahiro Okada[2], Ken Hirano[1], Takuya Matsumoto[2] (1.National Institute of Advanced Industrial Science and Technology, 2.Okayama University)

[MIS17-P04] Conversion from a stable crystal to a metastable crystal by grinding

*Hiroyasu Katsuno[1], Makio Uwaha[2] (1.Institute of Low Temperature Science, Hokkaido University, 2.Center for General Education, Aichi Institute of Technology)

[MIS17-P05] Improvement of transmission electron microscope images by neural network model

*Hiroyasu Katsuno[1], Shizuka Hirakawa[1], Tomoya Yamazaki[1], Ichigaku Takigawa[2], Yuki Kimura[1] (1.Institute of Low Temperature Science, Hokkaido University, 2.RIKEN, Center for Advanced Intelligence Project)

[MIS17-P06] Development of an early detection method of nucleation in in-situ liquid-cell TEM observation

*Yuki Kimura[1], Hiroyasu Katsuno[1], Tomoya Yamazaki[1], Ichigaku Takigawa[2,3] (1.Institute of Low Temperature Science, Hokkaido University, 2.AIP, RIKEN, 3.ICReDD, Hokkaido University)

[MIS17-P07] In-situ observation at the moments of bubble nucleation using a liquid-cell transmission electron microscope

*Yuki Kimura[1], Tomoya Yamazaki[1], Hiroyasu Katsuno[1], Shizuka Hirakawa[1] (1.Institute of Low Temperature Science, Hokkaido University)

[J] Poster | M (Multidisciplinary and Interdisciplinary)：M-IS Intersection

5:15 PM - 6:30 PM JST | 8:15 AM - 9:30 AM UTC | Ch.20_3

[M-IS20] Ocean Plastics, an earth science perspective

convener:Atsuhiko Isobe(Research Institute for Applied Mechanics, Kyushu University), Kiichiro Kawamura(Yamaguchi University), Yusuke Okazaki(Department of Earth and Planetary Sciences, Graduate School of Science, Kyushu University), Masashi Tsuchiya(Research Institute for Global Change, Japan Agency for Marine-Earth Science and Technology)

[MIS20-P01] Automatic detection for Nile Red-stained microplastic particles

*Masashi Tsuchiya[1], Tomo Kitahashi[1], Yosuke Taira[2], Hitoshi Saito[2], Kazumasa Oguri[1,3], Ryota Nakajima[1], Dhugal J. Lindsay[4], Katsunori FUJIKURA[1], Tomohiko Fukushima[1,5] (1.Research Institute for Global Change, Japan Agency for Marine-Earth Science and Technology, 2.NEC Corporation, 3.Danish Center for Hadal Research, University of Southern Denmark, 4.Institute for Extra-cutting-edge Science and Technology Avant-garde Research, Japan Agency for Marine-Earth Science and Technology, 5.Deep Ocean Resources Development Co., Ltd.)

[MIS20-P02] Deep sea Macro plastics in the Northwestern Pacific Ocean

*Tomoaki Kitayama[1], Takashi Hosono[1], Hideaki Saito[1] (1.Japan Agency for Marine-Earth Science and Technology)

[J] Poster | U (Union)：Union

Sat. Jun 5, 2021 5:15 PM - 6:30 PM JST | Sat. Jun 5, 2021 8:15 AM - 9:30 AM UTC | Ch.01_2

[U-14] Current status and issues of the earth education necessary for living on the changing earth

convener:Hiroshi Ichikawa, Saori Nakai(kyoto koka womens university department of child education), Hidenori Kumagai(Japan Agency for Marine-Earth Science and Technology), Hiroshi Nishi(The Center for Academic Resources and Archives, The Tohoku Museum Tohoku University)

A proposal entitled by "Importance of Earth Education in Elementary and Secondary School Education and Lifelong Education: for learning essential knowledge to live on a changing earth" was published by the Science Council of Japan on June 23, 2020. This proposal points out that, for all people living in the Japanese archipelago frequently attacked by severe natural disasters, it is important to increase the chances to acquire "the essential knowledge to live on a changing earth" in school learning of the nature, and learn it lifelong. Responding to this proposal, this session is held by WG for Studying on Teacher Training System, established for studying complex and diverse issues related to teacher training and others in May 2019 in the Education Committee, JpGU. This session aims to deepen discussions on the current situation and issues of elementary and secondary school teachers responsible for earth education in the fields of Geosciences and Geography regarding the teacher training and recruitment system and self-improvement of knowledge and skills.

[U14-P01] WG for Studying on Teacher Training System in JpGU

*Hidenori Kumagai[1], Saori Nakai[2], Teacher's training WG JpGU Education Comittee (1.Japan Agency for Marine-Earth Science and Technology, 2.Kyoto Koka Women's University)

[U14-P02] Current state of Geoscience education in primary school teacher training courses to obtain a Type II teacher’s license

*Hiroo Nemoto[1] (1.Ritsumeikan University)

WG for Studying on Teacher Training System in JpGU

*Hidenori Kumagai[1], Saori Nakai[2], Teacher's training WG JpGU Education Comittee

1. Japan Agency for Marine-Earth Science and Technology, 2. Kyoto Koka Women's University

See abstract written in Japanese.

Keywords: Teacher Training System, limitation of lessons available for geology

©2021. Japan Geoscience Union. All Right Reserved.

Current state of Geoscience education in primary school teacher training courses to obtain a Type II teacher’ s license

*Hiroo Nemoto[1]

1. Ritsumeikan University

The purpose of this study is to clarify current state of Geoscience education in teacher training courses in order to obtain a teacher’ s license for primary schools or RIKA (natural science) and/or geoscience teachers at secondary schools in Japan. As the first step, I investigated the syllabi and its related system of primary school teacher training courses at junior colleges in Japan which can be obtained a Type II teacher’ s certificate for primary schools.

As a result, it was revealed that at least about 50 out of around 2,000 graduates in 2019 school year at these junior colleges became primary school teachers without learning RIKA or geoscience while they were junior college students. Moreover, about half of graduates who obtained its certificate had not learnt RIKA or geoscience while at the junior college.

Therefore, we need to discuss and to adopt opinions as below in order to make a recommendation toward reduce internal problems related to teacher training programmes at junior colleges:
- We should propose that “Type II teacher’ s certificate for primary schools” will be limited license such as its for pupils year 1 to 2 class only because there is not subject RIKA on year 1 and 2.
- Subjects which are related to RIKA will be compulsory subjects to obtain “Type II teacher’ s certificate for primary schools” at junior colleges.

Keywords: primary school teacher training courses, Type II teacher’ s certificate for primary schools, Type II TCPS, RIKA (Natural Science), Geoscience

©2021. Japan Geoscience Union. All Right Reserved.

[J] Poster | P (Space and Planetary Sciences)：P-PS Planetary Sciences

Sat. Jun 5, 2021 5:15 PM - 6:30 PM JST | Sat. Jun 5, 2021 8:15 AM - 9:30 AM UTC | Ch.02_2

[P-PS07] Formation and evolution of planetary materials in the Solar System

convener:Megumi Matsumoto(Graduate School of Science, Tohoku University), Shin Ozawa(Department of Earth Science, Graduate School of Science, Tohoku University), Yuki Hibiya(Submarine Resources Research Center, Japan Agency for Marine-Earth Science and Technology), Noriyuki Kawasaki(Department of Earth and Planetary Sciences, Graduate School of Science, Hokkaido University)

In this session, we will discuss the material evolution in the Solar System based on extraterrestrial sample analyses and experimental works. We will overlook recent knowledge from primitive materials such as chondrites, interplanetary dust particles, and returned samples by space missions. Research works on meteorite parent body processes such as aqueous alteration, thermal metamorphism, shock metamorphism, volcanic activity, and core-mantle-crust differentiation will also be discussed. The topics of this session include experimental studies which, together with meteorite studies, help us to understand the material formation/evolution in the Solar System as well as processes on meteorite parent bodies. Presentations on new innovative analytical and theoretical techniques in various research fields (chemistry, theoretical calculation, physical property) are highly welcome to improve future studies of the Solar System evolution. This session is J (Japanese) session but English talks are also welcomed.

[PPS07-P01] Study of porosity change of simulated chondrite materials by impact experiments

*Akiko Nakamura[1], Yuki Hanzawa[2], Tomomi Omura[3], Sunao Hasegawa[4] (1.Graduate School of Science, Kobe University, 2.Faculty of Science, Kobe University, 3.Osaka Sangyo University, 4.Japan Aerospace Exploration Agency)

[PPS07-P02] Formation process of a multi-layered chondrule rim and relationship of fine-grained rim and matrix in two LL chondrites

Yukina Hashimoto[1], *Tomoki Nakamura[1], Megumi Matsumoto[1] (1.Department of Earth and Planetary Materials Sciences, Faculty of Science, Tohoku University)

[PPS07-P03] Mineralogical variations of CM chondrites revealed from X-ray diffraction method: Application to the parent body evolution

*Naoya Imae[1,2], Makoto Kimura[1], Akira Yamaguchi[1,2] (1.Antarctic Meteorite Research Center, National Institute of Polar Research, 2.The Graduate University for Advanced Studies (SOKENDAI))

[PPS07-P04] Combined XRD-XCT-FIB-TEM analysis of experimentally heated Murchison CM chondrite

*Megumi Matsumoto[1], Junya Matsuno[2], Akira Tsuchiyama[2,3], Yuri Fujioka[1], Tomoki Nakamura[1], Akira Miyake[4], Masahiro YASUTAKE[5], Shota Okumura[4], Kentaro Uesugi[5], Akihisa Takeuchi[5] (1.Graduate School of Science, Tohoku University, 2.Research Organization of Science and Technology, Ritsumeikan University, 3.Guangzhou Institute of Geochemistry, Chinese Academy of Science GIG, CAS , 4.Graduate School of Science, Kyoto University, 5.Japan Synchrotron Radiation Research Institute/SPring-8)

[PPS07-P05] Variations in initial 26Al/27Al ratios among condensate CAIs from CV chondrites

*Noriyuki Kawasaki[1], Naoya Sakamoto[2], Hisayoshi Yurimoto[2] (1.Department of Earth and Planetary Sciences, Graduate School of Science, Hokkaido University, 2.Hokkaido University)

[PPS07-P06] Petrology and mineralogy of a coarse-grained CAI “TTA01” from Allende

*Tadakatsu Yamasaki[1], Noriyuki Kawasaki[1], Hisayoshi Yurimoto[1] (1.Hokkaido University)

[PPS07-P07] Development of a chemical separation procedure for determining the initial niobium-92 abundance of chondritic components

*Yuki Hibiya[1] (1.Submarine Resources Research Center, Japan Agency for Marine-Earth Science and Technology)

[PPS07-P08] Motion of silicate particles in protoplanetary disk

*Tamami Okamoto[1], Shigeru Ida[1] (1.Earth-Life Science Institute, Tokyo Institute of Technology)

[PPS07-P09] Thermal history of andesitic achondrite Erg Chech 002

*Akira Yamaguchi[1], Atsushi Takenouchi[1], Jean-Alix Barrat[2] (1.National Institute of Polar Research, 2.UBO-IUEM)

[PPS07-P10] Excess silica in plagioclase in some mesosiderites

*naoji sugiura[1], tomoko Arai[1] (1.Chiba Institute of Technology)

[PPS07-P11] The petrological and mineralogical descriptions of nakhlites NWA 6148 and NWA 10153

*Kakeru Kukihara[1], Masaaki Miyahara[1], Akira Yamaguchi[2], Yoshio Takahashi[3], Yasuo Takeichi[4], Naotaka Tomioka[5], Eiji Ohtani[6] (1.hiroshima university , 2.National Institute of Polar Research, 3.Tokyo university, 4.Institute of Materials Structure Science, High-Energy Accelerator Research Organization (KEK), 5.Kochi Institute for Core Sample Research, Japan Agency for Marine-Earth Science and Technology (JAMSTEC), 6.Tohoku university)

Study of porosity change of simulated chondrite materials by impact experiments

*Akiko Nakamura[1], Yuki Hanzawa[2], Tomomi Omura[3], Sunao Hasegawa[4]

1. Graduate School of Science, Kobe University, 2. Faculty of Science, Kobe University, 3. Osaka Sangyo University, 4. Japan Aerospace Exploration Agency

Primordial small bodies formed by the aggregation of matrix and chondrules have a porous structure that depends on the matrix fraction. Compression due to self-gravity alone is not sufficient for the reduction of porosity from those of the primordial small bodies to the porosity of chondrites [1, 2]. In addition to thermal evolution and aqueous alteration, compression by impact is considered to be a factor of porosity reduction. In a previous study, analogue materials of chondrite parent body consisting of dust and beads sealed in a cylindrical vessel was compressed by an impact of an aluminum cylinder to examine the degree of compaction due to impact [1]. In this study, we investigate the porosity change during the crater formation and material ejection process by impact on the surface of the chondrite parent body.

Samples were prepared by mixing 1.5 μm irregularly shaped silica particles and 4.3 μm fly-ash as matrix simulants, and glass beads of 220 μm in diameter as chondrules, adding water to the mixture, compressing the mixture at 7 -10 kPa, and then drying the mixture at 50 ˚C. The volume ratio of glass beads was 13% (Sample A) and 35% (Sample B). The porosity after drying was 62% (Sample A) and 38% (Sample B), respectively.

For these samples, SUS and aluminum spheres 3.2 mm in diameter were impacted at a speed of 4.5 km/s using a two-stage light gas-gun at the Institute of Space and Astronautical Science (ISAS). Flash X-ray transmission images were acquired at several timings during 6 ~ 3000 μs after the impact. In all samples, the growth of the crater cavity over time was captured. In Sample A, a compacted layer was formed just below the cavity, and it was observed that the compacted layer expanded after a lapse of time from the impact. It is considered that the porosity of the compacted layer depends on the distance from the impact point. However, assuming that it is constant for simplicity, the average porosity of the compacted layer was calculated to be 23 ~ 54%. On the other hand, in the sample B, the compacted layer could not be detected. This is considered to be because the spatial resolution and S/N of the flash X-ray image were not sufficient to capture the change in the porosity.

This research was supported by the Hypervelocity Impact Facility (former facility name: The Space Plasma Laboratory) of ISAS, JAXA.

[1] Beitz, et al., Icarus 225, 558-569, 2013.

[2] Omura, T. and Nakamura, A. M. Planetary Science Journal, accepted.

Keywords: chondrite, porosity, impact, compaction, small bodies

©2021. Japan Geoscience Union. All Right Reserved.

Formation process of a multi-layered chondrule rim and relationship of fine-grained rim and matrix in two LL chondrites

Yukina Hashimoto[1], *Tomoki Nakamura[1], Megumi Matsumoto[1]

1. Department of Earth and Planetary Materials Sciences, Faculty of Science, Tohoku University

Chondrules in primitive chondrites are commonly surrounded by two types of rims: coarse-grained rims and fine-grained rims. Many studies of CM chondrites suggest that fine-grained rims are formed by the accretion of dust onto chondrules in the solar nebula (e.g., Metzler et al., 1992). However, recent studies of CV chondrites show that fine-grained rims formed by parent-body process (e.g., Tomeoka and Ohnishi, 2015). No conclusions are obtained so far as to whether the rims were formed by the parent body process or the nebular process.

In this study, to uncover the origin of fine-grained rims and the relationship of fine-grained rim and matrix material in ordinary chondrites, we investigated mineralogy and chemical composition of coarse-grained rims, fine-grained rims and matrix material in Y-75273 (LL3.2) and Y-74660 (LL3.0) using an optical microscope, FE-SEM, and FE-EPMA.

Many chondrules in Y 75273 are surrounded by fine-grained rims. Among them, we found a multi-layered chondrule rim. The rim consists of five layers made up with four inner coarse-grained rims (1-4th layer) and one outermost fine-grained rim (5th layer). Mineral combination of 1-4th layer is similar, but relative mineral abundance, grain size, and chemical composition of the minerals differ among the four rims. The boundaries between the 3rd and 4th layer, between the 4th and 5th layer are distinct and smooth (no topographic depressions).

Defocused (10 μm diameter) electron beam analysis of each layer shows compositional variation in individual rims: in a Si–Mg–Fe ternary diagram, the 2nd layer data distribute close to the solar abundance and the 1st- and 2nd- layer data make a trend from solar toward the Si-apex suggestive of addition of Si-rich material such as silicate glass, while the 3rd and 4th layer data distribute from solar to the Fe-apex indicative of addition of Fe-rich material such as Fe sulfide and Fe–Ni metal. On the other hand, the 5th-layer data fall on the different compositional field in Fe-rich areas relative to solar. The compositional field of the 5th layer overlaps those of the single rims formed on many other chondrules in this meteorite and both rims show irregular-shape surface morphology, suggesting that they were produced by brecciation in the same meteorite parent body. Texture, mineralogy, and chemical compositions of the multi-layered rim in the Y-75273 suggest that the outermost fine-grained rim was formed by parent-body process after inner coarse-grained rims were formed by multiple heating in the solar nebula.

Defocused electron beam analysis of fine-grained rims and matrix shows compositional variation: in a Si–Mg–Fe ternary diagram, the fine-grained-rims fall on the Fe-rich areas relative to solar, while matrix falls on the Si-rich areas relative to solar, suggesting that the fine-grained rims and matrix are different material. The constituent minerals of the fine-grained rims and matrix, such as olivine and pyroxene, differ in the chemical composition. Olivine composition of the fine-grained rim (Fa_{77-80}) differs from matrix (Fa_{38-48}), indicating that these olivines are not chemically equilibrated during thermal metamorphism. The mesostasis glass of the chondrules which is the most susceptible to alteration, is clear and seems not to have altered, suggesting that aqueous alteration did not cause the exchange of elements between the chondrules and the fine-grained rims and between the chondrules and the matrix. This suggests that the

©2021. Japan Geoscience Union. All Right Reserved.

difference in chemical composition between the fine-grained rim and the matrix was not established by secondary alteration, rather they are originally different material.
This compositional difference between matrix and fine-grained rims is observed in both Y-75273 and Y-74660. This suggests that the fine-grained materials in the LL chondrite formation region could have changed over time or location, because earlier-formed fine-grained rims differ from later-formed matrix material.

Keywords: Chondrule rim, LL chondrites, Fine-grained rim

©2021. Japan Geoscience Union. All Right Reserved.

Mineralogical variations of CM chondrites revealed from X-ray diffraction method: Application to the parent body evolution

*Naoya Imae[1,2], Makoto Kimura[1], Akira Yamaguchi[1,2]

1. Antarctic Meteorite Research Center, National Institute of Polar Research, 2. The Graduate University for Advanced Studies (SOKENDAI)

Introduction
CM chondrites have been characterized by aqueous alteration in the parent body [e.g.,1,2], and subtypes have been identified [3,4]. Findings of dehydrated [5,6] and unaltered samples [7] added new views. We studied the significant variations. We newly modeled the parent body evolution.

Experiments
Samples are QUE 97990 (subtype, 2.6), Murchison (2.5), DOM 03183 (2.5), Y-791198 (2.4), QUE 99355 (2.3), SCO 06043 (2.0), MET 01070 (2.0), Y 980036 (2.4-2.5 and heating stage II), Y 980051 (2.4-2.5 II), and Jbilet Winselwan (2.4-2.7 II). Three types of equipment were mainly used: X-ray diffractometer (XRD), field emission scanning electron microscope, and electron probe microanalyzer. The measurement conditions for XRD are the same as [8]. Focused Miller indices for XRD are the same as [9].

Results and Discussion
Systematic change is observed for subtypes of unheated CMs: The intensities of olivine, pyroxenes, and kamacite plus troilite decrease with decreasing subtypes—instead, serpentines (antigorite and cronstedtite) increase. Tochilinite abundance is the highest at the intermediate subtype (2.5-2.3). The relative intensity of antigorite to cronstedtite increases with decreasing subtype. Y 980036 and Y 980051 are entirely dehydrated, and matrices are low-crystalline. The sulfide assemblages correspond to category B [10]. Chondrule phenocrysts of forsterite olivine, ferroan olivine, and clinoenstatite have not been altered. Although the mesostasis has been altered. Cronstedtite and tochilinite in Jbilet Winselwan are decomposed, but antigorite is partly survived. [11] also showed that Jbilet Winselwan is a regolith breccia. We also confirmed that textures and analyzed compositions are consistent with XRD.

Application to the parent body evolution
Based on the observed mineralogical variations of CM chondrites, we will consider the evolutional processes of the parent body, focusing on dehydration. The hydrous alteration degree may be related mainly to temperature, potential of hydrogen, and water/rock ratio [2,12]. On the other hand, after once hydrated, dehydration has been theoretically predicted in the early history of the parent body's interior in a few million years after the formation [13]. Due to the latent heat of water, the peak metamorphic temperature is limited to be 600-800 K for the hydrous parent body with 100 km diameter, lower than that of anhydrous parent body [13]. The textures and compositions for dehydrated CM should be controlled by the diffusion length of Mg-Fe diffusion of olivine. The diffusion feature between forsterite and ferroan olivines is not noticed from intermediately heated CM. The absence of the diffusion is consistent with the estimation that any significant diffusion for the intermediate depth is not expected within the cooling time scale of 1-10 million years from 600-700K. The present model on parent body evolution is seemingly consistent with our observations.

References
[1] Tomeoka K. and Buseck P. R. 1985. Geochim. Cosmochim. Acta 49:2149. [2] Zolensky M. et al. 1993.

©2021. Japan Geoscience Union. All Right Reserved.

Geochim. Cosmochim. Acta 57:3123. [3] Rubin A. 2007. Geochim. Cosmochim. Acta 71:2361. [4] Howard K. T. 2011. Geochim. Cosmochim. Acta 75:2735. [5] Nakamura T. 2005. J. Min. Pet. Sci. 100:260. [6] King A. et al. 2019. Meterit. Planet. Sci. 54:521. [7] Kimura M. et al. 2020. Polar Sci. 17:100565. [8] Imae N., et al. 2019. Meterit. Planet. Sci. 54:919. [9] Imae N. and Kimura M. 2020. Polar Science Symp. abstract. [10] Kimura M. et al. 2011. Meterit. Planet. Sci. 46:431. [11] Zolensky M., et al. 2016. 47th LPSC. #2148. [12] Brearley A. J. 2006. In Meteorites and the Early Solar System II. [13] Grimm R. E. and McSween H. Y. 1989. Icarus 82:244.

Keywords: CM chondrites, X-ray diffraction, hydrous minerals, Antarctic meteorites, meteorite parent body, metamorphism

©2021. Japan Geoscience Union. All Right Reserved.

Combined XRD-XCT-FIB-TEM analysis of experimentally heated Murchison CM chondrite

*Megumi Matsumoto[1], Junya Matsuno[2], Akira Tsuchiyama[2,3], Yuri Fujioka[1], Tomoki Nakamura[1], Akira Miyake[4], Masahiro YASUTAKE[5], Shota Okumura[4], Kentaro Uesugi[5], Akihisa Takeuchi[5]

1. Graduate School of Science, Tohoku University, 2. Research Organization of Science and Technology, Ritsumeikan University, 3. Guangzhou Institute of Geochemistry, Chinese Academy of Science GIG, CAS , 4. Graduate School of Science, Kyoto University, 5. Japan Synchrotron Radiation Research Institute/SPring-8

Hayabusa2 spacecraft succeeded to touchdown on the surface of C-type asteroid 162173 Ryugu and brought Ryugu surface materials to the earth in the last December. Spectroscopic observations [1] suggested that Ryugu surface consists of materials which are similar to partially dehydrated carbonaceous chondrites. This means that heated hydrous carbonaceous chondrites are the closest analogues to Ryugu surface material. Recently, we performed synchrotron radiation-based X-ray diffraction (SR-XRD) and X-ray computed nanotomography (SR-XCT) of unheated and experimentally heated (400 ˚C-50 hrs and 600 ˚C -50 hrs) Murchison CM chondrite particles (~50 μm in size) [2] as rehearsal analyses [3]. The SR-XCT results will be presented by Matsuno et al. and Sun et al. in this JpGU meeting. The synchrotron analyses revealed that hydrous phases, tochilinite-cronstedtite intergrowth (TCI) and Mg-rich serpentine, in the Murchison matrix were partially decomposed by 400 ˚C -50 hrs heating without significant changes in CT images. In this study, we extracted an ultrathin section from a 400 ˚C -50 hrs heated Murchison particle, which was previously analyzed by SR-XCT, using a focused ion beam system (FIB), and analyzed it by transmission electron microscopy (TEM) to investigate microstructural changes in the matrix caused by the heating.

The target slice section in the 400 ˚C -50 hrs heated Murchison particle for TEM observation was selected based on CT images. In the selection, we set a few mineral grains (0.5 to a few μm in size) in the CT images as specific phases which should be included in the ultrathin section. Then, the Murchison particle was mounted on the FIB sample stage appropriately and sliced carefully by comparing the FIB cutting surface images and the CT slice images one by one. Finally, we successfully obtained an ultrathin section (~20 ×20 μm) containing all the specific grains.

TEM observation revealed that the ultrathin section contains partially decomposed TCIs, which were replaced by relatively large (a few hundred of nm) Fe-Mg rich silicates and clusters of 10-20 nm sized magnetite. Previous SR-XRD analysis [3] suggested the presence of abundant magnetite in 400 ˚C -50 hrs heated Murchison samples, and is consistent with the TEM observation. The XRD peaks of magnetite were characteristic to 400 ˚C heated samples and were not found for unheated and 600 ˚C heated Murchison samples [3]. Therefore, the magnetite nano-grains replacing TCIs may be able to use as an indicator of relatively low degrees of heating for CM type chondrites. We will perform further FIB-TEM analysis and summarize microstructural changes in the Murchison matrix by 400 ˚C -50 hrs heating and other degrees of heating.

[1] Kitazato et al. (2019) *Science* **364**. [2] Mogi et al. (2017) *The 80th Annual Meeting of the Meteoritical Society*, Abstract #6225. [3] Matsumoto et al. (2020) *The JpGU-AGU joint meeting 2020*, Abstract PPS10-P09.

©2021. Japan Geoscience Union. All Right Reserved.

Keywords: heated CM chondrite, Hayabusa2 mission, synchrotron XCT, synchrotron XRD, FIB-TEM

©2021. Japan Geoscience Union. All Right Reserved.

Variations in initial 26Al/27Al ratios among condensate CAIs from CV chondrites

*Noriyuki Kawasaki[1], Naoya Sakamoto[2], Hisayoshi Yurimoto[2]

1. Department of Earth and Planetary Sciences, Graduate School of Science, Hokkaido University, 2. Hokkaido University

Fine-grained Ca-Al-rich inclusions (FGIs) and fluffy Type A CAIs (FTAs) in CV chondrites are suggested to be condensates formed directly from the solar nebular gas (e.g., MacPherson and Grossman, 1984; Krot et al., 2004). Al–Mg mineral isochrons of seven FGIs and two FTAs from reduced CV chondrites Efremovka, Vigarano, Thiel Mountains 07007, and Northwest Africa 8613 were obtained via in situ Al–Mg isotope measurements using secondary ion mass spectrometry (Cameca ims-1280HR at Hokkaido University). The slopes of the mineral isochrons for seven FGIs and two FTAs exhibit statistically significant variations in initial 26Al/27Al ratios, (26Al/27Al)0, ranging from (5.19 ±0.17) to (3.35 ±0.21) ×10^−5, which correspond to a relative age spread of 0.44 ±0.07 Myr. Inferred upper limit of (26Al/27Al)0 for them is identical to the Solar System (26Al/27Al)0 of ˜5.2 ×10^−5 as determined by whole-rock Al–Mg isochron studies for CAIs in CV chondrites. The intercepts of the mineral isochrons, the initial 26Mg/24Mg ratios, are consistent with Mg-isotope evolution path of a solar-composition nebular gas. The observed variations in (26Al/27Al)0 for condensate CAIs are essentially similar to those (˜5.2 to ˜4.2 × 10^−5) for coarse-grained, igneous CAIs of CV chondrites that are formed by melting and solidification (MacPherson et al., 2012, 2017). If 26Al was distributed homogeneously in the forming region, then our data indicate that thermal processes of condensation and melting for CAI formation occurred contemporaneously and continued for at least ˜0.4 Myr at the very beginning of the Solar System. Alternatively, the observed variations in (26Al/27Al)0 also indicate the possibility of heterogeneous distributions of 26Al in the forming region, corresponding to a range of over at least 3.4 ×10^−5 < (26Al/27Al)0 < 5.2 ×10^−5.

Fig. 1. Variations in initial 26Al/27Al ratios among CAIs in CV chondrites (after Kawasaki et al., 2020). Colored symbols indicate data from this study. Other data are from Jacobsen et al. (2008), Larsen et al. (2011), MacPherson et al. (2010, 2012, 2017), Kita et al. (2012), and Kawasaki et al. (2018).

©2021. Japan Geoscience Union. All Right Reserved.

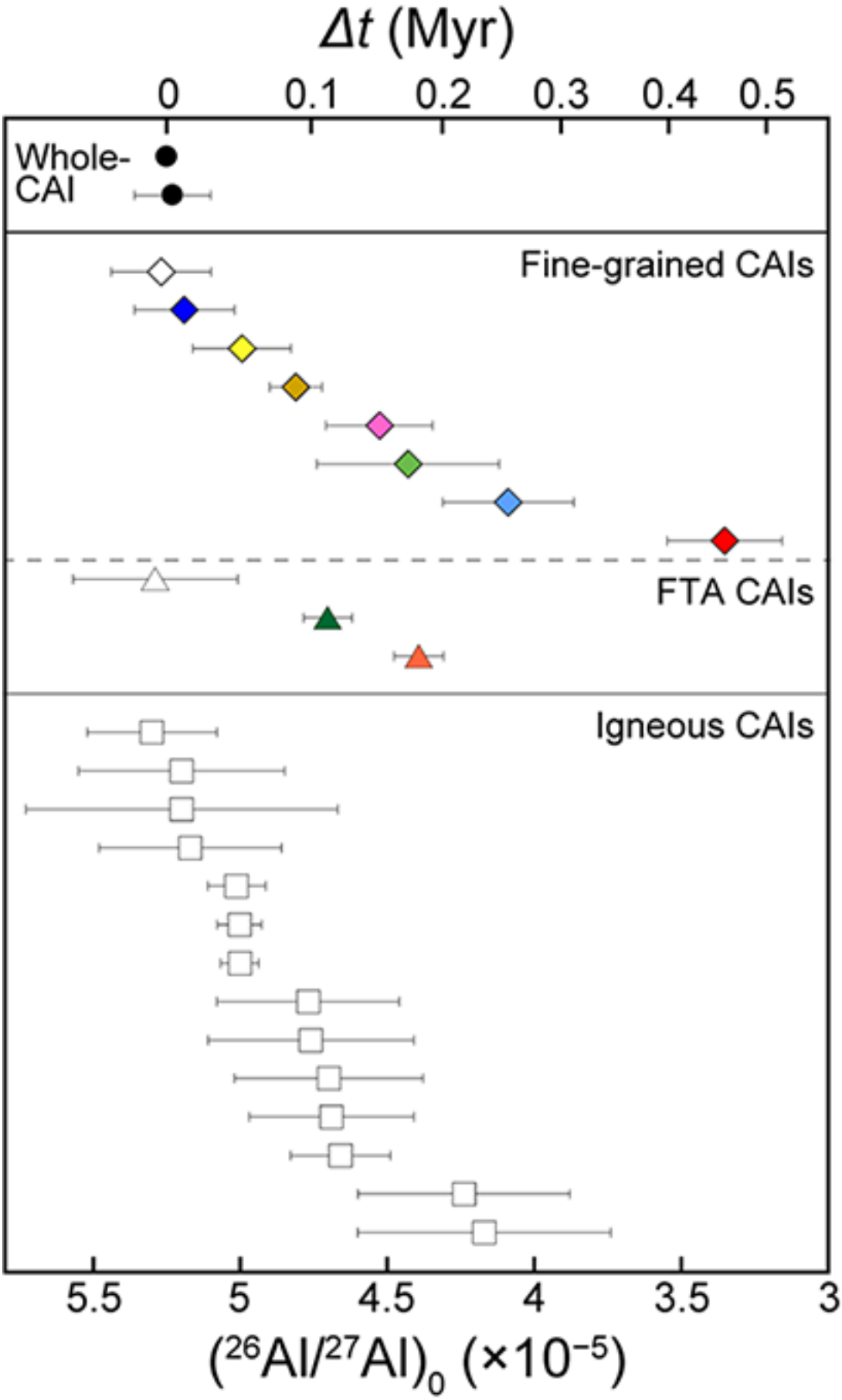

©2021. Japan Geoscience Union. All Right Reserved.

Petrology and mineralogy of a coarse-grained CAI “TTA01” from Allende

*Tadakatsu Yamasaki[1], Noriyuki Kawasaki[1], Hisayoshi Yurimoto[1]

1. Hokkaido University

Ca-Al-rich inclusions (CAIs) in meteorites are the oldest objects formed in the Solar System (Connolly et al., 2012) and composed of high-temperature condensate minerals from a solar-composition gas (e.g., Grossman, 1972). Coarse-grained CAIs in CV chondrites are divided into Type A, Type B and Type C CAIs according to their petrography. Fine-grained inclusions and fluffy Type A CAI are suggested to be condensates from the solar nebular gas (e.g., MacPherson and Grossman, 1984), while compact Type A, Type B and Type C CAIs formed by melt crystallization (e.g., MacPherson and Grossman, 1981; Yurimoto et al., 1998). In this study, we conduct petrographic observations of a coarse-grained CAI from Allende, TTA01 (Imai and Yurimoto, 2000), which has two regions with distinct petrographic signatures, using FE-SEM-EDS system (JEOL JSM-7000F; Oxford X-Max 150) installed at Hokkaido University.

TTA01 has an elliptical shape with a size of ~3.5 x 2.5 mm on the polished section of Allende. It is mainly composed of spinel, melilite, anorthite, and fassaite and contains secondary minerals of sodalite, nepheline, grossular, and monticellite. TTA01 can be divided into two regions. “Region A” is enriched in fassaite and anorthite. Subhedral anorthite (~1 mm long) and anhedral melilite and fassaite poikilitically enclose spinel crystals. A bulk chemical composition of region A is Type C CAI-like and plotted on the spinel + anorthite area of the ternary phase diagram of CAIs by Stolper (1982). Åkermanite contents of melilite in region A are ~50-70 mol%.

“Region B” is enriched in melilite. Small melilite and spinel grains (5-50 μm) are poikilitically enclosed in anorthite and fassaite crystals. Melilite also contains finer spinel grains. A bulk chemical composition of region B is Type B CAI-like and plotted on the spinel + melilite area of the Stolper diagram. Åkermanite contents of melilite in region B are ~15-50 mol%. Small melilite crystals often contain Al-rich grains with åkermanite contents of < 25 mol% and they are surrounded by melilite with > 30 mol%.
According to the petrographic observations, crystallization orders for region A is from spinel, anorthite, to melilite + fassaite, while those for region B is from spinel, melilite to anorthite + fassaite. These crystallization orders are consistent with the bulk chemistry of each region. The bulk chemistry and distinct åkermanite contents of melilites in regions A and B suggest that the two regions could not have formed from a homogeneous, single melt. Type C CAI-like precursor and Type B CAI-like precursor may have been accreted together and then remelted to form TTA01. A liquids temperature of anorthite in region A is 1340℃ while that of melilite in region B is 1430℃ (Stolper, 1982). The melting of precursors of TTA01 at 1340-1430℃ is consistent with the above observations; spinel and a part of melilite in region B were relict of the melting event.

©2021. Japan Geoscience Union. All Right Reserved.

Development of a chemical separation procedure for determining the initial niobium-92 abundance of chondritic components

*Yuki Hibiya[1]

1. Submarine Resources Research Center, Japan Agency for Marine-Earth Science and Technology

Introduction

One of the long-standing issues in the study of material evolution in the early solar system is "where did the nuclides come from, when were they injected into the solar system, and how were they transported to form the planets?" The short-lived nuclide niobium-92 (^{92}Nb), which originated from core-collapse Type II supernovae (SNII) [1], holds the key to solving this issue.

In this study, I investigate the initial abundance of ^{92}Nb amongst the chondritic components and determine the distribution of SNII origin components in the early solar system. A special focus is on the oldest solid material Ca-Al-rich inclusion (CAI) which is likely to have existed over a wide area in the protoplanetary disk [2], and the initial abundance of ^{92}Nb including the genetic information of CAI is determined by combining the results from the high-precision Cr and Ti stable isotope measurements.

In order to clarify a detailed picture of the SNII-origin-material influx and transportation processes at the birth of the solar system by applying this method to various primitive components in the future, I develop here a chemical separation of Cr, Ti and Zr from a single digest for the high precision isotope measurements of chondritic components using mass spectrometry.

Results & Discussion

Samples were prepared by mixing terrestrial basalt (JB-1b) and peridotite (JP-1) in ratios that would yield the approximate compositions (for major elements and Zr) of chondrules and CAIs. The typical compositions of chondrules and CAIs were calculated based on the sizes and major element compositions reported in the previous studies [3, 4]. Following digestion with conc. HF-HNO_3, samples were dried down and re-dissolved in 6 M HCl for the first step of column chemistry. The chemical separation and purification of Cr, Ti and Zr from the samples were established based on the procedure described by [5-7].

The newly developed separation procedure comprises four steps: (i) Fe removal using AG1-X8 anion exchange resin; (ii) Zr separation using Ln-resin; (iii) Ti separation using TODGA resin; (iv) Cr separation using AG50W-X8 cation exchange resin. In the first step, Fe was separated using small resin volumes of ~0.5 mL. The recovery rates for Cr, Ti, and Zr were 93-100% for all studied samples. The elution was evaporated until the total volume reached ~1 mL and then converted to 3 mL of ~2 mol L^{-1} HCl solution by dilution with H_2O. Subsequently, Cr and Ti were separated from the column using 2 mol L^{-1} HNO_3 + 1 wt.% H_2O_2, followed by the elution of Zr in 0.5 mol L^{-1} HCl + 0.06 mol L^{-1} HF. The recovery rates for Cr and Ti were ~100%, and that for Zr was 97-98% for all the studied samples. The elution containing Cr and Ti was then evaporated to dryness and dissolved in 1 mL of 12 mol L^{-1} HNO_3 for the third separation step. In the third step, Ti was separated from Cr-fraction using the pre-packed 1 ml cartridges containing TODGA resin associated with the cartridge reservoirs. The recovery rates for Cr and Ti were 95-100% for

©2021. Japan Geoscience Union. All Right Reserved.

all the studied samples. Prior to the final step, I used a Cr pretreatment procedure [8] involving exposure to 1 mol L^{-1} HNO_3 + 1 wt.% H_2O_2 >3 days so that Cr(III) remained as the dominant species in the acid. In the final step, Cr was purified from matrix elements. The recovery rates of Cr were 98-100% for all the studied samples.

Hence, we can expect that the above new method separates Cr, Ti, and Zr with >88%, >93%, and >90%, respectively. I am now planning to apply this method to individual CAIs extracted from primitive meteorites and assess the nature of proto-planetary disk through the combined Cr, Ti, and Zr isotope analyses.

[1] Hibiya et al. (2019) *82nd Metsoc meeting, #6370*, [2] Hezel et al. (2008) *MAPS* **43** 1879–1894, [3] Goresy et al. (2002) *GCA* **66** 1459–1491, [4] Alexander et al. (2005) *Chondrites and the protoplanetary disk* **341** 972, [5] Iizuka et al. (2016) *EPSL* **439** 172–181, [6] Münker et al. (2001) *G-cube.* **2**, [7] Hibiya et al. (2019) *GGR* **43** 133–145, [8] Larsen et al. (2016)*J. Chromatogr. A* **1443** 162–174.

Keywords: niobium-92, Type II supernova, CAIs, column chromatography, mass spectrometry

©2021. Japan Geoscience Union. All Right Reserved.

Motion of silicate particles in protoplanetary disk

*Tamami Okamoto[1], Shigeru Ida[1]

1. Earth-Life Science Institute, Tokyo Institute of Technology

Forsterites are crystallized by annealing of amorphous precursors (~1000 K) or sublimation and recondensation (~1400 K) in inner protoplanetary disk. On the other hand, the observation showed that comets include crystalline forsterites. Therefore, there must be some mechanism that transports them from the inner area to the outer area in the disk. In this study, we investigate the motion of dusts in steady protoplanetary disk, considering that dusts stick to icy pebbles. From the result, we discuss the dependence of surface density of silicate dusts on the distance from the central star and compare a calculation result of the ratio of crystallized silicates to amorphous precursors to the observation result of comets.

©2021. Japan Geoscience Union. All Right Reserved.

Thermal history of andesitic achondrite Erg Chech 002

*Akira Yamaguchi[1], Atsushi Takenouchi[1], Jean-Alix Barrat[2]

1. National Institute of Polar Research, 2. UBO-IUEM

Petrologic and geochemical study of asteroidal achondrites is essential to understand the earliest volcanism on planetesimals and protoplanets. These differentiated bodies were likely covered by crust formed by the melting of the parent bodies. Such crustal rocks are divided into basaltic and andesitic types. The majority of basaltic types are eucrites. In contrast, the andesitic type is very rare. We present the petrology of a newly-found andesitic achondrite Erg Check 002 (EC 002) and discuss its petrogenesis and thermal history. We studied polished sections of EC 002 using an FE-SEM equipped with EDS/EBSD/CL system, an EPMA, and a Raman spectrometer.

The section of EC 002 is an unbrecciated rock with medium-grained groundmass with pores. It consists of lath-shaped feldspar, anhedral pyroxene, silica minerals, with minor minerals such as spinel, ilmenite, Ca-phosphate, troilite, and FeNi metal. Silica minerals are cristobalite and tridymite (PO), with no quartz, confirmed by Raman spectra and CL observations. Groundmass pyroxenes are partly equilibrated and consist of relict augite with fine exsolution lamellae of low-Ca pyroxene or relict low-Ca pyroxene with fine exsolution lamellae of augite. In addition, EC 002 also contains angular to rounded pyroxene or olivine xenocrysts. EC 002 is slightly shocked. Bulk groundmass pyroxene compositions are generally augitic (Wo27.7-33.0En36.9-38.5). Feldspars are albitic (Or2.0-7.1Ab75.8-87.4) and contain lamellae of K-rich feldspar. The pyroxene xenocryst has a chemically homogeneous core (Wo4.7En76.8) with zoned rims. There is no difference in the FeO/MnO ratios (~21) between the xenocryst and groundmass pyroxene. The texture of the second section is slightly different, which contains four xenocrysts (1-7 mm in size). One elongated xenocryst is surrounded by a fine-aggregate of pyroxene and feldspar. Compared to the first one, this section contains little amounts of pores. The textural difference may have resulted from the difference of local cooling rates. A further petrologic study of this sample is still in progress. The bulk major chemical compositions of the groundmass are andesitic (58 wt% SiO2 and 4.54 wt% Na2O and K2O). Other REE abundances are low and of the order of 5 or 6 times the chondritic reference.

The petrologic and geochemical data indicate that EC 002 experienced two-stage cooling history. The first stage is the crystallization from lava at ~1200 to ~1000 ˚C at ~5˚C/year, estimated from the compositional profile of Mg# in the pyroxene xenocryst. The second stage is the rapid cooling from ~900 ˚C, estimated from the occurrence of silica minerals. The sudden change of cooling rates can be explained by rapid cooling caused by impact excavation, consistent with the shock features. The presence of xenocrysts (olivine and pyroxene) gives an impression that EC 002 is an impact melt breccia. However, we do not have a definitive answer to this question. The identical FeO/MnO ratios may indicate the genetic linkage of the pyroxene and xenocryst. The groundmass compositions can only be explained by partial melting, not by impact melting unless the target was andesitic crust.

Keywords: achondrite, andesite, planetesimal, volcanism

©2021. Japan Geoscience Union. All Right Reserved.

Excess silica in plagioclase in some mesosiderites

*naoji sugiura[1], tomoko Arai[1]

1. Chiba Institute of Technology

Introduction: Excess silica in plagioclase has been reported in lunar rocks [1] and chondrules [2]. It is absent in terrestrial plagioclase and the presence of the excess is considered as evidence against metamorphism and/or slow cooling at temperatures where cations could move around. Here we report excess silica in plagioclase in some mesosiderites (Dong Ujimqin Qi (B1), NWA1878 (B0), NWA2924, NWA4747, Bondoc (B4)), and absence of the excess in Estherville(A3/4).

Instrumental: Plagioclase compositions were measured by SEM-EDS. The measurements were made without standards and normalized to 100%. Since excess silica is produced by vacancies [1] this is problematic, but until measurements with EPMA are made we have to abide this ambiguity. The differences in apparent excesses in mesosideritic plagioclase and those in other plagioclase (terrestrial and achondrites) at the same anorthite number (An#) are considered as true excess silica.

Results: Similar to lunar plagioclase, silica excesses in mesosideritic plagioclase increase with decreasing anorthite number [1]. The excess silica evaluated at the same An# varies considerably among the mesosiderites. It decreases in the order of, NWA1878 > Dong Ujimqin Qi > Bondoc > NWA2924 > NWA4747> Estherville. The excess is practically nil in Estherville, within the error (standard deviation) of the measurement (about +/- 1% which is not significantly larger than those reported for lunar rocks). A typical excess in NWA1878 is ~4.5 % at An90, which is significantly higher than those in lunar rocks [1].

Discussion: In the case of lunar rocks, the excess silica is explained as a result of a high silica activity during crystallization of increasingly Na-rich plagioclase from a melt. Most mesosiderites experienced brief reheating to near-solidus temperatures after the mixing of metal. Also, the silica activities in most mesosiderites were high during reheating as a result of phosphate formation reactions. (Note that this requires reheating after the formation of phosphates.) Therefore, the excess silica in mesosideritic plagioclase may be understood to have been produced by a mechanism similar to that in lunar rocks. The variation in the excess among mesosiderites could be due to difference in the thermal histories (cooling rate or multiple reheating). The higher excesses in mesosideritic plagioclase than those in lunar rocks may be due to difference in the thermal histories. Dissecting the mesosiderite data in detail, however, it is found that the vacancy corresponding to the silica excess seems to be mostly created by Na deficiency. Merrillite in mesosiderites is known to be deficient in Na [3]. Therefore, both merrillite and plagioclase competed for limited supply of Na. This may have contributed to the high excess silica in mesosideritic plagioclase. A peculiar feature of mesosideritic plagioclase with high excess silica is the presence of fine silica particles. This is observed in NWA1878, Dong Ujimqin Qi and Bondoc. (A caveat on the reported excesses in these mesosiderites is that they could be due to hidden silica particles. Some of the data are likely to be affected by such hidden silica particles, but we believe many of the excesses are authentic.) Investigations of excess silica, exsolved silica particles, and the compositional relationship between plagioclase and merrillite would clarify the reheating history of mesosiderites.

References:

[1] D.W. Beaty and A.L. Albee, 1980, Silica solid solution and zoning in natural plagioclase. Am. Mineral.

©2021. Japan Geoscience Union. All Right Reserved.

65, 63-74.

[2] T.J. Tenner+, 2014, Silica excess in anorthitic plagioclase from type 3.00 chondrite chondrules: Evidence for retaining primary 26Al-26Mg systematics. 45th LPSC, 1187.pdf.

[3] N. Sugiura and T. Arai, 2020, Volatile loss from mesosiderites. 11th Symposium on Polar Science, OAp12_Sugiura_00260_01.pdf.

Keywords: mesosiderites, plagioclase, silica

©2021. Japan Geoscience Union. All Right Reserved.

The petrological and mineralogical descriptions of nakhlites NWA 6148 and NWA 10153

*Kakeru Kukihara[1], Masaaki Miyahara[1], Akira Yamaguchi[2], Yoshio Takahashi[3], Yasuo Takeichi[4], Naotaka Tomioka[5], Eiji Ohtani[6]

1. hiroshima university , 2. National Institute of Polar Research, 3. Tokyo university, 4. Institute of Materials Structure Science, High-Energy Accelerator Research Organization (KEK), 5. Kochi Institute for Core Sample Research, Japan Agency for Marine-Earth Science and Technology (JAMSTEC), 6. Tohoku university

We conducted a petrological and mineralogical study of nakhlites NWA 6148 and NWA 10153 to clarify an aqueous alteration in the nakhlites complex. NWA 6148 is suggested to have derived from the deeper part of the nakhlite complex [1]. NWA 10153 was hardly investigated and its position in the nakhlites complex is unknown. For the petrological and mineralogical descriptions, microtextural observations by an FE-SEM and chemical composition analysis by an EMPA were conducted. We used a FIB system to prepare the foils of alteration textures found in the samples. The chemical species of iron, oxygen, carbon, and sulfur in the foils were analyzed by XANES. The microtextures, chemical compositions, and crystal structures of minerals in the foils were analyzed using an FE-STEM-EDS.

NWA 6148 consists mainly of olivine, low-Ca pyroxene, plagioclase, K-feldspar, pyrrhotite, and Fe-Ti oxides. Plagioclase, K-feldspar, pyrrhotite, and Fe-Ti oxides occur in a mesostasis. NWA 6148 has a higher fraction of a mesostasis (55.2 vol.%) than other nakhlites (7–24 vol.%) [2]. The low-Ca pyroxene has normal compositional zoning. The Ca content increases toward the rim in some pyroxene grains. Alteration texture is not found in NWA 6148. NWA 10153 also has a high fraction of a mesostasis (36.3 vol.%), and its major constituents are low-Ca pyroxene, plagioclase, K-feldspar, pyrite, and Fe-Ti oxides. Only a small amount of olivine occurs as small grains ($< 100\ \mu m$) in the mesostasis. Alteration textures are found between low-Ca pyroxene grains and/or plagioclase grains. The alteration textures can be divided into four types: i) Fe-rich, ii) Si-Fe-rich, iii) Fe-S-rich, and iv) Carbonate-rich types. Based on Fe L-edge XANES, Fe^{3+} is dominant in the Fe-rich portion. Considering the SAED pattern and chemical compositions, the Fe-rich portion consists mainly of goethite. The absorption peaks both of Fe^{2+} and Fe^{3+} are observed in the Si-Fe rich portion. The Si-Fe-rich portion seems to consist mainly of smectite. Fe^{3+} is dominant and SO_4^{2-} is included in the Fe-S rich portion. Considering the SAED pattern and chemical compositions, the Fe-S rich portion consists mainly of Na/K-jarosite.

Cohen et al. (2017) [3] suggest that the nakhlite complex formed through several lava flows. The high proportions of mesostasis in NWA 6148 and NWA 10153 mean low crystallization degrees, suggesting that both of them were originated from lava flows that rapidly cooled and solidified near a surface. The Ca zoning in a pyroxene grain is observed in other nakhlites NWA 5790 and MIL 03346 along with NWA 6148 [1, 2]. The petrological similarities indicate that NWA 6148 and NWA 5790 might have formed by the same lava flow. However, more detailed investigations are necessary for the conclusion, because the proportion of a mesostasis in NWA 6148 (55.2 vol.%) is higher than NWA 5790 (36.3±3 Vol.%)[2]. NWA 6148 seems to be escaped from an aqueous alteration.

By contrast, NWA 10153 includes goethite, smectite, and carbonates as alteration minerals. Considering the formation conditions of the alteration mineral assemblage, two different aqueous alteration events likely occurred. In the first event, a hot neutral-basic fluid containing carbon dioxide gas formed smectite and carbonates. In the second event, a weak acidic fluid dissolved pyrite, which made the fluid to become

©2021. Japan Geoscience Union. All Right Reserved.

more acidic. Jarosite formed under very low-pH. With increasing the pH again due to the reaction between the surrounding minerals and the strongly acidic fluid, goethite precipitated from the fluid finally.

References:

[1] Jambon et al. (2016) Geochimica et Cosmochimica Acta 190, 191–212.

[2] Mikouchi et al. (2006) 37thLPSC, abstract no.1865.

[3] Cohen et al. (2017) Nature Communications 8, 1–8.

Keywords: Aqueous alteration, NWA 6148, NWA 10153, Chemical condition of the fluid

©2021. Japan Geoscience Union. All Right Reserved.

[J] Poster | P (Space and Planetary Sciences)：P-EM Solar-Terrestrial Sciences, Space Electromagnetism & Space Environment

Sat. Jun 5, 2021 5:15 PM - 6:30 PM JST | Sat. Jun 5, 2021 8:15 AM - 9:30 AM UTC | Ch.03_2

[P-EM14] Heliosphere and Interplanetary Space

convener:Kazumasa Iwai(Institute for Space–Earth Environmental Research (ISEE), Nagoya University), Yasuhiro Nariyuki(Faculty of Education, University of Toyama), Ken Tsubouchi(University of Electro-Communications), N Masaki Nishino(Japan Aerospace Exploration Agency, Institute of Space and Astronautical Science)

This session aims to secure comprehensive insights into physical processes of plasmas and fields in the heliosphere. Presentations of the recent studies from any approaches (integrated observation/theoretical modeling/massive numerical simulation) are welcomed. Topics are not restricted to any specific issues: phenomenological studies on solar flares/CME/solar wind, and related fundamental physics problems such as shocks/waves/turbulence/particle transport and acceleration can be the main target, including heliospheric high-energy phenomena and their impact on the Earth's environment.

[PEM14-P01] Relationship between solar type III radio bursts and electron energy spectra in solar impulsive electron events

Tatsuya Fujimoto[1], *Hiroaki Misawa[1], Fuminori Tsuchiya[1], Takahiro Obara[1] (1.Planetary Plasma and Atmospheric Research Center, Graduate School of Science, Tohoku University)

[PEM14-P02] Occurrence dependence on solar activity cycle for ordinary type III bursts and micro-type III bursts

*Yuichiro Seki[1], Hiroaki Misawa[1], Takahiro Obara[1], Fuminori Tsuchiya[1] (1.Tohoku University)

[PEM14-P03] Simple Estimation of the Global Solar Wind Structure

*Ken'ichi Fujiki[1], Munetoshi Tokumaru[1], Kazumasa Iwai[1] (1.Institute for Space-Earth Environmental Research)

Relationship between solar type III radio bursts and electron energy spectra in solar impulsive electron events

Tatsuya Fujimoto[1], *Hiroaki Misawa[1], Fuminori Tsuchiya[1], Takahiro Obara[1]

1. Planetary Plasma and Atmospheric Research Center, Graduate School of Science, Tohoku University

Solar Energetic Particles (SEPs) are protons, electrons, and heavy ions of 10 keV to several tens GeV generated with flares and coronal mass emissions (CMEs), which are explosive phenomena near the solar surface. SEPs are classified into two types; i.e., impulsive and gradual types, based on the elemental abundances and the time profile of ion flux variations. Impulsive SEPs, also known as electron-based events. In particular, electron events, in which the electron flux increases for a short period, have been understood to be the result of electrons accelerated by flares propagating through interplanetary medium and observed near the Earth. It has been reported that spectral shapes of electrons observed in electron events are frequently show broken power laws at the break energy of several tens of keV. Reid & Kontar [2013] proposed an explanation for the generation of the break: low energy electrons lose their kinetic energy during their propagations due to wave-particle interaction, which converts their kinetic energy into Langmuir wave energy. They also reported that type III radio bursts, which are suddenly appearing emissions caused by flares, are almost always observed in electron events in the several tens meter to kilometer wave bands. Type III radio bursts are thought to be generated by non-thermal electrons accelerated by magnetic reconnections, which propagate along open magnetic field lines. That is, an injection of energetic electrons into interplanetary medium leads to excite Langmuir waves, and the waves are converted into radio waves as type III bursts where the radio wave frequency is as same as the local plasma frequency. Type III bursts are therefore interpreted as being excited by energetic electrons causing electron events, and their characteristics have information on properties of energetic electrons. However, precise relationship between energetic electrons and Type III bursts in solar impulsive electron events has not been clarified.
In order to reveal the relationship by a statistical approach, we have made analyses for characteristics of energetic electrons and Type III radio bursts using solar electron spectral data of the 3DP instrument and type III bursts of the WAVES instrument onboard the WIND spacecraft. Among the significant single-event electron events observed by the WIND satellite from 1994 to 2005, we identified 37 events that simultaneously showed both a bend in the electron energy spectrum and type III burst spectrum with simple spectral form. As the results, we confirmed that the power law indices of electrons below the spectral break energy show a positive correlation with radio wave intensities/energies and the electron beam velocity calculated from the frequency drift features of type III bursts. On the other hand, no correlation was found between the kinetic energy of the electrons, which is assumed to be converted to wave energy and lost during the propagation, and the radio wave energy. These results suggest that 1) the electrons on the lower side of the break energy are responsible for the excitation of the type III bursts, and the spectral shape of energetic electrons is an important factor to control intensity and energy of Type III radio waves, and 2) the spectrum shapes of electrons with the break energy cannot be explained only by the energy loss process in the wave-particle interaction generating Type III bursts.

Keywords: sun, solar energetic particle, electron event, type III burst

©2021. Japan Geoscience Union. All Right Reserved.

Occurrence dependence on solar activity cycle for ordinary type III bursts and micro-type III bursts

*Yuichiro Seki[1], Hiroaki Misawa[1], Takahiro Obara[1], Fuminori Tsuchiya[1]

1. Tohoku University

Type III bursts are one of intense solar radio emissions and show a large negative frequency drift. Some of them originate above solar active regions and appear with solar flares. These type III bursts are hereafter referred to as ordinary type III bursts. On the other hand, type III bursts sometimes appear as clusters which are characterized by thousands of short-lived type III bursts lasting for a few days or more than a week. Morioka et al. (2007) proposed the term ‘micro-type III bursts’, which are elements of type III storms. It is suggested that micro-type III bursts originate near the edge of coronal streamers and are not just weaker versions of the ordinary type III bursts because a distribution of emitted power flux is different from that of ordinary bursts.

Generation processes of both ordinary and micro type III bursts are thought that high energy electrons originally generated with magnetic reconnections excite Langmuir waves in the solar corona and/or interplanetary space, then the Langmuir waves are converted into electromagnetic waves observed as type III bursts. It is therefore generally assumed that the frequency of type III bursts reflects the plasma density in the solar corona and/or interplanetary space where the radio waves are generated, and their frequency drift reflects the plasma density distribution and the velocity of high-energy electrons.

It is well known that density distributions of the solar plasma differ depending on the activity of solar surface area (ex. Aschwanden and Acton, 2001). This implies that the plasma density distribution roughly varies with the solar activity cycle and therefore the frequency drift rates of type III bursts might show solar cycle dependence since the drift rates should reflect plasma density distributions. Although the occurrence rates of type III bursts are known to show a positive correlation with solar activity, our knowledge for solar cycle dependence of the drift rates has been still limited (ex. Zhang et al., 2018). Moreover, there has been no study that clearly classifies ordinary type III bursts and micro-type III bursts, and simultaneously analyzes the long-term variation of their drift rates.

In this study, we have investigated occurrence features of drift rates for ordinary type III bursts and micro-type III bursts to clarify their solar cycle dependences. For this purpose, we have tried to make statistical analyses of type III bursts using a database of solar radio spectra observed with the Nancay Decameter Array (NDA). We have analyzed the low-resolution data (175 kHz frequency resolution, 1 second time resolution) of the NDA. Although the observation frequency range of NDA is 10MHz-80MHz, we have used the spectra for 30-80MHz to avoid noises below 30MHz.

An automatic burst detection system was newly developed to make the statistical analyses. Threshold methods, Convolution Neural Network (CNN) methods, and least squares methods with curve fitting are applied to our detection system. From candidates of type III bursts detected by this system, we finally selected ordinary type bursts and micro-type III bursts through a visual check.

Using the developed automatic detection system, we have analyzed 7 years of solar activity cycle 24, 2012-2014(around solar maximum) and 2017-2020(around solar minimum) so far, and detected 1145 ordinary type III bursts and 1021 micro-type III bursts in total and a preliminary result shows for ordinary

©2021. Japan Geoscience Union. All Right Reserved.

type III bursts, drift rates (|df/dt|) in 2019 and 2020 are lower than those in other years, and for micro-type III bursts, lower solar activity is, higher drift rates are. In the presentation, we will show solar cycle dependence for the occurrence characteristics of both ordinary and micro type III bursts with the discussion of their background processes.

Acknowledgments: The solar radio spectrum data was provided by the Nancay Observatory, Observatoire de Paris, France. We would appreciate Dr. L. Lamy and the NDA operation group.

Keywords: Radio emission, Particle acceleration, Nancay decameter array, Type III bursts, Micro-type III bursts

©2021. Japan Geoscience Union. All Right Reserved.

Simple Estimation of the Global Solar Wind Structure

*Ken'ichi Fujiki[1], Munetoshi Tokumaru[1], Kazumasa Iwai[1]

1. Institute for Space-Earth Environmental Research

The solar wind is composed of a slow wind (~450 km/s) and a fast wind (~800 km/s), which is known as the bimodal signature of the solar-wind velocity. These slow and fast wind are the main components of the solar wind in the low-mid and high latitudes of the heliosphere, respectively. The solar wind structure is stratified by latitude. For example, the slow wind is confined in a narrow band around the solar equator (or heliospheric current sheet with a small tilt angle) during the solar minimum. The width of the narrow slow wind band increases in rising and declining phases then the tilt angle of HCS becomes larger. During solar maxima, the latitude structure is lost, and the heliosphere is dominated by slow solar wind and frequent CMEs.

In this study, we focus a variation of boundary latitudes of the slow-fast solar wind through three solar cycles by using the interplanetary scintillation (IPS) observation at the Institute for Space-Earth Environmental Research (ISEE). The latitudinal structure of the bimodal solar wind is derived from the solar wind synoptic map for each Carrington rotation and compared with the maximum tilt angle of the HCS derived from observations by the Wilcox Solar Observatory (WSO). The results show that the HCS tilt angle correlates well with the latitudinal average of the solar wind speed of 600 km/s (correlation coefficient of 0.8). The empirical results allow us to estimate the latitudinal structure of the solar wind by the bimodal solar wind velocity after the 1970s when continuous magnetic field observations of the Sun began.

Keywords: solar wind, long-term variation, magnetic field

©2021. Japan Geoscience Union. All Right Reserved.

[J] Poster | A (Atmospheric and Hydrospheric Sciences)：A-OS Ocean Sciences & Ocean Environment

Sat. Jun 5, 2021 5:15 PM - 6:30 PM JST | Sat. Jun 5, 2021 8:15 AM - 9:30 AM UTC | Ch.06_1

[A-OS14] Coastal physical processes associated with mixing, eddies, internal waves

convener:Eisuke Tsutsumi(Atmosphere and Ocean Research Institute, The University of Tokyo), Eiji Masunaga(Ibaraki University), Taira Nagai(Graduate School of Science, The University of Tokyo)

Recently developed observational and numerical approaches have revealed details of physical processes in coastal regions, which are keys to understanding global ocean circulations and ecosystems. This session aims to provide discussions of mixing, eddies, nonlinear internal waves in coastal and marginal oceans, estuaries and lakes. Observations, numerical modeling and laboratory experiments associated with these phenomena are encouraged to submit an abstract to this session. In addition, studies that consider linkages between coastal physical processes and large scale open ocean processes, e.g., the Kuroshio, global ocean circulations.

[AOS14-P01] Material transport and diffusion around Sagami Bay and Suruga Bay using a particle tracking model

*Takayoshi Inoue[1], Eiji Masunaga[1], Taichi Kosako[2], Yusuke Uchiyama[3] (1.Ibaraki University, 2.Port and Airport Research Institute, 3.Kobe University)

[AOS14-P02] Physical structure and mixing processes in the inner part of Tokyo Bay

*Haruki Itozu[1], Eiji Masunaga[1] (1.Ibaraki University)

[AOS14-P03] Secular variations of M_2 tide, its resonant amplification, and the associated energy dissipation in a semi-enclosed sea connected to the East China Sea (Ariake Sea, Japan), 1980–2019.

*Eisuke Tsutsumi[1], Matsuno Takeshi[2], Sachihiko Itoh[1] (1.Atmosphere and Ocean Research Institute, The University of Tokyo, 2.Research Institute for Applied Mechanics, Kyushu University)

Material transport and diffusion around Sagami Bay and Suruga Bay using a particle tracking model

*Takayoshi Inoue[1], Eiji Masunaga[1], Taichi Kosako[2], Yusuke Uchiyama[3]

1. Ibaraki University, 2. Port and Airport Research Institute, 3. Kobe University

In this study, material transport and diffusion processes in Sagami Bay and Suruga Bay were evaluated using the ROMS model with a 3-D Lagrangian particle tracking model. The model was run for the summer season performed with long term averaged climatological reanalyzed data. We also investigated effects of horizontal diffusion by a random walk model.

Particles that flowed out from Sagami Bay were mainly transported to the east (70%) caused by the Kuroshio Current. For Suruga Bay, particles were mainly outflowed on the west side of the bay mouth (75%). Most of the model cases showed that the particle outflow from the inner part of the bays was lower than the bay mouths. The Kuroshio current directly influences particle transport in Sagami Bay, which results in a small difference in the particle flow rate from the bay mouth and inner part of the bay. The semi-closed shape of Suruga Bay suppressed the particle outflow rate. Particle transport between the inner part of Suruga Bay and bay mouth requires more than six days. Particles in Suruga Bay mouth tended to move toward the inner part of the bay as the horizontal diffusion increased, and the particle outflow rate decreased. Except for Suruga Bay mouth case, the particle outflow rate from the bays to the open ocean increased with increasing in the horizontal diffusion. Particles that flowed out from Sagami Bay (Suruga Bay) increased by 12 % (15 %) caused by the random walk when the horizontal diffusion was set at 10^{-1} ~ 10^{1} m^2 /s.

Keywords: ROMS model, Particle tracking model, Sagami Bay, Suruga Bay, Diffusion, Random walk

©2021. Japan Geoscience Union. All Right Reserved.

Physical structure and mixing processes in the inner part of Tokyo Bay

*Haruki Itozu[1], Eiji Masunaga[1]

1. Ibaraki University

Numerous physical processes are involved in coastal regions of freshwater influence, e.g., river plume dynamics, tidal mixing, internal waves. In the inner part of Tokyo bay, one of the regions of freshwater influence, strong stratification often appeasers resulting in hypoxia and blue tide, which significantly influences ecosystems. Although there have been numerous studies on physical structures in Tokyo bay, few studies have focused on mixing process in the inner part of the bay. In this study, we analyzed data from long term observations at the Chiba light beacon located at the inner part of Tokyo Bay to understand physical structures associated with mixing process. The observational data showed that hypoxia events occurred with appearances of high density water in the bottom layer. The ratio of the vertical density gradient and vertical shear, namely the Richardson number, well explains appearance of hypoxia events. The wind stress largely influenced vertical mixing, rather than tidal currents. We calculated modified versions of the horizontal Richardson number (R_x^{wt}) developed by Burchard [2009]. Bottom hypoxia events occurred when R_x^{wt} were over 2.1×10^{-3} of critical value of stable stratification. The horizontal physical structure can be used to explain the vertical physical structure. By comparing R_x^{wt} with zonal winds, R_x^{wt} was over approximately 2.1×10^{-3} when east wind below 5 m/s. This suggests that weak offshore winds promote the upwelling of bottom hypoxia water mass from offshore rather than mixing. Weak winds less than 5 m/s enhance stratification in the inner part of Tokyo bay.

Keywords: Tokyo Bay, Stratification, Mixing

©2021. Japan Geoscience Union. All Right Reserved.

Secular variations of M_2 tide, its resonant amplification, and the associated energy dissipation in a semi-enclosed sea connected to the East China Sea (Ariake Sea, Japan), 1980–2019.

*Eisuke Tsutsumi[1], Matsuno Takeshi[2], Sachihiko Itoh[1]

1. Atmosphere and Ocean Research Institute, The University of Tokyo, 2. Research Institute for Applied Mechanics, Kyushu University

After 2000, decrease in M_2 tidal elevation amplitude have been obverved in and around a semi-enclosed shallow embayment connected to the eastern East China Sea, Ariake Sea. In this study, we present an updated analysis of the secular variation of M_2 tide in Ariake Sea by introducing the bottom friction and its nonlinearity, which have not been explicitly considered in the tidal studies of the Ariake Sea. Over the last five decades, M_2 tidal elevation amplitude has decreased at an average rate of ~−11 % century^{-1} both inside and outside of the sea. The result of the analysis indicated that linear bottom drag coefficient had decreased at ~−10 % century^{-1}, suggesting that if the quadratic bottom drag coefficient was unchanged, mean M_2 velocity in the sea also had decreased at the same rate. Comparing 1997 and 2015, when the lunar nodal factor for M_2 tide was nearly at its maximum, we found that the energy dissipation of M_2 tide decreased by ~11 % in 2015. The possible causes of these decreasing trends were changes in the frictional resonance properties of the sea and change in the incoming M_2 tide from the East China Sea.

Keywords: Changing tides, Ariake Sea, Bottom drag, Tidal energy dissipation

©2021. Japan Geoscience Union. All Right Reserved.

[J] Poster | A (Atmospheric and Hydrospheric Sciences)：A-OS Ocean Sciences & Ocean Environment

Sat. Jun 5, 2021 5:15 PM - 6:30 PM JST | Sat. Jun 5, 2021 8:15 AM - 9:30 AM UTC | Ch.06_2

[A-OS16] Global ocean observing systems, their status, research results and future perspective

convener:Shigeki Hosoda(Japan Marine-Earth Science and Technology), Shuhei Masuda(Japan Agency for Marine-Earth Science and Technology), Yosuke Fujii(Meteorological Research Institute, Japan Meteorological Agency), Fujiki Tetsuichi(Japan Agency for Marine-Earth Science and Technology)

The global ocean is complementary covered by variable kinds of observing networks such as Argo, GO-SHIP, OceanSITES, earth observing satellite, then its observing network is crucial for research, monitoring and future predictions of climate changes and ocean environment. Besides, the ocean observing networks are also recognized as infrastructures for research, human societies, and industries in the SDGs and the UN Decade, which is suggested to achieve their goals and to develop the network within 10 years. In the session held previously, we discussed the status and future perspective on the ocean observing network, following themes in OceanObs19, etc., exchanging current information. After the previous session, the roadmap2020 for progress of the global ocean observation had been suggested, the GO BGC Argo project was accepted by the National Science Foundation in 2020, and the UN Decade starts from 2021. Under these circumstances, the target of this session is to host a meeting exchanging information on the recent status of the observing networks, and discussing for future perspectives regarding pilot studies of large-scale ocean observations, OSE and OSSE for the ocean observing networks, development of sensor and platform technologies. At the same time, we would like to share information of current research results regarding large-scale heat, freshwater, material transports, physical and biogeochemical mechanisms of water mass formation and modification, air-sea interaction, and developing measurement sensors and data quality controls contributing to those researches, overarching variable research fields.

[AOS16-P01] Spatiotemporal variability of vertical structures of temperature and salinity in the mid-latitude northwest Pacific Ocean based on unsupervised clustering

★Invited Papers

*Fumika Sambe[1], Toshio Suga[1,2] (1.Graduate School of Science, Tohoku University, 2.JAMSTEC)

[AOS16-P02] Temporal variations of Kuroshio transport based on a repeated hydrographic section along 137E

*Yuma Kawakami[1], Toshiya NAKANO[1], Atsushi Kojima[1], Kiyoshio Murakami[1], Shusaku Sugimoto[2] (1.Japan Meteorological Agency, 2.Tohoku University)

[AOS16-P03] Global distribution of 10-day differences of temperature and salinity around 2000 m depth observed with Argo floats

*Yoshimi Kawai[1] (1.Research Institute for Global Change, Japan Agency for Marine-Earth Science and Technology)

[AOS16-P04] GO-SHIP Easy Ocean: formatted and gridded ship-based hydrographic section data

*Katsuro Katsumata[1], Sarah Purkey[2], Rebecca Cowley[3], Bernadette Sloyan[3], Stephen Diggs[4], Thomas Moore, II[3], Lynne Talley[2], James Swift[4] (1.JAMSTEC, 2.Scripps Institution of Oceanography, 3.Oceans and Atmosphere, CSIRO, 4.CLIVAR and Carbon Hydrographic Data Office, Scripps Institution of Ocenaography)

[AOS16-P05] Salinity bias with negative pressure dependency caused by anisotropic deformation of CTD measuring cell under pressure examined with a dual-cylinder cell model

*Taiyo Kobayashi[1] (1.Japan Agency for Marine-Earth Science and Technology)

[AOS16-P06] pH measurement in the ocean

*Hajime Kayanne[1], Toshimasa Miyawaki[1], Nori Fujita[1], Kenta Suzuki[2], Hizuru Nakajima[2], Kazuhiro Morioka[3], Akihide Hemmi[4] (1.the University of Tokyo, 2.Tokyo Metropolitan Univ., 3.Tokyo Univ. Pharmacy Life Sci., 4.Möbius Advanced Tech.)

[AOS16-P07] Advances in the estimation of global surface net heat flux based on satellite observation: J-OFURO3 V1.1

*Hiroyuki Tomita[1], Kunio Kutsuwada[2], Masahisa Kubota[3], Tsutomu Hihara[4] (1.Institute for Space-Earth Environmental , Nagoya University, 2.School of Marine Science and Technology, Tokai University, 3.Institute of Ocean Research and Development, 4.Japan Fisheries Information Service Center)

[AOS16-P08] Keeping the PACE with the NASA Plankton, Aerosol, Cloud, ocean Ecosystem (PACE) mission

*Lachlan McKinna[1], Ivona Cetinić[2,3], Jeremy Werdell[3] (1.Go2Q Pty Ltd, 2.USRA, 3.NASA GSFC)

Spatiotemporal variability of vertical structures of temperature and salinity in the mid-latitude northwest Pacific Ocean based on unsupervised clustering

*Fumika Sambe[1], Toshio Suga[1,2]

1. Graduate School of Science, Tohoku University, 2. JAMSTEC

In the mid-latitude northwest Pacific Ocean, the transport, stirring and mixing of subtropical and subarctic water occur, resulting in multiple ocean domains characterized by a variety of unique oceanographic structures. Many studies were conducted on the characteristics and distribution of these ocean structures, and the boundaries of domains and characteristic water masses were defined. Most of subsequent studies on the ocean structure and water mass in this ocean region have been based on the existing definitions of the structure and water mass of interest based on spatiotemporally limited data. Even while a large amount of vertical profile data has become available evenly in space and time with the expansion of the Argo observing network, the basic research framework has not changed significantly. However, with the huge amount of data accumulated by Argo with a small spatiotemporal bias, it may be possible to objectively recapture the ocean structure by data-driven scientific methods, that is, machine learning. The Profile Classification Model (PCM) developed by Maze et al. (2017) is a machine learning method for vertical profile data in the ocean. The PCM classifies profiles by unsupervised clustering using Gaussian Mixture Model, and one of its main features is that it can perform analysis using a labeling metric that quantifies the certainty of the classification. Previous studies have shown that clustering with PCM represents the vertical structure and spatial distribution of each class representing a particular ocean structure and its main distribution area. In this study, PCM is applied for the first time to the temperature and salinity profiles by Argo floats in the mid-latitude northwest Pacific Ocean, and the results are compared with previous knowledge of ocean structure. In addition, we tried to understand the spatiotemporal variability of oceanographic structures from the results of PCM by grouping the results based on the Kuroshio Extension index (KE index), which is a measure of a stable and an unstable dynamic state of the KE, and discussing the characteristics of each group.
In this study, PCM clustering was performed on 57476 temperature and salinity profiles located between 30˚N and 60˚N and between 140˚E and 180˚E. Based on statistical criteria and the initial value dependence, the number of classes was set to five. The results showed that classes 1, 2, 3, 4, and 5 were distributed to form five regions: the subarctic region, the mixed water region, the subtropical subarctic intermediate region, the northwestern part of the subtropical gyre, and the downstream of the KE region. Each class has different oceanographic features. The relationship between the distribution area and the characteristics of each class corresponded to the relationship between the ocean structure and the area described in previous studies, which mainly focused on specific water masses and vertical structures. In addition, we investigated how the distribution of each class changed depending on the KE index. We found that the shape of the distribution area of class 4 and the degree to which classes other than class 5 coexist in the downstream of the KE region changed. This change in the distribution area was consistent with the results expected from the north-south shift of the KE position due to the dynamic state of the KE. The profiles with low labeling metrics were found to be concentrated near the boundaries of the main distribution areas of the classes. This may reflect “mixing” between different classes at the domain boundary. It was also confirmed that the proportion of profiles with low labeling metric to total profiles had a significant negative correlation with KE index, suggesting that the more unstable the KE dynamic state was, the more the interclass “mixing” became active.

©2021. Japan Geoscience Union. All Right Reserved.

Keywords: Mid-latitude Northwest Pacific Ocean, Kuroshio Extension, Argo float, Unsupervised Clustering, Data-driven Science, Oceanographic Structure

©2021. Japan Geoscience Union. All Right Reserved.

Temporal variations of Kuroshio transport based on a repeated hydrographic section along 137E

*Yuma Kawakami[1], Toshiya NAKANO[1], Atsushi Kojima[1], Kiyoshio Murakami[1], Shusaku Sugimoto[2]

1. Japan Meteorological Agency, 2. Tohoku University

Kuroshio is the western boundary current in the North Pacific subtropical gyre. It flows northeastward along the south coast of Japan. The Kuroshio has its origin in tropical region, and plays an important role for heat transport from low-latitude to mid-latitude North Pacific. Through its heat transport, the Kuroshio has a significant impact on basin-scale climate in the North Pacific. Therefore, in order to understand climate variability in the North Pacific, it is important to monitor and understand a temporal variation of the Kuroshio transport.

Past works reported that the Kuroshio transport fluctuates on decadal (about 10 years) and bi-decadal (about 20 years) timescales, responding to changes in the winter atmospheric field which reflects Aleutian Low activities. However, the length of Kuroshio transport time series used in the previous studies is about 35 years at most, and it cannot be said that low-frequency variations like decadal and bi-decadal timescale variations are detected robustly. The Japan Meteorological Agency has repeated ship-board observations along 137E across the Kuroshio since 1967 in winter and 1972 in summer. This long-term observational data is powerful tool to investigate the Kuroshio transport variation. In this study, we examine the Kuroshio transport variation based on the repeated hydrographic sections along 137E.

We estimate the Kuroshio transport by vertical and meridional integration of zonal geostrophic velocity. In this study, we focus on net eastward transport across the 137E section (hereafter, referred as net Kuroshio transport). The net Kuroshio transport is calculated by subtracting westward transports associated with the cold-core eddy and Kuroshio Counter current in the north and south of the Kuroshio from eastward Kuroshio transport.

The net Kuroshio transport fluctuates on inter-annual, decadal, and bi-decadal timescales. The inter-annual variation is detected before 1985 and after 2000, and the decadal variation is dominant before 2000. The bi-decadal timescale is detectable throughout the analysis period. As shown by previous studies, the net Kuroshio transport variation is caused by changes of the winter atmospheric forcing. We confirmed that the net Kuroshio transport responds to changes of winter wind stress curl (WSC) in the central North Pacific with a lag of two years.

To examine temporal variations of winter WSC field in the North Pacific subtropical gyre, we next performed an EOF analysis. As a result, the mode-1 is linked to a meridional movement of the Aleutian Low which has an inter-annual timescale before 1980 and after 1995, and the mode-2 reflects an Aleutian Low intensity fluctuation with a decadal timescale before 2000 and bi-decadal timescale throughout the analysis period. A correlation analysis shows that the winter WSC in the central North Pacific resulting in the net Kuroshio transport variation well reflects mode-2, especially before 2000 when the Aleutian Low intensity fluctuation has a decadal timescale. In addition, the winter WSC in the central North Pacific relatively well correlates to also mode-1 after 1985 and before 2000 when the meridional Aleutian Low movement has an inter-annual timescale. These results suggest that the winter WSC in the central North Pacific is determined by the Aleutian Low intensity fluctuation on decadal and bi-decadal timescales whereas influenced by the meridional movement of the Aleutian Low on an inter-annual

©2021. Japan Geoscience Union. All Right Reserved.

timescale.

From the above results, we concluded that the net Kuroshio transport variation on an inter-annual timescale is caused by the meridional Aleutian Low movement, and that on decadal and bi-decadal timescale results from the Aleutian Low intensity fluctuation. It can be also pointed out that temporal changes of timescales in the net Kuroshio transport derives from changes of timescales in the Aleutian Low activities.

Keywords: Kuroshio transport, Repeated hydrographic section along 137E, Aleutian Low

©2021. Japan Geoscience Union. All Right Reserved.

Global distribution of 10-day differences of temperature and salinity around 2000 m depth observed with Argo floats

*Yoshimi Kawai[1]

1. Research Institute for Global Change, Japan Agency for Marine-Earth Science and Technology

It has been indicated from repeat hydrographic observations up to the bottom that the warming of the oceans already spread to the global abyssal waters, not only near the surface. Investigating processes of energy and material transport and their variations is essentially important for global climate changes. It had been difficult to do that globally due to lack of observation, but now the observation system by the Argo floats covers almost the whole world. Previous studies have utilized the Argo data to investigate absolute geostrophic velocity, vertical diffusivity, warming trend, and intraseasonal oscillations globally around 1000-m depth or deeper, for example. Short-term variations induced by atmospheric cyclones and internal tides in the intermediate and deep layers are, however, not examined enough. In this study, the authors examines the variability of the layer around 2000 m depth, which is the “bottom” of the present, dense Argo observation system, using all of available Argo float data. In particular, this study focuses on the difference between two successive observations, that is, nearly 10-day variation, aiming to detect rapid changes, mainly due to developed cyclones or internal tides. Even 1-day sampling is too coarse to resolve the Ekman suction or near-inertial oscillations, but a large number of samples will highlight areas where the frequency of large changes in a short period is high.
All delayed quality controlled float data that were available as of 20 September 2020 were downloaded from the ftp site of Argo Global Data Assembly Center and analyzed only the measurements flagged as good. Each profile was vertically interpolated on a 10-dbar grid using the Akima spline. Then the author obtained differences in properties between two successive observations for each individual float at an isobaric or isopycnal surface. The differences with an observation interval of 9-12 days, $\Delta T_i=T_i-T_{i-1}$ for temperature, and $\Delta S_i=S_i-S_{i-1}$ for salinity, were selected and averaged on 2˚×2˚ grids. T and S are temperature and salinity, and subscript *i* denotes observation cycle. The average of the absolute value of ΔT or ΔS at 1000 dbar or 1950 dbar are mainly examined in this study.
Mean ΔT at 1000 dbar is large in the western boundary currents: the Gulf Stream, the North Atlantic Current, the Agulhas and Agulhas Return Currents, the East Australian Current, and the Kuroshio Extension. At 1950 dbar, ΔT is remarkable in the eastern North Atlantic Ocean west of Europe, the Argentine basin, and the northwestern Indian Ocean. Large ΔT is localized in some areas in the Southern Ocean: around 30ºE, 85ºE, 155ºE, 135ºW, and the Scotia Sea. For salinity, the spatial patterns are similar to those of temperature, but ΔS at 1000 dbar is also large in the east North Atlantic. There is no clear seasonality in the 10-day variations at 1000 dbar or deeper. The ΔT distribution at 1950 dbar shown by this simple procedure appears to reflect internal waves related with bottom topography, rather than atmospheric turbulence. The locally enhanced ΔT in the Southern Ocean are located over the ridges or leeward of the plateau, and may be caused by internal lee waves from geostrophic flows. On the other hand, the spatial distribution of ΔT in the North Atlantic Ocean is similar to that of the Mediterranean Outflow Water, which is a saline and warm water mass produced as a result of mixing the Mediterranean Sea Water and the ambient North Atlantic Central Water. The large ΔT in the North Atlantic Ocean would reflect the mixing and spreading processes of the saline water. The results of this study does not directly indicate the strength of ocean mixing, but is useful to infer where the mixing is vigorous in the intermediate layer, and will contribute to designing the observation system of the deep Argo float.

©2021. Japan Geoscience Union. All Right Reserved.

Keywords: Argo float, intermediate layer, 10-day change

©2021. Japan Geoscience Union. All Right Reserved.

GO-SHIP Easy Ocean: formatted and gridded ship-based hydrographic section data

*Katsuro Katsumata[1], Sarah Purkey[2], Rebecca Cowley[3], Bernadette Sloyan[3], Stephen Diggs[4], Thomas Moore, II[3], Lynne Talley[2], James Swift[4]

1. JAMSTEC, 2. Scripps Institution of Oceanography, 3. Oceans and Atmosphere, CSIRO, 4. CLIVAR and Carbon Hydrographic Data Office, Scripps Institution of Ocenaography

Despite numerous technological advances over the last several decades, ship-based hydrography remains the only method for obtaining high-quality, high spatial and vertical resolution measurements of a suite of physical, chemical, and biological parameters over the full water column essential for physical, chemical, and biological oceanography and climate science. The Global Ocean Ship-based Hydrographic Investigations Program (GO-SHIP) coordinates a network of globally sustained hydrographic sections as part of the global ocean observing system, building on previous programs. These data provide a unique data set that spans four decades, comprised of more than 40 cross-ocean transects, many with multiple repeats. The section data are, however, difficult to use owing to inhomogeneous format. The purpose of this data product is to increase the value of these data by better combining, reformatting and gridding in order to facilitate their use with less effort by a wider audience. The product is machine readable and readily accessible by many existing visualisation and analysis software packages. The data processing can be repeated with modifications to suit various applications such as analysis of deep ocean , validation of numerical simulation output, and calibration of autonomous platforms. This initial release includes temperature, salinity, and dissolved oxygen data from Conductivity-Temperature-Depth profiles, but the product will include other properties such as nutrients and carbon items in future releases.

Keywords: hydrographic data, ship observation, global

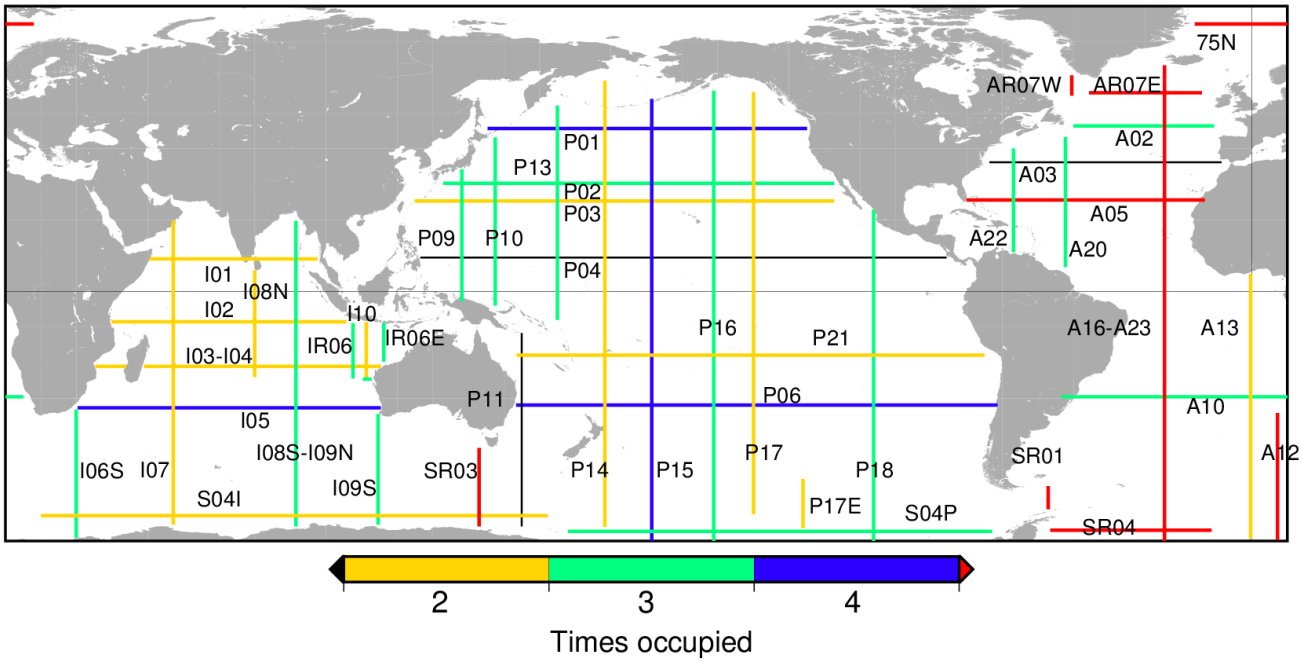

©2021. Japan Geoscience Union. All Right Reserved.

Salinity bias with negative pressure dependency caused by anisotropic deformation of CTD measuring cell under pressure examined with a dual-cylinder cell model

*Taiyo Kobayashi[1]

1. Japan Agency for Marine-Earth Science and Technology

Measurements made by deep floats had a salinity bias with a negative pressure dependency. Salinity is affected by conductivity measurements via changes in the CTD measuring cell geometry under pressure. To remove the effect, a canceling factor for pressure CPcor is prepared theoretically by the manufacturer considering the isotropic deformation of a single-cylinder measuring cell under pressure; the observed negative pressure dependency, however, requires an even smaller CPcor. This study examined the causes of the inconsistency for salinity measurements with a dual-cylinder cell model, considering that the actual CTD measuring cell is a glass cell covered by a polyurethane jacket. The dual-cylinder cell model clarifies that the CTD measuring cell deforms anisotropically to yield a smaller CPcor; mainly because the inner glass cell deforms radially to a greater extent than the single-cylinder model due to the radial stress from the outer cylinder (jacket) being stronger than the hydrographic pressure. The observed fresh bias at the sea surface is attributed to a slight shrinkage of the outer jacket because of compression set of polyurethane in deep ocean. The shrunken polyurethane jacket is elongated over time due to a creep phenomenon, which causes less-freshening of the fresh bias found at the sea surface. The observed linear relationship between the smaller CPcor and the fresher bias at the sea surface is attributed to the variation of the wall thickness of the polyurethane jacket when it shrinks similarly. The study suggests another idea to improve the salinity accuracy of CTD sensors greatly: a change of the jacket material into an elastomer. The improvement makes the present setting of CPcor be more valid and reliable, because the elastomer jacket hardly affects the change of the measuring cell geometry under pressure, which in turn removes the pressure effects on salinity measurements.

Keywords: Deep Argo, Salinity measurement, CTD sensor

©2021. Japan Geoscience Union. All Right Reserved.

pH measurement in the ocean

*Hajime Kayanne[1], Toshimasa Miyawaki[1], Nori Fujita[1], Kenta Suzuki[2], Hizuru Nakajima[2], Kazuhiro Morioka[3], Akihide Hemmi[4]

1. the University of Tokyo, 2. Tokyo Metropolitan Univ., 3. Tokyo Univ. Pharmacy Life Sci., 4. Möbius Advanced Tech.

For a century since Cremer (1906) discovered glass membrane potential and Sørensen and Palitzsch (1910) measured ocean pH for the first time, glass electrodes have been used universally to measure ocean pH.
The ion sensitive membrane of the indicator electrode is a thin fragile glass film. The principle behind the selective response of the glass membrane electrode to hydrogen ions is unknown, and manufacturing process is a black boxes varying among manufacturers. Since Ag-AgCl electrodes are used for both the indicator and reference electrodes, they react with the sample solution and deteriorate. In addition, the reference electrode is constantly leaking internal solution to maintain conductivity with the indicator electrode through the sample as a salt bridge, and the solution needs to be replaced. Despite the vast amount of pH data accumulated by glass electrodes, the values are considered less reliable than those obtained by spectrophotometry due to drift and degradation of the electrodes without proper calibration (Dickson 1993, McLaughlin et al. 2017). The measurement of ocean pH by spectrophotometry was established by Clayton and Byrne (1993). Seidel et al. (2008) evaluated a in-situ measurement system as a precision of 0.0007 and accuracy of 0.0017. However, spectrophotometric measurement requires mixing of reagents for coloring the sample, which poses a limitation of in-situ measurement.
Since 1970, a pH sensor using a solid-state semiconductor was developed and put into practical use (Bergveld 1970). This is called an ISFET (Ion Sensitive Field Effect Transistor), which measure the potential of the ion-selective membrane (e.g. Ta_2O_5) by the transistor. The principle of ISFET is electrochemically clear and there is no black box. The semiconductor sensor is durable and can be reduced its size. ISFETs are also applied in Argo Float for pH measurement. The most commonly used Durafet sensor has a short time accuracy (repeatability) of 0.0005, a multi-year accuracy of 0.005, and an accuracy of 0.01 (Martz et al. 2010, Johnson et al. 2016).
However, since the semiconductor should be immersed in the solution united with the membrane, the semiconductor must be tightly molded. For deep-sea measurements, a pressure resistance of 10 MPa or higher is required. Pressure dependancy of the semiconductor must be taken into consideration for measurement in deep sea. Also, there is a limit for reduction in size of the semiconductor. In addition, Ag-AgCl is used as the reference electrode, which reacts with the chloride ions in the solution, causing the electrode to deteriorate. KCl gel is used as the internal solution of the reference electrode, and its replacement is also necessary.
The pH is the most fundamental chemical variable in the ocean. In particular, ocean acidification due to rising atmospheric CO_2 has been recognized as a new issue related to global environmental change, and pH measurement has become increasingly important. In addition to pH, the three other variables of the four measurable ones of the ocean carbonate system (pH, CO_2, total inorgnic carbon, and alkalinity) can be determined by adding acid to the seawater sample (total inorgnic carbon and alkalinity) or by extracting CO_2 through a gas permeable membrane into the solution (CO_2, total carbon dioxide) and measuring its pH. The development of a pH sensor that can maintain stability and accuracy even in seawater and high-pressure deep waters will greatly advance the monitoring of the ocean's carbonate system, based on which ocean acidification and the ocean's CO_2 sink capacity would be evaluated. The new pH sensor must be small, have low power consumption, be reagent-free, be stable over the long term, not be altered by seawater, be resistant to high pressure, and have little been dependent on pressure. The

©2021. Japan Geoscience Union. All Right Reserved.

precision and accuracy must be within 0.0002 and 0.001 considering the propagation of errors in calculating the carbonate system.

Keywords: pH, ocean, measuement, Ocean Acidification, ISFET

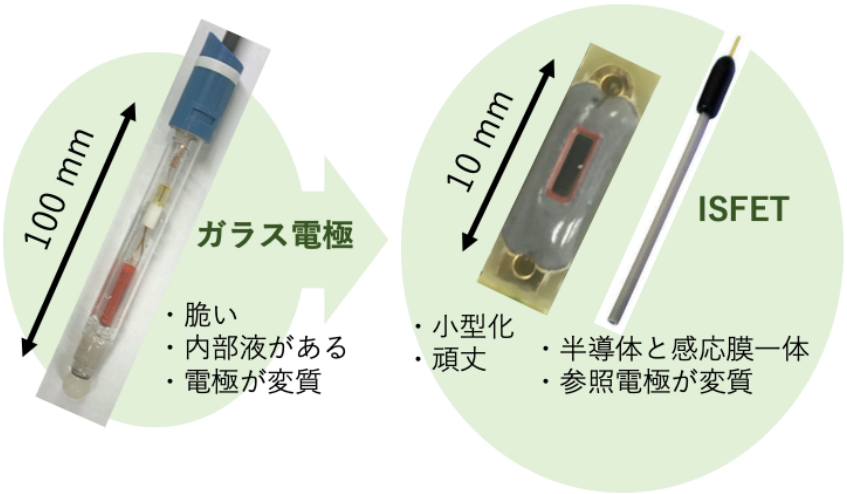

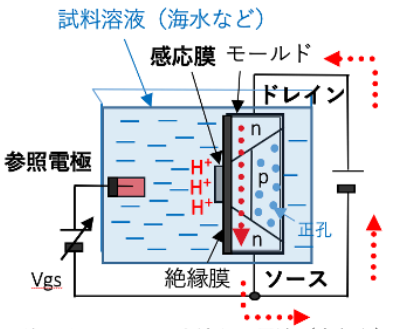

ドレインーソースを流れる電流（赤矢印）を一定にするゲート電位（Vgs）によって，感応膜の電荷（H^+; pH）を計測する．

ISFET の原理

©2021. Japan Geoscience Union. All Right Reserved.

Advances in the estimation of global surface net heat flux based on satellite observation: J-OFURO3 V1.1

*Hiroyuki Tomita[1], Kunio Kutsuwada[2], Masahisa Kubota[3], Tsutomu Hihara[4]

1. Institute for Space-Earth Environmental , Nagoya University, 2. School of Marine Science and Technology, Tokai University, 3. Institute of Ocean Research and Development, 4. Japan Fisheries Information Service Center

Surface net heat flux, defined as the total heat exchange between the atmosphere and oceans, affects both atmospheric and oceanic processes. Global estimates based on observations are necessary to understand long-term climate change and related responses and to validating climate model results. Consequently, estimating and improving surface net heat flux using satellite observations are of vital importance. The reliability of surface net heat flux data obtained from the latest satellite-based estimation (the third-generation Japanese Ocean Flux Data Sets with Use of Remote Sensing Observations [J-OFURO3, V1.1]) was investigated. Three metrics were utilized: 1) the long-term (30 years) mean for 1988–2017, 2) the local accuracy evaluation based on comparison with observations recorded at buoys located at 11 global oceanic points with varying climatological characteristics, and 3) the physical consistency with the freshwater balance related to the global water cycle. The globally averaged value of the surface net heat flux of J-OFURO3 was −22.2 W m^{-2}, which is largely imbalanced to heat the ocean surface. This imbalance was due to the turbulent heat flux being smaller than the net downward surface radiation. On the other hand, compared with the local buoy observations, the average difference was −5.8 W m^{-2}, indicating good agreement. These results indicate a paradox of the global surface net heat flux. In relation to the global water cycle, the balance between surface latent heat flux (ocean evaporation) and precipitation was estimated to be almost 0 when river runoff from the land was taken into consideration. The reliability of the estimation of the latent heat flux was reconciled by two different methods. Systematic ocean heating biases by surface sensible heat flux (SHF) and longwave radiation were identified. The bias in the SHF was globally persistent and especially large in the mid- and high latitudes. The correction of the bias has an impact on improving the global mean net heat flux by +5.5 W m^{-2}. Furthermore, since J-OFURO3 SHF has low data coverage in high-latitudes areas containing sea ice, its impact on global net heat flux was assessed using the latest atmospheric reanalysis product. When including the sea ice region, the globally averaged value of SHF was approximately 1.4 times larger. In addition to the bias correction mentioned above, when assuming that the global ocean average of J3 SHF is 1.4 times larger, the net heat flux value changes to the improved value (-11.3 W m^{-2}), which is approximately half the original value (-22.2 W m^{-2}).

Keywords: surface flux, air-sea interaction, satellite remote sensing

©2021. Japan Geoscience Union. All Right Reserved.

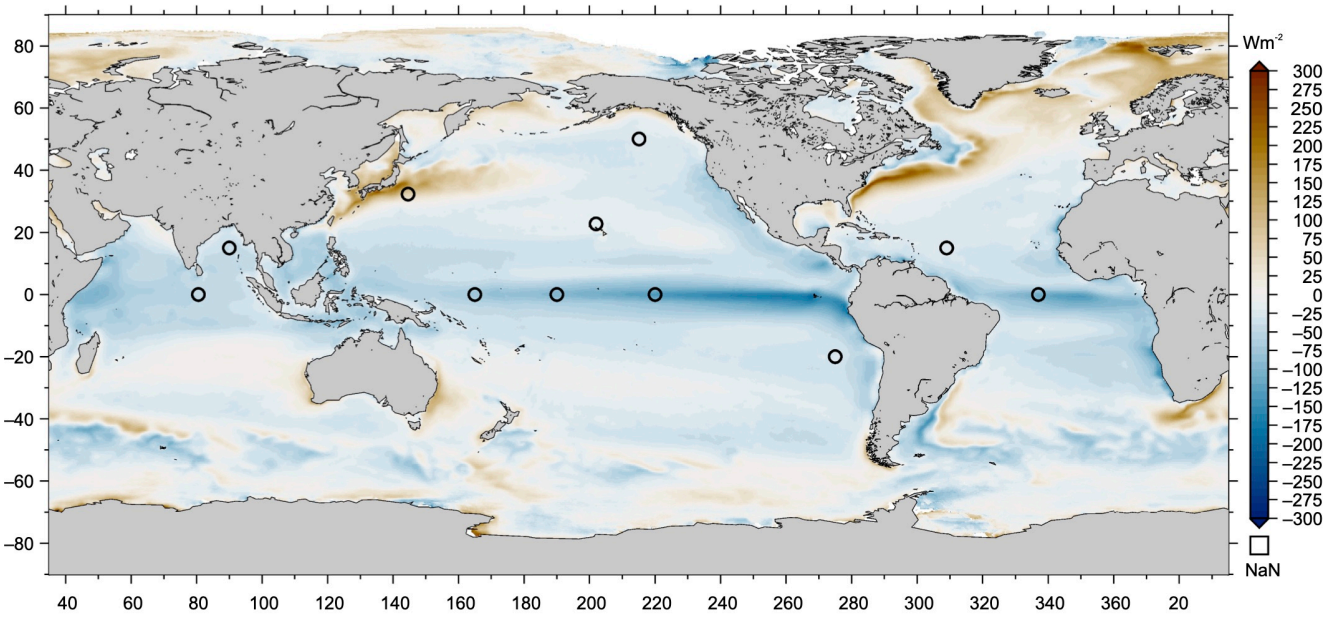

©2021. Japan Geoscience Union. All Right Reserved.

Keeping the PACE with the NASA Plankton, Aerosol, Cloud, ocean Ecosystem (PACE) mission

*Lachlan McKinna[1], Ivona Cetinić[2,3], Jeremy Werdell[3]

1. Go2Q Pty Ltd, 2. USRA, 3. NASA GSFC

This presentation will showcase the current status of the NASA Plankton, Aerosol, Cloud, ocean Ecosystem (PACE) mission. PACE is a strategic climate continuity activity that will not only extend key heritage ocean color, cloud, and aerosol data records, but also enable new insight into oceanographic and atmospheric responses to Earth's changing climate. PACE’ s primary instrument is a global spectrometer that spans the ultraviolet to near-infrared region in 2.5 nm steps and also includes seven discrete shortwave infrared bands from 940 to 2260 nm. This leap in technology will enable improved understanding of aquatic ecosystems and biogeochemistry, as well as provide new information on phytoplankton community composition and improved detection of algal blooms. PACE's spectrometer will also continue many aerosol and cloud capabilities from MODIS and VIIRS, which in combination with its ocean measurements, will enable improved assessment of aerosol impacts on ocean biology and chemistry. The PACE payload will be complemented by two small multi-angle polarimeters with spectral ranges that span the visible to near infrared spectral region, both of which will significantly improve aerosol and hydrosol characterizations and provide opportunities for novel ocean color atmospheric correction. Scheduled for launch in late 2023/early 2024, this PACE instrument suite will revolutionize studies of global biogeochemistry, carbon cycles, and hydrosols / aerosols in the ocean-atmosphere system.

Keywords: Ocean color, Hyperspectral, Remote sensing, Polarimetry, Biogeochemistry

©2021. Japan Geoscience Union. All Right Reserved.

[J] Poster | A (Atmospheric and Hydrospheric Sciences)：A-OS Ocean Sciences & Ocean Environment

Sat. Jun 5, 2021 5:15 PM - 6:30 PM JST | Sat. Jun 5, 2021 8:15 AM - 9:30 AM UTC | Ch.06_3

[A-OS19] Physical Oceanography (General)

convener:Yoshimi Kawai(Research Institute for Global Change, Japan Agency for Marine-Earth Science and Technology), Kitade Yujiro(Tokyo University of Marine Science and Technology)

This session invites presentations on a wide variety of topics related to physical oceanography, including observation, theory, technology, and numerical modeling.

[AOS19-P01] Long-term variability of summertime convective activity over the tropical northwestern Pacific and its influence on large-scale atmospheric circulation

*Shota Sera[1], Shusaku Sugimoto[1] (1.Graduate School of Science, Tohoku University)

[AOS19-P02] **Temporal variation of heat content within surface mixed layer in the western Arctic from Iridium-based autonomous thermistor strings**

*EunYae Son[1], Yusuke Kawaguchi[1] (1.University of Tokyo)

[AOS19-P03] Data and Sample Management for Marine Observation Cruises: Complaint can be Awareness

*Takayuki Tomiyama[1], Takako Sato[1], Kazuyo Fukuda[1], Hajime Kawakami[1], Makoto Ito[1], Chizuru Saito[1] (1.Japan Agency for Marine-Earth Science and Technology)

[AOS19-P04] Meridional heat transport in the North Pacific subtropical gyre -Analysis by ARMOR 3D-

*Yukina Fukaumi[1], Kazuyuki Uehara[1] (1.The Graduate School of Marine Science and Technology of Tokai University)

Long-term variability of summertime convective activity over the tropical northwestern Pacific and its influence on large-scale atmospheric circulation

*Shota Sera[1], Shusaku Sugimoto[1]

1. Graduate School of Science, Tohoku University

It is known that convective activity over the tropical northwestern Pacific during boreal summer affects atmospheric circulation around East Asia. Nitta (1987) showed that convective activity around the Philippine Sea influences the pressure field around Japan, and this teleconnection pattern is called the Pacific-Japan (PJ) pattern. On the other hand, there are few studies on the impact of convective activity in the South China Sea on the large-scale atmospheric circulation. In this study, we focused on the convective activity in the South China Sea, in order to obtain new insights into the fluctuations of atmospheric circulation around Japan.

The main data used in this study are NOAA Interpolated OLR, ERA5 850 hPa geopotential height, and AMeDAS surface air temperature. We used monthly mean values of 1979–2018. The years which OLR averaged over the South China Sea (110˚E-120˚E, 7.5˚N-22.5˚N) exceeds plus one standard deviation were classified as South China Sea weak convection years, and minus one standard deviation were classified as strong convection years for the composite analysis. The PJ index was calculated based on Wakabayashi and Kawamura (2004).

First, we examined the spatial distribution and variability of OLR around tropical northwestern Pacific. Results indicate that both the convective activity and the amplitude of the variability around the South China Sea in July tend to be getting strong in recent years. Therefore, we focused on July. A correlation coefficient between the PJ index and OLR in the South China Sea was 0.44, which does not necessarily indicate a well agreement. Next, we conducted a composite analysis of OLR. As a result, it was found that the center of activity for the South China Sea OLR was located locally over the South China Sea, and significant signal is not extracted over the Philippine Sea. The composite map for 850 hPa height between the strong and weak convective years indicates a north-south dipole structure appears, showing a westward shift/movement of atmospheric circulation pattern compared to the PJ pattern. The South China Sea OLR variability affects a wide area of Japan, including southwest Japan, thought the PJ pattern influences surface air temperature mainly over eastern Japan. These suggest that convective activity in the South China Sea may have a different impact from the PJ pattern.

In the presentation, we also introduce results of the LBM experiment that simulated convective activity in the South China Sea and discuss convective activity in the South China Sea under the future climate of CMIP6 outputs.

Keywords: PJ pattern, South China Sea

©2021. Japan Geoscience Union. All Right Reserved.

Temporal variation of heat content within surface mixed layer in the western Arctic from Iridium-based autonomous thermistor strings

*EunYae Son[1], Yusuke Kawaguchi[1]

1. University of Tokyo

In recent years, the delayed sea ice onset has been detected from satellite observations. The suspended sea ice onset can generate the longer sea surface exposure, which can enhance the kinetic energy input to the ocean from atmosphere. The increased kinetic energy can be a direct source to deepen the bottom of surface mixed layer (SML). We deployed two drifting buoys, with 17 thermistors and 3 pressure sensors on a 60 m long wire to investigate the heat and SML variation in the upper part of the Canada Basin, Arctic. The buoy collects the temperature, pressure, and GPS data with an hour interval and send it via the Iridium satellite. The deployment was done during the Mirai Arctic cruises of 2019 and 2020. Each buoy was deployed in the outer edge of pack ice in mid-October when the sea ice started to freeze up. The buoy deployed in 2019 survived only for three weeks and continued to report the cold surface water near -1.5 ˚C at 2.5 m depth. The surface temperature at the depth in the same season of 2020 showed warmer water near -1.2˚C than that collected in 2019. Another noticeable point is that the signal of the near-surface temperature maximum (NSTM), a thin warm water layer near 20 m, is more well-defined with the temperature of -0.5˚C in 2020 than in 2019. The upper water temperature showed that the signal of NSTM was weakened by a strong wind event. The difference between temperatures from the two buoys can also be found in the Pacific Summer Water layer (PSW) that forms the upper pycnocline. The PSW was located about 50 m depth in October 2020 where it was about 10 m deeper in October 2019. We found the several cases of upwelling and downwelling, which were recognized from the isothermal fluctuation, and which were driven by gale winds. In the data collected in 2020, periodic motion of sea ice showed variation according to ice formation. In melting phase when sea surface temperature is higher than the local freezing point, inertial motion is dominant in sea ice drift. When the surface temperature becomes colder than the point, the inertial motion disappeared. The detailed interpretation on the surface heat budget and SML thickness variation will be given in presentation.

Keywords: Western Arctic, Sea ice onset, Upper heat variation

©2021. Japan Geoscience Union. All Right Reserved.

Data and Sample Management for Marine Observation Cruises: Complaint can be Awareness

*Takayuki Tomiyama[1], Takako Sato[1], Kazuyo Fukuda[1], Hajime Kawakami[1], Makoto Ito[1], Chizuru Saito[1]

1. Japan Agency for Marine-Earth Science and Technology

Japan Agency for Marine-Earth Science and Technology (JAMSTEC) manages archives of data, samples and their metadata that are obtained during research cruises and submersible dives, and publicly distributes them for additional uses with research or educational purposes. These information services are accessible online through DARWIN website [1] and a series of surrounding online databases [2].

This activity has experienced continuous modifications since when it was founded more than a decade ago. For operating data and samples, we need to deal with new frameworks for organization, research project selection and funding, with volumetric growths of data and samples, and with developments and maintenances of information systems and workflows. Meanwhile, we have to keep the workflows in line as well, for collecting, processing, and distributing of data and samples. For example, as recent progresses, we have got enrolled into the JURCAOS Cooperative Research Cruises [3], introduced Digital Object Identifier (DOI) to our data management [4], and established newly integrated sample information management database [5]. It was not easy to apply these modifications to our work, because we have had reducing budget and human strengths for these years.

In addition, exceptional conditions are sometimes applied to individual research projects, because of contracts for research cooperation, inter-institutional agreements and official permission applications for research and observation. For such projects, we have to pay special care for ownership and handling of data and samples. The chances of having exceptional conditions are not necessarily rare, and their influences are not always small. We have to prepare for identifiable problems, and for unidentifiable problems, we have to develop a robust working system to avoid getting into serious troubles.

In this presentation, we will overview flows of data and samples of research cruises and submersible dives, with describing information systems and workflows, cooperation efforts among researchers, management offices, and institutional organizations. Then we will discuss future plans. For the better operation of data and samples, we have to cultivate cooperative relationship with researchers, by providing services that meet with the researchers needs, and by maintaining operation structure simple.

[1] JAMSTEC DARWIN website: http://www.godac.jamstec.go.jp/darwin/
[2] JAMSTEC NUUNKUI website: http://www.godac.jamstec.go.jp/jmedia/portal/
[3] AORI Tokyo Univ. Cooperative Research System Website: https://www.aori.u-tokyo.ac.jp/coop/
[4] Fukuda et al. (2020) https://doi.org/10.1002/essoar.10503966.1
[5] Tomiyama et al. (2020) https://doi.org/10.1002/essoar.10504056.1

Keywords: marine geological samples, data curation service

©2021. Japan Geoscience Union. All Right Reserved.

Meridional heat transport in the North Pacific subtropical gyre -Analysis by ARMOR 3D-

*Yukina Fukaumi[1], Kazuyuki Uehara[1]

1. The Graduate School of Marine Science and Technology of Tokai University

To clarify heat transports of the ocean interior is very important to understand the climate variability, because thermal inertia in the Ocean is larger than that of the atmosphere. In this study, we report the north-south ocean heat transports using ARMOR3D which are ocean three dimensional dataset and are based by in situ observations. First of all, we computed relative geostrophic velocities setting the reference level as the deepest layer from 3D-temperature and salinity fields. We then computed the volume transports and heat transports from these relative velocities. And we also computed the same two transports using the absolute geostrophic velocities in ARMOR3D. The northward relative volume and heat transports across the 25N-latitude line as one-year average in 2018 were calculated to be 57.2 Sv and 1.8 PW, respectivey. The northward absolute transports were 126.3 Sv and 2.8 PW. At the time of our presentaion on the day, we will discuss time variabilities of each transports of each ocean basins.

Keywords: heat transport, Subtropical gyre

©2021. Japan Geoscience Union. All Right Reserved.

[J] Poster | A (Atmospheric and Hydrospheric Sciences)：A-HW Hydrology & Water Environment

Sat. Jun 5, 2021 5:15 PM - 6:30 PM JST | Sat. Jun 5, 2021 8:15 AM - 9:30 AM UTC | Ch.07_3

[A-HW24] Water Environment and Geology in Urban Areas

convener:Takeshi Hayashi(Faculty of Education and Human Studies, Akita University), Akinobu Miyakoshi(Geological Survey of Japan, AIST)

The scope of this session is to create an interdisciplinary forum on the most recent advances in water environment and environmental geology research in urban areas. Various kinds of studies concerning environmental issues on water and geology in urban areas (e.g. water balance, water cycle, water resource development and management, inundations, hydrogeology, pollution and remediation, geohazard, basic law on the water cycle) are welcome from academia, industry, and government as well as wider geographic diversity.

[AHW24-P01] Variability of land-use in the catchments of spring water in the western marginal area of Kanto Plain

*Takeshi Hayashi[1], Masaya Yasuhara[2], Takashi Nakamura[3] (1.Faculty of Education and Human Studies, Akita University, 2.Department of Environment Systems, Rissho University, 3.ICRE, University of Yamanashi)

[AHW24-P02] Evaluation of subsurface warming in the Tokyo metropolitan area, Japan: Effective application of groundwater observation wells for subsurface temperature monitoring

*Akinobu Miyakoshi[1], Takeshi Hayashi[2], Hideki Hamamoto[3], Shoichi Hachinohe[3] (1.Geological Survey of Japan, AIST, 2.Faculty of Education and Human Studies, Akita University, 3.Center for Environmental Science in Saitama)

[AHW24-P03] Demonstration of Ground Source Heat Pump systems and variations of the subsurface temperatures in Saitama Prefecture

*Hideki Hamamoto[1], Hidetaka Shiraishi[1], Masaki Nakayama[2], Shingo Uchiyama[2], Shuhei Ishiguro[3], Junya Takeshima[3] (1.Center for Environmental Science in Saitama, 2.Environmental Energy Division, Environment Department, Saitama Prefecture, 3.OYO Corporation)

[AHW24-P04] Examination of groundwater level measurement method by microtremor array exploration

*Yuji Miyashita[1], Hideki Hamamoto[2], Shigeki Senna[3] (1.Hot Springs Research Institute of Kanagawa Prefecture, 2.Center for Environmental Science in Saitama, 3.National Research Institute for Earth Science and Disaster Resilience)

Variability of land-use in the catchments of spring water in the western marginal area of Kanto Plain

*Takeshi Hayashi[1], Masaya Yasuhara[2], Takashi Nakamura[3]

1. Faculty of Education and Human Studies, Akita University, 2. Department of Environment Systems, Rissho University, 3. ICRE, University of Yamanashi

Marginal areas of the Kanto plain are composed of several topographical units such as alluvial fans (e.g. Arakawa alluvial fan), uplands (e.g. Iruma-Musashino upland), and hills (e.g. Tama hills). These units show both topographical and geological variations. From the hydrological viewpoint, these units have various spring water that had been used as water resources in each area. Although a number of the springs were disappeared in the process of urbanization, there are still many springs in these areas. These existing springs have a wide variety of land-use such as woodlands, agricultural areas, and residential areas in each catchment area.

This study aims to evaluate the effect of land-use change on the water environment of these springs that still remain or are already depleted. In this study, topographical maps that have been published since the Meiji Period and Google Maps have used for understanding the land-use change. As for details of topography surrounding each spring water, 5m DEM published by the Geospatial Information Authority of Japan has been used.
As a result, we found both the existing spring water of which land-use in the catchment area has been historically changed and the disappeared spring water of which land-use has not been changed clearly. We will discuss the effects of land-use change on the processes of the water cycle and the sources of water for these springs.

This study was supported by JSPS KAKENHI Grant Number 19K12293-00.

Keywords: Kanto Plain, spring water, land-use change

©2021. Japan Geoscience Union. All Right Reserved.

Evaluation of subsurface warming in the Tokyo metropolitan area, Japan: Effective application of groundwater observation wells for subsurface temperature monitoring

*Akinobu Miyakoshi[1], Takeshi Hayashi[2], Hideki Hamamoto[3], Shoichi Hachinohe[3]

1. Geological Survey of Japan, AIST, 2. Faculty of Education and Human Studies, Akita University, 3. Center for Environmental Science in Saitama

Effects of urbanization-related changes in the environment and regional groundwater flow, on the subsurface thermal environment of the Tokyo metropolitan area in Japan, were evaluated. This was conducted by examining subsurface temperatures and their three-dimensional distribution as well as long-term changes. For this purpose, multiple observations of temperature-depth profiles from the year 2000 and subsurface temperature monitoring in observation wells from 2007 in Saitama Prefecture and 2013 in Tokyo Metropolis were used.

Subsurface warming was found at shallow depths throughout the study area in our previous study (Miyakoshi et al., 2010). Subsurface temperatures beneath the city center, such as those in central Tokyo, were particularly high, not only in the shallow parts but also in the deep parts. In contrast, relatively low temperatures were found beneath suburban areas. A comparison of past subsurface temperature data (2003–2005) and present subsurface temperature data (2013–2020) shows that subsurface warming has occurred in the shallow parts in the last 10 to 15 years. The increases in subsurface temperatures in the city center were found to be larger than those in the suburban area. The temporal differences in temperatures indicate an increasing trend of subsurface temperatures in both the areas. Additionally, present data indicate that subsurface warming occurred in deeper parts. This result suggests that the distribution of subsurface warming is expanding toward the deeper parts.

Based on the results of subsurface temperature monitoring, subsurface warming was confirmed to have occurred continuously. The warming rate varied depending on the location and depth. An almost-constant warming rate of 0.01–0.02 K/year was found to occur at a depth of 30 m in the observation wells in the southeastern area of Saitama Prefecture and the eastern area of Tokyo Metropolis(Miyakoshi et al., 2017). These observations were from the alluvial lowland, and the warming was driven mainly by heat conduction due to warming of the surface from urbanization.

In the Musashino upland, the southwestern area of Saitama Prefecture, the western area of Tokyo Metropolises, and the Arakawa alluvial fan in the northwestern part of Saitama Prefecture, continuous subsurface warming, similar to that in lowland, was found. However, the warming rate fluctuated with time in some observation wells. Additionally, significant temperature changes were observed at depths greater than 100 m. Comparing the Musashino upland and the Arakawa alluvial fan, the period, magnitude, and depth of these changes were different. Complex subsurface temperature changes were observed around areas where significant changes in hydraulic heads had occurred. It is considered that artificially induced change in groundwater flow is one of the main reasons for long-term changes in subsurface temperatures. Furthermore, the differences in the magnitude of subsurface temperature changes in the two regions reflect the differences in hydrogeological conditions and groundwater development. The mechanism of subsurface warming is expected to be evaluated by a combined analysis of changes in geological conditions, groundwater flow, and subsurface temperatures.

©2021. Japan Geoscience Union. All Right Reserved.

The research in Saitama Prefecture was conducted as a part of AIST- Akita University -Saitama Prefecture joint research. The utilization of the observation wells in the Tokyo Metropolis was supported by Civil Engineering Support and Training Center, Tokyo Metropolitan Government. The part of this study was supported by JSPS KAKENHI Grant Number 19K12364.

Keywords: subsurface temperature, groundwater flow, subsurface warming, observation well, urbanization, Tokyo metropolitan area

©2021. Japan Geoscience Union. All Right Reserved.

Demonstration of Ground Source Heat Pump systems and variations of the subsurface temperatures in Saitama Prefecture

*Hideki Hamamoto[1], Hidetaka Shiraishi[1], Masaki Nakayama[2], Shingo Uchiyama[2], Shuhei Ishiguro[3], Junya Takeshima[3]

1. Center for Environmental Science in Saitama, 2. Environmental Energy Division, Environment Department, Saitama Prefecture, 3. OYO Corporation

Geothermal energy systems are a type of renewable energy system. They are superior in energy conservation and are spreading in Japan and overseas. The ground-source heat-pump (GHP) system is widely used for room heating and cooling and hot water supply in large facilities and housings. It is important to quantitatively compare the operating efficiency, cost, and environmental effects of GHP and air source heat pumps (AHP) through experiments to promote the use of GHP in the future. The operating efficiency of both heat pumps varies with the weather conditions and heat loads at the installation sites and only the efficiency of GHP varies with the subsurface environmental conditions.
In 2018, the Local Government of Saitama Prefecture installed both GHP and AHP in five small-scale buildings in the prefecture. Among the five sites, four sites (Hanno City, Hanyu City, Miyashiro Town, and Kasukabe City) contain atmosphere-monitoring stations and the fifth (Kazo City) site is the Eco-Lodge of the Center for Environmental Science in Saitama. At the atmosphere-monitoring stations in four sites where the demonstration experiments were conducted, the continuous cooling and heating operation tests were conducted at the target room temperature (Cooling: 27˚C, Heating: 25˚C) of general housing to examine the operation efficiency of the GHP and AHP. Specifically, either of the HPs was operated alternately in summer and winter at 15-day intervals, and the SCOP was calculated by measuring the inlet/outlet temperatures, the circulating flow rate of the secondary circulating fluid, and power consumption. As a result, the average SCOP of the four sites in the cooling operation was 5.7 and 2.6 for the GHP and AHP, respectively, and 3.0 and 2.4 for GHP and AHP, respectively, in the heating operation. The efficiency of the GHP was higher than that of the AHP in all sites. The efficiency of the cooling operation was higher than that of the heating operation in the same site, and this tendency is consistent with the results of existing demonstration experiments.
In two sites (Kazo City and Miyashiro Town), observation wells (six wells at 2 m and one well at 5 m from the heat exchange well) were installed to investigate the temperature fluctuation in the vicinity of the heat exchange wells. In the eco-lodge, cooling and heating operations were conducted at the maximum load. The GHP was operated under a high load for 30 days to monitor the process of the rise and fall in subsurface temperature. The operation was halted for the next 60 days and the recovery process was monitored. This paper presents the results of the cooling operation. The temperature increased by 2˚C at the observation well, 2 m away from the heat exchange well (West 2 m well). And large temperature rise was not observed at the well 5 m away (West 5 m well). Next, assuming that the heat propagates from the heat exchange well to the surroundings by heat diffusion, the temperature variation was calculated using a numerical simulator (FEFLOW) and employing the finite element method. The attached figure shows the areal temperature distribution 90 days after starting the monitoring at a depth of 40 m. It was confirmed that heat spreads concentrically from the heat exchange well to the circumference. The measured and calculated values at the observation well 2 m west were compared and they are consistent. This could be well explained by assuming that the heat propagates by thermal diffusion. In more detail, however, the measured temperatures at the west 2 m observation well and the east 2 m well increased at the same rate during the heating process, whereas the temperatures differed by 0.5˚C in the recovery process (the east 2 m well was hotter than the west 2 m well). This suggests that variations in thermal properties and

©2021. Japan Geoscience Union. All Right Reserved.

groundwater flow influence the observed temperatures. These factors shall be considered in our future studies.

Keywords: ground source heat pump, subsurface temperature, groundwater flow

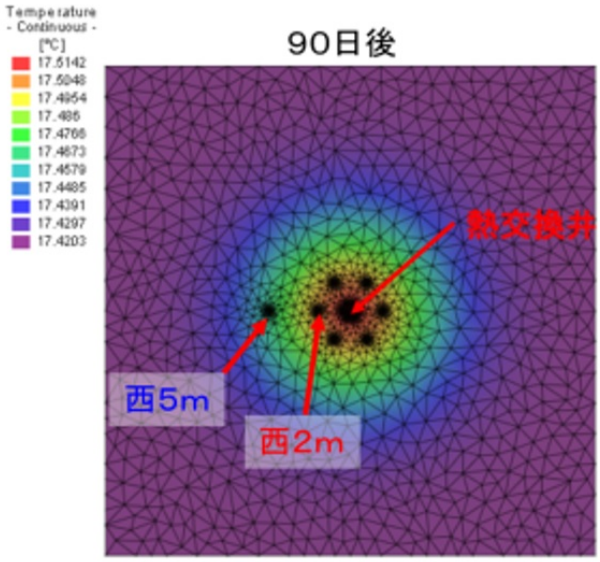

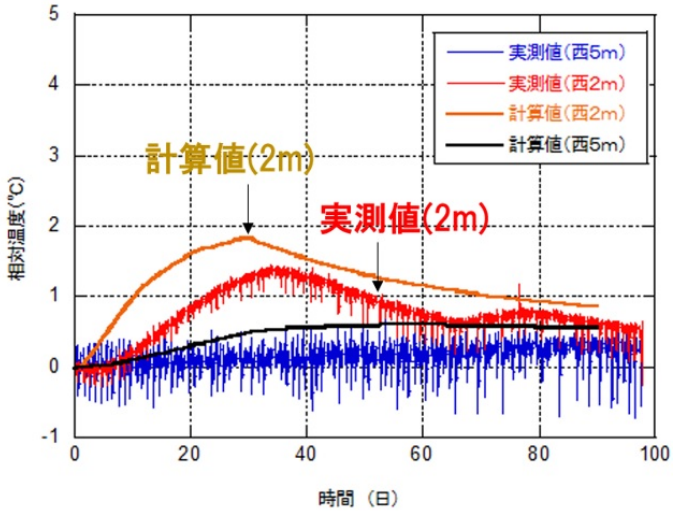

©2021. Japan Geoscience Union. All Right Reserved.

Examination of groundwater level measurement method by microtremor array exploration

*Yuji Miyashita[1], Hideki Hamamoto[2], Shigeki Senna[3]

1. Hot Springs Research Institute of Kanagawa Prefecture, 2. Center for Environmental Science in Saitama, 3. National Research Institute for Earth Science and Disaster Resilience

1. Introduction

One of the geophysical exploration methods is "microtremor exploration", which estimates the S wave velocity by constantly observing microtremors on the surface of the earth, and requires an S wave velocity structure in the vertical one-dimensional direction at the exploration point. Since the S wave velocity is determined by the physical properties of the ground, the geological structure such as the distribution of the aquifer and the basement can be grasped from the vertical distribution of the S wave velocity.

On the other hand, the ground is composed of three phases: a solid phase part such as soil and rock, a liquid phase part such as groundwater and soil water, and a gas phase part existing in the unsaturated zone near the ground surface. Therefore, if the ratio of the liquid phase portion in the ground (≈ groundwater level) changes, it is expected that the S wave velocity will change.

Takahashi (2019) reviewed and model-analyzed the relationship between S-wave velocity and saturation of rocks. From past experiments in the literature, in the case of sandstone and shale, the S wave velocity decreases with increasing water saturation, in limestone there is no change in S wave velocity due to water saturation, and in granite, S wave with increasing water saturation. It showed a tendency to increase in speed. On the other hand, although the experimental results for the unconsolidated sedimentary layer were not obtained, it is possible that the fluctuation of the water content has an effect on the S wave velocity from the large pore space in comparison with the consolidated layer.

Therefore, in this study, the relationship between the groundwater level change and the S wave velocity distribution was investigated by repeating the measurement of the groundwater level and the micro-array tremor exploration at the same point at the same time.

2. Method

Repeated tremor exploration at fixed points was conducted nine times from June to November 2014 and once each in August 2019 and January 2020 at two points (H54, R50) located in the alluvial fan area in the upper reaches of the Ashigara Plain. A total of 11 micro-array microtremor surveys were conducted. In addition, the groundwater level was continuously measured at the shallow groundwater observation wells attached to these points.

Microtremor observation was performed using JU210 and JU410 manufactured by Hakusan Kogyo with a sampling interval of 200 Hz. The results of microtremor exploration were analyzed according to the method of Senna et. al, (2014).

©2021. Japan Geoscience Union. All Right Reserved.

3. Results and discussion

As a result of 11 microtremor surveys, the maximum exploration depth was 68.9 m at H54 and 86.9 m at R50, and the S wave velocity at maximum depth was 965 m/s at H54 and 940 m/s at R50. It showed almost the same S wave velocity. The groundwater level during tremor exploration changed from -12.73 to -15.30 m at H54 and from -7.24 to -8.41 m at R50.

The S wave velocity near the groundwater table is 370 to 880 m/s at the H54 point and 230 to 370 m/s at the R50 point. The results show that the S wave velocity differs greatly depending on the exploration time. In addition, explorations in which the S wave velocity changed up and down across the vicinity of the water table were observed in 8 out of 11 explorations at H54 and 10 out of 11 at R50.

Factors that cause the S-wave velocity at the same depth to change significantly for each microtremor exploration include errors in exploration and analysis such as installation errors of microtremors for each microtremor exploration and waveform reading errors in analysis, as well as changes in soil temperature and inadequacy. Factors such as differences in soil moisture content in the saturated zone are possible. In the future, in addition to examining these error factors, we will also examine other geological and climatic conditions.

Keywords: Microtremor exploration, groundwater level, repeated measurements

©2021. Japan Geoscience Union. All Right Reserved.

[J] Poster | A (Atmospheric and Hydrospheric Sciences)：A-CG Complex & General

Sat. Jun 5, 2021 5:15 PM - 6:30 PM JST | Sat. Jun 5, 2021 8:15 AM - 9:30 AM UTC | Ch.08_3

[A-CG37] Biogeochemical cycles in Land Ecosystem

convener:Tomomichi Kato(Research Faculty of Agriculture, Hokkaido University), Kazuhito Ichii(Chiba University), Takeshi Ise(FSERC, Kyoto University), Munemasa Teramoto(Arid Land Research Center, Tottori University)

Terrestrial ecosystem influences global climate through cycles of water, carbon, and nitrogen between land surface and atmosphere. For better understanding of those behaviors, a great effort has been paid for developing varieties of approaches and techniques such as biometric survey, eddy and chamber methods, near and satellite remote sensing, biosphere modeling and so on.
In particular, the JapanFlux, founded in 2006 as a researchers network of CO2, H2O and other trace gas flux measurement, has promoted the multi-disciplinal studies not only for flux measurement community, but also for remote sensing and biosphere modeling communities. Moreover, the Research-Group-on-Integrated-Land-Processes, which was founded in 2006, also has contributed to build networks between Japanese researchers to better understanding of physical and biological processes on interactions between terrestrial surface and atmosphere.
This session unites those multi-disciplinal activities, and promotes the oral and poster presentations on the role of terrestrial ecosystem in material circulations of water, carbon, nitrogen, energy and other substances by any approaches and technics. This session takes over the former session in last year: A-CG54.

[ACG37-P01] Change in soil respiration rate and soil organic matter for three years after clear-cutting in a *Cryptomeria japonica* plantation

*Yukiko Abe[1], Naishen Liang[2], Munemasa Teramoto[3], Takeshi Tange[1] (1.The University of Tokyo, 2.National Institute for Environmental Studies, 3.Tottori University)

[ACG37-P02] Continuous measurement of atmospheric methane mixing ratio at a cool-temperate deciduous forest site, Takayama, Japan

*Shohei Murayama[1], Shigeyuki Ishidoya[1], Tomoyuki Hori[1], Shinpei YOSHITAKE[2], Takahisa Maeda[1] (1.National Institute of Advanced Industrial Science and Technology, 2.Waseda University)

[ACG37-P03] Seasonal variation and controlling factors of stem methane emissions from *Alnus japonica* revealed by continuous measurements

*Ayaka Sakabe[1], Kenshi Takahashi[1], Wakana Azuma[2], Masayuki Itoh[3], Makiko Tateishi[1], Yoshiko Kosugi[1] (1.Kyoto University, 2.Kobe University, 3.University of Hyogo)

[ACG37-P04] Spatio-temporal variation of soil respiration in coastal sand dunes and the mechanisms

*Munemasa Teramoto[1], Toru Hamamoto[1], Naishen Liang[2], Takeshi Taniguchi[1], Takehiko Y. Ito[3], Richa Hu[4], Norikazu Yamanaka[1] (1.Arid Land Research Center, Tottori University, 2.Center for Global Environmental Research, National Institute for Environmental Studies, 3.International Platform for Dryland Research and Education, Tottori University, 4.The United Graduate School of Agricultural Sciences, Tottori University)

[ACG37-P05] Validation of Two Vegetation Indices: NDVI and PRI Derived from GCOM-C/SGLI

*Sasagawa Taiga[1], Tomoko Kawaguchi Akitsu[2], Kenlo Nishida Nasahara[2] (1.Graduate School of Science and Technology, University of Tsukuba, 2.Faculty of Life and Environmental Sciences, University of Tsukuba)

[ACG37-P06] Seasonal variation in Solar Induced chlorophyll Fluorescence detected by multi-vertical layer spectroscopy in a canopy of cool-temperate deciduous broadleaf forest in Takayama, Gifu

*Tomoki Morozumi[1], Tomomichi Kato[1], Katsuto Tsujimoto[2], KANOKRAT BUAREAL[3], Naohisa Nakashima[1], Yuma Sakai[4], Hideki Kobayashi[4], Kenlo Nasahara[5], Tomoko Akitsu[5], Shohei Murayama[6], Hibiki M Noda[7], Hiroyuki Muraoka[8] (1.Research Faculty of Agriculture, Hokkaido University, 2.Graduate School of Life Sciences, Tohoku University, 3.Graduate School of Global Food Resources, Hokkaido University, 4.Institute of Arctic Climate and Environment Research, Japan Agency for Marine-Earth Science and Technology, 5.Faculty of Life and Environmental Sciences, University of Tsukuba, 6.Environmental Management Research Institute, National Institute of Advanced Industrial Science and Technology, 7.Center for Global Environmental Research, National Institute for Environmental Studies, 8.River Basin Research Center, Gifu University)

[ACG37-P07] On the factors affecting reproducibility of GPP estimated by the Earth System Model MIROC-ES2L

*Akira Kurisu[1], Toru Nozawa[2], Manabu Abe[3], Tomohiro Hajima[3] (1.Faculty of Science, Okayama University, 2.Graduate School of Natural Science and Technology, Okayama University, 3.Japan Agency for Marine-Earth Science and Technology)

[ACG37-P08] Estimation of forest above ground biomass from PALSAR Data

*Hantao Li[1], Tomomichi Kato[2], Lan Wu[3], Masato Hayashi[4] (1.Graduate School of Agriculture, Hokkaido University, 2.Research Faculty of Agriculture, Hokkaido University, 3.College of Ecology and Environment, Hainan University, China, 4.Earth Observation Research Center, Japan Aerospace Exploration Agency)

[ACG37-P09] Development of process-based model for estimating wheat production MATCRO-Wheat

*Maki Nakaguki[1], Tomomichi Kato[2], Yuji Masutomi[3], Leilei Liu[4], Seiji Shimoda[5] (1.Hokkaido University, 2.Research Faculty of Agriculture, Hokkaido University, 3.National Institute for Environmental Studies, 4.National Engineering and Technology Center for Information Agriculture, Nanjing Agricultural University, 5.Hokkaido Agricultural Research Center, National Agriculture and Food Research Organization)

Change in soil respiration rate and soil organic matter for three years after clear-cutting in a *Cryptomeria japonica* plantation

*Yukiko Abe[1], Naishen Liang[2], Munemasa Teramoto[3], Takeshi Tange[1]

1. The University of Tokyo, 2. National Institute for Environmental Studies, 3. Tottori University

Clear-cutting of forests significantly alters the carbon dynamics in soil, with the large temporary supply of litter and dead roots, followed by significant decline. In this study, we measured soil respiration rates, amount of litter on soil surface, dead root, and soil carbon contents at 20 measurement points in a sugi (*Cryptomeria japonica*) plantation of Tokyo University of Agriculture Okutama Forest from May 2017 (just before clear-cutting) to August 2019. Litter and soil at 0-5 cm in depth were collected at soil respiration measurement points approximately every three months. After soil sampling, the measurement points were reestablished at new locations. Weeding had been done once a year in the study site, and the herbaceous vegetation that entered the measurement points was removed.
Soil respiration rate at 20 ˚C (R_{20}) was estimated using the exponential functions of soil respiration rate and soil temperature at 5 cm in depth. The mean R_{20}s of 20 measurement points in 2018 and 2019 were not significantly different from that of 2017. The dead root amount of sugi fine root in measurement points did not decreased until May 2018 compared to the fine root biomass before clear-cutting (0.33 ± 0.27 t ha^{-1}) significantly. After that, the dead root amount from September 2018 to August 2019 decreased significantly to 35.7-52.0% before clear-cutting. The amount of sugi leaf litter was 6.24±1.98 t ha^{-1} before clear-cutting, but decreased significantly to 2.03±1.74 t ha-^{1} three months after clear-cutting, which may have been affected by the ground preparation after clear-cutting. The amount of sugi leaf litter after March 2018 has decreased significantly compared to August 2017, and it was 20.9-54.9% in August 2017. The fact that the soil respiration rate in the third year after clear-cutting did not decrease compared to the first year after clear-cutting could be due to the continuous supply of organic matter to the soil by litter and dead roots.

Keywords: litter, dead root, soil carbon

©2021. Japan Geoscience Union. All Right Reserved.

Continuous measurement of atmospheric methane mixing ratio at a cool-temperate deciduous forest site, Takayama, Japan

*Shohei Murayama[1], Shigeyuki Ishidoya[1], Tomoyuki Hori[1], Shinpei YOSHITAKE[2], Takahisa Maeda[1]

1. National Institute of Advanced Industrial Science and Technology, 2. Waseda University

Methane (CH_4) is a greenhouse gas that contributes to global warming next to carbon dioxide (CO_2). Forest ecosystems other than wetlands are considered to be CH_4 sinks due to the oxidative activities by soil microbes while it has also been pointed out that CH_4 may be released from trees. However, the factors governing CH_4 budgets in the ecosystem are not fully understood. To examine the variations in the atmospheric mixing ration and the budgets of CH_4 in the forest ecosystem and the factors governing them, continuous measurement of the atmospheric CH_4 mixing ratio has initiated at a cool-temperate deciduous forest site in the central Japan, Takayama (TKY: 36°08'N, 137°25'E, 1420 m) since July 2020. TKY is the longest monitoring site in the AsiaFlux network.

The continuous CH_4 measurement was made using a laser spectroscopy analyzer (Ultra-Portable GGA, Los Gatos Research). Meteorological instruments and air intakes for the CH_4 mixing ratio measurement were mounted on a 27-m tower. Sample air was collected from six different heights (27, 18, 8.8, 5.8, 2.0 and 1.3 m); the top level was above the canopy, the second just above the canopy and the other four below the canopy. The air was drawn by a diaphragm pump and introduced into the analyzer after removing aerosol particles and water vapor. The sample flow rate and the pressure in the sample cell of the analyzer were stabilized, and the analyzer was placed in a temperature-controlled box to reduce output drift. The analyzer was calibrated using three air-based CO_2-CH_4 standards with different mixing ratios every three hours. The overall precision was estimated to be less than 0.8 ppb, and the measured CH_4 values were almost in agreement with those measured by a flask sampling method using an FID-GC.

The atmospheric CH_4 observed at all heights did not show clear diurnal variation but fluctuations with a period of several days while the atmospheric CO_2 showed clear diurnal variation from summer to early fall reflecting photosynthesis and respiratory activities. The variation patterns of the atmospheric CH_4 observed at all heights were very similar, but the mixing ratios were lower at 1.3 m than at 27 m during most of the observation period. The vertical CH_4 difference between 27 m and 1.3 m above the ground clearly showed positive correlation with soil temperature near the ground surface, which is consistent with the seasonal variation in intensity of soil CH_4 sink observed at TKY using a soil chamber. The vertical difference also showed negative correlation with soil moisture, which suggests that the oxidation of CH_4 is enhanced under dry conditions. Significant sources of CH_4 from the above-ground parts of trees were not detected from the observed vertical profiles.

On the other hand, it was found from backward trajectory analyses that the observed high and low CH_4 on the several-day scale described above were related to long-range atmospheric transport originated from the Asian Continent and the North Pacific Ocean, respectively. The results suggest that the high CH_4 reflects the CH_4 emissions originated from wetlands and anthropogenic activities on the continent.

We plan to further investigate the mechanism governing variations in the CH_4 mixing ratio and the CH_4 budgets in the forest ecosystem at TKY through data accumulation, genetic analyses of soil microbes, etc.

©2021. Japan Geoscience Union. All Right Reserved.

Acknowledgements

We would like to thank members of River Basin Research Center of Gifu University and AIST for their support for our observation. A. Kudo and C. Abe for their technical support for our measurements. This research was supported by JSPS KAKENHI Grant Numbers JP18H03365, JP19H03301 and JP19H01975.

Keywords: Methane, Forest ecosystems

©2021. Japan Geoscience Union. All Right Reserved.

Seasonal variation and controlling factors of stem methane emissions from *Alnus japonica* revealed by continuous measurements

*Ayaka Sakabe[1], Kenshi Takahashi[1], Wakana Azuma[2], Masayuki Itoh[3], Makiko Tateishi[1], Yoshiko Kosugi[1]

1. Kyoto University, 2. Kobe University, 3. University of Hyogo

Recent studies suggest that tree-mediated methane emissions have the potential to offset the soil methane sink and may convert the forest from a net sink to a net source. However, tree-mediated CH_4 emissions represent an uncertain pathway of the total CH_4 flux from forested ecosystems. We measured the stem CH_4 fluxes from *Alnus japonica* in a riparian wetland of a temperate forest for a year using automated chambers. Three mature *Alnus japonica* trees grown naturally in the riparian wetland were selected for this study. Dissolved CH_4 concentrations in groundwater at two depths beneath each tree were measured biweekly. The sap flux for each tree was measured with Granier-type sensors.

The stem CH_4 fluxes seasonally vary, showing summertime maxima and wintertime minima. The stem CH_4 fluxes positively correlate with dissolved CH_4 concentration in groundwater beneath the trees. In addition, stem CH_4 emissions were observed when the sap flux diminished during the defoliation period. These results indicate that CH_4 in the rhizosphere is transported in the gaseous form through intercellular space in trees. On the other hand, CH_4 transport by sap flux also likely exists based on our observations; stem CH_4 fluxes showed diurnal variation. We also observed that rainfall caused a clear increase in the stem CH_4 emissions. Temporal changes in the groundwater flow paths by rainfall would have affected the belowground CH_4 concentrations and the stem CH_4 flux. Dynamic changes in soil environmental conditions (soil temperature, groundwater flow) controlled dissolved CH_4 concentrations in groundwater, thus, stem CH_4 flux. Our findings highlight the need for continuous stem CH_4 flux measurements to better understand the controlling factors and future response of CH_4 dynamics in forests to climate change.

Keywords: Stem methane emission, Alnus japonica, closed chamber

©2021. Japan Geoscience Union. All Right Reserved.

Spatio-temporal variation of soil respiration in coastal sand dunes and the mechanisms

*Munemasa Teramoto[1], Toru Hamamoto[1], Naishen Liang[2], Takeshi Taniguchi[1], Takehiko Y. Ito[3], Richa Hu[4], Norikazu Yamanaka[1]

1. Arid Land Research Center, Tottori University, 2. Center for Global Environmental Research, National Institute for Environmental Studies, 3. International Platform for Dryland Research and Education, Tottori University, 4. The United Graduate School of Agricultural Sciences, Tottori University

Coastal sand dunes are unique ecosystems where zonal distribution of coastal vegetations is typically observed. Globally, costal sand dunes are decreasing the area because of development and climate change. On the other hand, coastal sand dunes are gathering attention as multipurpose green infrastructure for mitigation and adaptation against global climate change. Studies for carbon cycle in coastal sand dunes can contribute to add a new value for the unique ecosystems from the viewpoint of carbon sequestration and sustainable ecosystem management.

Soil respiration (R_s) is one of the largest carbon flux components in terrestrial carbon cycle. Many field observations were conducted until now, and those observation data have been used for global estimation of R_s. However, observations were mainly conducted in forests, croplands and grasslands, major terrestrial ecosystems. Observations for R_s in coastal sand dunes are totally limited, and there is no example of R_s measurement in coastal sand dunes with consideration for zonal distribution of coastal vegetation.

To examine the spatio-temporal variation of R_s and related mechanisms in coastal sand dunes, we conducted field observations for R_s and environmental parameters from June to December in 2020 in coastal sand dunes in Tottori, Japan. We set four measurement plots (n = 10 in each plot) in the study site representing bare sand (plot 1), clusters of *Vitex rotundifolia* (plot 2), Mixture of *V. rotundifolia* and *Artemisia capillaris* (plot 3) and boundary area between a pine forest (*Pinus thunbergii*) and coastal vegetation zone (plot 4). In those measurement plots, we conducted R_s measurement once in two weeks using portable automated chamber measurement system. At the same time, environmental parameters like air temperature, soil temperature and soil moisture were continuously measured using environmental measurement system that composed of car battery, data logger (CR1000, Campbell Scientific Inc.), solar panel, temperature (thermocouples) and soil moisture sensors (CS616, Campbell Scientific Inc.).

R_s was exponentially increased along with the temperature rise in plot 1 and 2. Such exponential increase was also confirmed in plot 3 and 4 if we excluded data in August (remarkably small R_s) under drought stress because of little rainfall. In addition, significant relationships between soil moisture and temperature-normalized R_s were also confirmed in plot 2, 3 and 4. Those results suggested that soil temperature is the primary environmental factor caused for seasonal variation of R_s, but soil moisture can also demonstrate strong influence on R_s as drought stress in summer period in this study site. In this presentation, mechanisms for spatio-temporal variation of R_s will be also discussed including the analysis for sand CN, root biomass and microbial community.

Keywords: Chamber, Drought stress, Zonal distribution, Coastal vegetation, Carbon cycle

©2021. Japan Geoscience Union. All Right Reserved.

Validation of Two Vegetation Indices: NDVI and PRI Derived from GCOM-C/SGLI

*Sasagawa Taiga[1], Tomoko Kawaguchi Akitsu[2], Kenlo Nishida Nasahara[2]

1. Graduate School of Science and Technology, University of Tsukuba, 2. Faculty of Life and Environmental Sciences, University of Tsukuba

Forests play a significant role in terrestrial ecosystems and greatly influence the material cycle in terrestrial ecosystems. Therefore, an accurate understanding of forest conditions is fundamental and indispensable for understanding terrestrial ecosystems. In order to accurately understand the state of forests, which cover a large area, local observations are often insufficient. An example of such a method that can cover a large area is satellite remote sensing.
One example of satellite that is used for observation of terrestrial ecosystems is GCOM-C (Global Change Observation Mission-Climate), which was recently launched by JAXA (Japan Aerospace Exploration Agency). GCOM-C is equipped with a sensor called the SGLI (Second-generation Global Imager). This sensor is capable of observing a larger number of spectral bands than the sensors on other earth observation satellites. This means that GCOM-C/SGLI has a higher wavelength resolution. In addition, GCOM-C/SGLI has a wide observation range, which means that the frequency of observations is high, and thus the temporal resolution is high. Therefore, it is expected that GCOM-C/SGLI can be used for more detailed and frequent observation of forest conditions.
Usually, various indices are calculated from satellites' data to understand the condition of vegetation, such as forests. From the GCOM-C/SGLI data, several indices can be calculated, and typical indices derived from the GCOM-C/SGLI data are NDVI (Normalized Difference Vegetation Index) and PRI (Photochemical Reflectance Index).
The NDVI is widely used in remote sensing of vegetation and can be calculated from many earth observation satellites, but the NDVI derived from GCOM-C/SGLI has a feature that multiple NDVI can be calculated.
That is, it is possible to calculate four NDVIs: two in the red region and two in the near-infrared region since GCOM-C/SGLI has two observation bands each. This is a major feature of GCOM-C/SGLI, and the use of these four NDVIs will enable more detailed remote sensing of forests.
PRI is an indicator that reflects the chemical changes of xanthophylls in chloroplasts (xanthophyll cycle). Xanthophylls are closely related to the heat dissipation of excess energy in photosynthesis, and by quantitatively evaluating the xanthophyll cycle and combining it with other vegetation indices, it is thought that the gross primary production of forests can be estimated. Therefore, PRI, which reflects the xanthophyll cycle, is one of the most important indices in remote sensing of forests. However, the PRI is calculated from the reflectance of very close wavelengths, 531 nm and 570 nm, which requires high wavelength resolution. Therefore, it is not easy to calculate PRI from satellite data. Nevertheless, the GCOM-C/SGLI is able to observe these wavelengths independently. So observing the PRI is a great advantage of the GCOM-C/SGLI.
As described above, although the GCOM-C/SGLI data can be used to calculate the NDVI (four types) and PRI, which are significant vegetation indices, the detailed validation of the accuracy of the data has not been done so far. In this study, we focused on two vegetation indices: NDVI and PRI, which can be calculated from GCOM-C/SGLI observation data, and aimed to validate their accuracy.
For the accuracy verification, we used the ground validation data for three years from 2018 to 2020 at several sites in Japan (Teshio, Tomakomai, Takayama, Mase, Fuji-yoshida, and Fuji-hokuroku). These ground validation data were acquired by spectroradiometers installed at each site. In addition, the

©2021. Japan Geoscience Union. All Right Reserved.

phenology change of the forest was detected by the photographs of the forest taken by the fisheye camera installed with the spectroradiometer. The relationship between the phenological changes and the changes in each index was investigated.
The results of ground-based verification suggested that NDVI and PRI can be obtained from GCOM-C/SGLI. However, the difference between the ground-based measurements and satellite data was sometimes large, especially for PRI. It was also found that each vegetation index had a unique relationship with changes in forest phenology.
In the future, it will be necessary to develop a method to detect and remove the outliers of NDVI and PRI obtained from GCOM-C/SGLI.

Keywords: Remote Sensing, Forest, GCOM-C/SGLI, NDVI, PRI

©2021. Japan Geoscience Union. All Right Reserved.

Seasonal variation in Solar Induced chlorophyll Fluorescence detected by multi-vertical layer spectroscopy in a canopy of cool-temperate deciduous broadleaf forest in Takayama, Gifu

*Tomoki Morozumi[1], Tomomichi Kato[1], Katsuto Tsujimoto[2], KANOKRAT BUAREAL[3], Naohisa Nakashima[1], Yuma Sakai[4], Hideki Kobayashi[4], Kenlo Nasahara[5], Tomoko Akitsu[5], Shohei Murayama[6], Hibiki M Noda[7], Hiroyuki Muraoka[8]

1. Research Faculty of Agriculture, Hokkaido University, 2. Graduate School of Life Sciences, Tohoku University, 3. Graduate School of Global Food Resources, Hokkaido University, 4. Institute of Arctic Climate and Environment Research, Japan Agency for Marine-Earth Science and Technology, 5. Faculty of Life and Environmental Sciences, University of Tsukuba, 6. Environmental Management Research Institute, National Institute of Advanced Industrial Science and Technology, 7. Center for Global Environmental Research, National Institute for Environmental Studies, 8. River Basin Research Center, Gifu University

Solar Induced chlorophyll Fluorescence (SIF) is a quantitative remote sensing signal relating to the photosynthetic activity including gross primary productivity (GPP) of terrestrial ecosystems. After excitation by solar photon, chlorophyll pigment emits a part of unusable excess energy as fluorescence, which equals to SIF. On the contrary to other remote sensing vegetation indices (VIs), SIF has an advantage to be able to explain both diurnal and seasonal GPP variations with relating to photosynthetic active radiation (PAR), leaf absorptance, and photochemical reaction. Previous studies in a deciduous broadleaf forest argued that decrease at the canopy top VIs had lagged after that in the photosynthetic capacity in senescence period, although understory photosynthesis could be activated after crown leaf-off. Recent heavy rainfall events also may affect photosynthetic activity. Therefore, rapidly responding SIF can be expected to be an aid of monitor real-time suppression of photosynthetic activity in the vertical layer of forest canopy. The purpose of this study is to examine whether the ground-based SIF could respond at an autumn-winter senescence period and rainfall events when GPP supposed to decline. We continuously observed ultra-fine (full width at half maximum < 0.4 nm) spectral radiation in a deciduous broadleaf forest ecosystem, at TKY flux site (36.15˚N, 137.42˚E), Takayama, Gifu since August 2019 to December 2020. A spectrometer (QEpro, Ocean Optics, Dunedin, FL, USA) was equipped of 7 optical fiber cables via optical fiber switch and captured the upward and downward spectral radiation at three heights: 8, 14, and 18m (canopy top) with field of view (FOV) of 180˚ and FOV of 25˚. SIF was retrieved using spectral fitting method for O_2-A absorption band (759-767 nm). Half-hourly SIF varied 1.5-0.5 to 0.1-0 (mW m^{-2} nm^{-1} sr^{-1}) from summer to winter. Decreasing SIF besides almost stable VIs variations were shown at heavy rainfall events in late September 2019 and in early July 2020. A timing of SIF decline was earlier at the canopy top, and SIF signal remained detectable from understory till the end of senescence period. The result also suggests that there is a potential contribution of evergreen understory (< 8 m) in snowless winter periods.

Keywords: Chlorophyll Fluorescence, Heavy Rain Event, Remote Sensing, Tower Observation

©2021. Japan Geoscience Union. All Right Reserved.

On the factors affecting reproducibility of GPP estimated by the Earth System Model MIROC-ES2L

*Akira Kurisu[1], Toru Nozawa[2], Manabu Abe[3], Tomohiro Hajima[3]

1. Faculty of Science, Okayama University, 2. Graduate School of Natural Science and Technology, Okayama University, 3. Japan Agency for Marine-Earth Science and Technology

Earth System Models (ESM) that include biogeochemical cycles in land and marine ecosystems have come to be used for global warming simulations. Reproducibility of the biogeochemical cycles in the ESM, however, does not seem to be sufficient. For example, the MIROC-ES2L, one of the ESM developing in Japan, has some problems on the reproducibility of the Gross Primary Production (GPP); the terrestrial GPP has very little seasonality over the tropics. In this study, focusing on the African continent, we investigated that biases (defined as differences between the MIROC-ES2L outputs and satellite observations) in what kind of variables are related to the biases in the GPP.

We analyzed datasets of historical runs done by the MIROC-ES2L and those obtained by satellite and in-situ observations. The MIROC-ES2L data has horizontal resolutions of 2.8 degrees in longitude times 2.8 degrees in latitude. The horizontal resolutions of the observation datasets are converted into the same ones of the MIROC-ES2L. We investigated relationships between biases in the GPP and those in Leaf Area Index (LAI), surface downward shortwave radiation, surface temperature, surface soil moisture content, and precipitation.

Latitude-time distributions of the GPP biases over the African continent show that they are larger in June-October on the south of the Equator whereas larger in December-March on the north of the Equator. Comparing geographical distributions of the GPP biases with those of the LAI ones, both biases have the same sign in June-October on the south of the Equator and in December-March on the north of the Equator. On the other hand, both biases have the opposite sign in June-October on the north of the Equator and in December-March on the south of the Equator. Therefore, the GPP biases seems to be largely explained by the LAI biases, especially in December-March. However, in June-October over the tropical area, the GPP biases cannot be explained by the LAI biases only. The GPP biases in that case might be largely related to the other climatic variables in addition to the LAI biases.

Keywords: Earth System Models, GPP

©2021. Japan Geoscience Union. All Right Reserved.

Estimation of forest above ground biomass from PALSAR Data

*Hantao Li[1], Tomomichi Kato[2], Lan Wu[3], Masato Hayashi[4]

1. Graduate School of Agriculture, Hokkaido University, 2. Research Faculty of Agriculture, Hokkaido University, 3. College of Ecology and Environment, Hainan University, China, 4. Earth Observation Research Center, Japan Aerospace Exploration Agency

Under climate change and increasingly prominent environmental issues, the estimation on forest carbon stock has become hot research topic. Huge volume and high carbon content of tree is the main carbon storage reservoir of the terrestrial biosphere and plays an important role in the global carbon cycle. Therefore, accurate estimation of forest biomass enables us to evaluate and track the status of forest carbon stocks, and to predict the role and feedback of forests in the regional and global carbon cycle, and to provide an important basis for specifying policies to response climate change.

Remote sensing approach offers considerable contribution to forest monitoring via long-term and repetitive observations over vast area (Mermoz et al 2015). Synthetic aperture radar (SAR) is one of the most promising remote detectors to map the global forest above ground biomass (AGB). Especially, the L-band SAR is widely used to retrieve forest biomass, primarily based on a positive correlation between SAR backscatter and in situ AGB. A few studies have successfully used SAR data to map AGB, such as in Madagascar by Minh et al (2018), in Matang Mangroves, Malaysia b Hamdan et al (2014), in Africa by Bouvet et al (2018). These proved that the L-band SAR had a significant relationship with forest biomass, however, many studies have also proved that when AGB reaches a certain level, the correlation between it and the signal will decrease, which is also called saturation phenomenon. Inevitably, SAR shows poor accuracy in high biomass. In addition, satellite attitudes will also bring considerable noise to the inversion results. Although these noises can be avoided by geometric correction and extraction of areas with better local incident angle conditions, a relatively high-precision inversion result can still be hard to achieve.

The purpose of this study is to try to improve the inversion accuracy through filtering calculations and machine learning methods.
This study takes Hokkaido as the research area, based on ALOS-PALSAR and optical remote sensing data, combined with field survey data of forest resources, extracts a variety of remote sensing data modeling variables, and uses random forest and support vector machine methods to target the forest biomass of different tree species. Noted that there are two sets of variables for modeling, which are optical remote sensing data and SAR data. The forest coverage rate in Hokkaido is over 70%, with abundant vegetation types and species. Naturally distributed species mainly include Pinus densiflora, Abies sachalinensis, Cryptomeria japonica, Picea jezoensis, Fagus crenata, oak, etc., covering broad-leaved forests, coniferous forests, Coniferous and broad-leaved mixed forest. In this study, the sample plot data we used are the forest resource survey data provided by the Japanese Forestry Agency. The field data collection time was from 2004 to 2008, a total of 2907 sample sites were collected, and the area of each sample site was 1 ha. The main investigation factors of the field data of the Japanese Forestry Agency include tree height, tree age, volume per ha, tree types, slope, aspect, etc. In this study, the forest aboveground biomass is calculated by the biomass-accumulation relationship equation (Xu et al, 2007). In order to match the acquisition time of the field sample location as much as possible in time, we selected PALSAR data from 2007 to 2008, with two polarization modes, HH and HV, with a resolution of 25 meters. The accuracy of forest biomass estimation by different modeling methods, different tomographic parameters and different forest types was compared. Finally mapping the forest aboveground biomass in Hokkaido.

©2021. Japan Geoscience Union. All Right Reserved.

Keywords: forest aboveground biomass, ALOS, random forest, support vector machine, Landsat-8 OLI

©2021. Japan Geoscience Union. All Right Reserved.

Development of process-based model for estimating wheat production MATCRO-Wheat

*Maki Nakaguki[1], Tomomichi Kato[2], Yuji Masutomi[3], Leilei Liu[4], Seiji Shimoda[5]

1. Hokkaido University, 2. Research Faculty of Agriculture, Hokkaido University, 3. National Institute for Environmental Studies, 4. National Engineering and Technology Center for Information Agriculture, Nanjing Agricultural University, 5. Hokkaido Agricultural Research Center, National Agriculture and Food Research Organization

Crop yield has been significantly influenced by climate change (Schindeler et al .2001). In recent years, there is a concern that crop yields will decline due to rising temperatures and extreme weather events caused by global warming. Under the assumption that rapid population growth could cause food shortages in near future, therefore, many crop models have been developed though most of them are statistical models or site-based models. Statistical model is generally not able to show each process in the interaction between climate change and crops because they do not take into account the material cycle based on plant physiology. On the other hand, though site-based model has the elaborate representation of crop growth, they rarely have been applied at global scales (Zhang et al .2017), probably due to lack of high precision input data and representative parameter sets. Therefore, this study aims to develop a process-based crop model, extended version of Minimal Advanced Treatment of Surface Interaction and Runoff (MATSIRO; Takata et al., 2003) for wheat yield estimation at a global scale, named here as MATCRO-Wheat.

To estimate the wheat yields, MATCRO-Rice model (Masutomi et al. 2016) for rice yield, was modified and added new function specialized for wheat. First, the model parameters were newly set for wheat and a vernalization process was newly introduced. Second, the model was validated with observational data in 5 field sites: Memuro, Hokkaido in Japan (Hokkaido Agricultural Research Center), Nanjing in China (Nanjing Agricultural University), Wongan Hills in Australia, Valcarce in Argentina, and Wanningen in Netherland (AgMIP wheat for last three sites; Benchmark data set for wheat growth models: field experiments and AgMIP multi-model simulations). Model parameters were adjusted to match the modeled biomass evolution and yield to the measured ones as much as possible. Finally, MATCRO-Wheat was run at global scale with adjusted parameter with vernalization process with the spatial resolution of 0.5 degree x 0.5 degree and with the simulation period from 2009 to 2010. Yield per unit land area was calculated by weighting rain-fed and irrigated yields according to the fraction of irrigated area which is drive from AQUASTAT (FAO. AQUASTAT –Global Map of Irrigation Areas), and were validated with the national yields survey according to the GDHY-aligned version v1.2+v1.3 dataset (Iizumi et al .2020).

Results showed that wheat yields were generally well represented of field observations. In the Netherland and Japan, the overestimation of crop growth was improved by introducing vernalization treatment during winter. The global simulation indicated that wheat yields were overestimated in higher latitudinal zones and in summer wet regions. These would be caused as much photosynthate was produced because MATCRO-Wheat does not consider vernalization and growth restriction due to high humidity. Therefore, further improvement of MATCRO-Wheat is required for accurate representation of wheat growth and yield.

©2021. Japan Geoscience Union. All Right Reserved.

Keywords: Process-based model, climate change, vernalization

©2021. Japan Geoscience Union. All Right Reserved.

[J] Poster | H (Human Geosciences)：H-QR Quaternary research

Sat. Jun 5, 2021 5:15 PM - 6:30 PM JST | Sat. Jun 5, 2021 8:15 AM - 9:30 AM UTC | Ch.09_1

[H-QR04] Quaternary, Diachronic dynamics of human-environment interactions

convener:Mamoru Koarai(Earth Science course, College of Science, Ibaraki University), Yusuke Yokoyama(Atmosphere and Ocean Research Institute, University of Tokyo), Koji Okumura(Graduate School of Letters, Hiroshima University), Yasufumi Satoguchi(Lake Biwa Museum)

Humans have attained their specific development by indigenous cultures and evolved through environmental adaptation. The session raises issues of human-environmental interactions, views from diverse changes of climate, ocean, land and biota having made striking influence on humans. It welcomes various fields from human-environment change and their chronometric dating among Quaternary disciplines.

[HQR04-P01] Formation age of mire on marine terraces in Nemuro Peninsula, Hokkaido, Japan

*Reisuke Kondo[1], Minoru Yokochi[2], Takashi Inoue[5], Kazuhiro Kaneko[4], Hiroko Fujita[3], Mari Sumita[6], Yosuke Miyairi[1], Yusuke Yokoyama[1] (1.Atmosphere and Ocean Research Institute, The University of Tokyo, 2.Graduate School of Global Food Resources, Hokkaido University, 3.The Field Science Center for Northern Biosphere, Hokkaido University, 4.Graduate School of Agriculture, Hokkaido University, 5.Research Faculty of Agriculture, Hokkaido University, 6.GEOMAR Helmholtz Centre for Ocean Research Kiel)

[HQR04-P02] Changes in sedimentary environment during the Holocene in a wetland in Chanai area on Konsen plateau, eastern Hokkaido

*Ren Tsuneoka[1], Yusuke Yokoyama[1], Reisuke Kondo[1], Kosuke Ota[1], Minoru Yokochi[2], Kazuhiro Kaneko[3], Hiroko Fujita[4], Takashi Inoue[5], Norio Kito[6], Mari Sumita[7], Kyota Uemura[8], Yosuke Miyairi[1], Arata Momohara[9] (1.Atmosphere and Ocean Research Institute, The University of Tokyo, 2.Graduate School of Global Food Resources, Hokkaido University, 3.Graduate School of Agriculture, Hokkaido University, 4.The Field Science Center for Northern Biosphere, Hokkaido University, 5.Research Faculty of Agriculture, Hokkaido University, 6.International and Regional Studies, Hokkaido University of Education, 7.GEOMAR Helmholtz Centre for Ocean Research Kiel, 8.College of Humanities and Sciences, Nihon University, 9.Faculty of Horticulture, Chiba University)

[HQR04-P03] Holocene coastal evolution and vertical deformation in the Hachinohe plain, NE Japan, inferred from sedimentary analyses

*Yuichi Niwa[1], Toshihiko Sugai[2] (1.Faculty of Science and Engineering, Chuo University, 2.Department of Natural Environmental Studies, Graduate School of Frontier Sciences, The University of Tokyo)

[HQR04-P04] Landform evolution and estimation of crustal movement since MIS 12 in the central-northern part of the Kanto Plain

*Tatsuki Miyamoto[1], Toshihiko Sugai[1], Yuichi Niwa[2], Toshimichi Nakanishi[3], Tetsuya Komatsu[4], Yuki Hiura[4] (1.Department of Natural Environmental Studies, Institute of Environmental Studies,Graduate School of Frontier Science, The University of Tokyo, 2.Chuo Univ., 3.Museum of Natural and Environmental History, Shizuoka, 4.JAEA)

[HQR04-P05] Rock surface dating of granodiorite cobbles obtained from fluvial terrace deposits in the Chichibu Basin, central Japan

*Yuji Ishii[1], Takayuki Takahashi[2], Kazumi Ito[1] (1.National Institute of Advanced Industrial Science and Technology, 2.Tohoku Univ.)

[HQR04-P06] Identification of reworked volcaniclastic deposits composing the upper Alluvium along the Moto-arakawa River, east part of the Saitama Prefecture, Central Japan

*Masanori Murata[1], Takayuki Takahashi[2], Kaori Aoki[1], Fumikatsu NISHIZAWA[3], Makoto Kobayashi[4], Takehiko Suzuki[1,5] (1.Research Center for Volcanic Hazards and Their Mitigation, Tokyo Metropolitan

University, 2.International Research Institute of Disaster Science, Tohoku University, 3.Kanagawa Prefectural Museum of Natural History, 4.Mt. Fuji World Heritage Centre, Shizuoka, 5.Department of Geography, Tokyo Metropolitan University)

[HQR04-P07] Tephrostratigraphy during the past 30,000 years in the Jaishi Oike Moor, southern Izu Peninsula, Japan.

*Tatsuki Watanabe[1], Takehiko Suzuki[1], Daisuke Ishimura[1] (1.Department of Geography, Tokyo Metropolitan University)

[HQR04-P08] Landform evolution since the Middle Pleistocene estimated at the lower reaches of the Himekawa River, central Japan

*Jun Matsukaze[1], Masaaki Shirai[1] (1.Tokyo Metropolitan University)

[HQR04-P09] Radiocarbon dating using pollen fossils and its potential in Quaternary studies

*Keitaro Yamada[1], Takayuki Omori[2], Ikuko Kitaba[3], Takeshi Nakagawa[3] (1.Research Organization of Science and Technology, Ritsumeikan University, 2.The University Museum, The University of Tokyo, 3.Research Centre for Palaeoclimatology, Ritsumeikan University)

[HQR04-P10] Identification of middle to late Pleistocene marine sediments inferred from electric conductivity analysis of the Bando observation well core in Tokushima Plain, western Japan

*Yoshiki Sato[1], Kiyohide Mizuno[1], Yuki Haneda[1], Koretaka Nakatani[1], Rei Nakashima[1] (1.Advanced Industrial Science and Technology, Geological Survey of Japan)

Formation age of mire on marine terraces in Nemuro Peninsula, Hokkaido, Japan

*Reisuke Kondo[1], Minoru Yokochi[2], Takashi Inoue[5], Kazuhiro Kaneko[4], Hiroko Fujita[3], Mari Sumita[6], Yosuke Miyairi[1], Yusuke Yokoyama[1]

1. Atmosphere and Ocean Research Institute, The University of Tokyo, 2. Graduate School of Global Food Resources, Hokkaido University, 3. The Field Science Center for Northern Biosphere, Hokkaido University, 4. Graduate School of Agriculture, Hokkaido University, 5. Research Faculty of Agriculture, Hokkaido University, 6. GEOMAR Helmholtz Centre for Ocean Research Kiel

Large-scale mires are distributed on the marine terraces in Nemuro Peninsula, eastern Hokkaido. These mires are different in scale and morphology from mires / wetlands at the alluvial lowland of the floodplain in the valley and coastal lowland. The main part of the Habomai mire in the eastern part of the Nemuro Peninsula is located on several marine terraces at an altitude of about 20 to 40 m, and part of mire is hilly and sloping. There are no rivers in the Habomai mire, and erosional valleys are distributed the marginal area of the mire. In the Habomai mire, peat layers are known to be distributed on slopes, and historical botany has been studied (Igarashi et al., 2001; Momohara et al., 2009). However, the characteristics of peat covering on terraces and their relationship with the geomorphological development are unknown. The purpose of this study is to clarify the formation age and the geomorphological development of the Habomai mire.

Field surveys were conducted on the Habomai mire and the marine terraces of the Nemuro Peninsula. A cross-sectional surveys of the line transects were performed in the Habomai moor, and the sediments collected by the peat sampler, boring stick and borehole cores. And the marine terrace deposit were sampled at several outcrops around the Habomai mire. Tephrochronology, 14C dating and pIRIR dating were applied to date mire and terrace sediments.

In the Habomai mire, it was observed that the peat layer not only covers the gently sloping terrace surface, but also covers the buried depressions and terrace cliffs. In addition, the sedimentary environment often changes from wetland to peatland after the tephra deposition from Mashu volcano in the Middle Holocene (Ma-f~j). Around the locations where the buried depression and the terrace cliff, the peat layer above the Ma-f~j tephra is relatively thick, and the buried peat layer is intermittently deposited below. The Habomai mire is considered to be a blanket mire because the peat layer covers not only the sloped terrace surface but also the terrace cliffs. As a result of 14C dating, peat deposition started before the LGM. Since then, peatland environments have occurred intermittently at restrictive areas, such as buried depressions and terrace cliffs. From the results of pIRIR dating at the marine terraces around the Habomai mire, it is considered that the main part of marine terraces was formed during the Middle Pleistocene, and that periglacial environment contributed after the LGM. Therefore, it is considered that 1) the terrace surface became gentler due to solifluction during the last glacial period and the previous cold period, 2) subsequently, peat deposition began to accumulate locally at the base of terrace cliffs and buried depressions from an older age, 3) after that, peat deposition crawls up from the depression to the flat area, forming the present blanket mire.

Keywords: mire, marine terraces, 14C dating, pIRIR dating, tephra, Numuro peninsula

©2021. Japan Geoscience Union. All Right Reserved.

Changes in sedimentary environment during the Holocene in a wetland in Chanai area on Konsen plateau, eastern Hokkaido

*Ren Tsuneoka[1], Yusuke Yokoyama[1], Reisuke Kondo[1], Kosuke Ota[1], Minoru Yokochi[2], Kazuhiro Kaneko[3], Hiroko Fujita[4], Takashi Inoue[5], Norio Kito[6], Mari Sumita[7], Kyota Uemura[8], Yosuke Miyairi[1], Arata Momohara[9]

1. Atmosphere and Ocean Research Institute, The University of Tokyo, 2. Graduate School of Global Food Resources, Hokkaido University, 3. Graduate School of Agriculture, Hokkaido University, 4. The Field Science Center for Northern Biosphere, Hokkaido University, 5. Research Faculty of Agriculture, Hokkaido University, 6. International and Regional Studies, Hokkaido University of Education, 7. GEOMAR Helmholtz Centre for Ocean Research Kiel, 8. College of Humanities and Sciences, Nihon University, 9. Faculty of Horticulture, Chiba University

Widespread peatland and wetland distribution is common in eastern Hokkaido, Japan. However, few studies of paleoenvironmental transition history in small alluvial lowland marsh groups located on the Konsen plateau have been reported. A major obstacle is the reconstruction of a robust age model. Peat radiocarbon dating must be employed with caution due to the reservoir effect, since peat and wetland sediments contain not only plant remains at the time of sedimentation but also various organic materials such as roots that are mixed from the layer above after sedimentation (Shinozaki, 2013). If known tephra are identified in strata, accuracy of stratigraphically constrained ages increases. However, accurate ages from radiocarbon dating on macrofossils and marker tephra cannot always be found from wetland sediments.

In this study, we measured radiocarbon from pollen fossils contained in the sediments in a wetland of Chanai area in southern part of Konsen Plateau. This study marks the first use of large pollen on radiocarbon measurements using flow cytometry devices. To reconstruct paleoenvironments, we conducted high resolution elemental analysis on sediments to interpret the origin of the wetland sediments, in particular interpreting the origin of organic matter and its decomposition rate.

Tephra stratigraphy of the core sample indicate that the transition to a wetland setting at the study site occurred between about 7.5~2.5 ka. Results from elemental analysis showed that Total Organic Carbon (TOC) fluctuated between 20 and 40 % at depths of -90 to -60 cm, and between 40 and 50 % at -40 to -5 cm, with a peak of 53 % at -36 cm. Total Sulfur (TS) gradually rose from the bottom to the top, with 0.3~0.4 % at the base and 0.5~0.8 % at the top of the core. The resulted carbon and nitrogen (C/N) ratio was about 14~20 between -90 and -40 cm, and was about 25 in the upper 40 cm of the core, with a sharp rise around -40 cm. This suggests the changes in sedimentary preservation status occurred at around -40 cm, since the C/N ratio decreases with the decomposition of peat (Kondo et al., 1997).

From the C/N ratio, the degree of peat decomposition was highest at the core bottom and lower at the core top, suggesting a change in the decomposition rate or organic material depositional rate. We will further examine the transition of sedimentary environment in the wetland together with the results of radiocarbon dating.

Keywords: wetland, peat, radiocarbon dating, elemental analysis, wetland sedimentary environment, Chanai area on Konsen plateau

©2021. Japan Geoscience Union. All Right Reserved.

Holocene coastal evolution and vertical deformation in the Hachinohe plain, NE Japan, inferred from sedimentary analyses

*Yuichi Niwa[1], Toshihiko Sugai[2]

1. Faculty of Science and Engineering, Chuo University, 2. Department of Natural Environmental Studies, Graduate School of Frontier Sciences, The University of Tokyo

We report geomorphological and sedimentological analyses in the Hachinohe plain (northernmost Sanriku coast, NE Japan) that yield new insights into vertical deformation around the source region of the 2011 Tohoku-oki earthquake. Landform classification and analyses of seven sediment cores document the transgression and regression of the sandy barrier and back-barrier estuary during the Holocene.

Fluvial environment, which prevailed at lower part of the plain at 10,000 to 9,500 cal BP, changed to tidal river environment at 9,500 to 9,000 cal BP. Further transgression induced deeper bay environment at seaward site at 8,500 cal BP, whereas fluvial environments prevailed at upper part of the plain at that time. Because the Hachinohe plain is surrounded by Pleistocene marine terraces and the Mabechi River narrowly crosses them, we suggest that a wave-dominated estuary enclosed by a barrier formed in the present Hachinohe plain during the Middle Holocene. Transgressive lag sand and gravel layers and overlaying shoreface and foreshore sandy sediments imply that a barrier, which had been offshore during the Early Holocene, transgressed and truncated the back-barrier sediments. Consequently, the barrier has been located at present coastline after middle Holocene. The existence of barrier and upward-coarsening silt to sand layer, which filled in water area behind the barrier, indicates progradation of bay-head delta during the Middle Holocene. After progradation of the bay-head delta, fluvial environments again prevailed behind the barrier.
Comparison of height of a surface of the onset of tidal river environment (-22.76 m) at 9,460 cal BP, when sea-level was on or higher than the depositional surface, with hydro-isostatic sea-level prediction that do not account for tectonic deformation suggests maximum subsidence rate on a millennial scale in the Hachinohe plain is 0.7 mm/yr, if there is a millennial-scale subsidence trend at all. Similarly, comparison of a surface of onset of marsh environment (4.51 m) at 6,340 cal BP with hydro-isostatic sea-level predictions suggests that maximum uplift rate in the plain is 0.7 mm/yr. Therefore, the vertical deformation rate on a millennial scale in the Hachinohe plain ranges from -0.7 to 0.7 mm/yr (uplift positive). This vertical deformation is consistent with relative uplift in Kuji and Omoto, northern Sanriku coast and contrasts with subsidence along central to southern Sanriku coast. Our results also support a variation along the Sanriku coast in vertical deformation during the last 100 kyr; the southern part is subsidence while northern part has uplifted at least relative to southern part. Agreement of this trend with deformations during/before the 2011 Tohoku-oki earthquake that the amount/rate of subsidence decreased from south to north implies that effect of subduction and slip on megathrust for coastal deformation persist at least during 100 kyr around the source region of the 2011 earthquake.

Keywords: Sanriku coast, Holocene, millennial-scale crustal movements, sediment core, 2011 Tohoku-oki earthquake

©2021. Japan Geoscience Union. All Right Reserved.

Landform evolution and estimation of crustal movement since MIS 12 in the central-northern part of the Kanto Plain

*Tatsuki Miyamoto[1], Toshihiko Sugai[1], Yuichi Niwa[2], Toshimichi Nakanishi[3], Tetsuya Komatsu[4], Yuki Hiura[4]

1. Department of Natural Environmental Studies, Institute of Environmental Studies,Graduate School of Frontier Science, The University of Tokyo, 2. Chuo Univ., 3. Museum of Natural and Environmental History, Shizuoka, 4. JAEA

Kanto plain is one of the most studied tectonic basins in terms of landform evolution and crustal movement during the Late Quaternary in Japan, but the tectonic trends in the northern part of the plain, from Sashima to Takaragi terrace, have been little clarified. Miyamoto et al. (2020) and Nakanishi et al. (2020), based on the analysis of three all cores (GC-OY-1, OY-2 and NG-1), divided the cores into 19 sedimentary units, and compared Units 15-17 of GC-OY-2 and OY-1 to the Jizodo Formation, and Units 12-14 of GC-OY-2 and OY-1 are compared to the Yabu Formation. This presentation reports the outlines of landform evolution in this area since MIS 12 and the average crustal deformation rate during this period.

The upper surface elevation of the marine stratum in MIS 11 is -20.17 m above sea level for GC-OY-2 (foreshore) and -41.15 m above sea level for GC-OY-1 (delta front). Since the eustatic sea level in MIS 11 was about 6 m to 13 m higher than the present (Raymo and Mitrovica, 2012), the fluctuation amount since MIS 11 is estimated to be about -26 m to -33 m for GC-OY-2 (foreshore) and about -47 m to -54 m for GC-OY-1 (upper shoreface to foreshore). The water content ratio of the core does not decrease vertically downward, so the effect of consolidation is ignored. In addition, since the study area is located at the northern limit of the Paleo-Tokyo Bay expansion area and is heavily supplied by river sediments, it is assumed that the sea level at the time of the formation of the detached surface of the marine stratum approximates the highest sea level of the relevant evolution. From these results, the average rate of vertical change from MIS 11 to the present is estimated to be -0.08 mm/yr for GC-OY-2 and -0.13 mm/yr for GC-OY-1, indicating that the sediments have been settling at an average rate of about 0.1 mm/yr during this period.

The upper surface elevation of the marine stratum in MIS 9 is -9.74 m above sea level for GC-OY-2 and -24.13 m above sea level for GC-OY-1. Since the eustatic sea level in MIS 9 was about 9 m higher than the present (Spratt and Lisiecki, 2016), the fluctuation amount since MIS 9 is estimated to be about -19 m for GC-OY-2 and about -33 m for GC-OY-1. From these results, the average rate of vertical fluctuation during the period from MIS 9 to the present is calculated to be -0.06 mm/yr for GC-OY-2 and -0.11 mm/yr for GC-OY-1, indicating that the average rate of sedimentation during this period has been around 0.08 mm/yr.

The settling rate and the amount of settling are larger in the southern part of the region. This trend is in harmony with the fact that the center of settling is located around Kuki City, Saitama Prefecture in the southern part of the Sashima terrace (Kaizuka, 1987). The amount and rate of settling decrease with increasing age (MIS 11 and 9). This may reflect the shallowing and uplifting of the forearc basin throughout the Quaternary (Sugai et al., 2013).

©2021. Japan Geoscience Union. All Right Reserved.

Acknowledgements: This study used a part of the results of the research and developments funded by the Ministry of Economy, Trade and Industry (METI), Japan as part of its R&D supporting program titled “Establishment of Advanced Technology for Evaluating the Long-term Geosphere Stability on Geological Disposal Project of Radioactive Waste (Fiscal Years 2018 and 2019)

References: Miyamoto et al. 2020 AJG spring. Nakanishi et al. 2020 JpGU. Kaizuka 1987 Jour. of Geography. 96, 51-68. Sugai et al 2013 Jour. of Geography. 122(6), 921-948. Raymo and Mitrovica 2012 Nature 483, 453-456. Spratt and Lisiecki 2016 Climate of the Past 12, 1079-1092.

Keywords: Middle Pleistocene, crustal movement, Kanto plain

©2021. Japan Geoscience Union. All Right Reserved.

Rock surface dating of granodiorite cobbles obtained from fluvial terrace deposits in the Chichibu Basin, central Japan

*Yuji Ishii[1], Takayuki Takahashi[2], Kazumi Ito[1]

1. National Institute of Advanced Industrial Science and Technology, 2. Tohoku Univ.

Fluvial fill terraces are common in middle reach of Japanese rivers, and they were formed in the last glacial period. Ages of terraces have been investigated mainly based on the tephrochronology, but it may have some problems; abandonment ages of terraces may be underestimated because some part of the tephra deposits might have been eroded, or conversely, may be overestimated because tephra layers overlying terrace deposits only indicates the minimum age of the terraces. These problems should be overcome to correctly estimate the uplift rate in the middle reach of rivers as well as to understand the development of fluvial terraces. Optically-stimulated luminescence (OSL) dating could provide depositional ages of fluvial terraces, which may improve the chronology of fluvial terraces. We need to examine the validity of OSL dating of fluvial terrace deposits based on the comparison of tephra chronology.

Sand-sized grains or silt grains are usually used for OSL dating, but recently, cobble dating method have been developed and applied. Fluvial terrace deposits in the middle reach of Japanese rivers are mainly composed of gravels, and sand layers are sometimes difficult to find. Furthermore, cobbles might be better bleached compared to sand-sized grains because of long residence time in river channels. This study examines the luminescence dating of granodiorite cobbles obtained from the uppermost part of terrace deposits formed in the last glacial period in the Chichibu Basin, central Japan.

We obtained three granodiorite cobbles from an outcrop and treated them in a darkroom. We obtained three cores (with 10 mm diameters and 20–30 mm depths) for each cobble and sliced them using water-cooled, diamond-edged wafering blade, and rock slices of 1.2 or 0.65 mm thickness were produced. Measurements were conducted using Risø TL/OSL DA-20 and a post-IR $IRSL_{50/225}$ SAR protocol was used to estimate the depositional ages of cobbles. We also obtained samples from a silty sand layer and obtained post-IR $IRSL_{50/225}$ age of sand-sized K-rich feldspars (180–250 μm) and OSL age of fine-grained quartz grains (4–11 μm).

The OSL age of fine-grained quartz was ca. 9.4 ka, which is 5 ka younger than the UG tephra (16–15 ka) found in the lowest part of the loess deposits overlying the terrace. The decay curve of the quartz OSL signal suggests significant contribution of the medium component, which is thermally unstable, and led to age underestimate. The IR_{50} age of K-rich feldspars is ca. 46 ka and we infer that the luminescence signal was not completely bleached. Three cobbles yielded IR_{50} ages of 19–17 ka, which is consistent with the tephra age. The post-IR $IRSL_{50/225}$ ages of cobbles are considerably different between cobbles (125–34 ka). We introduce and discuss the calculation of dose rate and fading correction methods in the presentation.

Keywords: OSL dating, rock surface dating, fluvial terrace, Pleistocene

©2021. Japan Geoscience Union. All Right Reserved.

Identification of reworked volcaniclastic deposits composing the upper Alluvium along the Moto-arakawa River, east part of the Saitama Prefecture, Central Japan

*Masanori Murata[1], Takayuki Takahashi[2], Kaori Aoki[1], Fumikatsu NISHIZAWA[3], Makoto Kobayashi[4], Takehiko Suzuki[1,5]

1. Research Center for Volcanic Hazards and Their Mitigation, Tokyo Metropolitan University, 2. International Research Institute of Disaster Science, Tohoku University, 3. Kanagawa Prefectural Museum of Natural History, 4. Mt. Fuji World Heritage Centre, Shizuoka, 5. Department of Geography, Tokyo Metropolitan University

In order to study the impacts of the reworking of volcanic products of volcanoes in the northern Kanto region on the Nakagawa and Tokyo Lowlands, we investigated the secondary volcanic products in the alluvial deposit along the Moto-arakawa River. According to the "Borehole map using WebGIS" published by Center for Environmental Science in Saitama, many pumice clasts have been found in the sediments at a depth of less than 5 m from the ground surface. along the Moto-arakawa River. These pumice clasts are considered to have been transported by the Tone River, because the lowland along the Moto-arakawa River was the former channel of the Tone River for some time from the beginning of the 8th century. We carried out borehole investigations at two locations, Iwatsuki Bunka Park, Saitama City (Iwatsuki Bunka Park core) and Koshigaya, Koshigaya City (Koshigaya 2236 core). Based on the analysis of the volcanic products in the two cores, it was found that the upper Alluvium at the depths of 4-5 m in Iwatsuki Bunka Park, and 2-5 m in Koshigaya, Koshigaya City contains secondary volcanic products originated from Hr-FP and Asama tephras. This suggests that the reworking of volcanic products from the upper reaches of the Tone River had a significant impact on the development of the alluvial lowland in the central part of the Kanto Plain during the late Holocene. In the future, we plan to reconstruct the ages and paleoenvironments of the sediments using radiocarbon dating, and to assess the spatial and temporal impacts of the reworking of volcanic products in the Nakagawa and Tokyo Lowlands.

Keywords: alluvial lowland, volcanic hazard, Saitama Prefecture

©2021. Japan Geoscience Union. All Right Reserved.

Tephrostratigraphy during the past 30,000 years in the Jaishi Oike Moor, southern Izu Peninsula, Japan.

*Tatsuki Watanabe[1], Takehiko Suzuki[1], Daisuke Ishimura[1]

1. Department of Geography, Tokyo Metropolitan University

Recently, detailed tephrostratigraphic studies using lacustrine and moor sediment records have been conducted both in the Japanese Islands and overseas, providing more widespread distributions and eruption ages of tephras and contributing to studies of volcanic eruptive history (e.g., McLean et al. 2018; Albert et al. 2018, 2019). Such studies focusing on lacustrine sediment core records in the Japanese Islands are concentrated in the Kinki and Chubu regions. There are a limited number of lakes and moors suitable for the establishment of a detailed tephrostratigraphy in the Tokai and South Kanto coastal regions, where many tephras from Quaternary volcanoes in southwest Japan are expected to be distributed due to westerlies. In this study, we focused on the Jaishi Oike Moor in the southwestern part of the Izu Peninsula in order to establish the detailed tephrostratigraphy of the Jaishi Oike Moor, including cryptotephras (Lowe and Hunt 2001). We conducted particle size analysis, particle composition analysis, tephra analysis (measurement of refractive index of volcanic glass shards and amphiboles, and major element compositions of volcanic glass shards) using a JIS core (core length is 12 m) drilled in September 2020. In particular, the content of volcanic glass shards, amphiboles, and morphological classification of volcanic glass shards were used as indicators to identify the tephric particle concentration horizons.

The sediments of the JIS core are mostly composed of silt deposited under lake to moor environments. Additionally, we also identified tephra layers and coarse-grained sediments deposited by debris flows interbedded within silty sediments. Two visible tephra layers were identified based on tephra analysis: the Amagi-Kawagodaira tephra (Kg, 3,151-3,126 cal yrs BP: Tani et al. 2013) and Aira-Tn tephra (AT, 30,078± 96 cal yrs BP: Smith et al. 2013). In addition, nine cryptotephras were identified from seven layers of tephric particle concentration horizons. They are a widespread tephra of the Kikai-Akahoya tephra (K-Ah, 7,307-7,196 cal yrs BP: McLean et al. 2018), the newly discovered tephra in this site are shown from the top as follows: the Niijima-Miyatsukayama Nanbu tephra (Nj-Mts, 5.5 ka: Kobayashi et al. 2020), Niijima-Shikinejima tephra (Nj-Sk, 8 ka: Kobayashi et al. 2020), one tephra that may be correlated with Daisen Sasaganaru tephra (DSs, 29,837 ±96 cal yrs BP or 29,830 cal yrs BP: Albert et al. 2018) or Daisen Higashidaisen tephra (DHg, 28,895 ±72 cal yrs BP or 28,888 ±72 cal yrs BP: Albert et al. 2018), and one uncorrelated tephra from Izu Islands.

The distribution of Nj-Mts and Nj-Sk in the Honshu Island is identified for the first time. Therefore, JIS core can provide a type tephrostratigraphy in the Izu Peninsula for studying the distribution of tephras from the Izu Islands. On the other hand, the eastern end of the distribution of DSs and DHg in the previous studies is Lake Biwa (Takemura et al. 2010). Therefore, it is likely that the distribution area of either DSs or DHg is expanded to 250 km further east from Lake Biwa by this study and the main axis of them is east-southeast direction from the source volcano. In this study, we analyzed the moor sediments continuously and identified the tephric particle concentration horizons by several indicators, and showed the detailed tephrostratigraphy during the past 30,000 years in the southern part of the Izu Peninsula.

Keywords: Moor sediment, Cryptotephra, Jaishi Oike Moor

©2021. Japan Geoscience Union. All Right Reserved.

Landform evolution since the Middle Pleistocene estimated at the lower reaches of the Himekawa River, central Japan

*Jun Matsukaze[1], Masaaki Shirai[1]

1. Tokyo Metropolitan University

Studies on fluvial terrace have been conducted in many areas of the Japanese islands, and their relationship with climate changes and sea-level changes has been discussed. However, studies focusing on gravel shape (form and roundness) of fluvial terrace deposithave been seldom carried out. In addition to topographic classification and construction of chronology, the authors compared gravel shape of fluvial terraces in the lower reaches of the Himekawa River in the western Niigata Prefecture with gravel shape of the present Himekawa river bed.

Throughout the study, some results were obtained;
(1) The form of the pebbles on the present Himekawa River show that ratio of spherical (cubic) and disc shapes decrease and rod shape increases downstreamward. Local increase in ratio of spherical (cubic) and disc shapes in the middle reaches near by the confluence with the Urakawa River should be influenced by a giant slope-failure “Hieda-Yama-Kuzure” where lots of breccia and boulders were supplied AD1911. It suggests that the effects of giant slope-failure and debris flow may be detected from shape of fluvial gravels.
(2) Fluvial terrace in the studied area are divided as H1~3, M1~3, and L surface in descending order. Volcanic glass shards and minerals originated from AT, DKP, Aso-4, K-Tz, and Tt-D were detected from the tephric loess (so-called loam) in this area. Detection of K-Tz and Tt-D from the basal part of the loam layer on the M2 terrace means that the ages of the M1 and M2 terraces become older than the previous estimation.
(3) A buried valley was discovered on the eastern side of the present Himekawa River as a result of the field survey. The buried valley is estimated as the paleo-Himekawa River channel during the Middle Pleistocene.
(4) The H1~H3 terraces contain sub-angular cubic andesite pebbles just like as the middle reaches of the present Himekawa River, so it is considered that sub-angular cubic andesite pebbles were transported by debris flow from the Umikawa volcanic rocks area near the study area.

Consequently, landform evolution in the lower reaches of the Himekawa River is estimated as follow; Himekawa River flows eastern side of the present Himekawa River valley separated by the ridge of the basement rock during the Middle Pleistocene. The interglacial sea-level rise buries the basement ridge below the alluvial plain deposits. Then, downward valley erosion during the subsequent sea-level fall made the present Himekawa River valley due to tilting to north–northwest direction. During the middle Pleistocene, a large amount of andesite gravels derived from slope failures in the Umikawa volcanic rocks area.

Keywords: Fluvial terrace, Himekawa River

©2021. Japan Geoscience Union. All Right Reserved.

Radiocarbon dating using pollen fossils and its potential in Quaternary studies

*Keitaro Yamada[1], Takayuki Omori[2], Ikuko Kitaba[3], Takeshi Nakagawa[3]

1. Research Organization of Science and Technology, Ritsumeikan University, 2. The University Museum, The University of Tokyo, 3. Research Centre for Palaeoclimatology, Ritsumeikan University

Radiocarbon dating is one of the most widely used dating methods in Quaternary science, including paleoclimatology, archaeology, and hazard protection. Macrofossils (e.g., leaves, wood fragments, and shells) and bulk sediment samples have been used for dating in terrestrial studies. However, macrofossils are not always included in sediments. Moreover, depending on the sedimentary and post-depositional processes, these materials are often not suitable for dating. Therefore, the possibility of radiocarbon dating using small plant fragments and microfossils, which are generally expected to have better radiocarbon integrity, has been explored.

Fossil pollen grains are often found in terrestrial sediments and are one of such materials that have potential to yield more robust radiocarbon ages. Pollen membranes consists of sporopollenin, a physicochemically stable organic polymer. Sporopollenin contains ca. 60% of carbon and has been studied since the 1990s as a potential material for radiocarbon dating. While these studies have successfully shown that fossil pollen grains are potentially suitable for ^{14}C dating, their applications in actual researches have been very limited.

One of the limiting factors is the difficulty of extracting fossil pollen grains from sediment matrixes in high purity. We need to concentrate fossil pollen grains because they comprise very small part of the sediments. However, the characteristics of pollen fossils, such as size, specific gravity, and chemical tolerance do not differ significantly from those of other organic materials in sediments. Therefore, it is difficult to isolate pollen grains using only conventional physicochemical treatments. In this study, we established a novel method to extract fossil pollen grains using “cell sorter” in combination with new physicochemical treatments. Cell sorters can separate individual particles based on scattered light and fluorescence.

In this study, we used SG06 core obtained from Lake Suigetsu, Fukui prefecture, Japan, Radiocarbon ages of >800 terrestrial leaf fossils have been measured, making the core almost ideal target for comparison to assess robustness of the radiocarbon dates obtained on fossil pollen pellets.

The extracted pellets are composed almost exclusively of pollen grains, with almost no solid impurities. The size of the extracted pollen grains depends on the specs of the cell sorter. Therefore, the extracted pollen fossils consist of grains with diameters of 10-50 μm, such as *Cryptomeria* and *Alnus*, and do not retain the original percentage composition of fossil pollen assemblage.

The radiocarbon ages obtained on fossil pollen pellets prepared by cell-sorter precisely reproduced those from leaf macro fossils, regardless of the taxa percentage composition. These agreements were maintained even near the radiocarbon limit (ca.50 ka). The fossil pollen grains extracted by our method were useful as materials for radiocarbon dating, as is also the case with the terrestrial leaf fossils. Our method enables robust radiocarbon dating of the sediments that do not contain macro remains suitable for radiocarbon dating.

We also confirmed that fossil pollen grains could be extracted from not only lacustrine deposits, but also peat and volcanic soils. The extraction method can be applied to a range of terrestrial sediments deposited in various environments. Combined with Bayesian modeling, radiocarbon dating of strategically chosen horizons can provide much stronger age constraints to event deposits such as volcanic ash and tsunami deposits.

©2021. Japan Geoscience Union. All Right Reserved.

Keywords: radiocarbon, pollen

©2021. Japan Geoscience Union. All Right Reserved.

Identification of middle to late Pleistocene marine sediments inferred from electric conductivity analysis of the Bando observation well core in Tokushima Plain, western Japan

*Yoshiki Sato[1], Kiyohide Mizuno[1], Yuki Haneda[1], Koretaka Nakatani[1], Rei Nakashima[1]

1. Advanced Industrial Science and Technology, Geological Survey of Japan

Tokushima Plain is a coastal plain located on the western coast of the Kii Channel. Along the northern margin of the plain, the Median Tectonic Line Fault Zone is distributed, and displaces fans and Pleistocene terraces. The fault zone is a reverse fault with large right-lateral displacement and uplift of the northern side around the plain (Okada, 2020). This suggests and the plain can be regarded as a tectonic basin by the MTL fault zone. Since 1960s, many studies about the subsurface geology of the plain have been conducted (Kawamura & Nishiyama, 2019). The Quaternary subsurface geology can be roughly divided into two formations, the Tokushima and Kitajima Formations, which are related to Alluvium and the middle to late Pleistocene, respectively. However, detail sedimentary periods and environments have not been clarified.

We attempted to identify the marine sediments in the Kitajima Formation based on electrical conductivity [EC] analysis of the Bando observation well core, 502 m long core drilled in the plain in 1995 by GSJ. Matsumoto & Arai (2021) reported stratigraphic description and pollen fossil and paleomagnetic analyses of the core. These indicate that several glacial-interglacial cycles are preserved, and the Brunhes-Matsuyama [B-M] boundary may be located between 339 and 440 m depth. In this study, EC analysis was carried out on subsamples collected from lower than 90 m depth. Sample treatment and interpretation were based on Yokoyama & Sato (1987) and Niwa *et al.* (2009).

As the results, we found five marine sediments; M1, 93.4–102.45 m depth; M2, 228.08–237.00 m; M3, 258.83–263.98 m; M4, 2 88.06–288.60 m depth; M5, 305.50 m. Comparison with the pollen fossil stratigraphy of the Osaka Group (Hongo, 2009), the M1 layer probably deposited during the MIS5e because of the high abundance of *Lagerstoemia* (Matsumoto & Arai, 2021). High abundance of *Cyclobalanopsis* in the M3 layer (Matsumoto & Arai, 2021) suggests that this layer deposited during the MIS11. Assuming these interpretations are correct, M2 layer, located between the M1 and M3 layers, should be corresponding to the MIS 7 or 9 marine sediment. In addition, the M4 and M5 layers might deposit during the MIS 13, 15, or 17 because these are above the B-M boundary.

These insights suggest that glacial-interglacial cycles sediments after the middle Pleistocene had been recorded in the subsurface geology of the Tokushima Plain. The average subsidence rate is estimated to be ˜0.7 to ˜0.8 mm/yr. For clarifying detail stratigraphy of the subsurface geology in the plain, we will conduct volcanic ash, pollen fossils and paleomagnetic analyses of the core materials in future.

References

Hongo, M. (2009) Middle Pleistocene pollen biostratigraphy in the Osaka sedimentary basin, southwest Japan, with special reference to paleoenvironmental change. The Journal of the Geological Society of Japan, **115**, 64–79.

Kawamura, N. & Nishiyama, K. (2019) Correlation study of the late Pleistocene and Holocene deposits underlying the major coastal plains of Shikoku, Southwest Japan. The Journal of the Geological Society of

©2021. Japan Geoscience Union. All Right Reserved.

Japan, **125**, 87–105.
Matsumoto, N. & Arai, T. (2021) Report on construction of facilities and equipment for groundwater monitoring for earthquake prediction in 1995, No.2*. Open-File Report of the Geological Survey of Japan, AIST, no.713.
Niwa, Y. et al. (2009) Evidence for late Holocene coseismic subsidence identified in drilling cores along the Yoro fault system, western margin of the Nobi plain, central Japan. Daiyonki-Kenkyu, **48**, 339–349.
Okada, A. (2020) Median Tectonic Line Fault Zone. 368p. Kokon-Shoin, Tokyo.
Yokoyama, T. & Sato, M. (1987) Analysis of paleo-environments based on electric conductivity of stirred clayey sediments into water -On two drilled cores of Osaka Group in Senriyama Hills and Biwako Group at bottom of Lake Biwa, Japan-. The Journal of the Geological Society of Japan, **93**, 667–679.

Keywords: Tokushima Plain, subsurface geology, Kitajima Formation, Median Tectonic Line Fault Zone

©2021. Japan Geoscience Union. All Right Reserved.

[J] Poster | H (Human Geosciences)：H-DS Disaster geosciences

Sat. Jun 5, 2021 5:15 PM - 6:30 PM JST | Sat. Jun 5, 2021 8:15 AM - 9:30 AM UTC | Ch.10_2

[H-DS07] Seismic hazards on subduction earthquakes and active faults in the Central Japan

convener:Takashi Azuma(National Institute of Advanced Industrial Science and Technology), Yasuhiro Suzuki(Nagoya University)

This session focuses on seismo-tectonics and disasters prevention for large earthquakes in the Central Japan. We would like to discuss possible hazards with low probability, problems related to quantatitive evaluation, such as modellings and evaluation of uncertainties, utilization of hazard information, and so on.

[HDS07-P01] Issues for long-term evaluation of Byobu-yama/Ena-san fault zone

*Yasuhiro Suzuki[1] (1.Nagoya University)

[HDS07-P02] Paleoseismological trenching surveys on the Enasan-Sanageyamakita fault zone, Central Japan

*Takashi Azuma[1], Norio Shigematsu[1], Rei Nakashima[1], Ken-ichi Yasue[2], Ryo Tateishi[2], Daisuke Hirouchi[3] (1.National Institute of Advanced Industrial Science and Technology, 2.Toyama University, 3.Shinshu University)

[HDS07-P03] Questionnaire survey for experts on long-term evaluation of active faults and evaluation of ground motion (Part 1)

*Noa Mitsui[1], Takeshi Sagiya[1] (1.Disaster Mitigation Research Center, Nagoya University)

Issues for long-term evaluation of Byobu-yama/Ena-san fault zone

*Yasuhiro Suzuki[1]

1. Nagoya University

Introduction

The Headquarters for Earthquake Research Promotion selected the northern part of the " Byobuyama/Enasann Fault and Sanageyama Fault" as the target of intensive research (2020-2022). The purpose of this survey is to improve active fault evaluation and strong motion evaluation. The research group led by Nagoya University summarized the problems of the conventional evaluation of the fault and formulated a research plan to improve them.

Issues and research objectives

The "Byobuyama/Enasann Fault and Sanageyama Fault" is a long active fault zone with a total length of over 100 km from the Ena Mountains through the Okazaki Plain to the Chita Peninsula. The faults that make up the fault zone are close to each other, and it is difficult to decide a source fault scenario. Around the fault, there are densely populated areas such as Nagoya City and industrially concentrated areas such as Toyota City.

In Japan, the survey on this fault zone was once carried out from 1995 to 2000, however the activity history and fault structure data are scarce. Based on such data, in the previous long-term evaluation, the Enasan-Sanageyama north fault zone was ranked A *, the Byobuyama fault and the Kagiya fault were ranked A, the Sanage-Takahama fault was ranked Z, and the Akagawa fault was ranked X. "Fault near Nagoya City" was unknown.

The conventional active fault evaluation has the following problems.

1) Comparing the active fault map of the Geographical Survey Institute (1996-2016), the detailed digital map of the active fault (2002), and the active fault map of Gifu Prefecture (2010), there is a difference in trace identification.

2) It is assumed that the Enasan fault and the Sanageyama north fault, which have different geometrical characteristics, activate together.

3) There is no specific activity history for the Byobuyama fault. Since the earthquake occurrence probability is calculated by the Poisson process model, it cannot be compared with the probability of other faults based on the renewal process model.

4) The northern part of the Sanage-Takahama fault zone is evaluated as Z rank in calculation, while it is assumed that the activity confirmed at one point is regarded as the latest activity and that the total length of 51 km causes a 4 m displacement.

Keywords: active fault, earthquake, long-term evaluation

©2021. Japan Geoscience Union. All Right Reserved.

Paleoseismological trenching surveys on the Enasan-Sanageyamakita fault zone, Central Japan

*Takashi Azuma[1], Norio Shigematsu[1], Rei Nakashima[1], Ken-ichi Yasue[2], Ryo Tateishi[2], Daisuke Hirouchi[3]

1. National Institute of Advanced Industrial Science and Technology, 2. Toyama University, 3. Shinshu University

We conducted paleoseismological trench surveys at 2 sites on the Enasan-Sanageyamakita fault zone. This fault zone is consisted with the Enasan fault (38 km in length) and the Sanageyamakita fault (22 km). One site is Tomida on the Enasan fault, where is close to a previous trenching survey site by Gifu Prefecture in 2001. In our trench, 2 fault planes with high angle were recognized, whereas this fault is evaluated as a reverse fault.Another site is Higashi-shirasaka on the Sanageyama-kita fault, where is same site with a previous trenching survey by Aichi Prefecture in 1996. In the trench, low-angle fault planes were recognized, whereas this fault is evaluated as a high-angle right-lateral strike-slip fault. It cut sand-silt sediments and covered with gravels. We will discuss faulting histories these sites on this fault zone. This survey was a part of the Comprehensive Research Project for the Enasan-Sanageyama-Kita Fault Zone by MEXT.

Keywords: active fault, Central Japan, Paleoseismological trenching survey

©2021. Japan Geoscience Union. All Right Reserved.

Questionnaire survey for experts on long-term evaluation of active faults and evaluation of ground motion (Part 1)

*Noa Mitsui[1], Takeshi Sagiya[1]

1. Disaster Mitigation Research Center, Nagoya University

Regarding earthquakes occuring on active faults, the Headquarters for Earthquake Research Promotion has evaluated the long-term earthquake occurrence potentials based on surveys of active faults conducted nationwide since 1996. In addition, evaluations of strong ground motion is also published. Since the frequency of earthquakes on active faults is very low and the quantity and quality of information obtained from active fault surveys are limited, long-term evaluation of active faults has large uncertainty. Therefore, when disseminating long-term evaluations of active faults and evaluation of strong ground motion to the residents as earthquake risk information, it is necessary to consider the appropriate content and transmission method from various viewpoints. The viewpoints are such as scientific validity, understanding and utilization of information in disaster prevention administration, and understanding of local residents who receive the information.
Opinions of experts in active faults and earthquakes are reflected in the work process of long-term evaluation and evaluation of strong ground motion. In addition, surveys are conducted on the residents and local governments regarding the published results. On the other hand, regarding the published results, the degree of recognition and evaluation as a group of experts including non-committee members has not been clarified.
Therefore in this research, as part of the survey on the method of transmitting information of earthquake evaluation with uncertainty, we will first conduct a survey targeting experts in active faults and earthquakes. We conducted a questionnaire survey to member of the Japanese Society for Active Fault Studies and councillor of the Seismological Society of Japan to collect opinions based on the scientific validity about information that should be conveyed to residents and about the proper method regarding active faults and strong ground motion.

Keywords: active fault, long-term evaluation, evaluations of ground motion, risk

©2021. Japan Geoscience Union. All Right Reserved.

[J] Poster | H (Human Geosciences)：H-DS Disaster geosciences

Sat. Jun 5, 2021 5:15 PM - 6:30 PM JST | Sat. Jun 5, 2021 8:15 AM - 9:30 AM UTC | Ch.10_3

[H-DS10] Geohazards in humid, tectonically active countries and their precursors

convener:Satoru Kojima(Department of Civil Engineering, Gifu University), Taro Uchida(University of Tsukuba), Yoshihiko Kariya(Department of Environmental Geography, Senshu University)

This session covers mass movements of landslide, slope failure, debris flow, and gravitational slope deformation in tectonically active, humid countries, and aims to discuss on their mechanisms, characteristics of occurrence sites, the significance in geological time scale, and the methodology to mitigate their affects by researchers with various related research fields.

[HDS10-P01] Large-scale collapse of permafrost waste dump at Kumtor gold mine in Kyrgyz republic

*Ayano Aoki[1], Chiyuki Narama[1], Tsutomu Yamanokuchi[2], Murataly Duishonakunov[3] (1.Niigata university, 2.Remote Sensing Technology Center of Japan, 3.Kyrgyz National University)

[HDS10-P02] Relationship between landslide distribution and topographic feature and subsurface structure for the case of the 2018 Hokkaido Eastern Iburi Earthquake

*Junichiro Furuyama[1], Issei Doi[1], Toshitaka Kamai[1], Yuki Matsushi[1] (1.Kyoto University)

[HDS10-P03] Sediment movement on landslide slopes and river channel after the 2018 Hokkaido Eastern Iburi Earthquake

*Takashi Koi[1], Yasutaka Tanaka[1], Shin'ya Katsura[2], Norifumi Hotta[3] (1.Center for Natural Hazards Research, Hokkaido University, 2.Research Faculty of Agriculture, Hokkaido University, 3.Graduate School of Agricultural and Life Sciences, The University of Tokyo)

[HDS10-P04] Surface changes of Ganpei landslide in Joetsu region

*Yutaka Inoue[1], Chiyuki Narama[2], Chunxiang WANG[3], Eiji Takita[3] (1.Graduate Student,Niigata University, 2.Niigata University, 3.KITAK Corporation)

[HDS10-P05] Surface changes of rock slopes in the Hakuba-Daisekkei Valley, northern Japanese Alps

*Hirotaka Sugiyama[1], Chiyuki Narama[1], Hiroshi Inoue[2] (1.Niigata University, 2.NIED)

[HDS10-P06] Revisiting stratigraphy and age of so-called Otsukigawa debris avalanche deposits in the upper Otsukigawa and Yukawa Rivers on the eastern side of Yatsugatake Volcano in central Japan

*Takahiro Kurimoto[1], Yoshihiko Kariya[2] (1.Graduate School of Humanities, Senshu Univ., 2.Senshu Univ.)

[HDS10-P07] Relationship between a natural dam at the Yomogisawa River in the headwater area of the Abe River and the Oya-Kuzure rockslide with reference to new chronological information

*Keiju Kimura[1], Yoshihiko Kariya[2] (1.Graduate, Senshu Univ., 2.Senshu Univ.)

[HDS10-P08] Activities of landslides and their precursors: Case studies in Okutabora, Gujo, Gifu Prefecture and in Kuchisakamoto, Shizuoka Prefecture, central Japan

*Satoru Kojima[1], Kazuhide Sawada[1], Mizuki Tatekawa[1] (1.Department of Civil Engineering, Gifu University)

Large-scale collapse of permafrost waste dump at Kumtor gold mine in Kyrgyz republic

*Ayano Aoki[1], Chiyuki Narama[1], Tsutomu Yamanokuchi[2], Murataly Duishonakunov[3]

1. Niigata university, 2. Remote Sensing Technology Center of Japan, 3. Kyrgyz National University

Large-scale collapse of mine waste dump occurred at the Kumtor gold mine in Kyrgyz Republic on 1 December 2019 and killed two mine workers. The Kumtor gold mine (4000m) is located in Ak-Shiyrak massif of inner Tien Shan. This area is permafrost and active glacier zone. In the Kumtor gold mine, mine dumps are composed of permafrost and glacier ice. The mine dumps are made on permafrost slope, moraine-complex including permafrost and glacier ice, and glacier. Before this collapse, unstable flows are reported in the terminus of the dump in 2013 (Jamieson et al.,2015). In this study, we investigated the collapse of the mine dump at the Kumtor gold mine using satellite image analysis. Furthermore, we compared three dumps in the Kumtor gold mine to consider the factor of the collapse.

Keywords: collapse, permafrost, satellite image

©2021. Japan Geoscience Union. All Right Reserved.

Relationship between landslide distribution and topographic feature and subsurface structure for the case of the 2018 Hokkaido Eastern Iburi Earthquake

*Junichiro Furuyama[1], Issei Doi[1], Toshitaka Kamai[1], Yuki Matsushi[1]

1. Kyoto University

The 2018 Hokkaido Eastern Iburi Earthquake caused numerous (> 6000) shallow tephra landslides with the regional differences in the number and density of their occurrences (Ito et al., 2020). Wang et al. (2019) suggested that the heterogeneous patterns of landslide distribution are attributed to base geology, while Tajika et al. (2020) pointed out that low landslide density is observed along anticline axes.
We estimated the ridge intervals and slope degree by topographic analysis based on Parron et al. (2008) as well as the S-wave velocity structure by microtremor array survey for the partitioned areas according to the base geology and/or the density of landslide distribution.
The ridge intervals were found to be different according to the landslide distribution and base geology. It was suggested that the topography was affected by base geology and also affected landslide generation. We also obtained S-wave velocity structure to the depths of 300 m. We will further estimate the S-wave velocity data in a wider area and discuss them in connection with the topographic feature as well as landslide distribution.

Acknowledgement: We used DEM data provided by Geospatial Information Authority of Japan.

Keywords: 2018 Hokkaido Eastern Iburi Earthquake, Coseismic landslide

©2021. Japan Geoscience Union. All Right Reserved.

Sediment movement on landslide slopes and river channel after the 2018 Hokkaido Eastern Iburi Earthquake

*Takashi Koi[1], Yasutaka Tanaka[1], Shin'ya Katsura[2], Norifumi Hotta[3]

1. Center for Natural Hazards Research, Hokkaido University, 2. Research Faculty of Agriculture, Hokkaido University, 3. Graduate School of Agricultural and Life Sciences, The University of Tokyo

The Hokkaido Eastern Iburi Earthquake that occurred before dawn on September 6, 2018 caused shallow landslides in more than 6,000 locations, mainly in Atsuma Town and Abira Town, Hokkaido, Japan. Most of the sediment and driftwood produced from the collapsed area remain in the basin, and it is thought that sediment movement occurs at the time of flooding, but the magnitude, frequency and spatial distribution of the movement is not clear. The surface soil in areas where many shallow landslides occur is mainly covered with volcanic ejecta, and the constituent materials of the produced sediment are relatively fine grains. Therefore, if the landslide sediment flows out to the downstream area, it may affect the turbidity of running water and changes in water quality. In this study, we focused on the surface erosion of the landslide slope and the landslides deposited on the river channel in the Habiu River catchment (0.38 km^2) of the Atsuma River system where shallow landslides occurred frequently due to the Hokkaido Eastern Iburi earthquake, and clarified the sediment movement for two years after the earthquake. The sediment movement of the catchment was grasped from the field survey and topographical analysis. Using the laser profiler data taken immediately after the earthquake (2018) and the elevation data acquired using the UAV in 2020, the amount of change in elevation values on the slope and in the river channel was calculated from the difference analysis between the two periods. From the field survey, it was confirmed that a large amount of landslide sediment and driftwood produced during the earthquake were deposited in the river channel. In addition, from the differential analysis of the elevation data of the two periods, the landslide slope was eroded as a whole, while the eroded area and the deposited area were mixed in the river channel within a range of several tens of centimeters. Even after the earthquake, the newly produced sediment from the landslide slope was supplied to the river channel, and it was considered that sediment movement occurred in the river channel at the time of flooding. On the other hand, as for the landslide slope, the south-facing slope was more eroded than the north-facing slope, and the gully was also well developed. The progress of such gully erosion could be confirmed from the field survey. The predominant erosion on the south-facing slopes may be due to the effects of freezing, thawing and snowmelt in winter season due to differences in the amount of solar radiation.

Keywords: the 2018 Hokkaido Eastern Iburi Earthquake, shallow landslide, sediment movement, slope-channel coupling, volcanic area

©2021. Japan Geoscience Union. All Right Reserved.

Surface changes of Ganpei landslide in Joetsu region

*Yutaka Inoue[1], Chiyuki Narama[2], Chunxiang WANG[3], Eiji Takita[3]

1. Graduate Student,Niigata University, 2. Niigata University, 3. KITAK Corporation

Unique topography and vegetation can be observed around the landslide. The surface changes reflect the internal structure and sliding morphology of landslides. However, there are few cases which the surface changes of landslides are observed spatially and many times.
In this study, we repeatedly conducted field surveys including UAV aerial photography and GNSS survey in the Ganpei area in the eastern part of the Takada Plain, Joetsu City, Niigata. We discussed the relationship between the surface change and motion of landslide based on our results.

Keywords: Landslide, GNSS, Surface change

©2021. Japan Geoscience Union. All Right Reserved.

Surface changes of rock slopes in the Hakuba-Daisekkei Valley, northern Japanese Alps

*Hirotaka Sugiyama[1], Chiyuki Narama[1], Hiroshi Inoue[2]

1. Niigata University, 2. NIED

Introduction

In the northern Japanese Alps, rock slope failure has caused mountaineering accidents frequently. In Hakuba-Daisekkei Valley, rock slope failure with victims occurred in 2005 (Kariya, 2006). However, the process and geomorphological characteristics of rock slope failure are unclear. As a reason, it is difficult to investigate the steep rock slope directly. The purpose of this study is to clarify the process of rock slope failure on different rock types in Hakuba-Daisekkei Valley using UAV and SfM methods.

Study area

Hakuba-Daisekkei is a perennial snow patch located at the bottom of the Hakuba-Daisekkei Valley. The valley is a popular mountaineering route to Mt. Hakuba-dake (2932 m asl). More than 10,000 people pass the route every year. Hakuba-Daisekkei Valley is surrounded by Mts. Shakushi-dake and Hakuba-dake. Mt. Hakuba consisted of felsic tuff and tuff breccia. Mt. Shakushi consisted of Felsite. Hakuba-Daisekkei Valley is high annual precipitation through summer and heavy snow climate in Japan.

Methods

We observed the retreat process of rock slopes using images of UAV, Cessna and aerial photography with SfM (Structure from Motion) technology.

Results

We confirmed the difference in the retreat process between Mt. Shakushi-dake and Mt. Hakuba-dake. On the rock slope of Mt. Shakushi-dake, we observed the discriminatory retreat that depended on rock joint density. On the other side, we observed the sudden retreat process with a tension crack opening on the rock slope of Mt. Hakuba-dake.

Keywords: rockfall, rock slope failure, SfM, UAV, freezing and thawing, ICP

©2021. Japan Geoscience Union. All Right Reserved.

Revisiting stratigraphy and age of so-called Otsukigawa debris avalanche deposits in the upper Otsukigawa and Yukawa Rivers on the eastern side of Yatsugatake Volcano in central Japan

*Takahiro Kurimoto[1], Yoshihiko Kariya[2]

1. Graduate School of Humanities, Senshu Univ., 2. Senshu Univ.

On the east side of Yatsugatake Volcano, large-scale landslide features with a long and clear head scarp and undulated emplacement bodies with hummocks exists. This spectacle landforms and their forming materials have been called "Otsukigawa debris avalanche (ODA)" and "Otsukigawa debris avalanche deposit (ODAD)", respectively (Kawachi 1983). The cause of ODA has been attributed to the AD887 Ninna mega-earthquake generated from the Suruga-Nankai submarine troughs based on conventional ^{14}C dates and interpretation of historical documents. However, the recent novel study by Yamada et al. (2021) using oxygen isotope dendrochronology of ODAD suggests that there is doubt about the age of ODA. Therefore, based on field investigations, we reexamined ODA and ODAD in the upper reaches of Otsukigawa and Yukawa Rivers on the east side of the volcano. We reconfirmed a previous study by Machida and Tamura (2010) that ODAD is distributed along the Otsukigawa River and its tributaries, from Midori-ike Pond immediately below the head scarp to the confluence point between Otsukigawa and Chikuma Rivers. ODAD consists of non-sorted breccias, dominantly bearing hornblende andesite, and yellowish white to dark brown fine-grained matrix with a hydrogen sulfide odor. We carried out new age determination of the upper part of ODA by ^{14}C, all wood samples gave the range from AD772 to 976. Additionally, an unreported mudflow deposit was newly found in the east of Inagoyu Spa, showing 42 to 48 ^{14}C ka. We name this "Inagoyu mudflow deposit (IMD)". The age of IMD coincides with the Last Glacial period around MIS4 and one of activated periods of Yatsugatake Volcano, suggesting that IMD would be derived from snowmelt or icemelt lahar. We also found another landslide deposit different from ODAD and IMD on the banks of Yukawa River near Honzawa Spa. We call this "Honzawa debris avalanche deposit (HDAD)". The fossil wood collected from HDAD shows 3.6 to 2.8 cal ka. From these results, it is considered that large to middle scale landslide phenomena have occurred repeatedly in the period from 48 ka to 1 ka on the eastern side of Yatsugatake Volcano. Our data suggest that the thick debris, which was conventionally called as ODAD, was not produced by single large-scale landslide event, and the ages of ODAD span widely from the late Pleistocene to the recent millennia. However, it should be emphasized that debris avalanche occurred in the period from AD772 to 976 in the upper Otsukigawa River. The latest event in AD772 to 976 may be caused by AD887 Ninna earthquake or AD762 Mino/Hida/Shinano earthquake, as well as AD841 Shinano earthquake. Aftershocks by these earthquakes were also possible triggers. More information on the stratigraphy and ages of "so-called" ODAD is required.

Keywords: Yatsugatake Volcano, Otsukigawa debris avalanche, AD887 Ninna earthquake, Paleoearthquake

©2021. Japan Geoscience Union. All Right Reserved.

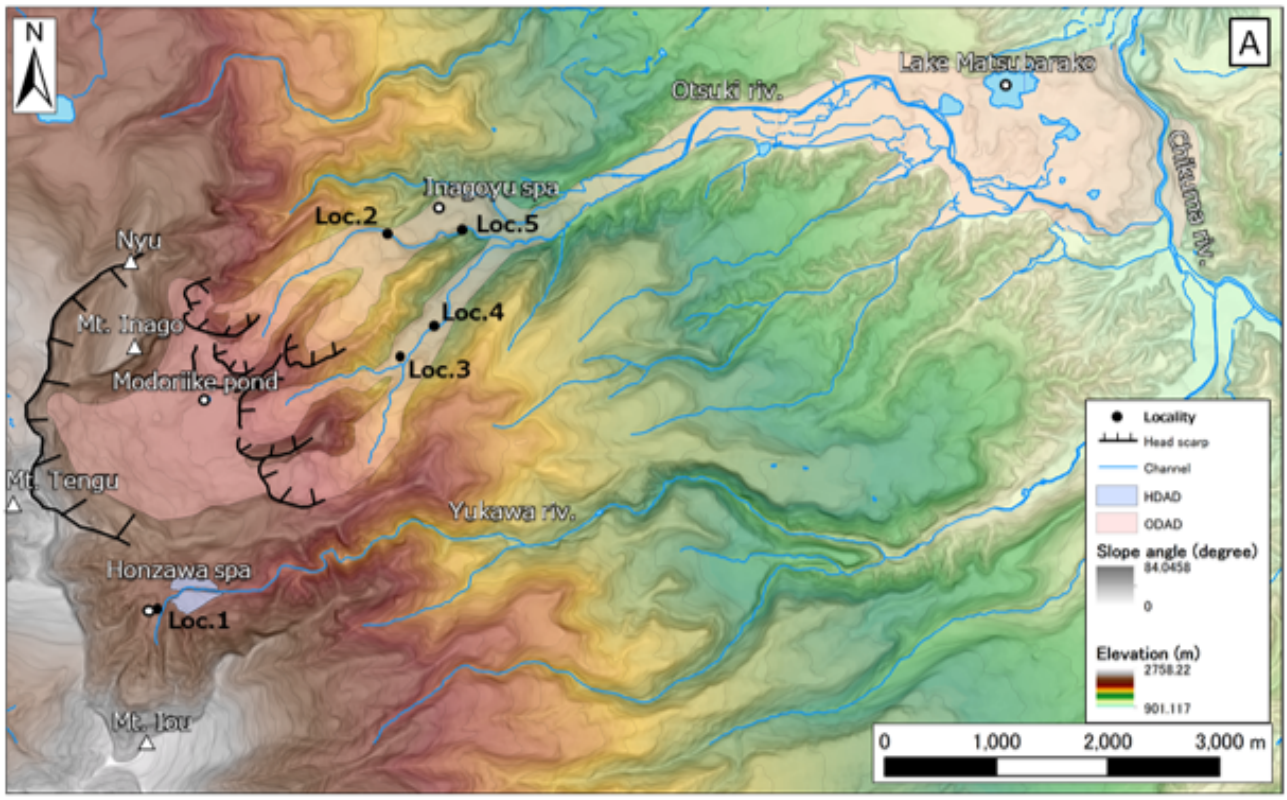

Figure and picture A to C ; A)Topography of the study area. Contour interval is 20 m. B)Picture of Outcrop(HDAD). C)Picture of Outcrop(ODAD).

©2021. Japan Geoscience Union. All Right Reserved.

Relationship between a natural dam at the Yomogisawa River in the headwater area of the Abe River and the Oya-Kuzure rockslide with reference to new chronological information

*Keiju Kimura[1], Yoshihiko Kariya[2]

1. Graduate, Senshu Univ., 2. Senshu Univ.

1. Introduction

The Oya-Kuzure is a huge landslide site located at the headwaters of the Abe River in Shizuoka Prefecture. This landslide is believed to be triggered by the CE1707 Hoei earthquake (est. M 8.6) (Shizuoka River Office, Ministry of Construction, 1988). There are, however, other arguments about the age of Oya-Kuzure, and all of them are based solely on historical documents without geological and chronological data. Machida (1959; Geogr. Rev. Jpn.) pointed out that lacustrine sediments are buried under the present riverbed near the confluence of the Oya and Mikochi Rivers upstream of the Abe River. He also showed that other lacustrine sediments are distributed along a few tributaries, whereas details were unknown.

In this presentation, we report landslide sediments originating from Oya-Kuzure and a resultant, natural dams, as well as the dammed lacustrine sediments found in Yomogisawa River, one of small tributaries of the Oya River, and show radiocarbon ages of those sediments. Then we will discuss the age of the Oya-Kuzure.

2. Landforms and geology

Oya-Kuzure has a following an area of 1.8 km^2, a headscarp width of 1.8 km, and a vertical difference of 800 m. The Oya River originates from the Oya-Kuzure, and the Mikochi River is combined to form the Abe River. As Oya-Kuzure has supplied a large number of debris, fill terrace is developed in this area.

The geology is mainly composed of alternating beds of sandstone and shale, but igneous rocks and serpentinite are limitedly distributed in the upper reaches of Yomogisawa River (Sugiyama and Matsuda, 2014).

3. Description of landslide and lacustrine sediments

An outcrop locality consisting of gravel layers and sandy silt layers is present on the left bank of Yomogisawa River, at which 1.1 km upstream from the confluence of Yomogisawa and Oya Rivers. The top surface (ground surface) of this outcrop corresponds to the terrace surface about 4 m high from the present riverbed of Yomogisawa River.

A paleosol layer S with a large amount of deformed wood fragments is confirmed at the bottom of outcrop. The paleosol S continues subsurface of outcrop and its thickness is estimated to 0.3 m or more. Above the paleosol S, an angular gravel layer A (max. thickness ca. 3 m) consisting of granule to boulder clast is observed. The gravel layer A becomes thinner in the upstream side. A sandy silt layer X (max. th. 0.6 m) and a sand layer Y (max. th. 0.5 m) are laid on the gravel layer A in this order, and both layers X and Y gradually become thinner in the downstream side contrary to the layer A. Layers X and Y abut on layer A and are finally disappear. Layers X and Y are covered by a gravel layer B (max. th. 1.5 m) with granule to boulder of debris flow origin.

Layers A and B can be distinguished by roundness and lithology of clastic materials. Layer A shows a lower degree of roundness than that of layer B, suggesting that layer A was caused by and moved by rock avalanche behavior. Layer B contains serpentinite and igneous rocks derived from the upper part of

©2021. Japan Geoscience Union. All Right Reserved.

Yomogisawa River, suggesting its source is restricted to the Yomogisawa River watershed.
Layer A is thought to be rock avalanche sediments supplied from the Oya-Kuzure and formed a natural dam obstructing the stream of Yomogisawa River. Layers X and Y are considered to be dammed lacustrine sediments by this natural dam. In addition, it is considered that the paleosol S is derived from disturbed soil at which layer A moved down and flowed into Yomogisawa River, or from a small-scale landslide occurred nearby the outcrop before formation of the natural dam.
Paleosol S, and layers A and X contain fossil wood fragments. We consequently measured ^{14}C age of those samples.

4. ^{14}C age

The wood samples showed the following ages. The calendar year was calculated by OxCal and INTCAL20 and shows a 2 σ error interval (1 σ for ^{14}C year). Paleosol layer S= cal CE1396-1441 (521±23 ^{14}C) BP, gravel layer A = cal CE1506-1596/1616-1655 (297±23 ^{14}C) BP, sandy silt layer X = cal CE1644-1680/1740-1753/1762-1800 (220±20 ^{14}C) BP.

5. Discussion

No stratigraphic reversal of ^{14}C ages are confirmed. Our age data can be considered as appropriate. Layer A may be up to 200 years older from CE1707, and it is probable that a landslide activity of Oya-Kuzure had preceded several hundred years before CE1707. On the other hand, the age of layer X includes CE1707, but it has a wide range and may have been deposited from the middle of CE1600’s to around CE1800. Therefore, in addition to 1707 Hoei earthquake, CE1498 Meio Tokai (est. M8.2-8.4), CE1605 Keicho Tokai (est. M7.9), and CE1703 Genroku (M7.9-8.2) earthquakes are candidate triggers of rock avalanche from the Oya-Kuzure site.

Keywords: Oya-Kuzure, lacustrine sediment, 14C age

©2021. Japan Geoscience Union. All Right Reserved.

Activities of landslides and their precursors: Case studies in Okutabora, Gujo, Gifu Prefecture and in Kuchisakamoto, Shizuoka Prefecture, central Japan

*Satoru Kojima[1], Kazuhide Sawada[1], Mizuki Tatekawa[1]

1. Department of Civil Engineering, Gifu University

Forecasting the slope movement is important for the mitigation of landslide disasters. After the landslide disaster in 2011 by the Typhoo Talas in Kii Peninsula, central Japan, the landforms formed by the process of deep-seated gravitational slope deformation (DSGSD) have been expected to be useful for the prediction of deep-seated landslides. We conducted researches on DSGSD in several regions of Japan, and in this session presented the results of two case studies analyzing the relationship between the DSGSD development and landslide activity. One of them is the landslide in the Okutabora Valley, Gifu Prefecture. About 20,000 m^3 debris slipped down along the valley in July 2018 by a rainstorm. In June 2020 a fissure, a type of DSGSD, was found above the main scarp of the landslide by the field survey after a strong rainstorm, and after that the LiDAR measurement was performed in order to grasp the total feature of the DSGSD. Another landslide occurred along the fissure in July 2020. Another case study examined three landslides named A-, B-, and No.2-landslides in the Kuchisakamoto area, Shizuoka Prefecture. Countermeasures against the A-landslide started in 1960, and the activity has calmed down recently. The B-landslide started the active in 1988, and has been active until now in spite of the extensive countermeasures for more than 30 years. The No.2-landslide started the activity in 2013. Double ridges, one of the typical DSGSD landforms, occur on the crests or slopes above the three landslides. Although the development histories of these DSGSD features are unknown, we estimate that they formed several thousand years ago on the basis of our research results on the similar double ridges located about 10 km north of this area. The double ridges above the A- and B-landslides have no signs of deformations, though the landslide scarps have reached just below the ridges. The ground extensometer installed on the uphill-facing scarplet, also one of the typical DSGSD landforms, of the No.2-landslide have recorded no movements during the last six years. These lines of evidence indicate that the DSGSD topographies stable for many years have not affected by the landslide activities below them. We need standardization of this model by more case studies. The data used in this study were provided by Gifu and Shizuoka Prefecture offices.

Keywords: landslide, deep-seated gravitational slope deformation (DSGSD)

©2021. Japan Geoscience Union. All Right Reserved.

[J] Poster | H (Human Geosciences)：H-TT Technology & Techniques

Sat. Jun 5, 2021 5:15 PM - 6:30 PM JST | Sat. Jun 5, 2021 8:15 AM - 9:30 AM UTC | Ch.11_3

[H-TT18] Environmental Remote Sensing

convener:Naoko Saitoh(Center for Environmental Remote Sensing), Hitoshi Irie(Center for Environmental Remote Sensing, Chiba University), Hiroto Shimazaki(National Institute of Technology, Kisarazu College), Teppei Ishiuchi(Miyagi University)

Measuring environmental changes at various spatio-temporal scales is the key to improve our understanding of the relationship between human activities and environmental problems. Remote sensing is a powerful tool to acquire information on the earth's surface frequently and repeatedly over a broad spatial scale, enabling us to find the changes which might be related to the cause and consequence of environmental degradation. This session discusses the applications of remote sensing to the detection and monitoring of environmental changes in time and space, and aims to promote the knowledge-sharing for better management of the environmental problems and natural disaster in any place in the world.

[HTT18-P01] Feasibility of observations of middle and upper tropospheric and lower stratospheric ozone concentrations by GOSAT/TANSO-FTS

*Eito Seki[1], Naoko Saitoh[1] (1.Center for Environmental Remote Sensing, Chiba University)

[HTT18-P02] Data quality of GOSAT-2/TANSO-FTS-2 GHG profile data retrieved from the V102.102 radiance spectra

*Naoko Saitoh[1], Ryoichi Imasu[2], kei Shiomi[3] (1.Center for Environmental Remote Sensing, Chiba University, 2.Atmosphere and Ocean Research Institute, The University of Tokyo, 3.Japan Aerospace Exploration Agency)

[HTT18-P03] Land use and land cover change of illegal settlements by landless peasants in the Brazilian Amazon

*Sayaka Yoshikawa[1,3], Kanae Ishimaru[2] (1.Ibaraki university , 2.Fukui Prefectural University, 3.Tokyo institute of technology)

[HTT18-P04] Evaluation of heterogeneity in growth of black pines planted for artificial coastal forests in the Sendai Plain

*Takuto Kajiwara[1], Masayuki Kawahigashi[2] (1.Graduate Student of Tokyo Metropolitan University, 2.Tokyo Metropolitan University)

[HTT18-P05] Accounting for atmospheric factors to estimate photosynthetically active radiation from surface solar irradiance

*YAJIE DAI[1], Hitoshi Irie[1], Alessandro Damiani[1] (1.chiba university)

[HTT18-P06] Data-assimilation-based Estimation of Infectivity Parameter of COVID-19 Epidemic Model and its Relation to NO2 satellite observation.

*Osamu Kabayama[1], Okazaki Atsushi[2], Shunji Kotsuki[1] (1.Centre for Environment Remote Sensing, Chiba University, 2.The Pennsylvania State University)

[HTT18-P07] Changes in the NO2 weekly cycle under COVID-19 pandemic

*Alessandro Damiani[1], Hitoshi Irie[1], Saito Hikaru[1], Ying Cai[1], Dmitry Belikov[1], Raul R. Cordero[2] (1.CEReS, Chiba University, 2.Santiago de Chile University)

Feasibility of observations of middle and upper tropospheric and lower stratospheric ozone concentrations by GOSAT/TANSO-FTS

*Eito Seki[1], Naoko Saitoh[1]

1. Center for Environmental Remote Sensing, Chiba University

Ozone vertical profiles are simultaneously retrieved from thermal infrared (TIR) spectra observed with Thermal and Near infrared Sensor for Carbon Observation (TANSO)- Fourier Transform Spectrometer (FTS) on board Greenhouse Gases Observing Satellite (GOSAT) in the data processing of the Version 1 CO_2 product [Saitoh et al., 2016]. Focusing on polar regions where severe ozone depletions occur, we have analyzed characteristics of the TANSO-FTS ozone profiles and compared them with ozone data obtained with Atmospheric Chemistry Experiment (ACE)-FTS on board SciSat-1, which is a solar occultation sensor with higher vertical resolutions, for validating the TANSO-FTS ozone data.

First, we selected TANSO-FTS ozone data obtained in the latitude range of 70˚N–80˚N from 2009 to 2014 and calculated zonal means for each 10-day period for each month. We found that TANSO-FTS ozone concentrations in lower stratosphere (35–29 hPa) in February and March in 2011, when large-scale ozone destructions occurred, were significantly lower than ozone concentrations of a priori data used in the TANSO-FTS retrieval processing [McPeters et al., 2007] and lowest of the other years.

Next, we calculated averages of the TANSO-FTS ozone concentrations for each 15˚ longitude for shorter period in the northern high latitudes in 2011, and analyzed the ozone data by dividing them into the two regions: ozone-depleted region and no ozone-depleted region. The area of ozone depletion was determined from ozone column data of Ozone Monitoring Instrument (OMI) on board AURA; here, the region in the longitude of 0˚ to 30˚E from March 26 to 31, 2011 was selected as the “ozone-depleted region” because severe ozone depletions were continuously observed there. TANSO-FTS ozone concentrations were much lower than the a priori concentrations in the ozone-depleted region, while TANSO-FTS ozone concentrations were in contrast closer to the a priori data in the no ozone-depleted region. We then compared TANSO-FTS ozone data with SciSat-1/ACE-FTS ozone data in northern high latitudes (60˚N–70˚N) in 2011. Comparison results showed that the TANSO-FTS ozone concentrations were closer to the SciSat-1/ACE-FTS ozone concentrations than the a priori concentrations in the lower stratosphere (around 60-20 hPa) in the ozone-depleted region, which could demonstrate the possibility of capturing a detailed structure of ozone depletion in the polar lower stratosphere by the TIR band of GOSAT/TANSO-FTS.

Keywords: GOSAT, TANSO-FTS, ozone, Arctic ozone depletion

©2021. Japan Geoscience Union. All Right Reserved.

Data quality of GOSAT-2/TANSO-FTS-2 GHG profile data retrieved from the V102.102 radiance spectra

*Naoko Saitoh[1], Ryoichi Imasu[2], kei Shiomi[3]

1. Center for Environmental Remote Sensing, Chiba University, 2. Atmosphere and Ocean Research Institute, The University of Tokyo, 3. Japan Aerospace Exploration Agency

Greenhouse Gases Observing Satellite-2 (GOSAT-2), the successor of GOSAT launched in 2009, was successfully launched on 29th October, 2018 and started its regular operation on 1st February, 2019. Thermal infrared (TIR) bands of Thermal and Near Infrared Sensor for Carbon Observation-Fourier Transform Spectrometer-2 (TANSO-FTS-2) on board the GOSAT-2 can provide information on vertical structures of GHG concentrations and temperature in the atmosphere [Saitoh et al., 2009, 2016].

We have retrieved GHG concentrations and temperature in several atmospheric layers (up to 30 layers) from the TIR bands of GOSAT-2/TANSO-FTS-2 by adopting a non-linear maximum a posteriori (MAP) method with linear mapping. In the retrieval processing, we used the Level 1B V102.102 radiance spectra of TANSO-FTS-2. We have used 9, 10, and 15 μm bands for CO_2, O_3, and temperature retrieval and 7 and 8 μm bands for CH_4, N_2O, and H_2O retrieval, basically following the GOSAT/FTS TIR algorithm [Saitoh et al., 2009, 2016]. We have taken into account the EOF components of spectral residuals and simultaneously retrieved surface parameters. As the signal-to-noise ratio (SNR) values of the TIR bands of TANSO-FTS-2 are significantly larger than those of TANSO-FTS, we can expect TANSO-FTS-2 to observe greenhouse gases concentrations with higher accuracy and precision.

Retrieved CO_2, CH_4, and N_2O concentrations showed reasonable latitudinal gradients over the ocean. Over the land, the retrieved CH_4 and N_2O concentrations had larger variabilities than expected; they clearly had positive biases over the Sahara, which could be attributable to the inappropriate setting of surface emissivity there in the retrieval processing.

Keywords: satellite remote sensing, GHG, retrieval algorithm

©2021. Japan Geoscience Union. All Right Reserved.

Land use and land cover change of illegal settlements by landless peasants in the Brazilian Amazon

*Sayaka Yoshikawa[1,3], Kanae Ishimaru[2]

1. Ibaraki university , 2. Fukui Prefectural University, 3. Tokyo institute of technology

In Legal Amazon, land use and land cover changes have been reported to occur over large areas due to the introduction of large-scale mechanized agriculture, extensive cattle ranching and uncontrolled slash-and-burn cultivation since the 1980s. Around the same time, movements which landless peasants (or poor people) settle into abandoned land have been very active in Brazil. In many cases, these people lack agricultural experiences to yield sufficient production for livelihoods. Thus, it leads to abandon the land and repeat forest clearance. In this study, we specifically aimed at clarifying changes in land use and land cover using ground observation data, remote sensing (Geo-Eye-1) data and GIS techniques. We focus on two different settlements: established settlement (30 years) and productive settlement (14 years). These settlements were located at Santa Barbará province, about 40 km northeast from the center of Belé m, the Pará state capital, in the northern part of Brazil. This research is motivated by the following three questions: i) How much forest areas have disappeared due to the activities of landless peasants? ii) Can they get compliance with Brazilian Forest Code? iii) How much are agricultural lands developed? For the answering these questions, we clarified changes in land use and land cover under five approaches which employs original spectral data and lacunarity index.

Keywords: Amazon deforestation, Agrarian settlements by landless peasants, Lacunarity Index

©2021. Japan Geoscience Union. All Right Reserved.

Evaluation of heterogeneity in growth of black pines planted for artificial coastal forests in the Sendai Plain

*Takuto Kajiwara[1], Masayuki Kawahigashi[2]

1. Graduate Student of Tokyo Metropolitan University, 2. Tokyo Metropolitan University

1. Introduction
The 2011 tsunami caused by the Great East Japan Earthquake hit the coastal area, resulting in fatal damage to the black pine coastal forest in the Sendai Plain, which has been developed since the 17th century. Although the Forestry Agency immediately launched a coastal forest restoration project in the damaged area after the tsunami, there were many drawbacks to grow plants, such as high salinity due to seawater inundation and high groundwater level. The Forestry Agency constructed an embankment to raise basement for planting using excavated soil from the hilly areas surrounding the Sendai Plain. Seedlings of black pines planted on the basement showed uneven growth rates in the area after several years. Since the constant growth of trees has been required to function as embankment for alleviation of tsunami impact, negative factors should be urgently removed to promote their satisfactory growth. The present growth condition was evaluated by the normalized difference vegetation index (NDVI) calculated by satellite images.
2. Research method
The survey site was set in the Arabama Coastal Forest, Wakabayashi-Ku, Sendai City, Miyagi Prefecture. Totally 35 plots with different planting years were targeted to calculate NDVI. The NDVI value was calculated from satellite images taken by Sentinel-2 on 20 August, 2020. Distribution of NDVI values was mapped using ArcMap 10.5.1. The range of NDVI values in each planting plot was estimated by the kernel density estimation, which is an algorithm to estimate a probability density by extrapolating data of finite samples, based on the NDVI values of all pixels. Statistical significance for differences in normality, homoscedasticity, and mean values was evaluated to compare the non-uniformity of the growth status at each site.
3. Results and Discussion
There were statistically significant differences in NDVI values between planting plots established in the same year, indicating that different growth rate of black pines even under same growth condition. Again, the spatial distribution of NDVI differed depending on planting plots and the growth of the black pine varied even in the same plot with same planting year. Since there is no difference in the climatic conditions, such as sunshine and precipitation between planting plots, the differences in the growth of black pine could be growth factors in soil affected by microtopography and micro-scale variation in soil. Therefore, constant and detail surveys are necessary to elucidate the cause of the growth differences in black pines.

Keywords: satellite image, vegetation index, tree planting, embankment materials

©2021. Japan Geoscience Union. All Right Reserved.

Accounting for atmospheric factors to estimate photosynthetically active radiation from surface solar irradiance

*YAJIE DAI[1], Hitoshi Irie[1], Alessandro Damiani[1]

1. chiba university

Photosynthetically active radiation (PAR) is the energy source for organic matter production in plants. To analyze the long-term PAR changes where no proper PAR data are available, it has been proposed to build the long-term PAR data set using the ratio of PAR to surface solar irradiance (SSI) (PAR/SSI). However, the PAR/SSI is affected by local atmospheric factors. Particularly, the identification of weather conditions is necessary to estimate PAR, but accurate cloud segmentation is challenging. We propose a simple methodology to distinguish clear sky, overcast, and partial cloudy conditions. We exploited the broad range of meteorological instruments available at the SKYNET super site of Chiba University (Japan) to develop a reconstruction method accounting for the atmospheric factors more accurately than previous methods based on annual or monthly averages of PAR/SSI. Using high-temporal-resolution data, we optimized our PAR estimation under clear sky, overcast, and partial cloud conditions. Then, we achieved that the average deviation of the estimated PAR from the quantum sensor PAR-01D is less than 10% when the solar zenith angle is small. This study is expected to make more PAR data available, providing a basis for understanding the impact of microclimate changes on plant photosynthesis.

Keywords: Photosynthetically active radiation, the ratio of PAR to surface solar irradiance, atmospheric factors, identification of weather conditions

©2021. Japan Geoscience Union. All Right Reserved.

Data-assimilation-based Estimation of Infectivity Parameter of COVID-19 Epidemic Model and its Relation to NO2 satellite observation.

*Osamu Kabayama[1], Okazaki Atsushi[2], Shunji Kotsuki[1]

1. Centre for Environment Remote Sensing, Chiba University, 2. The Pennsylvania State University

With COVID-19 spreading around the world, it is necessary to understand the relationship between its infectivity and political decisions. This study uses data assimilation techniques and satellite observations to clarify the relevance. First, modified epidemiological model based on a commonly used compartment model is developed. The model assigns population into five compartments, Susceptible, Exposed, Infectious, Recovered, and Death (here after SEIRD model). In contrast to influenza epidemics, daily reports of deaths are issued by governments in COVID-19 outbreak. Therefore, Death compartment is explicitly separated to utilize the observation information. Ensemble data assimilation of SEIRD model revealed that the time series of infectivity of COVID-19 corresponded with political decisions such as the lockdowns, economic activity resume in the United States and economic restraints in Japan. In addition, satellite observations of NO2 also imply the economic restraint in Japan. We are now investigating the relationship between infectivity and political decisions based on estimated infectivity parameter of SEIRD and NO2 satellite observations. This presentation will include the most recent progress up to the time of the conference.

Keywords: COVID-19, NO2 satellite observation, mathematical epidemic model, Ensemble Data Assimilation, Data Assimilation

©2021. Japan Geoscience Union. All Right Reserved.

Changes in the NO2 weekly cycle under COVID-19 pandemic

*Alessandro Damiani[1], Hitoshi Irie[1], Saito Hikaru[1], Ying Cai[1], Dmitry Belikov[1], Raul R. Cordero[2]

1. CEReS, Chiba University, 2. Santiago de Chile University

Urban nitrogen dioxide (NO_2) concentrations arise from anthropogenic activities, mainly from traffic sources. In Chiba and Tsukuba cities, within the Great Tokyo Region (GTR, Japan), partial column MAX-DOAS (Multi-Axis Differential Optical Absorption Spectroscopy) NO_2 observations (at 0-1 km) usually show a reduction of about 45-50 %, compared with the business days, during the end of the year holiday season. Corresponding ozonesonde observations carried out in a close location showed enhanced ozone (O_3) concentrations during holiday peaking at the surface (+15 %) and decreasing with the altitude. This suggests that titration processes, under saturated NO_2 conditions, usually occur in the investigated urban region and affect the surface and the lowest atmospheric layers. Keeping this in mind, we examined the so-called weekend effect in MAX-DOAS NO_2. We noted that its extent is getting smaller over the last years, characterized by decreasing NO_2 trends. An evident exception occurred in 2020 when the strongest weekend effect on records has been recorded. This was confirmed by S5P/TROPOMI NO_2 observations showing a weekend effect in 2020 clearly larger than in 2019 over the GTR. In this talk, we will put such findings into context by analyzing the changes in other large urban areas both in Japan and abroad (e.g., US, Europe, South America). We will then examine the results in light of the different responses of the population to COVID-19 as view in mobility data, changes in meteorology, and recent results pointing to enhanced surface ozone during lockdowns.

Keywords: Remote sensing, Tropospheric gases, NO2, O3

©2021. Japan Geoscience Union. All Right Reserved.

[J] Poster | H (Human Geosciences)：H-CG Complex & General

Sat. Jun 5, 2021 5:15 PM - 6:30 PM JST | Sat. Jun 5, 2021 8:15 AM - 9:30 AM UTC | Ch.12_2

[H-CG23] Nuclear Energy and Geoscience

convener:Eiji Sasao(Tono Geoscience Center, Japan Atomic Energy Agency), Shinji Takeuchi(Department of Earth and Environmental Sciences, College of Humanities & Sciences, Nihon University), Takuma HASEGAWA(Central Research Institute of Electric Power Industry)

Peaceful use of nuclear power is one of the most promising ways to solve energy problems and environmental problems. On the other hand, various problems are upcoming after nuclear disasters of Fukushima-Daiichi Nuclear Power Plant. The session provides a forum to deal with various aspects of scientific and engineering aspects of nuclear power. The session in this year focuses on radioactive waste disposal and covers not only scientific aspect such as characterization of geological environment but also engineering aspects such as microbe-nuclide, mineral-water, and cement-water interactions. In addition to this, themes on seismic hazards at nuclear facilities, environmental behavior of radionuclides emitted from nuclear power plants, and volume reduction and reuse of cesium contaminated soils are welcomed. Through these presentations, we promote intercultural communication and collaboration between science, engineering and social science.

[HCG23-P01] Modeling of Radial Dikes by Topographical Analysis using GIS for Quaternary Volcanoes

Yuki Hiura[1], *Makoto Kawamura[1], Umeda Koji[2], Masakazu Niwa[1] (1.Japan Atomic Energy Agency, 2.Hirosaki Univ.)

[HCG23-P02] Three-dimensional resistivity distribution by magnetotelluric survey to evaluate the distribution of fossil seawater

*Naomi Satoh[1], Akira Hayano[1], Minoru Teshima[2], Tateyuki Negi[2], Terumasa Yamane[3], Shinji Kawasaki[3] (1.Japan Atomic Energy Agency, 2.Nittetsu Mining Consultants Co., Ltd., 3.JGI, Inc.)

[HCG23-P03] Microbial community analysis of deep-seated fluids: Do microbes live in slab-derived fluid?

*Ayumi Sugiyama[1,2], Yuichi Tomioka[1], Shin-ichi Hirano[1], Tokihiro Kurita[1] (1.Central Research Institute of Electric Power Industry, 2.Asano Taiseikiso Engineering Co., Ltd.)

[HCG23-P04] Constructions of hydrogeological structure and mass transport model around hydraulic conductive fractures

*Ai Hamada[1], Kimio Miyakawa[1], Yasuharu Tanaka[1] (1.Central Research Institute of Electric Power Industry)

[HCG23-P05] Development of multi-scale modeling for estimation of inflow volume into tunnels of the geological disposal facility

*Naoki Katsumata[1], Satoru Suzuki[1], Hiromitsu Saegusa[1], Tatsuya Tanaka[2], Yoshito Kitagawa[1] (1.Nuclear Waste Management Organization of Japan, 2.OBAYASHI CORPORATION)

[HCG23-P06] Introduction of the “KiNa” international project of natural analogue studies of the long-term stability of bentonite

*Satoru Suzuki[1], Tsutomu Sato[2], Tsubasa Otake[2], Kikuchi Ryosuke[2], Fujimura Tatsuya[2], Takahiro Goto[1], Yusuke Ogawa[1], Patrik Sellin[3], Daniel Svensson[3], Albert H. Gilg[4], Ulf B. Andersson[5], Elizaveta Klein[6], Olivier X. Leupin[6], Simon Norris[9], Russell W. Alexander[10], Mehran Behazin[7], Nicolas Michau[8] (1.Nuclear Waste Management Organization of Japan , 2.Hokkaido University, 3.SKB, 4.TU Munich, 5.Luossavaara-Kiirunavaara AB, 6.Nagra, 7.NWMO, 8.ANDRA, 9.RWM, 10.Bedrock Geosciences)

[HCG23-P07] Interaction at the interface between compacted bentonite and carbon steel plate in artificial seawater

*Tatsuya Fujimura [1], Tsutomu Sato[2], Tsubasa Otake[2], Kikuchi Ryosuke[2], Satoru Suzuki[3], Takahiro Goto[3]
(1.Graduate School of Engineering, Hokkaido University, 2.Faculty of Engineering, Hokkaido University, 3.Nuclear Waste Management Organization of Japan)

Modeling of Radial Dikes by Topographical Analysis using GIS for Quaternary Volcanoes

Yuki Hiura[1], *Makoto Kawamura[1], Umeda Koji[2], Masakazu Niwa[1]

1. Japan Atomic Energy Agency, 2. Hirosaki Univ.

One of the technical issues related to volcanic and igneous activities is the sophistication of technology for grasping the range of influence of magma. To address this issue, it is important to accumulate survey cases, especially when the dike develops over a radius of 15 km from the center of the Quaternary volcano, but it lies beneath the existing volcanic body. It is practically difficult to grasp the distribution of the conduits and the dikes derived from them. Therefore, the purpose of this study was to develop a method for estimating the distribution range of dikes distributed under the Quaternary volcanic body based on topographical data such as digital elevation models. In this study, we used digital maps and GIS software to target six volcanoes, such as stratovolcanoes and calderas. The parameters were measured, and modeling of the three-dimensional distribution range of radial dikes was examined from each parameter for each altitude. As a result, the transition of the center of gravity position for each altitude suggests the transition of the center of activity in the process of forming the volcanic body to some extent, and it is possible to extract not only the activity of the central crater but also the activity of lateral volcanoes. This suggests the possibility of quantitative evaluation of the transition and stability of the conduit even in volcanoes whose activity history is not clear by applying this method.

Keywords: Quaternary Volcanoes, Volcanic Conduit, Radial Dikes, Topographical Analysis, GIS

©2021. Japan Geoscience Union. All Right Reserved.

Three-dimensional resistivity distribution by magnetotelluric survey to evaluate the distribution of fossil seawater

*Naomi Satoh[1], Akira Hayano[1], Minoru Teshima[2], Tateyuki Negi[2], Terumasa Yamane[3], Shinji Kawasaki[3]

1. Japan Atomic Energy Agency, 2. Nittetsu Mining Consultants Co., Ltd., 3. JGI, Inc.

Introduction

The hydrological regime with “a slow groundwater movement that minimizes the transport of radioactive materials” is considered one of the most suitable geological conditions in the site selection of the geological disposal of high-level radioactive waste [1]. Fossil seawater is groundwater whose composition has been altered during the burial diagenetic process but has not been affected by the infiltration of meteoric fresh water [2]. Its presence indicates that the groundwater movement of the area is sufficiently slow. Thus, developing a workflow in the geological disposal project for investigating the distribution of fossil seawater is essential to determine where groundwater movement is sufficiently slow.
This study reports the preliminary results of the magnetotelluric (MT) survey aiming to evaluate the three-dimensional distribution of fossil seawater in the Horonobe area that is composed of the Neogene sedimentary rocks. Moreover, fossil seawater is characterized by high salinity. Consequently, the low resistive domain obtained by the MT survey can provide information about its distribution [3]. The audio-magnetotelluric (AMT) survey, where the depth of exploration is shallow, was applied in most of the previous electromagnetic surveys conducted in the Horonobe area. This study applied the MT survey, which can explore the deeper layers with high accuracy, to improve the resolution of fossil seawater distribution.

Materials and methods

The survey was conducted in a 9-km^2 area adjacent to the Horonobe Underground Research Laboratory of Japan Atomic Energy Agency. Moreover, 60 points were arranged in a grid pattern within the area to effectively estimate the three-dimensional distribution of fossil seawater. Consequently, the MT data were obtained at each point. In the three-dimensional inversion, 99 points including 39 existing points were used to estimate the resistivity distribution.

Results and future perspective

The overall distribution of resistivity was generally low, consistent with the geology of the Horonobe area, which consists mainly of mudstone and shale. However, resistivity appeared to vary following the geological structure. The resistivity was relatively high (>10 Ω-m) until 50 m in depth, while it was relatively lower (1–5 Ω-m) at a depth of 50–1,000 m. The area adjacent to the Omagari Fault showed higher resistivity compared to the surrounding area, suggesting the infiltration of meteoric fresh water preferentially along the Omagari Fault similar to the previous AMT survey [4]. The Yuchi Formation, an upper stratum distributed to the southwest part of the survey area, also showed high resistivity, which may be due to the groundwater recharge.
Examining a more optimal resistivity distribution considering the geological structure is necessary for future work. Furthermore, the integration of the MT survey with borehole investigations is a critical issue to estimate the three-dimensional distribution of fossil seawater.

This study was conducted as a part of the project on “FY2020 Development and Improvement on groundwater flow evaluation technic in rock” funded by the Japanese Ministry of Economy, Trade and

©2021. Japan Geoscience Union. All Right Reserved.

Industry.

[1] Nuclear Waste Management Organization of Japan, 2011, NUMO-TR-13-05.
[2] Muramatsue et al., 2016, J. Hot Spring Sci., 65, 216-233.
[3] Mizuno et al., 2017, 58, 178-187.
[4] Ishii et al., 2006, Jour. Geol. Soc. Japan, 112, 301-314.

Keywords: Fossil seawater, Magnetotelluric survey, Neogene sedimentary rock, Geological disposal

©2021. Japan Geoscience Union. All Right Reserved.

Microbial community analysis of deep-seated fluids: Do microbes live in slab-derived fluid?

*Ayumi Sugiyama[1,2], Yuichi Tomioka[1], Shin-ichi Hirano[1], Tokihiro Kurita[1]

1. Central Research Institute of Electric Power Industry, 2. Asano Taiseikiso Engineering Co., Ltd.

Microbes are present under various environments and their distribution in the subsurface environment extend for several kilometers. The distribution of microbes in the environment reflects environmental conditions such as temperature, pH, nutrients. Understanding the microbial community in the groundwater might be elucidated the origin of groundwater and difference in the groundwater flow paths. However, little is known the microbial communities in slab-derived fluid, which is characterized by high temperature, high salinity and high CO_2 concentration. In this study, we analyzed the microbial community in groundwater, which is considered to be contribution of slab-derived water, and examined whether the origin and mixing of groundwater could be estimated from microbial analysis.

The 11 groundwater samples were collected from hot and cold springs at different locations. The temperature measured at the outflows ranged from 7.4°C to 41.2°C. The value of pH and the electric conductivity ranged from 6.26 to 8.14, from 129 mS/m to 5050 mS/m, respectively. The density of microbes ranged from 2.2 x 10^3 cells/mL to 9.3 x 10^5 cells/mL. 16S rRNA gene sequencing, 110,000 to 390,000 reads were obtained, and they belonged to 44 to 56 phyla. The relative ratio of archaea, which mainly live in extreme environments, accounted for 0.2% to 17.4%. At all sites, *Methanomicrobia*, *Methanobacteria* and *Methanococci* dominated. In some samples, hyper-thermophilic archaea, *Archaeoglobi* and *Thermococci*, and highly halophilic archaea, *Halobacteria*, were detected. The detection of these hyper-thermophilic and highly halophilic microbes suggests that the examined groundwater experienced a high temperature and high salinity environment, and the contribution of slab-derived water as the origin of the groundwater could be considered. We will perform further analysis and examine the possibility of evaluating the origin and mixing of groundwater using microbes.

This study was funded by the Ministry of Economy, Trade and Industry, Japan as part of its R&D supporting program titled “Establishment of Advanced Technology for Evaluating the Long-term Geosphere Stability on Geological Disposal Project of Radioactive Waste (FY 2020).

Keywords: density of microbes, next generation sequencing, deep-seated fluids, slab-derived fluid

©2021. Japan Geoscience Union. All Right Reserved.

Constructions of hydrogeological structure and mass transport model around hydraulic conductive fractures

*Ai Hamada[1], Kimio Miyakawa[1], Yasuharu Tanaka[1]

1. Central Research Institute of Electric Power Industry

In geological disposal of high-level nuclear waste, hydraulic conductive fractures in crystalline rock such as granite have been considered as a main pathway for radionuclides. Diffusion and absorption of radionuclide through microstructure in rock matrix can make mass transport to retard. Because the change of the characteristics of microstructure in rock matrix by structural movement and hydrothermal alteration have an effect on mass transport, it is important to understand hydrogeological continuity of fractures as well as their porosity and mass transfer characterizations by field survey and laboratory test and moreover to construct hydrogeological structure and mass transport model around hydraulic conductive fractures by reflecting their parameter from physical property values. For the purposes of effectiveness evaluation of technological development for estimating the interstitial structure of hydraulic conductive fractures in Japan, we have conducted the advancement of hydraulic fracture investigation methods for Toki granite of Mizunami Underground Research Laboratory of JAEA. In this study, we focus on hydraulic fractures of the western part around GL −300 m Measurement Niche off Ventilation Shaft and suggest that hydraulic geological structure and mass transfer model and their parameters for groundwater flow / nuclide migration analysis taking into account for nuclide diffusion / sorption behavior based on in-situ resin infiltration tests and diffusion and sorption tests.

In the rock around GL −300 m Measurement Niche off Ventilation Shaft, on the west side, NW fractures with hydrogeological continuity form higher-permeability zone through low dip angle fractures (Hamada, 2019). The hydraulic conductive fractures across multiple boreholes to the west sides, which were recognized as resin infiltrated fractures, mainly show NW fracture. They are open along cataclastic vein texture which consists of fractured rock-forming minerals, with euhedral calcite crystals between the surfaces of fracture. From the composition analysis by EPMA, minerals consisting of cataclastic vein texture do not include secondary minerals. It is considered that NW strike fractures were formed by opening along weak lines of the surface of the cataclastic vein structures after crustal movement, which were granulated by the grinding action. Low dip fractures are universally distributed at this depth and euhedral calcite crystals developing between fracture surfaces were thought to be originated from freshwater because of C-axis developing (Folk, 1974). From these, low dip fractures were formed by uploading after granite ascending and filled with euhedral crystals of calcite formed after the intrusion of surface water.

Based on the characteristics of hydraulic fractures as described above, we suggest mass transport models for analyzing groundwater flow / nuclide migration through mainly single fracture model in crystalline rock as follows. From both macroscopic and polarizing microscope observation of core samples, we recognized the traces of past shear activity and hydrothermal alteration in the range from the fracture surface (0 mm) to 30 mm in depth. From the results of laboratory tests (diffusion test, sorption batch test focusing on mineral ratio), the porosity is generally larger near the fracture surface within this range, and the porosity becomes smaller as the distance from the fracture surface increases, resulting in an effective diffusion coefficient. The partition coefficient seemed to change according to the amount of secondary minerals, especially sericite, contained in each matrix around the fracture. In the conceptual model proposed from this, the mass transfer parameters obtained from the laboratory test are set for the range from the fracture surface to 30 mm for each width of 10 mm from the fracture surface. The region separated from the fracture surface by 30 mm or more is considered appropriate to introduce the value of non-alteration rock

©2021. Japan Geoscience Union. All Right Reserved.

as a reference value.
This study is commissioned by the Agency for Natural Resources and Energy in the Ministry of Economy, Trade and Industry. Core sampling were conducted as a part of a collaborative research with JAEA.

Keywords: geological disposal, hydrogeological structure, hydraulic conductive fracture, Toki granite, Mizunami Underground Research Laboratory, mass transport model

©2021. Japan Geoscience Union. All Right Reserved.

Development of multi-scale modeling for estimation of inflow volume into tunnels of the geological disposal facility

*Naoki Katsumata[1], Satoru Suzuki[1], Hiromitsu Saegusa[1], Tatsuya Tanaka[2], Yoshito Kitagawa[1]

1. Nuclear Waste Management Organization of Japan, 2. OBAYASHI CORPORATION

During the construction and operation of underground tunnels for geological disposal, groundwater inflow into the tunnels may occur. It is necessary to drain the inflow of groundwater to the ground surface. In case if inflow volume is large, the hydrochemical environment around the tunnel may be disturbed by up-corning the deeper water such as brine and/or drawing in the near surface water into the disposal depth. Therefore, it is important to estimate the inflow volume and to prepare measures to effectively reduce the inflow volume, prior to the construction of the underground tunnels. We therefore developed a method for estimation of inflow volume into the tunnels and effect of its decrease by applied countermeasures.

We developed the hydrogeological model for plutonic rocks, Neogene sedimentary rocks, and pre-Neogene sedimentary rocks, which are widely distributed in Japan and the modeled areas have suitable features for geological disposal. In this report, an application of our evaluation method of estimating inflow volume to the plutonic rocks model is reported.

In the case of Plutonic rocks, faults and fractures are to be characterized during site investigations since these may be the major pathway of groundwater flow. In order to develop a hydrogeological model, distribution of faults and fractures, and their transmissivity were stochastically generated using the discrete fracture network method. The hydrogeological model is composed of two different domains with different discretized mesh size; a repository scale (set to 5 km x 5 km x 1.5 km) including the underground tunnels, which is for modeling detail hydraulic heterogeneity, and a regional scale (set to 50 km x 50 km x 5 km) for setting hydraulic boundary conditions for the repository scale model.

Underground tunnels will be placed in an area where safety can be ensured during the construction, operation and after closure, taking into consideration of properties of the host rocks and distribution of the faults and fractures at the targeted depth. During construction and operation, disposal zones are divided into the ones for construction and the one for operation, and the works are carried out in parallel. It is thus important that the safety of workers is ensured in both zones. For example, there is a possibility of having abnormally large inflow when high conductive fault and tunnel are intersected each other. In order to lower the risk, the disposal zone in which many disposal tunnels are lined up in parallel should not be located where a water-conductive fault exists and the zones for construction and operation are not directly connected to avoid potential interactions, e.g. large amount of water flows in each other.

In this study, inflow volumes considering several types of tunnel layouts were estimated. As results, inflow volume into the access tunnels, which connects from surface to underground, was the largest and inflow volume into the disposal tunnels were relatively small. The reason of this result is analyzed that the disposal tunnels are located in parallel, thus local drawdown of the water table occurred around these tunnels, which result in the inflow volume is smaller than that evaluated for a single disposal tunnel. On the other hand, the access tunnel was open throughout the period of construction and operation, so the inflow volume was relatively large. The measures for reducing inflow volume such as grout at the access tunnel are effective.

©2021. Japan Geoscience Union. All Right Reserved.

The key-finding of this study was that the developed multi-scale modeling method is effective in estimating the groundwater inflow volume taking into account variation of tunnel layouts and application of measures of water inflow control. As further R&D, we are also trying to apply this method to estimate how the hydro-chemical environment changes with groundwater inflow during construction and operation of the repository.

©2021. Japan Geoscience Union. All Right Reserved.

Introduction of the “KiNa” international project of natural analogue studies of the long-term stability of bentonite

*Satoru Suzuki[1], Tsutomu Sato[2], Tsubasa Otake[2], Kikuchi Ryosuke[2], Fujimura Tatsuya[2], Takahiro Goto[1], Yusuke Ogawa[1], Patrik Sellin[3], Daniel Svensson[3], Albert H. Gilg[4], Ulf B. Andersson[5], Elizaveta Klein[6], Olivier X. Leupin[6], Simon Norris[9], Russell W. Alexander[10], Mehran Behazin[7], Nicolas Michau[8]

1. Nuclear Waste Management Organization of Japan , 2. Hokkaido University, 3. SKB, 4. TU Munich, 5. Luossavaara-Kiirunavaara AB, 6. Nagra, 7. NWMO, 8. ANDRA, 9. RWM, 10. Bedrock Geosciences

Disposal of high level radioactive waste is based on multi-barrier systems, where the barriers are supposed to retain their properties for hundreds of thousands of years. To demonstrate long term stability, experimental results can be complemented with the studies of natural systems (Natural Analogues). Bentonite is a common barrier material in many repository concepts and the aim of this natural analogue project is to assess the long-term behaviour of bentonite and its interaction with iron-minerals at the repository-like conditions.
Significant clay alteration zones have been encountered in the Kiruna (Lapland, Sweden) magnetite(-hematite)-apatite deposits, which are hosted in weakly to strongly metamorphosed intermediate to acid volcanic and subvolcanic rocks. These up to 50 m thick soft clay alteration zones occur within ores and within the country rocks along the ore contact of the southern parts of the Kiirunavaara ore body. They are found at various levels to depths of at least 1200 m below the surface, in zones further into the hanging wall and footwall lithologies of the deposit. The predominant clay mineral in the alteration zones of all deposits is a dioctahedral Fe-poor montmorillonite (Rieger 2017). K-Ar data of various Na-exchanged size fractions from two clay-altered gneiss samples from the nearby Johannes ore body, Malmberget, which are dominated by R3-ordered illite-smectite, yield age values ranging from 837 ±14 Ma to 941 ±15 Ma (Gilg et al. 2017, Rieger 2017).
In many respects, the clay layers in the Kiruna deposits resembles a bentonite barrier in a repository: the clay layers are in the meter scale, the surrounding is fractured rock under the water table and the magnetite could serve as an analogue for an iron corrosion product. A project has been initiated to further study the Kiruna clay with focus on:
geological site description and genesis of smectite-dating, mineralogical and chemical investigation understanding the very long-term behavior of bentonite under conditions of direct relevance to deep geological disposal; examination of long-term iron oxide minerals - bentonite interaction; the potential erosion properties of bentonite; and Microbiological investigation.
NUMO-Hokkaido University Joint Team is now responsible for mineralogical and geochemical investigations of iron oxide-bentonite interactions. So far, preliminary investigations have confirmed a high degree of montmorillonite, a substantial swelling pressure at high dry density, a low hydraulic conductivity and somewhat surprisingly low interaction with the magnetite.

References

Gilg HA, Rieger P, Wampler JM, Andersson UB (2017) Origin of clays in Kiruna-type iron ore deposits, Sweden. Living Clays: Clay Minerals Society Meeting, June 5th, 2017, NAIT, Edmonton, Alberta, Canada. Conference abstracts p. 22.
Rieger P (2017) Low-temperature alteration in the iron ore deposits of Norrbotten, Sweden. Master thesis. Ludwig-Maximilians University Munich, Germany, 100 pp.

©2021. Japan Geoscience Union. All Right Reserved.

Keywords: Benotnite, Iron ore, Natural Analogue

©2021. Japan Geoscience Union. All Right Reserved.

Interaction at the interface between compacted bentonite and carbon steel plate in artificial seawater

*Tatsuya Fujimura [1], Tsutomu Sato[2], Tsubasa Otake[2], Kikuchi Ryosuke[2], Satoru Suzuki[3], Takahiro Goto[3]

1. Graduate School of Engineering, Hokkaido University, 2. Faculty of Engineering, Hokkaido University, 3. Nuclear Waste Management Organization of Japan

Geological disposal of high-level radioactive waste is definitely based on multi-barrier system. The barrier system will be composed many kinds of materials such as borosilicate glass, stainless steel, carbon steel, bentonite, rock and so on. Whereas previous studies have aimed to understand respective longevity and alteration of materials, understanding of the interaction between the constituent materials in multi-barrier system is crucial for long-term safety assessments of the disposal. In this context, iron-bentonite interaction has been studied to understand alteration of bentonite by interaction with iron materials. According to some of the previous studies, montmorillonite, main constituent mineral of bentonite was changed to non-swelling clay minerals such as berthierine, iron-serpentine. Of course, this mineralogical change was clearly one of results due to the iron-bentonite interaction. However, it is not available to be assumed berthierinization for mineralogical evolution at the interface because this alteration was observed in the experiment in the system by using deionized water, powder bentonite and powder or fibrous iron to accelerate reaction, which is completely different from real situation at the interface in multi-barrier system.

This study focuses on interaction at the interface between compacted bentonite and carbon steel plate in artificial seawater to observe the alteration of minerals in the bentonite and the extent of alteration at the interface. Interface of the sample immersed in artificial seawater for three years at 80˚C under anaerobic condition was target for analyses by XRD, SEM-EDS, TEM-EDS and EPMA.

Color of the bentonite contacted with carbon steel plate was change from gray to black during the immersion in artificial seawater. Therefore, it can be easily recognized the area occurring some chemical reactions between two materials. In this area, migration of constituent element in the iron plate such as Fe and Mn into the bentonite was observed by SEM-EDS and EPMA. However, non-swelling clay minerals such as serpentine, kaolinite and chlorite were not observed based on XRD analysis. Montmorillonite was still survived in the altered area, even though small change of 060 reflection in the XRD pattern was observed, indicating change in octahedral chemistry of the montmorillonite. On the contrary, several metal carbonates such as siderite, calcite and rhodochrosite were observed in the altered area. From SEM-EDS analysis, dissolved iron reached 700 mm away from the carbon steel plate. According to iron depth profile from the line analysis, the apparent diffusion coefficient of Fe was estimated to be $3.59\times10^{-16}m^2/s$, which was clearly smaller than that obtained in previous studies for compacted bentonite (Arima et al., 2004 and Kozaki et al., 1995). Observations by electron microscopes showed formations of solid solution carbonate phases consisting Fe, Mn, Mg, Ca and Cr in the area around 100 mm away from the carbon steel plate and Fe-rich montmorillonite. The smaller apparent diffusion coefficient may be attributed to the secondary Fe-carbonate formations at the interface. Observations by electron microscopes also showed Cl ion concentrated area just at the interface. Thus, the reaction and mineralogical evolution at the interface between compacted bentonite and carbon steel plate in artificial sea water were completely different from the previous studies. Further studies including geochemical reaction and transport modeling are necessary to reproduce the above observed phenomena and to understand why there is difference in different experimental systems.

©2021. Japan Geoscience Union. All Right Reserved.

References
Arima, T., Idemitsu, K., Xia, X., Ishidera, T., & Iijima, K. (2004). Diffusion of Iron and Neptunium in Buffer Material. Evaluation.
Kozaki, T., Imamura, Y., Takada, J., Sato, S., & Ohashi, H. (1995). Corrosion of iron and migration of corrosion products in compacted bentonite.

Keywords: Iron-Bentonite interaction, Geological disposal, Engineering barrier

©2021. Japan Geoscience Union. All Right Reserved.

[J] Poster | H (Human Geosciences)：H-CG Complex & General

Sat. Jun 5, 2021 5:15 PM - 6:30 PM JST | Sat. Jun 5, 2021 8:15 AM - 9:30 AM UTC | Ch.12_3

[H-CG24] Coastal wetlands: geomorphologic, biologic and anthropogenic processes

convener:Kiyoshi Fujimoto(Nanzan University)

Coastal wetlands are very fragile environment against external environmental changes such as sea-level rise and anthropogenic impacts. On the other hand, coastal wetlands have a significant role as a place for carbon sequestration in the belowground as well as the aboveground. This session will discuss the geomorphologic, biologic and anthropogenic processes on the coastal wetlands in the various climate zones during the Holocene. For example, coastal wetlands in the tropics have evolved with the development of wetland forests such as mangrove forest, peat swamp forest and fresh water swamp forest. The most significant process for habitat formation and maintenance of the former two forests are peat production and decomposition, which are also significant processes on the coastal lowlands in the temperate and subarctic zones, though the mechanism of the processes might be different. Geomorphological processes such as sedimentation and erosion by fluvial and marine processes are also important for all of coastal wetlands. However, the environment of coastal wetlands has been destroyed by various human activities such as deforestation, agriculture land development, peat mining, and shrimp firming in and around mangrove forests in recent years. We would like to invite the wide discipline of research papers on not only the natural processes but also the anthropogenic processes in order to offer the scientific basis for creating sustainable management systems on the coastal wetlands in the future.

[HCG24-P01] Mapping of mangrove species and communities using UAV photography and high-resolution satellite data to evaluate surface erosion induced by sea-level rise on Pohnpei Island, Micronesia

*Kiyoshi Fujimoto[1], Takeki Yaguchi[1], Yasumasa HIrata[2], Shin Watanabe[3], Kodai Hasada[4], Kenji Ono[2], Shingo Taniguchi[3], Keita Furukawa[5], Saimon Lihpai[6] (1.Nanzan University, 2.Forestry and Forest Products Research Institute, 3.University of the Ryukyus, 4.Hosei University, 5.Association for Shore Environment Creation , 6.Pohnpei State Government, FSM)

[HCG24-P02] Consideration of sea level rise effect on sediment transport process in mangrove forest -preliminary attempt for long-term analysis-

*Keita Furukawa[1,2], Kiyoshi Fujimoto[3], Kenji Ono[4], Shin Watanabe[5], Shingo Taniguchi[5], Yasumasa Hirata[4], Kodai Hasada[6], Renpei Suwa[7], Saimon Lihpai[8] (1.Association for Shore Environment Creation, 2.Ocean Policy Research Institute, Sasakawa Peace Foundation, 3.Nanzan University, 4.Forestry and Forest Products Research Institute, 5.Ryukyu University, 6.Hosei University, 7.Japan International Research Center for Agricultural Sciences, 8.Pohnpei State Government)

[HCG24-P03] Comparison of Fine Root Production among Several Types of Tropical Mangrove Stands in the Federated States of Micronesia using the Continuous Inflow Estimation Method

*Kenji Ono[1], Kiyoshi Fujimoto[2], Yasumasa Hirata[3], Ryuuichi Tabuchi[3], Shingo Taniguchi[4], Shin Watanabe[4], Keita Furukawa[5], Rempei Suwa[6], Saimon Lihpai[7] (1.Tohoku research center, Forestry and Forest Products Research Institute, 2.Nanzan Univ., 3.Forestry and Forest Products Research Institute, 4.Univ. of Ryukyu, 5.Association for Shore Enviromnent Creation, 6.Japan International Research Center for Agricultural Science, 7.Phonpei State Gov. FSM)

Mapping of mangrove species and communities using UAV photography and high-resolution satellite data to evaluate surface erosion induced by sea-level rise on Pohnpei Island, Micronesia

*Kiyoshi Fujimoto[1], Takeki Yaguchi[1], Yasumasa HIrata[2], Shin Watanabe[3], Kodai Hasada[4], Kenji Ono[2], Shingo Taniguchi[3], Keita Furukawa[5], Saimon Lihpai[6]

1. Nanzan University, 2. Forestry and Forest Products Research Institute, 3. University of the Ryukyus, 4. Hosei University, 5. Association for Shore Environment Creation , 6. Pohnpei State Government, FSM

In the western Pacific low-latitude region between the Philippines and Micronesia, the sea level has been rising at over 10 mm/yr (IPCC 2013). In the mangrove habitat situated in the low sediment inflow environment, *Rhizophora* pure forest is generally formed as a pioneer community and mangrove peat is created. However, the mangrove peat accumulation rate is considered to decrease with the vegetation succession because of the decline of tree density of *Rhizophora* sp. The mangrove communities decreased mangrove peat accumulation rate is possibly affected by sea-level rise first. In Pohnpei Island, Micronesia, the surface erosion is not recognized in the *Rhizophora stylosa* and *Rhizophora apiculata* communities yet, while it is recognized in the communities dominated by other species.

In this study, we create canopy projections for existed permanent plots using UAV photography and ground data first. Secondly, we examine an auto-detect method for mangrove species using the high-resolution satellite data by reference to the canopy projections. Finally, we zone communities based on Mochida et al. (2006) using the mangrove species distribution maps.

UAV photography enable us to identify mangrove species from the size, shape and color of crown. *R. apiculata* has round and relatively small crown with green and brownish to yellowish green. *R. stylosa* has similar features, though their crown loose shape with more brownish color. The two species can be identified from the distribution pattern, i.e., the former widely distribute to the interior, while the latter develop along the seaward forest edge only. *Sonneratia alba* has large and irregular shape crown with yellowish green. *Bruguiera gymnorrhiza* has relatively roundish crown with blueish green and appear in the space among other species with relatively low tree height. *Xylocarpus granatum* has irregular shape crown with emerald green and appear among other species as with *B. gymnorrhiza*.

Pan sharpening using Panchromatic ortho image (ground resolution: 40 cm) and 8 bands multispectral ortho image (ground resolution: 1.6 m) by WorldView-3 (taken on October 17, 2018) enable us to identify some mangrove species automatically. ArcGIS Pro was used for the Pan sharpening and GIMP 2.10.22 was used for auto-detect of mangrove species. As the result, three groups, i.e., 1) *R. apiculata* or *R. stylos* a, 2) *S. alba* and 3) *B. gymnorrhiza* or *X. granatum* were identified automatically. We can create mangrove community map by considering the distribution pattern for *R. stylosa* and *X. granatum*, i.e., the former distributes along seaward edge only and the latter appears in a climax forest with low tree density. The mangrove community map will enable us to create an evaluation map of surface erosion induced by sea-level rise with consideration for tree density of *Rhizophora* species and distance from the seaward forest edge.

Keywords: Mangrove, Sea-level rise, UAV photography, High-resolution satellite data, Species distribution map, Vegetation community map

©2021. Japan Geoscience Union. All Right Reserved.

©2021. Japan Geoscience Union. All Right Reserved.

Consideration of sea level rise effect on sediment transport process in mangrove forest -preliminary attempt for long-term analysis-

*Keita Furukawa[1,2], Kiyoshi Fujimoto[3], Kenji Ono[4], Shin Watanabe[5], Shingo Taniguchi[5], Yasumasa Hirata[4], Kodai Hasada[6], Renpei Suwa[7], Saimon Lihpai[8]

1. Association for Shore Environment Creation, 2. Ocean Policy Research Institute, Sasakawa Peace Foundation, 3. Nanzan University, 4. Forestry and Forest Products Research Institute, 5. Ryukyu University, 6. Hosei University, 7. Japan International Research Center for Agricultural Sciences, 8. Pohnpei State Government

Preliminary measurement for detecting sea level rise (SLR) effects on mangrove forests has been observed at Iriomote Island, Japan and Ponpei Island, Federal States of Micronesia since 2018. The short term SLR effects were measured by surface erosion and sedimentation. If sedimentation rate on a mangrove forest floor is faster enough to catch up with SLR, the forest will adapt on the change (Fujimoto et.al. 1989). Nevertheless, if it is slower than SLR, or erosion rate becomes greater than sedimentation rate, the forest will NOT adapt on the change (Furukawa et.al. 2002).

According to the observations, existence of following sediment transport mechanisms was suggested i.e. the existence of a sheet-flow transport mechanism in a short period of time when seawater is flooded and drained, the occurrence of steady erosion due to tidal transports, and the temporally and spatially uneven transport mechanism (Furukawa et al. 2019). In particular, it is necessary to clarify the effects of sediment supply from the upstream and micro-topography (creeks) existing on the forest floor.

Therefore, we attempted to measure two-dimensional sedimentation rate and sediment transport in the plot with complex topography conditions in 2019 (Pompeii PK plot: Fujimoto et al. 2019). In particular, we attempted to measure the effects of sediment supply from the upstream side, microtopography (creeks) existing on the forest floor, two-dimensional deposition rate, and sediment transport. In order to examine the effects of tides and rainfall, we observed the spring tide period (during fine weather) and the low tide period (during rainfall) and conducted a short-term trend analysis (Furukawa et al. 2020).

We adapted the typified segment transport mode to the climate data in the area and examined the methodology for examining the long-term trend of change in the plot. It was shown that it is indispensable to carry out long-term continuous observations or use a so-called outflow model in the future.

This research has been done as a part of “Mangrove forests community situation understanding against SLR.”

Keywords: Sea Level Rise, Mangrove Forest, Sediment Transport

©2021. Japan Geoscience Union. All Right Reserved.

Comparison of Fine Root Production among Several Types of Tropical Mangrove Stands in the Federated States of Micronesia using the Continuous Inflow Estimation Method

*Kenji Ono[1], Kiyoshi Fujimoto[2], Yasumasa Hirata[3], Ryuuichi Tabuchi[3], Shingo Taniguchi[4], Shin Watanabe[4], Keita Furukawa[5], Rempei Suwa[6], Saimon Lihpai[7]

1. Tohoku research center, Forestry and Forest Products Research Institute, 2. Nanzan Univ., 3. Forestry and Forest Products Research Institute, 4. Univ. of Ryukyu, 5. Association for Shore Enviromnent Creation, 6. Japan International Research Center for Agricultural Science, 7. Phonpei State Gov. FSM

The dynamics of blue carbon (BC), that is sequestered and stored in the ocean ecosystems (IPCC 2009), has gained considerable attention due to recent alarming concern about global warming. The BC stocks are substantial in the ocean ecosystems and they play an important role in global climate change mitigation (Alongi 2018). Mangrove forests are major components of coastal ecosystems in the tropical and subtropical zones. They are highly productive ecosystems with mean sequestration rates of organic carbons in the earth as well as salt marsh and seagrass ecosystems (Alongi 2020). Donate et al. (2011) described mangrove ecosystems as “among the most carbon(C)-rich forests in the tropics.”
Previous studies suggest that the high ability of C accumulation and sequestration in submerged soils of mangrove ecosystems are ensured by the high productivity of biomasses above and below the ground, especially that of root production. However, our understanding about the contribution of fine root production in mangrove ecosystems due to C sequestration and its fluxes is that blue carbons are limited by difficulties and uncertainties associated with fine root dynamics, such as their stocks, fluxes, and longevity in the invisible belowground root systems (Majdi and Kangas 1997).
On the other hand, recent reports proposed new approaches for estimating fine root dynamics in terrestrial forest ecosystems (Osawa and Aizawa 2012, Do et al. 2016). These approaches include continuous inflow estimate methods, which can provide more accurate and comprehensive evaluations of the fine root dynamics estimated by a simple mass balance model with compartments (i.e., stocks of living and dead masses) and flow (production, mortality, and decomposition) of organic materials originating from fine roots.
In this study, we tried to clarify the contribution of fine root dynamics including the processes of production, mortality, and decomposition to net primary production in mangrove ecosystems and carbon sequestration in BC ecosystems. To achieve this purpose, we performed continuous inflow estimates of fine root dynamics at several types of mangrove stands in Pohnpei Is., Federated States of Micronesia (FSM), by using a simple mass balance model with a combination of an ingrowth core method and litterbag experiment according to a study by Osawa and Aizawa (2012). In this presentation, we will report our findings related to these topics.

Keywords: Mangrove, Sea level rise, Fine root production, Blue carbon

©2021. Japan Geoscience Union. All Right Reserved.

[J] Poster | H (Human Geosciences)：H-CG Complex & General

Sat. Jun 5, 2021 5:15 PM - 6:30 PM JST | Sat. Jun 5, 2021 8:15 AM - 9:30 AM UTC | Ch.12_4

[H-CG27] Nuclear Power and Geoscience in Japan: 10 years after the 3.11 complex disaster

convener:Daisuke Suetsugu(institute for Marine Geodynamics, Japan Agency for Marine-Earth Science and Technology), Kohta Juraku(Department of Humanities, Social and Health Sciences, School of Engineering, Tokyo Denki University), Satoshi Kaneshima(Department of Earth and Planetary Sciences, Kyushu University), Takeshi Sagiya(Disaster Mitigation Research Center, Nagoya University)

Nuclear Power and Geoscience in Japan: 10 years after the 3.11 complex disaster
We have organized sessions in the JpGU meeting on the risk of nuclear power utilization in Japan mainly from the point of view of geoscience since 2013. It has shed new light on various aspects of the risk of nuclear power related to earthquakes, volcanic activities and tsunamis. The 2021 JpGU meeting will be held 10 years after the 3.11 complex disaster: the Great East Japan Earthquake with the Fukushima-Daiichi nuclear accident. On this occasion, we propose a reflexive session to review what we have discussed and understood through the past sessions or public debates: What should geoscience take the stance on the issue of scientific uncertainty and nuclear risk? How could scientists and engineers work together for public goods? We are also welcome to papers of other topics relevant to relationship of geoscience and nuclear utilization.

[HCG27-P01] Nuclear Power and Geoscience in Japan

*Daisuke Suetsugu[1], Satoshi Kaneshima[2], Takeshi Sagiya[4], Kohta Juraku[3] (1.institute for Marine Geodynamics, Japan Agency for Marine-Earth Science and Technology, 2.Department of Earth and Planetary Sciences, Kyushu University, 3.Department of Humanities, Social and Health Sciences, School of Engineering, Tokyo Denki University, 4.Disaster Mitigation Research Center, Nagoya University)

[HCG27-P02] Model and “Unexpected”

*Manabu Hashimoto[1] (1.Disaster Prevention Research Institute, Kyoto University)

[HCG27-P03] Does science give us THE answer? (2)
Issues centering on scientific advice

*Kohta Juraku[1] (1.Department of Humanities, Social and Health Sciences, School of Engineering, Tokyo Denki University)

[HCG27-P04] A personal summary of JPGU sessions about earth science and nuclear power plants in Japan

*Satoshi Kaneshima[1] (1.Department of Earth and Planetary Sciences, Kyushu University)

[HCG27-P05] Has the situation surrounding nuclear power generation and earth science changed during the last decade?

*Takeshi Sagiya[1] (1.Disaster Mitigation Research Center, Nagoya University)

Nuclear Power and Geoscience in Japan

*Daisuke Suetsugu[1], Satoshi Kaneshima[2], Takeshi Sagiya[4], Kohta Juraku[3]

1. institute for Marine Geodynamics, Japan Agency for Marine-Earth Science and Technology, 2. Department of Earth and Planetary Sciences, Kyushu University, 3. Department of Humanities, Social and Health Sciences, School of Engineering, Tokyo Denki University, 4. Disaster Mitigation Research Center, Nagoya University

Severe accident of the Fukushima-Daiichi nuclear power plant was caused by the 2011 Great East Japan earthquake and tsunami. Looking at the seriousness and broad extent of the accident, many geoscientists, including the authors, realized ourselves as those who have to consider the risk of nuclear power plants seriously, which motivated us to organize sessions in the JpGU meeting on the risk of nuclear power utilization in Japan mainly from the point of view of geoscience since 2013. It has shed new light on various aspects of the risk of nuclear power related to earthquakes, volcanic activities and tsunamis. The 2021 JpGU meeting will be held 10 years after the 3.11 complex disaster: the Great East Japan Earthquake with the Fukushima-Daiichi nuclear accident. On this occasion, we review what we have discussed and understood through the past sessions or public debates: What should geoscience bear geoscience hazard and risk of nuclear power plants to engineers, policy-makers, and Japanese people, with an emphasis on inevitably great uncertainty? Issues of the nuclear power plants in Japan are not only geoscientific risk, but including energy balance, economics and environment problems. How can we create a ‘public space’ consisting of all the stake-holders to discuss future of the nuclear power in Japan?

Keywords: Nuclear power plants, Geoscience

©2021. Japan Geoscience Union. All Right Reserved.

Model and “Unexpected”

*Manabu Hashimoto[1]

1. Disaster Prevention Research Institute, Kyoto University

Since the occurrence of the Great East Japan Earthquake Disaster, I have participated in several committees for the reexamination of earthquake countermeasures including the Nankai Trough earthquake. Under the banner of "No More Unexpected", model of the largest possible earthquake was asked to be discussed there, and various models were proposed. Ground motion and tsunami were calculated on the basis of these models, to estimate damages. As a result, the forecast of extremely large damage was announced, which shook the society. Since then, experts in surrounding fields and media have repeatedly used this estimate along with their arguments, which makes only these numbers prevalent. I guess some people are disgusted with the current situation.

By the way, what is a model on earth? In earth science, a wide variety of models are used, from conceptual qualitative models to precise numerical models with multiple degrees of freedom and analog models using actual materials. Just as the sand pile model, which is composed only of addition and subtraction calculations, creates a power law, even a highly abstracted model can show us the essence of the phenomenon. The analog model is constructed on a laboratory scale in order to understand the mechanism of phenomena that cannot be reproduced on a real scale. The model is extremely useful for understanding the phenomenon, because similar results can be obtained even if a third party executes them with the same settings.

On the other hand, the society counts on model’s predictability. Models of atmospheric phenomena have been used for future forecasts of weather and climate for many years, and information based on these forecasts are now a part of our lives. Following this success, models of generation of earthquakes and related disasters, such as long-term probabilistic forecast, strong ground motion prediction and tsunami forecast, are used. Based on these results, countermeasures are established, and building codes for important structures such as nuclear power plants and bridges are set.

However, the model is based on assumptions where complex factors are omitted. Therefore, the application of the model should be limited, but there are discussions that unconsciously go beyond, aren’t there? For example, the dislocation model, which is widely used in earthquake research, is also an approximate solution; the assumption of infinitesimal deformation is broken in the close vicinity of the fault. Long-term probability is calculated as a point process in which only earthquakes of a certain size or larger are extracted from the time series of earthquake occurrence. In the prediction of strong ground motion and tsunami, many assumptions such as homogeneous semi-infinite medium or stratified structure are made in the analysis, and the shape of the fault is an extremely simple rectangle. Real faults and structure are very complicated, but such complexities are stripped off. There is no assessment of the impact of the stripped elements and it is treated as an uncertainty that is difficult to quantify. Perhaps the "unexpected" is lurking there. We cannot rule the “unexpected” out.

Only researchers can criticize the validity of the model on which damage estimation is based from a professional viewpoint. Why not just make a statement, not just bitter?

©2021. Japan Geoscience Union. All Right Reserved.

Keywords: model, unexpected, earthquake science

©2021. Japan Geoscience Union. All Right Reserved.

Does science give us THE answer? (2) Issues centering on scientific advice

*Kohta Juraku[1]

1. Department of Humanities, Social and Health Sciences, School of Engineering, Tokyo Denki University

It has been discussed the relationship between the risk of nuclear utilization and geoscience, the role of scientist and engineer in the previous sessions. The author has analyzed those issues from the perspectives of interactions and gaps between science and engineering, their views on risk and safety behind the social mechanism and their senses of vocation, and pursued the better way to overcome the obstacles centering on them. This year, he would like to discuss the issues centering on so-called "scientific advice" in geo science field, in comparison with the case of the COVID-19 pandemic.

Before the 10th anniversary of the 3.11 complex disaster, the world faced the pandemic. The role, function and method of effective scientific advice to the policy has been attracted the public attention.

We have witnessed a wide-spread suspicion among the public that the relevant "experts" distort their scientific advice to government and society because of their own political and social interests, or politicians and bureaucrats cherry-pick or just neglect the expert's advices to protect themselves from public criticism. Very similar arguments were observed in the 3.11 disaster. We even saw the word *Goyo-gakusha* (lap-dog expert) again when people criticized the governmental public health advisors, exactly same to the Fukushima nuclear disaster case.

It was reasonable to use the word to criticize nuclear experts because they had a strong interest to trivialize the magnitude of the nuclear disaster to protect their nuclear technology, however, epidemiologist, virologist and pharmacologist could never share the interest with the COVID virus itself nor COVID-19 syndrome. Rather, it should even be advantageous to them to build a social consensus that the pandemic is more serious than the other people thought. Thus, it is questionable to use the same *Goyo-gakusha* rhetoric to critically analyze the problems behind the shortcomings of (Japanese) government's counter measures.

It must have a universal implication to answer this question for geoscientists who are involved in or interested in the relationship between the geoscience and the risks of nuclear technology. By touching upon the relevant frameworks on scientific advice in the field of STS, this paper try to answer the question.

Keywords: scientific advice, COVID-19, risk of nuclear technology, science and technology studies (STS)

©2021. Japan Geoscience Union. All Right Reserved.

A personal summary of JPGU sessions about earth science and nuclear power plants in Japan

*Satoshi Kaneshima[1]

1. Department of Earth and Planetary Sciences, Kyushu University

In this poster I discuss about the issues regarding the uncertainty of the scientific knowledge that earth scientists can provide for our society in order to help mitigate hazards associated with nuclear power plants. Through the series of our JPGU sessions held since 2013 about the relation between nuclear power plants and earth science, a consensus seems to have been reached among the participants. It is the recognition of substantial uncertainty inherent in the forecasts and/or evaluations on important issues such as the maximum size of earthquake at the trenches, the maximum ground motions anticipated at specific nuclear sites, and the long term safety of the nuclear waste deposition sites. Although this recognition seemingly is also shared by our society to some extent since the 2011 great Tohoku earthquake, the earth science community has to relentlessly keep announcing serious difficulties that any attempts to give reliable assessment must face. As long as the earth science issues mentioned above are concerned, the earth science community present day should not recommend a specific scientific model or evaluation for the society or policymakers to take, but rather should provide with the range of uncertainty in the models as clearly as possible. The community now needs to specifically develop an efficient system that can objectively and reasonably define the uncertainty ranges about those issues.

Keywords: nuclear power plants, earth scientific khowledge, uncertainty

©2021. Japan Geoscience Union. All Right Reserved.

Has the situation surrounding nuclear power generation and earth science changed during the last decade?

*Takeshi Sagiya[1]

1. Disaster Mitigation Research Center, Nagoya University

10 years have passed since the 2011 Great East Japan Earthquake and its disaster. After this disaster, The Seismological Society of Japan launched a special committee to discuss responses to this disaster and I served as the chair. We concluded with the following recommendation. "The seismological community should recognize the situation surrounding their research with sound criticism and we need to improve communication both inside and outside of the academic society" (Sagiya, 2012). After that, as a part of an attempt to put this recommendation in practice, we have been organizing a JpGU session where relationship between nuclear power generation and earth science is discussed. Looking back on these sessions, we can recognize various advances in earth science research and more interdisciplinary communication. On the other hand, the gap between the nuclear power generation side and general earth scientists sill exists. Scientists can mention possible future disasters, but such claim has a large uncertainty. The actual decision differs greatly depending on the treatment of the uncertainty. In order to make a proper decision, multidisciplinary discussion in a "public" space is indispensable, which has not been established yet. Considering such a situation, I would argue that the recommendation in 2012 is still valid.

Keywords: earth science, nuclear power generation, public space, social responsibility of scientists

©2021. Japan Geoscience Union. All Right Reserved.

[J] Poster | S (Solid Earth Sciences)：S-SS Seismology

Sat. Jun 5, 2021 5:15 PM - 6:30 PM JST | Sat. Jun 5, 2021 8:15 AM - 9:30 AM UTC | Ch.13_2

[S-SS09] Seismic wave propagation: Theory and Application

convener:Kaoru Sawazaki(National Research Institute for Earth Science and Disaster Resilience), Kiwamu Nishida(Earthquake Research Institute, University of Tokyo), Takao Nibe(JAPEX), Kyosuke Okamoto(National Institute of Advanced Industrial Science and Technology)

Seismic wave propagation provides rich information on earth's heterogeneities and the excitation sources. Understanding of this information requires various research fields: mathematical/numerical studies based on wave theory, physical experiments using rock samples, seismic data analysis, etc. With recent developments of observational techniques, various wave phenomena have been elucidated: seismic waves, acoustic waves, traveling ionospheric disturbances, and tsunamis. New frameworks will be crucial for comprehensive understanding of these phenomena. This session widely invites presentations about the theories and applications related to seismic and other geophysical waves.

[SSS09-P01] Temporal variation in seismic velocity at the shallow part of the overriding plate in the Japan Trench

*Takashi Tonegawa[1], Ryota Takagi[2], Kaoru Sawazaki[3], Katsuhiko Shiomi[3] (1.Japan Agency for Marine-Earth Science and Technology, 2.Tohoku University, 3.National Research Institute for Earth Science and Disaster Resilience)

[SSS09-P02] Estimation of instrumental clock errors at 46 active volcanoes in Japan based on seismic interferometry

*Takashi Hirose[1] (1.National Research Institute for Earth Science and Disaster Resilience)

[SSS09-P03] On the factors influencing ambient-noise passive seismic imaging

*Xin Guo[1], Zhihui Zou[1,2], Yongjun Rui[3], Qinghui Cui[3], Xinmin Shang[3] (1.College of Marine Geosciences, Key Lab of Submarine Geosciences and Prospecting Techniques. MOE, Ocean University of China, Qingdao 266100, China, 2.Evaluation and Detection Technology Laboratory of Marine Mineral Resources, Qingdao National Laboratory for Marine Science and Technology, Qingdao 266061, China, 3.Geophysical Research Institute of Shengli Oilfield, Sinopec, Dongying, China 257022)

[SSS09-P04] Migration of fluid during oil recovery revealed by Reverse Time Imaging

*Runbi Yuan[1], Zhihui Zou[2,1], Cui Qinghui[3], Rui Yongjun[3], Shang Xinmin[3] (1.College of Marine Geosciences, Key Lab of Submarine Geosciences and Prospecting Techniques. MOE, Ocean University of China, Qingdao 266100, China, 2.Evaluation and Detection Technology Laboratory of Marine Mineral Resources, Qingdao National Laboratory for Marine Science and Technology, Qingdao 266061, China, 3.Geophysical Research Institute of Shengli Oilfield, Sinopec, Dongying, China 257022)

[SSS09-P05] Effects of fine-scale heterogeneity distribution in the Pacific slab on the generation of anomalously large intensities from deep-focus earthquakes

*Takashi Furumura[1], Brian LN Kennett[2] (1.Earthquake Research Institute The University of Tokyo, 2.Research School of Earth Sciences The Australian National University)

[SSS09-P06] Scattering properties in Japanese volcanoes as inferred from the peak ratio analysis of teleseismic P waves using the JMA seismometer network data

*Gugi Aucklandi Ganefianto[1], Hisashi Nakahara[1], Takeshi Nishimura[1] (1.Tohoku University)

[SSS09-P07] Crack source and volcanic structural heterogeneity inferred from oscillatory waveforms of long-period seismic events: Application at Kusatsu-Shirane Volcano

*Nakano Masayuki[1], Hiroyuki Kumagai[1] (1.Nagoya University)

[SSS09-P08] Applying the shortest path method to anisotropic media in order to calculate ray paths

*Shoji Sekiguchi[1] (1.National Research Institute for Earth Science and Disaster Resilience)

[SSS09-P09] Numerical simulations of weak localization of scalar waves based on the finite difference method (2)

*Jun Kawahara[1], Masanobu Sato[1] (1.Graduate School of Science and Engineering, Ibaraki University)

[SSS09-P10] Observability of seismic radial anisotropy parameters by the analysis of surface waves and receiver functions based on the MCMC analysis

*Jumpei Maruyama[1], Hitoshi Kawakatsu[1], Nozomu Takeuchi[1] (1.University of Tokyo, Earthquake Research Institute)

Temporal variation in seismic velocity at the shallow part of the overriding plate in the Japan Trench

*Takashi Tonegawa[1], Ryota Takagi[2], Kaoru Sawazaki[3], Katsuhiko Shiomi[3]

1. Japan Agency for Marine-Earth Science and Technology, 2. Tohoku University, 3. National Research Institute for Earth Science and Disaster Resilience

Ambient noise correlation technique is now a powerful tool for detecting temporal variation in seismic velocity. Because such studies require long-term continuous seismic records, they have been often used to land-based seismic records. However, permanent seismic observations have recently deployed offshore areas, particularly around Japan, this technique can be applied to temporal variation in seismic velocity structure at the subseafloor (e.g., Ikeda and Tsuji, 2018). In particular, Tonegawa et al. (2020, JpGU; AGU) has reported that seismic velocity and heterogeneity changes are induced by tectonic compression and fluid migration at the subseafloor structure in the Nankai subduction zone. In this study, we applied ambient noise correlation technique to the continuous records observed at S-net deployed around the Japan Trench, and investigated the relationships among temporal variation in seismic structure, seismic activities, and tectonic settings.

We calculated cross correlation functions (CCFs) at a frequency band of 0.5–1.0 Hz using ambient noise records in the vertical component. Here, the three-component seismograms were synthesized using a method of Takagi et al. (2019). The CCFs show ocean acoustically-coupled Rayleigh waves whose propagation velocity is slightly less than 1.5 km/s. The time length of the time series for calculating CCFs was 3600 s, but the time series was subtracted by those in the next 3600 s for removing instrumental noises, according to the method of Takagi et al. (2021). The calculated CCFs are stacked over 1 year for the reference CCF and 30 days for individual CCFs. We measured seismic velocity change (dv/v) by a stretching method (Wegler and Sens-Schönfelder 2007) and also seismic heterogeneity change (CC) by cross correlating the reference and individual CCFs (Obermann et al. 2013).

Our results show temporal changes in dv/v near the Japan Trench, while such changes cannot be observed in the region close to land. The maximum change of dv/v over 4 year was 0.3 % around the latitude of 39ºN. It is considered that the gradual change primarily corresponds to the recovery process of a velocity reduction associated with the 2011 Tohoku-oki earthquake. Another candidate is tectonic compression in the overriding plate near the trench at this region, which induces a seismic velocity increase due to fluid drainage at shallow depths to the sea water.

Our results also show abrupt reductions in CC, but the areas of the changes are wide compare with those observed in the Nankai area. Some of them correspond to the timing of relatively large earthquakes, indicating that seismic heterogeneity at shallow depths was varied with seafloor motion due to the earthquakes. However, it appears that other CC reductions do not correspond to the large earthquakes. It is necessary to investigate the CC reductions in more details.

Data citation

S-net: doi:10.17598/NIED.0007

©2021. Japan Geoscience Union. All Right Reserved.

Keywords: Seismic velocity, Temporal variation, Japan Trench

©2021. Japan Geoscience Union. All Right Reserved.

Estimation of instrumental clock errors at 46 active volcanoes in Japan based on seismic interferometry

*Takashi Hirose[1]

1. National Research Institute for Earth Science and Disaster Resilience

The correct absolute timing of seismograms is crucially required in many seismological analyses. In recent years, seismic interferometry [e.g., Curtis et al., 2006; Shapiro, 2004] has been widely used to detect structural changes related to large earthquakes and volcanic activities [e.g., Brenguier et al., 2008; Wang et al., 2019; Hirose et al., 2020; Nishida et al., 2020]. Some previous studies have investigated the use of seismic interferometry to correct seismometer clocks [e.g., Stehly et al., 2007; Sens-Schönfelder, 2008; Hable et al., 2018]. Estimating instrumental clock errors are also important for continuous seismic monitoring of active volcanoes. I develop an estimation method of instrumental clock errors based on seismic interferometry and apply this method to 46 active volcanoes in Japan.

I computed seismic ambient noise cross-correlation functions (CCFs) using continuous seismograms at V-net and JMA stations of 46 active volcanoes in Japan between Jan. 1, 2020, and Jan. 31, 2021. Continuous seismic records on vertical component were divided into 10-minutes-long segments and applied spectral whitening [e.g., Shapiro et al., 2006; Bensen et al., 2007] and one-bit normalization [Larose et al., 2004]. Daily CCFs (DCCFs) were obtained by stacking CCFs every 10 minutes. I measured delay times between a reference 3-days-stacked CCF and a current 3-days-stacked CCF for each station pair and lag time at a 0.2-4 Hz band using the windowed cross-correlation method [e.g., Snieder et al., 2012]. A clock error will cause the same delay times between the reference and current CCFs at all lag times. Therefore, I fitted a straight line to the delay times at each lag time and assumed the straight line's intercept as the clock difference for that station pair. On the straight-line fitting, I used L1 norm optimization to suppress the effect of outliers. Finally, I estimated clock errors at each seismic station by linear least-squares inversion with the estimated clock differences.

In this study, clock errors were estimated for the time period between Jan. 1, 2020, and Jan. 31, 2021. Significant clock errors were detected at some volcanoes: At Nasu volcano, the clock of station N.NSOV started to drift with about 0.009 s/day in early Jan. 2021. This drift was caused by a malfunction of the GPS antenna from Jan. 8, 2021. At Asama volcano, a clock jump of about 1.0 s occurred at station V.ASME during Apr.-Jun. 2020, and the clock of station V.ASMG had a drift of about 0.005 s/day during Aug.-Oct. 2020. At Miyakejima volcano, the clock of station V.MYKO repeatedly drifted with 0.002 to 0.006 s/day during May-Jul. 2020, Aug.-Nov. 2020, and Dec. 2020-Jan. 2021. Repeated clock drifts (0.003-0.096 s/day) also occurred at Kusatsu-Shirane volcano. Maximum clock errors of station V.KSHA at Kusatsu-Shirane were estimated to be 1.55 s in Aug. 2020 and 0.84 s in Nov. 2020. Estimated clock errors in this study could improve the results of various seismological analyses at the 46 volcanoes, for example, hypocenter determination of volcanic earthquakes and seismic interferometry analysis.

Acknowledgment: I used seismograms recorded by Japan Meteorological Agency (JMA).

©2021. Japan Geoscience Union. All Right Reserved.

Keywords: seismic interferometry, clock error, volcano monitoring

©2021. Japan Geoscience Union. All Right Reserved.

On the factors influencing ambient-noise passive seismic imaging

*Xin Guo[1], Zhihui Zou[1,2], Yongjun Rui[3], Qinghui Cui[3], Xinmin Shang[3]

1. College of Marine Geosciences, Key Lab of Submarine Geosciences and Prospecting Techniques. MOE, Ocean University of China, Qingdao 266100, China, 2. Evaluation and Detection Technology Laboratory of Marine Mineral Resources, Qingdao National Laboratory for Marine Science and Technology, Qingdao 266061, China, 3. Geophysical Research Institute of Shengli Oilfield, Sinopec, Dongying, China 257022

The passive seismic imaging method extracts the subsurface reflected signals using the cross-correlation of ambient noise. It has the advantages of low cost and little environmental damage, and can image the subsurface continuously. The passive seismic method has been applied in the fields of time-lapse monitoring the changes in petroleum reservoirs and mining processes. One of the effective passive seismic method is developed on the base of the seismic interferometry. The basic idea of seismic interference was proposed by Claerbout (1968) firstly, in which case the Green's function was estimated through the auto-correlation of seismic records generated by underground sources. In the exploration geophysics, Schuster et al. (2001) reconstructed the seismic wave field from the cross-correlation information using a generalized correlation of seismic data. Draganov et al. (2009) proposed a method based on cross-correlation to passively reconstruct the reflections using the seismic waveforms radiated from the underground sources. The workflow of passive seismic imaging is as follows: firstly, the seismic record is divided into a small time window for filtering analysis; secondly, select the panel dominated by body wave noise, and normalize each trace each panel; thirdly, select one trace as the position of virtual source shot to cross-correlate with other all traces; finally, stack them together to create one channel of the seismic record. A new seismic record is created by stacking the negative and positive parts. The main factors influencing the process of reflection extraction include: ①source distribution; ②wavelet type; ③ seismic recording time; ④wavelet coherence. These factors are essential for the successful extraction of reflected signals, but systematic studies in this area are still lacking.

To analyze the influencing factors of the quality of passive reflected signals, we conduct a series of numerical tests. The effects of various factors on the quality of the reflection waves are compared and analyzed by synthesizing the virtual source seismic records from the transmitted wave response of underground passive sources. The results show that the denser the distribution of the seismic sources, the longer the recording time, and the stronger the incoherence of the seismic source, the better the quality of the synthetic reflection wave recording. By analyzing the factors that influence the construction of reflection waves, the processing flow of passive seismic exploration can be optimized to improve the quality of passive seismic imaging.

©2021. Japan Geoscience Union. All Right Reserved.

Migration of fluid during oil recovery revealed by Reverse Time I maging

*Runbi Yuan[1], Zhihui Zou[2,1], Cui Qinghui[3], Rui Yongjun[3], Shang Xinmin[3]

1. College of Marine Geosciences, Key Lab of Submarine Geosciences and Prospecting Techniques. MOE, Ocean University of China, Qingdao 266100, China, 2. Evaluation and Detection Technology Laboratory of Marine Mineral Resources, Qingdao National Laboratory for Marine Science and Technology, Qingdao 266061, China, 3. Geophysical Research Institute of Shengli Oilfield, Sinopec, Dongying, China 257022

The goal of microseismic source location method is to determine the spatial location and time of origin of a seismic event (Thurber 2011), which has significant value in the study of active faults, earth's internal structure, and shale gas production. Traditional seismic source location method mainly depends on the first arrival time, which requires picking the first arrival time accurately. Such seismic event location methods have limitations, because it is difficult to pick up the first arrival time in the records of the microseismic events that has low signal-to-noise (S/N) ratio. Reverse Time Imaging (RTI) method is an alternative event location method that is based on reconstructing wavefront and constructive stacking of seismic waveforms. The RTI method does not need first-arrival time and is suitable for data with low S/N (Gajewski and Tessmer 2005).

After its invention, the RTI method was continuously developed and broadly used. Steiner et al. (2008) used low-frequency information to identify reservoirs locations and provides a possible method for reservoir localization. Zou et al. (2014) successfully identified a doublet of earthquakes in the TGR region. Zhu (2014) discussed the RTI using the acoustic wave equation in attenuation media and proposed a method to overcome the influence of attenuation on the result of event location. Ge et al. (2019) combined the travel time location and RIT methods, and proposed the reverse travel time imaging (RTTI) method. Zhu (2019) developed a hybrid multiplicative time-reversal imaging (HyM-TRI) algorithm, for automatically tracking the spatiotemporal distribution of microseismic events. For its applicability in low SNR situation, the RTI has potential to image the noise generated by the movement of fluid in petroleum reservoir.

In this paper, RTI is applied to study the dynamic evolution of subsurface fluid during the steam injection for petroleum production. The real data before and after steam injection are processed respectively, and then compared to show the changes beneath the oil field. Since the noise surrounding the petroleum reservoir generated by the injection process usually has a relatively stable energy in a period of several minutes, the data of the two parts are superimposed in the time domain to suppress the influence of the random noise. Two images that are before and during the injection are normalized into the same background, and then subtracted with each other to show the difference that reflects the microseismic information generated by fracturing in the steam injection process.

©2021. Japan Geoscience Union. All Right Reserved.

Effects of fine-scale heterogeneity distribution in the Pacific slab on the generation of anomalously large intensities from deep-focus earthquakes

*Takashi Furumura[1], Brian LN Kennett[2]

1. Earthquake Research Institute The University of Tokyo, 2. Research School of Earth Sciences The Australian National University

From the analysis of OBS records in northwest Pacific and 3-D FDM simulations of high-frequency oceanic *Pn/Sn* (*Po/So*) wave propagations, lateral variations in fine-scale heterogeneity in the oceanic lithosphere have been revealed in detail (Furumura & Kennett, SSJ2020 Fall meeting). The *Po/So* propagation variability can be explained with a von Karman distribution function for elastic properties in the lithosphere with a longer correlation distance of 20 km in the NE direction, and much shorter correlation distances in the perpendicular (0.5 and 2 km) direction and in depth (0.5 km), with standard deviation from the background wavespeed of 2%. Since the longer axis of the heterogeneity distribution aligns with the observed *Pn/Sn*-wavespeed anisotropy in the northwest Pacific, it is highly likely that it was also developed during the formation and growth of the oceanic plate. Such a structure is very effective to guide high-frequency *Po/So* with long codas by multiple forward scattering in the direction parallel to the elongated heterogeneity.

The complex heterogeneity in the Pacific plate is expected to be carried by subduction deep beneath Japan, and can then produce unusually large signals in certain directions from deep earthquakes within the subducted slab. For example, on 2007 July 16, a 378 km deep Mw 6.8 earthquake beneath the Sea of Japan, produced anomalously large shaking over central to northern Japan. The shaking intensity near the epicenter was less than 1 (JMA), but the maximum intensity of 4 occurred in Obihiro, Hokkaido (Fig.1a).

Usually, such a peculiar intensity pattern occurs from deep earthquakes, as high-frequency (>1-2 Hz) signals traverse the cold, high-*Q* slab. In addition, the waveguide effect is reinforced by multiple forward scattering of seismic waves in the heterogeneous slab that captures high-frequency signals (e.g., Furumura & Kennett, 2005, JGR; Kennett & Furumura, 2015, G3). For this earthquake the significantly extended PGA contours into Hokkaido, more than 1000 km away from the hypocenter, is rather anomalous compared to other deep-focus earthquakes, indicating that an additional directional waveguide effect is needed.

We have undertaken 3-D FDM simulations of high-frequency wave propagation (up to 4.6 Hz) using the heterogenous slab structure (Fig.1b) that was identified from the *Po/So* propagation variability in the northwest Pacific. The area of simulation was 1536 km by 768 km in horizontal direction and 665 km in depth (Fig.1c), discretized by a uniform grid of 0.875 km. The crust and mantle structure was based on Crust 1.0 (Laske et al., 2013) and deeper structure was *ak135* (Kennett et al., 1995) with earth flattening. The Pacific plate model was based on Yokota et al. (2017).

The simulation results show that the presence of an elongated fine-scale heterogeneity in N45^{o}E direction in the Pacific slab (Model A in Fig.2a) can reproduce the main pattern of larger PGA extending to Hokkaido, similar to the observations, though the level of simulated ground motion was about a half of observation due to high-frequency limitations in the FDM simulation. The importance of the orientation of

©2021. Japan Geoscience Union. All Right Reserved.

the heterogeneity distribution for enhanced waveguide effects is demonstrated by comparison with the results using another model (Model B) in which the longer correlation length is orthogonal (N135°E; Fig. 2b). The simulation for Model B displays large PGA contours from Tokyo to the offshore of Tohoku, but these do not extend to Hokkaido.

A further deep event beneath Sakhalin (2013 July 23; depth=487 km, Mw6.8) did not display large PGA over Japan. FDM simulation shows that this effect arises from the propagation of seismic waves to Japan perpendicular to the elongated heterogeneity in the Pacific slab.

Keywords: Deep earthquake, Fine-scale heterogeneity, Oceanic lithosphere

©2021. Japan Geoscience Union. All Right Reserved.

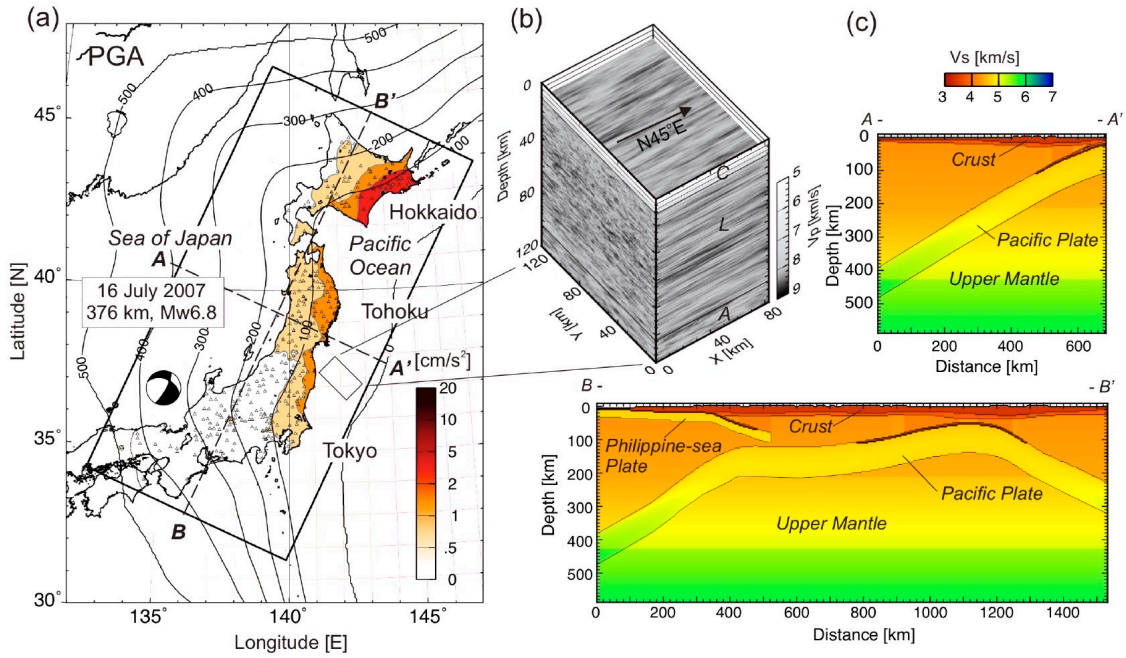

Figure 1. (a) Distribution of peak ground acceleration (PGA) for horizontal motions during the 376 km deep, Mw6.8 earthquake of 16 July 2007 that occurred in the subducting Pacific slab beneath the Sea of Japan. The black square outlines the area used for 3-D FDM simulation. (b) A 3-D view of a segment of *P*-wavespeed model of oceanic crust (*C*), lithosphere (*L*) and asthenosphere (*A*) with fine-scale heterogeneity is shown. (c) Vertical cross sections along A--A′ and B--B′, and *S*-wavespeed without fine-scale heterogeneity are shown.

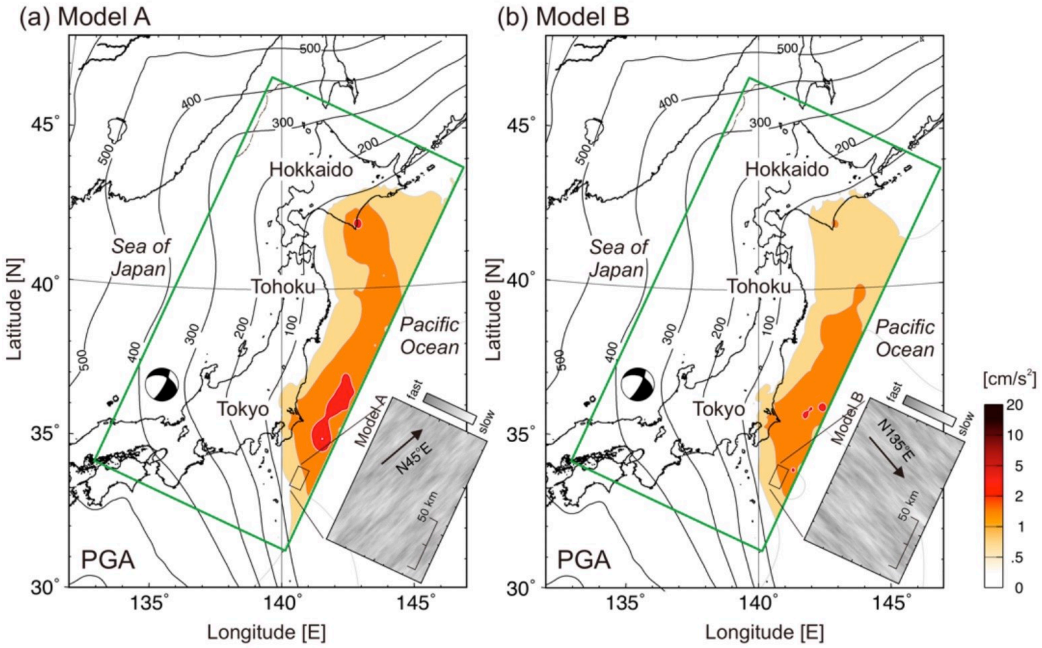

Figure 2. Comparison of the simulated PGA distribution for a deep earthquake beneath Sea of Japan obtained by simulation using different heterogeneity models; (a) Model A with a horizontally elongated heterogeneity in N45°E direction and (b) Model B in N135°E direction (illustrations of the velocity fluctuations at the crust-lithosphere boundary of the Pacific slab are shown to the right). The green rectangle indicates the area used for the 3-D FDM simulation and solid lines denote the iso-depth contours of the Pacific slab at 100 km interval.

©2021. Japan Geoscience Union. All Right Reserved.

Scattering properties in Japanese volcanoes as inferred from the peak ratio analysis of teleseismic P waves using the JMA seismometer network data

*Gugi Aucklandi Ganefianto[1], Hisashi Nakahara[1], Takeshi Nishimura[1]

1. Tohoku University

Stochastic approaches to study the small-scale medium heterogeneities are based on seismic scattered waves invoked by them. One approach is to use the partition of teleseismic P wave energy into the transverse component seismogram. The parameter used to measure the strength of this seismic wave scattering is the peak energy ratio, which is defined as the ratio of the maximum P wave energy in the transverse component seismogram envelope, to that of the sum of the transverse, radial, and vertical components. According to Sato (2006), the peak ratio can be approximated as $1.81 \varepsilon^2 h/a$ where ε, h, and a are fractional fluctuation in seismic velocity, thickness of the heterogeneous medium, and correlation distance respectively.

The quantification of the small-scale velocity heterogeneities through the computation of the peak ratio has been done by Kubanza et al., (2007) on a global scale. Nishimura (2012) estimated the peak ratio values at the Hi-net seismometer network in Japan. There are two significant observations that can be made from these two studies. One is that the peak ratio increases with increasing frequency. The second is that the more active regions, such as those in the proximity of quaternary volcanoes, yield higher peak ratios. The first observation has been explored by Ganefianto et al. (2020 SSJ meeting) through our estimation of the frequency gradient which characterises the power spectral density function of the small-scale heterogeneity. In this study, we would like to further examine the second observation, by calculating the peak ratios at JMA stations in many volcanoes of Japan. Through this approach, we would like to test the conjecture that the peak ratio gets higher at stations closer to a volcanic centre, in line with the increase in geological activity.

Data from 99 teleseismic events, recorded between 2010 and 2019 were considered. These earthquakes have depths of >300 km, magnitudes of roughly 5 to 6.5, and range between 0° to 60° epicentral distance from Japan. Analyses were performed under four separate frequency bands: 0.5-1, 1-2, 2-4, and 4-8 Hz. Source-receiver pairs with the signal-to-noise ratio of <10 were discarded. We computed seismogram envelopes of the remaining pairs. Finally, for individual stations that record >10 earthquakes, we stacked their envelopes together to obtain the mean-squared envelopes.

Our results show that the peak ratio of the JMA stations mostly range from roughly 0.16-0.44, 0.22-0.52, 0.24-0.54, and 0.30-0.60 for the 0.5-1, 1-2, 2-4, and 4-8 Hz band, respectively. The average and median value is increasing with the frequency as well. These ranges are on the high-end scale of what was found for the corresponding Hi-net peak ratios (e.g. Nishimura, 2012). As a result, on average, the peak ratio of the JMA network is larger than the Hi-net network in all frequency bands. This is also true when comparing only the Hi-net stations that are near quaternary volcanoes. We differentiate the JMA stations in our study according to the volcano they monitor. We see that most JMA stations indicate larger peak ratios than what was estimated for the quaternary volcano stations in the previous study. Furthermore, we differentiate the JMA stations into borehole and surface stations. And we observed that the peak ratios at the surface stations are higher than those at the borehole stations. All of these observations are verified to

©2021. Japan Geoscience Union. All Right Reserved.

be statistically significant from the t test. In other words, this suggests that it is highly unlikely that the patterns that we see are simply due to chances.

We speculate that there are two interdependent causes for such observations. One is because the JMA stations are positioned much closer to the volcanic centre which exposes them to richer heterogeneous elements created by volcanism. The second is due to the topography where it may convert P wave energies into surface waves, which can also excite the station’ s transverse component. This second cause seems to be much more prevalent at the surface stations compared to the borehole stations, owing to the penetration depth of surface waves.

Acknowledgement: We would like to thank the National Research Institute for Earth Science and Disaster Resilience (NIED) and the Japan Meteorological Agency (JMA) for the access to the data of the high sensitivity seismograph network (Hi-net) and the JMA volcanic seismometer network.

Keywords: Heterogeneity, Seismic scattering, Volcanoes, JMA seismometers, Hi-net, Surface wave conversion

©2021. Japan Geoscience Union. All Right Reserved.

Crack source and volcanic structural heterogeneity inferred from oscillatory waveforms of long-period seismic events: Application at Kusatsu-Shirane Volcano

*Nakano Masayuki[1], Hiroyuki Kumagai[1]

1. Nagoya University

Long-period (LP) events observed at active volcanoes are interpreted as oscillations of fluid-filled resonators in magma and hydrothermal systems. The fluid-filled crack model has been used to interpret LP waveforms. However, the crack source was estimated for only specific LP events due to technical difficulty in synthetic waveform calculations and poor understanding of volcano heterogeneity. To solve these problems, we developed a method to estimate crack sources of LP events and volcano heterogeneity easily by using multiple spectral peaks in LP events. We used peak-to-peak amplitudes of observed and synthetic waveforms to obtain stable inversion results. First, we performed numerical tests to verify the waveform inversion method using the analytical solution of Green's functions in an infinite homogeneous medium. We used OpenSWPC (Maeda et al., EPS, 2017) based on a finite difference method (FDM) accommodating topography and heterogeneity, and calculated synthetic waveforms for a horizontal crack, which were regarded as observed waveforms. By assuming the source mechanism as a crack, we conducted inversion using synthetic waveforms calculated with the analytical solution. As a result, the source depth was estimated to be shallower, but the crack inclination was estimated to be within errors of 10º. Thus, the analytical solution may be used to estimate LP sources, although there are some errors. Next, we applied our inversion method to an LP event observed on 26 April, 1992 at Kusatsu-Shirane volcano, Japan. Our result indicates that the estimated crack angles are similar to those of Nakano and Kumagai (GRL, 2005) which used synthetic waveforms calculated with a homogeneous half-space, although the source depth is slightly shallower than the previous estimate. Our application of the inversion method to other three LP events at this volcano, of which source mechanisms were not estimated before, indicates that the crack angles of the four LP events are similar, suggesting that these events were excited by the same crack. Taguchi et al. (JGR, 2018) considered that steam generated by degassing from magma entered into a crack repeatedly. Therefore, our results support this source model. By assuming that the source mechanism for multiple spectral peaks is same as the crack for the lowest frequency peak, we estimated normalized residuals by fitting observed waveforms at individual spectral peaks to synthetic waveforms calculated with the analytical solution. We found that the estimated residuals increased with increasing frequency. To evaluate this trend, we conducted FDM simulations using a von Kármán-type heterogeneity model characterized by the correlation distance (a) and heterogeneity fluctuation (ε). Volcano heterogeneity is characterized by smaller a and larger ε than those in the crust, and a = 50 m and ε = 0.2 were used by Morioka et al. (JGR, 2017). Wegler (JGR, 2004) and Kumagai et al. (JGR, 2018) indicated that strongly heterogeneous layers at volcanoes are limited to a depth of 1 km. Using a heterogeneous layer with a = 50 m and ε = 0.2 to a depth of 1 km from topography surface, we calculated synthetic waveforms with FDM for individual spectral peaks in 3–8 Hz, and fitted them to the synthetic waveforms calculated by the analytical solution. Their normalized residuals were, however, much smaller than those estimated for the observed LP events. The mean free path (l_0) for a = 50 m and ε = 0.2 around 5–10 Hz is about 1700 m, but l_0 at volcanoes around 5–10 Hz has been estimated to be about 100–200 m (Wegler, JGR, 2004; Kumagai et al., JGR, 2020). The heterogeneity used in our simulations may not be appropriate and weaker than the actual heterogeneity. We cannot use large values of ε because such FDM calculations are unstable. Monte Carlo simulations

©2021. Japan Geoscience Union. All Right Reserved.

(e.g., Yoshimoto, JGR, 2000) based on the radiative transfer theory may be required to estimate the heterogeneity.

©2021. Japan Geoscience Union. All Right Reserved.

Applying the shortest path method to anisotropic media in order to calculate ray paths

*Shoji Sekiguchi[1]

1. National Research Institute for Earth Science and Disaster Resilience

Calculating ray paths in anisotropic media in travel-time tomography is carried out in only a few studies. It is meaningful to apply the shortest path method to anisotropic media in order to calculating ray paths. Applying the shortest path method is easy, because nodes distributed in the media and ray paths between nodes are given and only the travel-time along the path need to be evaluated. However, it should be noted that it is important that ray (group) velocity in a given ray path direction can be easily evaluated in order to save calculation time. Generally, in ray tracing algorithms of anisotropic media, determinant of elastic parameter tensor in a given phase slowness direction is solved at first. The obtained phase slowness, etc. are substituted into the ray tracing equation. From the ray tracing equation, ray path and travel-time are calculated. Ray (group) velocity and its direction are also evaluated, but not input parameters. Here, in advance, we calculate ray (group) velocity in various phase slowness direction at each node by solving the determinant numerically, smooth them by Spline function and save them as linear function of two parameters: group velocity directions (colatitude, longitude). Using them when needed, we can easily obtain the ray (group) velocity of a given ray direction. The phase slowness is not needed anymore, but it is used in travel-time tomography. In such a case, three vector components of the phase slowness are saved as linear functions of the two parameters: group velocity directions. Next, to confirm that our way of the calculation is correct, we calculate ray (group) velocity in homogeneous transversely isotropic media, and compare our results with analytic solutions. We use elastic parameters of PREM at depth of 24.4km (at the top of LID layer). Our results are almost same as the analytic ones, which shows our calculation works fine. Anisotropic media produce two S phases (qS1 and qS2), but, only one travel-time as an S phase is picked in most observed data processing. To adjust to the actually available data, we assume the picked S data correspond to the first S arrivals, and adopt the faster group velocity of two S phases at each node to calculate the travel-time of the first S arrival.

Keywords: shortest path method, anisotropy, ray tracing

©2021. Japan Geoscience Union. All Right Reserved.

Numerical simulations of weak localization of scalar waves based on the finite difference method (2)

*Jun Kawahara[1], Masanobu Sato[1]

1. Graduate School of Science and Engineering, Ibaraki University

Short-wavelength random heterogeneities in the Earth’ s lithosphere scatter seismic waves propagating therein. In most cases, we can consider scattered waves to be incoherent. Nevertheless, there exists an interference phenomenon due to multiple scattering called weak localization (WL), if a wave source and a receiver are located at the same position. WL is caused because a pair of waves, which propagate along reciprocal paths via identical scatterers, have the same phase and hence constructively interfere. Margerin et al. (2001) theoretically investigated WL of scalar waves and concluded that the intensity at around the source is enhanced twice as large as that in a distant position, the diameter of the volume of intensity enhancement corresponds to the wavelength of the input wave, and the emergence time of this volume is governed by the scattering mean-free time (SMFT).

In our previous study (2019, SSJ fall meeting), we simulated WL of scalar waves in 2-D von Karman-type random media, using the finite difference method (FDM). We confirmed that the obtained intensities at the sources were nearly doubled as time passed. The peak widths of intensity were about half the dominant wavelength of the input waves. However, we found no systematic relationship between the peak emergence times and the SMFTs predicted based on the Born approximation (Sato et al., 2012). A possible reason may be the breakdown of the approximation under the present model setting.

In this study, we simulated WL of scalar waves in media with randomly distributed discrete scatterers, like cracks or inclusions. In contrast to random media, the total scattering cross section (TSCS) of a discrete scatterer can be defined without approximations. If scatterers with TSCS σ_0 are distributed with a number density n, then the SMFT is given as $(n\sigma_0 V_0)^{-1}$, where V_0 is the background wave velocity.

We adopted again a velocity-stress scheme FDM (Virieux, 1984). We modeled scatterers as small low-velocity squares with the side length of several grid intervals. These scatterers were distributed randomly, but without overlapping, in an area on the grid. We repeated simulations for many such areas with the same number density, and then calculated the ensemble average of intensity distributions from synthesized wavefields. We also estimated the TSCS of each scatterer after Suzuki et al. (2006). We repeatedly simulated plane waves propagating in areas with scatterers, and then evaluated scattering Q^{-1} as a function of wavenumber k from the spectra of the ensemble-averaged waves. We then obtained the TSCS $\sigma_0(k)$ via the relation $Q^{-1}=n\sigma_0/k$. Here we assumed the sparse distributions of scatterers and the wavelength much longer than the scatter size, which means nearly isotropic scattering.

Our simulations denoted again the intensity enhancement at the sources, with the relative peak heights of intensity being about two. The peak widths of the intensity were close to the dominant wavelength of the input waves. The peak emergence times were fairly smaller than the SMFT, but we found positive correlation between them. The peaks tended to emerge earlier for denser distribution of scatterers, that is, stronger scattering.

Keywords: weak localization, scalar waves, finite difference method, discrete scatterers

©2021. Japan Geoscience Union. All Right Reserved.

©2021. Japan Geoscience Union. All Right Reserved.

Observability of seismic radial anisotropy parameters by the analysis of surface waves and receiver functions based on the MCMC analysis

*Jumpei Maruyama[1], Hitoshi Kawakatsu[1], Nozomu Takeuchi[1]

1. University of Tokyo, Earthquake Research Institute

Although recent studies have reported the existence of strong radial anisotropy (RA) in the upper mantle/crust beneath the ocean and in the shallow crust directly under volcanos (e.g., Ekstrom & Dziewonski, 1998; Nettles & Dziewonski, 2008; Russell et al., 2019; Jaxybulatov. et al., 2014; Nagaoka, 2020), no constraint for its origin has been obtained from seismic observations. This is partly because the Rayleigh wave sensitivity kernels for vertical S wave velocity β_V and dimentionless parameter η_K, which is recently defined to represent the incident angle dependence of the bodywave phase velocity in RA, are similar, and thus, it is difficult to estimate each independently by surface wave analysis (Kawakatsu 2016). It should be also noted that the inaccuracy of η_K may mean β_V is not determined exactly.
In this study, we try to evaluate the observability of the new parameter η_K using Markov chain Monte Carlo (MCMC) method. In order to confirm the independence of estimations for multiple parameters, the Metropolis-Hastings method analysis is performed using surface wave dispersion data and receiver functions with multiple different incident angles. As a result of preliminary tests on a simple two-layer structure model with radial anisotropy, the trade-off between η_K and β_V can be resolved and both can be estimated accurately in the case that incident angles range between 20-30 [deg] for the S-wave and 20-50 [deg] for the P-wave receiver functions. This result may suggest that the RA parameters can be estimated by combining surface waves and receiver functions even in a more complicated structural model. In the presentation, we plan to clarify how the observability of radial anisotropy changes depending on data corresponding to various observation environments, which may further contribute to future analysis and/or observation.

Keywords: radial anisotropy, surface wave, receiver function , MCMC

©2021. Japan Geoscience Union. All Right Reserved.

[J] Poster | S (Solid Earth Sciences)：S-GL Geology

Sat. Jun 5, 2021 5:15 PM - 6:30 PM JST | Sat. Jun 5, 2021 8:15 AM - 9:30 AM UTC | Ch.15_1

[S-GL23] Geologic structure and tectonic history of East Asia and Japanese Islands

convener:Makoto Otsubo(Geological Survey of Japan, Research Institute of Earthquake and Volcano Geology), Jun Hosoi(Geological Survey of Japan, Institute of Geology and Geoinformation, AIST)

The main aim of this session is to discuss geologic structure and tectonic history of East Asia, especially of Japanese Islands, on the basis of the recent results of geology and other earth sciences.

[SGL23-P01] Estimation of fluid migration along the Out of Sequence Thrust from quartz vein geometric information
-Estuimation of permeability at Nobeoka Thrust in Kyushu, southwest Japan-

*Hinako Hosono[1], Takato Takemura[1], Makoto Otsubo[2] (1.Nihon University Colledge of Humanities and Sciences, 2.Geological Survey of Japan, Research Institute of Earthquake and Volcano Geology)

[SGL23-P02] Detrital zircon geochemistry in the Shimanto Accretionary Complex: Tectonic constraints on formations of the Jurassic to Cretaceous batholiths in the eastern Asian margin

*Shogo Aoki[1], Kazumasa Aoki[2], Mayuko Fukuyama[3], Masatsugu Ogasawara[4] (1.Graduate School of International Resource Sciences, Akita University, 2.Center For Fundamental Education, Okayama Univerisity of Science, 3.Graduate School of Engeneering Science, Akita University, 4.Institute of Geology and Geoinformation, Geological Survey of Japan, National Institute of Advanced Industrial Science and Technology)

[SGL23-P03] Itayama Nappe, meta-chert and gabbro in the Ryoke Belt of the Takato-Itayama area, central Japan

*Akira Ono

[SGL23-P04] Publication of the 1:50,000 geological map of the Ikeda District

*Atsushi Noda[1], Kazuhiro Miyazaki[1], Kiyohide Mizuno[1], Mitsuhiro Nagata[2] (1.National Institute of Advanced Industrial Science and Technology, 2.Japan Atomic Energy Agency)

[SGL23-P05] Tectonic slices at the Anko outcrop of Median Tectonic Line, Oshika Village, Nagano Prefecture, Japan

*RYOSUKE ISAJI[1], HIDEO TAKAGI[1] (1.Waseda University)

[SGL23-P06] Zircon U–Pb age of Paleoproterozoic granite gneiss from the Ogcheon Belt, Geumsan area and Paleoproterozoic leucogranite and quartzite from the Yeongnam Massif, Seolcheon area, South Korea

*Kenichiro Iwamizu[1,2], Yasutaka Hayasaka[1], Ji-Hoon Kang[3], Kosuke Kimura[1,4], Tomoyuki Shibata[1] (1.Hiroshima Univ., 2.The Univ. of Tokyo, 3.Andong National Univ., 4.National Inst. of Tech., Kure College)

Estimation of fluid migration along the Out of Sequence Thrust from quartz vein geometric information
-Estuimation of permeability at Nobeoka Thrust in Kyushu, southwest Japan-

*Hinako Hosono[1], Takato Takemura[1], Makoto Otsubo[2]

1. Nihon University Colledge of Humanities and Sciences, 2. Geological Survey of Japan, Research Institute of Earthquake and Volcano Geology

Slow slip earthquake has been attracting attention as a phenomenon that induces a megathrust earthquake along the plate boundary. The existence of fluid as well as the surrounding rock physical properties is an important factor for the slow slip earthquake. Geophysics studies demonstrated that the region storing the fluid and seismogenic zones are well overlapping, however, the heterogeneities of spatial fluid distribution and the processes of the increasing fluid pressure are poorly understood. In order to discuss the fluid migration and increasing fluid pressure along the out-of-sequence thrust based on permeability, numerical analysis was carried out using the geometric information of the quartz veins measured at the outcrop at Nobeoka, southwest Japan.
Footwall consisted of muddy melange with maximum paleo-temperature of 250 ˚C and hanging wall consisted of sand and mudstone with maximum paleo-temperature of 320 ˚C locate in the west and east part respectively of the Nobeoka thrust. The depth of the Nobeoka thrust fault is estimated to be 9.1 to 7.0 km from the geothermal gradient(Kondo et al., 2005). In this study, the following a) to c) were carried out at the Nobeoka thrust fault. a) observation of thin sections: The thin sections of the mineral veins took at the outcrop were observed, and the constituent minerals were identified and the mineral veins were classified. b) measuring veins: 8 square grids (A to G in the footwall, H in the hanging wall) with a side of 2.5m to the east-west direction across the Nobeoka thrust were generated and width, length, strike, and dip of the mineral veins in the grid were measured. c) Calculation of permeability by the numerical analysis: The permeability k_1, k_2, k_3 and flow direction are calculated from three-dimensional geometry information of veins measured in b) using the tensor analysis method proposed by Oda (1983).
As a result, the veins mainly consisted of quartz and calcite. The three-dimensional geometric distribution of the veins at the footwall could be classified into two groups, A to D and E to G. From the estimated permeability and its flow direction, it was found that the maximum permeability k_1 was almost perpendicular to the fault, and the fluid was easy to flow in this direction. The order of the maximum permeability k_1 was 10^{-9} to 10^{-10}. In the grid from E to G, it is difficult to flow in the direction orthogonal to the fault plane (k_3 is in the direction orthogonal to the fault plane), and the magnitude of the permeability was $k_1 = k_2 >> k_3$. On the other hand, in the A to D grids, permeabilities were almost $k_1 = k_2 = k_3$. These permeabilities estimated from outcrops are expected to enable us to consider the fluid behavior along the fault when considering the Fault valve model by Sibson (1992) using a specific permeability.

Keywords: Quartz vein, Permeability, Accretionary prism, Permeability tensor, Nankai Trough, Subduction zone

©2021. Japan Geoscience Union. All Right Reserved.

Detrital zircon geochemistry in the Shimanto Accretionary Complex: Tectonic constraints on formations of the Jurassic to Cretaceous batholiths in the eastern Asian margin

*Shogo Aoki[1], Kazumasa Aoki[2], Mayuko Fukuyama[3], Masatsugu Ogasawara[4]

1. Graduate School of International Resource Sciences, Akita University, 2. Center For Fundamental Education, Okayama Univerisity of Science, 3. Graduate School of Engeneering Science, Akita University, 4. Institute of Geology and Geoinformation, Geological Survey of Japan, National Institute of Advanced Industrial Science and Technology

Most of the Phanerozoic granite batholiths in the North and South China blocks have a tectonical-petrogenetical relation to the Pacific-type orogeny. In connection with this aspect, the major orogenic components including the batholiths of the Jurassic and Cretaceous are relatively well preserved especially in SW Japan. However, it is difficult to estimate the paleo-geologic structures even in the Jurassic and Cretaceous components, because they suffered from later disturbances such as tectonic and surface erosions. In this study, we compared the detrital zircon U–Pb ages and Hf isotopic ratios obtained from fifteen terrigenous clastic rocks in the Cretaceous Shimanto Accretionary Complex of the Shikoku, SW Japan. This comparison is a key to understand the Jurassic-to-Cretaceous spatial-temporal distributions of the batholiths connected with the inner structures of the subduction zone.
The zircon age spectra from the formations before ca. 100 Ma show two age clusters of Permian to middle Jurassic (from ca. 280 to 160 Ma) and early-to-middle Cretaceous (ca. 130 to 100 Ma). On the other hand, those from the formations after ca. 100 Ma show a single age peak of middle-to-late Cretaceous (< ca. 130 Ma). The major change in the age distributions suggests an oceanward migration of the magmatic front in the late Cretaceous (ca. 100 Ma), and the large batholiths formed after 100 Ma played a role in controlling terrigenous supply routes between coeval back-arc and fore-arc domains.
The Hf isotopic ratios ($\varepsilon_{Hf(t)}$) obtained from the analyzed zircons show characteristics values in corresponding to their crystallization ages; moderate juvenile to intermediate values (+6 to -4) for ca. 220 to 200 Ma, moderate juvenile to highly evolved values (+10 to -26) for ca. 200 to 180 Ma, moderate to highly evolved values (-4 to -30) for ca. 180 to 130 Ma, moderate juvenile to intermediate values (+10 to -4) for ca. 130 to 100 Ma, and intermediate to moderate evolved values (+4 to -10) for < ca. 100 Ma.
Integration of these results with the U–Pb age spectra leads to suggestion that the late Jurassic to early Cretaceous granites were generated from the older materials at the inland areas of the China blocks; on the other hand, the late Cretaceous granites were originated from the younger materials at the coastal areas. Moreover, subducting oceanic crusts and/or asthenospheric materials are also suggested to be involved in the early Cretaceous granites. Probably, the major change of source materials in relation to each granite was close to the transition in the position of magmatic front at the time in the North and South China blocks.

Keywords: zircon, U–Pb dating, Hf isotopic ratio

©2021. Japan Geoscience Union. All Right Reserved.

Itayama Nappe, meta-chert and gabbro in the Ryoke Belt of the Takato-Itayama area, central Japan

*Akira Ono

Itayama Nappe, meta-chert and gabbro are distributed near the Median Tectonic Line (MTL) of the Itayama area, Takato Town. Here, we introduce these geological bodies. Small Nappe occurs in the Itayama area [1]. Here, this is called Itayama Nappe. The Itayama Nappe is composed of various rocks derived from the Ryoke and Sanbagawa Belts. However, low-grade metamorphic rocks and sedimentary rocks in the Itayama Nappe are not exposed in the nearby Ryoke and Sanbagawa Belts. The Itayama Nappe is sandwiched between two faults, MTL-E and MTL-W (Figure A). However, there is a problem with the geology of the northern part of the Itayama Nappe. In this area an outcrop of MTL exists near the Miyadonosawa dam [2]. That is, the blue fault in Figure A is the MTL. The two MTLs do not exist in this area. Hence, the Itayama Nappe is a narrow geological body extending from north to south that has entered the Kashio mylonite zone (Figures B and C).
Narrow and long meta-chert is distributed in the vicinity of MTL [3]. To the west of the long meta-chert, mylonitized pelitic and siliceous rocks are exposed as xenoliths of Hiji tonalite. For example, various siliceous rocks are exposed almost continuously over about 120 m along a small valley to the east of the Kajimura village (Figure C). These mylonites are derived from the Hase Unit of the accretionary complex [4]. Sizes of quartz grains are about 100 μm for the quartz-rich portion of a siliceous mylonite (Figures D and E) near the red dotted line in Figure C. The red dotted line is the western margin of the Kashio mylonite zone for granitic rocks [3]. The psammitic hornfels in Figure C are not metamorphic rocks derived from the Hase Unit.
Small hornblende gabrro is exposed in two places along the forest road leading to Mt.Gatsuzozan (Figure F). The gabbro intrudes into banded tonalite (Figure G). The Hiji tonalite in the Itayama area has a relatively uniform lithology, but tonalites near the gabbro exhibit remarkably diverse lithologies (Figures H and I). The geological relationship between the Hiji tonalite and Katsuma quartz diorite is unknown, but in the Shioku to the north of Itayama, an outcrop was found in which these granitoids are almost vertically in contact with each other.
The Itayama Nappe is a geological body that has entered the Kashio mylonite zone. The existence of allochthonous geological body in the Kashio mylonite zone was first reported from the Kashio area. Watanabe & Kinugasa [5] reported the occurrence of metamorphic rocks which are thought to be the Sanbagawa metamorphic rocks. Next, microbreccia is found near the Bungui Pass of the Hase area [6]. Subsequently, Awasawa metamorphic rocks were reported which belong to neither Sanbagawa metamorphic rocks, Kashio mylonite nor microbreccia [7]. Microbreccia is a fractured Awasawa metamorphic rock. The Awasawa metamorphic rocks are mainly composed of garnet-biotite-muscovite schist. This pelitic schist is finer than the Sanbagawa schist containing garnet and biotite. Moreover, white mica is not phengite.The (FeO+MgO) content of muscovite is not high as compared with that of the Sanbagawa schist.

[1] Hara et al., 2004, Struc. Geol, No 48, 1. [2]Ono, 2013, GSJ Meeting, R5-P-13. [3]Makimoto et al, 1996, Geology of the Takato district, Geol.Surv.Jpn. [4] Ono, 2018, GSJ Meeting, R15-P-13.[5] Watanabe & Kinugasa, 1970, GSJ Meeting, p.286. [6] Takagi, 1984, Geol. Soc. Jpn, 81. [7] Ono, 2002, Geol. Soc. Jpn, 733.

©2021. Japan Geoscience Union. All Right Reserved.

Keywords: Ryoke belt, Takato-Itayama, Median Tectonic Line, Kashio mylonite, Hase unit

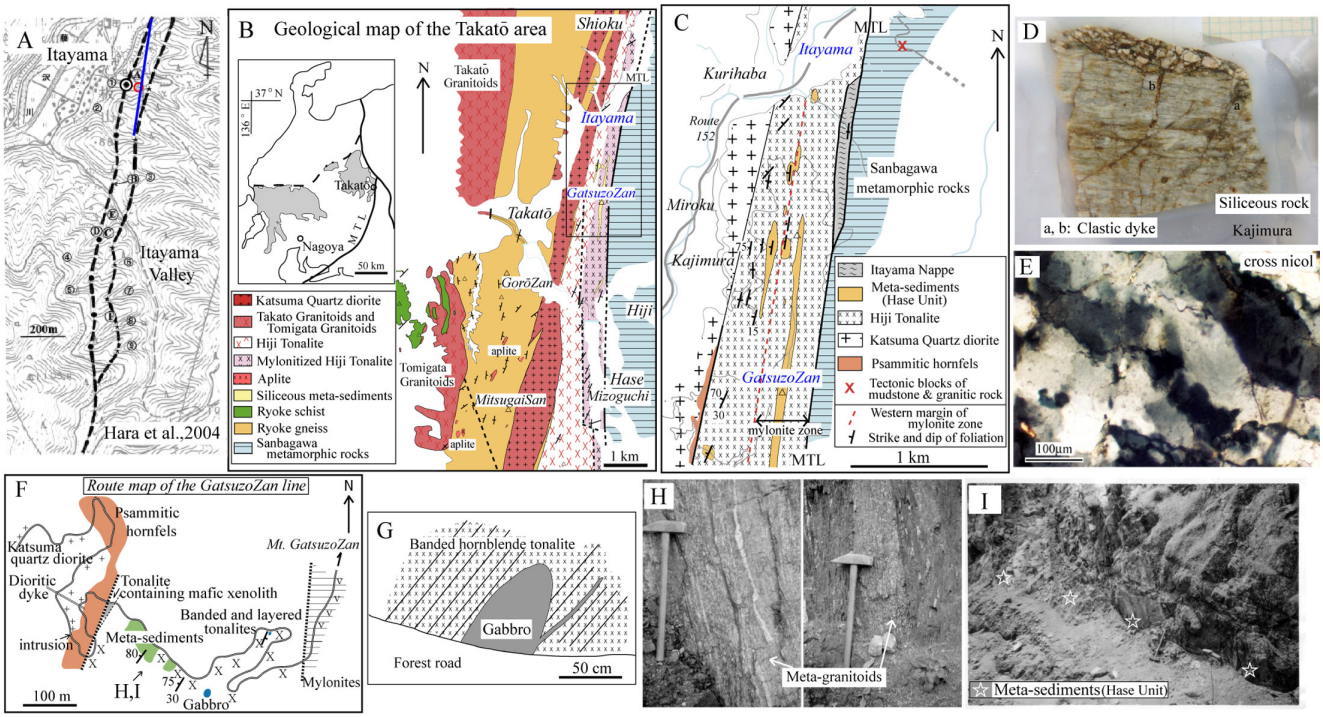

©2021. Japan Geoscience Union. All Right Reserved.

Publication of the 1:50,000 geological map of the Ikeda District

*Atsushi Noda[1], Kazuhiro Miyazaki[1], Kiyohide Mizuno[1], Mitsuhiro Nagata[2]

1. National Institute of Advanced Industrial Science and Technology, 2. Japan Atomic Energy Agency

Geological map of the Ikeda District, which is located in the northeastern part of Shikoku Island, has been published. The basement rocks are divided into the Inner and Outer zones of Southwest Japan by the Median Tectonic Line (MTL). The Inner Zone is composed of the Ryoke Complex, the Izumi Group (Upper Cretaceous), the Setouchi volcanic rocks (Miocene), and the Mitoyo Group (Lower Pleistocene). The Outer Zone comprises the Sanbagawa Complex (Upper Cretaceous–Paleogene) and the Dochu Formation (Lower Pleistocene). The southern margin of the Sanuki Mountain Range is bounded by active faults of the MTL, which include the Ikeda, Mino, and Hashikura faults, and they cut the lower terrace deposits (Upper Pleistocene) and the Holocene. The northern margin of the mountain range is bordered by Takenari, Ebata, and Kashihara faults; the Takenari Fault deformed the Mitoyo Group (Lower Pleistocene), and the Ebata Fault partly cut the lower terrace deposits (Upper Pleistocene). Landslide deposits are common in this district, especially in the southern part of the mountain range. Therefore, this district is an important area in terms of understanding of the basement geology as well as geohazards of earthquakes and landslides.

The Ryoke Complex comprises high-T/P metamorphic rocks, granitic rocks (Kan-onji Granite), and dikes. The protolith age of the metamorphic rocks is Late Permian based on the youngest peak age (258 Ma). The zircon U–Pb ages of granites and dikes range between 94 and 88 Ma. The Izumi Group unconformably overlies the Kan-onji Granite, which is composed of the northern marginal facies and the main facies. The northern marginal facies is characterized by conglomerate and massive mudstone, while the main facies is composed of alternating beds of sandstone and mudstone with felsic tuff beds. Ammonite fossils (*Metaplacenticeras subtilistriatum* zone) and zircon U–Pb ages (79–78 Ma) of felsic tuff beds indicate that the depositional age is the middle Campanian, Late Cretaceous. The Sanbagawa Complex is subdivided into the Itano, Minawa, and Koboke units from north to south. They are composed of mafic, pelitic, and psammitic schist. U–Pb ages of detrital zircons extracted from psammitic schists (93–81 Ma for Minawa unit and 76–74 Ma for Koboke unit) and K–Ar ages of phengite (74–72 Ma for Minawa unit and 65–62 Ma for Koboke unit). The Lower Pleistocene includes the Mitoyo Group (Saita, Koda, and Yakeo formations), Norouchi and Dochu formations. Formations of the Mitoyo Group are interfingered each other. Two widespread tephras constrain the depositional ages (2.4–2.3 Ma for the Yakeo and 1.75 Ma for the Saita). The *Metasequoia* sp. fossils also occur in the Mitoyo Group and the Dochu Formation.

Based on the above evidences, the geological history in this district can be summarized as follows. In the arc side, granitic magmas continuously provided to the lower crust that caused high-temperature and low-pressure metamorphism during the Late Cretaceous (94–88 Ma). At the same time (93–74 Ma), trench-fill deposits subducted beneath a forearc wedge to the depths of 20–35 km along the plate boundary, and then experienced low-temperature and high-pressure metamorphism at the later stage of subduction (74–62 Ma). In addition, the Kan-onji Granite was exposed on the seafloor and unconformably overlain by the Izumi Group (79–78 Ma). The simultaneous occurrences of magmatic, metamorphic, and depositional events recognized in this district imply an importance of flow/transport paths of materials in a forearc, which include supply of continuous magma to the lower crust, uplift and exhumation of the upper crust, sediment transport and deposition on the arc, subduction of trench-fill sediments beneath

©2021. Japan Geoscience Union. All Right Reserved.

the arc. Finally, in response to the regional stress change in Southwest Japan since early Pleistocene, the Sanuki Mountain Range began to uplift and the Mitoyo Group and Dochu Formation deposited at the both sides of the mountain range.

Keywords: Geological map, Ryoke Complex, Izumi Group, Sanbagawa Complex, Mitoyo Group, Median Tectonic Line

©2021. Japan Geoscience Union. All Right Reserved.

Tectonic slices at the Anko outcrop of Median Tectonic Line, Oshika Village, Nagano Prefecture, Japan

*RYOSUKE ISAJI[1], HIDEO TAKAGI[1]

1. Waseda University

The Median Tectonic Line (MTL) divides low-grade Sanbagawa schists and high-grade Ryoke metamorphic rocks with large amount of granitic rocks. The fault rocks along the MTL in the Anko outcrop in Oshika Village, Nagano Prefecture, is highly deformed and altered. Therefore, there was some ambiguity about the exact location of the MTL, it was determined by chemical analysis and microscopic observations conducted by Kawamoto et al. (2013). When the black gouge of the MTL is designated as G1, there are three black gouge on the Ryoke side of the MTL, which the authors call G2 (1.4 m thick), G3 (1.6 m thick), and G4 (Anko West outcrop in Takagi et al., 2015: 5.0 m thick) in order of northwestward direction. In this report, we determined the attribution of the gouge (G2, G3) using small rock fragments that had been randomly collected in the gouges, and conducting microscopic observations of the plagioclase fragments there. The plagioclase fragments derived from the Sanbagawa schist are rather fresh albite with inclusions, whereas those from the Ryoke rocks are highly altered because of original Ca content in the plagioclase.
As a result of above observations, albite with inclusions was observed in all five samples of the gouge G3, and in three samples in the gouge G2, but the attribution was uncertain for other two samples, because the fracturing and alteration were particularly severe. In addition, the cataclasite between G2 and G3, which is considered to belong to the Ryoke Belt, showed significant alteration of plagioclase porphyroclasts and was distinctly different from that from the Sanbagawa schist. From the observations mentioned above, it is clear that the black gouge in G2 and G3 is almost exclusively attributed to the Sanbagawa Belt. At G4 (Anko-west outcrop), located 40 m northwest from the MTL, rocks derived from the Sanbagawa schist have been recognized (Ishikawa et al., 2014), and at Anko-Sawa outcrop, about 24 m northwest from the MTL, rocks derived from the Sanbagawa belt are also recognized in the Ryoke belt.
In the Anko outcrop, at least three gouge zone derived from the Sanbagawa schist are intercalated in the Ryoke Belt near the MTL. In this outcrop, variations of strikes exist among the gouges including exact MTL gouge (G1: N25˚E) and another gouges such as G4 (N10˚E ; Takagi et al., 2015) which involves Quaternary activity history. The cataclasites and a slightly consolidated fault gouge shows sinistral shear sense, while the G4 gouge shows younger dextral slip sense. These lines of evidence suggest that the Sanbagawa schist were intercalated into the Ryoke Belt as tectonic slices due to the repeated strike-slip activities of the MTL in the study area.

References

Ishikawa, T., Hirono, T., Matsuta, N., Kawamoto, K., Fujimoto, K., Kameda, J., Nishio, Y., Maekawa, Y., Honda, G, 2014*, Planets and Space*, **66**: 36.
Kawamoto, K., Ishikawa, T., Matsuta, N., Hirono, T., 2013, *Natural history reports of Inadani*, **14**, 1-17.
Takagi, T., Sugiyama, K., Kawamoto, K., Kitazawa, N., 2015, Abstracts, *the 122nd Annual Meeting of the Geological Society of Japan,* R14-O12.

Keywords: Median Tectonic Line, fault gouge, Anko outcrop, tectonic slice

©2021. Japan Geoscience Union. All Right Reserved.

Zircon U–Pb age of Paleoproterozoic granite gneiss from the Ogcheon Belt, Geumsan area and Paleoproterozoic leucogranite and quartzite from the Yeongnam Massif, Seolcheon area, South Korea

*Kenichiro Iwamizu[1,2], Yasutaka Hayasaka[1], Ji-Hoon Kang[3], Kosuke Kimura[1,4], Tomoyuki Shibata[1]

1. Hiroshima Univ., 2. The Univ. of Tokyo, 3. Andong National Univ., 4. National Inst. of Tech., Kure College

Jurassic Daebo granite is widespread in the Geumsan area, Ogcheon Belt, South Korea, and Precambrian rocks are present on a small scale in it (Hong and Choi, 1978). Precambrian rocks are mainly composed of biotite gneiss and granite gneiss. Iwamizu et al. (2021, in press) reported that the granite gneiss (Gn) has an igneous age of ca. 2.5 Ga and two metamorphic ages of ca. 1.89 Ga and 174 ±74 Ma by LA-ICP-MS zircon U–Pb analysis. Gn is one of the second oldest rocks in south Korea, along with the granite gneisses which have the same igneous ages reported by Lee et al. (2016) in the southern Gyeonggi Massif.

The zircon U–Pb ages of Gn that Iwamizu et al. (2021, in press) reported are mostly the result of analysis of the zircon core and mantle data. The cores have various internal structures and show a wide range of ages of 2.5–1.9 Ga. The older the age, the higher the Th/U ratio and the smaller the discordance. Therefore, the igneous age is expected to be ca. 2.5 Ga. The 1.9–1.8 Ga mantle data show vague and round oscillatory zoning and all the Th/U ratios are lower than 0.04. A discordia line can be defined by 1.9–1.8 Ga mantle data in the Tera-Wasserburg concordia diagram. The upper intercept age and the lower intercept age are ca. 1.89 Ga and 174 ±74 Ma, respectively, which are interpreted to be metamorphic ages related to Paleoproterozoic and Jurassic magmatism, respectively. The upper intercept age is consistent with metamorphic ages of the Gyeonggi and Yeongnam Massif (Lee and Cho, 2012). The lower intercept age is consistent with surrounding Jurassic granite. All the zircon U–Pb data are discordant because of the Jurassic metamorphism. Since the detailed location of SKTL (South Korean Tectonic Line) in the Geumsan area is unknown, it is unknown whether the Gn is derived from the Gyeonggi or Yeongnam Massif.

In addition to the above, we newly report Paleoproterozoic leucogranite and quartzite in the Seolcheon area, Yeongnam Massif, which is about 25 km east of the Geumsan area.

The leucogranite looks white because it does not have biotite. It contains approximately 73 wt% SiO_2. It exhibits metaluminous whole rock chemical composition, which is different from the leucogranitoids that have peraluminous whole rock chemical composition reported by Lee et al. (2010) and Lee et al. (2019) in the Yeongnam Massif. Its zircons exhibit two layered structures, core and mantle. The cores (5 points) have homogeneous or banded zoning, concordant U–Pb ages of ca. 2.5–2.4 Ga and high Th/U ratios higher than 0.1. The mantle data (12 points) have oscillatory or banded zoning, concordant U–Pb ages concentrating near 2 Ga and Th/U ratios higher than 0.1. The mean age of the concordant mantle data concentrating near 2 Ga is 1997 ±10 Ma, which is interpreted to be an igneous age. This age is close to an igneous age of 1985 ±10 Ma of the leucogranite gneiss in the Muju area (Lee et al., 2019). The 2.5–2.4 Ga cores are considered to be inherited zircons. Metamorphic age has not been obtained.

The quartzite is mainly composed of coarse quartz and contains a small amount of muscovite. It contains approximately 98 wt% SiO_2. Its detrital zircons mainly show oscillatory zoning. The zircon U–Pb ages (63 points) show a wide range of ages of ca. 3.5–1.9 Ga. Most data are concordant, and all the discordances

©2021. Japan Geoscience Union. All Right Reserved.

are smaller than ca. 7.7 %. The oldest age is 3505 ±28 Ma. The youngest age is 1902 ±31 Ma, which is an upper limit of deposition. The detrital zircons of the quartzite have the biggest age peak at ca. 2.5 Ga, which is the same as the Paleoproterozoic Yuli Group, Yeongnam Massif (Lee et al., 2011) and the Cambrian Jangsan Formation, Taebaeksan zone (Kim et al., 2019).

From the above, ca. 2.5 Ga granite gneiss exists in the Geumsan area, Ogcheon Belt (Iwamizu et al., 2021, in press) and ca. 2.5 Ga inherited or detrital zircons are dominant in the Seolcheon area, Yeongnam Massif (this study). Therefore, extensive magmatism at ca. 2.5 Ga can be suggested in the Geumsan–Seolcheon area if Gn is located southeast of SKTL. If Gn is located northwest of SKTL, Gn can be correlated with the same age granite gneiss in the southern Gyeonggi Massif (Lee et al., 2016), which indicates ca. 2.5 Ga extensive magmatism there.

[References]
Hong, S.-H. and Choi, W.-C. (1978) Geumsan Sheet. Korea Research Inst. of Geoscience and Mineral Resources.
Iwamizu, K. et al. (2021) *J. Geol. Soc. Japan*, **127**, in press, doi: 10.5575/geosoc.2020.0057
Kim, H.-S. et al. (2019) *Int. J. Earth Sci.*, **108**, 1509–1526.
Lee, B.-C. et al. (2016) *Precambrian Res.*, **283**, 169–189.
Lee, B.-C. et al. (2019) *Gondwana Res.*, **72**, 34–53.
Lee, S.-G. et al. (2010) *Chem. Geol.*, **276**, 360–373.
Lee, S.-R. and Cho, K. (2012) *J. Petrol. Soc. Korea*, **21**, 89–112.
Lee, Y.-I. et al. (2011) *J. Geol. Soc. Korea*, **47**, 81–87.

Keywords: Korea, Ogcheon Belt, Yeongnam Massif, zircon, granite, quartzite

©2021. Japan Geoscience Union. All Right Reserved.

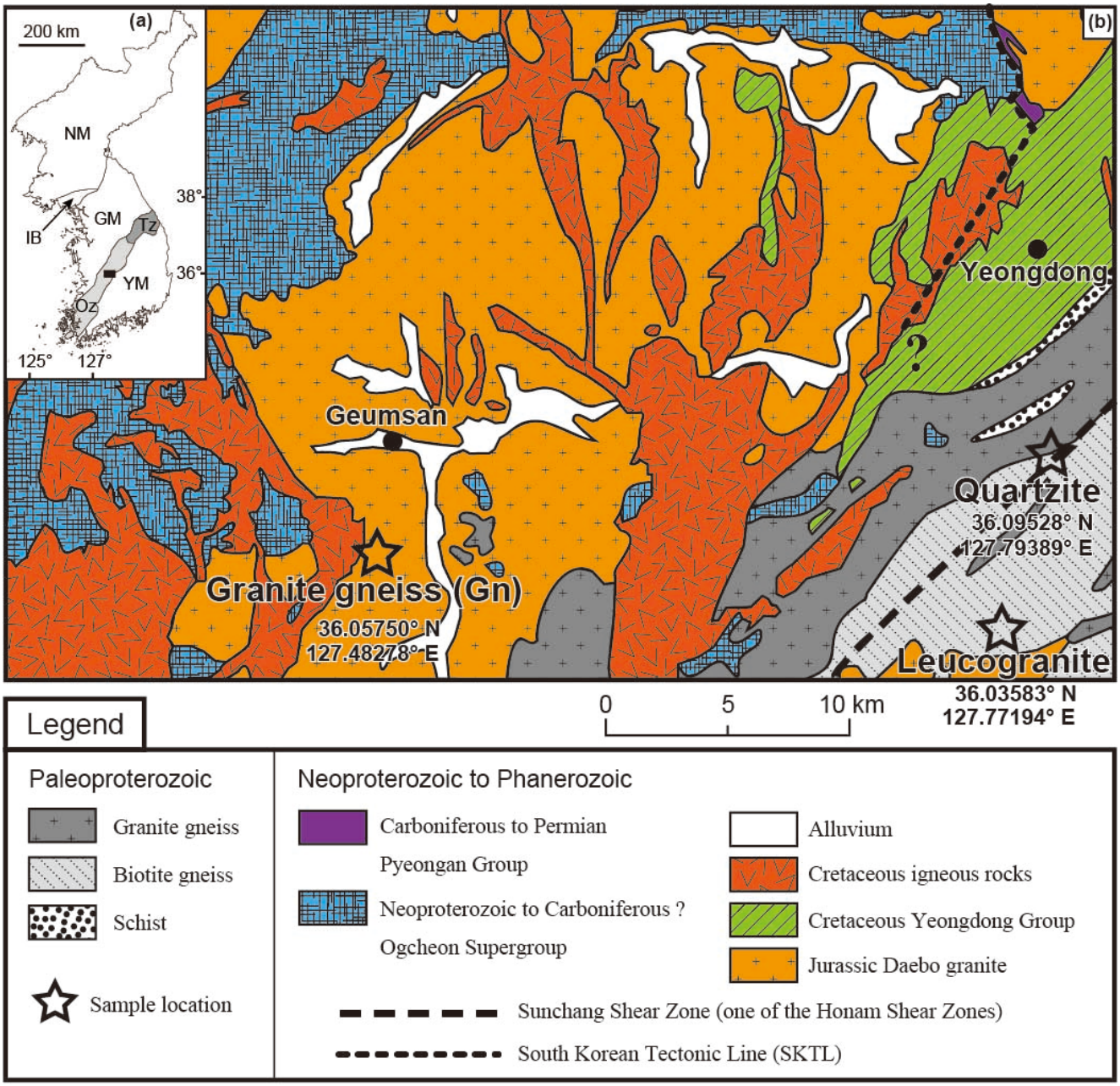

Fig. 1. based on Iwamizu et al. (2021, in press) and references therein.

(a) Tectonic province map of Korea. Black rectangle is study area (b). NM: Nangrim Massif, IB: Imjingang Belt, GM: Gyeonggi Massif, Oz: Ogcheon Metamorphic zone, Tz: Taebaeksan zone, YM: Yeongnam Massif.

(b) Geological map around the Geumsan–Seolcheon area, South Korea.

©2021. Japan Geoscience Union. All Right Reserved.

[J] Poster | S (Solid Earth Sciences)：S-VC Volcanology

Sat. Jun 5, 2021 5:15 PM - 6:30 PM JST | Sat. Jun 5, 2021 8:15 AM - 9:30 AM UTC | Ch.16_1

[S-VC28] Active Volcanism

convener:Yuta Maeda(Nagoya University), Takahiro Miwa(National research institute for earth science and disaster prevention), Takeshi Matsushima(Institute of Seismology and Volcanology, Faculty of Science, Kyushu University)

This session discusses various aspects of active volcanisms including, but not limited to, rec ent and historical eruptions, various phenomena associated with the volcanic activities, und erground structures of the volcanoes, and developments of new instruments based on geop hysical, geochemical, geological, and multidiscipline approaches. We also welcome studies o n understanding and predicting the transitions of the eruptive activities from observational, theoretical, and experimental approaches.

[SVC28-P01] Local deformation at Mt.Tokachi detected by TS-InSAR

*Satoshi Okuyama[1], Shinobu Ando[1] (1.Meteorological Research Institute)

[SVC28-P02] Volcanic tremor source location at Tokachidake volcano from cross-correlation analysis of 2018-2020 seismic data

*Theodorus Permana[1], Hiroshi Aoyama[1] (1.Institute of Seismology and Volcanology, Faculty of Science, Hokkaido University.)

[SVC28-P03] Time-series of crustal deformation on Azuma volcano revealed by PALSAR-2 data

*Yuji Himematsu[1], Taku Ozawa[1] (1.National Research Institute for Earth Science and Disaster Resilience)

[SVC28-P04] Existence of deep pressure sources and its behaviors during recent volcanic activity at Azumayama, NE Japan

*Jun Okada[1], Yu Nihara[2], Yuji Miyagawa[3], Susumu Seki[3], Takuya Yamamura[2], Shin Chikasawa[3] (1.Volcanology Research Department, Meteorological Research Institute - Japan Meteorological Agency, 2.Regional Volcanic Observation and Warning Center, Sendai Regional Headquarters - Japan Meteorological Agency, 3.Seismology and Volcanology Division, Sendai Regional Headquarters - Japan Meteorological Agency)

[SVC28-P05] Amorphous silica coating on flank deposits of the 1783 CE (Tenmei) eruption at Asama volcano

*Takayuki Nakatani[1], Sarina Sugaya[2], Maya Yasui[3], Satoshi Okumura[2], Michihiko Nakamura[2] (1.Geological Survey of Japan, National Institute of Advanced Industrial Science and Technology, 2.Department of Earth Science, Graduate School of Science, Tohoku University, 3.Department of Earth and Environmental Sciences, College of Humanities and Sciences, Nihon University,)

[SVC28-P06] **Monitoring of underground temperature in Jigokudani, Midagahara volcano using LPWA devices**

*Tohru Watanabe[1] (1.Faculty of Sustainable Design, University of Toyama)

[SVC28-P07] Formation of N_3 member from the younger Ō-shima group distributed around the Habu area, southeastern part of Izu-Ō-shima Island.

*Ryota Uchiyama[1], Izumi Sakamoto[1] (1.School of Marine and Technology, Tokai University)

[SVC28-P08] Banded Tremors Activity at Miyakejima Volcano

*Yoshihiro Otsuka[1], Shinya Nagato[1] (1.Japan Meteorological Agency)

[SVC28-P09] Estimating the underground pressure source of Miyakejima volcano by integrated processing of GNSS and leveling data

*Haruna Watanabe[1], Takeshi Matsushima[2], Miyo Fukui, Atsushi Watanabe[3], Jun Oikawa[3], Takashi OKUDA[4], Taku Ozawa[5], Yosuke Miyagi[5] (1.Department of Earth and Planetary Sciences, Graduate School of Science, Kyushu University, 2.Institute of Seismology and Volcanology, Faculty of Sciences, Kyushu University, 3.Earthquake Research Institute, University of Tokyo, 4.Earthquake and Volcanology Research Center, 5.National Research Institute for Earth Science and Disaster Resilience)

[SVC28-P10] Three-Dimensional Crustal Structure beneath Hachijojima Island using dense seismic observation data

*Shotaro Kanke[1], Hiroyuki Azuma[1], Yoshiya Oda[1] (1.Tokyo Metropolitan Univ.)

[SVC28-P11] Ground deformation between eruptions at Nishinoshima Island using InSAR time series analysis

*Shinobu Ando[1], Satoshi Okuyama[1] (1.Volcanology Research Department, Meteorological Research Institute)

[SVC28-P12] Abrupt change in eruption style during the 2019-2020 eruption of Nishinoshima, Ogasawara

*Fukashi Maeno[1], Takayuki Kaneko[1], Natsumi Hokanishi[1], ATSUSHI YASUDA[1], Yoshihiko Tamura[2] (1.Earthquake Research Institute, University of Tokyo, 2.Japan Agency for Marine-Earth Science and Technology)

[SVC28-P13] The depth of the air-magma interface and the sound velocity in the shallow conduit of Aso volcano inferred from seismic and infrasound signals

*Kyoka Ishii[1], Akihiko Yokoo[1] (1.Graduate School of Science, Kyoto University)

[SVC28-P14] Estimation of source location of high-frequency tremor at Aso volcano by array analysis

*hirotaka tanaka[1], Takahiro Ohkura[2], Hiroyuki Inoue[2], Shin Yoshikawa[2] (1.kyoto university, 2.Aso Volcanological Laboratory)

[SVC28-P15] Debris avalanche deposits and the stratigraphy on the outcrop to north east from Mt.Unzen

*Daisuke Nagai[1] (1.Mt.Unzen disaster memorial hall)

[SVC28-P16] Vault-housed extensometers and tiltmeters recorded continuous crustal movement during the eruption of Kirishima Shinmoe-dake in 2018

*Koki Yoshinaga[1], Takeshi Matsushima[2], Hiroshi Shimizu[2], Yusuke Yamashita[3], Shintaro Komatsu[3], Ken'ichi Yamazaki[3] (1.Department of Earth and Planetary Sciences, Graduate School of Science, Kyushu University, 2.Institute of Seismology and Volcanology, Faculty of Sciences, Kyushu University, 3.Miyazaki Observatory, Disaster Prevention Research Institute, Kyoto University)

[SVC28-P17] Two experiments using a small-aperture infrasonic array at Kirishima

*Kazuya Yamakawa[1], Mie Ichihara[1], Dan Muramatsu[2], Takeshi Matsushima[2], Ruka Wada[3], Hideki Takahashi[3], Isao Shimoyama[4] (1.Earthquake Research Institute, University of Tokyo, 2.Institute of Seismology and Volcanology, Faculty of Science, Kyushu University, 3.Department of Mechanical Engineering, Faculty of Science and Technology, Keio University, 4.Department of Intelligent Robotics, Toyama Prefectural University)

[SVC28-P18] Estimating the source of volcanic earthquakes during eruption events at Kirishima Volcanos, in 2018, using spatial distribution of earthquake amplitude.

*Daiki Goshima[1], Satoshi Matsumoto[2], Ayaho Mitsuoka[1], Yuhei Yuasa[4], Yuta Kawamura[1], Mie Ichihara[3] (1.Department of Earth and Planetary Sciences, Graduate School of Science, Kyushu University,

2.Institute of Seismology and Volcanology, Faculty of Sciences, Kyushu University, 3.Earthquake Research Institute, University of Tokyo, 4.Osaka Regional Headquarters, Japan Meteorological Agency)

[SVC28-P19] S-wave attenuation structure of Mt.Kirishima estimated using coda of S-wave

*Takuji Watanabe[1], Ayaho Mitsuoka[1], Yuhei Yuasa[1], Yuta Kawamura[1], Daiki Goshima[1], Satoshi Matsumoto[2], Mie Ichihara[3] (1.Department of Earth and Planetary Sciences, Graduate School of Science, Kyushu University, 2.Institute of seismology and Volcanology, Faculty of Sciences, Kyushu University, 3.Earthquake Research Institute, University of Tokyo)

[SVC28-P20] Estimate of magma supply beneath Aira caldera during the last 10 years based on ground deformation observation and amount of volcanic ejecta

*Daisuke Miki[1], Tomoki Tsutsui[1], Masato Iguchi[1] (1.Sakurajima Volcano Research Center, Disaster Prevention Research Institute, Kyoto University)

[SVC28-P21] Temporal changes of seismic velocities and scattering properties at Suwanosejima volcano inferred from seismic interferometry

*Takashi Hirose[1], Hideki Ueda[1], Eisuke Fujita[1] (1.National Research Institute for Earth Science and Disaster Resilience)

[SVC28-P22] Development of volcano deformation calculation system using boundary element method (2)

*Ryohei Kawaguchi[1] (1.Meteorological Research Institute)

[SVC28-P23] Estimation of seismic scattering coefficients at active volcanoes

*Mare Yamamoto[1] (1.Research Center for Prediction of Earthquakes and Volcanic Eruptions, Graduate School of Science, Tohoku University)

[SVC28-P24] Temporal Change in Coda-Q at the upper East Rift Zone of Kīlauea volcano, Island of Hawai‘i

*Takuji Yamada[1], Paul G Okubo[2] (1.Faculty of Science, Graduate School of Science and Technology, Ibaraki University, 2.University of Hawai‘i at Mānoa)

[SVC28-P25] A prototype of advanced Multi-GAS for unmanned aircraft systems

*Masaaki Morita[1], Toshiya Mori[2] (1.Geological Survey of Japan, AIST, 2.Graduate School of Science, The University of Tokyo)

Local deformation at Mt.Tokachi detected by TS-InSAR

*Satoshi Okuyama[1], Shinobu Ando[1]

1. Meteorological Research Institute

Introduction

Mt.Tokachi is one of the most active volcanoes in Hokkaido, Japan. Its notable eruptions took place around every 30 years; in 1926, 1962 and 1988-89 (4th edition of National Catalogue of the Active Volcanoes in Japan). 32 years have passed since the last eruption, which implies that Mt.Tokachi is at a preparation stage for the next eruption.

GNSS observation revealed the local inflation since 2006, and as much as 10cm of displacement is observed at Mae-Tokachi GNSS station established by Geological Survey of Hokkaido. After that, inflation slowdowned in 2017, then turned to deflation in 2018.

We have been monitoring the activity of Mt.Tokachi through SAR interferometry and reported about the deformation at western flank (Okuyama et al., 2019). In this presentation, we report the result of time-series analysis using GIAnT (Agram et al., 2012).

Data and Method

We composed 58 pairs of path 122 (Ascending, Right-looking), path 17 (Descending, Right-looking) and path 18 (Descending, Right-looking) observed by ALOS-2/PALSAR-2. We could not collect large number of SAR images due to low observation frequency and the fact that the target area is covered by snow for more than 6 months. Hence, to increase the number of pairs, we regard path 17 and 18, whose incidence angles differ by about 10 decimal degrees, as same path of which incidence angle is the average of those. We applied NSBAS method to those pairs to detect time evolution of the deformation, linearly interpolated between observation dates, then calculated two-dimensional displacement.

Result

The result timeseries show two main characteristics –upheaval around Furikozawa fumaroles and complex deformation at the slope located at the west of Mae-Tokachi. The former turns into subsidence in late 2017, then became stagnant after 2018. This trend is same as the displacement observed at Mae-Tokachi GNSS station. The latter, on the other hand, shows partial correspondence with the topography, which implies the effect of landslide. However, as we reported in Okuyama et al. (2019), the pattern includes local upheaval, which cannot be explained by the landslide. Unlike the deformation around Furikozawa fumaroles, these deformation progress at a uniform rate.

Acknowledgement

PALSAR-2 SLC data are shared among PIXEL (PALSAR Interferometry Consortium to Study our Evolving Land surface), and provided from JAXA under a cooperative research contract with ERI, Univ., Tokyo. The ownership of PALSAR-2 data belongs to JAXA. We used RINC (Ozawa et al., 2016) and Fundamental Geospatial Data (Elevation) published by GSI for interferogram processing. We used GSI tile for displaying displacement map.

©2021. Japan Geoscience Union. All Right Reserved.

Keywords: Mt.Tokachi, SAR Interferometry, Crustal Deformation

©2021. Japan Geoscience Union. All Right Reserved.

Volcanic tremor source location at Tokachidake volcano from cross-correlation analysis of 2018-2020 seismic data

*Theodorus Permana[1], Hiroshi Aoyama[1]

1. Institute of Seismology and Volcanology, Faculty of Science, Hokkaido University.

Volcanic tremors are known to be related to the processes that involve the movement of magma and gas within a volcano. During the 1988-1989 eruptive activity at Tokachidake volcano, Hokkaido, Japan, volcanic tremors were observed accompanying explosive eruptions. Volcanic tremors were sometimes associated with other phenomena such as low-frequency earthquakes and tilt changes. Considering that past major eruptive activities have occurred with an interval of a few tens of years, and the risk the volcano imposed on the surrounding inhabited areas, monitoring of volcanic tremors is important among other phenomena that could provide us with insights into the ongoing volcanic activity at Tokachidake. However, volcanic tremors are challenging to locate due to their complex seismic waveforms showing unclear onset of seismic phases. We use cross-correlation analysis of seismic data that measures the travel time differences between seismic stations and avoid picking the arrival time of seismic phases. We compute stacked cross-correlation functions and find the most probable source location using a grid-search scheme. We analyzed tremors that occurred during 2018-2020, mainly those who are reported by the Japan Meteorological Agency (JMA). Specifically, we determine the source location of every 1-minute seismic data in WIN format used in Japanese monitoring system and focus on 1-minute data that contain volcanic tremors. We find that tremor source locations are located beneath the northwest flank of Tokachidake and the 62-II and Taisho craters at shallow depths of about 0.5 km from the ground surface. The distribution area of volcanic tremor sources is generally consistent with that of the hypocenter of volcanic earthquakes. We also show the possibility to detect more tremors at Tokachidake by measuring the spatial coherency of seismic signals. Our results show that the seismic correlation-based volcanic tremor location method is applicable at Tokachidake and could be used together with other monitoring techniques to gain insights into volcanic activity.

Keywords: volcanic tremor, seismic data, cross-correlation, volcano monitoring, Tokachidake

©2021. Japan Geoscience Union. All Right Reserved.

Time-series of crustal deformation on Azuma volcano revealed by PALSAR-2 data

*Yuji Himematsu[1], Taku Ozawa[1]

1. National Research Institute for Earth Science and Disaster Resilience

Azuma volcano is an active volcanic complex in central Japan and comprises pyroclastic cones and/or volcanic craters aligning in the northwest-southeast direction. Several previous papers have reported increases of the volcanic earthquake and uplifts around Oana crater, one of the most active craters of the Azuma volcano in 2015 and 2018-2019, and sulfur combustion in 2020.

We applied multi-temporal InSAR analysis of ALOS-2/PALSAR-2 data observed in 2014-2020 for investigating the time-series of crustal deformation of the Azuma volcano. We report the spatiotemporal variety of line-of-sight (LOS) changes on Azuma volcano during 2014-2020 using PALSAR-2 data, which were acquired from both right-looking ascending and descending orbits.

Time-series of both ascending and descending LOS changes on Oana crater shows peaks of LOS shortening in 2015 and 2019, implying intermittent uplift. It takes about a year to reach the peak of LOS shortening, while about two years to reach zero for the 2015 LOS shortening. The northwest-southeast cross-section of the ascending LOS change revealed a peak of LOS shortening in 2015 on the northern rim of Oana crater and that in 2019 on the point of 200 m away from Oana crater for the northwest direction. We expect that the observed crustal deformation in Oana crater was driven by pressure change of the shallow hydrothermal system because the spatial extent of LOS changes is consistent with that of ground thermal activity and active fumaroles with steam/volcanic gas emission.
Acknowledgment: ALOS-2/PALSAR-2 data in this study are sharing among the PIXEL consortium, and are provided from JAXA under a cooperative research contract with ERI, the University of Tokyo.

Keywords: SAR, Crustal deformation, Azuma volcano

©2021. Japan Geoscience Union. All Right Reserved.

Existence of deep pressure sources and its behaviors during recent volcanic activity at Azumayama, NE Japan

*Jun Okada[1], Yu Nihara[2], Yuji Miyagawa[3], Susumu Seki[3], Takuya Yamamura[2], Shin Chikasawa[3]

1. Volcanology Research Department, Meteorological Research Institute - Japan Meteorological Agency, 2. Regional Volcanic Observation and Warning Center, Sendai Regional Headquarters - Japan Meteorological Agency, 3. Seismology and Volcanology Division, Sendai Regional Headquarters - Japan Meteorological Agency

Recent volcanic activity of Azuma volcano, NE Japan is characterized by the repetitive unrests where the shallow seismic activities coincide with ground deformation attributed to the various depths. In the volcanic activities of 2014-2015 and 2018-2019, there are two types of ground deformation such as (1) months-long inflation at both shallow and deep parts and (2) short-term shallow inflation and deep deflation during the volcanic tremors (Okada *et al*., 2019, JpGU). This indicates that both shallow and deep parts beneath the volcano are related each other. Regarding (2), the shallow inflation preceded the deep deflation at least for the 2018-2019. The recent studies of Tohoku University (2019) and Seki *et al*. (2020) pointed out long-period events with the frequency lower than 0.1 Hz exist during the above-mentioned short-term deformation. Their results show the shallow volcanic activities might have affected the deeper parts. The existence of deep inflation sources (BSL 3-4km and/or more) is suggested by Seki *et al*. (2020) in order to explain the entire activity of the 2018-2019. Similar deep inflation episode exists during 2003-2004, 2006-2007 and 2014-2015, and all these cases resulted in volcanic unrests with intense seismic activities beneath Oana crater. However, the volcanic episodes of the 2008-2012 and the March-October 2020 seem exceptional. The former episode misses a clear deep inflation but shows the significant thermal activity on the surface. The latter episode shows deep inflation but does not lead any clear volcanic unrests hitherto (February 2021). Different behaviors of deep pressure sources may address the feasibility of magma ascent/supply from the depth and provide important constraints on the changeable condition of the shallow hydrothermal system such as wet/dry environments or with/without sealing of the preexisting conduits/vents.

Reference:
1. Okada *et al*. (2019) Ground deformation associated with the 2014-2015 and the 2018-2019 volcanic activities at Azumayama. SVC38-P02, Japan Geoscience Union Meeting 2019.
2. Seki *et al*. (2020, accepted) Volcanic activity in 2018-2019 at Azumayama Volcano, Japan. Kenshin-Jiho, 35pp.
3. Tohoku University (2019) Seismic activity of Azumayama, Report of the 144th Coordinating Committee for Prediction of Volcanic Eruption (No. 5) additional material, 9-10.

Keywords: Azumayama, GNSS, deformation, deep pressure sources, magma resorvoirs

©2021. Japan Geoscience Union. All Right Reserved.

Amorphous silica coating on flank deposits of the 1783 CE (Tenmei) eruption at Asama volcano

*Takayuki Nakatani[1], Sarina Sugaya[2], Maya Yasui[3], Satoshi Okumura[2], Michihiko Nakamura[2]

1. Geological Survey of Japan, National Institute of Advanced Industrial Science and Technology, 2. Department of Earth Science, Graduate School of Science, Tohoku University, 3. Department of Earth and Environmental Sciences, College of Humanities and Sciences, Nihon University,

Recently, rock coatings have attracted attention in the broader field of geosciences because of their potential to record the changes in their immediate environment. Despite the potential for silica-rich rock coatings to evaluate past volcanic activity and its impacts on the surface environment, detailed reports on the silica-rich rock coatings at the proximal area are still rare, and its occurrence and formation processes are not fully understood. In this study, we report the amorphous silica-rich coating on the juvenile volcanic lapilli and blocks of the 1783 CE (Tenmei) pyroclastic flow deposits 1.9–3.6 km northeast of the Maekake crater of Asama volcano in Central Japan. These coatings are up to 660 μm in thickness and composed of fine-grained volcanic ash particles with silica-rich cement. Raman spectroscopic measurements showed that the interstitial silica-rich phase is hydrous amorphous silica and is considered to be a reaction product of ash particles with acidic volcanic rain and fog like volcanic smog (vog) as it has been recorded in Hawaii. The formation of amorphous silica without jarosite and the preferential alteration of plagioclase compared with pyroxene indicate that the reaction occurred with a sulfuric acid solution of pH < ~3. The dissolution of sintered volcanic ash and the resultant precipitation of amorphous silica would have been facilitated by the porous structure and large surface area of the ash layer. The thickness of the coating and degree of alteration in the plagioclase phenocrysts adjacent to the coating tend to decrease with an increase in distance from the volcanic crater, which is consistent with the absence of fumarolic areas in the flank. Since 1783 CE, the Asama-Maekake volcano has repeated Vulcanian and phreatic eruptions, especially in the first half of the 20th century. The amorphous silica coating recognized in this study is assumed to have formed mainly during this period, which can thus be an indicator of the acidity and distribution of past acidic volcanic rain and fog.

Keywords: Rock coating, Amorphous silica, Acid rain, Vog, Asama volcano

©2021. Japan Geoscience Union. All Right Reserved.

Monitoring of underground temperature in Jigokudani, Midagahara volcano using LPWA devices

*Tohru Watanabe[1]

1. Faculty of Sustainable Design, University of Toyama

Jigokudani is an active geothermal area in Midagahara volcano, Toyama prefecture, central Japan. It was formed as a result of repeated phreatic eruptions over 40,000 years. Increased volcanic activity in this area has been observed since 2011. In order to detect a precursory signal of a phreatic eruption, observations should be conducted on seismicity, ground deformation, geothermal activity, volcanic gas, etc. A monitoring system of underground temperature using LPWA (Low Power, Wide Area) devices has been tested since 2018. LPWA devices (netvox, R718CX2) for measuring underground temperature were deployed at 8 points in Jigokudani. One device has two thermocouples at the depths of 10 and 50 cm. Underground temperature is sent every 30 minutes to a gateway to the internet situated in Hotel Tateyama. Short-period (~10 hours) variations in temperature are remarkable at 10 cm, while quite weak at 50 cm. Short-period variations come from the temporal change in the surface temperature. The heat flux can be estimated from temperatures at different depths. Jigokudani has heavy snow fall in winter. The operation of this system has been tested since October 2020. Temperature data can still be received at least until February 2021.

Keywords: Midagahara volcano, Jigokudani, underground temperature

©2021. Japan Geoscience Union. All Right Reserved.

Formation of N_3 member from the younger Ōshima group distributed around the Habu area, southeastern part of Izu-Ōshima Island.

*Ryota Uchiyama[1], Izumi Sakamoto[1]

1. School of Marine and Technology, Tokai University

Izu-Ōshima island is an active volcano located at the northernmost point of the Izu-Bonin Arc. In Izu-Ō shima Island, outcrops of lava and volcanic sediments flowing from eruptions of mainly low-alkaline tholeiite series basalts can be seen in many places. In this study, we describe the outcrops and lithology of the area from Habu Port to Ryuozaki in the southeastern part of Izu-Ōshima Island, and examine the activity patterns that formed the Habu Port and Ryuozaki area.

The volcanic ejecta exposed on the sea cliffs distributed from the Ryuozaki to the Habu area can be classified into the Ryuozaki Lava, the Ryuozaki layer, the Suribachi layer, the M layer, the Habu lava and the Habu breccia layer.

Based on the stratigraphic sequence of each layer and the characteristics of the rock fragments collected, it is considered that the activities from the northern part of Habu Port to the Ryuozaki area occurred in the following order: 1) eruption of the Ryuozaki lava, which is the basement rock, 2) formation of the Ryuozaki layer by magmatic steam explosion off Ryuozaki, 3) activities of the Suribachi layer and the M layer, 4) eruption of the Habu lava, and 5) magmatic steam explosion (formation of the Habu Conglomerate layer) caused by the contact of the Habu lava with seawater. 5) magma generated by the contact of Habu lava with seawater, and steam explosion (formation of the Habu breccia layer).

©2021. Japan Geoscience Union. All Right Reserved.

Banded Tremors Activity at Miyakejima Volcano

*Yoshihiro Otsuka[1], Shinya Nagato[1]

1. Japan Meteorological Agency

Introduction

Since the 2000 eruption, volcanic tremors (banded tremors) that occur intermittently in 2000-2006, 2011 (September-October) and 2015 (October-December) have been observed on Miyakejima Volcano. Banded tremors are characterized by volcanic tremors with a maximum duration of about 20 minutes and a predominant cycle of about 0.2 seconds, which occur repeatedly at intervals of about 30 minutes (some events exceed 1 hour). The maximum amplitude (maximum during in the Oyamahokutou) was 16 μm / s from 2000 to 2006, 30 μm / s in 2011, and 62 μm / s in 2015. We considered the relationship between the changes in the location of banded tremors since 2000 and volcanic activity.

Discussion

Otsuka et al. (2012) estimate that the location of banded tremors from 2000 to 2011 is about 2 km near the crater. Similarly, when estimating the location of occurrence in 2015, the depth near the crater was about 1 km. It is possible that these occur in shallower areas than before 2011 (Fig.1). Slightly low-frequency earthquakes (BH-type earthquakes) tend to be shallower than 2 km in 2004, shallower than 1.5 km in 2011, and shallower than 1 km in 2015. Low-frequency earthquakes (BL-type earthquakes) have a small number of events, but are often found shallower than 1.5 km.

In order to consider the occurrence of banded tremors, we divided the transition of volcanic activity into three periods from seismic activity and crustal deformation after the 2000 eruption. The period (1) "2000-2007", the banded tremors that had been observed since the start of the eruption disappeared after April 2006 as the thermal activity decreased. However, from around this time, the pressure source in the deep part turned to inflation. The period (2) "2008-2012", eruptions accompanied by BH-type and BL-type earthquakes were repeated until July 2010. The inflation of the deep part has continued since around 2006, but the deflation of the shallow part has been stagnant since about October 2010, and banded tremors have been observed since then. The period (3) "2013-present", deep inflation continues. The stagnation in the shallow part changed to inflation from around September 2014, but banded tremors occurred during the temporary stagnation from around May 2015 (Report of Coordinating Comittee for Prediction of Volcanic Eruptions, 2018). After the banded tremors subsided in the first half of 2016, crustal deformation showing rapid inflation were observed. After that, volcanic gas ejection event with tilt change occurred in May 2016 (Nagato et al., 2017).

Since all banded tremors occur during the period when the temperature inside the crater and the volcanic fume index (Q) are high, it is considered to be related to thermal activity (Fig.2). The epicenter of the BH-type earthquakes became shallow from around 2013. The GNSS baseline associated with the shallow pressure source began to shift from deflation to stagnation and then inflation from around 2013. From these facts, it is possible that the location of thermal activity, which is the cause of banded tremors, has moved in the shallow direction due to seismic activity and movement of the pressure source. In addition, the period (1) is the period when volcanic activity such as deflation of the pressure source is low, the period (2) is the period when the deflation of the shallow part is temporarily stagnated, and the period (3) is the period when the gradual inflation of the shallow part is temporary. After stagnation, banded tremors occur. From these facts, it is possible that the supply balance of volcanic fluid underground changes. On the other hand, in the 1962 and 1983 eruptions, continuous tremors occurred for several days, but no records of volcanic tremors have been observed since then. From this, banded tremors are considered to be a peculiar phenomenon of the 2000 eruption.

©2021. Japan Geoscience Union. All Right Reserved.

Keywords: Miyakejima Volcano, Banded Tremors

Fig1

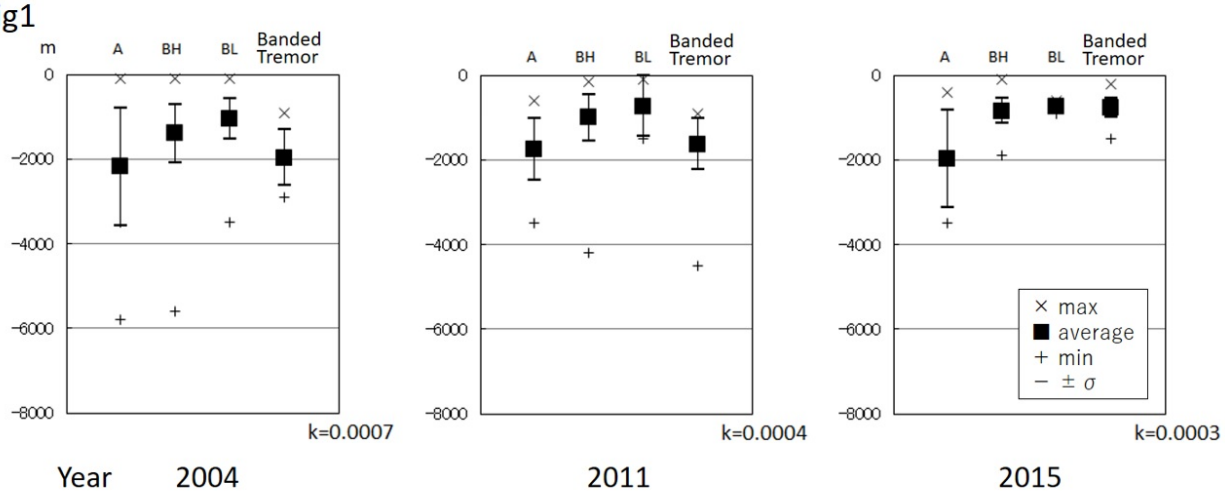

Fig2

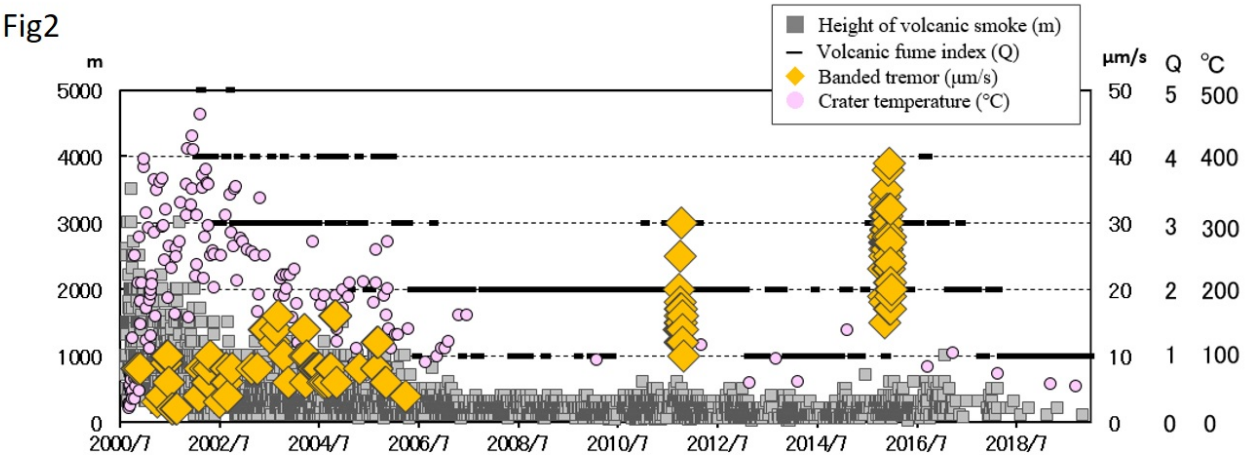

©2021. Japan Geoscience Union. All Right Reserved.

Estimating the underground pressure source of Miyakejima volcano by integrated processing of GNSS and leveling data

*Haruna Watanabe[1], Takeshi Matsushima[2], Miyo Fukui, Atsushi Watanabe[3], Jun Oikawa[3], Takashi OKUDA[4], Taku Ozawa[5], Yosuke Miyagi[5]

1. Department of Earth and Planetary Sciences, Graduate School of Science, Kyushu University, 2. Institute of Seismology and Volcanology, Faculty of Sciences, Kyushu University, 3. Earthquake Research Institute, University of Tokyo, 4. Earthquake and Volcanology Research Center, 5. National Research Institute for Earth Science and Disaster Resilience

Miyakejima is an active volcano located about 180 km south of Tokyo, and since the 20th century it erupted at intervals of about 20 years (1940, 1962, 1983, and 2000). Although there are continuous GNSS stations on Miyakejima, the number is limited and detailed crustal movements have not been obtained. Therefore, we conducted dense GNSS campaign observations six times from 2011 to 2019. Fukui et al. (2015) estimate the position and volume change of the pressure source on Miyakejima based on the observation results from 2011 to 2013, but consider only the data of the horizontal component of GNSS observation. This study accurately grasps the crustal movement of Miyakejima by enhancing GNSS observations and using leveling data during the latest 2013-2019 period, and we estimated in detail the location and temporal changes of the pressure source under Miyakejima volcano.

In September 2013, 2015, 2016 and 2019, we conducted GNSS campaign observations at benchmark points (up to 30 points) arranged so as to be distributed almost evenly over Miyakejima. In this study, 12 points of continuous data obtained from this GNSS campaign observation and 10 points of data during the same period of continuous observation points set up by the Geospatial Information Authority of Japan, Japan Meteorological Agency, and National Research Institute for Earth Science and Disaster Resilience used. We also used the data from the Miyakejima leveling survey conducted by the Tokyo Metropolitan Government almost every two years, and used the vertical fluctuations during the same period.

We used RTKLIB ver.2.4.2 (Takasu et al., 2007) to analyze the GNSS data, and we obtained the coordinate values of the GNSS stations. The horizontal displacement of GNSS from 2013 to 2019 showed radial displacement centered on the southwestern part of Miyakejima during all periods. On the other hand, the vertical displacement of leveling survey from 2014 to 2019 showed sedimentation on the northeastern side of Miyakejima with respect to the southwestern side during all periods.

The pressure source was estimated based on the GNSS horizontal displacement from 2013 to 2019 and the vertical displacement of leveling survey from 2014 to 2019. The optimum values of the position and volume change of the pressure source were obtained by using MaGCAP-V software (Meteorological Research Institute, 2008) for analyzing crustal activity for volcano. As a result, two pressure sources with different depths were estimated. One is a horizontal plate-shaped sill just below the Miyakejima crater and 0.3 km below sea level, and the other is a spherical pressure source located about 2.5 km southwest of the Miyakejima crater and 9.0 km below sea level. The volume change of each volume was -3.3×10^5 m^3/yr for sill and $+1.2 \times 10^7$ m^3/yr for spherical pressure source. It is presumed that the sill in the shallow part contracts due to degassing from the crater, and the spherical pressure source in the deep part accumulates and expands due to the rise of magma from the deeper part.

In this study, the position of the pressure source in the island could be accurately determined by

©2021. Japan Geoscience Union. All Right Reserved.

analyzing the fluctuation of the vertical components by leveling survey. The deep spherical pressure source was estimated at almost the same position as the result of Nishimura et al. (2002). In the addition, Nishimura et al. (2002) estimated that the volume accumulation rate of magma chamber deep underground during the last eruption rest period (1983~2000) was 10.2×10^6 m^3/yr. On the other hand, the volume accumulation rate between 2000 and 2019 was estimated to be 12.6×10^6 m^3 / yr from the Geospatial Information Authority of Japan data (2011), Fukui et al. (2015), and this study. Therefore, in the 2000 eruption, a caldera crater was formed, which is very different from previous eruptions, but since then, the deep underground magma chamber have been in the same position as in the 1983-2000 period, and have been increasing at about the same rate.

This work is partly supported by MEXT under its The Second Earthquake and Volcano Hazards Observation and Research Program, and also supported by Earthquake Research Institute, The University of Tokyo under JURP (2016-B-09). Continuous GNSS data was provided by GSI and JMA. Leveling survey data was provided by the Bureau of General Affairs of the Tokyo Metropolitan Government. Many member of the Japanese University Consortium for GPS Research (JUNCO) cooperated in the GNSS campaign observation. We would like to express our gratitude to all.

Keywords: Miyakejima, GNSS observation, leveling survey

©2021. Japan Geoscience Union. All Right Reserved.

Three-Dimensional Crustal Structure beneath Hachijojima Island using dense seismic observation data

*Shotaro Kanke[1], Hiroyuki Azuma[1], Yoshiya Oda[1]

1. Tokyo Metropolitan Univ.

Hachijojima Island is a volcanic island belonging to the Izu Islands, and in 2002, a volcanic earthquake swarm and a crustal movement were observed. Because of these volcanic activity, Hachijojima Island has been monitored by JMA. In order to interpret volcanic activity correctly, it is effective to understand the underground structure of the volcano by means of geophysical method.

Hagiwara and Watanabe (2019) have estimated the underground structure beneath Hachijojima Island from earthquakes data observed by permanent stations. In this study, in order to estimate the underground structure of Hachijojima Island in more detail, we installed 46 stations of 1Hz velocity seismograph (LE-3Dlite) on Hachijojima Island and Hachijo-kojima Island and conducted temporary seismic observation from September 2019 to March 2020 (182 days). We have picked P-wave and S-wave first arrivals manually on the seismic waveform data processing system, WIN system (Urabe and Tsukada, 1992), and the hypocenter determination by hypocenter determination program hypomh (Hirata and Matsu'ura, 1987).

We used the tomography program, SIMULPS12 (Evans et. al., 1994) to estimate the underground velocity structure. As a result of 3D analysis, we found that the high Vp anomaly at the depth of 2-5km just beneath Nishiyama. In particular, P-wave velocity structure was estimated with high resolution up to the depth of 4km. We compared our results with previous studies and discussed the validity of the analysis results and the effect of dense seismic observation on the resolution.

Keywords: natural earthquake tomography, velocity structure, dense seismic observation, Hachijojima Island

©2021. Japan Geoscience Union. All Right Reserved.

Ground deformation between eruptions at Nishinoshima Island using InSAR time series analysis

*Shinobu Ando[1], Satoshi Okuyama[1]

1. Volcanology Research Department, Meteorological Research Institute

The eruptive activity of Nishinoshima Island in the Ogasawara Islands, which began erupting in November 2013, is largely classified into the following phases: Phase I: 2013.11-2015.12, Phase II: 2017.4-2017.8, Phase III: 2018.7-2018.8, and Phase IV: 2019.12-2020.8. In Phase III, the lava flow did not reach the coast, but in all other phases, the lava effused a large amount of lava and expanded the land area. The second half of Phase IV was the most active eruptive activity in the series of eruptions, with a large amount of ash fall (Ando et al. 2020, JPGU or Geodetic Society of Japan).

The Meteorological Research Institute (MRI) has been analyzing large-scale earthquakes and volcanic eruptions since August 2014, when the ALOS-2/PALSAR-2 data became available. In the area around Nishinoshima Island, we have been conducting analysis using spotlight mode (SPT: resolution 3m ×1m (Range ×Azimuth)) data, which is particularly frequently observed. In general, the interferometric SAR analysis becomes significantly worse with increasing the perpendicular baseline (Bperp) distance. However, in the case of ALOS-2, the Bperp is generally very well controlled (Bperp < 500m), and the interferometric analysis is possible for almost all pairs except for the degradation of temporal coherence.

In this paper, we report the results of InSAR time series analysis to investigate the fine ground deformation between eruption phases of Nishinoshima Island. For example, in the case of phase III-IV, we set a one-year period from the end of November 2018, when the most recent differential interferometric pair showed no significant phase change, to the end of November 2019, just before the start of phase IV eruption. There were 25 scenes imaged by PALSAR-2 in SPT mode during this period, and a total of 129 pairs of data were obtained by creating pairs of data within about three months. For the individual interferometry analyses, tropospheric and ionospheric delay corrections were not processed, except for the baseline re-estimation, because the land area of Nishinoshima Island is very small. Using these results, an InSAR time series analysis using the SBAS method was applied to detect temporal varies in local ground deformation. As a result, the phase difference of elongation in the constant line-of-sight direction of about 14 mm/year can be confirmed locally around the east side of the central pyroclastic cone, and the elongation deformation decreases exponentially at the south end of the lava flowed in Phase III. In this presentation, we also present the results of the analysis of Phases I-II and II-III.

The PALSAR-2 data were prepared by the Japan Aerospace Exploration Agency (JAXA) via Coordinating Committee for the Prediction of Volcanic Eruption as part of the project 'ALOS-2 Domestic Demonstration on Disaster Management Application' of the SAR analysis of volcano Working group. The PALSAR-2 data belongs to JAXA. PALSAR-2 was analyzed using Gamma, RINC (Ozawa et al., 2016), and LiCSBAS (Morishita et al., 2020). Topographic data generated from GSI Technical Document C1-No.463, 478, and 489 were used in the processing process.

Keywords: ALOS-2/PALSAR-2, spotlight mode, InSAR time analysis, Nishinoshima

©2021. Japan Geoscience Union. All Right Reserved.

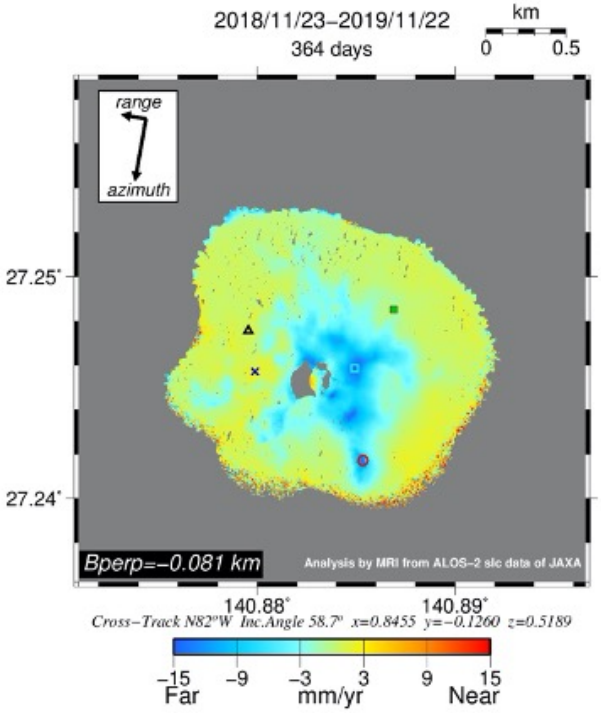

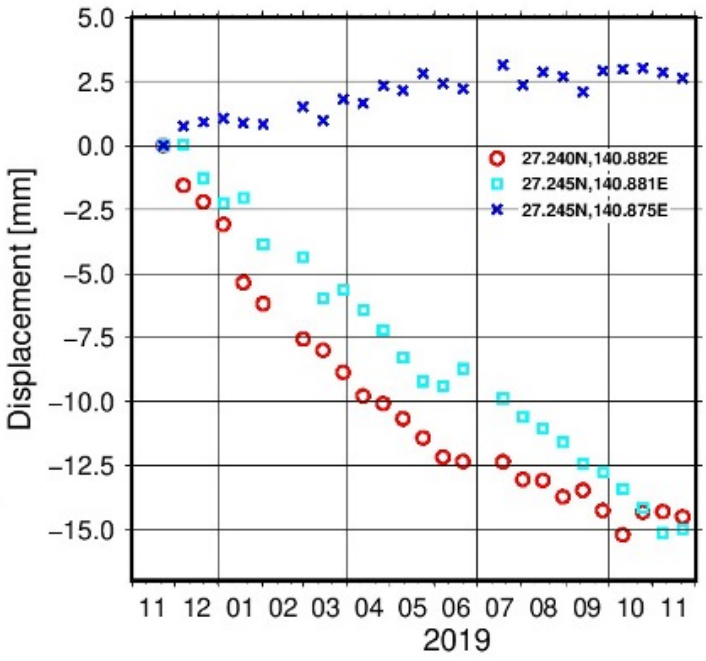

Fig. Time series of displacement

©2021. Japan Geoscience Union. All Right Reserved.

Abrupt change in eruption style during the 2019-2020 eruption of Nishinoshima, Ogasawara

*Fukashi Maeno[1], Takayuki Kaneko[1], Natsumi Hokanishi[1], ATSUSHI YASUDA[1], Yoshihiko Tamura[2]

1. Earthquake Research Institute, University of Tokyo, 2. Japan Agency for Marine-Earth Science and Technology

The style of volcanic eruption often changes significantly during a series of activity. Elucidation of the causes of such changes of eruption is important in prediction of eruption sequence. In the latest eruption of Nishinoshima, Ogasawara, magma discharge rate abruptly increased in June-July 2020, and the eruption style changed from lava flow-dominated to pyroclast-dominated one. In this presentation, we will report geological and geomorphological features and current state of volcanic activity of Nishinoshima, which was clarified by survey and observation on KR20-E06 cruise conducted in December 2020. Also we will discuss the eruption sequence and the causes of the change of volcanic activity based on the results of analysis of eruptive materials obtained by sample return with drone.

The most notable feature on the activity in 2019-2020 is that the entire island was covered with pyroclastic deposits due to the change in eruption style to explosive one. As a result of producing a DEM based on still images acquired by drone and estimating the amount of topographical change before and after the latest eruption, it was unveiled that the new pyroclastic cone accounts for ~60% of the increased volume of ~100 million m^3. This value is significantly larger than before the eruption, ~10%. Although lava flows were thickly covered with pyroclastic deposits, some parts are eroded, and lava interior is exposed. In such places, fumarolic activity and high temperature regions are recognized. This situation that even six months after the eruption high temperature regions are widely recognized on the entire surface of the island has not been observed in the previous activity of Nishinoshima. One of plausible reasons is that cooling of lava flows has been delayed due to low thermal conductivity of porous pyroclastic deposits.

Lapilli and ash were collected at multiple locations on the western side of the island by drone. Analysis of the whole rock chemical composition revealed that they are basaltic andesite with 54-55 wt.% in SiO_2. This result is almost the same as the value of bulk ash chemistry for samples collected by Meteorological Research Institute, JMA, in July 2020. Thus it is understood that the magma composition has changed significantly from andesite with 59-60 wt.% in SiO_2. There are also major changes in phenocrysts, such as increase in An# of plagioclase and the presence of olivine. In addition, changes of incompatible element concentration ratios such as Zr/Y in whole rock composition are identified. Such changes in eruption patterns and magma characteristics suggest that new undifferentiated magma was involved in the latest eruption, apart from the mafic magma that was steadily involved in the previous eruptions. Specifically, there are possibilities that undifferentiated magma rich in volatile components accidentally ascended from the deeper part, or the discharge of a large amount of magma from the shallow magma reservoir due to long-term eruptive activity triggered the movement, redistribution and ascent of deeper magma.

Keywords: Nishinoshima, Eruption, Drone, Basaltic andesite, Pyroclastic deposits, Lava flows

©2021. Japan Geoscience Union. All Right Reserved.

The depth of the air-magma interface and the sound velocity in the shallow conduit of Aso volcano inferred from seismic and infrasound signals

*Kyoka Ishii[1], Akihiko Yokoo[1]

1. Graduate School of Science, Kyoto University

The depth of the air-magma interface in the shallow conduit can be used as an indicator of the volcanic activity of open-vent volcanoes. Although there are many methods for the estimation of such depth, most of them are unable to constrain the depth into the narrow range due to multiple unknown parameters. In order to estimate the depth more accurately, we combine two methods; one is using the time delay (Δt) of arrivals between seismic and infrasound signals of explosions (Ishii et al., 2019), and another is using the resonant infrasound in the conduit observed as the peak frequency (f_0) (e.g., Johnson et al., 2018). The time delay of the signals is controlled by the depth of the air-magma interface (i.e., the depth of the explosive source) and the sound velocity in the conduit, and the peak frequency of infrasound is also controlled by the same two parameters. Therefore, this combined method provides both estimations of the depth and the sound velocity in the conduit simultaneously. The seismic and infrasound data were acquired at the vicinity of Nakadake 1st crater of Aso volcano, Japan in April 2015. A high-frequency seismic arrival is followed by an infrasound compressional phase accompanied by each Strombolian explosion at the vent. The infrasound signals are characterized by clear peaked frequency spectra (f_0, 0.5 Hz), which are derived from acoustic resonance in the gas-filled conduit (Yokoo et al., 2019). In this study, 318 events are used for analysis. Before combining the two methods, some effects have to be considered regarding the relationship between the infrasound peak frequency f_0 and the estimated depth, such as the conduit shape (cylinder or frustum), the sound velocity profile in the conduit, and the topography between a source and a station. Therefore, the estimation of the depth is performed by the following procedures. First, the conduit shape is determined by the infrasound frequency ratio of the fundamental resonant mode and overtone. The frequency ratio is theoretically related to the ratio of radii between open and closed ends of a pipe (Ayers et al., 1985). The observed frequency ratio of the peak frequency and overtone (2 Hz) suggests that the shape of the conduit wall is like a frustum of which the small end is open. Then, 3-D FDTD simulation is conducted to test how the sound velocity profile in the conduit and the topography of the propagation path affect the observed peak frequency of infrasound. High-resolution topographic data and 1-D profiles of sound velocity are assumed in the simulation. There is a transition zone from sound velocity in the conduit to that in the air at shallow depth within the 1-D profiles of sound velocity. The results of the 3-D simulation show the synthetic peak frequency of infrasound at a station is lower than the theoretical value (Ayers et al., 1985), especially in the case that sound velocity in the conduit is faster than that in the air. Based on this result, the calibrated relationship among the three parameters, the peak frequency of infrasound, the depth, and the sound velocity in the conduit, are acquired. Finally, two methods, using time delay of seismo-acoustic signals (Δt) and infrasound peak frequency (f_0), are combined. The depth and the sound velocity in the conduit estimated by the combined method are <100 m and 300-600 m/s, respectively. This estimated depth is constrained in the narrower range than the estimates by using only Δt (Ishii et al., 2019). However, only 10 % of all events are used for the estimation because the observed pair of Δt and f_0 of the other events are not explained by any realistic depths and sound velocities. This problem may be solved by considering the horizontal location of the explosive source.

©2021. Japan Geoscience Union. All Right Reserved.

Keywords: Shallow conduit, Infrasound, Aso volcano

©2021. Japan Geoscience Union. All Right Reserved.

Estimation of source location of high-frequency tremor at Aso volcano by array analysis

*hirotaka tanaka[1], Takahiro Ohkura[2], Hiroyuki Inoue[2], Shin Yoshikawa[2]

1. kyoto university, 2. Aso Volcanological Laboratory

1.Introduction
Volcanic microtremors are closely related to the movement of fluids such as magma, hydrothermal fluids and volcanic gases, and it is important to understand the generation process of volcanic microtremors in order to understand volcanic phenomena and predict eruptions. In Aso volcano, microtremors such as long-period tremor, isolated tremor, and continuous tremor have been observed. The new high-frequency tremor precedes the long-period tremor, suggesting that this tremor has a mechanism to excite the crack oscillation, which is the source of the long-period tremor. Furthermore, the amplitude of the high-frequency tremor and the time difference from the long-period tremor are time-varying and that is expected to be closely related to the changes in volcanic activity.
In this study, in order to investigate the source mechanism of the high-frequency tremor, we investigated the temporal variation of the tremor generation pattern and estimated the source location using the data from several seismometer arrays including a 3D array installed near the first crater of Nakadake and broadband seismographs from 23 February to 31 July 2020.

2.Observation and data analysis
In this study, several arrays were installed near the first crater of Nakadake to observe the high-frequency tremors. The arrays are located about 1 km away from the first crater and consist of four stations: South (SUN), Northwest (WES), North (UMA) and Southwest (HND). At SUN, WES and UMA, a 2D array consisting of six vertical seismometers with a spacing of 10-30 m and a natural frequency of 2 Hz was installed. At HND, a 3D array consisting of 13 three-component seismometers with a horizontal spacing of 10-15 m and a vertical spacing of about 30 m and a natural frequency of 2 Hz was installed above the ground and in an observation tunnel located about 30 m below the surface.
In this study, we first tried to extract the high-frequency tremors from the band-pass filtered waveforms of 2Hz to 6Hz by the correlation coefficient with the reference waveform. The amplitude of the extracted tremor and the time difference from the long-period tremors were investigated. We also analyzed the source location using the semblance method assuming plane waves, and estimated the epicenter using the 2D arrays at SUN, WES and UMA, and then estimated the epicenter depth using the 3D array at HND.

3.Result and consideration
The epicenters of the high-frequency tremors are estimated to be the west wall of the first crater of Nakadake and do not change with time estimated from the results of the apparent velocity and the direction of arrival of the tremors from the semblance analysis of 2D arrays. The depth of the source is estimated to be about 200 m to 500 m from the semblance analysis of the 3D array. Furthermore, it is found that the high-frequency tremors have the large amplitude when the time difference from the long-period tremors is short, and that the frequency of high-frequency tremors increase or decrease due to the temperature change at the source or the heavy rainfall.
The estimated region of the source of the high-frequency tremors coincides with a highly conductive region estimated from electromagnetics observations (Kanda et al., 2018). In this region, it is considered that continuous tremors are generated by the inflow of volcanic fluid from deep underground, which destroys the sulfide precipitated to seal the fractures (Kanda et al., 2018). The high-frequency tremors

©2021. Japan Geoscience Union. All Right Reserved.

analyzed in this study occur in the same region as the continuous tremors and the spectra of the high-frequency tremors are well correlated with the spectra of the continuous tremors, suggesting that they are generated by the same process. On the other hand, Yamamoto (2005) reported that volcanic fluid flows constantly into the cracks-like conduit from the deep underground, and that the inflow of volcanic fluid causes a disturbance near the top of the cracks, which in turn vibrates the cracks and generates long-period tremors. In addition, it was found that the inflow of volcanic fluid into the shallower part of the cracks cause cylindrical deformation at the upper end of the cracks, and isolated tremors is generated.
These suggest that the high-frequency tremors are caused by the breakdown of sulfides blocking the fluid path in the upper part of the crack-like conduit, which perturbs the outflow of volcanic fluid from the inside to the upper part of the crack, causing the crack to vibrate and generating long-period tremors.

Keywords: Aso volcano, volcanic tremor, array analysis

©2021. Japan Geoscience Union. All Right Reserved.

Debris avalanche deposits and the stratigraphy on the outcrop to north east from Mt.Unzen

*Daisuke Nagai[1]

1. Mt.Unzen disaster memorial hall

Unzen Volcano is a stratovolcano which repeatedly grew through the formation of lava dome, the generation of pyroclastic flow and the mountain collapse. Pyroclastic flow deposits originating from Mt. Fugen have been found in the northeastern foot of Mt. Fugen (Kobayashi and Kato,1985,Kobayashi and Nakada,1991, Watanabe and Hoshizumi,1995). It is important to investigate what kind of activity the Unzen Volcano is going to do in the future and the past ejecta to consider future disaster prevention measures. In Nagai (2019), this paper reports on the debris avalanche deposit which has never been seen before in the Tateno area which is located about 5km in the northeast foot of Mt. Fugen. This time, another debris avalanche deposit was newly found in Ide no Kawamachi (About 7 km from Mt. Fugen), Mie district, northeast foot of the same mountain. The stratigraphy of ejecta was compared with that of outcrops in the Tateno area. The newly discovered debris avalanche deposit is found to be a newer age debris avalanche different from the one reported in Nagai (2019). This debris avalanche is thought to have occurred during a series of eruptions of the Kureishibaru pyroclastic flow at about 19000 years ago. There are unclear points, such as the identification of the source of the mountain collapse, which has become a subject of future research. We hope the results will be useful for future disaster prevention measures.

Keywords: active volcano, Debris avalanche deposits, Unzen Volcano

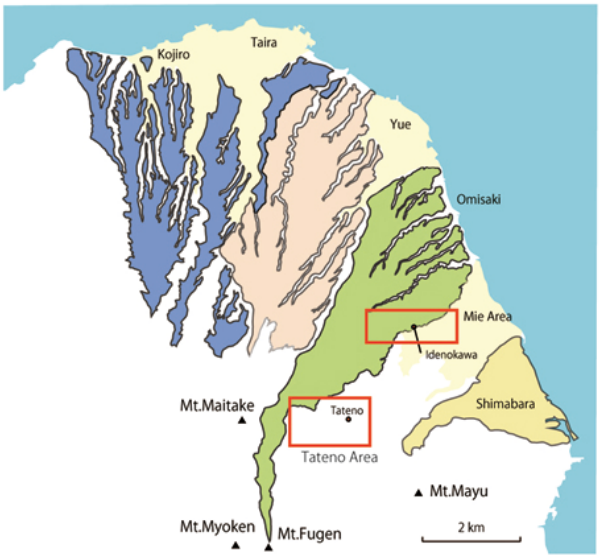

Fig.1 Location map of study area and alluvial fan related volcanic eruptions on the north-east flank of Mt.Unzen

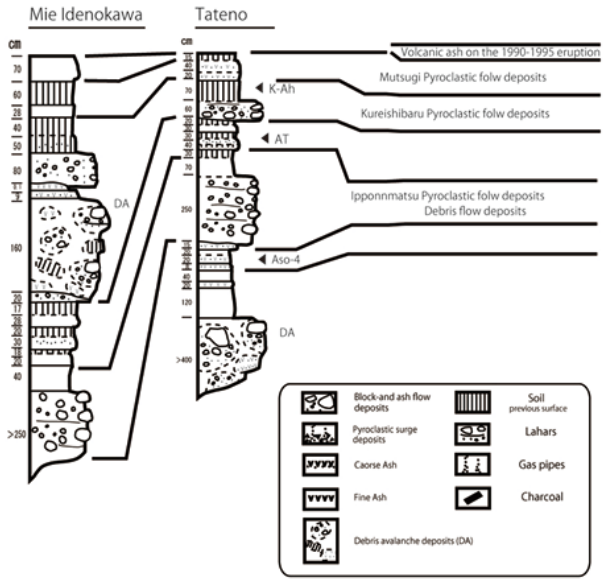

Fig.2 Columnar sections of pyroclastic deposits and stratigraphy

©2021. Japan Geoscience Union. All Right Reserved.

Vault-housed extensometers and tiltmeters recorded continuous crustal movement during the eruption of Kirishima Shinmoe-dake in 2018

*Koki Yoshinaga[1], Takeshi Matsushima[2], Hiroshi Shimizu[2], Yusuke Yamashita[3], Shintaro Komatsu[3], Ken'ichi Yamazaki[3]

1. Department of Earth and Planetary Sciences, Graduate School of Science, Kyushu University, 2. Institute of Seismology and Volcanology, Faculty of Sciences, Kyushu University, 3. Miyazaki Observatory, Disaster Prevention Research Institute, Kyoto University

Shinmoe-dake is one of the volcanoes constituting the Kirishima volcanic group in southern Kyushu, and it is an active volcano with major eruptions in 2011 and 2018 in recent years. In this study, we use vault-housed extensometer and tiltmeter data to analyze the ground deformation recorded during the Shinmoe-dake eruption in 2018. The purpose of this study is to clarify what occurred underground during the eruption with high spatial and temporal resolution.
We used the vault-housed extensometer data installed at the Isa Observatory (ISA), Kyoto University. The ISA consists of tunnels in three directions, E1, E2, and E3. Each extensometer made up of 30m lengths of super-invar rods. E1 extends in the direction of the presumed contraction source of the 2018 eruption, and E2 in the direction orthogonal to E1. The tiltmeter data were obtained from three stations: Takachihokawara (KITK) station of the Japan Meteorological Agency (JMA), Hinamoridai (KRHV) station and Manzen (KRMV) station of the National Research Institute for Earth Science and Disaster Resilience (NIED). We resampled the original data at 1 hour by simple averaging and removed tidal components from the original time series using the tidal analysis software BAYTAP-G (Ishiguro *et al.*, 1984). According to the Japan Meteorological Agency (JMA), the deep point source of the 2018 eruption contracted at the beginning of March, and we focused this period and compared each data and arranged its character.
The tilt at the KITK and the KRHV started to change around 9:00 a.m. on March 6, while the strain at Isa and the tilt at KRMV started to change in the morning of March 5. New lava was found in the crater on March 6, and the changes in Isa and KRMV were detected earlier than that. Strain variations in ISA were characterized by an extension in the E1 component and by contraction in the E2 component, which can be interpreted as the contraction of the pressure source estimated by the JMA to be located about 6 km northwest of Shinmoe-dake. In addition, the tilt in KRMV changed in the direction of subsidence from north to northeast until 9:00 a.m. on the 6th, and the strain rate in ISA also changed after 9:00 a.m. on the 6th.
In summary, we think that the first contraction occurred at depth on the morning of the March 5th, before new lava was found in the crater, and the second contraction occurred at a shallower depth on the northeast side during the 2018 eruption.

Keywords: Shinmoe-dake, Extensometers, Tiltmeter, Ground deformation

©2021. Japan Geoscience Union. All Right Reserved.

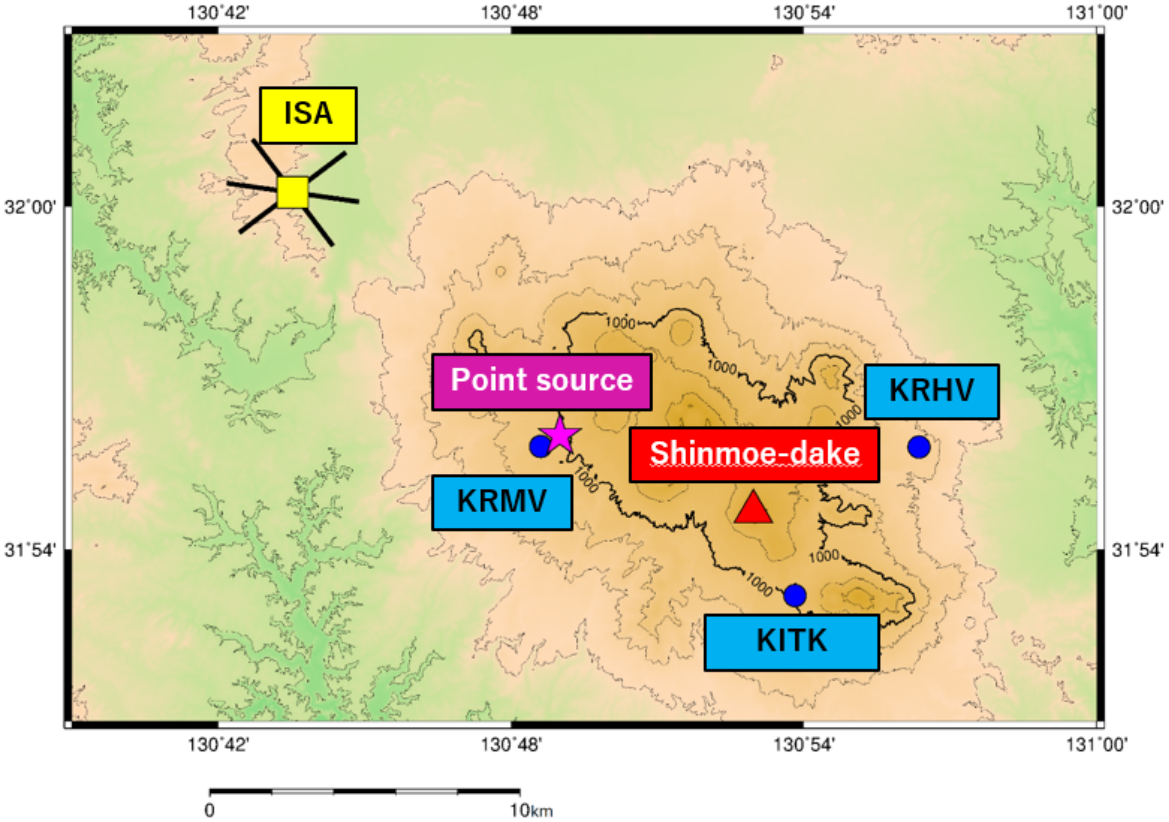

Fig.1 Map showing the location of Shinmoe-dake volcano crater and observation sites. The red triangle indicates the Shinmoe-dake volcano crater. The yellow square indicates the extensometers site (ISA), and the blue circle indicates the tiltmeter sites, respectively. The pink star represents the source location inferred from GNSS data (JMA., 2018).

©2021. Japan Geoscience Union. All Right Reserved.

Two experiments using a small-aperture infrasonic array at Kirishima

*Kazuya Yamakawa[1], Mie Ichihara[1], Dan Muramatsu[2], Takeshi Matsushima[2], Ruka Wada[3], Hideki Takahashi[3], Isao Shimoyama[4]

1. Earthquake Research Institute, University of Tokyo, 2. Institute of Seismology and Volcanology, Faculty of Science, Kyushu University, 3. Department of Mechanical Engineering, Faculty of Science and Technology, Keio University, 4. Department of Intelligent Robotics, Toyama Prefectural University

Infrasound, which is the air vibration with sub-audible frequency (< 20 Hz), is generated by various geophysical phenomena and is used for monitoring them. A small-aperture (10-30 m) infrasonic array with high-performance microphones is shown to have a practical resolution of the direction of arrival of an incident signal [Johnson & Palma, 2015; Yamakawa et al., 2018]. Also, a new infrasonic MEMS (Micro Electro Mechanical Systems) microphone is being developed, which is inexpensive and has a reasonably good performance [Wada and Takahashi, Japanese Journal of Applied Physics, 2020]. In this study, we conducted two experiments using a small aperture array at Kirishima volcano in 2020.

The first experiment examined the performance of the MEMS microphones [Wada and Takahashi, 2020]. It was conducted for 19 hours from 5 p.m. on 19 October 2020 at Kirishima Ioyama, where several fumaroles were active. The MEMS microphones were compared with the latest model of infrasound microphones (Type 7744N, ACO CO., LSD., hereafter referred to as ACO microphone) that had been used in several infrasonic studies. We installed two identical three-element infrasonic arrays with an aperture of 15 meters (Figure 1). The one consisted of the MEMS microphones and the other of the ACO microphones. At each array element, a MEMS microphone and an ACO microphone were put in the same box. There were two active fumaroles around the array. One was Iwo-yama West Craters, 150 m northeast of the array, and the other was Iwo-yama South Crater, 270 m northwest of the array [Tajima et al., 2020; Muramatsu et al., 2021]. Here we refer to the fumarole of Iwo-yama West Craters as NW fumarole and the fumarole of Iwo-yama South Crater as NE fumarole. We also placed a microphone (Type SI104, Hakusan Co., hereafter referred to as SI microphone) near the NW fumarole.
The recorded waveforms and the array processing results were excellently matched between the MEMS microphone array and the ACO microphone array, confirming that the MEMS microphones are practically useful.
The array processing showed that the infrasound from the NE fumarole was dominant at the arrays. We found that the NW fumarole also emanated infrasound by the combined analysis of the array data with the data from the SI microphone located close to the NW fumarole. The NW signals were weak compared to the NE signals: the cross-correlation coefficient between the array microphones and the SI microphone was 0.13 for the NE and 0.01 for the NW (Figure 2). With the monopole source assumption and the ratio of the correlation coefficient, the NW-to-NE amplitude ratio was approximately 0.06-0.1.

The second experiment was a mobile array survey for infrasound noise. It was conducted around Makizono-cho, Kirishima city, from 3 p.m. to 5 p.m. on 20 October 2020. While traveling by car, we stopped at an observation point, deployed the small-aperture (15 m) array for several minutes, retrieved them, and then moved to the next point. We used the ACO microphones that were used in the first experiment. We obtained the infrasonic array data at four locations in 2 hours.
The results indicated that the dominant infrasound noise was from the fumarolic area (Iodani Fumarolic Area Park) at the P1, P2, and P4 (Figure 3). At the P3, the estimated source direction was deviated. This deviation should have been brought by the topographical barrier of a hill between P3 and the fumarolic

©2021. Japan Geoscience Union. All Right Reserved.

area. Fumarolic noise is persistent and can disturb infrasonic monitoring of volcanoes. The array survey for background noise will be useful for designing infrasound observations for volcanoes.

Two experiments were successful. In the first experiment, new MEMS microphones was proven as practical. This new and inexpensive microphone will benefit the infrasonic studies. The first experiment also succeeded in detecting the existence of the infrasound signals that were masked by another signals. In the second experiment, we proved the movability of a small infrasonic array, and succeeded to identify the infrasonic noise source in a short time. These two experiments demonstrated the wide usage of a small infrasonic array.

Keywords: Infrasound, array, volcano

©2021. Japan Geoscience Union. All Right Reserved.

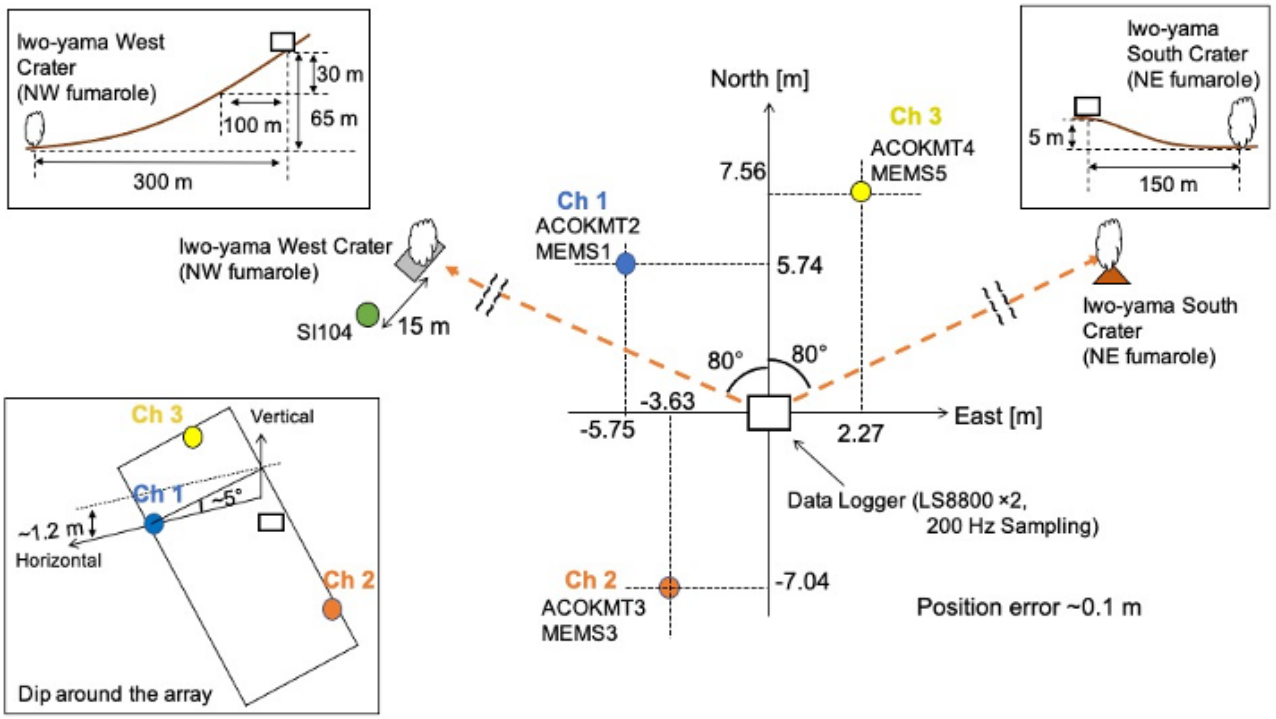

Figure 1. Experiment at Kirishima Ioyama. The colored circles show the positions of microphones.

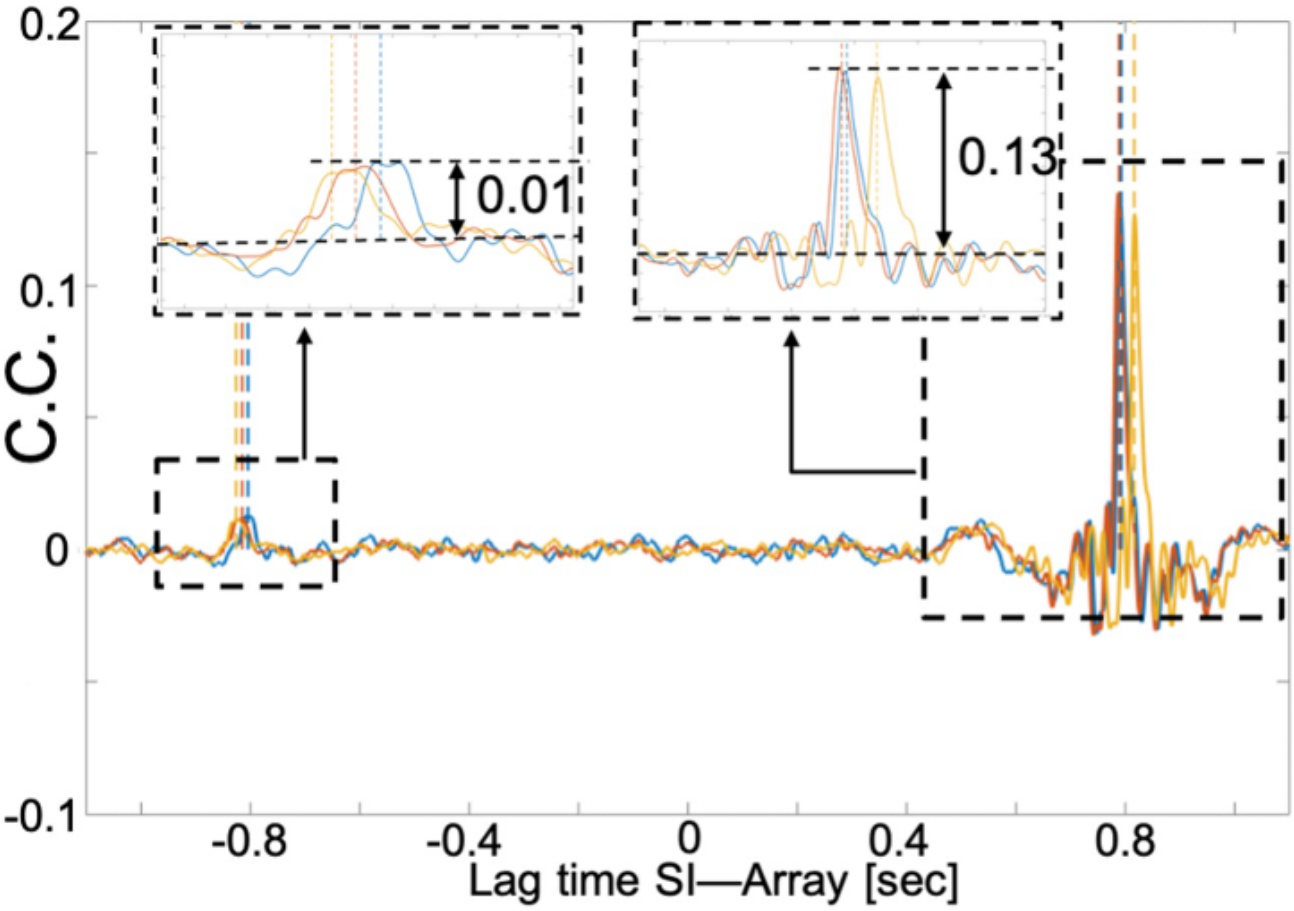

Figure 2. Correlation coefficient between the SI microphone and each array components (Figure 1). The solid lines show the correlation coefficient (blue: SI-Ch1, red: SI-Ch2, yellow: SI-Ch3). The dashed lines show the lag times corresponding to the northeast fumarole (right) and the northwest fumarole (left). In this figure, the ACO microphones' data were used. Note that the MEMS microphones' data also produced the similar result.

©2021. Japan Geoscience Union. All Right Reserved.

©2021. Japan Geoscience Union. All Right Reserved.

Estimating the source of volcanic earthquakes during eruption events at Kirishima Volcanos, in 2018, using spatial distribution of earthquake amplitude.

*Daiki Goshima[1], Satoshi Matsumoto[2], Ayaho Mitsuoka[1], Yuhei Yuasa[4], Yuta Kawamura[1], Mie Ichihara[3]

1. Department of Earth and Planetary Sciences, Graduate School of Science, Kyushu University, 2. Institute of Seismology and Volcanology, Faculty of Sciences, Kyushu University, 3. Earthquake Research Institute, University of Tokyo, 4. Osaka Regional Headquarters, Japan Meteorological Agency

Kirishima volcanic area consists of about 20 volcanoes and is located around the border of Kagoshima and Miyazaki prefectures. Ichihara et al (2017) analyzed the volcanic tremors associated with volcanic activity in 2011 eruption. They obtained tremor sources just below the crater and discussed its relationship with surface phenomena. However, source of tremor that might be associated with magma migration to the crater have not been determined and their relationships are not known well. The location of magma chamber of the Kirishima Volcanos was inferred from pressure source detected by GPS observations, which is located at 5 km northwest of Shinmoe-dake and depth of 8 km (Nakao et al., 2013). On the other hand, Aizawa et al (2014) discussed the location to be 5 km northeast of Iwo-yama. In this study, we attempt to detect magma behavior associated with the 2018 eruptions of Shinmoe-dake and Iwo-yama through detection of volcanic tremor.

In order to detect tremor and determine source location, we use seismic stations around the volcano. Tremor location is determined from amplitude distribution at the seismic stations. Generally, seismic signal is affected by source, path, and site factors. Then, we estimate the site amplification characteristics at the stations using the distant earthquake occurred in Shimane Prefecture on 9 April 2018, and remove the effect from amplitude data. After that, we estimate the source location of tremor. The location was determined by spatial amplitude distribution through grid-search processing for trial source locations.

Prior to tremor detection, we performed source determination for events at known location. At the same time, we estimated optimal attenuation factor to eliminate propagation path effect. We used two natural earthquakes and two volcanic eruptions for the checking. The result of the check showed that the processing could not determine the depth of the source well but the horizontal location of the source can be estimated by it. Undetermined depth might be attributed to the effect of radiation pattern from the natural earthquake source. Therefore, we confirmed the processing can be used for the determination of tremors.

Keywords: volcanic tremor, amplitude distribution

©2021. Japan Geoscience Union. All Right Reserved.

S-wave attenuation structure of Mt.Kirishima estimated using coda of S-wave

*Takuji Watanabe[1], Ayaho Mitsuoka[1], Yuhei Yuasa[1], Yuta Kawamura[1], Daiki Goshima[1], Satoshi Matsumoto[2], Mie Ichihara[3]

1. Department of Earth and Planetary Sciences, Graduate School of Science, Kyushu University, 2. Institute of seismology and Volcanology, Faculty of Sciences, Kyushu University, 3. Earthquake Research Institute, University of Tokyo

Mt.Kirishima is a volcanic group located on the border of Kagoshima prefecture and Miyazaki prefecture in Japan. Shinmoe-dake in the center of Mt.Kirishima has been active in 2011 and 2018. Therefore, it is important to estimate the underground structure of Mt.Kirishima in order to consider volcanic activities in the future.

When seismic waves go through the fluid such as a magma reservoir, the energy of waves is absorbed and scattered and the amplitude is attenuated. In this study, we estimated the underground structure of Mt.Kirishima by comparing the amplitudes of S-waves that normalized by coda-waves.

In this study, we used the data were obtained from 23 stations (Kyushu University, Tokyo University, JMA and NIED). We used seven earthquake events (M=1.3~2.3). These station and event were located around Mt.Kirishima. In the analysis, we used coda-normalization method which removes the source effect and site effect by amplitude of coda-wave. We used method (1) that image range of attenuation by comparing amplitude of S-wave and method (2) that estimate Q-value by ratio of root mean square amplitude of coda-wave (C_RMS) and root mean square amplitude of S-wave (S_RMS). In the method (1), we made amplitude of coda-wave recorded all station the same size that maximum amplitude of coda-wave for 3 seconds after the arrival time of coda-wave recorded at the station farthest from the hypocenter and we compared amplitude for 1 second after the arrival time of S-wave recorded at each station. In the method (2), we calculated C_RMS for 3 seconds after the arrival time of coda-waves (twice the travel time of S-wave) at each station and S_RMS for 1 second after the arrival time of S-waves at each station. We divided S_RMS calculated at each station by respective C_RMS and calculated the amplitude ratio. In the method (1), we connected hypocenter and station that amplitude of S-wave is smaller than standard on the map. We did the same procedure each events and imaged attenuation range where the lines overlapped. In the method (2), we divided the range where include hypocenters and stations into blocks in two dimensions and estimated Q-value in each blocks by least squares method.

In our results, attenuation range located south of Karakuni-dake in both methods. The hypocenters of volcanic earthquake distribute neighborhood of this attenuation range. Therefor we suggested there is heterogeneous structure related to volcanic activity at south of Karakuni-dake.

Keywords: Coda-wave, Attenuation structure

©2021. Japan Geoscience Union. All Right Reserved.

Estimate of magma supply beneath Aira caldera during the last 10 years based on ground deformation observation and amount of volcanic ejecta

*Daisuke Miki[1], Tomoki Tsutsui[1], Masato Iguchi[1]

1. Sakurajima Volcano Research Center, Disaster Prevention Research Institute, Kyoto University

We applied a composite analysis of spherical pressure source at around Aira caldera, Kyushu Japan. Horizontal displacements obtained from GNSS observations and vertical displacements from leveling survey, during 2017 to 2019, were used for the analysis. A volume increase source of 15.2 $\times 10^6$ m^3 was estimated at a depth of 11.2 km near the central part of Aira Caldera. The volume change during the last 10 years was calculated based on the estimated location of the pressure source beneath Aira caldera and change in horizontal distance between MAKI and YOSI, which crosses the central part of Aira caldera from east to west. The amount of magma supplied to Aira caldera was estimated by adding the amount of volcanic ash ejected from Sakurajima volcano, to volume change of pressure source. Estimated magma supply during the last 10 years are 70 $\times 10^6$ m^3 and 93 $\times 10^6$ m^3, respectively, assuming equivalent densities of 2500 kg/m^3 and 1000 kg/m^3. The average magma supply rate is close to the 10 $\times 10^6$ m^3/yr obtained in previous studies.

Keywords: Aira caldera, ground deformation, magma supply

©2021. Japan Geoscience Union. All Right Reserved.

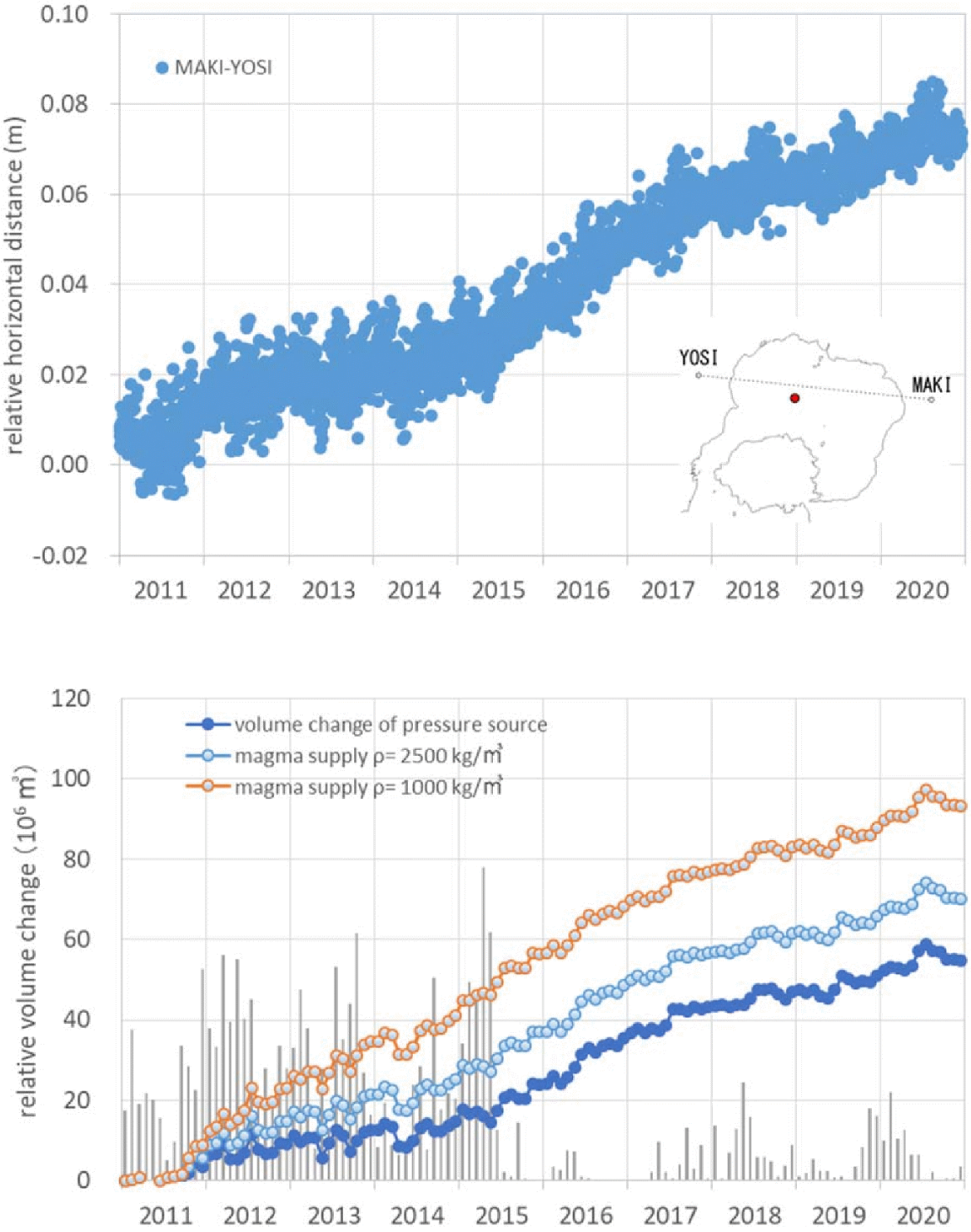

Daily change in horizontal distance between MAKI and YOSI (upper figure) and monthly variation of magma supply to Aira caldera (lower figure). The lower figure also shows the volume change at the pressure source and amount of volcanic ejecta.

©2021. Japan Geoscience Union. All Right Reserved.

Temporal changes of seismic velocities and scattering properties at Suwanosejima volcano inferred from seismic interferometry

*Takashi Hirose[1], Hideki Ueda[1], Eisuke Fujita[1]

1. National Research Institute for Earth Science and Disaster Resilience

In recent years, seismic interferometry [e.g., Curtis et al., 2006; Shapiro, 2004] has been widely used to detect seismic velocities and/or scattering properties related to large earthquakes and volcanic activities. Some previous studies succeeded in detecting precursory changes in volcanic regions 10 days - a few days before eruption/increase in activity [e.g., Budi-Santoso and Lesage, 2016; Obermann et al., 2013a; Olivier et al., 2018]. Increasing the number of applications will be important to improve volcano monitoring with seismic interferometry. In this study, we conduct seismic interferometry analyses at Suwanosejima volcano, where the number of eruptions increases in the last few months, and discuss temporal changes of seismic velocities and scattering properties.

We used seismic ambient noise data of three JMA stations during Jan. 2018 - Feb. 2021 at Suwanosejima volcano and estimated temporal changes of seismic velocities and scattering properties during that period. A reduction of waveform correlation (decorrelation) will indicate a seismic scattering property change. We firstly divided continuous seismic records on vertical component into 10-minutes-long segments and applied spectral whitening [e.g., Shapiro et al., 2006; Bensen et al., 2007] and one-bit normalization [Larose et al., 2004]. Daily CCFs (DCCFs) were obtained by stacking CCFs every 10 minutes. Finally, we measured relative velocity change and waveform correlation (CC) between a reference CCF and 3-days-stacked CCF at 0.5-1 Hz, 1-2 Hz, and 2-4 Hz bands by using stretching method [Lobkis and Weaver, 2003]. Where the reference CCF is computed by stacking DCCFs between Jun. 10, 2020, and Jan. 31, 2021.

At the 0.5-1 Hz band, seismic velocity decreased by 2.6-2.9 % from 12 days before the explosion on Dec. 28, and significant decorrelations were detected 5-15 days before this explosion. Seismic velocity decreased by 2.1 % at the maximum of 9 days before the eruption on Jan. 20. Significant decorrelations were detected from 7 days before to 3 days after this eruption. Estimated seismic velocity changes just before those eruptions have large errors caused by significant decorrelations. Therefore, it is difficult to discuss seismic velocity changes related to those explosions. Although the seismic velocity changes and the decorrelations were also detected at 1-2 Hz and 2-4 Hz bands, further investigation is required because CCs at these frequency bands show large fluctuations. To investigate temporal changes of CC values in more detail, we directly computed CCs between each DCCF. CC values between DCCFs around those eruptions have relatively high, suggesting that scattering properties at the shallow region of the volcano in those periods of time are similar to each other.

To discuss possible causes of significant decorrelations, we compared temporal changes of CC with other observations. No heavy precipitations were observed at AMeDAS station in Suwanosejima during Dec. 2020 - Feb. 2021, indicating the significant decorrelations should not have been caused by heavy rains. No geodetic data showed precursory changes related to the explosions. Finally, we checked temporal changes of SO_2 flux. Daily SO_2 flux increased to 2,500 tons on Dec. 26, 2020 [JMA, 2021], suggesting that volcanic gas moved to the shallow region of Suwanosejima. The inflow of volcanic gas to cracks at the shallow part of Suwanosejima might have caused significant decorrelations.

©2021. Japan Geoscience Union. All Right Reserved.

Acknowledgments: We used seismograms recorded by Japan Meteorological Agency (JMA) and AMeDAS data provided by JMA.

Keywords: seismic interferometry, scattering property change, Suwanosejima volcano

©2021. Japan Geoscience Union. All Right Reserved.

Development of volcano deformation calculation system using boundary element method (2)

*Ryohei Kawaguchi[1]

1. Meteorological Research Institute

Volcanic deformation data observed by tilt meter and/or GNSS stations were useful for monitoring and evaluating the volcanic activities. The Japan Meteorological Agency (JMA) has been constructing such observation stations around volcanoes, and these observed data were used for monitoring operation of volcanic activities. Because these observation stations around volcanoes were located on the steep topography of the volcano, the observed data were affected by the topography. It was important to consider the effect of the topography in the analysis of the observation data. To investigate the influence of topography on the analysis results of volcanic deformation data, we have developed a program for calculating volcanic deformation which considering the effect of topography by using the boundary element method (BEM). As a result, when the depth of the deformation source was about the same as the elevation of the observation station, the analysis result assuming an elastic half space was overestimated or underestimated the depth and the magnitude of the deformation source (Kawaguchi, 2020, JpGU). To utilize the developed program for the volcano monitoring operation by the JMA, we have developed functions for creating the mesh model of volcanic topography and converting the calculation results for data at observation station. In this study, we introduce the developing system and report the examples of its application.

The volcano deformation calculation system was consisted by the functions of creating a mesh model of the topography of volcano, calculating the volcanic deformation using the BEM, and converting of the calculation results into observational data. The mesh model of the topography of volcano and pressure sources was made by setting some parameters such as the name of the volcano and the location of the pressure source. The topography of the volcano was created using a 10-meter mesh digital elevation model (DEM) of the Geospatial Information Authority of Japan. A spherical or ellipsoidal pressure source can be set as the deformation source. The calculated results were output as displacement for each coordinate of the mesh model. These results were converted into the tilt change and displacement of each observation station for analysis. The converted tilt changes and displacements were output in the format of input files of MaGCAP-V developed by the Meteorological Research Institute, JMA. We have developed the program that can be applied to 20 volcanoes.
As an example of application of this system, we created the topographic model of Izu-Oshima volcano and calculate the volcanic deformation. Assuming a dike penetration, we set a pressure source below the summit area. The tilt changes and displacements at the observation stations at Izu-Oshima volcano were numerically calculated. As a result, when the depth of the pressure source was 1,000 m below sea level, the difference in calculated tilt changes and displacements were small compared to the those obtained by assuming the elastic half space. When the elevation of the pressure source was set to 0 m above sea level, the calculated tilt changes and displacements were more than twice as large as those obtained by assuming the elastic half space at some stations.

Keywords: volcano deformation, BEM

©2021. Japan Geoscience Union. All Right Reserved.

Estimation of seismic scattering coefficients at active volcanoes

*Mare Yamamoto[1]

1. Research Center for Prediction of Earthquakes and Volcanic Eruptions, Graduate School of Science, Tohoku University

Volcanoes are considered one of the most heterogeneous field in the Earth’ s crust, and the understanding of such small-scale inhomogeneities in volcanoes may provide us important information on the various volcanic processes including fluid transport related to past and present volcanic activities. In heterogeneous media, like shallow volcanic structure, the seismic wave propagation is strongly affected by the scattering, and the conversion scattering between P and S waves and their multiple scattering play an important role in wave propagation and energy transportation. Such mode conversion and multiple scattering are also important to consider the applicability of seismic interferometry and Green’ s function extraction which are often related to the requirement of equipartitioning. In our previous work, we estimated the total scattering coefficients including those of conversion scattering using the spatial distribution of propagating energy from an active seismic source at Asama volcano, Japan (Yamamoto and Sato, 2010). In this presentation, we report the results of systematic estimation of the scattering coefficients at several volcanoes and discuss the relation between the estimated scattering coefficients and the structure of each volcano.

In this study, we estimated the scattering coefficients at Aso, Bandai, Iwate, and other volcanoes using the data of active seismic experiments which were conducted as a part of the national project for the prediction of volcanic eruptions in 1990s and 2000s. The most remarkable characteristic of observed seismograms is the existence of long and dominant coda waves after the onset of P wave, and the spatial distribution of propagating energy at fixed time shows a clear pattern exhibiting two slopes which are indicative of multiple scattering P and S modes having different scattering coefficients. From the comparison between the observed energy distributions and those calculated by the radiative transfer model considering the mode conversions between P and S energies and the multiple isotropic scattering of these two modes in the full space, we found that the total scattering coefficients of P-S scattering at 4-8 Hz and 8-16 Hz bands are approximately 1.5 km at all volcanoes we examined. These estimated values of the total scattering coefficients were close to those estimated in our previous study at Asama and are also consistent with those estimated by an array observation at Sakurajima. In this study, we also verified the validity and reliability of the use of the radiative transfer model in the full space by analyzing the energy propagation in the half space and the layered models which are computed by numerical means (i.e., finite-difference and Monte Carlo methods). We found that the maximum error of the estimated total scattering coefficients is about 40%, and thus the wave scattering at shallow volcanic structure is still one or two order stronger than that in the ordinary crust.

These results suggest that the conversion scattering between P and S waves and significant multiple scattering of each mode have an indispensable effect in the modeling and analysis of seismic wave propagation in heterogeneous volcanic environments. Since we have been assuming the scattering caused by statistical random fluctuations, it is also necessary to consider the scattering by discrete cavities as pointed out by Sato (2019, GJI; 2020, JpGU) for a better understanding of wave scattering in the shallow volcanic structure in the future.

©2021. Japan Geoscience Union. All Right Reserved.

Keywords: Shallow volcanic structure, Seismic scattering, Active seismic experiments

©2021. Japan Geoscience Union. All Right Reserved.

Temporal Change in Coda-Q at the upper East Rift Zone of Kīlauea volcano, Island of Hawai‘i

*Takuji Yamada[1], Paul G Okubo[2]

1. Faculty of Science, Graduate School of Science and Technology, Ibaraki University, 2. University of Hawai‘i at Mānoa

1. Introduction

Quality factor coda-Q, or Qc, is measured from the decay rates of coda-wave amplitudes for local earthquakes. The decay of the coda amplitude is independent of the distance and path between source and receiver (Aki, 1969) and can be used as an indicator of subsurface complexity, such as the density of cracks and other wave scatterers. Lower suggests higher density of cracks and scatterers.

Elevated volcanic activity at Kīlauea volcano has persisted for decades, with essentially continuous eruption in its middle East Rift Zone from the Pu‘u O‘o vent from 1983 to mid-2018. A vent within Halema‘uma‘u Crater in the Kīlauea summit region was formed in 2008, and a lava lake occupied the vent also until mid-2018. In May 2018, magma intruded into and erupted from Kīlauea’s lower East Rift Zone for much of the summer of 2018. Punctuating Kīlauea’s sustained eruptions from the vents at its summit and East Rift Zone were intervals when the summit lava lake formed, a fissure eruption between the summit and Pu‘u O‘o, and two overflows of the lava lake within Halema‘uma‘u. During such intervals, we presume that magma rising toward the surface or migrating through the volcano will activate and fill cracks and fractures in the shallow crust. This suggests that changes in Qc could be detected prior to visible changes in the eruptions.

In this study, we focused on the upper East Rift Zone, now being referred to as the east rift connector between the summit and rift zone, where occasional elevation of seismicity has been detected. We analyzed waveforms of 462 earthquakes (M ≧ 2.0) that occurred at the upper East Rift Zone from 2009 to 2015 (Figures 1a and 1b) and investigated temporal change in Qc.

2. Methods

We first applied band-pass filters with five different frequency bands for S-coda waves, which were 1-2, 2-4, 4-8, 8-16, and 16-32 Hz. We then calculated the root-mean-square amplitude Ac of a S-coda wave in a moving time window with a duration of 4/fc, where fc is the center frequency of each frequency band. From the single backscattering model (Aki and Chouet, 1975), Ac and Qc will obey the following equation, $\ln Ac + \ln t = -\pi(fc/Qc)t + const.$, where t is the lapse time from the origin time of the earthquake. We finally estimated values of Qc for individual frequency bands and hypocenter-station pairs from waveforms of 462 earthquakes (M ≧ 2.0) and investigated temporal change in the values.

3. Results and Discussion

Figure 1c shows temporal change in Qc for the east-west component of the seismogram at a station (HV.PAU) for the five analyzed frequency bands. Figure 1d shows a temporally smoothed result in each

©2021. Japan Geoscience Union. All Right Reserved.

month for a frequency band of 2 to 4 Hz. We observed no clear change associated with elevated seismicity in 2009, 2011, and 2015. On the other hand, a long-term decrease in Qc was detected at some stations and frequency bands. We interpret this as suggesting an increasing density of cracks and scatterers associated with a raised volcanic activity at the upper East Rift Zone.

Keywords: Kīlauea volcano, Coda-Q, scatterer density

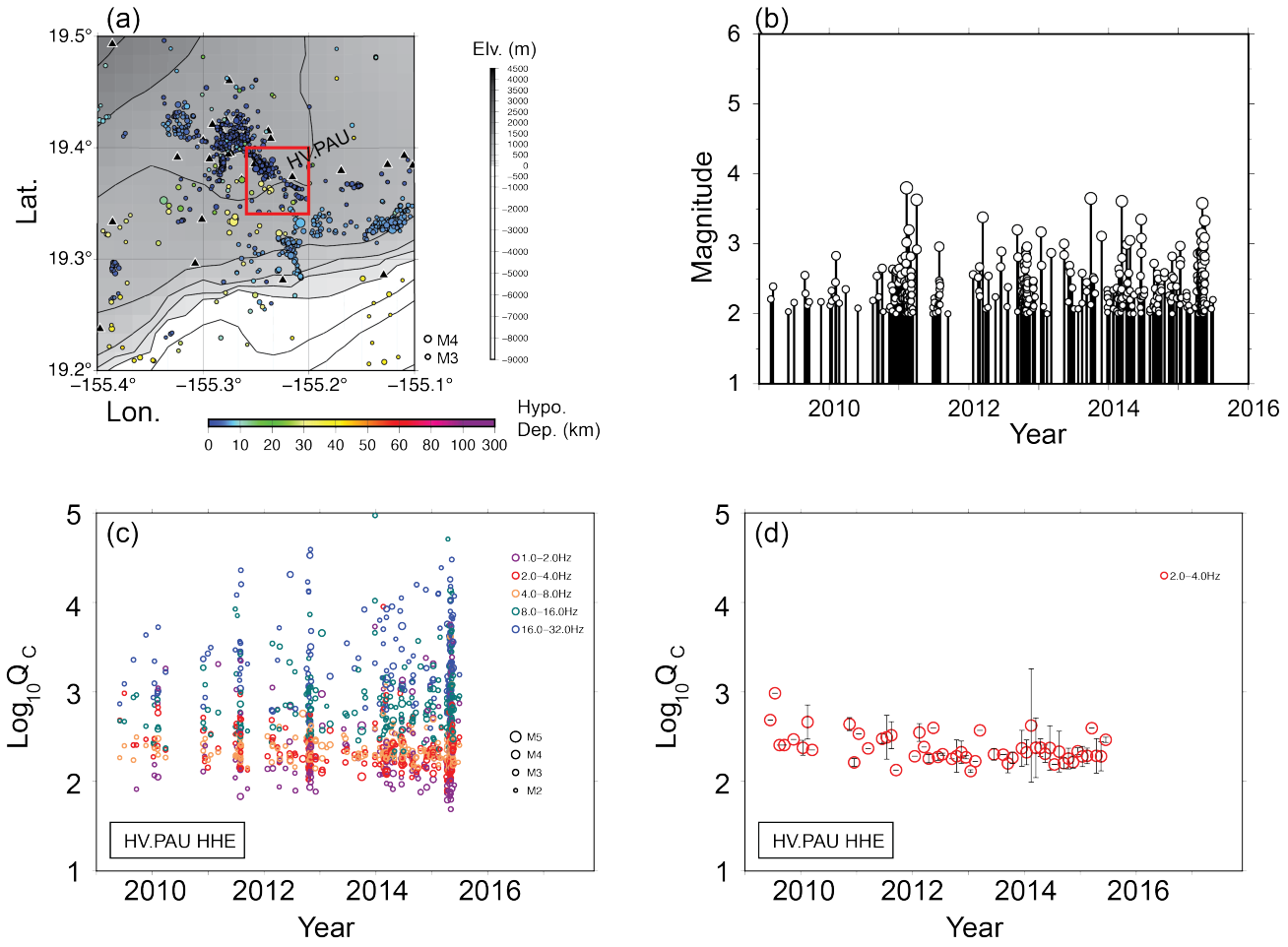

Figure 1. (a) Seismicity around Kīlauea volcano from 2009 to 2015 (Matoza et al., 2020). Circles and triangles indicate hypocenters and seismic stations, respectively. Earthquakes in the red square were used for the coda-Q analysis in this study. (b) Magnitudes of earthquakes as a function of time in the study area. (c) Estimated values of coda-Q for individual earthquakes at a station HV.PAU for the five analyzed frequency bands. (d) A temporally smoothed result in each month for a frequency band of 2 to 4 Hz. Vertical bars indicate standard errors.

©2021. Japan Geoscience Union. All Right Reserved.

A prototype of advanced Multi-GAS for unmanned aircraft systems

*Masaaki Morita[1], Toshiya Mori[2]

1. Geological Survey of Japan, AIST, 2. Graduate School of Science, The University of Tokyo

The composition of volcanic gases reflects the temperature and pressure where they exsolved from magma and the chemical equilibrium reactions during their ascent to the surface. A measurement of their composition is essential to understand the supply system of volcanic gases and their fluctuations during the volcanic unrest. In addition to a conventional method of the volcanic gas composition measurement (sampling and wet chemical analysis), in-situ measurement of plume composition using multiple gas sensors (Multi-GAS: Shinohara et al., 2005, JVGR; Aiuppa et al., 2005, GRL) has become possible. A smaller and lighter Multi-GAS has been recently made with minimal gas sensors, batteries, and data loggers. It has been installed on unmanned aircraft systems (UASs, drones) and has operated at volcanoes with limited access to the craters or volcanoes that are inaccessible due to eruptions (Mori et al., 2016, EPS; Rüdiger et al., 2018, AMT; Stix et al., 2018, JGR; Liu et al., 2018, G-cubed).

In Multi-GAS measurements, the sensor detects changes in the concentration of each component relative to the surrounding atmosphere, and the composition is calculated by the concentration ratio of each component based on the correlation of the concentration changes. It is currently necessary to balance the payload of the drone and the type and accuracy (signal-to-noise ratio) of the onboard gas sensors depending on the situation. At present, it is difficult to measure the main components of volcanic gases comprehensively and accurately with a small drone for general use, and on the other hand, even if a large drone for industrial use can mount high-quality sensors, it is difficult to carry the drone and its peripheral equipment, and the mobility of the drone must be sacrificed to some extent. Therefore, in this study, we have tried to create a lightweight and highly functional drone-borne Multi-GAS that can measure the major components of volcanic gases comprehensively and accurately.

The prototype of drone-borne Multi-GAS (size: L 16 cm ×W 21 cm ×H 14 cm) consisted of a non-dispersive infrared spectroscopic CO_2 sensor and a solid-state H_2O sensor (SBA-5, PP Systems, Amesbury, USA), controlled potential electrolysis SO_2 and H_2S sensors (KTS-512P and KHS 5TA, Komyo Rikagaku Kogyo, Kawasaki, Japan), and a semiconductor H_2 sensor (SB-19, Nissha FIS, Osaka, Japan). The analog output of each sensor was recorded to an SD card inside the Multi-GAS by using a microcomputer Lazurite Sub-GHz (LAPIS Technology, Yokohama, Japan; 12 bit AD converter) and a data logging shield for Arduino (Adafruit Industries, New York, USA). The data were also transferred to the pilot in real-time via specified low-power radio communication (920 MHz band). The weight of the Multi-GAS alone was about 600 g, and it is possible to fly safely within the allowable payload of a small industrial drone that can be carried by researchers at volcanoes (e.g., DJI's Matrice 200 V2, 4.69 kg weight with batteries, 1.45 kg maximum payload).

In the future, we will conduct a flight test at an actual volcano to evaluate the measurement accuracy of the new drone-borne Multi-GAS and the data transfer by radio communication. Also, it is necessary to conduct comparative observations with a conventional Multi-GAS to evaluate its performance.

Keywords: Multi-GAS, Volcanic gas, Volcanic plume, UAS, Drone

©2021. Japan Geoscience Union. All Right Reserved.

[J] Poster | S (Solid Earth Sciences)：S-VC Volcanology

Sat. Jun 5, 2021 5:15 PM - 6:30 PM JST | Sat. Jun 5, 2021 8:15 AM - 9:30 AM UTC | Ch.16_2

[S-VC31] Dynamics of volcanic eruptions and their physical and chemical processes

convener:Yujiro Suzuki(Earthquake Research Institute, The University of Tokyo), Atsuko Namiki(Graduate School of Environmental Studies, Nagoya University), Masatoshi Ohashi(Earthquake Research Institute, the University of Tokyo)

A Volcanic eruption is a hazardous phenomenon that results from a sequence of coupled processes, including storage in the subsurface and ascent to the surface. The volcanic gas exsolving from the ascending magma generates bubbles, which influence both the potential energy of the magma (density) and its resistance to flow (viscosity). Bubbles can sometimes deform and/or fragment the surrounding magma, leading up to explosive eruptions that develop volcanic plumes and/or pyroclastic flows. A broad range of approaches is required to tackle these processes and better understand the factors that govern the physics of explosive eruptions. We welcome contributions from interdisciplinary approaches, including, geophysical observations of active/quiet volcanoes, geochemical measurements of eruptive products, theoretical approaches, and numerical simulations, and laboratory experiments designed to explore the fundamental processes underlying explosive volcanism.

[SVC31-P01] PHENO-BUBBLE NUMBER DENSITY (PBND) AS INDICATOR OF OVERPRESSURE IN PRE-ERUPTIVE MAGMA CHAMBER

*Indranova Suhendro[1], Atsushi Toramaru[1] (1.Department of Earth and Planetary Sciences, Graduate School of Sciences, Kyushu University)

[SVC31-P02] Crystal Fracture in the Youngest Toba Tuff (74 ka) Pumices

*Gabriela Nogo Retnaningtyas Bunga Naen[1], Atsushi Toramaru[1], Haryo Edi Wibowo[2] (1.Department of Earth and Planetary Science, Kyushu University, Fukuoka, Japan, 2.Geological Engineering Department, Universitas Gadjah Mada, Yogyakarta, Indonesia)

[SVC31-P03] Textural study of the 7.3 ka caldera-forming eruption of Kikai Caldera: Correlating bulk density to bubble-size observations

*Selvia Novianty[1], Masatoshi Ohashi[1], Atsushi Toramaru[1] (1.Department of Earth and Planetary Sciences, Graduate School of Science, Kyushu University)

[SVC31-P04] Factors controlling bulk density of pumice in explosive eruption deposits

*Atsushi Toramaru[1], Miki Ogata[1], Haruka Ino[1], Indranova Suhendro[1], Gabriela Bunga Naen[1] (1.Department of Earth and Planetary Sciences, Faculty of Sciences, Kyushu University)

[SVC31-P05] Eruptive style and sequence of the 1235 eruption of Ohachi volcano, Kirishima, Japan -constraints from distribution, shape, and texture of pyroclasts-

*Sayaka Shohata[1], Fukashi Maeno[2], Natsumi Hokanishi[2], ATSUSHI YASUDA[2] (1.Department of Earth and Planetary Science, School of Science, The University of Tokyo, 2.Earthquake Research Institute, The University of Tokyo)

[SVC31-P06] Conduit ascent process of mafic subplinian eruption: Constraints from plagioclase microlites in the 1235 scoria of Kirishima-Ohachi volcano, Japan.

*Yoshiharu Iwaki[1], Hidemi Ishibashi[1], Natsumi Hokanishi[2], ATSUSHI YASUDA[2], Toru Ishikawa[3], Taketo Shimano[4] (1.Shizuoka University Graduate School of Integrated Science and Technology, 2.Earthquake Research Institute, University of Tokyo, 3.Kirishima Geopark Council, 4.Graduate School of Environment and Disaster Reserch, Tokoha University)

[SVC31-P07] Texture of ejecta of summit eruptions in Izu-Oshima

*Yuya Ikenaga[1], Fukashi Maeno[1], ATSUSHI YASUDA[1] (1.Earthquake Research Institute, The University of Tokyo)

[SVC31-P08] Shallow conduit process of Strombolian eruption: A case study of Izu-Omuroyama monogenetic volcano, Japan

*Hidemi Ishibashi[1], Risako Hatakeyama[1], Ryuta Sakamoto[1], Natsumi Hokanishi[2], ATSUSHI YASUDA[2] (1.Faculty of Science, Shizuoka University, 2.Earthquake Research Institute, The University of Tokyo)

[SVC31-P09] **Parameters to control bubble - crystal interaction styles**

*Kyoko Ikeda[1], Atsushi Toramaru[2] (1.Department of Earth and Planetary Sciences, Graduate School of Science, Kyushu University, 2.Department of Earth and Planetary Sciences, Faculty of Science, Kyushu University)

[SVC31-P10] 3D crystal size distributions of pyroxene nanolites plotted against short-axis length reflect magma ascent dynamics

*Shota Okumura[1], Mayumi Mujin[2], Akira Tsuchiyama[3,4], Akira Miyake[1] (1.Department of Geology and Mineralogy, Graduate School of Science, Kyoto University, 2.Division of Earth and Planetary Materials Science, Department of Earth Science, Tohoku University, 3.Research Organization of Science and Technology, Ritsumeikan University, 4.Guangzhou Institute of Geochemistry, Chinese Academy of Sciences)

[SVC31-P11] Petrological characteristics of the Kawago-daira rhyolite lava, Izu Peninsula, Japan

*Hiroshi Oka[1], Motohiro Tsuboi[1], Kuniyuki Furukawa[2] (1.Kwansei Gakuin University, 2.Aichi University)

[SVC31-P12] Determination of water solubility in the rhyolitic melt at 650°C and its interpretation by "hydrogen bonding model"

*Mizuki Nishiwaki[1], Takahiro Miwa[2] (1.Department of Earth and Planetary Sciences, Graduate School of Sciences, Kyushu University, 2.National Research Institute for Earth Science and Disaster Resilience)

[SVC31-P13] Flowage of the 1991 Unzen lava: Discussion to Goto et al.(2020) Rigid migration of Unzen lava rather than flow. JVGR

*Hiroaki Sato[1], Shigeru Suto[2], Tadahide Ui[3], Toshitsugu Fujii[4], Takahiro Yamamoto[2], Shinji Takarada[2], Keiichi Sakaguchi[2] (1.Kobe Univ., 2.Geological Survey of Japan, 3.Hokkaido Univ., 4.Mount Fuji Research Institute)

PHENO-BUBBLE NUMBER DENSITY (PBND) AS INDICATOR OF OVERPRESSURE IN PRE-ERUPTIVE MAGMA CHAMBER

*Indranova Suhendro[1], Atsushi Toramaru[1]

1. Department of Earth and Planetary Sciences, Graduate School of Sciences, Kyushu University

Magma chamber overpressure which caused by the oversaturation of preexisting bubbles (hereafter referred as “pheno-bubble” as a mimic of “phenocryst” in the common terminology of crystals in magma chamber) has been considered as one of the most important factors for triggering explosive volcanic eruptions. However, such qualitative and quantitative information of pheno-bubbles which are preserved in juvenile materials (e.g. pumice and scoria) is not yet provided. Therefore, in this study, we present the qualitative and quantitative study of pheno-bubble by examining natural samples which were obtained from 16 volcanoes, ranging from the VEI (volcanic explosivity index) 3 to 8 eruptions with various eruption style (subplinian to caldera forming eruptions) and various magma compositions (basaltic andesite to rhyolite). Based on our 2D-bubble size distributions (BSDs) data, we confirm that pheno-bubble can be defined as bubbles with diameter larger than approximately 0.1 mm, regardless to its compositions. We found that the number densities of pheno-bubble (PBND) in pre-eruptive magma chamber exhibit positive correlation with VEI. Particularly, VEI 3-5 eruptions have typically smaller PBNDs value (0.07 to 0.3x10^{11} m^{-3}) compared to VEI 6-8 eruptions (0.8 to 2x10^{11} m^{-3}). This suggest that the large and long-lived magma chambers experience with more intense heterogeneous nucleation of bubbles (or second boiling) thus results in more intense supersaturation of volatiles and provides larger amount of overpressure. In addition, we also found that bulk density has strong dependence on PBND value, as supported by the fact that juvenile materials from VEI 3-5 eruptions are typically denser than VEI 6-8 eruptions (avg. 0.6-1.4 gr/cm^3 and 0.3-0.8 gr/cm^3, respectively).

Keywords: Pheno-bubble, Pheno-bubble number density, Magma chamber, Overpressure, Explosive eruptions, Bulk density

©2021. Japan Geoscience Union. All Right Reserved.

Crystal Fracture in the Youngest Toba Tuff (74 ka) Pumices

*Gabriela Nogo Retnaningtyas Bunga Naen[1], Atsushi Toramaru[1], Haryo Edi Wibowo[2]

1. Department of Earth and Planetary Science, Kyushu University, Fukuoka, Japan, 2. Geological Engineering Department, Universitas Gadjah Mada, Yogyakarta, Indonesia

Pumice clasts from the enormous eruption of the Youngest Toba Tuff (YTT) contain crystals that are fragmented. That special texture is commonly seen as a product of large caldera-forming eruptions, thus understanding the origin of it can help to reveal the factors that lead to the eruptions. This study focuses on white pumices from non-welded YTT, especially feldspar (plagioclase and alkali feldspar) as the most abundant crystal and is expected to record the dynamic processes of YTT super eruption.

YTT white pumices consist of transparent (TWP: mainly containing larger vesicles, > 0.1 mm) and non-transparent pumices (NTWP: mainly containing smaller vesicles, < 0.1 mm). We studied 25 thin sections of pumice clasts with optical microscope. Textural analysis was carried out using microphotographs taken by SEM and further analysed using image processing software to extract the number of crystal fragments, pheno-bubble number density (PBND), and matrix-bubble number density (MBND). Chemical analysis for feldspar chemistry was conducted using EPMA.

First, we define a fragmented crystal (hereafter “crystal”) as a region containing broken pieces that preserve the initial form as one single crystal. We tentatively classify the size of feldspar into two groups based on crystal size namely microphenocryst (< 1mm), and phenocryst (> 1mm). In addition, we quantified fractured-crystals by classifying them into two classes in terms of number of fragments included in a “crystal”: type A includes 2 –9 fragments, and type B does more than 10 fragments. Then, we examined the correlation among the average number of fragments in one thin section with total individual crystals in the same thin section, MBND, PBND, and chemical composition (anorthite content).

YTT feldspar is mostly characterized by crystal fractures (58.6%), especially up to 85.8% in phenocryst. Broken melt inclusions and melt inclusions containing vapor bubbles are observed in some of the crystals, especially associated with type B crystals. TWP is dominated by crystal type A with low average of crystal fragments per one thin section (2 –10.5) and low MBND (10^4 mm^{-3}). On the other hand, NTWP is dominated by crystal type B, which shows various values of average crystal fragments per one thin section (2 –67) and has high MBND (10^5 mm^{-3} –10^7 mm^{-3}). However, the PBND is not so much different between the two types of pumices. Furthermore, crystal type B exhibits slightly higher anorthite content (An_{35-45}) compared to less fragmented crystal type A (An_{25-35}), and occasionally crystal type B occurs with some disequilibrium textures like patchy zoning, reverse zoning, and hollow texture.

Crystal fracture in YTT is thought to be formed by several mechanisms. YTT, as a crystal-rich magma system, experienced intensive collision of crystals. Phenocrysts, compared with microphenocrysts, are characterized by high number of crystal fragments. This could be explained by their longer times in magma chamber, which expose them to various dynamic processes as implied by the disequilibrium texture. These processes facilitate the formation of the cleavage planes that accommodate the crystals to be broken. From the correlation between MBND and the crystal fragmentation class, it is found that higher decompression rates make crystals fractured more, whereas lower decompression rates make less fractured crystals. In addition, magma decompression causes the volatile explosion of melt inclusions trapped in the crystals, which forces the crystal to be broken into many pieces, as was observed in crystal

©2021. Japan Geoscience Union. All Right Reserved.

type B. Moreover, crystals with high anorthite content are characterized by high average number of fragments, suggesting that the crystal composition influences the strength of crystals which affects the crystal fracture formation.

Keywords: YTT Pumices, Crystal fracture, Feldspar, Bubble, Textural study

©2021. Japan Geoscience Union. All Right Reserved.

Textural study of the 7.3 ka caldera-forming eruption of Kikai Caldera: Correlating bulk density to bubble-size observations

*Selvia Novianty[1], Masatoshi Ohashi[1], Atsushi Toramaru[1]

1. Department of Earth and Planetary Sciences, Graduate School of Science, Kyushu University

The 7.3 eruption of Kikai Caldera is one of the catastrophic events that cause devastating damage on southern Kyushu, Japan (Maeno et al., 2007). A comprehensive study on the detailed stratigraphy and transport-mechanism of its products has been carried out by Maeno et al. (2007). Regardless, the textural study of the 7.3 ka eruptive deposits of Kikai Caldera hasn't been conducted yet. In addition to the detailed description of the stratigraphic sequence of the eruptive deposits, the bubble size observation in the pumice is useful to characterize the vesicle texture and to gain insights into the eruption dynamics such as decompression rate in the conduit and overpressure condition in the magma chamber prior to the eruption. Integrating the bulk density data to the bubble-size observation for pumices is the aim of this study.

Samples were collected from all of the layers of Unit A, Unit C, and Unit D of the 7.3 ka caldera-forming eruption of Kikai Caldera at three localities, Southern Kyushu (Distal Locality), Takeshima Island (Proximal Locality), and Satsuma-Iojima Island (Proximal Locality). From all the localities, we had confirmed the stratigraphy which is coherent with the results by Maeno et al. (2007). Bulk density analyses were conducted for the pumice grains with the selected size range (2-16 mm) by 3D scanner (Medit Solutonix D700) and measuring software (Hira 3D viewer).

We selected 1131 pumice grains from all localities and measured the wide range (0.17 g/cm^3 –1.31 g/cm^3) of pumice bulk density from Unit A, Unit C, and Unit D. From the observation of pumice grains, we identified some physical characteristic such as bubble size, bubble shape, and crystal abundance. We compared each unit and analysed the different physical characteristics from its appearance qualitatively. Thus, from the measured bulk density, Unit A (0.17 g/cm^3 –1.14 g/cm^3) has a relatively lower bulk density compared to Unit C (0.27 g/cm^3 –1.31 g/cm^3) and Unit D (0.22 g/cm^3 –1.24 g/cm^3). We observed the dominant mode bulk of Unit A (0.45 g/cm^3) angular and spherical bubble shape, crystal poor, and relatively has smaller bubble size, sometimes has a foamy appearance. On the other hand, the dominant mode of Unit C (0.54 g/cm^3) and Unit D (0.50 g/cm^3) have similar physical characteristics such as have sub-angular and frequently stretched to elongated bubble shape, have a bigger bubble size, and have prismatic jointing appearance in some grains. The ranges of densities and physical characteristics in pumices may imply that each unit has a different vesiculation and fragmentation process such as different quenching. Thus, the difference fragmentation process affects measurable properties such as shape, vesicularity, permeability, bubble, and crystal size distribution (Rust et al., 2011). In this study, we attempt to reveal the eruption dynamic between each unit by connecting the bulk density with the bubble-size observation that comprises measurement of vesicularity, bubble size distribution (BSD), bubble number density (BND); and crystal contents.

Keywords: Kikai Caldera, Textural Analyses, Bulk Density, Bubble, Fieldwork

©2021. Japan Geoscience Union. All Right Reserved.

Factors controlling bulk density of pumice in explosive eruption deposits

*Atsushi Toramaru[1], Miki Ogata[1], Haruka Ino[1], Indranova Suhendro[1], Gabriela Bunga Naen[1]

1. Department of Earth and Planetary Sciences, Faculty of Sciences, Kyushu University

The bulk density of pumice clasts produced by explosive eruptions has thought to have the significant information on vesiculation processes that the magmas experience in the volcanic conduits and the magma chambers. As known well, there are the wide variations of bulk density even in the single eruption deposits. However, it is unclear that what causes the variation in bulk density, e.g., vesicularity or crystallinity. To reveal factors controlling the bulk density variations, we examine the correlation between the bulk density and other textural properties such as vesicularity, phenocryst-crystallinity, pheno-bubble abundance, and matrix bubble abundance for three eruptions; Aira caldera forming eruption, Japan, Mount St. Helens 1980 eruption, USA, and Manijau caldera-forming eruption, Indonesia. We determine the bulk density of pumice clasts (mainly 8 –16 mm) from the volume by 3D scanner and the weight by electric balance, and conduct the textural analysis for vesicularity (pheno-bubble (PB) (>0.1 mm) and matrix-bubble (MB) (< 0.1 mm)), phenocryst-crystallinity by the 2D image analysis for the SEM microphotographs. In the case of the Aira caldera-forming eruption, both PB and MB abundance have negative correlations with the bulk density and bulk vesicularity, the crystallinity has no correlation with bulk density. In the case of the Mount St. Helens 1980 plinian eruption, PB abundance has no correlation with bulk density, whereas MB abundance has a negative correlation and crystallinity has a positive correlation with bulk density. In the case of Maninjau caldera-forming eruption, both PB and MB abundance have negative correlations with bulk densities, whereas the crystallinity has no correlation with bulk density. Thus, in two large-volume caldera-forming eruptions among these three eruptions, only vesicularity controls the bulk density. In smaller plinian eruption of Mount St. Helens 1980 eruption, in addition to vesicularity, the crystallinity controls the bulk density. In the presentation, data for other eruptions such as Toba YTT caldera forming eruption will be shown to discuss the processes to make such PB, MB and crystallinity.

Keywords: pumice, bulk density, vesicularity, phenocryst, pheno-bubble, matrix-bubble

©2021. Japan Geoscience Union. All Right Reserved.

Eruptive style and sequence of the 1235 eruption of Ohachi volcano, Kirishima, Japan -constraints from distribution, shape, and texture of pyroclasts-

*Sayaka Shohata[1], Fukashi Maeno[2], Natsumi Hokanishi[2], ATSUSHI YASUDA[2]

1. Department of Earth and Planetary Science, School of Science, The University of Tokyo, 2. Earthquake Research Institute, The University of Tokyo

The diversity of the eruptive styles of basaltic magma is still poorly understood. In particular, it is necessary to understand the processes that determine eruptive events, such as explosive eruptions and pyroclastic flows. Ohachi volcano, Kirishima, is known to have had multiple explosive eruptions during the historical period due to the presence of tephra layers. Although the general framework of the time-series change of the eruptions have been described, the details of the style change and the factors of the change have not been fully understood. In this study, we investigate Takaharu tephra associated with the 1235 eruption in detail, and discuss the eruption transition and its driving process based on the re-examination of the eruption volume and changes in rock shape, density, and textural characteristics along the time series.

Takaharu tephra is divided into three units (A-B) based on the characteristics of the constituent pyroclasts. The total volume of the tephra is estimated to be 1.5 to 2 times larger than previously estimated, indicating that the 13th century eruption may have been larger than previously thought. Furthermore, field observations unveiled that each unit can be further divided into two or three layers. We collected samples of pyroclastic flow (PDC) deposits from the stage of Unit C and each subdivided layer, and measured the apparent density and grain density (density excluding connected voids). We also carried out quantitative evaluation of grain shape, textural observation by polarized light microscopy, and identification of phenocrysts.

The apparent density measurement results showed different peaks for below the lower of Unit C and for above the middle of unit C. The lower part showed low values (0.8-1.0 g/cm3) and the upper part showed high values (1.0-1.2 g/cm3). PDC clasts also showed high values. The results of grain density measurement showed low values (about 2.6 g/cm3) for unit B and below, and high values (about 2.9 g/cm3) for unit C and above, but PDC clasts showed low values as well as unit B and below. This suggests that the PDCs have smaller amount of connected porosity. The actual calculated connected porosity is 0.59 for PDCs compared to 0.62-0.69 for tephra layers.

The shape of scoria has different characteristics for each unit at the macroscopic observation level; A is flaky, B is relatively smooth, and C is intermediate. The three indices of circularity, roundness, and solidity (shape indices) were obtained from the projected images of the particle shapes, and were found to reflect the irregularities and other features in the observation.

There is no significant difference in the phenocrysts (plagioclase, pyroxene, and olivine) throughout the layers. However, the whole rock composition is slightly rich in SiO2 in the late stage of eruption (Unit C) (Miyamoto and Tsutsui, 1996). The groundmass crystallinity is high in the order PDC >B >C >A, and the lower the crystallinity, the larger the crystal size. Microscopic bubble texture shows that A is dominated by small isolated bubbles, B is dominated by large connected bubbles, C is dominated by large but

©2021. Japan Geoscience Union. All Right Reserved.

wall-separated bubbles, and PDC is dominated by small bubbles connected in a complex manner. The textures vary with stratigraphy.

A comparison of shape index and rock texture shows that there is a relationship between them, with the exception of pyroclastic density currents. For example, in Unit A, the low crystallinity and low connected pore fraction are seemingly reflected in the roughness of the particle surface. In this case, it can be interpreted that the low viscosity magma has a high ascent velocity and it was strecthed and broken apart by the explosion to form the specific shape. The relationship we have found between particle shape/density and rock texture may be an important constraint for understanding the origin of pyroclastic particles in different units and the eruptive sequence.

Keywords: eruptive style, scoria, Ohachi volcano

©2021. Japan Geoscience Union. All Right Reserved.

Conduit ascent process of mafic subplinian eruption: Constraints from plagioclase microlites in the 1235 scoria of Kirishima-Ohachi volcano, Japan.

*Yoshiharu Iwaki[1], Hidemi Ishibashi[1], Natsumi Hokanishi[2], ATSUSHI YASUDA[2], Toru Ishikawa[3], Taketo Shimano[4]

1. Shizuoka University Graduate School of Integrated Science and Technology, 2. Earthquake Research Institute, University of Tokyo, 3. Kirishima Geopark Council, 4. Graduate School of Environment and Disaster Reserch, Tokoha University

Mildly explosive eruption is common styles of high-temperature, less viscous mafic magma. However, many cases of Plinian eruptions of mafic magmas have been reported in this decade. Recent studies suggest that microlite crystallization at the shallow conduit depth significantly increases viscosity and causes the viscous-brittle transition of mafic magma, which induces sustained fragmentation and explosion. Therefore, it is important to clarify the processes of microlite crystallization during conduit ascent for understanding the eruption mechanism of mafic magmas. The 1235 subplinian eruption is the largest eruption of Ohachi volcano, which is one of the active volcanoes in Kirishima, Japan. During the eruption, basaltic andesite magma with bulk SiO_2 content ~51-55wt.% erupted and formed three thick fall scoria layers (ThT-a, ThT-b, and ThT-c) called Takaharu scoria (Tsutsui et al., 2007). Because the groundmass crystallization occurred at the shallow conduit depth, the groundmass texture is expected to have information about the conduit ascent process of the magma. In this study, we performed textural analyses of the plagioclase microlites in Takaharu scoria to clarify the conduit ascent process of mafic magma during a subplinian eruption.

In this study, we investigated glassy scoria grains (2-8 mm in size) in ThT-a, ThT-b, and ThT-c. FE-EPMA (JEOL JCXA-8530FPlus) at Earthquake Research Institute (ERI) of the University of Tokyo, Japan, was used to acquire backscatter electron (BSE) images of the groundmass of the samples. The BSE images were quantitatively analyzed to determine crystal volume fractions, crystal number densities, and crystal size distributions (CSDs) of plagioclase microlites.

Plagioclase, olivine, orthopyroxene, and clinopyroxene were found as phenocrysts in the Takaharu scoria, with a total phenocryst contents of ~19-22 vol.%. The groundmass is composed of plagioclase, mafic minerals and glass. Because olivine and pyroxene in the groundmass are difficult to distinguish on BSE images, we treated them together as mafic minerals. The microlite contents (Φ) of plagioclase are ~10-30 vol.% for ThT-a, ~10-37 vol.% for ThT-b, and ~6-33 vol.% for ThT-c, respectively. On the other hand, the microlite contents were less than 5 vol.% for mafic minerals.

Measured CSDs for plagioclase microlites are often inflected. Least-squares regression into the combination of two distinct log-linear CSD relations was done to determine the intercept, log $n_{0,}$ and the slope, $1/L_0$, of each CSD relation. The n_0 for the finer crystals ranges ~$10^{8.6\text{-}9.4}$ mm^{-4} for ThT-a, $10^{8.7\text{-}9.7}$ mm^{-4} for ThT-b, and $10^{9.1\text{-}10.2}$ mm^{-4} for ThT-c, respectively; it increases from ThT-A to C. On the other hand, the $1/L_0$ varies in the ranges of 78-169 mm^{-1} for ThT-a, 94-166 mm^{-1} for ThT-b, and 116-261 mm^{-1} for ThT-c, respectively; it also increases from ThT-A to C. The number densities of plagioclase microlite (N) were determined from the values of n_0 and $1/L_0$. The Ns of plagioclase microlites were ~3.8×10^{15}-$1.3\times10^{16}m^{-3}$ for ThT-a, ~7.6×10^{15}-$3.6\times10^{16}m^{-3}$ for ThT-b, and ~1.0×10^{16}-$6.8\times10^{16}m^{-3}$ for ThT-c, respectively. N

©2021. Japan Geoscience Union. All Right Reserved.

was almost constant regardless of Φfor ThT-a, whereas positive relations between Φand N are observed for ThT-B and C.

The microlite number density decompression-rate meter (Toramaru et al., 2008) was applied to the plagioclase microlites to estimate the conduit ascent rate of the magma. The decompression rates were estimated to be in the range of ~0.31-0.73 MPa/s for ThT-a, ~0.45-1.38 MPa/s for ThT-b, and ~0.34-1.24 MPa/s for ThT-c, respectively; these are comparable with those estimated for other mafic subplinian eruptions. The estimated decompression rate increases from ThT-a to ThT-b, and then decreases to ThT-c. These results are consistent with the relation of the dispersal areas between three scoria units (Tsutsui et al., 2007). Our results suggest that the eruption intensity is controlled by the conduit ascent rate of the mafic magma.

Keywords: plagioclase, mafic subplinian eruption, Kirishima, Ohachi volcano, shallow conduit process, microlite crystallization

©2021. Japan Geoscience Union. All Right Reserved.

Texture of ejecta of summit eruptions in Izu-Oshima

*Yuya Ikenaga[1], Fukashi Maeno[1], ATSUSHI YASUDA[1]

1. Earthquake Research Institute, The University of Tokyo

Izu-Oshima, which is an active volcano erupting basaltic magma, have caused many eruptions from both summit and flank craters. The eruptions which occurred in 1986 and 1950 are known as recent middle-scale eruptions. It is also known that large-scale eruptions have occurred every 150-200 years before recent middle-scale eruptions (Nakamura 1964, Isshiki 1984, Koyama and Hayakawa 1996, Endo et al. 1988). There are various kinds of geological and petrological research in Izu-Oshima, and the sequence and magma system of each eruption has gradually become revealed (Kawanabe 1991, Nakano and Yamamoto 1991, Hamada 2014, Ishizuka et al. 2015). On the other hand, there are few studies which analyze the textures of ejecta, and the relationship between eruption intensities and textures of ejecta is not clear. We focused on the summit eruptions in this study, and analyzed the bubble and microlite textures of scoriae of Strombolian eruption (1986 eruption) and sub-Plinian eruptions (Y1, Y2, Y4 and Y6 eruptions). In Y1 eruption, scoria deposits were divided into lower part (Unit A) and upper climax part (Unit C).

We measured scoria density of each eruption by glass beads, and selected one low-density, two middle-density and one high-density samples to create thin sections. Backscattered electron images of thin sections were obtained by FE-EPMA and analyzed by ImageJ.

Bubble textures changed according to the intensities of eruptions. In 1986 eruption, large bubbles were mainly observed. On the other hand, in the sub-Plinian (Y1, Y2, Y4 and Y6) eruptions, there were many small bubbles and the bubble number densities were higher than 1986 eruption. Bubble number density was especially high in Y1 Unit C. Scoria density was highest in Y1 Unit C. Microlites were observed in almost all eruptions, except Y1 Unit C.

From bubble textural analyses, there is a tendency that scoriae include many small bubbles in high-intensity eruptions. It is assumed that magma ascent rates were high and magma was supersaturated in volatiles and bubble nucleation progressed in high-intensity eruptions. In the low-intensity eruption such as 1986 eruption, there were many large bubbles and bubble number density was low as a result of growth, coalescence and degassing of bubbles. There were nearly no microlites in Y1 Unit C. Although it is estimated that magma was highly supersaturated in this Unit, there is possibility that liquidus temperature didn’t become lower sufficiently and crystallization of microlites didn’t occur because magma ascent rate was high and volatiles couldn’t precipitate enough as bubbles.

Keywords: Izu-Oshima, Bubble texture, Microlite

©2021. Japan Geoscience Union. All Right Reserved.

Shallow conduit process of Strombolian eruption: A case study of Izu-Omuroyama monogenetic volcano, Japan

*Hidemi Ishibashi[1], Risako Hatakeyama[1], Ryuta Sakamoto[1], Natsumi Hokanishi[2], ATSUSHI YASUDA[2]

1. Faculty of Science, Shizuoka University, 2. Earthquake Research Institute, The University of Tokyo

Izu-Omuroyama volcano is one of the monogenetic volcanoes in the Higashi-Izu monogenetic volcanic field (HIMVF) and was formed by the Strombolian eruption that occurred at 4ka. The eruption formed the largest scoria cone in HIMVF and simultaneously effused abundant lava flows. In this study, we performed quantitative textural analyses of minerals and chemical analyses of glasses in the groundmass of the Izu-Omuroyama scoria to clarify the shallow-conduit processes inducing the branch of the scoria-forming explosion and the lava effusion.

The scoria of the cone-forming stage was investigated. BSE images were acquired using FE-EPMA at ERI. We quantified volume fractions (Fs), number densities (NDs), and size distributions (CSDs) by image analyses for plagioclase (80 samples) and mafic minerals (40 samples), respectively. Because it is difficult to discriminate olivine and pyroxene in BSE images, we treated these minerals collectively as mafic minerals.

The groundmass of the scoria is composed of plagioclase, olivine, pyroxene, and glass. Fs of plagioclase and mafic minerals vary ~5-40 vol.% and ~3-20 vol.%, respectively. NDs are ~2000-20000 mm^{-1} for both minerals. An-rich, coarse and An-poor, fine plagioclase grains are found; the former and the latter are called microphenocryst and microlite, respectively. We discriminated against the microphenocrysts and the microlites based on CSDs. Inflected CSDs are found for both plagioclase and mafic minerals in the scoria; they are successfully explained by combinations of two linear CSD relations. The inflected sizes are determined for each sample. We regarded the mineral grains coarser and finer than the inflected size as microphenocrysts and microlites, respectively.

For microphenocrysts, Fs vary ~5-40 vol.% for plagioclase and ~0.4-20 vol.% for mafic minerals, respectively. NDs are 20-1000 mm^{-2} for both minerals. Positive relations are found between F and ND for both minerals. The ND of plagioclase microphenocryst increases from lower to higher units of the stratigraphy. The NDs of the higher units are similar to those of the lava flow, indicating that the groundmass texture of the lava flow can be explained by the crystal growth of microphenocryst without microlite crystallization. For microlites, Fs vary ~5-40 vol.% for plagioclase and ~2-20 vol.% for mafic minerals, respectively. The NDs are 1000-20000 mm^{-2} for both minerals. Contrary to the scoria case, the ND of plagioclase microphenocryst decreases from lower to higher units of stratigraphy. Fs of microphenocrysts are lower than ~40 vol.%, whereas those of all groundmass minerals are higher than ~40 vol.%. Previous experimental studies show that plagioclase-bearing magma behaves as solid when the F of suspended crystal is larger than ~40 vol.%, suggesting that the liquid-solid rheological transition was induced by microlite crystallization. The depth condition of microlite crystallization is constrained to be < 400m based on the chemical compositions of interstitial glasses and MELTS simulation.
Our results suggest that microlite crystallization at < 400m depth induced solidification of magma, which resulted in brittle fragmentation and explosion at the summit vent. On the other hand, the branch of the conduit to the flank vent occurred at a deeper depth than that of microlite crystallization, resulting in lava flow effusion. The increase and decrease of NDs of microphenocrysts and plagioclase microlite,

©2021. Japan Geoscience Union. All Right Reserved.

respectively, from the lower to the higher stratigraphic units can be attributed to the resupply of the deep-derived hot magma, which is consistent with the abundant lava effusion following the scoria cone formation.

Keywords: mafic magma, Strombolian eruption, microlite crystallization, Shallow conduit process, Higashi-Izu monogenetic volcano group, eruption style

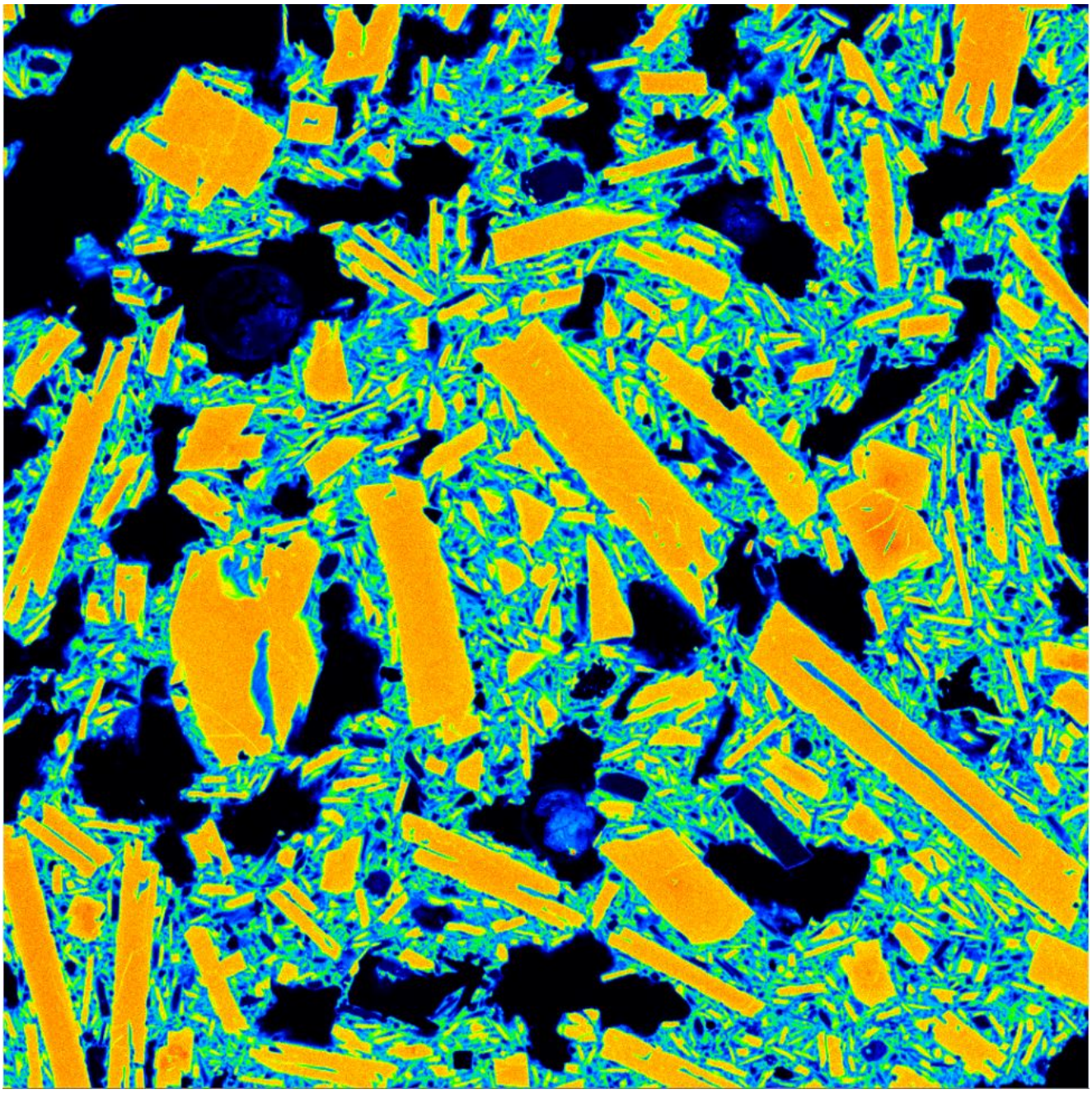

©2021. Japan Geoscience Union. All Right Reserved.

Parameters to control bubble - crystal interaction styles

*Kyoko Ikeda[1], Atsushi Toramaru[2]

1. Department of Earth and Planetary Sciences, Graduate School of Science, Kyushu University, 2. Department of Earth and Planetary Sciences, Faculty of Science, Kyushu University

In the magma, the interaction between suspended crystals and the rising bubble due to buoyancy is important because their stratification through the rheological properties and bulk densities. Belien et al. (2010) showed that there are three interactionstyleswithchangingbubblediameter bylaboratoryexperimentsusingan analog material: a single plastic cube and a controlled single bubble in viscous liquid. However, the crystal - bubble interaction is still poorly understood because factors determining the interaction styles have not been revealed in terms of dimensionless parameters. In order to solve this problem, we try to find the dimensionless parameters by the analogue experiments with varying viscosity and size ratio of solid cube to bubble.

The experiments are performed in the tank filled with viscous liquid (analog material of silicate melt) and prepared six different viscosity(0.041 Pa・s –47.2 Pa・s). The plastic cube (analog material of crystal) with 10 mm is suspended in liquid by a rod. The bubble is injected into the liquid from 11cm below the plastic cube from a syringe connected to a motor controlled by the PC program by which we can change the initial bubble size. We examine the probability of occurrence of three styles of interaction: "stuck", "pass", and "split"; "stuck" in which a bubble stays below the solid cube, "pass" in which a bubble passes around the cube and "split" in which a bubble splits into two bubbles. To determine the probabilities, we did the repetition of 10 times for the same condition of initial bubble radii and viscosity.

In our experiments, we observed two styles of the interaction of "stuck" and "pass" and not "split". It is found that the smaller bubble tends to “stuck”, on the other hand, the probability of “pass” became higher as the bubble radii are larger. To reveal the boundary of “stuck” and “pass”, we estimated three parameters in my previous research (Ikeda and Toramaru, 2020 JpGU meeting) ; the size ratio of the crystal and the bubble, the Bond number(Bo), which represents the deformation scale of the bubble caused by buoyancy, and the Reynolds number(Re), which is the ratio of inertial to viscous forces. In high Re regime, the bubble bounces back after impacting the crystal because of inertia force. In this region, the bubble is easily deformed because the Bo is large. Because of the both effect of inertial force and the bubble deformation, “pass” occurs even if the size ratio of crystal and bubble is smaller than in other regions. On the other hand, in low Re regime, rebounding does not occur because the viscous force is larger than inertia force. In this region, Bo is also small, therefore, bubble deformation is difficlut to occur. This indicates that "pass" does not occur unless the size ratio of bubble and crystal is larger than in other regions.

In this presentation, we measured the rheology of analog liquid used in this experiments. Using the measured viscosity for Re, it was found that the boundary value of the size ratio of crystal and bubble is constant as the Re increased. This indicates that the viscosity does not affect the interaction-style boundary. To be more precise in measuring the size of bubble, we used the bubble radius calculated from the area measured from the images. From these results, we propose the new criterion dividing “stuck” and “pass” as the critical value of product of Bo and the size ratio: in one regime, “stuck “occurs when both of Bo and the size ratio of crystal and bubble were small. in the other regime, “pass” occurs when the Bo and the size ratio of crystal and bubble were large.

©2021. Japan Geoscience Union. All Right Reserved.

Keywords: analog experiment, bubble-crystal interaction

©2021. Japan Geoscience Union. All Right Reserved.

3D crystal size distributions of pyroxene nanolites plotted against short-axis length reflect magma ascent dynamics

*Shota Okumura[1], Mayumi Mujin[2], Akira Tsuchiyama[3,4], Akira Miyake[1]

1. Department of Geology and Mineralogy, Graduate School of Science, Kyoto University, 2. Division of Earth and Planetary Materials Science, Department of Earth Science, Tohoku University, 3. Research Organization of Science and Technology, Ritsumeikan University, 4. Guangzhou Institute of Geochemistry, Chinese Academy of Sciences

Groundmass crystals indicate syn-eruptive magmatic conditions and thus their crystal size distributions (CSDs) reflect magma ascent histories via their crystallizing balance between nucleation and growth (e.g., Marsh 1998; Mujin and Nakamura 2014). 3D CSDs are most commonly estimated from 2D observations and plotted against long-axis length, *L* (e.g., Higgins 2000). *L*-plot CSDs of phenocrysts estimated from 2D observations were confirmed to agree well with those measured directly in 3D (e.g., Mock and Jerram 2005; Jerram et al. 2009). However, Castro et al. (2003) pointed out the possibility that largely varied shapes of groundmass crystals cause inconsistency among the CSDs in 2D and 3D.

Because *L*-plot CSDs require additional stereological corrections compared to CSDs plotted against *S* or *I* when they are estimated from 2D observations, the estimated *L*-plot CSDs should include large errors associated with the stereological corrections. Nevertheless, it has not been discussed fully whether *L* is the most representative size for CSDs of groundmass crystals in order to infer magma ascent conditions in conduits. Therefore, it is necessary to evaluate the influences of size criteria on the CSDs.

Here, we observed groundmass pyroxene crystals in pumices from sub-Plinian and Vulcanian eruptive phases during the 2011 eruption of Shinmoedake (Kirishima volcano group, Japan) by both a JEOL JSM-7001F field-emission scanning electron microscope (FE-SEM) at Kyoto University and synchrotron radiation-based X-ray computed nanotomography (SR-XCT) at beamline BL47XU of the SPring-8 synchrotron facility (Hyogo, Japan; Uesugi et al. 2006; Takeuchi et al. 2009). The SR-XCT observations with effective spatial resolution of 200 nm provided detailed 3D morphologies, triaxial lengths (*S*, *I*, and *L*), and true 3D CSDs of pyroxene crystals ranging from a few hundred nanometers to a few micrometers in width. We compared 3D CSDs estimated from 2D SEM observations (SEM-CSDs) with those measured directly by SR-XCT (CT-CSDs) to investigate whether the prevalent *L*-plot SEM-CSDs are accurate for groundmass crystals of various shapes. We also compared 3D CSDs plotted as a function of *S*, *I*, and *L* to explore which plot types are most representative of eruptive style.

The slopes of *S*- and *I*-plot SEM-CSDs were similar to the slopes of the CT-CSDs compared to *L*-plot SEM-CSDs. This inconsistency of *L*-plot CSDs results from the difficulty in estimating a representative 3D aspect ratio for fairly elongated groundmass crystals ($L/S = 1–40$) from 2D observations, which is critical for the accuracy of stereological conversion into 3D CSDs. Moreover, the slopes of *S*- and *I*-plot CT-CSDs differed more markedly according to eruption style (by ~20%) than those of *L*-plot CT-CSDs.

For estimating magma ascent histories, we propose that the optimum method for acquiring SEM-CSDs is to measure the cross-sectional widths of crystals and convert the 2D dataset into *S*-plot CSDs. By calculating *S*-plot CSD slopes from previous studies reporting *L*-plot SEM-CSDs and 3D aspect ratios, we show that plotting CSDs against *S* preserves their actual slopes, which more reliably reflect magma ascent conditions than those plotted against *L*.

©2021. Japan Geoscience Union. All Right Reserved.

Keywords: crystal size distribution, X-ray CT, nanolite, morphology, magma ascent

©2021. Japan Geoscience Union. All Right Reserved.

Petrological characteristics of the Kawago-daira rhyolite lava, Izu Peninsula, Japan

*Hiroshi Oka[1], Motohiro Tsuboi[1], Kuniyuki Furukawa[2]

1. Kwansei Gakuin University, 2. Aichi University

The explosive and effusive rhyolitic eruptions were occurred in Kawago-daira in 3000 years ago[1)], which relates to the Amagi volcanic group in the Izu peninsula, Japan[2)]. The eruptions began with pyroclastic density currents, which were followed by the lava effusion. The Kawago-daira lava is composed of obsidian and pumiceous lithofacies.
In this study, the whole-rock chemical compositions and water contents of the Kawago-daira lava were provided to reveal the development process of the lithofacies. All samples were collected from the distal part of the lava. Major and trace elements were determined by wavelength dispersive X-ray fluorescence spectrometry (WDXRF), and rare earth elements (REE) were determined by inductively coupled plasma mass spectrometry (ICP-MS). Water contents were estimated using micro-Fourier-transformed infrared spectroscopy (m-FT-IR). Thickness of double polished thin sections for m-FT-IR analysis were 108-208 μm. The absorbance at 1630 cm^{-1} (bending vibration of H_2O molecule) and 3580 cm^{-1} (stretching vibration of OH group) was measured 25 times for groundmass of each sample. The water content was calculated from the absorbance, using the Lambert-Beer's law. Molar absorption coefficients used are 55 L/mol・cm and 67 L/mol・cm for 1630 cm^{-1} and 3580 cm^{-1}, respectively[3)].
The whole-rock SiO_2contents of both lithofacies show 70.18-71.41 wt.%. In Harker diagrams and chondrite-normalized REE patterns, the results of pumiceous and obsidian lithofacies were indistinguishable from each other. A total amount of H_2O molecules and OH groups ranges from 0.23 to 0.25 wt.% for pumiceous lithofacies and from 0.18 to 0.31 wt.% for obsidian lithofacies. While the water contents of both lithofacies appear to be consistent, it is needed to assess the amount of secondary water to evaluate the accurate water contents. We will discuss the development process of the lithofacies from the chemical characteristics and the textures in thin sections.

1) Shigeru Shimada, *The Quaternary Research*, **39**, (2000) 151-164.
2) Konosuke Sawamura, EXPLANATORY TEXT OF THE GEOLOGICAL MAP OF JAPAN Scale1:50,000 SHUZENJI, *Tokyo*, **100**, (1954) 34-37.
3) Yohei Yoshimura, Kazuhiko Kano, Daizo Ishiyama, *Bulletin of the Volcanological Society of Japan*, **57**, (2012) 159-176.

Keywords: rhyolite, obsidian, pumice, infrared microspectrometry, Izu Peninsula

©2021. Japan Geoscience Union. All Right Reserved.

Determination of water solubility in the rhyolitic melt at 650℃ and its interpretation by "hydrogen bonding model"

*Mizuki Nishiwaki[1], Takahiro Miwa[2]

1. Department of Earth and Planetary Sciences, Graduate School of Sciences, Kyushu University, 2. National Research Institute for Earth Science and Disaster Resilience

We experimentally determined the water solubility in the rhyolitic melt at 650˚C with pressures of 30, 90, and 150 MPa. First, we hydrated a clear rhyolitic obsidian glass pellet with water of ~10 wt%, at 800 or 900℃ with arbitrary pressures for 21-48h in a cold-seal pressure vessel. Subsequently, we lowered the temperature to 650℃ at the isobaric condition and kept it for 0-120h. Then, the system was instantaneously decompressed to the pressures of 30, 90, and 150 MPa, and put for 24-96h to induce vesiculation. The run products, which did not contain any microlite or nanolite, were sliced into several pieces and double-polished. The content and distribution of water species of the run products were measured by using the doubly-polished thin sections and Fourier transform infrared (FT-IR) micro-spectroscopy (JASCO FT/IR-660 Plus spectrometer and a JASCO IRT-30 microscope in ERI, University of Tokyo). The total water contents (H_2O_m + OH^-) and its gradients around the bubbles were determined by transmittance and reflectance spectra, respectively. H_2O_m means H_2O molecule.

As a result of the experiment, we found the obtained solubility (2.70 ±0.25 wt% at 30 MPa, 5.84 ±0.54 wt% at 90 MPa, and 6.84 ±0.63 wt% at 150 MPa) is significantly higher than that calculated by the “Burnham model” (Burnham, 1979). In the Burnham model, the whole water is dissolved into melt as OH^- groups through the hydrolysis of Si-O bondings, despite the contribution of H_2O_m cannot be neglected in low temperature. Therefore we developed a new solubility model accounting for the dissolution of H_2O_m into the rhyolitic melt by considering a hydrogen bonding between hydrogen of H_2O_m and oxygen of the Si-O network. We analytically derived the pressure-temperature dependence of H_2O_m solubility in melt and substituted the molar enthalpy of formation of hydrogen bonding in water-saturated aluminosilicate melt $\Delta H = 10$ kJ/mol (Mysen, 2012). The solubility of total water is evaluated from the sum of the solubilities of H_2O_m and OH^- which is calculated from the equilibrium constant between H_2O_m and OH^- ($K = [OH^-]^2/[\text{oxygen}][H_2O_m]$). This new “hydrogen bonding model” can explain our experimental data very well when $K \fallingdotseq 0.040$-0.10.

Our new theoretical model can calculate the water solubility in low-temperature melt below 700℃, in that region extrapolation of conventional theoretical equations has not yielded reliable values until now. A precise study of the physicochemical properties of low-temperature magma, including the water solubility determined in this study, may provide further insights into the cooling process near the walls of magma reservoirs and volcanic conduits, the formation process of dikes and sills, and the behavior of obsidian lava flows.

Keywords: water solubility, 650℃, rhyolitic melt, vesiculation, hydrogen bonding model

©2021. Japan Geoscience Union. All Right Reserved.

Flowage of the 1991 Unzen lava: Discussion to Goto et al.(2020) Rigid migration of Unzen lava rather than flow. JVGR

*Hiroaki Sato[1], Shigeru Suto[2], Tadahide Ui[3], Toshitsugu Fujii[4], Takahiro Yamamoto[2], Shinji Takarada[2], Keiichi Sakaguchi[2]

1. Kobe Univ., 2. Geological Survey of Japan, 3. Hokkaido Univ., 4. Mount Fuji Research Institute

Goto et al. (2020) presented new rheological data on the bulk rocks and a groundmass glass synthetic sample of the ejecta of the 1991 Unzen dacite, and together with the previous rheological data of groundmass glass, they suggested that bulk viscosity of Unzen dacite is more than 1 order of magnitude larger than those obtained by Jeffreys model calculated from the apparent velocity of the lava front, slope inclination, lava height and density of the lava by Suto et al.(1993) and Yamamoto et al. (1993). Although they suggested possible effect of water in the lower part of the lava where higher pressure (ca. 1.4 MPa) affords retaining of water in the matrix glass, they suggested rigid migration of the lava from the video image analyses. Our discussion is concerned with more fluidal aspect of the lava from the pictures at the time of eruption, suggesting that at least some part of the lava flowed as viscous fluid, and that shear zone at the base of the lava, which Goto et al.(2020) suggested, is not likely.

Figure 9 of Goto et al.(2020) vaguely show that apparent advance of the lava lobe front is accompanied by crack widening in the lava lobe, and they suggested that apparent advance of the lava lobe represents rotation of the frontal block. However, our sequential pictures show that upstream area also advance nearly parallel to the frontal area, which indicate the deformation of the lava lobe. Other evidence of flowage of the lava lobe includes thickening of the lava lobe in the downstream area, protrusions of the front of the lava lobe, crease structure of the lava lobe near the site of upwelling, and wrinkle structure on the surface of the lava block. Thickening of lava lobe in the downstream area has been illustrated in Figure 7 of Nakada and Fujii (1993)jvgr and our pictures. Protrusive front is also described in Nakada and Fujii (1993) jvgr, Ohta (1992) and our photographs taken from helicopter of the Ground Self-Defence Force in August and November, 1991. Crease structure show viscous deformation of the upwelling lava from the source vent, and are often observed in the 1991 Unzen eruption. Wrinkle texture is sometimes observed on the surface of lava blocks of the Unzen lava lobes including the supplementary movie of Goto et al.(2020). Interval of wrinkles is generally 2-5 meters, and indicate much less viscous interior than the surface of the lava block (Fink and Fletcher, 1978 jvgr).

Several shear zones are observed in the section of lava lobe such as Figure 3 of Suto et al.(1993) and lava lobe-11. The presence of shear zones within the lava lobe together with protrusive front of the lava lobes suggest that basal boundary of the lava lobe is resistant to slide.

The discrepancy of the idea may be caused by slight difference in temperature and glass composition of the lavas: temperature Goto et al.(2020) used was ca. 850˚C, whereas experimentally duplicated temperature of Venezky and Rutherford (1999) gave 900±30˚C, and glass composition of Nakada and Motomura (1999) gave 1-2wt% lower SiO_2 and 0.3-0.4 wt% higher Na_2O, which result in the estimated viscosity difference of more than 1 log unit.

The experimental work of Goto et al.(2020) together with those of Cordonnier et al. (2009) and Coats et al. (2018) showed fairly large variation of viscosity on the bulk rock of Unzen lava samples (more than 2 orders of magnitude at 900˚C), which may correspond to wide variations of fluidity/rigidity as pictures of

©2021. Japan Geoscience Union. All Right Reserved.

the 1991 Unzen lava lobes show. Viscosity of effusing lava is delicately influenced by dewatering, cooling, and crystallization during effusive action, and application of the rheological experimental results to natural lava behavior should be carried out with much more caution.

Keywords: Unzen volcano, Lava lobe, Viscosity, Flowage of lava, Magma temperature, Groundmass glass composition

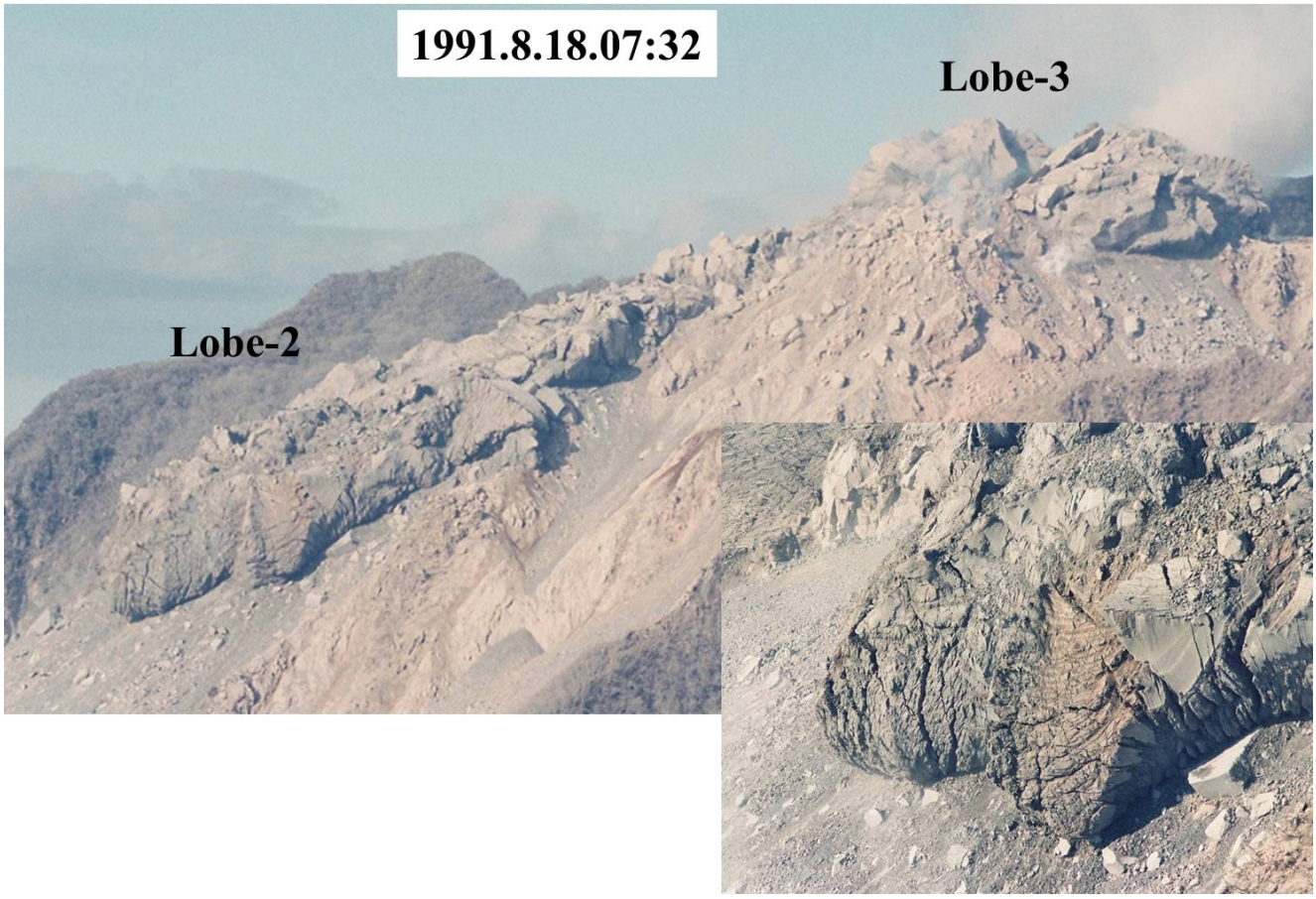

©2021. Japan Geoscience Union. All Right Reserved.

[J] Poster | S (Solid Earth Sciences)：S-GC Geochemistry

Sat. Jun 5, 2021 5:15 PM - 6:30 PM JST | Sat. Jun 5, 2021 8:15 AM - 9:30 AM UTC | Ch.17_2

[S-GC33] Solid Earth Geochemistry, Cosmochemistry

convener:Gen Shimoda(Geological Survey of Japan, AIST), Katsuhiko Suzuki(Submarine Resources Research Center, Japan Agency for Marine-Earth Science and Technology), Katsuyuki Yamashita(Graduate School of Natural Science and Technology, Okayama University), Akira Ishikawa(Department of Earth and Planetary Sciences, Tokyo Institute of Technology)

Solid Earth Geochemistry, Cosmochemistry" session aims at evaluating processes during the 4.6 billion years of the solar system and the Earth. Any approaches to this issue is welcomed, including, geochemistry, geophysics, geology, mineralogy and petrology.

[SGC33-P01] Origin of intra-plate magmatism in Kamchatka constrained by noble gas isotopes

*Masao Fukagawa[1], Hirochika Sumino[2], Anna O Volynets[3], Yuri Taran[3] (1.Department of Integrated Science, College of Arts and Science, the University of Tokyo, 2.Department of General Systems Studies Graduate School of Arts and Sciences, The University of Tokyo, 3.Russian Academy of Sciences)

[SGC33-P02] Rare earth elements composition of carbonate concretion in the Miocene Morozaki Group, southwestern Japan

*Ryosuke Kitanaka[1], Motohiro Tsuboi[1] (1.Kwansei Gakuin University)

[SGC33-P03] Investigation of Validity for Evaluation Particle numbers on Characterization of Soil Particle Morphology Using Automated Particle Image Analysis and Computed Simulations.

*Daisuke Sasakura[1] (1.Malvern Japan ,Div of Spectris Co.Ltd,.)

[SGC33-P04] Role of fluid rock reaction for the production of FOZO isotopic composition

*Gen Shimoda[1], Tetsu Kogiso[2], Katsuhiko Suzuki[3], Akira Ishikawa[4], Norikatsu Akizawa[5] (1.Geological Survey of Japan, AIST, 2.Kyoto University, 3.Japan Agency for Marine-Earth Science and Technology, 4.Tokyo Institute of Technology, 5.University of Tokyo)

Origin of intra-plate magmatism in Kamchatka constrained by noble gas isotopes

*Masao Fukagawa[1], Hirochika Sumino[2], Anna O Volynets[3], Yuri Taran[3]

1. Department of Integrated Science, College of Arts and Science, the University of Tokyo, 2. Department of General Systems Studies Graduate School of Arts and Sciences, The University of Tokyo, 3. Russian Academy of Sciences

Introduction: In Kamchatka, three volcanic chains (the first is volcanic front, the second is back-arc chain and the third is Sredinny Range, SR) are identified, and the former two are considered to result from the subduction of Pacific plate. On the other hand, several origins have been proposed for intra-plate magmatism in SR: ascent of deep mantle plumes, back-arc spreading in response to trench rollback, etc. The purpose of this study is to constrain the origin of magmatism in SR by using noble gas isotopes, which have different features in different geochemical reservoirs, such as convecting MORB-source mantle, deep-mantle-derived plume, and crust.

Samples and analysis: We extracted noble gases (He, Ne, Ar, Kr, and Xe) from fluid/melt inclusions in olivines and pyroxenes separated from basalts and andesites collected from SR by crushing in vacuum, and analyzed their abundances and noble isotope ratios. After that we heated in vacuum the recovered powders after crushing to melt the sample for complete noble gas extraction, and then analyzed in the same way.

Results and discussion: Helium isotope ratios ($^3He/^4He$ ratios) obtained with the crushing of olivines were in general around 8 Ra, where Ra denotes atmospheric $^3He/^4He$ ratio. The values are in the range of MORB-source mantle (8±1 Ra), which is similar to He in mantle-derived xenoliths from Avacha volcano in the volcanic front [1]. On the other hand, crush-released $^3He/^4He$ ratios of pyroxenes were systematically lower than those of olivines in the same host rocks. Because pyroxene crystallization is generally later than that of olivine in magma, the lower $^3He/^4He$ ratios of pyroxenes than olivines would have resulted from interaction of magma with surrounding crustal rocks, which have low $^3He/^4He$ ratios, between olivine and pyroxene crystallization. A few olivines showed lower $^3He/^4He$ ratios than MORB value during the crushing experiment, which would be trace of the slab fluids enriched in U and Th. Higher $^3He/^4He$ ratios than the MORB value were also observed during crushing of another fer olivines samples Because He extracted by heating of crushed powder yielded much higher $^3He/^4He$ ratio (>100 Ra), the high $^3He/^4He$ ratios obtained with crushing would be due to a small release of cosmic-ray produced He having accumulated in the sample after the eruption.

Based on the above observations, we conclude that the origin of magma erupted in SR is the convecting mantle, and the possibility of plume’ s involvement is low. We also conclude that there are significant traces of slab fluids in some regions in SR.

Reference: [1] Kobayashi et al., EPSL, 2017.

Keywords: Noble gasses, kamchatka

©2021. Japan Geoscience Union. All Right Reserved.

Rare earth elements composition of carbonate concretion in the Miocene Morozaki Group, southwestern Japan

*Ryosuke Kitanaka[1], Motohiro Tsuboi[1]

1. Kwansei Gakuin University

Carbonate concretions are observed in marine sedimentary rocks from all over the world, and are generally spherical in shape. They are mainly composed of calcium carbonate, and resistant to weathering. The formation of carbonate concretions may be related to the organic matters of marine life and formed rapidly in the pores of sediments (1). It sometimes contains well-preserved ammonite or other fossils. In this study, we measured rare earth elements (REE) composition of carbonate concretions and investigate the formation processes of concretion. The studied concretion samples are approximately 1.5 m in scale and the matrix is tuffaceous fine sandstones and mudstones of the Miocene Morozaki Group (15–18 Ma), Chita Peninsula, Aichi Prefecture, Japan. REE are measured by inductively coupled plasma mass spectrometry (ICP-MS). The core, mantle and front part of concretion and, matrix sedimentary rocks were analyzed. REE concentrations were normalized by CI chondrite, deep seawater and matrix sedimentary rocks. The REE patterns normalized by CI chondrite shows negative Eu anomaly and abundant light rare earth elements (LREE) in all samples. It shows negative Ce anomaly in the matrix. REE patterns of concretion, except for core, normalized by the matrix show flat curve. At the core part, LREE show higher value, while heavy rare earth elements (HREE) show lower value in all REE patterns. This may be due to the elemental mobility process or the original organism matters.

(1) Yoshida, H., Ujihara, A., Minami, M., Asahara, Y., Katsuta, N., Yamamoto, K., Sirono, S., Maruyama, I., Nishimoto, S. and Metcalfe, R., 2015, Early post-mortem formation of car-bonate concretions around tusk-shells over week-month timescales. Scientific Reports **5**, 14123.

Keywords: carbonate concretion, rare earth elements (REE)

©2021. Japan Geoscience Union. All Right Reserved.

Investigation of Validity for Evaluation Particle numbers on Characterization of Soil Particle Morphology Using Automated Particle Image Analysis and Computed Simulations.

*Daisuke Sasakura[1]

1. Malvern Japan ,Div of Spectris Co.Ltd,.

[Introduction]

Particle morphology, such as particle size and shape aspects are well known that to give affect to various bulk characteristics on mechanics aspect of grounds. Hence, to characterize particle morphology, an Image Analysis (IA) using a manually microscopic technic is commonly used to investigate particle morphology.
However, one of the major challenges of a conventional IA is the near impossible of measuring a statistically significant number of particles. Typically, realistic particle morphology in natural field should has aspects as broadly distribution. Indeed, ISO and JIS statements suggested to measuring over than tens of thousands of particles. Furthermore, reason of importance to concern of a deviation matter is as well as supported from that typical model of particle size distribution should follow with a lognormal distribution. Recent advances in computer technology have allowed for the development of a new automated particle image analysis (APIA) approach that uses digital imaging technology. This technology is based on allowed acquisition of a calculation of binarized (2D) particle projection images on each individual particle from on over than ten thousand particles within at least few hours. Hence, these approaches are allowed for the calculation of the various morphological parameters using graphical comparison, such as various distribution graph, such as frequency curve and cumulant curve. However, even if recently progress as mentioned above, it is still only limited suggestion for enough particles to determine distribution on realistic particles which has various aspects. This study will suggest and discussion for a practical investigation of relationship of particle number and distribution on soil particle by APIA combined with using statistically modeling and simulation.

[Method]

Tohoku Keisya and Milled Silica sand were used as model samples. APIA analyses were conducted on a Morphologi G3SE as automated image analysis system (Malvern Instruments, Worcestershire, UK). Sample was subsequently dispersed with an SDU using a short duration pulse of compressed air. Measurements were collected automatically using standard operating procedures (SOPs), which clearly define the software and hardware settings used during the measurement process. The measurement sample was dispersed on a glass plate, which was used as a sample carrier to minimize environmental exposure within the enclosed sample chamber unit.
A computer simulation was carried out mainly Scilab platform with implemented own programming to calculate various numerical model, MS Excel used as supportive.

[Simulation Design]

Regarding size distributions, determined any statistical numbers from over than 10,000 particle images were calculated by distribution graph and mean analysis. It was compared that statistical specific numbers from experiment and simulated results based on lognormal random distribution due to step-upped number. Regarding shape matters were not only used as statistical number approach and also fitting approach were carried out.

©2021. Japan Geoscience Union. All Right Reserved.

Keywords: Particle Size, Particle Shape, Image Analysis

©2021. Japan Geoscience Union. All Right Reserved.

Role of fluid rock reaction for the production of FOZO isotopic composition

*Gen Shimoda[1], Tetsu Kogiso[2], Katsuhiko Suzuki[3], Akira Ishikawa[4], Norikatsu Akizawa[5]

1. Geological Survey of Japan, AIST, 2. Kyoto University, 3. Japan Agency for Marine-Earth Science and Technology, 4. Tokyo Institute of Technology, 5. University of Tokyo

It has been noted that Pb-Nd-Sr isotopic compositions of OIB converge on a small space. Definitions of the convergent space were proposed by several groups, such as the Focus Zone (FOZO; Hart et al., 1992), the Common component (C; Hanan and Graham, 1996), Prevalent Mantle (PREMA; Zindler and Hart, 1986), *etc*. The convergent space has relatively small Nd and Sr isotopic variation but relatively large Pb isotopic range, resulting in vertical trend in 3D isotopic plot with $^{143}Nd/^{144}Nd$ (x axis), $^{87}Sr/^{86}Sr$ (y axis) and $^{206}Pb/^{204}Pb$ (z axis). A recent geochemical study proposed cause of isotopic convergence, in which reaction between subducted oceanic crust and fluid released by serpentinite dehydration can produced chemical composition that is suitable for the production of FOZO isotopic compositions when the recycling age of oceanic crust was about 1.0 Ga (Shimoda & Kogiso, 2019).
In this presentation, we estimated isotopic range of recycled oceanic crusts modified by subduction process, including dehydration and fluid-rock reaction. Isotopic variation was estimated with wide variety of geochemical conditions, such as chemical variation of oceanic crust, variable degree of dehydration, fluid rock ratios, recycling ages and different subduction conditions. We calculated isotopic compositions of recycled oceanic crust about a million sets of Pb-Sd-Sr-Hf isotopic compositions. The calculated isotopic compositions distributed near FOZO and PREMA. Although the tested subduction conditions were varied widely, isotopic compositions of recycled oceanic crust show small isotopic variation, indicating that isotopic composition of FOZO simply reflect isotopic variation of subduction modified oceanic crust. It may follow that focusing isotopic distribution of OIB simply express isotopic variation of recycled oceanic crust with variable subduction conditions and recycling ages.

Keywords: FOZO, mantle, isotopic composition

©2021. Japan Geoscience Union. All Right Reserved.

[J] Poster | S (Solid Earth Sciences)：S-TT Technology & Techniques

Sat. Jun 5, 2021 5:15 PM - 6:30 PM JST | Sat. Jun 5, 2021 8:15 AM - 9:30 AM UTC | Ch.18_1

[S-TT36] Synthetic Aperture Radar and its application

convener:Yohei Kinoshita(University of Tsukuba), Takahiro Abe(Graduate School of Bioresources, Mie University), Shoko Kobayashi(Tamagawa University), Yuji Himematsu(National Research Institute for Earth Science and Disaster Resilience)

ALOS-2 and Sentinel-1, which have highly enhanced capacity compared to previous SAR satellites, were launched in 2014, and their utilization has been widely expanding as data have accumulated for approximately six years. Other long-operating SAR satellites like TerraSAR-X and Cosmo-SkyMed also contribute to expanding the SAR utilization. Now we are facing a new and abundant era of the satellite SAR, along with a worldwide trend to an open and free data policy of satellite data, under the situation of next-generation advanced and/or constellated SAR satellite plans by both public agencies (e.g. ALOS-4 and NISAR) and private sectors. In addition, SAR technologies with other platforms, such as ground-based SAR with high temporal resolution and UAV (Unmanned Aerial Vehicle) SAR with flexible operability, have also been developed and used for various targets. These facts indicate that the SAR utilization has become widespread in both basic researches (e.g., earth science) and diverse applications (e.g., disaster prevention and forest monitoring). In this session, we would like to invite various kinds of research and application results with regard to SAR, sharing our knowledge and having a discussion for the advancement of the SAR utilization.

[STT36-P01] Long-term crustal deformation of domestic volcanoes detected by InSAR time series analysis

*Kano Mikihara[1], Takaaki Inukai[1], Nobuhiro Ishikura[1], Kumi Shimazaki[1], Masayoshi Ishimoto[1], Tomokazu Kobayashi[1] (1.GSI of Japan)

[STT36-P02] Surface displacement in Hachijojima Island since 2014 by InSAR analysis and GNSS

*yusei Hamamura[1], HIROYUKI AZUMA[1], Yoshiya Oda[1] (1.Tokyo Metropolitan University)

[STT36-P03] Observing Crustal Deformation Using Interferometric Synthesis Aperture Rader and Estimating Magma Chamber Associating with the 2018 Eruption of Shinmoedake of Kirishima Volcanoes, Japan.

*Takahisa Tashiro[1], Koichi Suzuki[2] (1.Cooperative Program for Resources Engineering, Graduate School of Engineering, Hokkaido University, 2.Research Group of Geoenvironmental Engineering, Division of Sustainable Resource Engineering, Faculty of Engineering, Hokkaido University)

[STT36-P04] Using InSAR for evaluating the accuracy of earthquake location determination, Comparison of Iranian and Japanese cases

*Nematollah Ghayournajarkar[1], Yo Fukushima[2] (1.Graduate School of Science, Tohoku University, 2.International Research Institute of Disaster Science, Tohuku University)

[STT36-P05] Progress on developing a GNSS-based InSAR atmospheric delay correction model

*Yohei Kinoshita[1] (1.University of Tsukuba)

[STT36-P06] Ship Detection Using Synthetic Aperture Radar

*Kengo Iwata[1], Masanobu Shimada[1] (1.Tokyo Denki University)

Long-term crustal deformation of domestic volcanoes detected by InSAR time series analysis

*Kano Mikihara[1], Takaaki Inukai[1], Nobuhiro Ishikura[1], Kumi Shimazaki[1], Masayoshi Ishimoto[1], Tomokazu Kobayashi[1]

1. GSI of Japan

GSI (Geospatial Information Authority of Japan) has been monitoring crustal and ground deformation all over Japan with ALOS-2 data by applying two-pass synthetic aperture radar Interferometry (InSAR) method. But, it is difficult to detect small deformations, because InSAR results often have errors due to tropospheric disturbances and ionospheric disturbances.
To overcome the flaw, in recent years, InSAR time series analysis that is statistically processing a number of images has been conducted. This is because InSAR time series analysis can effectively reduce errors contained in image and resultantly improves the measurement accuracy. Persistent Scatter Interferometry method (PSI method) and Small Baseline Subset algorithm method (SBAS method) are typical examples of InSAR time series analysis. GSI has developed the InSAR time series analysis system (GSITSA) which includes both PSI method and SBAS method (Kobayashi et al., 2018). Hayashi et al., (2019) conducted InSAR time series analysis using GSITSA for domestic volcanic areas and land subsidence areas. They confirmed that the SBAS method using ALOS-2 data is an effective analysis method for crustal deformation monitoring even in mountainous areas, in which they demonstrated that it could detect temporal changes on small ground deformations. In addition, with Advanced Land Observing Satellite-4 (ALOS-4), which is scheduled to be launched in 2022, the observation frequency will be increased five times more than ALOS-2. ALOS-4 is expected to enable more accurate measurement of deformations by applying InSAR time series analysis.
With the background, for the effective utilization of ALOS-4 data, we conducted InSAR time series analysis for the domestic volcanic area using ALOS-2 data accumulated since 2014. In this presentation, we will show the results of InSAR time series analysis of Mt. Kusatsushirane, Mt. Yakedake and Kuchino-Erabujima Is.. As a result of the analysis, we detected ground displacement away from the satellite in and around Kagamiike. We found that the deformation occurred slowly before an eruption that occurred in January 2018, and that the deformation speed changed after the eruption and continued to deform until around the summer of 2019. Around the summit of Mt. Shindake on Kuchino-Eerabujima Is., deformations away from the satellite were detected during the two periods from the eruption in May 2015 to around January 2018 and from the eruption in January 2019 to around August 2019. In addition, we found that near the summit of Mt. Yakedake, there was a deformation approaching the satellite at a speed of about 2 cm per year from 2016 to 2020. By applying InSAR time series analysis, we were able to significantly detect the temporal changes in small crustal deformations that have not been detected with sufficient accuracy by the conventional InSAR method.

Acknowledgments
ALOS-2 data were provided based on the joint research agreement with JAXA (Japan Aerospace Exploration Agency). The ownership of ALOS-2 data belongs to JAXA.

Keywords: “DAICHI-2” (ALOS-2), SAR, Volcanic activity, Crustal deformation

©2021. Japan Geoscience Union. All Right Reserved.

Surface displacement in Hachijojima Island since 2014 by InSAR analysis and GNSS

*yusei Hamamura[1], HIROYUKI AZUMA[1], Yoshiya Oda[1]

1. Tokyo Metropolitan University

In this study, as a volcanic disaster prevention study, the surface displacement of Hachijojima Island, a volcanic island belonging to Tokyo Metropolitan, has been estimated by InSAR time series analysis, ALOS-2 PALSAR-2 data observed during the period from August 2014 to August 2020 are used for InSAR analysis. In this study, we employed SBAS(Small Baseline Subset) method, which in one of the methods for InSAR time series analysis. 83 pairs for Descending, and 26 pairs for Ascending are used for SBAS analysis. In addition, we analyzed GNSS data observed at JMA “South mountainside of Nishiyama” station to verify the results.
The results of InSAR analysis, it is not possible to confirm significant displacement above noise level. In addition, it was not possible to find the long-term sueface displacement trend.
The results obtained by InSAR time series analysis are described. On Hachijojima Island, no regions with surface displacement of 4 cm or more was observed in 6 years. But it was confirmed that analysis results of both Descending and Ascending showed uplifting surface displacement in the flat area between Nishiyama and Higashiyama and near the summit of Nishiyama. Specifically, a displacement of about 4 cm was confirmed on the flat land, and a displacement of about 2 cm was confirmed near the summit of Nishiyama. Those area correspond to the area of the lavas of the Senjojiki stage and Okoshigahana Scoria fall.

©2021. Japan Geoscience Union. All Right Reserved.

Observing Crustal Deformation Using Interferometric Synthesis Aperture Rader and Estimating Magma Chamber Associating with the 2018 Eruption of Shinmoedake of Kirishima Volcanoes, Japan.

*Takahisa Tashiro[1], Koichi Suzuki[2]

1. Cooperative Program for Resources Engineering, Graduate School of Engineering, Hokkaido University, 2. Research Group of Geoenvironmental Engineering, Division of Sustainable Resource Engineering, Faculty of Engineering, Hokkaido University

Shinmoedake of Kirishima Volcanoes in Southern Kyushu, Japan is reported to be eruptive around March 2018. We investigated crustal deformations before (17th Oct. 2017 –8th Feb. 2018), while (8th Feb. 2018 –8th Mar. 2018) and after (8th Mar. 2018 –7th Feb. 2019) of this eruption using Interferometric Synthetic Aperture Rader (InSAR). We also applied a spherical source deposited in a half-space model, called Mogi Model (Mogi, 1958), to presume the pressure source that caused eruptions as well as its latitude, longitude, depth and volume changes. To obtain fitting parameters, we considered Pearson's X^2 test and assumed the smallest magnitude would be valid. We used grid searching as hyperparameter optimisation when finding them.

The InSAR observations revealed that LOS were 2.41 [cm] in pre-eruptive, -3.75 [cm] in syn-eruptive and 3.93 [cm] in post-eruptive periods. These results were harmonic to baseline estimations of GNSS performed by JMA (2019) and GSI (2019).

Estimated volume changes were 0.37 [m^3] in charging, -0.69 [m^3] in discharging and 0.79 [m^3] in re-charging process. We assumed the magma chamber that caused crustal deformations was located at the depth of 7.5 km at approximately 6 km away from the summit of Shinmoedake. These values are equivalent to JMA (2019), who obtained -0.66×10^7 [m^3] (1st Mar. –10th Mar. 2018), which applied Mogi Model to GNSS dataset. Since Shinmoedake is characteristic of its relatively spacious crater, NIED (2018) carried out SAR observations from 6th Mar. to 9th Mar. 2018 and determined the volume of accumulated ejecta was 1.32×10^7 [m^3]. All the values were on the same order (10^7 [m^3]).

Based on our analysis, we conclude that the 2011 events' magma chamber (*e.g.* Kobayashi *et al.*, 2011; Miyagi, Ozawa, and Kohno, 2013) could be attributed to 2018 events.

Acknowledgement

PALSAR level 1.0 data are shared amongst PIXEL and provided by JAXA under a cooperative research contract with ERI, Univ. of Tokyo. The ownership of PALSAR belongs to METI and JAXA.

References

GSI, *Rep. Coordinating Comm. Prediction Volcan. Erupt.*, **132**, 338-351, 2019. (in Japanese)
JMA, *Doc. Coordinating Comm. Prediction Volcan. Erupt.*, **144**, 89-101, 2019. (in Japanese)
Kobayashi, T. *et al.*, *Bull. GSI*, **121**, 195-201, 2011. (in Japanese)
Miyagi, Y., Ozawa, T. and Kohno, Y., *Kazan* (*Bull. Volcanol. Soc. Japan*), **58**(2),341-351, 2013. (in Japanese)
Mogi, K., *Bull. Earthq. Res. Inst. Univ. Tokyo*, **36**, 99-134, 1958.

©2021. Japan Geoscience Union. All Right Reserved.

NIED, https://www.bosai.go.jp/info/saigai/2017/pdf/20180309_01.pdf, 2018. (in Japanese)

Keywords: Shinmoedake of Kirishima Volcanoes, InSAR, Mogi Model

©2021. Japan Geoscience Union. All Right Reserved.

Using InSAR for evaluating the accuracy of earthquake location determination, Comparison of Iranian and Japanese cases

*Nematollah Ghayournajarkar[1], Yo Fukushima[2]

1. Graduate School of Science, Tohoku University, 2. International Research Institute of Disaster Science, Tohuku University

Accurate location and extent of the earthquake rupture provide fundamental information for seismic hazard evaluation. Interferometric Synthetic Aperture Radar (InSAR) is a promising technique to constrain fault parameters because it has high spatial resolution in the epicentral area for shallow earthquakes, and the fault model derived from InSAR can be taken as the ground truth. In this study, we compared the fault location derived from InSAR to the epicenters determined by local and global seismic networks. We focused on shallow earthquakes that occurred in Iran and Japan, where the station density of the local seismic networks differs significantly, in order to evaluate how the station density and azimuthal coverage influence the accuracy of the earthquake location determination. On each of the five Iranian and five Japanese earthquakes, we obtained the coseismic interferograms, applied a Particle Swarm Optimization (PSO) method assuming a rectangular finite fault with uniform slip to obtain the optimal rupture location, and then calculated the distance between seismic-derived epicenters and InSAR-derived surface-projected fault plane for each earthquake. The results for the Iranian earthquakes showed that the distance between IRSC (Iranian Seismological Center)-derived epicenter and the fault plane was larger than that between the USGS-derived epicenter and the fault plane. Since the spatial density of the IRSC network is better than the USGS network, we can attribute the higher accuracy of the USGS epicenters to the better azimuthal coverage of the USGS network. For the case of the Japanese earthquakes, the epicenter determined by JMA (Japan Meteorological Agency), which has good azimuthal coverage and much denser spatial coverage than the USGS network, was closer to the InSAR-derived fault plane compared to the USGS epicenter. These results indicate that 1) good azimuthal coverage of the seismic network is fundamentally important in obtaining accurate epicenters, and 2) the dense station coverage leads to improving the accuracy.

Keywords: InSAR, Finite rectangular fault, Earthquake location accuracy

©2021. Japan Geoscience Union. All Right Reserved.

Using InSAR for evaluating the accuracy of earthquake location determination, Comparison of Iranian and Japanese cases

Nematollah Ghayournajarkar[1], Yo Fukushima[2]

1: Department of Geophysics, Graduate School of Science, Tohoku University;

2: International Research Institute of Disaster Science, Tohoku University

Accurate location and extent of the earthquake rupture provide fundamental information for seismic hazard evaluation. Interferometric Synthetic Aperture Radar (InSAR) is a promising technique to constrain fault parameters because it has high spatial resolution in the epicentral area for shallow earthquakes, and the fault model derived from InSAR can be taken as the ground truth. In this study, we compared the fault location derived from InSAR to the epicenters determined by local and global seismic networks. We focused on shallow earthquakes that occurred in Iran and Japan, where the station density of the local seismic networks differs significantly, in order to evaluate how the station density and azimuthal coverage influence the accuracy of the earthquake location determination. On each of the five Iranian and five Japanese earthquakes, we obtained the coseismic interferograms, applied a Particle Swarm Optimization (PSO) method assuming a rectangular finite fault with uniform slip to obtain the optimal rupture location, and then calculated the distance between seismic-derived epicenters and InSAR-derived surface-projected fault plane for each earthquake. The results for the Iranian earthquakes showed that the distance between IRSC (Iranian Seismological Center)-derived epicenter and the fault plane was larger than that between the USGS-derived epicenter and the fault plane. Since the spatial density of the IRSC network is better than the USGS network, we can attribute the higher accuracy of the USGS epicenters to the better azimuthal coverage of the USGS network. For the case of the Japanese earthquakes, the epicenter determined by JMA (Japan Meteorological Agency), which has good azimuthal coverage and much denser spatial coverage than the USGS network, was closer to the InSAR-derived fault plane compared to the USGS epicenter. These results indicate that 1) good azimuthal coverage of the seismic network is fundamentally important in obtaining accurate epicenters, and 2) the dense station coverage leads to improving the accuracy.

©2021. Japan Geoscience Union. All Right Reserved.

Progress on developing a GNSS-based InSAR atmospheric delay correction model

*Yohei Kinoshita[1]

1. University of Tsukuba

Correcting the InSAR atmospheric delay noise is one of the problem for InSAR researches. In teh last year, Kinoshita (2020, GSJ) proposed a new InSAR atmospheric delay model by use of the GNSS zenith total delay (ZTD) and its horizontal gradient data, in which we referred the method proposed by Arief and Heki (2020). The preliminary result of our proposed model showed a better performance compared with a traditional correction approaches such as the GACOS global mode and the JMA's MSM based model. Here we investigated parameter sensitivities of our model in terms of the grid spacing and the use of the delay gradient.

We at first investigated the model sensitivity in the grid spacing. As a default, we have set it to 5 km spacing, although this setting may not be the best value. In this experiment, we changed the grid spacing ranging from 2 km to 30km while other parameters were fixed. The result showed that the InSAR phase reduction was most significant with the 4 km grid spacing. Even if the grid spacing were set to be finer such as 2 km and 3 km, the delay correction effectiveness slightly worsened. This would indicate the limitation of the resolvable ability of using the GNSS ZTD and gradient.

We next investigated the sensitivity to the GNSS station density. In this experiment, we performed model simulations under conditions that reduced the number of GNSS stations. Other parameters were fixed as a default and the grid spacing was set to 5 km as being the same as the original model run. The result showed the monotonical decrease of the phase reduction ability with decreasing the number of GNSS stations as expected. An interesting feature was that the decreasing ratio of the model correction ability done not worsened significantly until the GNSS station density was reduced to 20 % of the original number (average distance between stations was aproximately 50km). This result indicated that our proposed model would have an applicability for regions where only small numbers of GNSS stations are installed like south-eastern Asia and Africa.

In addition, we compared the model's correction ability with that of the model without using delay gradients. Contrary to our expectation, the InSAR phase reduction was slightly better in the model without using gradients (corrected phase standard deviation was 25.62 mm) than the model with using gradients (25.75 mm). This difference may be not significant statistically, but the cause of this may be 1) an overfitting to the observed gradients for the small scale (an order of kilometers) in the inversion, 2) an inadequacy of the smoothing hyper-parameter value that was set manually, or 3) inappropriate value of the scale height that we used the scale height value of 2.5 km which is for atmospheric water vapor.

In the presentation, we will discuss our model characteristics shown above.

Keywords: InSAR, delay correction, GNSS

©2021. Japan Geoscience Union. All Right Reserved.

Ship Detection Using Synthetic Aperture Radar

*Kengo Iwata[1], Masanobu Shimada[1]

1. Tokyo Denki University

Synthetic aperture radar image includes waves, internal waves, vessel detection, and tides. With regard to the ship detection, the synthetic aperture radar PALSAR-2 mounted on ALOS-2 and AIS (Automatic Identification System), which transmits and receives identification codes, ship names, positions, speeds, etc., will cooperate. Surveillance is being conducted to identify suspicious vessels.

In last year's study, we measured the average ($\sigma^0_{Avg.}$) of the backscatter coefficient (σ_0) in a small area and determined the area with a coefficient above a threshold (σ_{th}) as a vessel. As a result, the threshold of the directional scattering coefficient was set to -8.0 dB, and the number of detected vessels with AIS (Automatic Identification System) location information was 27/29 (95%) and 25/25 (100%), and many other points that were considered to be vessels were detected. In addition, we found problems related to the determination of the threshold value and the appearance of false detection points mainly in coastal areas. In this study, we compared the two methods in order to improve the detection accuracy.

The first is the fixed threshold method. We improved the threshold calculation method compared to the algorithm used in last year's study. We cut out a 500 x 500 pixel area (1) that shows one large ship and a 1000 x 1000 pixel area (2) that shows five small ships as samples from the image, and determined the threshold value based on the histograms of the sea surface and ships in areas (1) and (2). We applied this threshold to the entire image and detected pixels with a value greater than the threshold, which we considered to be ships.

The second method is the adaptive threshold method (ATM). In this method, a small region is set in the image and the threshold is calculated within this region. By scanning the entire image with this small region: the moving window, a threshold value is calculated for each region and the vessel is detected. In this study, we created an algorithm by referring to the formula for deriving the moving window and threshold used in the study by Mizukoshi, Ouchi, and Watanabe (2019).

We used one scene of November 18, 2019 in the waters from the Pacific Ocean in Wakayama Prefecture to the Kii Suido and Osaka Bay, taking into account the number of vessels traveling and the expected speed of navigation. At the same time, AIS information of the same area was used to compare ship detection .

We determined the threshold for the fixed threshold method to be DN=5000 based on the histograms of regions (1) and (2).The results of AIS and visual detection of the vessels were 33/33 (100%). The processing time of the algorithm was about 2 seconds.We set the ATM moving window as background window 81×81 and buffer window 41×41. The detection result was 33/33 ships (100%). The processing time of the algorithm was about 3 hours. The advantages of the fixed threshold method were the small number of false positives on the sea surface and the short processing time. In contrast, the advantages of ATM were clearer detection of small vessels and fewer false positives in coastal areas.

Keywords: Synthetic aperture radar, Ship Detection, Adaptive threshold method

©2021. Japan Geoscience Union. All Right Reserved.

©2021. Japan Geoscience Union. All Right Reserved.

[J] Poster | S (Solid Earth Sciences)：S-TT Technology & Techniques

Sat. Jun 5, 2021 5:15 PM - 6:30 PM JST | Sat. Jun 5, 2021 8:15 AM - 9:30 AM UTC | Ch.13_3

[S-TT38] Creating future of solid Earth science with high performance computing (HPC)

convener:Takane Hori(R&D Center for Earthquake and Tsunami, Japan Agency for Marine-Earth Science and Technology), Yuji Yagi(Graduate School of Life and Environmental Sciences, University of Tsukuba, Tsukuba), Katsuhiko Shiomi(National Research Institute for Earth Science and Disaster Resilience), Ryoichiro Agata(Japan Agency for Marine-Earth Science and Technology)

Due to the development in computer science and computational science, large-scale or many times forward simulations and/or inversion analyses have become available recently. In solid Earth science, large-scale seismic wave propagation and crustal deformation with high fidelity models based on high resolution observation data have been demonstrated; uncertainty in crustal deformation caused by material properties and structures can be investigated based on many-time calculations for different material properties and structures; fault slip inversion analyses for non-Gaussian error distribution, etc. Thus, we will invite researchers who are applying HPC technology in forward simulations and inversion analyses and discuss how to improve more the collaboration between computer & computational sciences and solid Earth science. We are welcome submission by the researchers who are interested in this scope, especially students and young researchers.

[STT38-P01] CMT catalog based on a local 3D structure model for simulations of long-period ground motions in the Kanto region, Japan

*Kazuo Yoshimoto[1], Kosuke Minamihama[1], Shunsuke Takemura[2], Katsuhiko Shiomi[3] (1.Yokohama City University, 2.Earthquake Research Institute, The University of Tokyo, 3.NIED)

[STT38-P02] Coordinate Independent Visualization Method for Stress Tensor Field by Using Principal Axis Line

*Sayako Hirobe[1], Kenji Oguni[1], Muneo Hori[1] (1.Japan Agency for Marine-Earth Science and Technology)

CMT catalog based on a local 3D structure model for simulations of long-period ground motions in the Kanto region, Japan

*Kazuo Yoshimoto[1], Kosuke Minamihama[1], Shunsuke Takemura[2], Katsuhiko Shiomi[3]

1. Yokohama City University, 2. Earthquake Research Institute, The University of Tokyo, 3. NIED

Long-period ground motions associated with shallow local and/or regional earthquakes have been observed in the Kanto region due to the excitation and amplification of the Kanto sedimentary basin structure. To improve the evaluation of the characteristics of long-period ground motions, it is necessary to have an accurate information on focal mechanisms of earthquakes. However, moment tensor inversion using a 1D velocity structure model had been commonly used to construct a focal mechanism catalog in Japan. In this study, we conducted centroid moment tensor inversion using a 3D velocity structure model (the Japan Integrated Velocity Structure Model version 1 (JIVSM) [Koketsu et al. 2012]) to estimate the focal mechanism solutions of earthquakes in and around the Kanto region more accurately. Then, we compared our focal mechanism solutions with the MT solutions of F-net.

For the 3D CMT inversion, we analyzed 82 earthquakes of magnitude 5.5 or greater occurred between January 2004 and June 2020 (Lat.: 34°N~38°N, Lon.: 138°E~142°E, Depth: 40 km or shallower). The broadband seismic waveforms recorded by F-net were used for our 3D CMT inversion, and the displacement waveforms in the period band of 25~100 seconds were used for waveform fitting. The Green's functions of the seismic motion for the 3D velocity structure model were evaluated by the reciprocal calculations via the OpenSWPC [Maeda et al., 2017]. In this calculation, source grids were uniformly distributed at a horizontal interval of 0.1° and vertical interval of 2 km from depth 6 km to 60 km. The Küpper wavelet with a duration of 1 s was employed as a source time function. The reproducibility of the observed waveforms was evaluated by the variance reduction (VRs), and the moment tensor, centroid location, and time of occurrence of the earthquake were estimated by searching for the solution with the maximum VRs. Other details are described in Takemura et al. (2021).

We compared our 3D CMT solution with the F-net MT solution, and found that the two solutions are highly consistent over the land area. The Kagan angle, which was calculated as an index value for comparison, is generally less than 30° for all earthquakes. However, the difference between the 3D CMT solution and the F-net MT solution is larger for earthquakes that occurred in the offshore region such as off the coast of Ibaraki Prefecture and near the triple junction off the Boso Peninsula. This result suggests that the use of an appropriate seismic velocity structure model is important in the estimation of focal mechanisms for offshore earthquakes, which occur in a more complex structure than the land area. Other than that, as pointed out by Takemura et al. (2021), our study confirmed that the seismic moments estimated using JIVSM are systematically slightly smaller than those estimated by using F-net 1D velocity structure model. The details of our results and ground motion simulations will be presented in the conference presentation.

Acknowledgements
We used F-net waveform data and the F-net MT catalog. The FDM simulations of seismic wave propagation were conducted using the computer system of the Earthquake and Volcano Information Center at the Earthquake Research Institute, the University of Tokyo, and Fujitsu PRIMERGY CX600M1/CX1640M1 (Oakforest-PAC) at the Information Technology Center, the University of Tokyo.

©2021. Japan Geoscience Union. All Right Reserved.

Keywords: CMT inversion, Focal mechanism solution, Kanto region, Long-period ground motion

©2021. Japan Geoscience Union. All Right Reserved.

Coordinate Independent Visualization Method for Stress Tensor Field by Using Principal Axis Line

*Sayako Hirobe[1], Kenji Oguni[1], Muneo Hori[1]

1. Japan Agency for Marine-Earth Science and Technology

The physical quantities in the physics problems are written in tensor. The scalar field written in the zeroth-order tensor and the vector field written in the first-order tensor are easily visualized and are implemented on various visualization tools.
On the other hand, in the three-dimensional space, the fields of physical quantities written in the symmetric second-order tensor (e.g., strain or stress in continuum) have the six independent components. For instance, in the conventional visualization method of the stress field, we need the set of six contour maps color-coded by the three normal stresses and the three shear stresses, or the set of the three contour maps color-coded by the three principal stresses (i.e., major, medium, and minor principal stress) and the three line segment maps showing the directions of three principal axes. Therefore, it is almost impossible to intuitively understand the whole second-order tensor field by comparing these several images.
To solve this problem, some topological-based visualization method have been proposed. In these method, a ellipsoid is defined at every point in the analysis domain. The axes of this ellipsoid are parallel to the three principal axes and the length of the axes are scaled by the absolute value of the principal value. Then, these ellipsoids or the tube obtained by connecting glyphs in the longitudinal axis direction are displayed in the analysis domain. However, these method is only effective as long as the all principal values are positive (e.g., diffusion tensor used in a tractography of MRI images). In the case of the stress or strain tensor, since the principal value becomes the negative under compression, these visualization methods cannot show the second-order tensor field correctly.
In this research, we propose the new visualization method and the algorithm to help the correct and intuitive understanding of the second-order symmetric tensor field in three-dimensional space. Here, for the sake of simplicity, we use the stress tensor for the explanation of the outline of the proposed method. In the proposed method, the visualization domain are divided into small domains arranged so as not to overlap with each other. If the constant stress tensor field is given in each small domain, the line segment tangent to the principal axis can be defined in each small domain. When this line segment passes through the boundary of the small domain, we select the line segment direction from the three principal axes direction in the next domain. Here, we select the direction so that the two line segments are connected with each other most smoothly. Then, we draw the next line segment tangent to the selected principal axis. It should be noted here that the selection of the line segment direction is not carried out to connect between the major (medium, minor) principal axes. The line segment is colored according to the principal value associated with the line segment direction. Performing the series of these drawing operations from several start points (called ‘seed’) placed in arbitrary position to three orthogonal principal axis direction, we can draw multiple lines (called ‘principal axis line’) in the visualization domain. These principal axis lines enable to show the six independent components of the second-order symmetric tensor in one figure.
According to these principal axis lines, we can understand the flow and magnitude of the second-order symmetric tensor field. Also, while the contour maps showing the components of the second-order symmetric tensor are completely changed by the rotation of the coordinate system, the principal axis lines given by the proposed method are independent from the rotation of the coordinate system.
In the conference, we will show some examples and will discuss about the application to the dynamic

©2021. Japan Geoscience Union. All Right Reserved.

wave field.

Keywords: Visualization, Tensor Field, Stress

©2021. Japan Geoscience Union. All Right Reserved.

[J] Poster | S (Solid Earth Sciences)：S-CG Complex & General

Sat. Jun 5, 2021 5:15 PM - 6:30 PM JST | Sat. Jun 5, 2021 8:15 AM - 9:30 AM UTC | Ch.19_1

[S-CG45] Ocean Floor Geoscience

convener:Kyoko Okino(Atmosphere and Ocean Research Institute, The University of Tokyo)

Most of Earth's volcanism and much of its tectonic activity occur on and beneath the s eafloor. Various phenomena on the seafloor are closely linked to plate tectonics, Earth s tructure and dynamics, and also related to Earth's environments through the hydrosphe re and atmosphere. Seafloor rocks and sediments record Earth's evolution and heat an d material fluxes on the Earth. Ocean Floor Geoscience session covers a broad range of research on seafloor such as mid-ocean ridge process, subduction dynamics, arc magm atism, hot spot and LIPs, crustal movement and structure etc. Every field of researches and every approaches are welcomed.The session aims to encourage discussion among scientists from different study fields and to integrate our understanding of ocean floor. The session is co-chaired by K. Tadokoro (Nagoya Univ.), O. Ishizuka (AIST), T. Toki (Univ . Ryukyus), and N. Takahashi (JAMSTEC).

[SCG45-P01] **Temporal variation of crustal accretion along the Vulcan Transform, the Southern Ocean: Preliminary results of KH-19-6 cruise**

*Kyoko Okino[1], Kenichiro Tani[2], Osamu Ishizuka[3], Hiroaki Koge[3], JINYU ZHOU[1] (1.Atmosphere and Ocean Research Institute, The University of Tokyo, 2.National Museum of Nature and Science, 3.National Institute of Advanced Industrial Science and Technology)

[SCG45-P02] S wave velocity structure at the Kairei Hydrothermal Vent Field near the Rodriguez Triple Junction in the Indian Ocean

*Ayato Morii[1], Toshinori Sato[1], Hiroyoshi Takata[1], Tomoaki Yamada[2], Masanao Shinohara[3] (1.Chiba Unv., 2.JMA, 3.ERI, Unv. Tokyo)

[SCG45-P03] **Deep-tow magnetics for 29–33 Myr seafloor of the Southeast Indian Ridge**

*Masakazu Fujii[1,2], Kyoko Okino[3], Chiori Tamura[3] (1.National Institute of Polar Research, 2.SOKENDAI (The Graduate University for Advanced Studies), 3.AORI, UTokyo)

[SCG45-P04] **Magnetic and gravity constraints on crustal structure of the Nosappu Fracture Zone, Northwestern Pacific**

*Mai Kintsu[1], Nobukazu Seama[1], Masakazu Fujii[2,3], Tomoko Hanyu[4] (1.Department of Planetology, Graduate School of Science, Kobe University, 2.National Institute of Polar Research, 3.SOKENDAI (The Graduate University for Advanced Studies), 4.Kobe Ocean-Bottom Exploration Center)

[SCG45-P05] Multibeam bathymetric and single-channel seismic surveys of the Mid-Slope Terrace off Sanriku in the northern Japan Trench

*Toshiya Fujiwara[1], Toshiya Kanamatsu[1], KanHsi Hsiung[1] (1.Research Institute for Marine Geodynamics, Japan Agency for Marine-Earth Science and Technology)

[SCG45-P06] Deformation of the upper plate within the Tohoku Region Pacific Coast analyzed by the top surface structure

*Hiroaki Koge[1], Ayanori Misawa[1], Toshiya Fujiwara[2], Yoshiaki Suzuki[1], Yusuke Sato[3], Ryosuke Komatsu[5], Chiori Tamura[4], Katsura Kameo[4] (1.AIST, 2.JAMSTEC, 3.Tokai Univ., 4.AORI. UTokyo, 5.MOL Marine Co., Ltd)

[SCG45-P07] Classification and estimation of petit-spot volcanos by multibeam backscatter data

*Matamura Yuki[1], Naoto Hirano[2], Masakazu Fujii[3,4] (1.Tohoku University, 2.Center for Northeast Asian Studies, Tohoku University, 3.National Institute of Polar Research, 4.SOKENDAI)

[SCG45-P08] Origin of Philippine Sea basins -Tectonic setting leading to subduction initiation of Izu-Bonin-Mariana arc-

*Osamu Ishizuka[1,2], Kenichiro Tani[3], Gen Shimoda[1], Yumiko Harigane[1], Taichi Sato[1], Rex Taylor[4], Susumu Umino[5], Tian Yu Ping[5], Izumi Sakamoto[6], Yuka Yokoyama[6], Sho Yatsuka[6], Ryota Uchiyama[6], Tomoaki Wakayama[6], Aimi Suzuki[6], Kana Narita[7], Chinatsu Ogawa[7], Yasuhiko Ohara[8,2,9], Chris Conway[1] (1.Geological Survey of Japan, AIST, 2.JAMSTEC, 3.NMNS, 4.University of Southampton, 5.Kanazawa University, 6.Tokai University, 7.Ehime University, 8.Japan Coast Guard, 9.Nagoya University)

[SCG45-P09] What happened to the seafloor around Nishinoshima volcano during deployment of OBEMs between September 2018 and December 2020?

*Noriko Tada[1], Kiyoshi Baba[2], Toshiya Fujiwara[1], Yoshihiko Tamura[1], Toshiya Kanamatsu[1], Kenta Yoshida[1], Akimichi Takagi[3], Fukashi Maeno[2] (1.Research Institute for Marine Geodynamics, Japan Agency for Marine-Earth Science and Technology, 2.Earthquake Research Institute, The University of Tokyo, 3.Japan Meteorological Agency)

[SCG45-P10] Estimation of the Active Faults from BSR-derived heat flow by Automated Velocity Analysis in the Nankai Trough, Japan

*Shuto Takenouchi[1], Kota Mukumoto[1], Takeshi Tsuji[1], Shuichi Kodaira[2], Gou Fujie[2], Yasuyuki Nakamura[2], Kazuya Shiraishi[2] (1.Kyushu-university, 2.Japan Agency for Marine-Earth Science and Technology)

[SCG45-P11] Precipitation process and early diagenesis after deposition of iron hydroxide in Nagahama Bay, Satsuma Iwo-Jima Island, Kagoshima, Japan.

*Koki Hori[1], Shoichi Kiyokawa[2], Minoru Ikehara[3] (1.Department of Earth and Planetary Sciences, Graduate School of Sciences, Kyushu University, 2.Department of Earth and Planetary Sciences Faculty of sciences, Kyuushu University, 3.Center for Advanced Marine Core Research, Kochi University)

[SCG45-P12] Geological structures in the southern part of the Okinawa Trough north off Ishigaki Island: Preliminary results of the KH-21-3 cruise

*Ayanori Misawa[1], Ryuta Arai[2], Masahiko Sato[3], Saki Ishino[1], Misaki Horiuchi[4], Keita Suzuki[4], Chiori Tamura[5], Katsura Kameo[5], Satoshi Okumura[6], Makoto Otsubo[1], KH-21-3 Shipboard Scientists (1.Geological Survey of Japan, National Institute of Advanced Industrial Science and Technology(AIST), 2.Research Institute for Marine Geodynamics, Japan Agency for Marine-Earth Science and Technology (JAMSTEC), 3.Department of Earth and Planetary Science, The University of Tokyo, 4.Nippon Marine Enterprises, Ltd., 5.Atmosphere and Ocean Research Institute, The University of Tokyo, 6.MOL Marine Co. Ltd.)

[SCG45-P13] **The link between volcanism and tectonics at back-arc rifting stage: analysis of three volcanic areas in the southern Okinawa Trough**

*JINYU ZHOU[1], Kyoko Okino[1], Masakazu Fujii[2,3] (1. Atmosphere and Ocean Research Institute, The University of Tokyo, 2.National Institute of Polar Research, 3.The Graduate University for Advanced Studies)

[SCG45-P14] Mineralogical and geochemical study of sediment cores collected from the Ieyama hydrothermal field in the Okinawa Trough

*Jun-ichiro Ishibashi[1], Takashi Miyamoto[1,3], Shuhei Totsuka[1,2], Kazuhiko Shimada[1], Toru Yamasaki[2], Ken Ikehara[2], Toshiro Nagase[4], Yutaro Takaya[5], Hideaki Machiyama[6], Koichi Iijima[6], Hirofumi Yamamoto[6], Hidenori Kumagai[6] (1.Department of Earth and Planetary Sciences, School of Science, Kyushu University, 2.National Institute of Advanced Industrial Science and Technology, 3.School of science, University of Tokyo, 4.Tohoku University Museum, 5.Waseda Research Institute for Science and Engineering, 6.Japan Agency for Marine-Earth Science and Technology)

[SCG45-P15] Geochemical and geochronological study of barite in sediment cores obtained from Higashi Izena hydrothermal field, Okinawa Trough

Yushi Itatani[1], *Jun-ichiro Ishibashi[1], Makiko Tomita[2], Shin Toyoda[2], Ryuichi Shinjo[3], Kazuno Arai[4], Taisei Fujiwara[5] (1.Department of Earth and Planetary Sciences, Graduate School of Science, Kyushu University, 2.Okayama University of Science, 3.Faculty of Science, University of Ryukyus, 4.Center for Advanced Marine Core Research, Kochi University, 5.Institute for Geology and Geochronology)

[SCG45-P16] Fin whale signals recorded by S-net

*Masashi Mochizuki[1], Takeshi Nakamura[2], Ryoichi Iwase[3], Kenji Uehira[1] (1.National Research Institute for Earth Science and Disaster Resilience, 2.Central Research Institute of Electric Power Industry, 3.Japan Agency for Marine-Earth Science and Technology)

[SCG45-P17] Effective removal of oceanic variation from ocean bottom pressure gauge data using the MSSA

*Kenta Shimizu[1], Toshinori Sato[1], Koichi Murata[1], Norihisa Usui[2], Hajime Shiobara[3], Tomoaki Yamada[4], Masanao Shinohara[3] (1.Chiba Univ., 2.MRI, 3.ERI. Univ. Tokyo, 4.JMA)

[SCG45-P18] Sampling process of seafloor sediments as a source of information on their rheology

*Nikita Dubinya[1,2], Sergey Tikhotskiy[1,2], Victor Nachev[1,3] (1.Moscow Institute of Physics and Technology, 2.Schmidt Institute of Physics of the Earth of the Russian Academy of Sciences, 3.Sadovsky Institute of Geosphere Dynamics of the Russian Academy of Sciences)

[SCG45-P19] Technical protocol for deep-sea environmental monitoring by the portable seafloor observation platform Edokko Mark 1

*Hiroyuki Yamamoto[1], Tetsuya Miwa[1], Shinsuke Kawagucci[1], Sangkyun Lee[2], Atsuo Oono[3], Kousuke Tsutsumi[3], Hideki Sugishima[3] (1.Japan Agency for Marine-Earth Science and Technology, 2.J-MARES/JGI, 3.J-MARES/idea)

Temporal variation of crustal accretion along the Vulcan Transform, the Southern Ocean: Preliminary results of KH-19-6 cruise

*Kyoko Okino[1], Kenichiro Tani[2], Osamu Ishizuka[3], Hiroaki Koge[3], JINYU ZHOU[1]

1. Atmosphere and Ocean Research Institute, The University of Tokyo, 2. National Museum of Nature and Science, 3. National Institute of Advanced Industrial Science and Technology

The Vulcan transform is a 120 km long, east-west trending strike-slip boundary between the Antarctic and Sur plates. The ridge axis offsets right-stepped, and the Sur plate moves westward at 15-16 mm/yr. relative to the Antarctic plate (MORVEL, DeMets et al., 2010). R/V Hakuho-maru KH-19-6 cruise conducted geophysical mapping along with this transform and conducted five dredge hauls along Antarctic side of transform wall from the present-day ridge axis to 120 km off-axis, that roughly corresponds 15 Ma crust assuming global plate motion model. As part of the project MOWALL (Moho Observation along transform fault WALLs), we try to investigate the temporal variation of the mid-ocean ridge process and the relationship with mantle heterogeneity by systematic rock sampling along with long oceanic transform, where the whole crustal section is exposed in chronological order. In this presentation, we present the preliminary analysis of geophysical data collected during the cruise.

The axial valley of the southern ridge segment shows an asymmetric structure. In the western part of the axial valley, ridge-parallel, inward-facing fault scarps develop to the ridge flank. In the eastern part, contrary, relatively smooth, doomed high forms the deeper part of the axial wall, and a large volcanic peak continues eastward. The doomed high is likely a detachment surface suggesting magma-starved spreading. A steep and oblique lineament develops about 20 km east of the axis. The abyssal hills are well-ordered east of 17˚W, showing typical magmatic seafloor.
The magnetic profiles along the TF were also collected, to obtain the exact history of the spreading rate. Our forward modeling (2D, assuming constant thickness magnetization layer draped the observed bathymetry) provides two possible scenarios of spreading. The preliminary result of age dating of dredged rock samples possibly supports one of these two models, assuming the change of spreading rate at 2~3 Ma. We also calculate mantle Bouguer anomaly (MBA) using newly collected multibeam bathymetry. Anomalous high positive MBA appears around the eastern axial wall, suggesting the exposure of high-density material. The variation of crustal thickness is also estimated from gravity anomalies. The result indicates that the thickness of crust shows a million-year order fluctuation, reflecting the temporal variation of melt supply at this ridge segment.

Keywords: mid-ocean ridge process, transform fault, oceanic crust

©2021. Japan Geoscience Union. All Right Reserved.

S wave velocity structure at the Kairei Hydrothermal Vent Field near the Rodriguez Triple Junction in the Indian Ocean

*Ayato Morii[1], Toshinori Sato[1], Hiroyoshi Takata[1], Tomoaki Yamada[2], Masanao Shinohara[3]

1. Chiba Unv., 2. JMA, 3. ERI, Unv. Tokyo

1. Introduction

The Kairei Hydrothermal Vent Field (KHF) is located at eastern area of the first segment of the Central Indian Ridge which is extended from the Rodriguez Triple Junction. The KHF extrudes fluid with rich H_2 content. Although the KHF itself exists above a basaltic rock massif (Hakuho Knoll), gabbro and mafic rocks such as peridotite were discovered on the seafloor around the KHF. These deep rocks may move upward, may be serpentinized by sea water, and may contribute to the high H_2 concentration of the Kairei vent fluid. To investigate seismic structure, we conducted a seismic survey with ocean bottom seismometers and an air-gun in 2013. Takata et al. (JpGU, 2015) reported the P wave velocity structure. They revealed high velocity areas with more than 6.0 km/s of the P wave velocity under 1-2 km from the seafloor at the Hakuho Knoll and the Yokoniwa Rise which is located north of the Hakuho Knoll. This result indicated uplift of deep rocks. To investigate these rock’ s properties, we determine the S wave structure using the air-gun.

2. Data acquisition and analysis methods

We conducted a seismic refraction/reflection survey from January 27 to March 19 in 2013 using S/V Yokosuka of Jamstec. In the experiment, we used 19 OBSs, an air-gun (G.I. gun) and a single channel steamer cable.

To make the S phase easer to see, we rotate the horizontal components of seismic sensors to the radial and transverse directions. We estimate horizontal direction of the sensors from trajectories of water waves. Using picking data of the S phase, we construct a 3D S wave velocity structure by the FAST program (Zelt and Barton, 1998).

3. Results

A provisional result is that the high P wave velocity areas under the Hakuho Knoll and the Yokoniwa Rise have high Vp/Vs ratio with about 2.0. This ratio is higher than those for gabbro (about 1.9) and peridotite (about 1.7). Since the Vp/Vs ratio of serpentine is about 1.8-2.2, this result may indicate serpentinization of these areas.

Acknowledgment

We thank the captain and crew of S/V Yokosuka of JAMSTEC for their support. This work was supported by Grant-in-Aid for Scientific Research on Innovative Areas of the Ministry of Education, Culture, Sports, Science and Technology (Grant Number 20109002, TAIGA project).

©2021. Japan Geoscience Union. All Right Reserved.

Keywords: S wave velocity structure, Vp/Vs ratio, Kairei hydrothermal vent field, serpentinization

©2021. Japan Geoscience Union. All Right Reserved.

Deep-tow magnetics for 29–33 Myr seafloor of the Southeast Indian Ridge

*Masakazu Fujii[1,2], Kyoko Okino[3], Chiori Tamura[3]

1. National Institute of Polar Research, 2. SOKENDAI (The Graduate University for Advanced Studies), 3. AORI, UTokyo

Knowledge of the Earth's magnetic field intensity variations provides an essential constraint on the age benchmark and geodynamo model. A record of absolute palaeointensity has been compiled from archaeomagnetic and volcanic materials, and long-term relative palaeointensity has been obtained from sedimentary sequences. Although geomagnetic intensity signal recorded as the oceanic crust's thermoremanence should provide a higher-time-resolution record of crustal accretion at mid-ocean ridges (e.g., Gee et al., 2000), available data is essentially limited due to observation difficulty. Here, we present new observation data of near-seafloor magnetic anomalies of 29–33 Myr seafloor at the Southeast Indian Ridge.

We conducted a deep-tow operation during the R/V Hakuho-maru cruise of KH-20-1 (Cape Town to Fremantle, January –February 2020). Underway geophysical data (e.g., multibeam bathymetry and total magnetic field) of the target area has been obtained during the KH-07-4 and KH-16-1 cruises. The deep-sea total magnetic fields were measured using the deep-tow cesium magnetometer developed by the Atmosphere and Ocean Research Institute, The University of Tokyo. The towed proton magnetometer data was simultaneously observed at the sea-surface. The deep-tow sensor was kept 30 m away from the mainframe using the electric cable. The stainless mainframe consists of the magnetometer body, a pressure sensor, a motion sensor, and a transponder for acoustic positioning. The mainframe is 100 m away from the 600kg-weight tied to the ship No.1 wire. Another transponder was also set to the ship No.1 wire 20 m above the weight. The data of total magnetic field, depth, and attitude are merged and recorded at 2Hz. This observation covers the signal from the northern off-axis area of the Southeast Indian Ridge on 13–14 February. The sensor reached ~4,500m deep. The total length of obtained data at >3,000m deep is up to 40 miles.

Obtained near-seafloor magnetic anomalies ranges 60,700 to 62,300 nT. This variation is three times larger than the total intensity variation observed at sea-surface. Long-wavelength signatures are well correlated with each other. Comparing with geomagnetic polarity chrons (Gee and Kent, 2015), previously obtained surface data (Quesnel et al., 2009), and globally picked isochrons (Seton et al., 2014), we individually picked magnetic isochrons of C11n12n, C11r, C12n, and C12r from obtained near-seafloor magnetic anomalies. The corresponding age is 29.401 to 33.058 Myr. Several tiny wiggles with an amplitude of up to 300 nT are remarkably observed in C12r. This result is generally consistent with summarized cryptochrons (Cande and Kent, 1992; Cande and Kent, 1995). A few tiny wiggles with an amplitude of up to 200 nT were also observed in C12n, which have never been reported. We consider that this result can be a new finding of short-term fluctuations in the geomagnetic field, but careful examination considering crustal processes is needed. In this presentation, we aim to discuss these observed tiny wiggles' origin by comparing our results with sea-surface anomaly data of faster spreading seafloor segments (western slopes of the East Pacific Rise 22–33°S and Pacific Antarctic Ridge 33–40°S). Besides, Oligocene sediment record from IODP Sites U1331, U1332, and U1333 (140°W Pacific equatorial high-productivity zone; Yamazaki et al., 2013; Yamamoto et al., 2013), and DSDP Site 522 (Walvis Ridge, South Atlantic Ocean; Hartl et al., 1993; Tauxe and Hartl, 1997) are utilized to discuss palaeointensity variation. We will also compare our results with 30Myr lava flow data from the Lima Limo

©2021. Japan Geoscience Union. All Right Reserved.

section of the Ethiopian trap (Ahn et al., 2021; Yoshimura et al., 2020).

Keywords: Near-seafloor magnetic anomaly, C11n12n, C11r, C12n, & C12r, Southeast Indian Ridge

©2021. Japan Geoscience Union. All Right Reserved.

Magnetic and gravity constraints on crustal structure of the Nosappu Fracture Zone, Northwestern Pacific

*Mai Kintsu[1], Nobukazu Seama[1], Masakazu Fujii[2,3], Tomoko Hanyu[4]

1. Department of Planetology, Graduate School of Science, Kobe University, 2. National Institute of Polar Research, 3. SOKENDAI (The Graduate University for Advanced Studies), 4. Kobe Ocean-Bottom Exploration Center

The structure and lithology of fracture zones (FZ) are essential for understanding long-term tectonic evolution of the seafloor as well as Earth water and material cycles. Widely obtained marine geophysical dataset such as magnetic anomalies can provide strong constraint on crustal structures, in which several historical information such as magnetic field variations, crustal accretion processes, and temporal change of lithology should be reserved. Here,we present analyses of magnetic dataset obtained along and across the Nosappu Fracture Zone (NFZ). The NFZ is located on the old Pacific lithosphere just before subducting into the Kuril trench. It extends over 1000 km NNE-SSW direction from around 33˚N,154˚E; the Shatsky Rise, to around 42˚ N,148˚E; the Kuril Trench. The horizontal distance of offset is about 350 km based on the magnetic isochron M5r, which is 6 Myr or more converted to age (Nakanishi, 1993). The purpose of this study is to understand the geophysical properties of the magnetic, as well as gravity and topography, in the NFZ for providing constraints on the crustal structure.

Multibeam bathymetry, total and vector magnetic fields, and gravity data were acquired along and across the NFZ during two research cruises; the KR06-03 with R/V Kairei and YK14-09 with R/V Yokosuka. The magnetic anomaly was calculated by subtracting the International Geomagnetic Reference Field (IGRF12; e.g., Thébault et al., 2015) from each magnetic field data point. The amplitude of the magnetic anomaly ranged from -500 to +600 nT for the east side of the NFZ, and from -200 to +400 nT for the west side. The clear magnetic stripes appeared in the magnetic anomaly map and were divided into the east and west sequences, which corresponds to each formation age of the crust in contact with the NFZ. The crustal magnetization structure was estimated from the calculated magnetic anomaly based on the well-established inversion methods (e.g., Macdonald et al., 1980; Parker & Huestis, 1974). The inversion calculation was carried out with a focus on the area where dense data were obtained, assuming a 1.0 km thick magnetized source layer without vertical variation of magnetization. No annihilator was added. For estimating paleo-latitude when the oceanic crust was formed, we examined various magnetization directions to determine the optimal one by comparing them with the results of the topography and gravity analysis. To determine the FZ area semi-objectively, slope angle was calculated from the multibeam bathymetric data using the Generic Mapping Tools (GMT; Wessel & Smith, 1991). Slope azimuth was also calculated to detect the strike of abyssal hills using GMT. We determined the east and west boundaries of the FZ area between normal oceanic crust by using the maximum value of the slope angle. The strike of abyssal hills around the NFZ was also detected by using the results of slope azimuth. In addition, mantle bouguer anomaly (MBA) was calculated from the satellite-derived free-air gravity anomaly (Sandwell et al., 2014) by subtracting the predicted gravity for the gridded multibeam bathymetry data and a constant thickness crust using the method of Parker (1973).

The low intensity of the crustal magnetization was observed along the FZ area. Two magnetic boundaries parallel to the NFZ were identified by the vector magnetic anomaly and the crustal magnetization. Assuming the magnetization inclination was -30˚, the magnetic boundaries almost coincided with the east and west boundaries of the FZ area based on the bathymetric results. The region where low MBA value appeared also corresponded to the FZ area. Inside the FZ area, several local areas with high

©2021. Japan Geoscience Union. All Right Reserved.

magnetization intensity were observed at the areas with local low value of the MBA. In this presentation, we aim to discuss geophysical insights to the formation background of crustal structure at regional scales.

Keywords: fracture zone, magnetic anomaly, marine geophysics

©2021. Japan Geoscience Union. All Right Reserved.

Multibeam bathymetric and single-channel seismic surveys of the Mid-Slope Terrace off Sanriku in the northern Japan Trench

*Toshiya Fujiwara[1], Toshiya Kanamatsu[1], KanHsi Hsiung[1]

1. Research Institute for Marine Geodynamics, Japan Agency for Marine-Earth Science and Technology

We conducted JAMSTEC R/V Kaimei KM19-03 cruise in 2019. During the research cruise, we carried out mulibeam bathymetry and single-channel seismic reflection surveys in the Mid-Slope Terrace (MST) off Sanriku in the northern Japan Trench (39-40˚N).

The Mid-Slope Terrace (MST) is a flat to gentle slope with an average slope angle of about 0-2˚. The MST is situated at a depth of 4000-6000 m and is a slope break between the steep upper and the lower trench landward slopes. The MST has the regional variation in the depth and width of the terrace from south to north along the trench. It may reflect regional differences in the dynamics of the upper plate in the subduction zone exerting on the landward slope, or differences in the stage of the tectonic evolution. Our study area is located at a depth of 4600-4800 m and has one of the largest east-west (trench to landward) widths of the MST, about 20 km, and is a region where the MST is well developed.

The Kaimei bathymetric data were obtained using a KM122 multibeam echo sounder. And also, cross-track bathymetric data were collected using a KM122 echo sounder by the German R/V Sonne SO251A cruise and using a SeaBeam 3012 echo sounder by the JAMSTEC R/V Mirai MR16-09 Leg 4 cruise, respectively. These bathymetric data have higher resolution compared with previous data, because the data were measured using recent echo sounders. Therefore, the complex topography of co-existing slope failures, steep scarps, minor ridges, and small sedimentary basins covering the MST (e.g., Sasaki, 2003) were mapped more clearly.

The slope failures suggest erosion and landslides, the steep scarps suggest faulting, the minor ridges suggest uplift, and the small sedimentary basins suggest subsidence. The single-channel reflection record shows that the thickness of sediment basin is about 75 m even in the thickest deposits. Considering the sedimentation rate of about 36-109 cm/kyr estimated from sediment cores obtained by piston coring in the sedimentary sub-basin in the study area, the sedimentary sub-basin on the MST has been formed within about 70-200 ka. The sedimentary layers located on the western and landward sides of the MST are inclined toward the landward in the lower part of the layer, suggesting that the western side of the MST has been tilted toward the landward while subsiding.

In this paper, we will describe features and relations of the seafloor and the sub-surface structures, and discuss the tectonic evolution of the upper plate in the Japan Trench.

We thank the officers and crew of R/V Kaimei for outstanding professionalism and dedication that made the cruise successful. We are indebted to marine technicians from Nippon Marine Enterprises, M. Takaesu, Y. Ohwatari, H. Iwamaru, and M. Morioka for their invaluable help to acquire data at sea.

Figure: Bathymetry of the Mid-Slope Terrace off Sanriku in the northern Japan Trench. Contour interval is 50 m.

©2021. Japan Geoscience Union. All Right Reserved.

Keywords: Japan Trench, Mid-Slope Terrace, Multibeam Bathymetric Survey, Single-Channel Seismic Reflection Survey

©2021. Japan Geoscience Union. All Right Reserved.

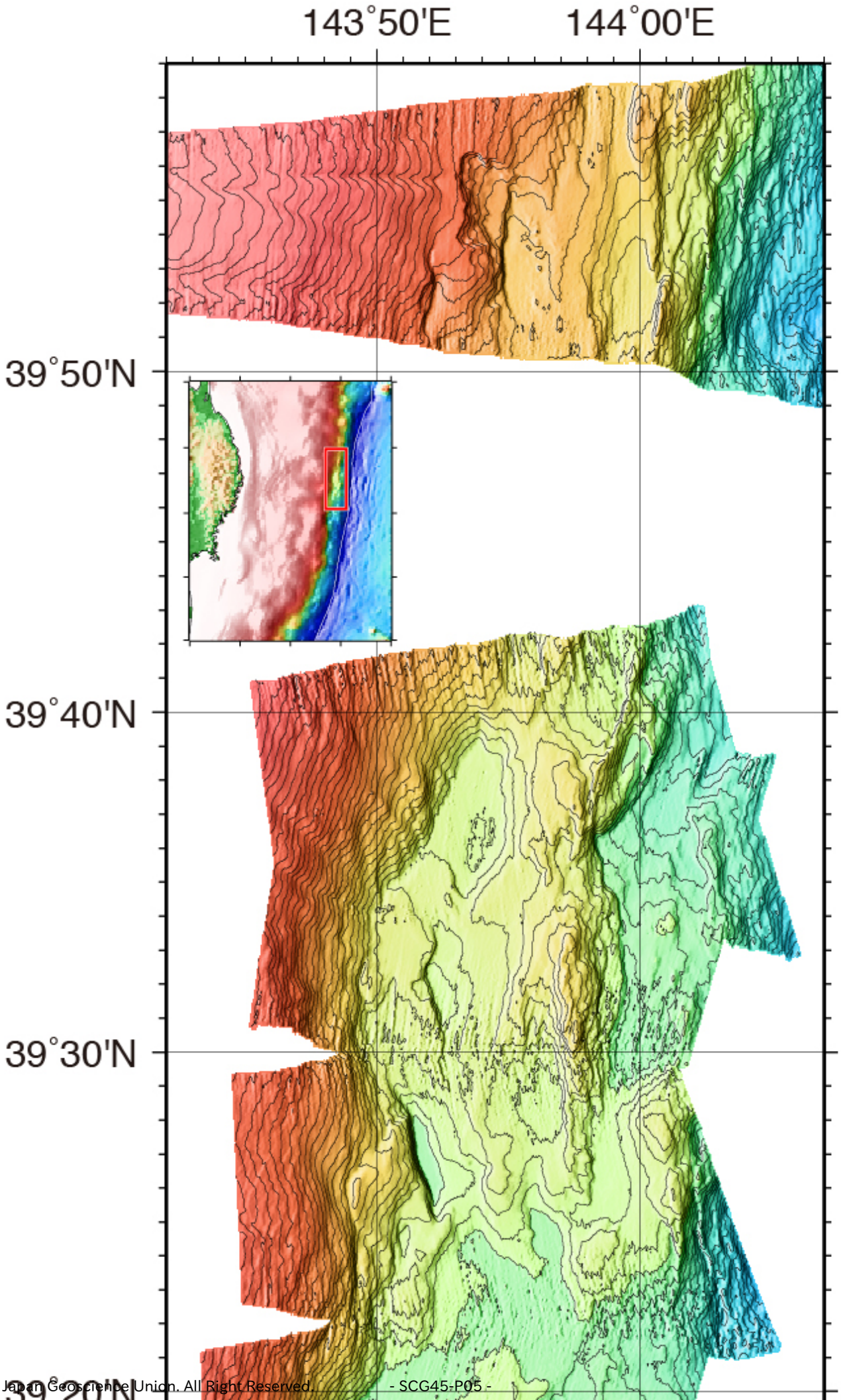

©2021. Japan Geoscience Union. All Right Reserved.

©2021. Japan Geoscience Union. All Right Reserved.

Deformation of the upper plate within the Tohoku Region Pacific Coast analyzed by the top surface structure

*Hiroaki Koge[1], Ayanori Misawa[1], Toshiya Fujiwara[2], Yoshiaki Suzuki[1], Yusuke Sato[3], Ryosuke Komatsu[5], Chiori Tamura[4], Katsura Kameo[4]

1. AIST, 2. JAMSTEC, 3. Tokai Univ., 4. AORI. UTokyo, 5. MOL Marine Co., Ltd

Large earthquakes and tsunamis have repeatedly occurred along the Japan Trench. In the 2011 Tohoku-Oki earthquake (Mw 9.0), the fault rupture extended to the shallow portion of the Japan Trench. These large slips on shallow decollement resulted in the huge tsunami that devastated much of the east coast of Japan. Therefore, it is key to understand the deformation of forearc for disaster prevention. Geodetic observations have provided insights into the deformation in the landward plate after the 2011earthquake. However, there are few kinds of research that throughout the direct observation of bathymetry or the shallow structure below the seafloor. Therefore, to discuss the following two purposes, we have conducted the shipboard geophysical observation in the KH-20-10 cruise; a multi-narrow beam echo sounder (MBES); proton precession magnetometer (PPM), shipboard three-component magnetometers (STCM), shipboard gravimeter, and sub-bottom profiler (SBP). 1)Subsidence in the forearc slope from the surface structure of the hollow-shaped sedimentary basin. To consider the development of normal faults on the sedimentary basin, we obtained the SBP cross-sections in sedimentary basins scattered in the forearc slope. 2) Revisit postseismic deformation in the forearc slope, The survey lines obtained from the seafloor topography cross-section of Fujiwara et al. (2011) were re-obtained in this cruise. We compare the three seafloor topography data before the 2011 earthquake, immediately after the 2011 earthquake, and approximately 10 years after the earthquake, and examine the presence or absence of postseismic deformation.
We were able to carry out all the planned observations on the KH-20-10 voyage, because of the good conditions of the sea and the equipment. In this presentation, we will introduce the preliminary results while the KH-20-10 voyage. In particular, our presentation will focus on the results related to the topic 2).

Keywords: japan trench, subduction zone, sub-bottom profiler, bahtymetry

©2021. Japan Geoscience Union. All Right Reserved.

Classification and estimation of petit-spot volcanos by multibeam backscatter data

*Matamura Yuki[1], Naoto Hirano[2], Masakazu Fujii[3,4]

1. Tohoku University, 2. Center for Northeast Asian Studies, Tohoku University, 3. National Institute of Polar Research, 4. SOKENDAI

Petit-spots are small monogenetic volcano generated on the outer rise system prior to subduction of oceanic plate. It shows several important features of the Earth (e.g. the composition of asthenosphere: Hirano et al., 2006). Although the geochemical composition of petit-spot basalts recently provides new insights both into lithospheric and asthenospheric mantle prior to subduction (e.g. Yamamoto et al., 2014; Machida et al., 2015; Pilet et al., 2016), the surface structure of volcanic distributions and lava-flowing patterns are not enough discussed in their tectonic regime. For example, the detail distribution of petit-spot volcano generally follows the tectonic lines of surface environment. Petit-spot volcanic province after the subduction plausibly controls the occurrence of interplate earthquake, contrasting the pelagic sediment of the surface of subducting plate. However, we have found only a few locations of petit-spot volcanic field. Previously, the acoustic backscatter images have been macroscopically checked to discover a petit-spot on the KR04-08 cruise in 2004 (Hirano et al., 2006). In this research, we aim to establish a method to find new petit-spots by acoustic measurement data and to classify petit-spots by topographic features such as their distributions and lava-flowing patterns.

As the petit-spot volcanic edifices are small and monogenetic of less than 1 km^3 and few hundred meters in height (Hirano et al., 2008), it is difficult to find them using onboard bathymetry for deep ocean floor. The acoustic backscatter image, on the other hand, is a powerful tool to visualize submarine lava flow. In this research, we picked up data from a petit-spot volcanic field Site C, off the Fukushima and Miyagi Prefecture, as a target area, where tens of strong backscatter zones has been recognized as the presence of petit-spot sites (up to 80 sites; Hirano et al., 2008). We conducted geophysical mapping of multibeam echo sounder in this area during three cruises (KR04-08, YK14-05 and KS18-09). The CARIS HIPS and SIPS software (Teledyne CARIS Inc., Ltd., Fredericton, Canada) was used for raw data processing. In this cleaning process, both CUBE algorism and manual editing were applied. The sound velocity was corrected by real-time data of the surface water velocity meter, and observations of XCTD (expendable conductivity, temperature, and depth) probe profiles.

Backscatter image shows many of high intensity locations that are similar to some locations of petit-spot that were already sampled. There is a variation of intensity. It is considered that sediments signature or measurement conditions (e.g., track direction, horizontal distance from the ship) can affect observed beam-pattern and scattering. Additionally, highly intensity zones have a variation of the area. Comparing with topography, small areas (approximately 1 km in diameter) are located flat field. In contrast, large areas (approximately 5 km in diameter) are located topographical height (approximately 500 m in height). Therefore, it is suggested that intensity variations are also caused by scattering on the slope or existing relatively large petit-spot. Furthermore, some of large areas show some peaks on topography. It suggests an eruption by multiple petit-spot activities.

In following analytical steps, we are applying clustering of gray level co-occurrence matrix (GLCM), in which the probability of neighboring some target pixel value with any neighbor pixel value can be estimated. It is calculated by each texel of any size subarea cut from image, then calculating some values

©2021. Japan Geoscience Union. All Right Reserved.

to explain textual feature (e.g. regularly pattern area, strong signal area). The features of backscatter image provide an effective means to compile topography before the clustering features by k-means clustering (e.g. Honsho et al., 2015; Fakiris et al., 2019). Based on results of the textural feature classes that describe rough surface, and intensity of backscatter image, we aim to discuss the correlation between our classified groups and the geochemical and physical variation of petit-spot lavas.

Keywords: petit-spot, GLCM, acoustic backscatter image, classification

©2021. Japan Geoscience Union. All Right Reserved.

Origin of Philippine Sea basins -Tectonic setting leading to subduction initiation of Izu-Bonin-Mariana arc-

*Osamu Ishizuka[1,2], Kenichiro Tani[3], Gen Shimoda[1], Yumiko Harigane[1], Taichi Sato[1], Rex Taylor[4], Susumu Umino[5], Tian Yu Ping[5], Izumi Sakamoto[6], Yuka Yokoyama[6], Sho Yatsuka[6], Ryota Uchiyama[6], Tomoaki Wakayama[6], Aimi Suzuki[6], Kana Narita[7], Chinatsu Ogawa[7], Yasuhiko Ohara[8,2,9], Chris Conway[1]

1. Geological Survey of Japan, AIST, 2. JAMSTEC, 3. NMNS, 4. University of Southampton, 5. Kanazawa University, 6. Tokai University, 7. Ehime University, 8. Japan Coast Guard, 9. Nagoya University

Robust tectonic reconstruction of the evolving Philippine Sea Plate for the period immediately before and after subduction initiation at ~52 Ma to form the Izu-Bonin-Mariana (IBM) arc is prerequisite to understand cause of subduction initiation (SI) and test competing hypotheses for SI such as spontaneous or induced nucleation. Understanding of nature and origin of overriding and subducting plates is especially important because plate density is a key parameter controlling SI based on numerical modeling (e.g., Leng and Gurnis 2015). There is increasing evidence that multiple geological events related to changing stress fields took place in and around Philippine Sea plate about the time of SI ~52 Ma (Ishizuka et al., 2011). For our understanding of the early IBM arc system to increase, it is important to understand the pattern and tempo of these geological events, particularly the duration and extent of seafloor spreading in the proto arc associated with SI, and its temporal relationship with spreading in the West Philippine Basin (WPB) and structural development of the Daito Ridge Group.

Recent cruises (KS-17-15 and YK19-07S cruises) in the Philippine Sea basins investigated origin and age of formation of ocean basins in and around the Daito Ridge group. The data are still preliminary, but some fresh basalt samples returned well-defined $^{40}Ar/^{39}Ar$ ages older than the age of onset of subduction along the IBM arc at c. 52 Ma. Combined with interpretation of seafloor magnetic anomaly data, this strongly implies that some part of the Philippine Sea basins such as the West Philippine Basin existed prior to the IBM arc, and this basin could be a part of overriding plate at subduction initiation.

Temporal variation of geochemical characteristics of basalts in the Philippine Sea basins appears to indicate that major compositional variation occurred in sub-Philippine Sea mantle subsequent to subduction initiation. This might imply that sinking of large volume of Pacific Plate along the entire IBM arc margin triggered counterflow of asthenospheric mantle and reorganization of sub-Philippine Sea mantle.

The Kita-Daito Basin separates the Amami Plateau and the Daito Ridge. No rock sampling has been reported from this basin to constrain its age and origin of this basin. The Vp model of the Kita-Daito Basin suggests the presence of a 4 –6 km thick crust, similar to the backarc basin oceanic crust in the Shikoku and Parece Vela Basins, as revealed by Nishizawa et al. (2011, 2013). These features seem to imply that rifting and seafloor spreading occurred between the Amami Plateau and Daito Ridge to form the Kita-Daito Basin. Dredge sampling and Shinkai 6500 submersible survey observed and recovered samples from the crustal sections exposed in the deepest part of the basin. Collected samples are mostly composed of volcanic rocks, porphyries and trace amount of sedimentary rock and conglomerate. The volcanic rocks are basalt to andesite clasts. These samples show geochemical characteristics implying influence of material released from subducting slab. This implies that these rocks are not part of ocean crust composed of MORB. These volcanic rocks gave ages of middle Eocene, which indicates that these

©2021. Japan Geoscience Union. All Right Reserved.

volcanic rocks formed after the period of subduction initiation of Izu-Bonin-Mariana arc. These observations seem to imply that the Kita-Daito Basin did not exist at the subduction initiation, and formed by rifting in middle Eocene accompanied by basaltic to andesitic volcanism.

Keywords: subduction initiation, Izu-Bonin-Mariana arc, Philippine Sea Plate

©2021. Japan Geoscience Union. All Right Reserved.

What happened to the seafloor around Nishinoshima volcano during deployment of OBEMs between September 2018 and December 2020?

*Noriko Tada[1], Kiyoshi Baba[2], Toshiya Fujiwara[1], Yoshihiko Tamura[1], Toshiya Kanamatsu[1], Kenta Yoshida[1], Akimichi Takagi[3], Fukashi Maeno[2]

1. Research Institute for Marine Geodynamics, Japan Agency for Marine-Earth Science and Technology, 2. Earthquake Research Institute, The University of Tokyo, 3. Japan Meteorological Agency

We have conducted geomagnetic and electric fields observation using OBEMs and VTMs (hereafter “OBEM” is used to express both instruments) on the seafloor around Nishinoshima volcano belonging to Bonin Islands since 2016 in order to find magma reservoirs and estimate an electrical conductivity structure beneath Nishinoshima. We totally deployed 22 instruments by January 2021, but five OBEMs, two of six OBEMs deployed in September 2018 and three of five OBEMs deployed in July 2019, were not able to be recovered.

Two OBEMs deployed in September 2018 were first tried to recover by self-pop-up in July 2019. Although they normally received the release commands of weights through underwater acoustic communication, they could not float up to the sea surface. We determined the position of the OBEMs both in September 2018 and in July 2019, which indicates both OBEMs shifted a few tens meters in about ten months. It might be possible that the OBEMs were partially buried in sediments by sector collapse or something like that. Two OBEMs were deployed in July 2019 and were safely recovered by self-pop-up in December 2020. Both of them were moved about 3 km in a direction away from Nishinoshima island. We tried to search and rescue three of five OBEMs which would be still on the seafloor by using KM-ROV (KM20-11 cruise in December 2020) and HPD (KS-21-2 cruise in January 2021), but could not find.

According to videos during the dives of KM-ROV and HPD, volcanic activities of Nishinoshima, especially violent Strombolian eruptions after December 2019 (Yanagisawa et al., 2020) might have some influence on the displacements and disappearances of OBEMs. We are analyzing bathymetric data obtained before May 2019 and since December 2020 to evaluate the effect of changing of bathymetric feature on the OBEMs quantitatively.

Keywords: Nishinoshima volcano, OBEM, VTM, bathymetric feature change

©2021. Japan Geoscience Union. All Right Reserved.

Estimation of the Active Faults from BSR-derived heat flow by Automated Velocity Analysis in the Nankai Trough, Japan

*Shuto Takenouchi[1], Kota Mukumoto[1], Takeshi Tsuji[1], Shuichi Kodaira[2], Gou Fujie[2], Yasuyuki Nakamura[2], Kazuya Shiraishi[2]

1. Kyushu-university, 2. Japan Agency for Marine-Earth Science and Technology

Along the Nankai Trough southwest Japan, the recurrence of great earthquakes with an interval of approximately 100 years have been identified from historical literature (Satake, 2015). Therefore, it is important to characterize the active faults for causing great earthquakes and tsunami in the Nankai Trough.

Previously, geophysical surveys have observed many faults in the Nankai Trough (e.g., Ashi et al., 2002). A seismic survey is one of the most effective methods to characterize the faults (e.g. Tsuji et al., 2014). Moreover, the joint interpretation of seismic reflection images and heat flow value estimated from the bottom-simulating reflector (BSR) makes it possible to identify the active faults (Yamano et al., 1982). In the Nankai subduction zone, the active faults cutting through accretionary prisms may act as permeable paths for pore fluid flow, and such localized fluid flow transports heat in an advective manner (Yamano et al., 2014). Especially, the active faults that have recently ruptured include open fractures and thus have higher permeability and higher heat flow. Therefore, if we identify the heat flow anomalies, we can infer the active faults there.

Some methods have evaluated heat flow in the Nankai Trough (e.g., heat flow probe (Christoffel et al., 1969); piston core samples (Kinoshita et al., 2008)). One of them is using the information of BSR (e.g., Yamano et al., 1982). On seismic profiles, BSR appears as the high-amplitude reverse-polarity waveforms parallel to the seafloor reflection: BSR indicates CH4 phase boundary between free gas and hydrate (Markl et al., 1970). The heat flow estimation method using BSR uses the depth of BSR from a seismic profile. Then from the depth information, we determine the temperature and the pressure of BSR. The temperature and depth finally estimate the spatial heat flow distribution. However, inaccurate depth information cannot lead us to accurate heat flow values. To obtain an accurate depth model and infer BSR, we have applied automated velocity analysis (Fomel et al., 2013; Chhun et al., 2018). This analysis yielded a high-resolution P-wave velocity structure (Mukumoto et al., 2019). In this analysis, P-wave velocity can be determined to all CMP gathers, and we could obtain accurate depth model for heat flow estimation.
When we applied this method to the seismic data in the Nankai Trough off Kii-suido, the heat flow mapping value was estimated approximately 40-80 (mW/m2). This result is consistent with previous studies (Ohde et al., 2018). Moreover, we interpreted the location of the active faults from the area based on high heat value. The inferred active fault is located in outer ridge region where the strike-slip faults are developed. The presence of such faults supports the interpretation of heat flow anomalies estimated by our approach.

Keywords: Heat Flow, Velocity Analysis, Nankai Trough, Seismic Reflection, Bottom-Simulating Reflector

©2021. Japan Geoscience Union. All Right Reserved.

Precipitation process and early diagenesis after deposition of iron hydroxide in Nagahama Bay, Satsuma Iwo-Jima Island, Kagoshima, Japan.

*Koki Hori[1], Shoichi Kiyokawa[2], Minoru Ikehara[3]

1. Department of Earth and Planetary Sciences, Graduate School of Sciences, Kyushu University, 2. Department of Earth and Planetary Sciences Faculty of sciences, Kyuushu University, 3. Center for Advanced Marine Core Research, Kochi University

Satsuma Iwo-Jima is a volcanic island located about 50 km south of Makurazaki City, Kagoshima Prefecture, on the northwestern edge of the Kikai caldera, and the size is about 6 km east to west and 3 km north to south. In Nagahama Bay on Satsuma Iwo-jima, iron hydroxide deposition is caused by the supply of acidic hot water rich in dissolved iron and free CO_2 (Shikaura and Tasaki, 2001; Sakamoto, 2015). However, there has never been a clear explanation for the oxidation-precipitation process in the bay, and mineral species after deposition. Therefore, in this study, we measured physicochemical properties of seawater, and observed and analyzed sediment samples or sediment porewater. And finally, we summarized a series of morphological changes from iron oxidation to the earliest diagenesis phase.

As a result of infrared thermography drone exploration in the bay, hydrothermal sources were identified at multiple locations, and we could observe that hot water spreads to the sea surface. The results of water quality measurement showed relatively low pH, ORP, EC values and high turbidity values near the water surface, and toward the deep part of the water mass, the former increased and the latter decreased. In particular, the pH and turbidity values showed a strong negative correlation, with the pH being the lowest and the turbidity being the highest near the sea surface. Correspondingly, it was confirmed from the captured water mass image that the sea surface layer was strongly turbid, and that the precipitation progressed toward the deep part (pH ≈8) and the turbidity became weaker. Furthermore, DO was higher than the metabolizable concentration of marine microaerobic iron-oxidizing bacteria (*zetaproteobacteria*) reported in previous studies (Krepski et al., 2013).
As a result of pH and dissolved element measurement of porewater from the sediment surface core sample with a length of about 40 cm collected from Nagahama Bay in 2020, the pH value changed from 7.5(near sea bottom) to 5.8(deepest part of core), and at that time concentrations of elements such as Fe, Mn, and Si increased. As a result of XRD of samples collected from another core sample collected in 2020 with a length of 1m, a peak of goethite was obtained from the upper part of the sediment (10 to 20 cmbsf) and a peak of siderite was obtained from the more deeper part. This siderite represented a rhombic euhedral shape in SEM observation. In addition, as a result of comparing the XRD peaks of the samples (5 sites) from same stratigraphy between above core and the core sample obtained in 2010, a clear siderite peak was identified at the shallowest sample from the new core, but not at the same stratigraphy sample from the past core.

Summarizing these above results, the following precipitation model can be considered in Nagahama Bay. It is suggested that abiotic oxidation of Fe (II) occurs near the surface of the water mass, and that it precipitates as ferrihydrite, which is a precursor of goethite. Also, the increase in pH toward deeper part caused by mixing with seawater is thought to strongly control the aggregation of iron hydroxide during precipitation. In addition, after deposition, parts of sediments are transformed into goethite near the sea bottom (a few cmbsf). In more deep part, dissolved iron derived from the reduction of iron hydroxide deposits and the supply of hydrothermal fluid from more deep part is contained in the pore water and it is

©2021. Japan Geoscience Union. All Right Reserved.

thought to be used for the precipitation of siderite.Especially, siderite crystals detected in shallow part are suggested to have grown in sediments over the last decade.

Keywords: Satsuma Iwo-Jima, iron hydroxide, siderite

©2021. Japan Geoscience Union. All Right Reserved.

Geological structures in the southern part of the Okinawa Trough north off Ishigaki Island: Preliminary results of the KH-21-3 cruise

*Ayanori Misawa[1], Ryuta Arai[2], Masahiko Sato[3], Saki Ishino[1], Misaki Horiuchi[4], Keita Suzuki[4], Chiori Tamura[5], Katsura Kameo[5], Satoshi Okumura[6], Makoto Otsubo[1], KH-21-3 Shipboard Scientists

1. Geological Survey of Japan, National Institute of Advanced Industrial Science and Technology(AIST), 2. Research Institute for Marine Geodynamics, Japan Agency for Marine-Earth Science and Technology (JAMSTEC), 3. Department of Earth and Planetary Science, The University of Tokyo, 4. Nippon Marine Enterprises, Ltd., 5. Atmosphere and Ocean Research Institute, The University of Tokyo, 6. MOL Marine Co. Ltd.

Backarc basins on continental margins are important constituents of the plate tectonic paradigm, and knowledge of their evolution is key to understanding the lithosphere’s development. Since the backarc basins in the rifting state at the continental margin are limited to the Okinawa Trough and the Bransfield Strait, they are not well understood due to the current rarity of such deformations. In the Okinawa Trough, intermittent rifting has been occurring since 2 Ma. Based on seismic profiles from the Yaeyama Rift, Arai et al. (2017) and Nishizawa et al. (2019) reported normal faults bounding the Yaeyama Rift and the stratigraphy of well-stratified trough-fill sediments. Arai et al. (2017) reported a magma intrusion directly beneath the narrow rift valley of the Yaeyama Rift. Arai et al. (2017) also identified a less reflective zone and a low-velocity zone in the trough-fill sediments and suggested an off-axis magma chamber in the Okinawa Trough. However, the spatial distribution of the normal faults around the Yaeyama Rift and the intrusive structure beneath the Yaeyama Rift has not yet been clarified.

To clarify the detailed geological structure of the southern part of the Okinawa Trough, an integrated marine geological and geophysical survey was conducted using *R/V Hakuho-maru* of JAMSTEC (KH-21-3 cruise) in January 2021. In this cruise, we conducted the following survey: swath bathymetric survey, multi-channel seismic (MCS) reflection survey, subbottom profiler survey, geomagnetic measurements (proton precession magnetometer and shipboard three-component magnetometers), and gravity measurement. The MCS survey used two 355 cubic inch GI guns (total volume of 710 cubic inches) and a 1,200 m 48ch streamer cable. In the MCS profiles, we could obtain clear images down to approximately 1.6 sec (Two-Way Travel Time: TWT) below the seafloor in the trough-fill sediments of the Okinawa Trough. In the Yaeyama Rift, the graben formed by innumerable normal faults were clarified. Moreover, total magnetic field data were acquired with a surface-towed proton magnetometer. The proton magnetometer sensor was towed approximately 290 m behind the ship to minimize magnetization effects from the ship. In this presentation, we will show the preliminary results of the KH-21-3 cruise in the southern part of the Okinawa Trough.

Keywords: Okinawa Trough, Backarc Basin, Yaeyama Graben, Normal fault

©2021. Japan Geoscience Union. All Right Reserved.

The link between volcanism and tectonics at back-arc rifting stage: analysis of three volcanic areas in the southern Okinawa Trough

*JINYU ZHOU[1], Kyoko Okino[1], Masakazu Fujii[2,3]

1. Atmosphere and Ocean Research Institute, The University of Tokyo, 2. National Institute of Polar Research, 3. The Graduate University for Advanced Studies

Back-arc basins are semi-closed seas developed under extensional stress field along subduction zones. Though the origin of the extensional field is still debating, the evolution generally follows the common process; arc or continental crust thinning, development of normal faults (=rifting), breaking off the pre-existed crust, and finally continuous oceanic crust formation. The initial rifting stage is sometimes accompanied by sporadic volcanism, but the link between arc/back-arc volcanism and rifting has not been well-understood. The Okinawa Trough was a back-arc basin at the rifting stage, where the Philippine Sea Plate subducts beneath the Yangtze Plate. The previous studies on the back-arc rifting mainly dealt with rifting in oceanic island arcs. Since the southern Okinawa Trough (OT) is one of few places where we can observe the back-arc rifting on the continental crust, it provides us a valuable opportunity to understand the details of the continental rifting process and its relationship with volcanism.

In our research, geophysical data of the Yonaguni Knolls, the Irabu Knolls, and the Tarama Knolls - three volcanic areas near the rifting axis locating in the southern Okinawa Trough are analyzed. These three volcanic areas are located in different tectonic settings. Through the bathymetry, gravity anomaly, magnetic anomaly, and other compiled data, I tried to elucidate the character of these knolls and the adjacent areas and then to discuss the relationship with their tectonic background.

The axial rift valley generally extends the E-W direction and segmented. The rift valley is 18 km-wide and is accompanied by a high Bouguer anomaly in the eastern Yonaguni area. Both the widths and the Bouguer anomalies of the rift valleys surrounding the Irabu and Tarama Knolls decrease eastward. These observations suggest that the rifting stage is more progressed in the western end of the Okinawa Trough. High magnetic anomalies are observed at minor ridge and knolls within the rift valley and along the rift walls, indicating magma injection. Three volcanic areas show different geophysical features, reflecting their tectonic settings.

The Yonaguni Knolls, located at the western end of the Okinawa Trough, forms an en echelon arrangement of the E-W trending knoll chain (row), likely controlled by the rift faults.

Irabu Knolls locates at the intersection of two differently trending segments of the Okinawa Trough. It may form many faults that enhance the magma intrusion.

Tarama Knolls is located on the arc side flat seafloor. Two types of volcanic eruption are presumed here; fissure-eruption with higher magnetic anomaly and explosive eruption with a large volume of pumice causing low gravity anomaly and no magnetic anomaly.

As the result of the forward modeling of magnetic anomalies, I estimated the magnetization of Yonaguni, Tarama, and Irabu Knolls as 14, 10, and 2 A/m, respectively. This result is consistent with previously collected rock samples.

©2021. Japan Geoscience Union. All Right Reserved.

Keywords: Gravity and magnetic anomalies, Back-arc basin, Okinawa Trough

©2021. Japan Geoscience Union. All Right Reserved.

Mineralogical and geochemical study of sediment cores collected from the Ieyama hydrothermal field in the Okinawa Trough

*Jun-ichiro Ishibashi[1], Takashi Miyamoto[1,3], Shuhei Totsuka[1,2], Kazuhiko Shimada[1], Toru Yamasaki[2], Ken Ikehara[2], Toshiro Nagase[4], Yutaro Takaya[5], Hideaki Machiyama[6], Koichi Iijima[6], Hirofumi Yamamoto[6], Hidenori Kumagai[6]

1. Department of Earth and Planetary Sciences, School of Science, Kyushu University, 2. National Institute of Advanced Industrial Science and Technology, 3. School of science, University of Tokyo, 4. Tohoku University Museum, 5. Waseda Research Institute for Science and Engineering, 6. Japan Agency for Marine-Earth Science and Technology

Ieyama hydrothermal field is located at the seafloor around a water depth of 1050-1100 mbsl (meters below the sea level) in the mid-Okinawa Trough. Semi-detailed exploration survey during YK17-18C cruise using AUV (Autonomous underwater vehicle) identified negative self-potential anomalies probably related to mineralization on and beneath the seafloor in this area (Kasaya et al., 2020). Moreover, ROV (Remotely operated vehicle) surveys conducted in the same and later durations observed and accessed present hydrothermal activities represented by high temperature fluid venting from mound structure consisted of sulfide and sulfate mineral deposits. Scientific drilling was performed by J-MARES during the SIP Integrated Ocean Resource Surveying System JM18-04 Cruise in September 2018. Sediment cores were obtained from 3 sites in the Ieyama field, employing BMS (Boring Machine System) installed on *Shincho-maru*. Lithology and mineralogy of the obtained sediment cores were studied based on VCD (Visual Core Description), measurements of physical properties, XRD (X-ray diffractometer) analysis, and electron probe microanalyzer (EPMA) analysis.

Sulfide mineralization was recognized in the layer from 50 to 65 mbsf (meters below the seafloor) of the sediment core collected from a bottom of circular depression of about 100 m diameter. This layer was overlaid by thick pile of pumice and pumiceous tuff, and underlaid by tuffaceous breccia. Mineralogical and chemical studies of sulfide minerals revealed several similarities to sulfide minerals collected from chimney and mound structures found in the vicinity of the drilled site.

Acknowledgements:

This study was conducted under the framework of the Next-Generation Technology for Ocean Resources Exploration Project, Cross-ministerial Strategic Innovation Promotion Program (SIP) funded by CSTI, Cabinet Office, Government of Japan. We are thankful to J-MARES (Research and Development Partnership for Next Generation Technology of Marine Resources Survey) for providing samples used in this study.

Keywords: seafloor massive sulfide deposits, sulfide and sulfate mineralization, subseafloor of hydrothermal field, scientific drilling using BMS(Boring Machine System)

©2021. Japan Geoscience Union. All Right Reserved.

Geochemical and geochronological study of barite in sediment cores obtained from Higashi Izena hydrothermal field, Okinawa Trough

Yushi Itatani[1], *Jun-ichiro Ishibashi[1], Makiko Tomita[2], Shin Toyoda[2], Ryuichi Shinjo[3], Kazuno Arai[4], Taisei Fujiwara[5]

1. Department of Earth and Planetary Sciences, Graduate School of Science, Kyushu University, 2. Okayama University of Science, 3. Faculty of Science, University of Ryukyus, 4. Center for Advanced Marine Core Research, Kochi University, 5. Institute for Geology and Geochronology

Ieyama hydrothermal field is located at the seafloor around a water depth of 1050-1100 mbsl (meters below the sea level) in the mid-Okinawa Trough. Scientific drilling performed by J-MARES during JM18-04 Cruise in September 2018 confirmed sulfide and sulfate mineralization in the layer from 50 to 65 mbsf (meters below the seafloor) of the sediment core collected from a bottom of circular depression of about 100 m diameter (Ishibashi et al., this meeting). We focused on barite in the sediment core and conducted measurement of strontium isotope ratio, gamma ray measurement to determine radium content, and geochronological studies employing ESR dating and 226Ra-210Pb radioactive disequilibrium dating. Vertical profile of radium content in barite showed monotonic change along the depth, as well as variation of strontium isotope ratio. These results suggest barite formation within the sediment layer by mixing of radium-rich hydrothermal fluid and seawater penetrated through a volcaniclastic sediment layer of high porosity. Results of radioactive disequilibrium dating barite within the sediment core showed similar age to barite obtained from hydrothermal mound on the seafloor where high temperature fluid venting. These results imply barite within the sediment layer is formed by present hydrothermal activity.

Keywords: seafloor massive sulfide deposits, strontium isotopic composition, radioactive disequilibrium dating, electron spin resonance dating

©2021. Japan Geoscience Union. All Right Reserved.

Fin whale signals recorded by S-net

*Masashi Mochizuki[1], Takeshi Nakamura[2], Ryoichi Iwase[3], Kenji Uehira[1]

1. National Research Institute for Earth Science and Disaster Resilience, 2. Central Research Institute of Electric Power Industry, 3. Japan Agency for Marine-Earth Science and Technology

S-net (Seafloor observation network for earthquakes and tsunamis along the Japan trench) is the online and real-time seafloor observation network of 150 observatories for earthquakes and tsunamis along the Japan Trench. It covers the focal region of the 2011 off the Pacific coast of Tohoku earthquake and its vicinity regions. All the data from 150 seafloor observatories are being transferred to the data center and being automatically processed for monitoring of earthquake activities in these regions.

We have investigated noise sources that contaminate seismic signals recorded by S-net and cause deteriorating of automatic earthquake detection capability. One of such noise sources is fin whale signal. Waveforms of fin whale signals have characteristic spectral peaks in narrow frequency bands of 14-25 Hz. They have a short duration of about one second and are repeated at regular intervals of several tens of seconds.

Nakamura and Iwase (2020) developed a method that automatically detect and count fin whale signals from continuous seismic records. This method was applied to the seismic data caught by the 150 observatories of S-net from 2017 to 2019. They found that the observatories, located at area off Kushiro and Aomori, recorded the fin whale signals frequently from early autumn to spring. The migration of the signals among the observatories from northeast to southwest direction in winter was also recognized.

Monitoring and counting the fin whale signals within S-net area with the method by Nakamura and Iwase (2020) have continued, in order to understand characteristics of observation environment at each of S-net observatories. We report spatiotemporal distributions of fin whale signals recorded by S-net observatories in the year of 2020 in this presentation.

Keywords: ocean bottom observation, S-net, fin whale

©2021. Japan Geoscience Union. All Right Reserved.

Effective removal of oceanic variation from ocean bottom pressure gauge data using the MSSA

*Kenta Shimizu[1], Toshinori Sato[1], Koichi Murata[1], Norihisa Usui[2], Hajime Shiobara[3], Tomoaki Yamada[4], Masanao Shinohara[3]

1. Chiba Univ., 2. MRI, 3. ERI. Univ. Tokyo, 4. JMA

1. Introduction

Ocean bottom pressure gauges (OBPs) can observe vertical movement of the seafloor continuously, and are useful to detect slow movement due to slow slip events. The OBP data include components such as oceanic tide, oceanic variation, and instrumental drift. To detect crustal movement, these components must be removed. To remove the oceanic variation, several methods were proposed in the previous studies such as average subtraction using neighboring OBPs (e.g. Suzuki et al. 2016), fitting of a parametric model (Sato et al. 2017), and subtraction of a data-assimilated oceanic model (e.g. Inazu et al. 2012). This study conducts the Multi-channel Singular Spectrum Analysis (MSSA) for the observed data and an oceanic model, and divides into components. Then, we remove only good correlation components of the oceanic model from the observed data. This method can extract vertical movement better, because this method may remove incompleteness of the oceanic model.

2. Method

As an oceanic model, we use a four-dimensional variational ocean reanalysis
for the Western North Pacific over 30 years (FORA-WNP30) (Usui et al. 2017). The OBP data are obtained at off Boso Peninsula from 2013-2015, which include the 2014 Boso slow slip event.
From the observed data, we remove the oceanic tide using Baytap08 (Tamura et al. 1991), and the drift using a linear fitting. We conduct the MSSA for the removed data and the FORA-WNP30 data, and calculate correlation between them for each component. We reconstruct oceanic model data using only good correlation components, then remove them from the removed data.

3. Results

The residual between the removed data and the reconstructed oceanic model has standard deviation of about 1.0 hPa. On the other hand, the residual between the removed data and the original oceanic model has about 1.6 hPa. This suggests that the present method can remove oceanic variation better than the previous methods.
We fit a parametric model to the residual between the removed data and the reconstructed oceanic model, and obtain standard deviation of about 0.8 hPa.

Acknowledgments

We thank the captains and crew of R/V Hakuho-maru and R/V Natsushima of JAMSTEC for their support. This work was supported by the Earthquake and Volcano Hazards Observation and Research Program authorized by the Ministry of Education, Culture, Sports, Science and Technology. This work was supported by JSPS (25287109).

Keywords: Multi-channel Singular Spectrum Analysis, ocean bottom pressure gauge, oceanic model

©2021. Japan Geoscience Union. All Right Reserved.

Sampling process of seafloor sediments as a source of information on their rheology

*Nikita Dubinya[1,2], Sergey Tikhotskiy[1,2], Victor Nachev[1,3]

1. Moscow Institute of Physics and Technology, 2. Schmidt Institute of Physics of the Earth of the Russian Academy of Sciences, 3. Sadovsky Institute of Geosphere Dynamics of the Russian Academy of Sciences

The study is related to the problem of offshore infrastructure construction with an especial focus on development of offshore hydrocarbon fields from the perspective of geomechanics. It is essential to have a model of mechanical properties of seafloor sediments for effective construction of safe infrastructure. The problem of creating such model is rather complicated as the rheological properties of seafloor sediments are nonlinear –mechanical behavior of sediments appears to be described by nonlinear visco-elasto-plastic models. At the same time there are limited opportunities to estimate these properties as engineering drilling –a valid source of information on mechanical properties –may be very expensive and complicated at offshore conditions.

Sediment sampling with various corers provides one of the most valuable sources of information regarding mechanical properties of seafloor sediments. The collected samples may be analyzed in laboratory conditions using various techniques. One of the problems with this procedure is related to difficulties in recreating mechanical conditions of the sample before coring procedure: any sample could have been significantly altered before arriving to the laboratory. There are various ways to deal with this problem –in the current study we focus on one of them.

In the current study we analyze the sampling process itself as a source of information regarding rheological properties of seafloor sediments. From the perspective of continuum mechanics the interaction between corer and seafloor may be considered as a contact problem –a rigid body (corer) penetrates into a visco-elasto-plastic medium (seafloor). It is clear that the dynamics of penetration is governed by a set of conditions, including initial conditions, setting distance, geometry and mechanical properties of the seafloor at the vicinity of the contact point. As rheological properties of the seafloor are included into this set of factors, one may postulate and try to solve the inverse problem: can mechanical properties of the seafloor sediments be estimated if all other factors mentioned above are known alongside with the changes of measurable corer acceleration with time?

In the current paper we analyze this question using numerical modeling. A numerical finite-element model has been constructed for the mentioned contact problem in the case of gravity tubular corer penetrating into plastic medium without hardening. A set of numerical experiments has been carried out to obtain the dependencies between changes in acceleration of the corer and mechanical properties of seafloor sediments: density, elastic moduli, and strength properties. The obtained dependencies revealed that it is possible to deal with the inverse problem mentioned above. There are nonlinear relationships between the corer penetration dynamics and mechanical properties of the seafloor. It appears that the postulated inverse problem may have more than one solution even without viscosity taken into account. Nevertheless, the obtained results prove that sampling process itself may provide information regarding the type of rheological model properly describing the mechanical behavior of seafloor sediments.

Keywords: Seafloor sampling, Indentation, Rheology, Geomechanics

©2021. Japan Geoscience Union. All Right Reserved.

©2021. Japan Geoscience Union. All Right Reserved.

Technical protocol for deep-sea environmental monitoring by the portable seafloor observation platform Edokko Mark 1

*Hiroyuki Yamamoto[1], Tetsuya Miwa[1], Shinsuke Kawagucci[1], Sangkyun Lee[2], Atsuo Oono[3], Kousuke Tsutsumi[3], Hideki Sugishima[3]

1. Japan Agency for Marine-Earth Science and Technology, 2. J-MARES/JGI, 3. J-MARES/idea

The mooring, lander, and cable connected station are conventional methods for deep-sea monitoring. Recently, increasing interest for seabed mining, requirement of environmental management, and demand for marine biodiversity raises the issue of seafloor monitoring techniques, especially for deep-sea environments. The portable seafloor observation platforms with standalone operation mechanisms have been developed. In Japan, the joint project of private companies and academia developed the portable seafloor observation platform Edokko Mark 1, consisting of grass spheres with a built-in HD video cameras system and an acoustic release mechanism (1). The Edokko Mark 1 has four types with unique abilities to adopt monitoring targets; HSG for anti-corrosion, 365 for long-term observation, COEDO for simple operation by human power. These products are commercially available from Okamoto Glass Co. Ltd. (https://ogc-jp.com/productinfo/glassball/).

The system of Edokko Mark 1 has been improved in the Japan projects for technology development on seabed mining. Since the trial to 8000m depth of Japan trench in 2013, the Edokko Mark 1 has been deployed on the seafloor of Okinawa Trough from 2014 to18 and off Minami Torishima from 2018 to 2021. The video image is commonly used for biological and ecological survey in deep-sea expedition, although the observation area is limited within lighting power. The hydrophone is an optional sensor of Edokko Mark 1, can record biological sound as well as anthropogenic and geological sources. The soundscape is complementary to image data, and enables the expand observation area for deep-sea communites. Electromagnetic current meter and acoustic current meter could be installed on Edokko Mark 1 at 1.5m position from the seafloor and measured bottom current. Another observation of 2019 in the Suruga Bay recorded deep-sea turbidity current triggered by heavy precipitation of the Super Typhoon Hagibis (2). In this case, a deep-water displacement phenomenon was determined and drastic turbidity change was quantified from video images.

The projects of marine environmental assessment anticipate the transportability and quick deployment capability of the portable seafloor observation platform such as Edokko Mark 1. The guidance for environmental impact assessment on seabed mining (ISBA/25/LTC/6/Rev.1) published by the International Seabed Authority recommends the Edokko Mark 1 as a suitable system adopted deep-sea observation protocol (https://www.isa.org.jm/). These knowledge on video observation strongly supported establishing the technical protocol and making the International Standard (ISO /DIS23730, 23731).
In this presentation we will explain the observation techniques and results from deep-seafloor surveys.

References:

1) Miwa, T., et al. 2016. Underwater Observatory Lander for the Seafloor Ecosystem Monitoring using a Video System. Pages 333-336 in Techno-Ocean. IEEE, Kobe.
2) Kawagucci, S., et al. 2020. Deep-sea water displacement from a turbidity current induced by the Super Typhoon Hagibis. PeerJ 8:e10429.

©2021. Japan Geoscience Union. All Right Reserved.

Keywords: seafloor monitoring, deep-sea environments, environmental impact assessment

©2021. Japan Geoscience Union. All Right Reserved.

[J] Poster | S (Solid Earth Sciences)：S-CG Complex & General

Sat. Jun 5, 2021 5:15 PM - 6:30 PM JST | Sat. Jun 5, 2021 8:15 AM - 9:30 AM UTC | Ch.18_2

[S-CG46] Rheology, fracture and friction in Earth and planetary sciences

convener:Shintaro Azuma(Department of Earth and Planetary Sciences, School of Science, Tokyo Institute of Technology), Ichiko Shimizu(Division of Earth and Planetary Sciences, Graduate School of Science, Kyoto University), Osamu Kuwano(Japan Agency for Marine-Earth Science and Technology), Miki Tasaka(Shizuoka University)

The aim of this session is to join people from various research area in the earth and planetary sciences and to stimulate discussion beyond the boundaries of each research area. Our goal is to deepen our understanding of dynamics in geosciences by looking over whole areas in the earth and planetary sciences from the viewpoint of PHYSICS OF DEFORMATION, FLOW, AND FRACTURE. We welcome any field (e.g., earthquake, volcano, earth surface, crust, mantle and the core, and other planets and satellites) and any approach (e.g., laboratory experiments, numerical simulations, field observations, and theories).

[SCG46-P01] Experimental investigation of the pyroxene-garnet and olivine-spinel transformations under shear deformation using synchrotron radiation and acoustic emission techniques

*Yuki Mori[1], Tomoaki Kubo[1], Rikuto Honda[1], Takuya Iwasato[2], Yuji Higo[3], Yoshinori Tange[3] (1.Kyushu Univ., 2.Shin-Nippon Nondestructive Inspection Co.,Ltd., 3.JASRI)

[SCG46-P02] Creep behavior during the post-spinel transformation in $(Mg, Fe)_2SiO_4$

*Yuta Goto[1], Tomoaki Kubo[1], Rikuto Honda[1], Yumiko Tsubokawa[1], Yuichiro Mori[2] (1.Kyushu Univ., 2.The University of Tokyo)

[SCG46-P03] SOR and AE study on the olivine-spinel transformation in $(Mg,Fe)_2SiO_4$ under uniaxial deformation with D111-type apparatus

*Rikuto Honda[1], Tomoaki Kubo[1], Yuichiro Mori[2], Goto Yuta[1], Yumiko Tsubokawa[1], Takuya Iwasato[3], Yuji Higo[4] (1.Kyushu University, 2.The University of Tokyo, 3.Shin-Nippon Nondestructive Inspection Co., Ltd., 4.JASRI)

[SCG46-P04] Frequency characteristics of acoustic emission in the fracture process of thermally cracked granite

*Sueyoshi Kazumasa[1], Manami Kitamura[2], Xinglin Lei[2], Ikuo Katayama[1] (1.Department of Earth and Planetary Systems Science, Hiroshima University, 2.National Institute of Advanced Industrial Science and Technology)

[SCG46-P05] Flow-to-fracture transition of linear Maxwell-type fluid by air injection

*Claudia Sanchez[1], Osamu Kuwano[2], Mie Ichihara[1] (1.Earthquake Research Institute, Tokyo University , 2.JAMSTEC)

[SCG46-P06] Role of lithology in deformation mechanisms of shallow-crustal active faults: Evidence from the Nahan thrust of Himalayas

*Dyuti Prakash Sarkar[1], Jun-ichi Ando[1], Kaushik Das[1], Gautam Ghosh[2], Prabir Dasgupta[3] (1.Hiroshima University, 2.Presidency University, 3.Durgapur Govt. College)

[SCG46-P07] Study of the mobile granular layer in bedload transport by laminar shearing flow in a tilted channel

*Chong-Wei Hong[1], Franco Tapia[2], Pascale Aussillous[3], Élisabeth Guazzelli[4], Chi-Yao Hung[1] (1.Department of Soil and Water Conservation, National Chung Hsing University, Taichung, Taiwan, 2.Department of Mechanical Engineering, Tokyo University of Agriculture and Technology, Tokyo, Japan, 3.Aix-Marseille

Université, CNRS, IUSTI, Marseille, France, 4.Université de Paris, CNRS, Matière et Systèmes Complexes (MSC) UMR 7057, Paris, France)

[SCG46-P08] Fracture behavior of silicate network phase-separating from aqueous fluid

*Takehito Koyama[1] (1.Institute of Industrial Science, the University of Tokyo)

[SCG46-P09] Evolution of patterns of hydraulically conductive natural fractures during inelastic deformation of rocks

*Nikita Dubinya[1,2] (1.Moscow Institute of Physics and Technology, 2.Schmidt Institute of Physics of the Earth of the Russian Academy of Sciences)

[SCG46-P10] Theoretical study on rock anelasticity;
Extension of a grain-boundary sliding model to two dimensions

*Mitsuyoshi Kunugihara[1], Yasuko Takei[1] (1.Earthquake Research Institute,The University of Tokyo)

[SCG46-P11] A DEM model of uniaxial and triaxial compression test of rocks

*Mikito Furuichi[1], Daisuke Nishiura[1], Yuzuru Yamamoto[2] (1.Japan Agency for Marine-Earth Science and Technology, 2.Kobe University)

[SCG46-P12] Relaxation of the frictional force in a statistical mechanical model of magnetic friction

*Komatsu Hisato[1] (1.National Institute for Materials Science)

Experimental investigation of the pyroxene-garnet and olivine-spinel transformations under shear deformation using synchrotron radiation and acoustic emission techniques

*Yuki Mori[1], Tomoaki Kubo[1], Rikuto Honda[1], Takuya Iwasato[2], Yuji Higo[3], Yoshinori Tange[3]

1. Kyushu Univ., 2. Shin-Nippon Nondestructive Inspection Co.,Ltd., 3. JASRI

Detection of acoustic emission (AE) has been recently performed combined with high-pressure deformation apparatus and synchrotron radiation to study the mechanisms of deep-focus earthquakes. To understand effects of large strains on shear localization and instability, deformation experiments in shear is more effective than uniaxial compression. However, the sample volume in shear deformation experiment is generally much smaller than that in uniaxial deformation experiment, which may make it difficult to conduct AE study with required accuracy. In this study, we carried out the pyroxene-garnet and olivine-spinel transformation experiments under shear deformation using AE techniques combined with deformation-DIA (D-DIA) apparatus and synchrotron radiation. Both pyroxene and olivine are major constituent minerals in subducting slabs, but their transformation processes are different. Here we report preliminary results on AE activities induced by these high-pressure transformations in shear.

The high-pressure shear deformation experiments were conducted using a uniaxial press (SPEED Mk. II) with a D-DIA type guide block installed at beamline BL04B1 in SPring-8, Japan. The 60 keV monochromatic X-ray was used to obtain 2D X-ray diffraction pattern and radiograph every 5 min during the experiments. We used MA 6-6 type AE measurement system attached with D-DIA guide block (Iwasato et al., 2020). Three kinds of starting materials of synthesized Al-rich clinopyroxene (Al-rich cpx), natural Al-poor clinopyroxene (Al-poor cpx), and synthesized fayalite were prepared for our study. They were sintered and cut to form polycrystalline disks (300 μm in thick and 1.3 mm in diameter). Each disk was assembled together with strain marker of gold foil between two 45˚-cut alumina pistons. The samples were first deformed to shear strains of ~30% at ~10 GPa and 650˚C for clinopyroxene and 475˚C for fayalite (stage 1), and then heated with a constant rate of 0.05 ℃/sec to cause the phase transformations (stage 2). The shear strain rates and the final shear strains were 1–5 x 10^{-4} /s and ~70-160%, respectively.

The pyroxene-garnet transformation already started during the deformation at 650˚C in Al-rich cpx and proceeded with increasing temperature. In contrast, no transformation was observed in Al-poor cpx up to ~850˚C. This is possibly originated from the difference in the Al content. We detected many AEs from the sample region at the stage 2 in the Al-rich cpx run, but no AEs at the stage 2 in the Al-poor cpx run, implying that AEs were induced by the pyroxene-garnet transformation in shear. FE-SEM observations of the recovered sample in the Al-rich cpx run revealed that garnet formed along grain boundary of clinopyroxene, and the shear deformation was localized in some regions. We also detected large AEs from the sample region in the fayalite run during the stage 2 associated with the olivine-spinel transformation. Thus, both the pyroxene-garnet and olivine-spinel transformations caused AE activity in our shear deformation experiments. We recognized two types of waveform of AE: AE with rapid increase in amplitude to the maximum (type 1), and AE with gradual increase in amplitude to the maximum (type 2). The type 2 is dominant in the Al-rich cpx run, whereas AEs in the fayalite run were type 1 only. The estimated locations of AE source were concentrated within the sample region in the case of type 1 AE, whereas those of type 2 AE were widely scattered from the sample to pressure medium. This is probably because the AIC pick is difficult in the type 2 AE. Our study demonstrated that both the pyroxene-garnet

©2021. Japan Geoscience Union. All Right Reserved.

and olivine-spinel transformations caused AE activity under shear deformation at ~10 GPa, however further investigations are necessary to understand why the waveform of AEs are rather different between theses transformations.

Keywords: Acoustic emission, In situ X-ray observation, Deep-focus earthquake, Pyroxene, Olivine

©2021. Japan Geoscience Union. All Right Reserved.

Creep behavior during the post-spinel transformation in $(Mg, Fe)_2SiO_4$

*Yuta Goto[1], Tomoaki Kubo[1], Rikuto Honda[1], Yumiko Tsubokawa[1], Yuichiro Mori[2]

1. Kyushu Univ., 2. The University of Tokyo

Seismological studies have shown large deformation and no deep earthquakes in the lower mantle slabs, which may be attributed to the post-spinel transformation (the decomposition reaction of $(Mg,Fe)_2SiO_4$ ringwoodite into $(Mg,Fe)SiO_3$ bridgmanite and (Mg,Fe)O ferropericlase). *Poirier et al.* (1986) reported that the post-spinel transformation is a eutectoid reaction with alternating fine lamellar structure in the colony texture. Based on microstructural observations, *Ito and Sato* (1991) suggested that aseismicity in the lower mantle is caused by superplastic flow of the fine-grained post-spinel assemblage. The weakening of the lower mantle slab has also been suggested from the degree of the grain-size reduction and diffusion creep viscosity (e.g., *Kubo et al.*, 2009). Syn-deformational reaction experiments using analog materials have shown that eutectoid reaction does not directly weaken the material, but the degeneration of eutectoid colony is an important process for rheological weakening (e.g., *Doi et al.* 2014; *Zhao et al.* 2012). However, there have been no direct experimental studies to understand effects of the post-spinel transformation on creep behavior.

In this study, syn-deformational post-spinel transformation experiments in $(Mg, Fe)_2 SiO_4$ were conducted by in-situ X-ray observation method using a D-111 type deformation apparatus (MAX-III) at PF-AR NE-7 beamline. The starting material is polycrystalline ringwoodite (grain size ~a few to 10 μm) that was synthesized from single crystalline San Carlos olivine. The ringwoodite sample was first uniaxailly deformed at ~27 GPa and 600˚C to ~3% strain, and then heated to around 1000˚C at a constant rate of 0.06˚C/s to cause the post-spinel transformation. 2D-XRD patterns and radiography images were taken every ~5 min to obtain stress-strain and transformation-time curves. Deformation and transformation microstructures in recovered samples were examined by FE-SEM.

We conducted two runs at the similar P, T, and strain rate conditions. The strain rates changed from 1.3-1.5e-5 s^{-1} to 4.9-5.6e-5 s^{-1} at the timing of the initiation of the transformation. The final strains and transformed fraction were ~27-37% and ~50-80%, respectively. Creep behaviors in ringwoodite suggested that it reached steady state at the strain of ~5% and the stress of ~4 GPa, and then exhibited weakening with the increase in temperature. The decrease in the flow stress of ringwoodite became more rapidly at higher than ~800-850˚C, which may be linked to the initiation of the transformation. However, the stress of bridgmanite newly transformed is larger than that of ringwoodite. FE-SEM observation revealed that many eutectoid colonies with the size of ~1 μm in diameter are present at grain boundaries of ringwoodite. The lamellar spacing in the colony is ~50 nm. It is noteworthy that the eutectoid colonies themselves are not deformed and degenerated after the deformation with nearly 30% strain. Both the colony size and lamellar spacing are much smaller than those observed in transformation experiments with similar overpressures but no deformation (e.g., *Kubo et al.*, 2011).

Each phase (bridgmanite and ferropericlase) in a eutectoid colony is thought to be an interconnected single crystal. No deformation in the eutectoid colonies implies that the stiffer bridgmanite supports the colony (i.e., isostrain in the two phase of the colony), which means that the transformed post-spinel colony is stiffer than the parental ringwoodite. Thus, it is unlikely that the reaction-induced weakening occurs in our experiments. The weakening of ringwoodite observed at higher than ~800-850˚C may be originated by the change of the dominant deformation mechanism from low-temperature plasticity to

©2021. Japan Geoscience Union. All Right Reserved.

dislocation creep (e.g., *Imamura*, 2018). Our study demonstrates that rheological weakening due to the post-spinel transformation is difficult at low temperatures ~1000°C and larger strains are required to degenerate the post-spinel colony.

Keywords: post-spinel transformation, eutectoid reaction, deformation experiment, in situ X-ray observation, deep slab deformation, rheological weakening

©2021. Japan Geoscience Union. All Right Reserved.

SOR and AE study on the olivine-spinel transformation in $(Mg,Fe)_2SiO_4$ under uniaxial deformation with D111-type apparatus

*Rikuto Honda[1], Tomoaki Kubo[1], Yuichiro Mori[2], Goto Yuta[1], Yumiko Tsubokawa[1], Takuya Iwasato[3], Yuji Higo[4]

1. Kyushu University, 2. The University of Tokyo, 3. Shin-Nippon Nondestructive Inspection Co., Ltd., 4. JASRI

In cold subducting slabs, it has been pointed out that olivine remains in metastable phase beyond the equilibrium boundary. The metastable olivine transforms into its high-pressure phases, such as wadsleyite or ringwoodite under non-equilibrium conditions. It has been suggested that this phenomenon leads to rheological weakening and shear instability causing large deformation and deep-focus earthquakes in subducting slabs. For example, Schubnel et al. (2013) reported AE activity following the olivine-spinel transformation with in-situ X-ray observation using D-DIA apparatus. However, they used olivine analogue, Mg_2GeO_4, which transformed to spinel phase at low pressures (~2 GPa). In the present study, we conducted deformation experiments with San Carlos olivine polycrystal under the mantle transition zone (MTZ) conditions using D111-type apparatus combined with synchrotron radiation to observe creep behavior during the phase transformation. In addition, we developed 8-channel Kawai-type AE measurement system attached with D111-type apparatus to observe shear instability at MTZ pressures. Here we report some preliminary results on these experimental studies.

We carried out deformation and transformation experiments with synchrotron X-ray using a D111-type apparatus (MAX-III) installed at PF-AR NE7 beamline. The starting material was polycrystalline San Carlos olivine sintered at 1323 K (grain size of ~100 μm, Run oldt11) and 1223 K (grain size of ~30 μm, Run oldt12). The sample was first uniaxially deformed to ~1-3 % strain with a constant anvil displacement rate of 300 μm/h at ~20 GPa and 773 K / 873 K, and then heated with a constant rate of 0.09 K/s to cause transformation during deformation. We obtained 2D-XRD patterns and radiography image every 5 minutes using a 60 keV monochromatic X-ray to measure stress-strain curves and reaction kinetics.

Transition to ringwoodite started at ~20 GPa and ~1000K with ~5% strain, and finally proceeded more than 90% transformation at 1273K with the final strain of ~20-35%. The strain rate was 0.4-7.5e-5 s^{-1}. The stress of olivine reached to ~5 GPa at most before the transition and gradually decreased to ~2-3 GPa with the increase in temperature and transformed fraction. In contrast, the stress of ringwoodite newly appeared was very small less than 1 GPa and subtly increased. The similar results have been reported in the RDA study (Mohiuddin et al., 2020), however, the strength of ringwoodite kept small in our experiments. The temperature dependence of the olivine stress was almost consistent with the flow law of Peierls mechanism constructed by Mei et al. (2010) at the initial stage, and the olivine got more weakened as the transformation proceeded especially in Run oldt11. These creep behaviors suggest that reaction-induced weakening occur, but not significant. It is unlikely that the interconnected weak layer was formed at the initial stage of the transformation. In the recovered samples, intracrystalline lamellae filled with fine ringwoodite grains were widely observed. Similar textures have been reported in shocked meteorite (Chen et al., 2004) and the syn-deformational olivine-spinel transition of fayalite (Mori et al., 2020).

We also have set up 8-channel Kawai-type AE measurement system attached with another D111-type apparatus (QDES2) newly installed at Kyushu University. This is almost similar to 6-channel MA6-6 type AE measurement system with D-DIA apparatus (Iwasato et al., 2020) for lower-pressure experiments. After the

©2021. Japan Geoscience Union. All Right Reserved.

verification of the performance by conducting cold compression runs using grass beads and single crystalline San Carlos olivine, we have started syn-deformational transformation experiment in San Carlos olivine under the MTZ conditions with the AE system. We have recorded AE from the sample during transformation, however no distinct faulting structure was observed so far except for lenses and thin lamellae filled with fine-grained ringwoodite.

Keywords: high-pressure deformation experiments, in-situ X-ray observation, acoustic emission, slab weakening , deep earthquakes, olivine-spinel transformation

©2021. Japan Geoscience Union. All Right Reserved.

Frequency characteristics of acoustic emission in the fracture process of thermally cracked granite

*Sueyoshi Kazumasa[1], Manami Kitamura[2], Xinglin Lei[2], Ikuo Katayama[1]

1. Department of Earth and Planetary Systems Science, Hiroshima University, 2. National Institute of Advanced Industrial Science and Technology

Fluid flow-induced seismicity has been observed in various engineering fields such as enhanced geothermal system (EGS). Especially, in the Pohang EGS project, the Mw 5.4 earthquake was likely induced by fluid injection after the events in the entire period of stimulations (Kim et al., 2018). To understand the processes of induced earthquakes due to fluid injection, it is necessary to research the propagation process of pre-existing cracks in thermally damaged granites. The acoustic emission (AE) is defined as elastic waves released by rapid cracking, which is a useful tool for investigating generation and propagation of rock fractures. The frequency of AE signals from fracturing provides information about internal structure of rock. In this study, we measure AE and P-wave velocity of thermally cracked granite during triaxial deformation under dry and fluid-saturated conditions.

We conduct triaxial compression tests at confining pressure of 22.5 MPa and strain rate of ~10^{-6} s^{-1} under dry and wet conditions using the loading system at AIST. Permeability is measured by a fluid flow method using water as a pore fluid, in which a constant upstream pore pressure was maintained at 4 MPa. Cylindrical coarse-grained Inada granite (50 mm in diameter and 125 mm in length), which are intact and thermally damaged at 550 ℃, are used as samples. We measure AEs with 28 piezoelectric transducers (PZTs) with variable resonance frequencies of 0.25 - 2 MHz. In the frequency spectrum obtained from the fast Fourier transform, the peak amplitude is defined as the largest amplitude in the spectrum, and the peak frequency is defined as the frequency at the peak amplitude.
Our result shows that wet samples behave elastically until the onset of dilatancy ranging from 27.1 to 32.7 % of the peak stress, and then shows inelastic behavior. After the peak stress of 357-413 MPa, post-yield behavior of the sample indicates brittle failure with drastic stress drop. AE activity was initiated at the crack damage stress ranging from 51.8 to 62.6 % of the peak stress. Frequency analysis based on the fast Fourier transform shows that the peak frequency was mainly distributed in the range of 0 to 0.6 MHz. Chen et al. (2020) has shown that low peak frequency signal with high peak amplitude normalized by the maximum value in the test (LH signal) reflected the formation of macrocracks. In our results of PZTs with resonant frequency of 1 and 0.5 MHz, LH signals were only recorded after 99 % of the peak stress for the thermally cracked sample, while LH signal began to appear after approximately 80 % of the peak stress for the intact sample. A comparison of the results indicates that stress-induced crack growth in the thermally cracked sample was not detected due to the large scale of thermal cracks.

Keywords: acoustic emission, frequency, triaxial compression

©2021. Japan Geoscience Union. All Right Reserved.

Flow-to-fracture transition of linear Maxwell-type fluid by air injection

*Claudia Sanchez[1], Osamu Kuwano[2], Mie Ichihara[1]

1. Earthquake Research Institute, Tokyo University , 2. JAMSTEC

Due to decompression during magma ascent, bubbles grow, rise, and burst. These behaviors are coupled with the rheology of the magma. The complex nature of magma and the conditions under which the bubbles develop may control the eruption styles, whether explosive or effusive. Among the complexity, the viscoelasiticy is considered essential for the flow and fracture transition. The linear Maxwell model is the simplest model to represent the magma viscoelasticity. It has a single relaxation time. Brittle fracture of magma is considered to occur when the deformation time scale is shorter than the relaxation time. Although this concept has been used in many eruption models, the ductile-to-brittle transition of flowing fluid has not been sufficiently investigated in the laboratory. We report the experimental study of using an aqueous solution of cetyltrimethylammonium bromide and sodium salicylate (CTAB/NaSal), which forms wormlike micelles known to have a simple Maxwell-type viscoelasticity. We inject air through the fluid and observe the elastic and viscous deformation of the fluid around the bubble. The brittleness of the bubble burst on the fluid surface is characterized by visualizing the elastic strain by the birefringence technic and by measuring the bursting sounds.

Keywords: Viscoelasticity, magma, bubble

©2021. Japan Geoscience Union. All Right Reserved.

Role of lithology in deformation mechanisms of shallow-crustal active faults: Evidence from the Nahan thrust of Himalayas

*Dyuti Prakash Sarkar[1], Jun-ichi Ando[1], Kaushik Das[1], Gautam Ghosh[2], Prabir Dasgupta[3]

1. Hiroshima University, 2. Presidency University, 3. Durgapur Govt. College

Research on deformation nature and fault rock geochemistry of shallow-crustal active faults has been widely studied for elucidating the stress accommodation mechanisms and response to the fault movement in terms of stress localizations, fault weakening, and earthquake nucleation. The heterogeneous nature of the fault in response to tectonic stresses is also reported by few researchers. The current study is focused on Nahan Thrust (NT), a shallow-crustal thrust fault within the Main Frontal Thrust (MFT) sheet of the Himalayan Fold Thrust belt. In the present study, we have attempted to elucidate the nature of deformation mechanisms inferred from detailed field mapping of the fault zone, microstructural observation, and characterization of deformation mechanisms. In the studied area, NT has developed within the alternation of quartz-rich and phyllosilicate-rich siltstone of the Paleogene Dagshai Formation. It forms a wide brittle fault zone with a damage zone of 110 m and a fault core of 40 m. The damage zone of NT shows dominantly brittle deformation with an increasing degree of brecciation toward the fault core. The fault core shows several layers of chaotic breccia-grey gouge and foliated red gouge with a single layer of black gouge ~1 m (forming black gouge). Calcite vein fragments present with the damage zone rocks and fault core show the development of deformation twins, which suggests a deformation temperature of ~170 ℃. The modal mineral analysis of the intact and gouge rocks, determined in conjunction with SEM-BSE, EPMA, and image processing by ImageJ software, as well as the obtained XRD patterns from intact and gouge rocks indicate that the formation of different gouges within the fault core is dependent on the intact rocks. Based on the microstructural observations, the quartz-rich intact rock has dominantly deformed by fracturing and cataclasis with minimum effects of fluid alteration (if any) during the fault activity. The phyllosilicate-rich layer, however, has exhibited pervasive alteration and generation of finer phyllosilicates, with deformation dominantly by pressure solution mechanisms. The phyllosilicate-rich layers also act as sealing zones, localizing stress and subsequent stress buildup within the quartz-rich layers, thereby narrowing the active zone of the fault during subsequent fault activity. Additionally, grain size analysis of the gouge rocks by ImageJ, and their XRD patterns indicate the presence of amorphous material in the black gouge. The presence of amorphous materials is also evident from Transmission Electron Microscopy (TEM) analysis of the black gouge. The black gouge in the studied area is, therefore a product of co-seismic frictional heating, indicated by the presence of amorphous materials, gas escape structures, and clay clast aggregates.

Keywords: NT, Fault gouge, CCA, Calcite e-twins

©2021. Japan Geoscience Union. All Right Reserved.

Study of the mobile granular layer in bedload transport by laminar shearing flow in a tilted channel

*Chong-Wei Hong[1], Franco Tapia[2], Pascale Aussillous[3], Élisabeth Guazzelli[4], Chi-Yao Hung[1]

1. Department of Soil and Water Conservation, National Chung Hsing University, Taichung, Taiwan, 2. Department of Mechanical Engineering, Tokyo University of Agriculture and Technology, Tokyo, Japan, 3. Aix-Marseille Université, CNRS, IUSTI, Marseille, France, 4. Université de Paris, CNRS, Matière et Systèmes Complexes (MSC) UMR 7057, Paris, France

Erosion is a natural phenomenon which moves materials from the earth's surface thanks to a shearing fluid, and has a significant effect on the morphodynamics of river beds. When sands and rocks are transported, this process is hard to clarify since we can only observe the surface motion. Following previous work to investigate experimentally the mobile layer of a granular bed due to a shearing fluid flow we use a refractive index matching technique. The experimental setup consists of a rectangular channel partially filled with particles as shown in the figure. We use index-matched combinations of spherical hydrogel particles and a mixture of water, citric acid, and ucon oil to control the hydrogel particles diameter (which have swelled in the fluid) and the fluid viscosity. The tube is tilted, between 20 deg and 40 deg, and we impose an upward fluid flow thanks to a pump, which ensures a stationary regime. Indeed, the upper layers of particles are transported upstream due to the fluid shearing flow whereas the granular bed tends to slide down due to gravity. Both particle and fluid velocity profiles are obtained using particle image velocimetry. The experimental results are compared with a two-phase continuum model having frictional rheology to describe particle-particle interactions. By varying the viscosity of the fluid, we study the influence of inertia while staying in a laminar regime. We also focus on the role of the elasticity of the particles on the frictional rheology.

Keywords: granular media, particle/fluid flow, sediment transport

©2021. Japan Geoscience Union. All Right Reserved.

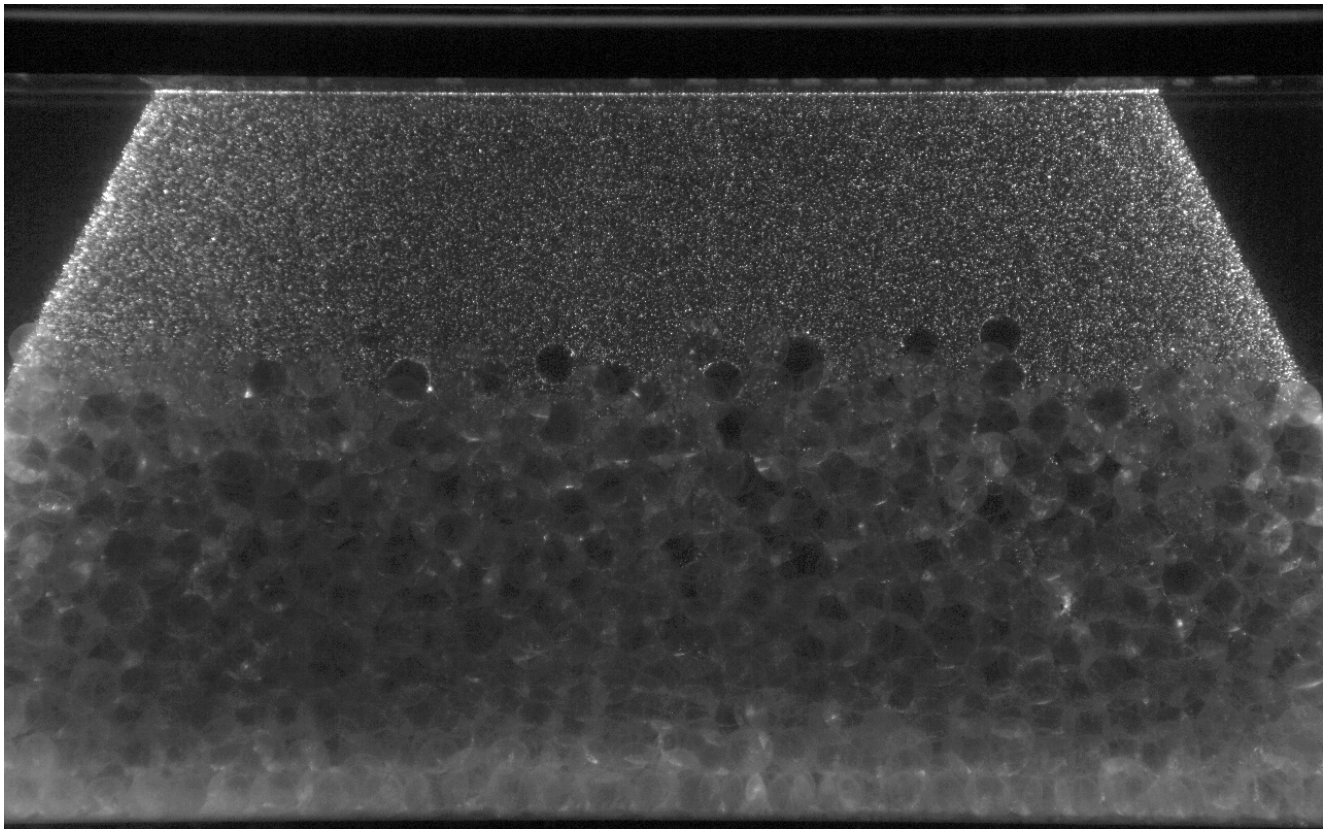

©2021. Japan Geoscience Union. All Right Reserved.

Fracture behavior of silicate network phase-separating from aqueous fluid

*Takehito Koyama[1]

1. Institute of Industrial Science, the University of Tokyo

Assuming the crustal structure with “actively-shrinking” lower crust of silicate network phase-separating from aqueous fluid below “passively-deformed” upper crust of usual rocks, I tried to explain the crustal activities including the intra-crustal seismicity in the short time scale and the crustal stabilization from its compaction in the long time scale (Koyama, JpGU 2019, JpGU-AGU2020, JPS2020, AGU2020). One of the important problems in the deformation of the “active” lower beneath the “passive” upper is the strength of the lower-crustal network solid filled with the fluid, because the fluid pressurized into cracks in rocks can weaken the rocks through inducing the fracture, which is a known fact (Hubbert and Rubey, 1959; Michaelske, 1982).
This fluid effect promotes mechanically and chemically fracture of crustal rocks: In the case of aqueous fluids, H_2O can slide the cracks through opening the impermeable crack walls with the pressure (Hubbert and Rubey, 1959) and can propagate the crack tips through disconnecting the bonds of the rock materials around there with the chemical reactions (Michaelske, 1982). These must result from the contact between the two materials originating from their different thermodynamic states, which create their impermeable interface for their counter pressures and their chemical potential gradient for their mutual dissolution around the interface.
Then, how do the fluid effect arises in the fluid-solid coexistence in the same single thermodynamic state? Phase separation between shrinking amorphous network solid and diffusing fluid realizes this situation (Tanaka, 2000, 2017; Koyama, 2009, 2018); In phase separation between shrinking silicate network and diffusing aqueous fluid, the question is whether the fluid effect on the network fracture are the same with the case of the contact between fluid and rock from different origin or not. I expect to be not, because thermodynamic relation between H_2O and SiO_2 in the phase separation is the opposite from that in the above fluid-rock contact: In the two coexisting phases from the same origin the pressure is common between them and the fluid can diffuse through the network, and chemical potential gradient demixing them in the phase separation, on the other hand, must prevent the reactions for network dissociation. Thus, the counter pressure and the crack tip propagation by the fluid must be difficult to arise on the coexisting network: The fluid must be difficult to weaken the network.
If these are true, the network coexisting with the fluid in the lower crust can keep its strength under the fluid-filled situation. On the other hand, the fluid diffusing from the shrinking lower-crustal network can weaken the usual upper-crustal rocks as a result of its permeation from the crustal lower to the upper. Thus, we can consider the possibility that the lower-crustal network is stronger than the upper-crustal rocks, and that the “actively-shrinking” former deform the latter one-sidedly.

Keywords: Fracture, Silicate netowrk, Aqueous fluid, Phase separation or phase demixing

©2021. Japan Geoscience Union. All Right Reserved.

Evolution of patterns of hydraulically conductive natural fractures during inelastic deformation of rocks

*Nikita Dubinya[1,2]

1. Moscow Institute of Physics and Technology, 2. Schmidt Institute of Physics of the Earth of the Russian Academy of Sciences

The study is focused on spatial orientations of hydraulically conductive natural fractures existing in rock masses subjected to varied stresses. Fluid conductivity of natural fractures is a serious issue in various fields as the opportunity to predict it is essential for such problems as assessing risks in underground infrastructure engineering or unconventional hydrocarbon reservoirs development. This problem is complicated as the inner structure of rock masses is often unknown with limited sources of information regarding it.

The current study is focused on establishing the relationship between deformation of naturally fractured rock samples and spatial orientations of hydraulically conductive fractures existing in them. Only geomechanical aspect of the problem is taken into account in the current study with other factors being outside of its scope.

The study is based on the results of series of laboratory experiments. A series of triaxial tests have been carried out using cylindrical samples of naturally fractured rocks. These samples were saturated and subjected to external stresses. Typical deformation curves –interrelationships between components of stress and strain tensors –were obtained for varied conditions. These dependencies proved to be nonlinear, so the results have been consequently analyzed through the concept of non-associated plastic flow law: a mathematical model to establish stress-strain relationship has been constructed. Plastic hardening resulting into varied elastic moduli and friction angle was taken into account within this model. The constructed model made it possible to estimate the preferable directions of natural fractures propagation during inelastic stage of rock deformation as the planes of optimally oriented fractures evolve alongside with friction angle. As a result, the constructed model made it possible to predict the statistics on spatial orientations of developed natural fractures in a rock sample subjected to inelastic deformation.

Nevertheless, this statistics itself is not enough to predict fluid conductivity of the developed natural fractures. Critically stressed fractures concept was used to analyze, which of the fractures existing in the rock are hydraulically conductive, and which are not. According to this concept, hydraulic conductivity of a natural fracture is governed by the relationship between normal and shear stress acting on its surface. There is an analytical solution providing spatial orientations of all fractures that are hydraulically conductive for a given arbitrary stress tensor. This solution is valid if critically stressed fractures concept is true and hydraulic conductivity of natural fractures is governed solely by relationship between stresses. Other cases are not within the scope of the current study. Application of the mentioned solution to the obtained statistics on spatial orientations of natural fractures existing in the rock sample may provide insights regarding the changes in hydraulically conductive natural fractures patterns caused by evolution of stress-strain state of naturally fractured rock mass. Laboratory experiments were analyzed with this technique: each stage of deformation process was characterized by such factors as current spatial orientations of all developed natural fractures alongside with spatial orientations of hydraulically conductive fractures; changes in relative number and total free surface of all developed fractures and hydraulically conductive fractures and so on.

©2021. Japan Geoscience Union. All Right Reserved.

The proposed approach of treating naturally fractured rock masses may be used for solving various problems. In the current study an example of such application is considered from the perspective of hydrocarbon reservoir development: the proposed approach made it possible to predict changes in fluid conductivity of natural fractures existing in oil reservoirs during various operations related to reservoir development.

Keywords: Plastic hardening, Critically stressed fractures, Non-associated flow rule

©2021. Japan Geoscience Union. All Right Reserved.

Theoretical study on rock anelasticity; Extension of a grain-boundary sliding model to two dimensions

*Mitsuyoshi Kunugihara[1], Yasuko Takei[1]

1. Earthquake Research Institute,The University of Tokyo

Rock anelasticity has a significant effect on seismic velocity and attenuation structure in the upper mantle. However, experiments are difficult and data are limited. Therefore, theoretical approaches to rock anelasticity are important. Existing experimental data indicate that grain boundary sliding is one of the major mechanisms of rock anelasticity under upper mantle conditions (e.g., Jackson & Faul, 2010; Takei et al., 2014). A model of grain boundary sliding was developed by Raj & Ashby (1971). Their model is a quasi-one-dimensional model that deals with the sliding between two elastic blocks with interlocking nonplanar boundary. When the amplitude of the nonplanarity is small, they analytically obtained the effective shear modulus and attenuation as functions of frequency. Their model successfully reproduced the seamless transition of a polycrystalline material from elastic, through anelastic, to viscous body with decreasing frequency. Morris & Jackson (2009) introduced a minute quantity ε to represent the amplitude of the nonplanarity, and reformulated the model of Raj & Ashby (1971) more rigorously using the perturbation method. In these previous quasi-one-dimensional models, the base state only represents the relaxation of shear stress applied to a single planar grain boundary, and does not represent the real grain boundary in a polycrystalline material where both normal and shear stresses act. In addition, the previous models predict the existence of a large peak on the high-frequency side, but experimental results using polycrystalline olivine (Jackson & Faul, 2010) and rock analogs (Takei et al., 2014) do not show such a peak. In this study, we develop a two-dimensional model for grain boundary sliding in a polycrystalline material. By modeling with a more realistic geometry, the base state reflects self-locking at the mineral grain scale, and hence we can consider atomic-scale steps along the grain boundary in the first order perturbation. For a quantitative prediction of the peak amplitude, it is important to consider a granular aggregate interlocked both at mineral grain scale and atomic scale.

In this study, we obtain the shear modulus and attenuation of a two-dimensional polycrystalline material with arbitrary grain shape as functions of frequency. Using the perturbation method proposed by Morris & Jackson (2009), we first solve for the case where the grain shape is a perfect circle as the base state. The general solution of the elastic displacement field and stress field of a circle was obtained by Love (1927). By adding boundary conditions for grain boundary diffusion and grain boundary viscosity, we can obtain the displacement and stress fields of a grain in the presence of matter diffusion and grain boundary sliding. For a grain of arbitrary shape deviating from the circle, the approximate solution depending on the detailed grain shape can be obtained analytically by using the perturbation method. So far, we have obtained the base state solution and found that it has the viscoelastic properties of the Burgers model. In the next step, we plan to obtain solutions up to the first order perturbation.

Keywords: anelasticity, grain-boundary sliding, seismic attenuation

©2021. Japan Geoscience Union. All Right Reserved.

A DEM model of uniaxial and triaxial compression test of rocks

*Mikito Furuichi[1], Daisuke Nishiura[1], Yuzuru Yamamoto[2]

1. Japan Agency for Marine-Earth Science and Technology, 2. Kobe University

The Discrete Element Method (DEM) is a fundamental simulation method to investigate solid earth dynamics. A simple friction model between the contacting particles is known to simulate the behavior of the sand layer which is the scaled analog model of accretionary prism formation. However, to simulate the mechanical behavior of rocks in such DEM-based geoscience simulation, we have to extend the model to support the bonding model between the particles. Here, we present the parametric study and technique to reproduce the uniaxial and triaxial compression test of rocks sampled in the Hota accretionary complex. Our model based on the ratios of tensile to compressive strength can reproduce essential behaviors of non-linear failure envelopes. We will discuss the role of bonding parameters in the normal and tangential direction in the pre-and post- failure processes.

Keywords: DEM, Compression test of rocks, Accretionary prism

©2021. Japan Geoscience Union. All Right Reserved.

Relaxation of the frictional force in a statistical mechanical model of magnetic friction

*Komatsu Hisato[1]

1. National Institute for Materials Science

Magnetic friction, the frictional force caused by the magnetic interaction between materials, is studied in recent years to investigate the microscopic mechanism of the friction. As part of these studies, we previously proposed a statistical mechanical model of magnetic friction obeying the Dieterich-Ruina law in the steady state with sufficiently weak external force(Komatsu 2019). This law is a well-known empirical law observed in the usual solid surfaces, so our previous study implies that the analogy between the magnetic and usual frictions exists.
In this presentation, we investigate the behavior of the magnetic friction in the non-steady state using a model similar to our previous one. Specifically, we consider a chain moving on the edge of a two-dimensional lattice, and let each lattice point of them have one spin variable interacting with each other. The chain is combined with a spring, and the other edge of the spring moves with a constant veocity v.
We investigate the responce of the frictional force to the sudden change of v by the numerical simulation. If the time scale of the spin relaxation is slower than that of the chain motion, the relaxation of the frictional force is divided into two processes: the sudden change accompanied by that of v called direct process, and the slow relaxation after that called indirect process. This behavior resembles that observed in the usual solid surfaces. In the case of the usual solid surfaces, it is said that these two processes result from the creep motion of the materials. In the case of our model, on the other hand, this behavior is caused by the slow relaxation of the magnetic structure. Hence, the change of the magnetic structure of our model has a similar role to the creep motion of usual solid surfaces.

Keywords: friction, magnetic materials, statistical mechanics

©2021. Japan Geoscience Union. All Right Reserved.

[J] Poster | M (Multidisciplinary and Interdisciplinary)：M-IS Intersection

Sat. Jun 5, 2021 5:15 PM - 6:30 PM JST | Sat. Jun 5, 2021 8:15 AM - 9:30 AM UTC | Ch.21_3

[M-IS12] Planetary Volcanology

convener:Rina Noguchi(Faculty of Science, Niigata University), Nobuo Geshi(Geological Survey of Japan, The National Institute of Advanced Industrial Science and Technology), Tomokatsu Morota(Department of Earth and Planetary Science, The University of Tokyo)

Volcanoes exist on solid planetary surface across the solar system. They tell insight into the interior, and the surface environment when they were formed and subsequent evolution. Recent high-resolution remote sensing data on extraterrestrial body allows us to analyze on outcrop scales. Now we are on the stage to share the research targets beyond fields of general volcanology and planetary science. Because some geomorphological and geological environments in other planets are similar to those on Earth, research on volcanic geomorphology and geology on Earth will provide good terrestrial analogues to understand planetary volcanology. The aim of this session is to discuss formation history and mechanism of volcanoes across the solar system.

[MIS12-P01] Review of duration and spatial heterogeneity of mare volcanism on the Moon

*Tomokatsu Morota[1] (1.Department of Earth and Planetary Science, The University of Tokyo)

[MIS12-P02] **Possible existence of lava tube cave and pit/fissure cave in the Moon and Mars**

*Tsutomu Honda[1] (1.Vulcano-speleological Society)

[MIS12-P03] Geomorphological and geological study of the summit caldera of Olympus Mons on Mars.

*Mayuko Nakamura[1], Tomohiro Tsuji[1] (1.Division of Earth Science The Graduate School of Sciences and Technology for Innovation , Yamaguchi University)

[MIS12-P04] The extent of shallow underground water-ice in the Amazonian period on Mars inferred from the distribution of rootless cones

*Rina Noguchi[1] (1.Institute of Space and Astronautical Science, Japan Aerospace Exploration Agency)

Review of duration and spatial heterogeneity of mare volcanism on the Moon

*Tomokatsu Morota[1]

1. Department of Earth and Planetary Science, The University of Tokyo

Unraveling the duration and spatial activity of mare volcanism on the Moon is fundamental to understand the thermal evolution of small terrestrial planets. Lunar mare basalts, which are the most common volcanic features on the Moon, cover 17% of its total surface area. We have investigated the eruption ages and volumes of mare basalts and the relationship between mare distribution and crustal thickness using geological and geophysical data obtained by the SELENE (Kaguya) and recent lunar missions. In this talk, we will review the results and discuss the thermal evolution of the Moon.

Keywords: Moon, Mare volcanism, Lunar dichotomy

©2021. Japan Geoscience Union. All Right Reserved.

Possible existence of lava tube cave and pit/fissure cave in the Moon and Mars

*Tsutomu Honda[1]

1. Vulcano-speleological Society

[Introduction]

There is a large number of lava tube caves(~150) on the foot of Mt. Fuji, though there are also some fissure/pit crater caves(~4)[1,2]. It is also thought that the lava tube cave is preponderant because of the vast lava flow on the Moon and the Mars, but the possibility of the existence of the fissure/pit crater cave cannot be denied. We compared the lava tube cave such as Banba ana cave and fissure/pit crater cave such as Kaminari ana cave on Mt.Fuji, then, examined the possible existence of fissure/pit crater caves on the Moon and Mars.

[Comparison of lava tube cave/Banba ana cave and fissure cave/Kaminari ana cave]

As shown in Fig. 1 and 2, horizontal cavities communicate with the vertical hole for both caves.
Banba ana cave has,under the32m-deep vertical hole. a tubular cavity of length of 1 km. Banba ana cave is formed in Futagoyama/Anmoyama lava flow erupted from the fissure vent of Futagoyama. Banba ana cave has lava shelves, ropy lava flow, and lava stalactite inside of the tubular cavity, indicating the characteristics of a typical lava tube cave(Photo 1). The obtained lava yield strength $f_B=H(\rho g \sin\alpha)/4$ of $3.4x10^3$ to $6.8x10^3$Pa for the slope angle:4.8˚and for the tube height 5m to 10m,is a reasonable value as a basalt.
Kaminari ana cave was formed in Kansuyama lava flow under with the vertical hole depth of 10 m. Kaminari ana cave has a horizontal fissure cavity of height of 3m to 6m with a width of 7m. it is a part of the fissure/pit vent. In the fissure/pit cavity of Kaminari ana cave, a scoria layer can be seen behind the collapsed side wall of the fissure cavity at the bottom (Photo 2). This cavity can be regarded as a fissure cave created by draining back of magma.

[Possibility of pit/fissure vent cave on the Moon/Mars]

The cavity height($H=4f_B/(\rho g \sin\alpha)$) as a lava tube cave is estimated for the vertical holes of the Moon and Mars[3,4,5]. For Lacus Mortis Pit in the Moon, the estimated tube height as the lava tube cave deviates greatly in comparison to the vertical hole depth (estimated tube height 2.5 m~9.8 m for a vertical hole depth of 112 m), so the cavity could be a pit/fissure cave where magma is drained back[3]. As for Arsia Mons on the Mars[4], the estimated value for the vertical hole on the steep slope of Arsia Mons (slope angle 1.0˚~3.5˚) has a large deviation from the vertical hole depth, so that there is a possibility to be a pit/fissure cave. On the other hand, the vertical holes on the gentle slope on the foot of Arsia Mons (slope angle 0.12˚ to 0.54˚) show almost the same value as the estimated tube height, suggesting that a lava tube cave is likely to exist. Regarding Elysium Mons[5], for the vertical holes on the steep slope of Elysium Mons (slope angle ~6˚), the difference between the vertical hole depth and the estimated tube cavity height is large, so it may be a pit/fissure cave.

[Conclusion]

Exploration of the internal structure of the vertical hole in order to clarify how the cavity under the vertical hole of the Moon and Mars is necessary at first for understanding the igneous activity and for possible future use as human base. It is expected that the fissure/pit cave and the lava tube cave will clarify the eruption mechanism and the behaver of lava flow after the eruption. In any case, both the lava tube cave and fissure/pit cave will be possible as underground bases of the Moon and Mars in the future.

References:

[1]Takanori Ogawa (1991): Volcanic cave of Fujimiya, Fujimiya City Folk Museum, Fujimiya City Board of

©2021. Japan Geoscience Union. All Right Reserved.

Education, [2]Takanori Ogawa (1991): Volcanic cave at the southern foot of Fuji, Susono city Education Committee,
[3]Tsutomu Honda(2019): PPS08-P0 Cave height of lava tube cave under the vertical hole estimated from the surface topography of the Moon, Japan Geoscience Union 2019 Meeting, [4]Tsutomu Honda(2017): P117 Mars Possibility of Lava Tube Cave in Vertical Hole of Asia Mons, Japan Volcanic Society Autumn Meeting,[5]Tsutomu Honda(2018): SVC43-P02 Lava yield strength and possibility of lava tube cave below the vertical hole of Mars Elysium volcano, Japan Geoscience Union 2018 Meeting

Keywords: Lava flow, Lava tube cave, Pit cave, Moon, Mars

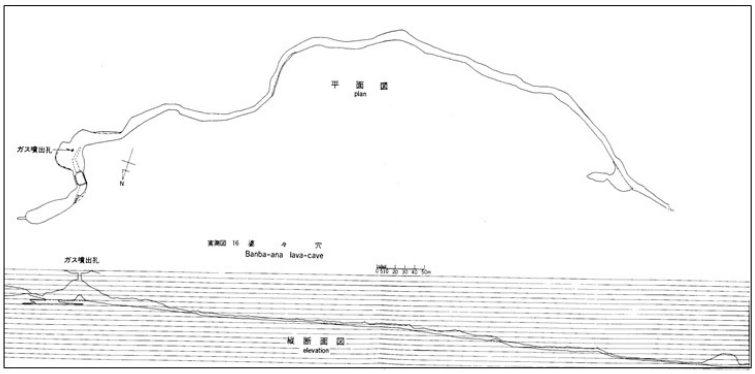

図1 婆々穴測量図(長さ621.2m部分,現在長さが1101.1mに更新)

写真1 婆々穴のチューブ状空洞の内部
©NPO法人火山洞窟学会

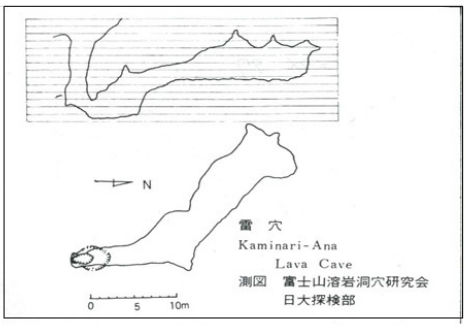

図2 雷穴測量図

写真2 雷穴の割れ目状空洞の内部©NPO法人火山洞窟学会

©2021. Japan Geoscience Union. All Right Reserved.

Geomorphological and geological study of the summit caldera of Olympus Mons on Mars.

*Mayuko Nakamura[1], Tomohiro Tsuji[1]

1. Division of Earth Science The Graduate School of Sciences and Technology for Innovation , Yamaguchi University

The Olympus Mons, located in the northwestern part of the Tharsis Highlands on Mars, is the largest volcano in the Solar System. It has a basal width of 840 ×640 km (Plescia, 2004), and an elevation of 21,241 m (MOLA DEM data). Olympus Paterae are located in the northern part of the summit and are divided into six calderas (Mouginis-Mark, 2019). In this research, we reconsider the formation of Hames Patera based on the geological and morphological study. The Hermes Patera, located in the center of the western part of Olympus Paterae, has diameters of ~40 km. It could be divided into the western (Hermes Patera-1) and the eastern patera (Hermes Patera-2)(Fig. 1. Hermes Patera-1 and 2).
The floor of Hermes-Patera-2 is ~ 200 m deeper than that of Hermes Patera-1. The boundary of them is a north-south-strike cliff in the central area of the Patera recognized by a 10 m-interval topographic map that has been recognized as a wide ridge by Mouginis-Mark (2018). The elevation of the east side of the cliff is ~200 m lower than that of the west side. This landform constitutes a cliff topography with a dense concentration of contour lines on the 10 m interval contour map. The cliff shows an arc shape that curves northeast-trend at the north and southeast-trend at the south end of the cliff. The entire floor of the western part slopes toward the east. In contrast, the eastern floor is circular and slopes toward the northeast. The eastern shows a circularly enclosed topography, it is necessary to consider the different landforms of the western and eastern parts. Consequently, it is necessary to consider different collapses in Hermes Patera-1 and 2. The cliffs deserve the Hermes Patera-2 caldera rim. In addition, circumferential graben (Zuber and Mouginis-Mark, 1992) are distributed in Olympus Patera. Above all, we Focus on the west of Zeus patera and the graben of Hera patera. This graben surrounding Hermes Patera-is divided in Graben-1 and 2 based on its circumferential curvature. The Graben-1 restricted to the floors of the Hera Patera (Fig. 1. Graben-1). It has a curvature that is subparallel to the western rim of the Hermes Patera-1. The Graben-2 exists along the eastern margin of Hermes Patera-2 (Fig. 1. Graben-2). It has a smaller curvature than Graben-1, and each one is smaller in size. These graben were cut by Hermes Patera-1 and 2, and don't extend to the subsequent collapse of Patera.
Patera and graben are considered to have been formed in the following formation order. Hermes Patera-2 shows a lower elevation than Hermes Patera-1, and thus Hermes Patera-1 considered to have subsidence before Hermes Patera-2. The first, Graben-1 formed on the floors of Hera Patera, which is the subsidence of Hermes Patera-1. Subsequently, Hermes Patera-2 did subsidence of the caldera floors. Graben-2 formed on the floors of Zeus Patera, which is the subsidence of Hermes Patera-2. It can be estimated that these graben were formed at the same time as Hermes Patera-1 and 2 on the geological time scale. Therefore, we need to reconsider Hermes Patera-1n the present proposed formation sequence of the Olympus Patera.

Keywords: Mars , Caldera, Planetary Volcano

©2021. Japan Geoscience Union. All Right Reserved.

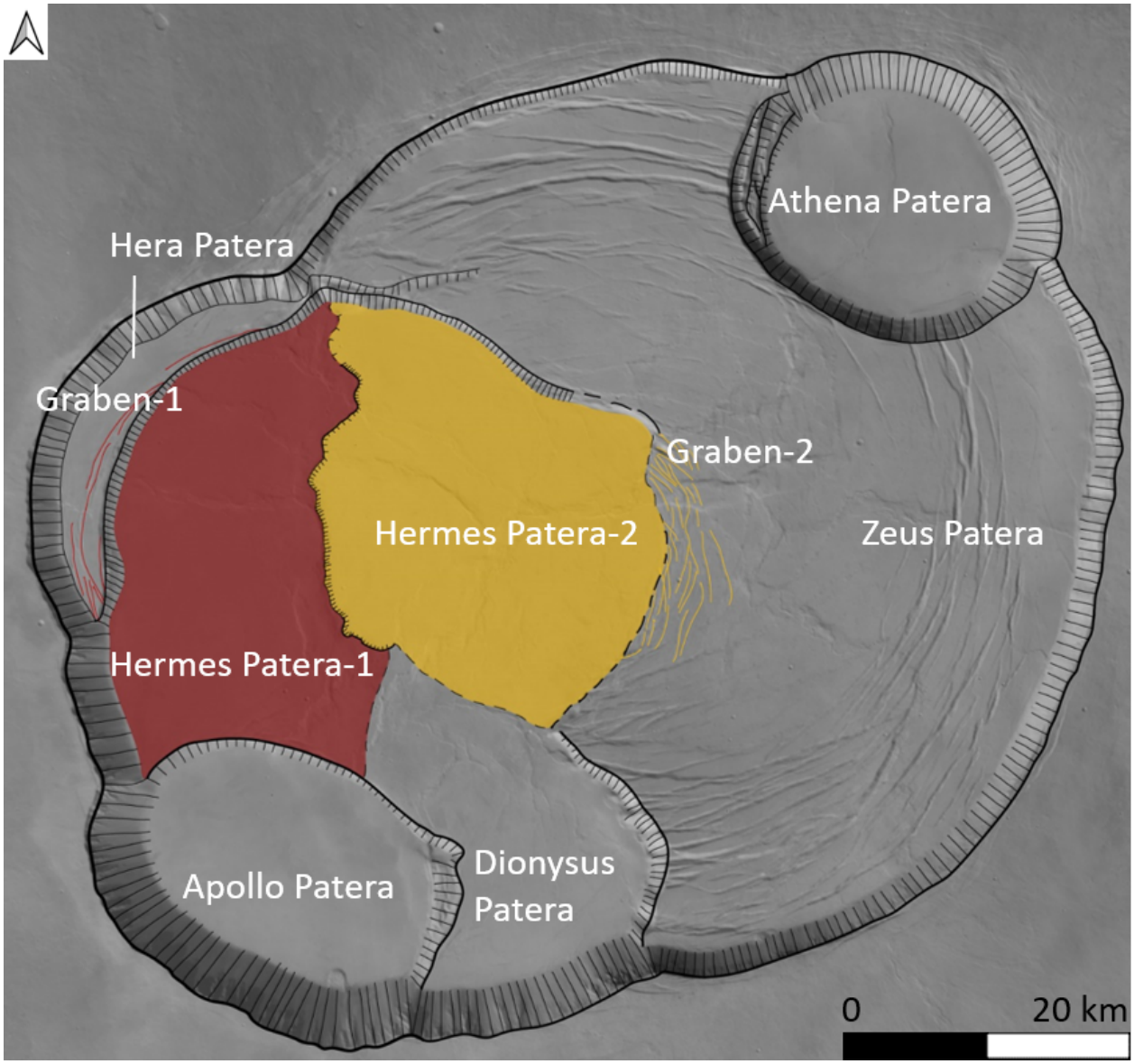

©2021. Japan Geoscience Union. All Right Reserved.

The extent of shallow underground water-ice in the Amazonian period on Mars inferred from the distribution of rootless cones

*Rina Noguchi[1]

1. Institute of Space and Astronautical Science, Japan Aerospace Exploration Agency

On Mars, volcanism in the Amazonian period is characterized by the emplacement of flood lava, contrasting to that of Noachian and Hesperian that built large shield volcanoes (e.g., Keszthelyi et al., 2006). Previous studies have found conical mounds on Amazonian lava flows which have been considered to be possible rootless cones (e.g., Greeley and Fagents, 2001; Fagents and Thordarson, 2007; Keszthelyi et al., 2010). Rootless cones are formed by intermittent explosions that occurred by the interaction of lava and water (ice)-logged sediments (Thorarinsson, 1953). Thus, the existence of rootless cones suggests not only volcanic activity but also the presence of water-ice in the shallow subsurface. Possible rootless cone fields have been described in several places. According to Fagents and Thordarson, 2007, candidates of rootless cone fields are mapped in Amazonis Planitia, Olympus Mons aureole, Acidalia Planitia, S. Utopia Planitia, Isidis Planitia, Hephaestus Fossae, Elysium Planitia, Cerberus, Marte Valles, and Arrhenius. Most of the fields are located in low-mid latitudes of the northern lowland plains. Since this mapping was based on studies before 2000 with low-resolution images, those rootless cone fields are uncertain and should be revised with higher resolution images. In the presentation, I update and summarize possible rootless cone fields on Mars, and discuss the extent of groundwater-ice in Amazonian.

Keywords: Mars, rootless cone, ground water-ice

©2021. Japan Geoscience Union. All Right Reserved.

[J] Poster | M (Multidisciplinary and Interdisciplinary)：M-IS Intersection

Sat. Jun 5, 2021 5:15 PM - 6:30 PM JST | Sat. Jun 5, 2021 8:15 AM - 9:30 AM UTC | Ch.22_1

[M-IS14] Aqua planetology

convener:Yasuhito Sekine(Earth-Life Science Insitute, Tokyo Institute of Technology), Takazo Shibuya(Japan Agency for Marine-Earth Science and Technology), Hidenori Genda(Earth-Life Science Institute, Tokyo Institute of Technology), Keisuke Fukushi(Institute of Nature & Environmental Technology, Kanazawa University)

This proposed session covers a wide range of topics related to aqua planetology, including chemical reactions involving water on planetary bodies, water-rock reactions within planetesimals, distribution of water in the early Solar system and the origin of water on terrestrial planets, hydrological and biogeochemical processes on Earth, geochemical cycles and habitability on Mars and icy moons, exploration of water in the solar system, and theory to understand how to build a habitable aqua planet.

[MIS14-P01] Experimental study of hypervelocity impact penetration of asteroids into the Ocean and benthic cratering

*Manabu Nishizawa[1] (1.Japan Agency for Marine-Earth Science and Technology)

[MIS14-P02] Experimental study on the growth process of iron rind in Fe-oxide concretions

*Hiroyuki Okamura[1], Sin-iti Sirono[1] (1.Department of Earth and Planetary Sciences, Nagoya University)

[MIS14-P03] Redox change by coseismic water-rock reactions in the interior of planets

*Takehiro Hirose[1], Ryoichi Nakada[1], Keishi Okazaki[1], Takazo Shibuya[1] (1.Japan Agency for Marine-Earth Science and Technology)

[MIS14-P04] Characterizations of mineralogy and infrared spectra of serpentinized samples in Oman ophiolite along with redox gradients in subsurface: Toward identification of redox gradients in Martian subsurface

*Takumi Sato[1], Yasuhito Sekine[1], Ikuo Katayama[2] (1.Tokyo Institute of Technology , 2.Hiroshima University)

[MIS14-P05] Experimental study of element dissolution to liquid CO_2 from artificial seawater and hydrothermal vent chimney

*Kaito Seo[1,2], Takazo Shibuya[2], Kosuke Fujishima[3], Ken Takai[2], Masaru Tomita[1,4] (1.Graduate School of Media and Governance, Keio Univ., 2.JAMSTEC, 3.ELSI, 4.IAB, Keio Univ.)

[MIS14-P06] Rocognition and classification of Martian chaos terrains using imagery marchine learning: Implications for groundwater distribution and hydrological cycles

Hiroki Shozaki[2], *Yasuhito Sekine[1], Nicholas Guttenberg[1] (1.Earth-Life Science Insitute, Tokyo Institute of Technology, 2.Dept. Earth Planetary Sci., Tokyo Institute of Technology)

[MIS14-P07] No effective oxychloride formations on Europa's surface inferred from UV/electron irradiation experiments onto salt-ice mixtures

*Shuya Tan[1], Yasuhito Sekine[1], Takashi Kikuchi[2], Hisayuki Suematsu[2], Tetsuya Hama[3], Yoshio Takahashi[4] (1.Earth-Life Science Institute, Tokyo Institute of Technology, 2.Nagaoka University of Technology, 3.Komaba Institute for Science, The University of Tokyo, 4.Department of Earth and Planetary Science, Graduate School of Science, The University of Tokyo)

[MIS14-P08] An experimental study on evaporite formation around the north pole of Titan

*Eito Hirai[1,2], Yasuhito Sekine[2], ZHANG NAIZHONG[2] (1.Department of Earth and Planetary Sciences, School of Science, Tokyo Institute of Technology, 2.Earth-Life Science Institute, Tokyo Institute of Technology)

[MIS14-P09] **Prediction of the composition of the primordial ocean just after its formation**

*Hisahiro Ueda[1], Takazo Shibuya[1] (1.JAMSTEC)

[MIS14-P10] **Formation conditions of magnetite and hematite in Sheepbed mudstone and bioavailable energies in lake water-groundwater mixing zone in Gale crater, Mars**

*Sakiko Kikuchi[1], Takazo Shibuya[1] (1.Japan Agency for Marine-Earth Science and Technology)

[MIS14-P11] Measurements of elastic wave velocity of mafic and ultramafic rocks below the freezing point: Consideration about reflectivity due to ice-water phase transition in Mars

*Haruna Wakabayashi[1], Ikuo Katayama[1] (1.Hiroshima University)

[MIS14-P12] Viscosity of aqueous MgSO4 solutions at high-pressure and low-temperature: implications for icy satellites

*Shunsuke Nozaki[1], Seiji Kamada[2,3], Akio Suzuki[2] (1.Division of Earth and Planetary Materials Science, Faculty of Science, Tohoku University , 2.Department of Earth Science, Graduate School of Science, Tohoku University, 3.Frontier Research Institute for Interdisciplinary Sciences, Tohoku University)

[MIS14-P13] Formation mechanism of spherical concretions in Tatsukushi area: Possible analogy with spherical nodule in Gale crater, Mars

*Saki Asai[1], Hitoshi Hasegawa[1], Hidekazu Yoshida[2], Minoru Ikehara[1], Nagayoshi Katsuta[3], Masakazu Nara[1], Yui Tomonao[1], Satoru Imai[4] (1.Kochi University, 2.Nagoya University, 3.Gifu University, 4.Tosashimizu GeoPark)

[MIS14-P14] Synthesis and reversible redox properties of iron-saponite

*Hiroshi Sakuma[1], Koki Morida[2], Keisuke Fukushi[2], Yoshio Takahashi[3], Natsumi Noda[3,4], Yasuhito Sekine[4], Kenji Tamura[1] (1.National Institute for Materials Science, 2.Kanazawa University, 3.University of Tokyo, 4.Tokyo Institute of Technology)

[MIS14-P15] Physical dependence of stable carbon and hydrogen isotopic ratio of methane gas in gas hydrate

*Kushi Kudo[1], Atsushi Tani[1], Keita Yamada[2], Naohiro Yoshida[3] (1.Graduate School of Human Development and Environment, Kobe University, 2.Department of Chemical Science and Engineering, School of Materials and Chemical Technology, Tokyo Institute of Technology, 3.Earth–Life Science Institute)

[MIS14-P16] **Clumped isotope signatures of abiotic methane formed via Fischer-Tropsch catalysis and their implications**

*ZHANG NAIZHONG[1], Yasuhito Sekine[1], Mayuko Nakagawa[1], Naohiro Yoshida[1] (1.Tokyo Institute of Technology)

[MIS14-P17] Possibilities of the rubidium stable isotope ratio as geochemical tools

*Rimi Konagaya[1], Hiroyuki Tsuboi[1], Takaaki Itai[1], Yoshio Takahashi[1] (1.The University of Tokyo)

[MIS14-P18] **Determination method of ^{13}C-labeled isotopomer ratio of dissolved organic acids by GC-MS analysis**

*Konomi Suda[1] (1.National Institute of Advanced Industrial Science and Technology)

[MIS14-P19] **Selectivity coefficient of Na^+-NH_4^+ exchange in saponite interlayer: Reconstruction of ammonium concentration in early ocean on Ceres**

*Hiroto Tokumon[1], Keisuke Fukushi[2], Yasuhito Sekine[3], Kosuke Inoue[1], Koki Morida[1] (1.Kanazawa University , 2.Institute of Nature and Environmental Technology Kanazawa University, 3.Tokyo institute of

technology)

Experimental study of hypervelocity impact penetration of asteroids into the Ocean and benthic cratering

*Manabu Nishizawa[1]

1. Japan Agency for Marine-Earth Science and Technology

The hypervelocity (measured in km/s) impact of extraterrestrial bodies in the marine environment is more common than that on land because ~70% of the Earth's surface is covered by oceans. Seafloor cratering is important for recording Earth's impact history, driving environmental, biotic, and climatic perturbations by ejecting crustal materials into the atmosphere (e.g., the K–T boundary event); impactors can also affect the fate of extraterrestrial organic matter and may have been key components of primitive life on early Earth (the so-called panspermia hypothesis). Herein, we simulated the oceanic hypervelocity impacts of asteroids in a laboratory to derive a scaling relationship for benthic cratering. The results are reported for experimental hypervelocity impacts of chondrite and other projectiles (olivine, stainless-steel, polycarbonate) on a water-covered iron target. In situ observations of 5-km/s impacts quantify the deceleration of projectiles in the water column by shock-induced deformation and fragmentation. The minimum water depths at which multiple craters appeared on the benthic target were two and four times the projectile diameter for chondrite and stainless steel, respectively. Based on the observed deceleration of projectiles in water, the cratering efficiency of a benthic target for a given impact velocity is predicted to follow an exponential decay law in terms of water depth normalized by projectile diameter (H/d), given by $\pi v \propto \exp(-(H/d)/\kappa)$, when a projectile of original mass collides with the target. Comparing the volume of the largest crater in the experiments and that derived from the scaling relation, mass ratios of the largest projectile fragment to original projectile in the 5-km/s impact were calculated to be 0.1–0.3 (H/d = 2–6) and 1.0 ±0.3 (H/d = 5.5) for chondrite and stainless steel, respectively. Using the scaling relationship, the volume of the transient crater on oceanic crust by an asteroid impact is estimated to be smaller than previously predicted by hydrocode simulation when the asteroid fragmentation in the water column controls seafloor cratering. Our results suggest that deformation and fragmentation of asteroid impactor control the water depth conditions that enable benthic cratering.

Keywords: Oceanic impact, scaling relation, chondrite

©2021. Japan Geoscience Union. All Right Reserved.

Experimental study on the growth process of iron rind in Fe-oxide concretions

*Hiroyuki Okamura[1], Sin-iti Sirono[1]

1. Department of Earth and Planetary Sciences, Nagoya University

Introduction

The Navajo Sandstone in Utah, U.S.A. and the Gobi Desert in Mongolia have geological formations containing Fe-oxide concretions. They are several mm to cm in size and have spherical shape. The surface is covered with a rind of iron and the interior is filled with sandgrain. An analog of Fe-oxide concretion was discovered on Mars by NASA's Opportunity rover. Fe-oxide concretions form only under limited conditions. Therefore, identification of the formation process of Fe-oxide concretions on Earth will lead to clarification of the ancient environment of Mars. In 2018, a research group at Nagoya University proposed a new model for the formation of Fe-oxide concretions on the Earth. The hypothesis is that Fe-oxide concretions were originally $CaCO_3$ concretions. They were replaced by iron through processes including (1) dissolution and (2) precipitation due to neutralization reactions with iron rich acidic groundwater (Yoshida et al., 2018). However, the growth rate and width of the iron rind have not been clarified in this model.

Objectives

The purpose of this study is to generate artificial Fe-oxide concretions and to measure the (1) growth rate (infiltration, precipitation, and dissolution rate) and (2) width of the iron rind.
Based on geological evidence, the formation process of Fe-oxide concretions on Earth can be applied to one on Mars. Thus, this study will provide clues to the ancient environment of Mars.

Methods

We used artificial $CaCO_3$ concretions that made by kneading $CaCO_3$ powder, glass beads with the same particle size as desert sand (150-180 μm), and distilled water. Also, groundwater was simulated with $FeCl_2$ solution (Molarity=1.07 [mol/l]). We fixed an artificial $CaCO_3$ concretion in a Petri dish and simulated the environment where groundwater with iron ion reacts with the $CaCO_3$ concretion. We set a sample on a fixed-point imaging system that we made ourselves.

Results and Discussion

We investigated the relationship between width of rind and time. We analyzed width of a rind on 300 images. The results showed that the solution rapidly penetrated the $CaCO_3$ concretion (about 5.2×10^{-4} [mm/s]) in five minutes, and the width slowly grew (about 3.4×10^{-7}[mm/s])(Fig.1). This indicates that the iron rind grows through the processes of (1) penetration, (2) dissolution, and (3) precipitation. We describe the relationship between natural $CaCO_3$ concretions and artificial $CaCO_3$ concretion. We performed the same experiment with the moisture content of the concretion set to 0[%] in another preliminary experiment. A thicker iron rind was formed than in this experiment. From the above, It is expected that the porosity (in artificial $CaCO_3$ concretions, moisture content) determines the penetration rate and width of rind. Porosity of natural $CaCO_3$ concretions is about 10.2[%]. It is technically difficult to reproduce this porosity in artificial $CaCO_3$ concretions. We will create an artificial $CaCO_3$ concretion with a feasible porosity about 15-25 [%] and calibrate the porosity, penetration velocity and width of rind. We use this as a basis for correcting the results of this experiment and can derive the penetration rate and width of rind for a porosity of 10.2 [%]. This mean that it is possible to estimate the reaction of natural $CaCO_3$ concretions. Also, The existence of a penetration process means that we need to consider a "dissolution from the part where the solution has finished penetration " model, rather than the traditional "dissolution from the surface" model.

©2021. Japan Geoscience Union. All Right Reserved.

Conclusion

We have succeeded in experimentally photographing the growth of the iron rind over time. As a result, we discovered a new process, " penetration " that was not previously hypothesized. We propose to incorporate the effects of penetration into numerical calculations and formation processes. In the future, we will conduct similar experiments by varying the soil concentration and moisture content. In addition, elemental mapping will be created using SXAM.

References

Yoshida et al., (2018) Fe-oxide concretions formed by interacting with carbonate-acidic waters on Earth and Mars. Sci. Adv. 4:eaau0872. doi:10.1126/sciadv.aau0872

Keywords: Fe-oxide concretion, CaCO3 concretion

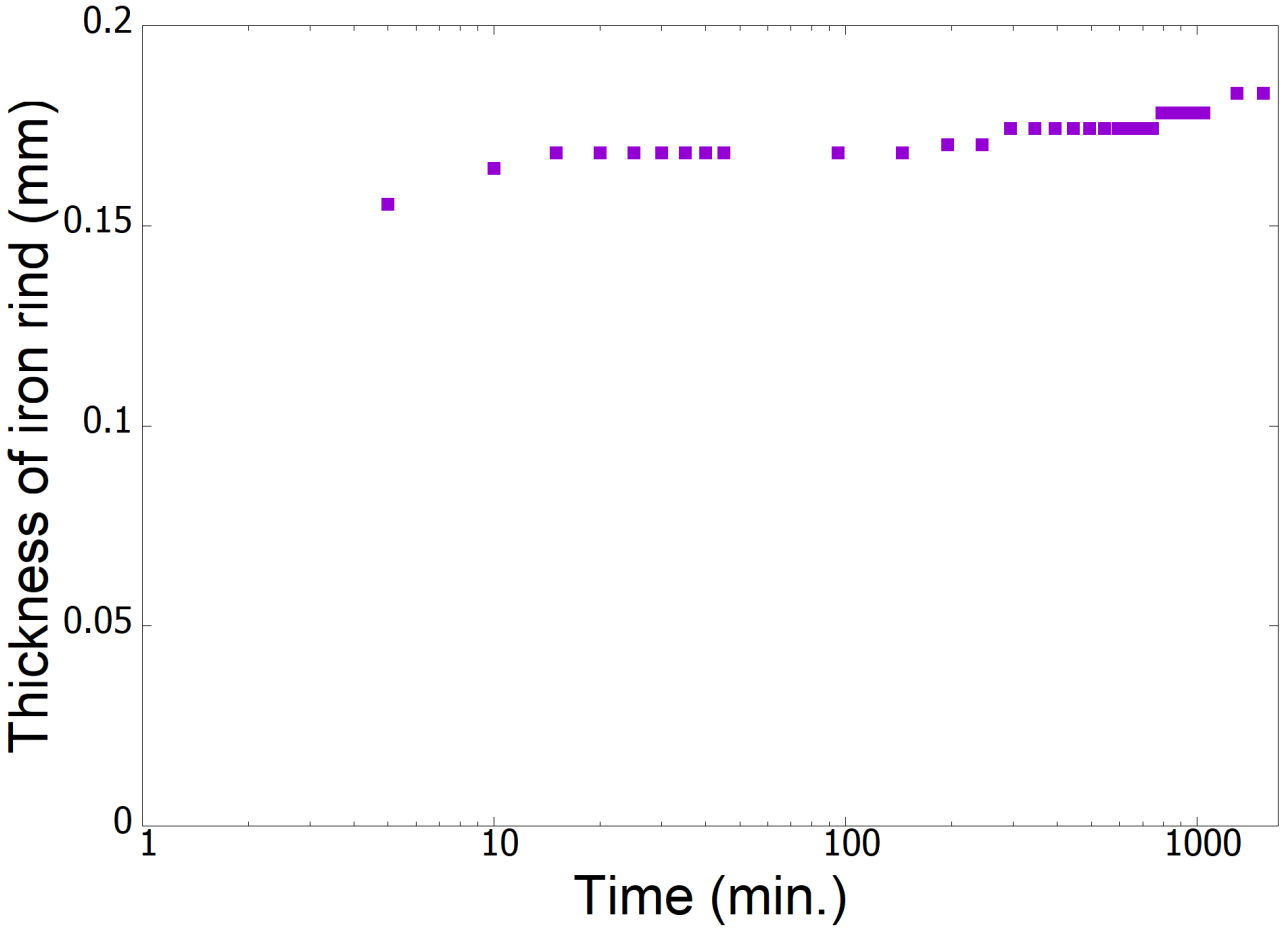

©2021. Japan Geoscience Union. All Right Reserved.

Redox change by coseismic water-rock reactions in the interior of planets

*Takehiro Hirose[1], Ryoichi Nakada[1], Keishi Okazaki[1], Takazo Shibuya[1]

1. Japan Agency for Marine-Earth Science and Technology

An earthquake releases elastic energy stored in the planets. The stored energy is dissipated mostly as a heat, which facilitates coseismic water-rock reactions along a fault and eventually changes in redox conditions in the planets. In this study we have reproduced earthquake faulting by laboratory friction experiments and determined redox change within a simulated fault by X-ray absorption near edge structure (XANES) analysis, in order to explore a hypothesis that the coseismic water-rock reactions could provide a potential metabolic energy for life on the planets.

Friction experiments have performed on San Carlos olivine powder with grain sizes of 100~180 μm and on clay-rich décollement materials from the Nankai Trough plate boundary using a rotary shear apparatus at Kochi/JAMSTEC. Earthquake faulting was reproduced at slip velocity of 1.0 m/s with different displacements of 2.6~18 m under normal stress and fluid pressure conditions of 30 and 25 MPa, respectively. After the experiments, the specimens were thin-sectioned to observe microstructures under FE-SEM and to determine how the ($Fe^{2+}/\Sigma Fe$) and ($S^{0}/\Sigma S$) ratios change with input shear energy by the XANES analyses using the BL27SU at SPring-8.

On the olivine specimen the mean value of $Fe^{2+}/\Sigma Fe$ in the fault zone decreases from 0.68 to 0.59 (i.e. oxidization) as increasing shear energy from 0 to ~34 MJ/m^2. In contrast, on the décollement specimen the $Fe^{2+}/\Sigma Fe$ ratio tends to increase with shear energy from 0.48 at 0 MJ/m^2 (starting material) to 0.51 at ~3.2 MJ/m^2 (i.e. reduction). However, the décollement specimen contains sulfide minerals (S^{-2}) in which the $S^{0}/\Sigma S$ increases from ~0.3 to 0.09 as increasing shear energy to ~3.2 MJ/m^2 (i.e. oxidization). Thus, both specimens oxidized during rapid coseismic faulting in several seconds. This is likely attributed to the reactions between minerals and water, that is enhanced by the formation of tens-nanometer-size minerals with fresh reactive surfaces by rapid faulting. Particularly in the olivine experiments with high shear energy inputs, frictional heat transforms liquid water into supercritical state, promoting the oxidization reactions. If seismicity in the planets could be monitored, the proposed correlation between the shear energy (equivalent to earthquake magnitude) and the oxidation progress enables us to estimate the quake-induced redox change in the interior of planets.

Keywords: earthquake, redox change, water-rock interaction

©2021. Japan Geoscience Union. All Right Reserved.

Characterizations of mineralogy and infrared spectra of serpentinized samples in Oman ophiolite along with redox gradients in subsurface: Toward identification of redox gradients in Martian subsurface

*Takumi Sato[1], Yasuhito Sekine[1], Ikuo Katayama[2]

1. Tokyo Institute of Technology , 2. Hiroshima University

Mars would have possessed liquid water on the surface, at least temporally, in late Noachian to early Hesperian in a dense CO2 atmosphere. In addition to surface water, groundwater is highly likely to have been abundant and interacted with mafic rocks that consisted of Martian crust. Hydrological cycles between these endmember waters would have generated redox and pH gradients in the subsurface, through vertical mixing of acidic, oxidizing surface water with alkaline, reducing groundwater. On Earth, chemoautotrophic life can live in the redox and pH gradients generated in subsurface. Thus, identifications of redox states of (sub)surface rocks on Mars through remote sensing is critical to select landing sites and to collect promising samples for microbial life in future missions to Mars. In this study, we aim to characterize mineralogical compositions and infrared spectra of serpentinized Semail Ophiolite, Oman, along with redox and pH gradients in the subsurface. Semail Ophiolite consists of basalt, gabbro, and upper mantle ophiolite, which are exposed on the surface. Oxidizing surface water infiltrates into the subsurface where in-situ serpentinization proceeds, generating steep redox and pH gradients. This geohydrological setting allows this area as a promising terrestrial analog of aqueous alterations in particular areas on Mars where ultramafic, olivine-rich rocks are exposed (e.g., Nili Fossae). We used core samples (Hole BA1B) from an area of active serpentinization of the Semail Ophiolite, drilled during the ICDP Expedition 5057 and stored at Hiroshima Univ. SEM-EPMA, XRD, and FTIR analyses were performed for the core samples. Based on mineralogical and chemical compositions of the samples, we classified core samples based on alteration stages. In the stage 1 (160–350 m in depth), samples contain unaltered minerals, e.g., olivine and diopside, and, thus, serpentinization was proceeding. The samples also contain secondary minerals of serpentine and brucite. Water chemistry of pore water at these depth were measured on site previously and reported as alkaline and reducing. The samples in the stage 1 exhibit characteristic steep slopes at 0.8–1.5 μm in infrared reflectance spectra. In the stage 2 (30–100 m in depth), serpentinization has completed without unaltered olivine or diopside. The samples are predominantly composed of serpentine and brucite. According to previous study, water chemistry of pore water was reported as alkaline and moderately oxidizing. The infrared spectra of the stage-2 samples have moderate slopes at 0.8–1.5 μm. In the stage 3 (10–30 m in depth), the samples are composed mainly of serpentine with trace Mg/Fe smectite. Fe(III) oxides appear in veins in the samples. These suggest alterations with high water-to-rock ratio with oxidizing surface water. Pore water was reported as highly oxidizing. The infrared spectra of the stage-3 samples have moderate slopes at 0.8–1.5 μm with absorption features at 1.4 and 1.9 μm owing to smectite. In the stage 4 (< 10 m in depth), the samples contain serpentine together with Mg/Fe smectite, Fe(III) oxides, and carbonate. Owing to the secondary minerals other than serpentine, the color of the samples was whitish red. The infrared spectra of the stage-4 samples have gentle slopes at 0.8–1.5 μm with clear absorption features at 1.4 and 1.9 μm. Our results show that we can distinguish the alteration stages of core samples solely based on infrared features (namely, slope gradient at 0.8–1.5 μm and absorptions at 1.4 and 1.9 μm). According to a previous microbiological study at the Semail Ophiolite site, methanogens and acetogens were found in depth of the stage 1 (and 2). Reflectance spectra features resembling to those of the stage 1 can be found in Nili Fossae regions on Mars, suggesting the importance of this area as a future landing site.

©2021. Japan Geoscience Union. All Right Reserved.

Keywords: Serpentine, Mars, Redox gradients

©2021. Japan Geoscience Union. All Right Reserved.

Experimental study of element dissolution to liquid CO_2 from artificial seawater and hydrothermal vent chimney

*Kaito Seo[1,2], Takazo Shibuya[2], Kosuke Fujishima[3], Ken Takai[2], Masaru Tomita[1,4]

1. Graduate School of Media and Governance, Keio Univ., 2. JAMSTEC, 3. ELSI, 4. IAB, Keio Univ.

Pools of carbon dioxide (CO_2) fluid have been found under the ocean floor in the vicinity of a few hydrothermal vent sites (Sakai et al., 1990; Konno et al., 2006; Lupton et al., 2006; Pedersen et al., 2010; Zhang et al., 2020). CO_2 fluid acts as hydrophobic solvent under a certain range of temperature and pressure due to its non-polar property (Hyatt, 1984). Because various hydrophobic compounds such as organometallic complex, amides, alcohols, carboxylic acids and phenols can dissolve into CO_2 fluid (Škerget et al., 2011; Knez et al., 2018), the pools of CO2 fluid have the potential to behave as a distribution and condensation field for those compounds. Indeed, Stensland et al., (2019) suggested that heavy metals are transported to shallower part of a water column by upwelling of CO_2 hydrate released from CO_2 pools and hydrothermal vents.

Even in the Hadean ocean, liquid/supercritical CO_2 is presumed to have acted as a solvent for hydrophobic molecules and elements related to origin of life and as a reaction field providing condensation, and as reaction field (Shibuya and Takai, 2017, Zhang et al., 2020). Despite utilization in industrial technologies such as extraction, dry cleaning, and homogenization, particularly in the form of supercritical CO_2 (Beckman, 2004), geochemical roles of CO_2 fluid in natural environments are poorly understood.

In this study, we developed a corrosion-resistant high-pressure reactor and extraction/analytical methods of CO_2 fluid. Then, we experimentally simulated distribution of major elements in artificial seawater and heavy metals included in hydrothermal vent chimney samples to liquid CO_2. As a result, dissolution of major elements; Na, Mg and heavy metals; Cu, Mg, Zn, and etc., were observed from artificial seawater and hydrothermal vent chimneys, respectively. The results suggest that transition metals and the elements in boron group (Al, Ga, In, Tl) form complexes with CO_2. We will further discuss about implications of modern and Hadean hydrothermal systems.

Keywords: liquid CO2, elemental distribution, hydrothermal vent, origin of life, Hadean eon

©2021. Japan Geoscience Union. All Right Reserved.

Rocognition and classification of Martian chaos terrains using imagery marchine learning: Implications for groundwater distribution and hydrological cycles

Hiroki Shozaki[2], *Yasuhito Sekine[1], Nicholas Guttenberg[1]

1. Earth-Life Science Insitute, Tokyo Institute of Technology, 2. Dept. Earth Planetary Sci., Tokyo Institute of Technology

Water activities have played central roles in the environmental evolution on Mars, through creating landforms and secondary minerals, driving geochemical cycles, and possibly supporting life. Knowledge on the distribution and activities of groundwater is critical in the hydrology, the habitability, and in-situ resource utilization for future manned missions. Chaos are fractured depressions that consist of broken blocks and locate on sources of outflow channels. Some of chaos are interpreted to have been formed through outbursts of groundwater triggered by melting of ground ice; thus, they can be clues to understand the distribution and activities of groundwater. On the other hand, other chaos may have been formed through an inflation-deflation of a magma chamber without water activities. A large number of chaos and chaos-like features have been found on Mars. However, the formation mechanisms of these chaos remained uninvestigated.

Here, we perform recognition and classification of chaos based on the formation mechanisms using imagery machine learning. We developed neural network models (i.e., classifiers) to classify chaos formed by water activities (called as water-related chaos), chaos formed by volcano-tectonic activities (called as volcano-tectonic chaos), and non-chaos surface features (e.g., valleys, plains, and craters) using remote-sensing data of chaos previously investigated. Our developed classifiers can recognize chaos and non-chaos surface features with ~97% of test accuracy and can classify water-related chaos and volcano-tectonic chaos with ~95% of test accuracy.
By applying our classifiers to a large number of unclassified chaos, we found two types of chaos terrains on Mars. One is hybrid chaos terrains, in which water-related chaos and volcano-tectonic chaos coexist in one terrain, and the other is water-dominant chaos terrains, in which water-related chaos are predominant. Hybrid chaos terrains are mainly found in the circum-Chryse outflow channels region. Based on our geomorphic analyses, hybrid chaos terrains would have formed through a combination of upwelling of magma and consequent melting of ground ice. The groundwater from the hybrid chaos terrains formed outflow channels and supplied water to water-dominant chaos terrains in the downstream. Water-dominant chaos terrains are mainly located near the dichotomy boundary. The locations of water-dominant chaos terrains coincide with the proposed regions of upwelling of groundwater on ancient Mars. The locations of water-dominant chaos terrains can be potential landing sites for future missions, where frozen ancient groundwater may be available near surface.

Keywords: Mars, hydrological cycles, machine learning

©2021. Japan Geoscience Union. All Right Reserved.

No effective oxychloride formations on Europa's surface inferred from UV/electron irradiation experiments onto salt-ice mixtures

*Shuya Tan[1], Yasuhito Sekine[1], Takashi Kikuchi[2], Hisayuki Suematsu[2], Tetsuya Hama[3], Yoshio Takahashi[4]

1. Earth-Life Science Institute, Tokyo Institute of Technology, 2. Nagaoka University of Technology, 3. Komaba Institute for Science, The University of Tokyo, 4. Department of Earth and Planetary Science, Graduate School of Science, The University of Tokyo

Recent observations of Europa's surface suggest that chlorides (e.g., NaCl, $MgCl_2 \cdot nH_2O$) exist on Europa's geologically active chaos regions (Fischer et al., 2015; Ligier et al. 2016). Europa's surface is irradiated by high-energy particles, such as electrons, and solar UV light. These irradiations would cause the oxidation of surface materials due to dissociation of H_2O ice and subsequent escape of H_2 into space. Through the irradiation, chlorides on the surface could be oxidized to form oxychlorides, such as chlorates (e.g., $Mg(ClO_3)_2 \cdot 6H_2O$) or perchlorates (e.g., $NaClO_4$, $Mg(ClO_4)_2 \cdot 6H_2O$) (e.g., Johnson et al., 2019). However, the oxidation reactions have been poorly investigated based on laboratory experiments.
Here, we perform laboratory experiments to investigate formation of oxychlorides on Europa. We irradiated ~10-keV electron or UV light onto mixtures of H_2O ice and chlorides at temperatures of ~120 K using a newly-developed irradiation experimental system. In addition, we irradiated MeV electron onto mixture of H_2O ice and chlorides using an electron-beam accelerator, ETIGO-III (Tokuchi et al., 1998). Our results show no significant formations of ClO_4 and ClO_3 from chlorides regardless of the experimental conditions. The upper limits of conversion efficiency from NaCl to $NaClO_4$ are estimated in our experiments. The estimated upper limits of conversion efficiency are 10^{-19}–10^{-20} /electron. Considering the upper limits of conversion efficiency, together with the fluxes of electrons or photons on Europa (Paranicas et al., 2009; Clare et al., 2012), an upper limit abundance of $NaClO_4$ are estimated as less than ~2 mol% relative to H_2O ice over Europa's surface age (30–100 Myr). Our experimental results and estimations suggest that oxychlorides are minor components as salts and oxidants on Europa's surface.

Keywords: Europa, Irradiation experiment, Perchlorate

©2021. Japan Geoscience Union. All Right Reserved.

An experimental study on evaporite formation around the north pole of Titan

*Eito Hirai[1,2], Yasuhito Sekine[2], ZHANG NAIZHONG[2]

1. Department of Earth and Planetary Sciences, School of Science, Tokyo Institute of Technology, 2. Earth-Life Science Institute, Tokyo Institute of Technology

Through the Cassini-Huygens mission, 5 μm-bright deposits are found at dried lakebeds and along paleo-shorelines of the north pole regions of Titan, which are inferred as organic evaporites (Barnes et al. 2009, 2011).

Evaporites on Titan can be formed when dissolved organic matter in liquid methane lakes is concentrated and precipitated upon drying (Barnes et al. 2009, 2011). Thus, they could be a proxy indicator of arid climates through effective evaporation of liquid methane. In addition, evaporative condensation promotes syntheses of complex organic molecules on Titan.

The previous study (Cordier et al. 2013) suggested that the main components of evaporites would be acetylene and butane solids based on results of photochemical calculation of precipitation rates of organic solids in Titan atmosphere (Lavvas et al. 2008).

However, spectral features of evaporites resembles to benzene and cyanoacetylene solids, rather than acetylene and butane solids (Clark et al. 2010).

Given that organic aerosols may be composed of PAHs, such as benzene, and nitriles, such as cyanoacetylene, dissolution of benzene and nitriles from organic aerosols by liquid methane could explain the enrichments of these molecules in evaporates on Titan. Nevertheless, there is no experimental study that investigates the solubility of organic aerosol analogs by liquid methane.

Here, we construct laboratory experimental system that can investigate interactions between organic aerosol analogues, called Titan tholin, and liquid methane. We developed a stainless-steel liquid methane generator that can keep liquid methane through controlling temperature inside the chamber. After immersing Titan tholin into liquid methane in the generator, dissolved species in liquid methane are analyzed with a gas chromatograph.

Keywords: Titan, Liquid methane, Evaporites, Organic aerosols, Tholin

©2021. Japan Geoscience Union. All Right Reserved.

Prediction of the composition of the primordial ocean just after its formation

*Hisahiro Ueda[1], Takazo Shibuya[1]

1. JAMSTEC

Hadean is an enigmatic period in the Earth's history when ocean formation and the emergence of life occurred. However, minimal geological evidence is left from this period. Regarding the ocean in the early Earth, previous research indicates that seawater had weak acidity (pH 4–7) because the carbon dioxide concentration in the atmosphere was high compared to that today (e.g., Walker, 1985; Grotzinger and Kasting, 1993; Macleod et al., 1994), or it was strongly acidic (pH 1–2) because a large amount of halogen substance in the high-temperature vapor atmosphere eventually dissolved into seawater (Maruyama et al., 2013). Previously, pH, CO_2 concentrations, and other elements were considered (Morse and Mackenzie, 1988) but these estimations did not provide information about the quantitative chemical compositions of seawater. To understand the primordial ocean's composition, we focused on the ocean's formation processes from CO_2- and HCl-bearing water vapor in the high-temperature atmosphere. When the temperature of the lower atmosphere fell below the critical point, high-temperature rain reached the ground surface. Then, hydrothermal reactions between the subcritical fluid and primordial crust started. Eventually, a liquid ocean emerged on the completely altered crust as the temperature decreased to approximately 25 ˚C until the ocean's temperature stabilized. Here, we conducted two experiments and modeling simulating the reactions between hypothetical primordial crustal rock (basalt or komatiite). The results indicate that the primordial ocean was mildly acidic and rich in CO_2, Mg, and Ca relative to Na, irrespective of the rock type, which is different from the modern equivalents. Therefore, unlike the present seawater, the primordial seawater could have been carbonic, bitter, and harsh rather than salty. The ocean's composition started to evolve once plate tectonics began on Earth.

Keywords: primordial ocean composition, ocean formation, water-rock reactions, Hadean, experiment

©2021. Japan Geoscience Union. All Right Reserved.

Formation conditions of magnetite and hematite in Sheepbed mudstone and bioavailable energies in lake water-groundwater mixing zone in Gale crater, Mars

*Sakiko Kikuchi[1], Takazo Shibuya[1]

1. Japan Agency for Marine-Earth Science and Technology

The Sheepbed mudstone of Yellowknife Bay, Gale crater was interpreted as an ancient habitable environment, based on its detailed mineralogical and geochemical composition analyses. However, the energetic availability for metabolic reactions is poorly constrained. Here, we propose the possible mixing of surface water and groundwater that (i) explains the formation of magnetite and hematite detected in Sheepbed mudstone and (ii) works as a potential habitable zone for aerobic Fe^{2+}-oxidizing microbes. Our thermodynamic modeling of water–rock reactions revealed that the formation of abundant Fe-rich saponite in Sheepbed mudstone may occur under various conditions of water-to-rock mass ratios, temperatures (5–300ºC) and initial fluid compositions (O_2/H_2+CO_2-bearing and gas-free fluids). In contrast, the formation of magnetite and hematite in the mudstone can be explained only by the mixing of Fe^{2+}-rich groundwater and oxygenated surface water, where the Fe^{2+}-rich groundwater can be generated by the low-temperature water–rock reactions with a CO_2-bearing initial fluid. The calculated free energy yield of aerobic Fe^{2+} oxidation in the fluid-mixing zone on Mars is similar to that estimated for a fluid-mixing zone on Earth actually inhabited by aerobic Fe^{2+}-oxidizing microbes. The findings will contribute to a better understanding of potential habitability on Mars.

Keywords: early Mars, saponite, bioavailable energy, water-rock reactions

©2021. Japan Geoscience Union. All Right Reserved.

Measurements of elastic wave velocity of mafic and ultramafic rocks below the freezing point: Consideration about reflectivity due to ice-water phase transition in Mars

*Haruna Wakabayashi[1], Ikuo Katayama[1]

1. Hiroshima University

It has been pointed out that a large amount of water existed on the surface of Mars in the past, and it is expected that life may have existed there. However, Mars is currently dry, with an average surface temperature of about -50 degrees Celsius, so water exists mainly as ice in the ice sheets and the deep underground cryosphere. On the other hand, the gravity of Mars is lower than that of the Earth, and rocks are less compressible. Therefore, Mars retains high porosity deep underground, and a phase transition from ice to water is predicted to occur underground from the heat flow rate. Therefore, in this study, we will measure the elastic wave velocity in the phase transition from ice to water in rocks, and verify whether water in the subsurface can be detected by seismic reflection surveys such as the InSight mission on Mars. Diabase, peridotite, and serpentinite which are considered to be the basement rocks of Mars, were used as samples to measure the elastic wave velocity. Elastic wave measurements were performed under dry, wet, and frozen conditions (-55˚C). In the measurements, the effect of porosity on elastic waves was examined. In order to examine the effect of porosity on elastic waves, thermal cracks were introduced into the samples. The porosity of the diabase was 0.14% at Intact, 0.55% at 600˚C and 1.17% at 800˚C. The porosity of the peridotite was 0.32% at Intact, 1.32% at 600˚C and 1.70% at 800˚C. Elastic wave velocities were calculated using the pulse transmission method by crimping a piezoelectric element with a resonant frequency of 2MHz to the sample. The elastic wave velocities of all rock samples decreased with increasing porosity, and increased as the pores were filled with water, with the highest velocities observed under frozen conditions. The Vp/Vs ratio was also calculated and showed a decreasing trend with increasing porosity in the dry condition, an increasing trend in the wet condition, and constant in the frozen condition. Using these results, the aspect ratio (short axis/major axis) of the voids was estimated from the effective medium theory (Kuster and Toksoz 1974), and the crack with aspect ratio of 0.01 is consistent with the experimental data. Using the results of this velocity measurement, we calculated the acoustic impedance and calculated the reflectivity at 5 km underground, where the ice-water phase transition is predicted to occur in the Martian subsurface. As a result, the reflectivity at the ice-water phase transition was 0.269 for diabase and 0.319 for peridotite. Thus, when the phase transition from ice to water occurs, high seismic wave reflectance is expected, and future seismic surveys on Mars may reveal the existence of water.

Keywords: Mars, Elastic wave velocity, Aspect ratio

©2021. Japan Geoscience Union. All Right Reserved.

Viscosity of aqueous MgSO4 solutions at high-pressure and low-temperature: implications for icy satellites

*Shunsuke Nozaki[1], Seiji Kamada[2,3], Akio Suzuki[2]

1. Division of Earth and Planetary Materials Science, Faculty of Science, Tohoku University , 2. Department of Earth Science, Graduate School of Science, Tohoku University, 3. Frontier Research Institute for Interdisciplinary Sciences, Tohoku University

Some icy satellites, such as Europa, Ganymede, Enceladus, and Titan, have a subsurface ocean under the thick crusts. Though transport properties are essential to discuss the fluid behavior in these subsurface oceans, there are few viscosity data within P-T conditions corresponding to the ocean. Because fluid viscosity is dependent on temperature, pressure, and concentration, understanding these relationships leads to a more accurate view of the subsurface ocean.

The viscosity data of 10 wt% aqueous magnesium sulfate solutions were measured using a diamond anvil cell (DAC). The solutions' viscosity was determined up to 1100 MPa in the temperature range from −10 to 40˚C from the falling sphere measurements with DAC by constructing apparatus with a rotating stage, microscope, and camera. The pressure was measured using the ruby fluorescence method (Piermarini et al., 1975), while the temperature was controlled by flowing cooling or warming water through the DAC. The obtained viscosity was in the range of 1−10 mPa s and showed high pressure dependence of viscosity as well as temperature-dependence. Assuming that the subsurface ocean is composed of 10 wt% magnesium sulfate and satisfies the high-pressure and low-temperature conditions of the ocean, the ocean's dynamic viscosity would be in the range from 1 to 10 mPa s in the pressure condition below 700 MPa, which is higher than the viscosity of Earth's seawater. Because viscosity affects convection, diffusion rate, chemical reaction rate, and flowing velocity through the seafloor, this property might change the predicted habitability and oceanic composition.

Keywords: Icy satellites, Subsurface ocean, Viscosity, Aqueous magnesium sulfate solution, Diamond anvil cell

©2021. Japan Geoscience Union. All Right Reserved.

Formation mechanism of spherical concretions in Tatsukushi area: Possible analogy with spherical nodule in Gale crater, Mars

*Saki Asai[1], Hitoshi Hasegawa[1], Hidekazu Yoshida[2], Minoru Ikehara[1], Nagayoshi Katsuta[3], Masakazu Nara[1], Yui Tomonao[1], Satoru Imai[4]

1. Kochi University, 2. Nagoya University, 3. Gifu University, 4. Tosashimizu GeoPark

On Earth, spherical carbonate ($CaCO_3$) concretions are widely recognized. Many of these concretions are centered on fossils, and thought to be formed by decaying of soft body organic matter as carbon source. On the other hand, carbonate concretions are also formed by inorganic precipitation of calcite-saturated groundwater in arid environment. In addition, Fe-oxide encrusted concretions are found both on Earth (Utah and Mongolia) and Mars (Meridiani Planum). Yoshida et al. (2018) proposed that Martian Fe-oxide concretions are formed by dissolution of pre-existing carbonate concretions. They further suggested that spherical-shaped nodules in Gale crater can also formed by similar process, although shape and size of the Gale nodules are more variable. Here we report that spherical and variable-shaped concretions in Tatsukushi area, western Kochi, whose shapes are resembling to Gale nodules. In order to understand formation mechanisms of concretions in Tatsukushi area, we performed analyses of X-ray CT scan, elemental mapping, and stable carbon and oxygen isotope on samples of variable shapes of concretion. The results reveal that large-sized spherical-shaped concretion can be formed by organic matter origin. In this presentation, we will discuss the similarity of both concretions in Tatuskushi area and Gale crater.

Reference

Yoshida, H., Hasegawa, H., et al. (2018). Fe-oxide concretions formed by interacting carbonate and acidic waters on Earth and Mars. *Science advances*, *4*(12), eaau0872.

Keywords: spherical concretion, organic matter origin, carbon isotope, Mars, Gale crater

©2021. Japan Geoscience Union. All Right Reserved.

Synthesis and reversible redox properties of iron-saponite

*Hiroshi Sakuma[1], Koki Morida[2], Keisuke Fukushi[2], Yoshio Takahashi[3], Natsumi Noda[3,4], Yasuhito Sekine[4], Kenji Tamura[1]

1. National Institute for Materials Science, 2. Kanazawa University, 3. University of Tokyo, 4. Tokyo Institute of Technology

Clay minerals widely distribute on the surface of Mars. In these clay minerals, (Fe,Mg)-smectites were commonly discovered and useful for understanding the history of Mars. The valence state of iron in smectite is one of the key properties to reveal the redox state at the smectite formation. It has been believed that the redox state can be revealed from the crystal structures of iron-rich smectite. In the smectite, ferrous (Fe^{2+}) ions fully occupy the octahedral sites, while the ferric (Fe^{3+}) can occupy only two third of the sites due to the charge balance. This difference should be identified from the X-ray diffraction (XRD) profile. From the XRD analysis, ferrous saponite can be an analogue of smectites discovered at Yellowknife Bay in Gale Crater [Chemtob *et al.*, 2015]. However, the natural iron saponite on the Earth can also explain the XRD pattern and surprisingly the most iron was characterized by ferric (Fe^{3+}) state [Treiman *et al.*, 2014]. A central question is whether the XRD analysis can provide the oxidation state on formation of smectite.

A hypothesis was proposed for the crystal structure of ferric iron-rich saponite [Treiman *et al.*, 2014]. The saponite was initially synthesized under reduced conditions and oxidized later. The oxidation may occur by the deprotonation from structural OH groups. If this is correct, the oxidation and reduction can occur reversibly without large deformation in the crystal structure. In this study, the reduction and oxidation of ferrian (ferric iron-rich) saponite were investigated to study the hypothesis.

Ferrian saponite was synthesized by the hydrothermal method similar to the method proposed for the synthesis of ferrous saponite [Baldermann *et al.*, 2014]. The precipitates were dispersed in ultrapure water for one to five days. These samples were analyzed by inductively coupled plasma optical emission spectrometry (ICP-OES), humidity-controlled X-ray diffraction (XRD), transmission electron microscopy (TEM), X-ray absorption fine structure (XAFS), and infrared spectroscopy.

The chemical composition of precipitates and their swelling behavior indicate that the precipitates are smectite. The crystal structure of synthesized samples is categorized to trioctahedral smectite which is characteristic to ferrous saponite, but the XANES and TEM-electron energy loss spectroscopy (EELS) analysis indicates that most iron is present as ferric iron. These results indicate that the smectite is ferrian saponite. The reduction treatment was conducted for the ferrian saponite for one hour. There is no difference in the XRD profile before and after the treatment, but about 40% of ferric ion was reduced to ferrous ion in the saponite. This reduction may be interpreted by the exchange of hydrogen in the crystal as proposed for the formation mechanism of natural ferrian saponite [Treiman *et al.*, 2014].

Our results indicate that the ferrian saponite preserves the oxidation state on formation in the crystal structure, and the redox state of iron ions can be changed without deformation in the structure.

References

©2021. Japan Geoscience Union. All Right Reserved.

A. Baldermann, R. Dohrmann, S. Kaufhold, C. Nickel, I. Leftofsky-Papst, M. Dietzel, *Clay Minerals*, (2014) **49**, 391-415.

S. M. Chemtob, R. D. Nickerson, R. V. Morris, D. G. Agresti, J. G. Gatalano, *J. Geophys. Res. Planets*, (2015) **120**, 1119-1140.

A. H. Treiman *et al.*, *Am. Mineral.*, (2014) **99**, 2234-2250.

Keywords: Smectite, Mars, Iron, Redox

©2021. Japan Geoscience Union. All Right Reserved.

Physical dependence of stable carbon and hydrogen isotopic ratio of methane gas in gas hydrate

*Kushi Kudo[1], Atsushi Tani[1], Keita Yamada[2], Naohiro Yoshida[3]

1. Graduate School of Human Development and Environment, Kobe University, 2. Department of Chemical Science and Engineering, School of Materials and Chemical Technology, Tokyo Institute of Technology, 3. Earth–Life Science Institute

Icy satellites have capability of having extra biota due to eruption of plume, which is consisted by sea ice particles including organic matter. The observation using Cassini clarified that this plume included hydrogen molecule (H_2), CO_2, methane (CH_4) and organic matter (e.g. Porco et al. 2006; Waite et al. 2006, 2009, 2017). Especially in plume gas species, methane (CH_4) is regarded as one of the candidate of signature of biological activity due to CH_4 formation reaction by methanogen. However, CH_4 gas in plume is consisted of not only microbial origin but also primitive and/or hydrothermal origin and this fact does not let CH_4 detection is sufficient for conclusion for existence of biological activity by microbe. Therefore, we consider that evaluation of the elementary process of CH_4 isotopic fractionation ($\delta^{13}C$ and δD of CH_4) via room experiment is important for isotopic observation of icy satellite in nearly future.

In this study, we focus on CH_4 hydrate which is reservoir to produce the plume (Kieffer et al. 2006; Kamata et al. 2019) and plan to evaluate isotopic fractionation with its formation. Isotopic fractionation with hydrate formation has been found at only δD of CH_4(liquid_water+CH_4: ~5‰; ice+CH_4: ~10‰) (P: 0–6 MPa) (Hachikubo et al. 2007; Lapham et al. 2012). In the case of condition of icy satellites, the pressure range is wider than of the Earth, and therefore we need to estimate isotopic fractionation.

We formed clathrate hydrate samples using hydrate formation equipment under the extreme environments, which can hold until 50 MPa. We lowered cell temperature from room temperature to 276 K, and then stirred CH_4 gas and pure water at 85 or 400 RPM stirring rotation speed to form hydrate sample. We inserted CH_4 gas at slightly higher pressure than the previous studies (4.4–9.7 MPa). We collected gas samples of primitive gas from CH_4 gas cylinder and remained gas samples from the high pressure cell after hydrate formation, and then we measured stable isotopic ratio ($\delta^{13}C$ and δD of CH_4) using GC-IRMS equipment. We used the working standard with $\delta^{13}C = -48.17$‰ and $\delta D = -178$‰ for isotopic measurement. Precision of $\delta^{13}C$ and δD value were estimated as 0.3‰ (n = 6, 1 σ) and 0.7‰ (n = 4, 1 σ), respectively, which were based on repeated analyses of the standards.

Results in isotopic measurements showed that the $\delta^{13}C$ value of remained gas phase was slight lower than of primitive gas phases ($|\varepsilon|$ ~1‰, which was almost same as a few previous studies) and became lower at higher pressure. This suggested that 1) $^{13}CH_4$ and $^{12}CH_4$ easily condensed into gas phase in hydrate and remained gas phase with clathrate hydrate formation, respectively, and 2) this condensation became stronger at higher pressure. On the other hand, results in the δD value of remained gas phase maximized at around 6–7 [MPa] (theoretical value). Hachikubo et al. (2007) reported that δD value of hydrate phase became lower than those of remained and primitive gas, and host–guest interaction did not cause the isotopic fractionation of δD. Furthermore, Casco et al. 2015 reported that CH_4 adsorption ratio and hydrate formation speed rapidly increased from 6 to 8 [MPa]. Above results and previous studies might suggest that isotopic fractionation of δD with hydrate formation was not caused by water molecule of host cage and CH_4 molecule, which had only H atom, was most easily taken at 6–7 [MPa]. Furthermore, results of remained gas phase showed that the $\delta^{13}C$ value and pressure of theoretical δD maxima

©2021. Japan Geoscience Union. All Right Reserved.

became lower at faster stirring rotation speed ($\delta^{13}C$ value at 85 and 400 [RPM]: $p < 0.05$, $n = 8$; pressure of theoretical δD maxima: 7.1 and 5.7 [MPa] at 85 and 400 [RPM], respectively). Since Wijayanti (2018) reported that stability and storage capacity of hydrate became higher at higher stirring rotation speed. Thus, above tendencies and previous study might suggest that faster stirring rotation speed caused stronger hydrate stability due to easiness of ^{13}C adsorption, and most easiness statement of only H atom having CH_4molecule adsorption easily occurred at lower pressure.

Therefore, we found that physical condition such as pressure and stirring rotation speed, which was concerned to flow velocity of internal ocean, might become important factor of effect of gas hydrate formation at icy satellites condition on transportation and release processes of CH_4 gas.

Keywords: gas hydrate, methane gas, icy satellite, stable isotope, isotopic fractionation, physical dependence

©2021. Japan Geoscience Union. All Right Reserved.

Clumped isotope signatures of abiotic methane formed via Fischer-Tropsch catalysis and their implications

*ZHANG NAIZHONG[1], Yasuhito Sekine[1], Mayuko Nakagawa[1], Naohiro Yoshida[1]

1. Tokyo Institute of Technology

Abiotic CH_4 has been widely observed in nature, such as in hydrothermal vents, springs and so on. However, our knowledge on pathways of their formation remains pool. The bulk isotopic compositions of CH_4, such as $\delta^{13}C$ and δD, are widely used as tracers for identifying the CH_4 formation processes. However, obvious defects are existent, such as partly overlapping of isotopic signatures for different CH_4 sources, difficulty in constraining CH_4 generated from two or more sources, suffering from post-processes and so on (Douglas et al., 2017). Very recently, CH_4 clumped isotope signatures have been regarded as helpful constraints to provide additional information on origins of natural CH_4 (e.g. Douglas et al., 2017; Young et al., 2017).

The clumped isotope refers to molecules substituted by two or more rare stable isotopes, e.g. $^{13}CH_3D$ and $^{12}CH_2D_2$, whose abundance relative to a random distribution is temperature dependent (Stolper et al., 2014). Therefore, the formation or bond reordering temperatures of CH_4 can be obtained if the clumped isotope signatures are presented at intra-species equilibrium. On the other hand, kinetic effect and secondary processes like mixing and diffusion, will introduce disequilibrium values, which can be used in identifying specific process/mechanism (Stolper et al., 2015; Young et al., 2017). Limited data derived from abiotic CH_4 synthesized by ruthenium (Ru) so far presented strongly depleted signals in both $\Delta^{13}CH_3D$ and $\Delta^{12}CH_2D_2$, and the mechanism has been explained by quantum tunneling effect, combinatory effect and/or kinetic effect (Young et al., 2017; Cao et al., 2019; Young, 2019). Nonetheless, a recent study on abiotic CH_4 samples from hydrothermal systems suggested near-equilibrium clumped signals, being attributed to bond reordering at local fluid temperatures (Labidi et al, 2020).

In this study, we will present the clumped isotopic signatures of laboratory produced abiotic CH_4 via series of gaseous FTT reactions, applying various experimental parameters and catalysts, such as Ni, Fe, Ru and Co. Both $\Delta^{13}CH_3D$ and $\Delta^{12}CH_2D_2$ values are analyzed by a 253 Ultra High Resolution Isotope Ratio Mass Spectrometer established in Earth-Life Science Institute (ELSI), Tokyo Institute of Technology, following the similar procedures described in Eldridge et al. (2019). Preliminary data presented similar depleted signal in $\Delta^{12}CH_2D_2$, both for Ni and Ru catalyzing reactions at 300-400 ˚C. The mechanism causing depleted clumped values in laboratory produced abiotic methane will be discussed based on our new results, as well as its implication in the natural abiotic CH_4 samples.

References: Douglas et al., 2017, Organic Chemistry; Eldridge et al., 2019, ACS Earth Space Chem.; Stolper et al., 2014, Geochim. Cosmochim. Acta.; Stolper et al., 2015, Geochim. Cosmochim. Acta.; Wang et al., 2018, Geochim. Cosmochim. Acta.; Young et al., 2017, Geochim. Cosmochim. Acta.; Cao et al., 2019, Geochim. Cosmochim. Acta; Young, 2019, Deep Carbon; Past to Present; Labidi et al., 2020, Geochim. Cosmochim. Acta

Keywords: Methane, Isotope, Clumped isotope

©2021. Japan Geoscience Union. All Right Reserved.

Possibilities of the rubidium stable isotope ratio as geochemical tools

*Rimi Konagaya[1], Hiroyuki Tsuboi[1], Takaaki Itai[1], Yoshio Takahashi[1]

1. The University of Tokyo

One of important aspects of molecular geochemistry is to develop new isotope tools of various processes by focusing on physico-chemical properties of elements from their atomic scales. There have been no studies so far on the isotope fractionation of rubidium (Rb) caused by Rb behavior during water-rock interaction, possibly due to general knowledge that the reactivity of Rb^+, or alkaline metal ion, is very low. This is not the case, however, if we think about its interaction with phyllosilicates. It has been clarified that cesium (Cs) is adsorbed on 2:1 type phyllosilicates as inner-sphere (IS) complex by analyzing extended X-ray absorption fine structure (EXAFS). It is considered that the specific adsorption structure is caused by the ionic radius of Cs. Therefore, it was predicted that Rb which is close to Cs in terms of ionic radius also forms IS complex on phyllosilicates. Therefore, in this study, it was aimed to clarify whether the concentration and isotopic ratio of Rb change by the formation of IS complex to phyllosilicate. Rb^+ was adsorbed on vermiculite, montmorillonite, and illite under various pH and ionic strength conditions, and the adsorption structure was analyzed by EXAFS. For comparison, the same experiment was carried out for the strongly acidic cation-exchange resin (SCR). After these adsorption experiments, Rb stable isotope ratios ($^{87}Rb/^{85}Rb$) in liquid and solid phases were measured with a multi-collector type inductively coupled plasma mass spectrometry (MC-ICP-MS) and the degree of the isotope fractionations were analyzed. The host phase of Rb^+ in marine sediment in the Pacific Ocean and the standard rock samples were also analyzed with EXAFS and their Rb stable isotope ratios were measured with MC-ICP-MS. In addition, dissolved Rb^+ and Rb^+ in suspended particles in river water samples collected in the Tone River were also analyzed with EXAFS and their Rb stable isotope ratios were measured with MC-ICP-MS. In this study, it was verified experimentally that Rb forms IS complexes in specific phyllosilicates (vermiculite and illite) and Rb stable isotope fractionation occurs during its adsorption. The lighter isotope (^{85}Rb) was concentrated in the solid phases in this isotope fractionation. On the other hand, Rb was mainly adsorbed as outer-sphere complexes in montmorillonite and strongly acidic cation-exchange resin, and the isotope fractionations were small. These results showed that the fractionation was clearly observed for the adsorption system with formation of IS complex (vermiculate and illite). EXAFS analysis also revealed that Rb in sedimentary rocks is also dominated by IS complexes with phyllosilicates. In the ocean system, it was revealed that the fractionation has occurred between marine sediment and seawater. The lighter isotope was concentrated in the solid phases in these systems. Hence, the Rb isotope fractionation observed in the laboratory experiments was also found in the marine environment. However, the mean Rb isotope ratio of seawater-marine sediments is significantly higher than the crustal average, suggesting that the Rb isotope ratio is higher in rivers before its inflow into the ocean. Actually, $\delta^{87}Rb$ of the Tone River water was fractionated between dissolved and suspended particle phases and this fractionation was consistent with the fractionation observed in the laboratory experiments for illite and vermiculite. Finally, $\delta^{87}Rb$ of seawater and marine sediment can be explained by considering adsorption reaction on phyllosilicates in both rivers and oceans in this study. Also, Illite and smectite are typical clay minerals in pelagic sediments, and these minerals are also ubiquitous in planetary materials such as meteorites. Therefore, I proposed that possible geochemical applications of the $^{87}Rb/^{85}Rb$ isotope ratio can be estimation of the record of sea water fluctuation and water-rock ratio. It has now been widely recognized that various planets had initially water, and the water-rock ratio is important for the study on the evolution of planets and asteroids within the solar system. Measurement of Rb isotope in clay minerals in meteorites and halite, which represents Rb remaining aqueous phase, may provide constraints on the water-rock

©2021. Japan Geoscience Union. All Right Reserved.

ratios in the parent body of the meteorites. If this method can be applied to the “Ryugu” return sample provided by the spacecraft “Hayabusa2”, it can be used to estimate the water-rock ratio of the parent body.

Keywords: rubidium, stable isotope, clay mineral, geochemistry

©2021. Japan Geoscience Union. All Right Reserved.

Determination method of ^{13}C-labeled isotopomer ratio of dissolved organic acids by GC-MS analysis

*Konomi Suda[1]

1. National Institute of Advanced Industrial Science and Technology

Organic acids, especially formic acid and acetic acid, have been predicted to form abiotically from inorganic precursors under certain aqueous conditions (e.g., McCollom, 2013, *Reviews in Mineralogy & Geochemistry* 75: pp. 467-494; Preiner et al., 2020, *Nature ecology & evolution* 4.4: pp. 534-542). Stable isotope tracers are powerful tool for visualizing a specific reaction pathway and distinguishing between experimental products and contamination. Laboratory experiments with stable-isotopically labeled starting materials require the determination of isotope enrichment of product materials. Gas chromatography-Mass spectrometry (GC-MS) technique with direct injection of aqueous sample has been a simple and rapid method for determining the isotope enrichment of underivatized acetic acid (Mulat and Feilberg, 2015, *Talanta* 143: pp. 56-63). However, the applicability of ^{13}C-tracer analysis by GC-MS to formic acid has still not been investigated adequately. Furthermore, the previous calculation method which estimates the ^{13}C-labeled mass isotopomer ratio of acetic acid by using ion intensities of m/z 60, 61 and 62 (Mulat and Feilberg, 2015) cannot distinguish between two kinds of singly labeled isotopomers, i.e., $CH_3{}^{13}COOH$ and $^{13}CH_3COOH$. In this study, I investigate a determination method for ^{13}C-labeled isotopomer ratio of formic acid and acetic acid in aqueous solution by using GC-MS data. Standard solutions were prepared from sodium formate and sodium acetate reagents. The unlabeled sodium salts with natural isotope abundance were purchased from Sigma-Aldrich. The ^{13}C-labeled sodium salts, which were artificially enriched in ^{13}C atom in some specific position with isotopic purity of 99%, were purchased from Cambridge Isotope Laboratories, Inc. Pure standard solutions (50 to 1000 μmol/L) were individually prepared; unlabeled formic acid (HCOOH), labeled formic acid ($H^{13}COOH$), unlabeled acetic acid (CH_3COOH), singly labeled acetic acids ($CH_3{}^{13}COOH$ and $^{13}CH_3COOH$) and doubly labeled acetic acid ($^{13}CH_3{}^{13}COOH$). Then, mixture solutions in which two or more isotopomers presented were prepared by mixing of these pure standards. The aqueous samples were analyzed by GC-MS (7890B gas chromatograph and 5977B mass spectrometer, Agilent Technologies) which was placed at the dedicated analysis laboratory for samples labeled with heavy stable isotopes such as ^{2}H, ^{13}C and ^{15}N…etc. in the Geomicrobiology Research Group (Geological Survey of Japan, AIST). Prior to direct injection of aqueous sample into the GC-MS system, sample was acidified to about pH 2 with phosphoric acid to improve peak sharpness and reduce ghost peaks (Pind et al., 2003, *Biotechnology and Bioengineering* 82: pp. 791-801; Mulat and Feilberg, 2015). Dissolved formic acid and acetic acid were detected with good peak sharpness at minimum concentration of 50 μmol/L and 4 μmol/L, respectively.
In this presentation, I will report the following results and discussions.
- Comparison of results from different data acquisition modes to assess the optimal GC-MS configuration; Profile mode vs. Selected Ion Monitoring (SIM) mode.
- Effectiveness assessment of new calculation approach by least-square method with GC-MS data for determining each mixing ratio of ^{13}C isotopomeric tracers of formic acid and acetic acid.

Keywords: GC-MS, Stable isotope tracer, 13C-label, Acetic acid, Formic acid

©2021. Japan Geoscience Union. All Right Reserved.

Selectivity coefficient of Na^+-NH_4^+ exchange in saponite interlayer: Reconstruction of ammonium concentration in early ocean on Ceres

*Hiroto Tokumon[1], Keisuke Fukushi[2], Yasuhito Sekine[3], Kosuke Inoue[1], Koki Morida[1]

1. Kanazawa University , 2. Institute of Nature and Environmental Technology Kanazawa University, 3. Tokyo institute of technology

Recent space explorations have revealed the existence of a subsurface ocean in early Ceres due to the melting of ice components by the decay heat of short-lived radionuclides. NASA's Dawn survey has also revealed the existence of ammonium-type saponite containing ammonium ions in the interlayer on Ceres. Recent theories of solar system formation as known as the Grand Tuck Model (Walsh et al., 2011) suggest that during the planet-forming period when protoplanets existed, large-scale mass transfer may have occurred as the orbits of gas giant planets such as Jupiter and Saturn evolved. Ceres may have been transported from a distant location to its present position by the migration of these gas giants. If we can estimate the ammonium concentration in the early ocean on Ceres, we can determine whether the location of early Ceres was outside of the ammonia snow line or not. Currently, a geochemical model has been developed that can reconstruct the chemical properties of water with the clay mineral smectite. The model can estimate the cation concentrations in ancient liquid water from the cation composition in smectite via selectivity coefficients of relevant cation. However, the Na^+-NH_4^+ selection coefficient of saponite, which is essential to reconstruct the water quality of the early Ceres' ocean, has not yet been estimated. In this study, we aim to quantitatively estimate the Na^+-NH_4^+ selection coefficient of saponite. Furthermore, from the obtained selection coefficients, we re-examine the water quality of the early Ceres' ocean as reported by De Sanctis et al. (2020).

Keywords: Saponite, Selectivity coefficient, Ceres

©2021. Japan Geoscience Union. All Right Reserved.

[J] Poster | M (Multidisciplinary and Interdisciplinary)：M-IS Intersection

Sat. Jun 5, 2021 5:15 PM - 6:30 PM JST | Sat. Jun 5, 2021 8:15 AM - 9:30 AM UTC | Ch.23

[M-IS16] Paleoclimatology and paleoceanography

convener:Yusuke Okazaki(Department of Earth and Planetary Sciences, Graduate School of Science, Kyushu University), Hitoshi Hasegawa(Faculty of Science and Technology, Kochi University), Atsuko Yamazaki(Faculty of Science, Kyushu University), Akitomo Yamamoto(Japan Agency for Marine-Earth Science and TechnologyAtmosphere and Ocean Research Institute)

Past environmental changes and events at interannual to tectonic timescale toward an understanding of Earth climate system by an integration of terrestrial and marine proxy studies and numerical modeling will be discussed. At JpGU2021, a series of presentations on "high-resolution" paleo data and model studies will be held. We welcome a variety of paleo-environmental studies from a wide range of background. We hope that this session will provide an opportunity to promote communication between participants from multidisciplinary field.

[MIS16-P01] Temperature effect on Japanese stalagmite $\delta^{18}O$ records from Hiroshima and Gifu

*Hirokazu Kato[1], Taiki Mori[2], Shota Amekawa[1], Akihiro Kano[1] (1.Department of Earth and Planetary Science, The University of Tokyo, 2.Chuo Kaihatsu Corporation)

[MIS16-P02] **Oxygen isotope equilibrium of the shallow-water benthic foraminifer *Hanzawaia nipponica* (Asano) in Tosa Bay, southwest Japan**

*Minoru Ikehara[1,2], Shigetaka Kita[2], SHUNGO KAWAGATA[3] (1.Center for Advanced Marine Core Research, Kochi University, 2.Graduate School of Integrated Arts and Sciences, Kochi University, 3.Faculty of Education, Yokohama National University)

[MIS16-P03] **Variations in shell morphology of the planktonic foraminifer *Globigerina bulloides* in the sediment off Kashima**

*Yuya Hashimoto[1], Takuya Sagawa[2] (1.Kanazawa University College of Science and Engineering, 2.Institute of Science and Engineering, Kanazawa University)

[MIS16-P04] Climate characteristics of Amami , Kagoshima , Japan over the past 200 years inferred from tree-ring cellulose oxygen isotope ratio data

*Akihiro Masuoka[1], Kenjiro Sho[1], Masafumi Ohata[2], Zhen Li[3], Takeshi Nakatsuka[3] (1.Nagoya Institute of Technology, 2.Taisei Corporation, 3.Nagoya University)

[MIS16-P05] Coral skeletal records reveal the relationship between Kuroshio variability and North Pacific climate

*Atsuko Yamazaki[1,2], Tsuyoshi Watanabe[2,3] (1.Kyushu University, 2.KIKAI institute for Coral Reef Sciences, 3.Hokkaido University)

[MIS16-P06] Reconstruction of environmental and flooding histories since AD1250 at Lake Kortta, an annually laminated lake at the Central Finland presumed by Diatom and Chrysophyceae assemblages

*Kaoru Kashima[1], Yu Fukumoto[2], Timo Saarinen[3] (1.Department of Earth and Planetary Sciences, Kyushu University, 2.Osaka City University, 3.University of Turku)

[MIS16-P07] **Sphagnum and grass cellulose oxygen isotopes in peat cores reveal climate changes in northern Japan over the past 4400 years and close relationship with human histories**

*Masanobu Yamamoto[1], Osamu Seki[2] (1.Faculty of Environmental Earth Science, Hokkaido University, 2.Insititute of Low Temperature Science)

[MIS16-P08] Can Sedimentary fish DNA track decadal to centennial scale fish abundance?

*Michinobu Kuwae[1], Hiromichi Tamai[1], Hideyuki Doi[2], Masayuki Sakata[3], Toshifumi Minamoto[3], Yoshiaki Suzuki[4] (1.Center for Marine Environmental Studies, 2.Graduate School of Simulation Studies, University of Hyogo, 3.Graduate School of Human Development and Environment, Kobe University, 4.Research Institute of Geology and Geoinformation, Geological Survey of Japan, National Institute of Advanced Industrial Science and Technology)

[MIS16-P09] Paleoenvironmental variations reconstructed by algal biomarker analysis of a sediment core from Lake Nakaumi, Japan

*Akiko Taneichi[1], Yuki Hattori[1], Ken Sawada[1], Takuto Ando[2], Hideto Nakamura[3], Kotaro Hirose[4] (1.Hokkaido Univ., 2.Shimane Univ., 3.Osaka City Univ., 4.Waseda Univ.)

[MIS16-P10] Paleoceanographic changes in the western part of the Arctic Sea based on ostracods

*Katsura Yamada[1], Kosuke Yamaguchi[1], Masao Uchida[2], Takuya Itaki[3], Kanako Mantoku[2] (1.Department of Geology, Faculty of Science, 2.National Institute for Environmental Studies, 3.National Institute of Advanced Industrial Science and Technology)

[MIS16-P11] **Mid- to late Holocene variability of the Aleutian Low Atmospheric Pressure Cell: Forcing by the Western Jet**

*Kana Nagashima[1], Jason Addison[2], Tomohisa Irino[3], Takayuki Omori[4], Kei Yoshimura[5], Naomi Harada[1] (1.Research Institute for Global Change, Japan Agency for Marine-Earth Science and Technology, 2.U.S. Geological Survey, 3.Faculty of Environmental Earth Science, Hokkaido University, 4.The University Museum, The University of Tokyo, 5.Institute of Industrial Science, The University of Tokyo)

[MIS16-P12] Sedimentary characteristics, age and event of a marine core collected from Uranouchi Bay, Kochi, Japan

*Masafumi MURAYAMA[1,3], Wataru Tanikawa[2], Akira Ijiri[2], Tatsuhiko Hoshino[2], Takehiro Hirose[2], Katsuya Nejigaki[3], Kazuno Arai[3], Go-Ichiro Uramoto[3], Kondo Yasuo[4], Hiromasa Ozaki[5], Minoru Yoneda[5] (1.Faculty of Agriculture and Marine Science, Kochi University, 2. Institute for Extra-cutting-edge Science and Technology Avant-garde Research, Kochi Institute for Core Sample Research, JAMSTEC, 3.Center for Advanced Marine Core Research, Kochi University, 4.Faculty of Science and Technology, Kochi University, 5.The University Museum,The University of Tokyo)

[MIS16-P13] Estimation of amount of meltwater discharge from the Laurentide to the Arctic Ocean during the MWP1a event

★Invited Papers

*Kenta Suzuki[1], Masanobu Yamamoto[1], Leonid Polyak[2], Tomohisa Irino[1] (1.Faculty of Environmental Earth Science, Hokkaido Univ., 2.Byrd Polar and Climate Research Center, The Ohio State Univ.)

[MIS16-P14] Millennial variability in precipitation in Papua New Guinea during the last deglaciation

*Gaku Sudo[1], Masanobu Yamamoto[1], Samantha Bova[2], Yair Rosenthal[2] (1.Faculty of Environmental Earth Science, Hokkaido Univ., 2.Rutgers Univ.)

[MIS16-P15] A paleoclimatic reconstruction of the southeastern Pacific last deglacial using geochemical proxies obtained from offshore Chile

*Karin Nemoto[1,2], Yusuke Yokoyama[1,2], Adam David Sproson[2], Yosuke Miyairi[2], Takahiro AZE[2], Hiroyuki Matsuzaki[3,4], Yair Rosentha[5], Samantha Bova[5] (1.Department of Earth and Planetary Science, The University of Tokyo, 2.Atmosphere and Ocean Research Institute, The University of Tokyo, 3.The University Museum,The University of Tokyo, 4.School of Engineering, The University of Tokyo, 5.Department of Marine and Coastal Sciences, School of Environmental and Biological Sciences, Rutgers University)

[MIS16-P16] Paleovegetation changes in the northern Mongolia since the last glacial

*Ryosuke Imaoka[1], Koji Shichi[2], Hitoshi Hasegawa[1], Niiden Ichinnorov[3], Nagayoshi Katsuta[4], Davaasuren Davaadorj[5], Masafumi MURAYAMA[1], Masao Iwai[1], masami izuho[6] (1.Kochi University, 2.Forestry and Forest Products Research Institute, 3.Paleontological Center of Mongolia, 4.Gifu University, 5.National University of Mongolia, 6.Tokyo Metropolitan University)

[MIS16-P17] Glacial–interglacial variations in the Leeuwin Current for the last 50,000 years based on Nd isotope records of benthic foraminifers

*Ryota Wako[1], Hideko Takayanagi[1], Shigeyuki Wakaki[2], Takeshige Ishiwa[4], Yusuke Yokoyama[5], Hitomi Uchimura Wakaki[3], Tsuyoshi Ishikawa[2], Yasufumi Iryu[1] (1.Department of earth science, Tohoku university , 2.Kochi Institute for Core Sample Research, JAMSTEC, 3.Center for Advanced Marine Core Research, Kochi University, 4.National Institute of Polar Research, 5.Atmosphere and Ocean Research Institute, University of Tokyo)

[MIS16-P18] Changes in carbonate dissolution and preservation in Southern Ocean sediment off Chilean margin during the last 140 kyrs based on fragmentation and size-normalized weight of planktic foraminiferal tests.

*Takuto Kasuya[1], Yusuke Okazaki[2], Shinya Iwasaki[3], IODP Expedition 383 Scientific Party (1.Department of Earth and Planetary Sciences, School of Science, Kyushu University , 2.Department of Earth and Planetary Sciences, Faculty of Science, Kyushu University, 3.MARUM Center for Marine Environmental Sciences and Department of Geosciences, University of Bremen)

[MIS16-P19] Examining MIS 5e Sea-Levels around Japan: 60+ Years of Sea-Level Proxy Analysis and Applied Dating Techniques

*Evan Tam[1,2], Yusuke Yokoyama[1,2] (1.University of Tokyo, Atmosphere and Ocean Research Institute, 2.University of Tokyo, Graduate Program on Environmental Science)

[MIS16-P20] Integrated stratigraphy of the sediment core retrieved from the Manihiki Plateau in the central Pacific and the paleotemperature change for the last 800 kyr

*MISAKI URAKAMI[1], Takuya Sagawa[2], Yoshimi Kubota[3] (1.College of Science and Engineering, Kanazawa University, 2.Institute of Science and Engineering, Kanazawa University, 3.National Museum of Nature and Science)

[MIS16-P21] Preliminary results of oxygen isotopic, paleomagnetic, and pollen analyses from a mid-Piacenzian marine succession in the Boso Peninsula, central Japan.

*Yuki Haneda[1] (1.Geological Survey of Japan, AIST)

[MIS16-P22] The mid-Pliocene Warm Period: climate sensitivity to atmospheric CO_2 levels and inclusion of dynamic vegetation in the MIROC4m model

*Wing-Le Chan[1], Ayako Abe-Ouchi[1,2] (1.Atmosphere and Ocean Research Institute, The University of Tokyo, 2.National Institute of Polar Research)

[MIS16-P23] Chemical weathering feedback during the early Paleogene hyperthermals based on osmium isotope analysis

*Kakeru Ikegami[1], Kazutaka Yasukawa[1,2], Erika Tanaka[1], Junichiro Ohta[1,2], Yusuke Kuwahara[1], Moei Yano[2,1], Koichiro Fujinaga[2,1], Yasuhiro Kato[1,2] (1.School of Engineering, The University of Tokyo, 2.ORCeNG, Chiba Institute of Technology)

[MIS16-P24] High latitude paleoenvironments in Southern Hemisphere during mid-Cretaceous

*Hiromichi Komiya[1], Takashi Hasegawa[1] (1.Kanazawa University)

[MIS16-P25] A study on the responses of the climate field in the Cretaceous to orbital parameter changes

★Invited Papers

*Taro Higuchi[1], Ayako Abe-Ouchi[1], Wing-Le Chan[1] (1.Atmospheric and Ocean Research Institute, the University of Tokyo)

[MIS16-P26] **Eccentricity paced increase in the continental weathering in the latest Hauterivian, Early Cretaceous**

★Invited Papers

*Hironao Matsumoto[1], Rodolfo Coccioni[2], Fabrizio Frontalini[2], Kotaro Shirai[1], Junichiro Kuroda[1] (1.Atmosphere and Ocean Research Institute, the University of Tokyo, 2.University of Urbino)

[MIS16-P27] Millennial-scale cyclicities recorded in the Cretaceous lacustrine core using Monte Carlo approach

*Hitoshi Hasegawa[1], Hirofumi Asahi[2] (1.Faculty of Science and Technology, Kochi University, 2.Center for Advanced Marine Core Research, Kochi University)

Temperature effect on Japanese stalagmite $\delta^{18}O$ records from Hiroshima and Gifu

*Hirokazu Kato[1], Taiki Mori[2], Shota Amekawa[1], Akihiro Kano[1]

1. Department of Earth and Planetary Science, The University of Tokyo, 2. Chuo Kaihatsu Corporation

Stalagmites from caves are excellent archives of terrestrial paleoclimate information. Stalagmite $\delta^{18}O$ values are basically controlled by two major factors, temperature of calcite formation and cave drip water $\delta^{18}O$ derived from the local precipitation. The latter factor involves the changes in climatic factors including the monsoon intensity, moisture trajectory, and seasonality of precipitation. It is, however, not easy to determine relative importance of two fundamental controls, by conventional isotopic compositions alone. Carbonate clumped isotope thermometry is a resolution to this problem, which can directly reconstruct paleo-temperature regardless of drip water $\delta^{18}O$.
Recently, stalagmite studies focusing on temperature signals were reported for the late Pleistocene to middle Holocene stalagmites from Japan (e.g., Mori et al., 2018). We recently measured carbonate clumped isotope (Δ_{47}) from 50 layers of Hiro-1 stalagmite (18–4 ka) from Hiroshima Prefecture and successfully separated signals of temperature changes and drip water $\delta^{18}O$ in the Hiro-1 $\delta^{18}O$ values (Kato et al., 2021) using equations of temperature-dependencies of $\delta^{18}O$ and Δ_{47} (Tremaine et al., 2011; Kato et al., 2019). An important finding in Kato et al. (2021) was that meteoric water $\delta^{18}O$ (drip water $\delta^{18}O$) per se changes depending on temperature.
In this study, the authors newly analyzed Δ_{47} values from more than 60 layers of OT-02 stalagmite (63–35, 8–3 ka) collected from Ohtaki cave, Gifu prefecture, of which U-Th ages and $\delta^{18}O$ values had been already analyzed by Mori et al. (2018). The Δ_{47} measurements were performed using a dual inlet mass spectrometer (Finnigan MAT-253) at Kyushu University.
In the relevant interval of mid-Holocene (8 to 4 ka), OT-02 stalagmite shows a similar Δ_{47} profile with Hiro-1, the peak of warming around the Hypsithermal (6–5 ka) after a slight cooling around 7 ka. This agreement suggests that Δ_{47} values of the two Japanese stalagmites are reliable proxies of terrestrial temperature. In the period of 63–35 ka, Δ_{47} values of OT-02 exhibit periodic fluctuation relating Dansgaard-Oeschger cycles with 3–5 ºC cooling in Heinrich events 4–6. As considered by Mori et al. (2018), temperature variation is likely a major controlling factor of OT-02 $\delta^{18}O$. Reconstructed paleo drip water $\delta^{18}O$ by subtracting temperature effect from OT-02 $\delta^{18}O$ shows a correlation with the reconstructed temperature, which was also recognized in Hiro-1 stalagmite in Hiroshima. However, the correlation in OT-02 is even stronger than that of Hiro-1. It can be assumed that the drip water $\delta^{18}O$ in Gifu reflect the precipitation ratio of summer rainfall with higher $\delta^{18}O$ and winter snow/rainfall with lower $\delta^{18}O$, which differs depending on climatic periods.

References

Kato, H. et al (2019) Seasonal temperature changes obtained from carbonate clumped isotopes of annually laminated tufas from Japan: discrepancy between natural and synthetic calcites. GCA 244, 548–564.
Kato, H. et al (2021) Influences of temperature and the meteoric water $\delta^{18}O$ value on a stalagmite record in the last deglacial to middle Holocene period from southwestern Japan. QSR 253.
Mori, T. et al (2018) Temperature and seawater isotopic controls on two stalagmite records since 83 ka from maritime Japan. QSR 192, 47–58.

©2021. Japan Geoscience Union. All Right Reserved.

Keywords: stalagmite, paleo climate, stable oxygen isotope , carbonate clumped isotope, terrestrial temperature

©2021. Japan Geoscience Union. All Right Reserved.

Oxygen isotope equilibrium of the shallow-water benthic foraminifer *Hanzawaia nipponica* (Asano) in Tosa Bay, southwest Japan

*Minoru Ikehara[1,2], Shigetaka Kita[2], SHUNGO KAWAGATA[3]

1. Center for Advanced Marine Core Research, Kochi University, 2. Graduate School of Integrated Arts and Sciences, Kochi University, 3. Faculty of Education, Yokohama National University

Oxygen isotopic compositions ($\delta^{18}O$) of benthic foraminifer tests are widely used for reconstructing paleoceanographic changes, such as global ice volumes during glacial–interglacial cycles. Although deep-sea benthic foraminifers have been well characterized and are considered reliable indicators, little attention has been paid to the geochemistry of shallow-water benthic foraminifers. In this study we evaluated $\delta^{18}O$ in the shallow-water benthic foraminifer *Hanzawaia nipponica* (Asano), which lives in surface sediments on continental shelves and upper slopes under the influence of two warm currents, the Kuroshio and Tsushima currents, in the East China Sea, northwest Pacific, and southwestern Japan Sea. To evaluate oxygen isotope equilibrium, we analyzed $\delta^{18}O$ of *H. nipponica* and ambient seawater on the continental shelf in Tosa Bay, southwest Japan. Seawater $\delta^{18}O$ and salinity in Tosa Bay are similar to those of surface and subsurface waters in the Kuroshio region in the Okinawa Trough and the northwest Pacific. Vertical profiles of seawater $\delta^{18}O$ show no variation with water depth (0–200 m) in Tosa Bay. However, tests of living *H. nipponica* (as determined by staining with Rose Bengal) and fossil (non-stained) *H. nipponica*, picked from samples of the top centimeter of seafloor sediment, yielded carbonate $\delta^{18}O$ values that clearly increase with water depth, suggesting a temperature-dependent relationship. A comparison of carbonate $\delta^{18}O$ values in living *H. nipponica* and those predicted on the basis of seawater $\delta^{18}O$ and annual mean bottom temperature shows that *H. nipponica* tests are in oxygen isotopic equilibrium with ambient seawater. This result additionally suggests that the life cycle of this species is longer than one year. Thus, we propose that the carbonate $\delta^{18}O$ of *H. nipponica* are useful proxies to reconstruct shallow-water paleoenvironmental changes in the northwest Pacific and its marginal seas.

Keywords: benthic foraminifer, oxygen isotope equilibrium, Tosa Bay, Kuroshio

©2021. Japan Geoscience Union. All Right Reserved.

Variations in shell morphology of the planktonic foraminifer *Globigerina bulloides* in the sediment off Kashima

*Yuya Hashimoto[1], Takuya Sagawa[2]

1. Kanazawa University College of Science and Engineering, 2. Institute of Science and Engineering, Kanazawa University

Planktonic foraminifer *Globigerina bulloides* inhabits a wide range of latitudes, especially in the mid-latitudes. Domitsu and Oda. (2005) focused on such shell morphology and reported that it can be divided into two major types, corresponding to warm and cold water masses in Japan Sea. However, there is no such comprehensive study on water masses and shell morphology in the Pacific Ocean. In this study, we focused on the waters off Kashima, where the temperature gradient in the latitudinal direction increases due to the mixing of the warm and cold water masses and examined the diversity of shell morphology of *G. bulloides* in response to such water mass mixing by observing and quantitatively measuring the shells. We used *G. bulloides* which is 180-250 μm size from 120 individuals each from Holocene, glacial, and last glacial samples. Measurements were made on images taken with a digital microscope. The following parameters were measured: short diameter [maximum distance between the first chamber from the last (F-1) and the third chamber from the last (F-3)], long diameter [maximum distance between the second chamber from the last (F-2) and the last chamber (F)], foraminiferal area (FA), the area of each foraminiferal chamber and the coiling direction of the shell. Cross-sectional observation by SEM was also conducted to see the difference in shell thickness. The ratio of short to long diameters (short diameter/long diameter) and the ratio of the area of F to the area of F-3 (F/F-3) were taken as quantitative indices to reflect the differences in shell morphology using the data obtained from the measurements. Histograms were made for each sample, and the values and shell morphology were compared among samples of different ages. As for F/F-3, there was an inverse correlation between the two indices, reflecting the difference in shell morphology. Although there was no significant difference in the shell morphology of the representative individuals of the populations located at both ends of the value range, observations showed that the shell thickness of the individuals from the warm period samples was thinner than that of the individuals from the cold period samples. This is consistent with Domitsu and Oda. (2005), who reported that thin-shelled individuals predominate in warm water masses and thick-shelled individuals predominate in cold water masses. It could not be adapted to the classification of Kashima. The mean values of short/long diameters were compared for each coiling direction, but no significant differences were found. So, we conclude quantitative data on thickness are also needed to classify *G. bulloides* with different water masses, and it is necessary to consider those with intermediate morphology off Kashima.

Keywords: Planktonic foraminifera, morphology, Kashima

©2021. Japan Geoscience Union. All Right Reserved.

Climate characteristics of Amami , Kagoshima , Japan over the past 200 years inferred from tree-ring cellulose oxygen isotope ratio data

*Akihiro Masuoka[1], Kenjiro Sho[1], Masafumi Ohata[2], Zhen Li[3], Takeshi Nakatsuka[3]

1. Nagoya Institute of Technology, 2. Taisei Corporation, 3. Nagoya University

It has become clear that the oxygen isotope ratios contained in tree-ring cellulose reflect oxygen isotope ratios in precipitation and relative humidity , regardless of physiological factors of the tree. It is a useful tool to reconstruct past climate. In this study, we investigate climate characteristics over the past 200 years in Amami Oshima Island(28˚22’ N 129˚29’ E), southwestern Japan, by measuring the oxygen isotope ratio contained in tree-ring cellulose.
We collected disk samples from three Ryukyu pine (*pinus luchuensis*) trees (namely, “Sennen”, ”Santera”, “Untera”). The disk samples were cut into transverse thin plates with a thickness of 2 mm using a diamond wheel saw to extract cellulose. The prepared cellulose specimen was divided into 12 segments for each ring along the growth direction using a binocular stereomicroscope and an ophthalmic knife. We used an online system of a pyrolysis elemental analyzer and an isotope ratio mass spectrometer (TCEA-Delta V Advantage) installed at the Graduate School of Environmental Studies, Nagoya University for isotope measurement. The measured period is Santera pine: 1799 to 1847,1951 to 1967, Sennen pine: 1951 to 1967,1914,1915,1923 to 1927, 1986 to 1994 and Untera pine: 1830 to 1975,1948 to 1952, 1971 to 1990, 2002 to 2013.
To determine the seasonal growth pattern of the three sample trees, we analyzed correlation between intra-ring $\delta^{18}O$ variation and 10-day rative humidity data at Naze Meteorological Station (28˚22’ N 129˚29’ E) using 37 rings within 1961-2012. As a result, it was estimated that the first segment, corresponding to the earliest stage of tree-ring formation, is formed from early March to mid-April, and the 12th segment, corresponding to the end of tree-ring formation, is formed from late November to late December.
Old document "Oshima Daikanki" (document of prefectural office at Amami Oshima Island) states that there was a long rain from late February to April in 1833, and our oxygen isotope ratio data indicate anomalous wet condition (low δ^{18}) for the first and second segments of the 1833 ring. Similar resalt was found for the 1804 and 1819 rings, implying about 15-year periodical occurrence of long rain in spring.

Keywords: Tree-ring cellulose, Oxygen isotope ratio, Relative humidity, Amami Oshima Island, Ryukyu pines

©2021. Japan Geoscience Union. All Right Reserved.

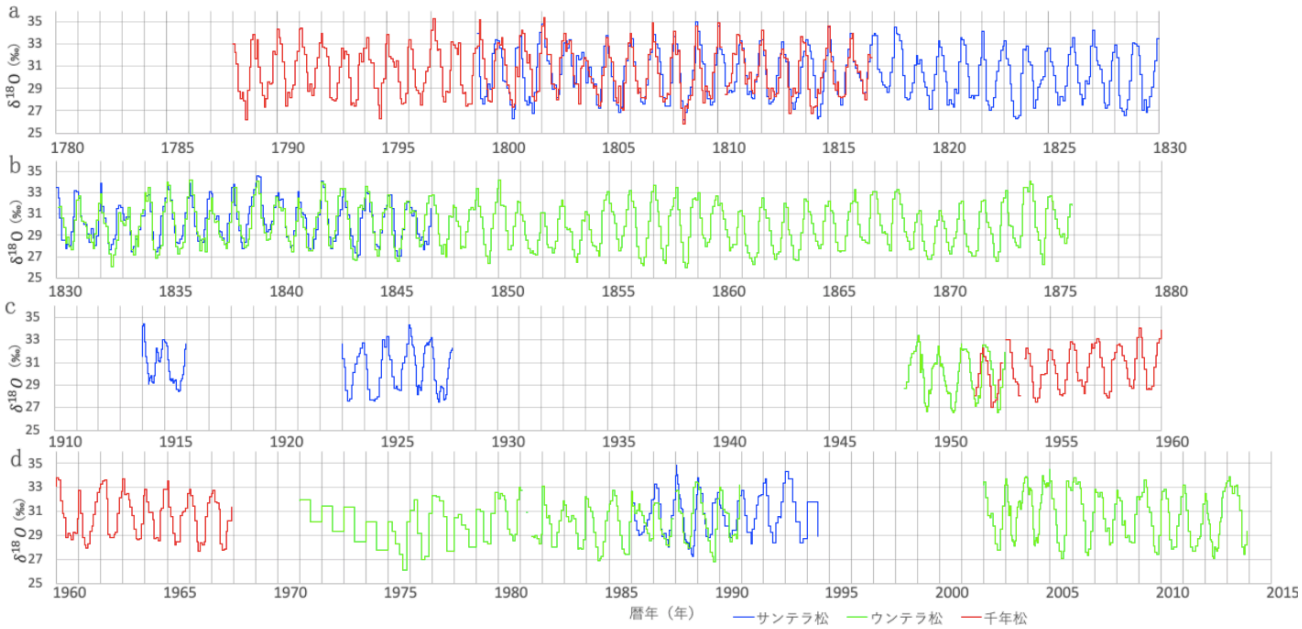

a.1780 年～1829 年，b.1830 年～1879 年，c.1910 年～1959 年，d.1960 年～2014 年における酸素同位体比データ

測定期間　千年松(赤線):1788 年～1816 年，1951 年～1967 年

サンテラ松(青線):1799 年～1847 年，1914，1915，1923 年～1927 年，1986～1994 年

ウンテラ松(緑線):1830 年～1975 年，1948 年～1952 年，1971 年～1990 年，2002 年～2013 年

©2021. Japan Geoscience Union. All Right Reserved.

Coral skeletal records reveal the relationship between Kuroshio variability and North Pacific climate

*Atsuko Yamazaki[1,2], Tsuyoshi Watanabe[2,3]

1. Kyushu University, 2. KIKAI institute for Coral Reef Sciences, 3. Hokkaido University

The Kuroshio Current is a western boundary current in the North Pacific Ocean. The variations of its transport and migration under the global warming condition have been debated because they have a high impact on the climate, ecosystem, and fishery in the northwestern Pacific. Here, we reconstructed the Kuroshio transport variability and its migration over 70 years using coral skeletal records. Coral cores were collected from Tatsukushi Bay in 2008 on the Pacific coast of Japan, located on the northern front of the Kuroshio Current. Another coral cores were drilled at Cape Shionomisaki is located on the Kuroshio meander site.
The nitrogen isotope proxy in coral skeletons was used as a proxy to record the nitrogen isotope of nitrate controlled by the upwelling of subtropical subsurface water (+2−+3 permil), and coral nitrogen isotope was negatively correlated with observations of the Kuroshio transport ($R = -0.69$, $P < 0.001$) and the two years lagged PDO index ($R = -0.63$, $P < 0.005$) from 1972 to 2007. The 150-year record of coral nitrogen isotopes suggested that the Kuroshio transport varied with ~25-year cycle, and the amplitude became stable, and the volume was intensified through the twentieth century.
The Kuroshio transport was intensified with the La Nina state in the early 1900s and with the El Nino-PDO state after the 1920s. Our results suggested that the Kuroshio transport was influenced by the combined climate modes of ENSO and PDO during the last century. To detect the migration of Kuroshio, we used oxygen isotopes in dual coral cores at Cape Shionomisaki and Tatsukushi Bay. During 1930-2007, the maxima of the oxygen isotopes in the CS core correlated with the winter East China Sea temperature. However, the minima and maxima of the TB core's oxygen isotopes varied with salinity and temperature at the sea surface along the subtropical gyre. The oxygen isotope anomaly in the CS core from the TB core highlights cool and dry conditions with Kuroshio meander events. It correlated with Kuroshio meander's observational proxy, the tide level differences from Kushimoto to Urakami ($R=+0.56$, $P<0.01$).
The reconstructed Kuroshio migration suggested that Kuroshio migration is positively correlated with Kuroshio transport in an 8-12 year cycle. The axis of Kuroshio leaves Cape Shionomisaki with large transport. The Kuroshio meander events are not related to ENSO, but they have positive PDO mode. The coral skeletal archives in the northwestern Pacific can detect the transport and migration of Kuroshio currents.

Keywords: Coral skeletons, Kuroshio, nitrogen isotope, oxygen isotope

©2021. Japan Geoscience Union. All Right Reserved.

Reconstruction of environmental and flooding histories since AD1250 at Lake Kortta, an annually laminated lake at the Central Finland presumed by Diatom and Chrysophyceae assemblages

*Kaoru Kashima[1], Yu Fukumoto[2], Timo Saarinen[3]

1. Department of Earth and Planetary Sciences, Kyushu University, 2. Osaka City University, 3. University of Turku

Lake Kortta, located at the central part of Finland, is a small freshwater lake with 1000m length and 400 width. It has continued more than 3000 years for the sedimentation of laminated lake deposits. The average sedimentation rate was about 4mm/year (after AD1950) and 0.8-1.0mm/year (before AD1950). In this paper, we used the 80cm sedimentary core which was taken in 2010. The age of the base of the core was presumed as AD1250.

The annually laminations of Lake Kortta was related to melting flooding at early spring. The flooding layers were composed of whitish gray sands and were contrast to dark gray clay at other seasons. Among the fine laminated layers, we recognized the several thick whitish flooding layers, dated AD1260, AD1460, AD1780, AD1914-1918, AD1967 and AD1986 respectively. AD1260, AD1460 and AD1780 were presumed to be cold winter in North Europa by historic records, and AD1967 and AD1986 were recorded as lowering of winter temperatures by Meteorological observation in Finland. AD1914-1918 was the period of WWI, and the huge deforestation occurred.

Diatom assemblages were dominated by freshwater planktonic diatoms as Aulacoseira ambigua, A. valida, Stauroneis spp., those presumed the freshwater lake environment has continued since AD1250 to the present. In addition to those lake living diatoms, *Eunotia* spp., *Pinnuralia* spp., peat living diatoms, were observed abundantly. They presumed to be enter into the lake from the surrounding peat lands during the flooding Early Spring season.
Cists of Chrysophyceae increased at cold climatic years as AD1260, AD1460, AD1780, and AD1986. In addition to them, the ratio of Cists of Chrysophyceae increased during the Little Ice Age, about AD1780-1900. Chrysophyceae made cists when lake water conditions became unsuitable for growing, and the ratio of cists was presumed to be related to the climatic and flooding histories at the lake for these 750 years.

Keywords: Annually laminated sediment, Finland, Climatic Change, Flooding sediments, Diatom, Chrysophyceae cists

©2021. Japan Geoscience Union. All Right Reserved.

Sphagnum and grass cellulose oxygen isotopes in peat cores reveal climate changes in northern Japan over the past 4400 years and close relationship with human histories

*Masanobu Yamamoto[1], Osamu Seki[2]

1. Faculty of Environmental Earth Science, Hokkaido University, 2. Insititute of Low Temperature Science

The cellulose $\delta^{18}O$ of plant tissues in peat is a potential climatic proxy to understand the atmospheric dynamics of the past. In this study, we analyzed the $\delta^{18}O$ values of sphagnum and vascular plant cellulose in 4.6- and 4-m long peat cores from the Minamihama moor in Rishiri Island, Japan, to understand paleoclimate changes in northern Japan over the past 4400 years. Cellulose $\delta^{18}O$ of sphagnum showed multi-centennial and millennial variation with higher values in 4500–3400, 2800–2300, and after 700 year BP, and lower values around 3000, and 2200–1000 year BP. The difference of $\delta^{18}O$ between vascular plants and sphagnum ($\Delta\delta^{18}O_{vp-sp}$), a proxy of relative humidity, was reversely correlated with $\delta^{18}O$, indicating humid climate in the periods with higher sphagnum $\delta^{18}O$. The factors controlling the climate in Rishiri Island changed between 2800 and 1300 years BP. In the older period, the development of the North Pacific High determined the climate of entire Hokkaido area *via* changes in the position of the westerly jet and the East Asian summer monsoon rainfall. In the younger period, this mechanism continued to determine the climate of eastern Hokkaido facing the Pacific Ocean, while the intensity of the Tsushima Warm Current determined the climate in Rishri Island. The weakening of the North Pacific High shifted the westerly jet south of Rishiri Island so that the position of the westerly jet did not influence the precipitated water $\delta^{18}O$ in the Rishiri Island. The climate changes in Rishiri Island corresponded to the evolution of human culture in Hokkaido Island.

Keywords: cellulose oxygen isotopes, Holocene, Climate

©2021. Japan Geoscience Union. All Right Reserved.

Can Sedimentary fish DNA track decadal to centennial scale fish abundance?

*Michinobu Kuwae[1], Hiromichi Tamai[1], Hideyuki Doi[2], Masayuki Sakata[3], Toshifumi Minamoto[3], Yoshiaki Suzuki[4]

1. Center for Marine Environmental Studies, 2. Graduate School of Simulation Studies, University of Hyogo, 3. Graduate School of Human Development and Environment, Kobe University, 4. Research Institute of Geology and Geoinformation, Geological Survey of Japan, National Institute of Advanced Industrial Science and Technology

Far too little is known about the long-term dynamics of the abundance of most macro-organism species. We used sedimentary DNA technology to quantify marine fish DNA abundance in sediment sequences spanning the last 300 years. This study first shows the existence of fish DNA in the sequences and proves that fish abundance can be tracked using sedimentary DNA, highlighting the utility of sedimentary DNA for researchers to acquire lengthy records of macro-organism species abundance.

Reference
Kuwae, M., Tamai, H., Doi, H., Sakata, M.K., Minamoto, T., and Suzuki, Y. (2020) Sedimentary DNA tracks decadal-centennial changes in fish species abundance. Communications Biology, 3, 558, https://doi.org/10.1038/s42003-020-01282-9

Keywords: sedimentary DNA, fish abundance, Beppu bay

©2021. Japan Geoscience Union. All Right Reserved.

Paleoenvironmental variations reconstructed by algal biomarker analysis of a sediment core from Lake Nakaumi, Japan

*Akiko Taneichi[1], Yuki Hattori[1], Ken Sawada[1], Takuto Ando[2], Hideto Nakamura[3], Kotaro Hirose[4]

1. Hokkaido Univ., 2. Shimane Univ., 3. Osaka City Univ., 4. Waseda Univ.

Diverse microalgae species inhabit brackish and lacustrine environments, and sensitively change their assemblages and compounds they produce in response to environmental changes. Algal biomarkers have been used to reconstruct the paleoenvironment in aquatic system: aquatic ecology and environmental factors such as temperature and salinity. In particular, long-chain alkenones, haptophyte-produced biomarker, have been widely used for temperature reconstruction in ocean, but there are few examples of their discovery in Japanese lakes such as Lakes Toyoni (Hokkaido), Ichinomegata (Akita), and Nakaumi - Shinji (Tottori-Shimane). Long-chain (C_{28}-C_{32}) alkyl diols are widely distributed in marine and lacustrine sediments and recently used as paleoenvironmental indicators. In particular, C_{32} 1,15-diol is considered to originate from freshwater eustigmatophytes and has been proposed as indicator of freshwater input in coastal area (Lattaud et al., 2016). In the present study, we conducted a biomarker analysis of a sediment core from the Lake Nakaumi to evaluate how the algal biomarkers long-chain alkenones and alkyl diols record the changes in algal assemblages and environments in the brackish lake.
The sediment core was collected from central area of the lake (Nk3C) during May 2017. The ages were determined by Cs and Pb isotopes, and the lowermost horizon was estimated to be about 600 years ago. Biomarker analysis was performed as follows; freeze-dried sediments were extracted by solvents and then separated into fractions by silica-gel column chromatography. Resulted ketone-containing and alcohol-containing fractions were analyzed by GC-MS and GC-FID. The Lake Nakaumi, has been strongly affected by anthropogenic rearrangements during the high economic growth in Japan. Perticularly, the land reclamation and desalination projects in the 1960s to 1980s are known to have had a significant impact on the ecosystem.
The long-chain alkenones and alkyl diols were detected in all the samples from the Nk3C core. The alkenone compositions were clearly different between the samples above and below the horizons affected by the reclamation and desalination project during 1960s. Below the horizons, $C_{37:2}$ alkenones were dominant and C_{40} homologues was absent. On the other hand, $C_{37:4}$ alkenones and C_{40} alkenones were relatively abundant above the horizons. We presume that the main alkenone-producers in sediments below and above the horizons in 1960s were typical marine (Group III) and lacustrine species (Group II), respectively. The compositions of long-chain alkyl diols are also different between the sediments above and below the horizons in 1960s; C_{30} 1,15-diol, common alkyl diol produced by marine eustigmatophyte, was predominant below the horizons, while C_{32} 1,15-diol, biomarker for freshwater eustigmatophyte, was dominant above the horizons in 1960s. From these results, it is suggested that typical marine species of haptophyte and eustigmatophyte inhabit shallow marine environment in the Lake Nakaumi by the middle 20th century, and subsequently, the freshwater species flourished as the dominant producers under brackish environment in the lake after the anthropogenic rearrangements during 1960s. Furthermore, the paleo-temperature (T) calculated by using lacustrine-specific alkenone unsaturation index ($U^{K'}_{37}$; Zheng et al., 2016) gradually increased through the horizon that alkenone-producing species were converted, whereas the common index (U^{K}_{37})-based T showed unexpected change (sudden 5ºC inclease). Although the resolution of the biomarker data is still low, the variations in $U^{K'}_{37}$-based T appear to be broadly consistent with historical record of climate-related events such as the four great famines during the Edo Period and the long-term divisions of climatic periods after 17th century. Thus, the algal biomarker proxies can be expected to apply to reconstructing paleoenvironmental, moreover paleoclimatic

©2021. Japan Geoscience Union. All Right Reserved.

variations in lacustrine sediments.

Keywords: Brackish lake, Lake Nakaumi, Algae biomaker, Alkenone, Alkyl diol, Paleoenvironmental Reconstruction

©2021. Japan Geoscience Union. All Right Reserved.

Paleoceanographic changes in the western part of the Arctic Sea based on ostracods

*Katsura Yamada[1], Kosuke Yamaguchi[1], Masao Uchida[2], Takuya Itaki[3], Kanako Mantoku[2]

1. Department of Geology, Faculty of Science, 2. National Institute for Environmental Studies, 3. National Institute of Advanced Industrial Science and Technology

Abrupt climate changes for a few thousand years are identified between Late Pleistocene and Holocene. Some of them are found in the Arctic Sea and northwestern Atlantic Ocean, suggesting that importance to understand paleoceanographic shifts accurately in the Arctic Ocean. However, oceanographic changes during the Holocene are ambiguous yet there. Thus, our aim is to clarify the Holocene oceanographic shifts in the area shallower than 200 m water depth in the western part of the Arctic Ocean. The study area is influenced by waters from the Pacific, Atlantic Oceans and river input. We used two cores; One was taken from the bottom at a water depth of 65 m in the Mackenzie trough located in river mouth of the Mackenzie river. Another was taken from the bottom in the northern part of the Chukchi shelf at a water depth of 197 m. This water depth is close to the depth bounding waters from the Atlantic and Pacific Oceans. Fossil ostracod assemblages and chemical compositions of the ostracod shells are investigated taken from the core sediments. Shallow marine ostracod taxa were dominated in the Mackenzie trough, and it is considered that the assemblage shifts related to water salinity changes. Conversely, samples from the Chukchi Sea contained ostracod taxa inhabiting in the Pacific and Atlantic Ocean waters. Mg/Ca of ostracod shells were measured by using ICP-AES. First, past water temperatures by using regression lines between Mg/Ca of the genus *Krithe* and water temperature in the previous study was calculated. Then, past water temperatures were reconstructed by relationships between Mg/Ca of *Semicytherura complanate* and the calculated water temperatures in both areas. The bottom water temperatures in the Chukchi shelf showed relative high values during 7000 and 2000 cal year BP. Dominance of ostracod taxa inhabiting in the Atlantic Ocean waters was identified in the two periods inferring intensification of the Atlantic Ocean water influence. Bottom water temperatures in the Mackenzie trough showed high value between 5500-4900 cal year BP and was stable after 4900 cal year BP. Salinity generally had increased from 7700 cal year BP to the present based on ostracod assemblage changes in the Mackenzie trough. Further, relative high salinity was recognized in 2600, 600, and 200 cal year BP. The long-term increase and temporal high values in salinity coincide with the timing of ice sheet expansions since the 5000 cal year BP in the Northern Hemisphere, implying that the salinity was affected by the glacier expansion in the trough.

Keywords: Holocene, Paleoceanography, ostracod

©2021. Japan Geoscience Union. All Right Reserved.

Mid- to late Holocene variability of the Aleutian Low Atmospheric Pressure Cell: Forcing by the Western Jet

*Kana Nagashima[1], Jason Addison[2], Tomohisa Irino[3], Takayuki Omori[4], Kei Yoshimura[5], Naomi Harada[1]

1. Research Institute for Global Change, Japan Agency for Marine-Earth Science and Technology, 2. U.S. Geological Survey, 3. Faculty of Environmental Earth Science, Hokkaido University, 4. The University Museum, The University of Tokyo, 5. Institute of Industrial Science, The University of Tokyo

The North Pacific Ocean is the largest geographic feature in the Northern Hemisphere and its interactions with the overlying atmosphere drives critical components of the global climate system. The Aleutian Low (AL) is one of the major atmospheric systems that determines environmental conditions during winter in the North Pacific Ocean, with impacts that affect the climates of both Asia and North America. However, the multi-centennial and longer scale dynamics of the AL during the Holocene is not fully understood.

The climate mechanism(s) that are responsible for generating AL intensity and position changes over recent instrumental timescales are also poorly understood. One important component is the Westerly Jet (WJ), which is closely associated with the AL through its alternations on cyclogenesis, monsoon development, and storm tracks (e.g., White and Barnett, 1972; Lau, 1988; Dole and Black, 1990; Nakamura et al., 2002; Yang et al., 2002; Athanasiadis et al., 2010; Park and An, 2014). However, at timescales that exceed the recent instrumental record, the interactions between the AL and the WJ are virtually unknown. Therefore, it is critical to reconstruct paleoclimatic history of the AL and examine its interactions with other components of the climate system.

Here we conducted principal component analysis (PCA) using published $\delta^{18}O$ records from Alaska, northwestern Canada, and the western United States, thus eliminating local environmental effects on each record. The analysis was used to 1) identify common pattern(s) of $\delta^{18}O$ anomalies across the study area since 7.5 ka in order to trace multi-centennial and longer AL variations; 2) compare the reconstructed AL variations with proxy reconstructions of the WJ in East Asia and the western North Pacific Ocean to determine linkages; and 3) use these combined AL and WJ datasets to better clarify dynamic changes in North Pacific atmospheric circulation and elucidate the potential triggers of Holocene climate variability (after Nagashima et al., 2021).

The extracted Principal Component 1 (PC1) represents a dramatic change from the mid- to late Holocene, and appears to reflect long-term intensified AL related to interactions between orbitally-driven southward shift of the Westerly Jet (WJ) over East Asia and the northwestern Pacific, and intensification of the El Niño–Southern Oscillation. In contrast, PC2 is characterized by multi-centennial to millennial-scale oscillations, with a spatial loading pattern that suggests PC2 reflects AL intensity and position shifts; AL intensification with a westward shift during 7.5–5.1, 2.4–1.2 and 0.7–0.4 ka. These oscillations are contemporaneous with both WJ latitude and/or the meandering path shifts over East Asia and solar activity change, suggesting that a decrease/increase in solar irradiance is related to AL variability via interactions with the WJ (Nagashima et al., 2021).

Keywords: Aleutian Low, Holocene, oxygen isotope, Westerly Jet

©2021. Japan Geoscience Union. All Right Reserved.

Sedimentary characteristics, age and event of a marine core collected from Uranouchi Bay, Kochi, Japan

*Masafumi MURAYAMA[1,3], Wataru Tanikawa[2], Akira Ijiri[2], Tatsuhiko Hoshino[2], Takehiro Hirose[2], Katsuya Nejigaki[3], Kazuno Arai[3], Go-Ichiro Uramoto[3], Kondo Yasuo[4], Hiromasa Ozaki[5], Minoru Yoneda[5]

1. Faculty of Agriculture and Marine Science, Kochi University, 2. Institute for Extra-cutting-edge Science and Technology Avant-garde Research, Kochi Institute for Core Sample Research, JAMSTEC, 3. Center for Advanced Marine Core Research, Kochi University, 4. Faculty of Science and Technology, Kochi University, 5. The University Museum,The University of Tokyo

Sediment cores collected from the inner part (10m depth) of Uranouchi Bay, Kochi Prefecture, have been analyzed to investigate the history of changes in the marine environment. Uranouchi Bay that extends in the east-west direction with 12 km is located in the central part of Tosa Bay, Kochi Prefecture facing to the north side of the Yokonami Peninsula. This is well known as a sinking bay caused by subduction-zone earthquakes. Two 4 m sediment cores were collected by vibro coring using the university research vessel "Neptune". These core samples are considered to have recorded detailed environmental changes in the bay having no affecting the surrounding river. These core samples were carried out X-ray CT and visual observation, physical properties, identification and ^{14}C dating of fossil shells. The lithology of the sediments was olive to gray colored silty clay with a lot of shell fragments. The most upper part of these cores was providing dark colored and had a strong hydrogen sulfide odor. In addition, a well-laminated sedimentary layer with a thickness of 8 cm was observed in the lower part of the core (around 306 m from the core top). This sedimentary layer was confirmed in a similar depth collected at a nearby water depth of 8 M, but no lamination was developed. Radiocarbon dating (AMS 14C age) of shell fragments from the 8 layer of sediment was performed. At the bottom of the core, showing about 3800 years ago, the estimated average deposition rate was 102 cm / kyr. In this presentation, we will introduce these results.

Keywords: Uranouchi Inlet Bay, Marine Core, Event sediment, 14C age

©2021. Japan Geoscience Union. All Right Reserved.

Estimation of amount of meltwater discharge from the Laurentide to the Arctic Ocean during the MWP1a event

*Kenta Suzuki[1], Masanobu Yamamoto[1], Leonid Polyak[2], Tomohisa Irino[1]

1. Faculty of Environmental Earth Science, Hokkaido Univ., 2. Byrd Polar and Climate Research Center, The Ohio State Univ.

The significant sea-level rise events are recognized during the last deglaciation period. The global sea-level rose by 12-18 m in ~340 years at the MWP1a event. However, the sources of meltwater during the MWP1a event are uncertain. In this study, we identified the event layers deposited by MWP1a event from the western Arctic Ocean sediment cores and estimated the amount of meltwater discharged into the Arctic Ocean during this period based on the extent and thickness of sediments.

In this study, we used seven sediment cores collected in the western Arctic Ocean. Event layers by meltwater pulse were identified based on the amount of IRD, mineral composition, sedimentary structure, grain size distribution, and organic matter composition. The amount of suspended matter discharged during this period was calculated from the thickness range of the layer in MWP1a event, and the amount of meltwater that transported this sediment was estimated.

An event layer with sharp boundaries with the upper and lower layers, containing IRD, coarse grained, kaolinite-rich and terrestrial organic matter was identified around 14.7 ka in several sediment cores from the western Arctic Ocean. The characteristics of this layers suggest that those sediments were transported by meltwater discharge during MWP1a event. Rough-estimation indicates the meltwater discharge rate during the MWP1a event was 2 ~ 4 times higher than that of today. The amount of meltwater calculated from the amount of sediment discharged during MWP1a event was equivalent to ~30 % of the relative sea level change at that time.

Keywords: Arctic Ocean, MWP1a

©2021. Japan Geoscience Union. All Right Reserved.

Millennial variability in precipitation in Papua New Guinea during the last deglaciation

*Gaku Sudo[1], Masanobu Yamamoto[1], Samantha Bova[2], Yair Rosenthal[2]

1. Faculty of Environmental Earth Science, Hokkaido Univ., 2. Rutgers Univ.

Millennial climate changes during the last deglaciation is attributed to changes in the Atlantic Meridional Overturning Circulation (AMOC). Although the millennial climate changes have been observed worldwide, the mechanism by which the AMOC change is transmitted is not clear. One plausible hypothesis is that the AMOC variability changes the heat balance in the northern and southern hemispheres, which in turn changes the mean position of the Intertropical Convergence Zone (ITCZ), which in turn changes global temperature and precipitation. Indeed, it has been reported that when the AMOC weakened the ITCZ shifted southward in the Atlantic and eastern Pacific regions. However, there is no conclusive evidence in the regions away from the Atlantic Ocean.

In this study, to test this hypothesis, we reconstructed the variability of the ITCZ in the western Pacific Ocean over the past 25,000 years by analyzing GDGT and long-chain fatty acid isotopes in marine sediments from IODP site U1485 in the Bismarck Sea off the northern coast of Papua New Guinea (PNG). In PNG, orogenic precipitation caused by the northwest monsoon increase when the ITCZ is located south of PNG. The detrital matter is delivered via the Sepik and Ramu rivers to the study site. Thus, the study site is ideal to capture ITCZ variability.

The CBT and BIT, which reflect river discharge, were higher during Bølling-Allerød (BA) period and lower in the Younger-dryas (YD) period. Stable hydrogen isotope ratios (δ D) of long-chain fatty acid, which reflect atmospheric convective activity (and thus precipitation), were lower in the BA period and higher in the YD period. These results indicate that precipitation in PNG was higher in the BA period and lower in the YD period. This is contrary to the results predicted by the above hypothesis, and suggests that the AMOC weakening did not cause the ITCZ to move southward in the western Pacific.

Keywords: ITCZ, Bismarck Sea, Last deglaciation

©2021. Japan Geoscience Union. All Right Reserved.

A paleoclimatic reconstruction of the southeastern Pacific last deglacial using geochemical proxies obtained from offshore Chile

*Karin Nemoto[1,2], Yusuke Yokoyama[1,2], Adam David Sproson[2], Yosuke Miyairi[2], Takahiro AZE[2], Hiroyuki Matsuzaki[3,4], Yair Rosentha[5], Samantha Bova[5]

1. Department of Earth and Planetary Science, The University of Tokyo, 2. Atmosphere and Ocean Research Institute, The University of Tokyo, 3. The University Museum,The University of Tokyo, 4. School of Engineering, The University of Tokyo, 5. Department of Marine and Coastal Sciences, School of Environmental and Biological Sciences, Rutgers University

The southeastern Pacific is a key location to understand the relationship between global climate change and Southern Ocean condition. The coast of Chile is ideally located to clarify the mechanisms behind local climate change. The Southern Westerly Wind belt (SWW) blows over central Chile and interacts with the Southern Annular Mode, the El Niño-Southern Oscillation (ENSO) and the Atlantic Meridional Overturning Circulation (AMOC). The Antarctic Circumpolar Current (ACC) diverts to the north and the south, causing steep latitudinal gradients off the coast of Chile.

A marine sediment core recovered from offshore Chile (44˚S, 75˚W) was used in this study. The age model of this core is based on 14C Accelerator Mass Spectrometry (AMS) dates. The 10Be and 9Be abundances were measured by AMS and High Resolution Inductively Coupled Plasma Mass Spectrometry, respectively. The organic elemental analyzer was used to measure organic C, N and S.

The variation in 10Be may reflect atmospheric conditions such as the location of the SWW and associated precipitation since 10Be is produced in the atmosphere. The amount of 10Be and 9Be are affected not only by the source but also by delivery. When 10Be is normalized by 9Be, the latter effect can be offset (Simon et al., 2016). The 10Be/9Be may reflect atmospheric processes since the ratio is highly controlled by 10Be. The results of 10Be/9Be and 10Be indicates the intensity of the SWW became stronger and the amount of precipitation was increased from 12 ka to 3 ka, which is antiphase to those in the core zone of the SWW (Lamy et al., 2010).

Most of the records from both this and previous research fluctuate around 12 ka, 8 ka and 3 ka. Climatic changes off the coast of Chile are associated with changes in the ACC and the SWW. The changes observed in this study clearly suggests close relationship with global climate indicating importance of coupling between atmosphere and ocean in this region.

References

Lamy F. et al. Modulation of the bipolar seesaw in the Southeast Pacific during Termination 1. Earth Planet. Sci. Lett. 259, 400-413 (2007).

Pike J., Swann G.E.A., Leng M.J. & Snelling A.M. Glacial discharge along the west Antarctic Peninsula during the Holocene. Nat. Geosci. 6, 199-202 (2013).

Simon Q. etal. Authigenic $^{10}Be/^{9}Be$ ratios and ^{10}Be-fluxes ($^{230}Th_{xs}$-normalized) in central Baffin Bay sediments during the last glacial cycle: Paleoenvironmental implications. Quat. Sci. Rev. 140, 142-162 (2016).

©2021. Japan Geoscience Union. All Right Reserved.

Keywords: paleoclimate, westerly, beryllium

©2021. Japan Geoscience Union. All Right Reserved.

Paleovegetation changes in the northern Mongolia since the last glacial

*Ryosuke Imaoka[1], Koji Shichi[2], Hitoshi Hasegawa[1], Niiden Ichinnorov[3], Nagayoshi Katsuta[4], Davaasuren Davaadorj[5], Masafumi MURAYAMA[1], Masao Iwai[1], masami izuho[6]

1. Kochi University, 2. Forestry and Forest Products Research Institute, 3. Paleontological Center of Mongolia, 4. Gifu University, 5. National University of Mongolia, 6. Tokyo Metropolitan University

Northern Mongolia is located at the boundary between northern permafrost and southern desert belts and is sensitive to climate change such as permafrost thawing. In this study, we aimed to reconstruct changes in paleoenvironment and paleovegetation in northern Mongolia since the last glacial based on the analysis for lake sediment record of Sangiin Dalai lake. We took lake bottom sediment by gravity core in August 2016 (16SD02; 84 cm length), and five boring cores in March 2019 (19SD01~05; ca. 13 m length). Using these sediment cores, we performed palynological analysis at Forestry and Forest Products Research Institute and elemental composition analysis using XRF core scanner at Center for Advanced Marine Core Research, Kochi University.
Based on palynological analysis and biome reconstruction (Tarasov *et al*., 2000), paleovegetation changes from steppe-desert biome dominated by *Artemisia* and Chenopodiaceae in the last glacial to steppe-taiga biome composed of mixture of *Artemisia* and *Pinus* in the Holocene were reconstructed. Elemental composition analysis reveals that higher Si/Ti ratio in sand layer and higher Mn/Fe ratio (oxic environment) and Ca/Ti ratio (saline lake) in silt layer during the last glacial, and low Ca/Ti ratio (less saline lake) during the Holocene. Thus, marked paleoenvironmental change from shallow lake and alluvial plain during the last glacial to high lake-level during the Holocene are reconstructed. These result, in conjunction with palynological data-sets in surrounding area (Kotokel lake in southern Siberia: Shichi *et al*., 2009; and Orog lake in southern Mongolia: Yu *et al*., 2019) suggests that predominance of steppe-desert vegetation in southern Siberia and northern/southern Mongolia during the last glacial, and turned to Forest vegetation in southern Siberia, steppe-taiga vegetation in northern Mongolia, and desert vegetation in southern Mongolia during the Holocene, which likely caused by permafrost thawing by insolation change and climatic warming in deglaciation period.

References

Shichi, K., *et al*. (2009). Late Pleistocene and Holocene vegetation and climate records from Lake Kotokel, central Baikal region. *Quaternary International*, *205*, 98-110.

Tarasov, P. E., *et al*. (2000). Last glacial maximum biomes reconstructed from pollen and plant macrofossil data from northern Eurasia. *Journal of Biogeography*, *27*, 609-620.

Yu, K., *et al*. (2019). Late Quaternary environments in the Gobi Desert of Mongolia: Vegetation, hydrological, and palaeoclimate evolution. *Palaeogeography, Palaeoclimatology, Palaeoecology*, *514*, 77-91.

Keywords: Pollen analysis, Vegetation reconstruction, Last glacial period, Permanent frost, Global warming

©2021. Japan Geoscience Union. All Right Reserved.

©2021. Japan Geoscience Union. All Right Reserved.

Glacial–interglacial variations in the Leeuwin Current for the last 50,000 years based on Nd isotope records of benthic foraminifers

*Ryota Wako[1], Hideko Takayanagi[1], Shigeyuki Wakaki[2], Takeshige Ishiwa[4], Yusuke Yokoyama[5], Hitomi Uchimura Wakaki[3], Tsuyoshi Ishikawa[2], Yasufumi Iryu[1]

1. Department of earth science, Tohoku university , 2. Kochi Institute for Core Sample Research, JAMSTEC, 3. Center for Advanced Marine Core Research, Kochi University, 4. National Institute of Polar Research, 5. Atmosphere and Ocean Research Institute, University of Tokyo

The Leeuwin Current (LC) is a major warm current flowing poleward from the equatorial region along the west coast of Australia. Variations in the air-sea interaction in its surrounding area (e.g., ENSO and wind strength) and the intensity of the Australian monsoon are known to have a strong influence on the strength and pathway of the LC at the seasonal to interannual time scales. However, it is still controversial how the LC responded to paleoclimate and paleoceanographic conditions at the millennial or longer time scales, such as glacial-interglacial climate changes. In this study, we analyzed neodymium (Nd) isotope composition (ε Nd) of bulk benthic foraminifers from shallow-water to hemipelagic carbonate sediment cores (IODP Exp. 356 sites U1460, U1461, and U1463 from south to north) collected off West Australia to understand water mass exchanges and variations in the strength and pathway of the LC for the last 50,000 years.

Nd isotope results indicate that the coastal current, which flows the surface between the LC and Australian continent, became predominant at least in coastal areas around U1461 in the latest Pleistocene. This may indicate that the pathway of the LC moved slightly offshore at northwestern Australia due to the stronger Australian monsoon and/or thickening of surface to sub-surface water masses during the postglacial period. While, during the last glacial maximum (MIS2), the ε Nd composition of all sites exhibited more radiogenic values than those of the postglacial period. Our results suggest that, although the ε Nd values of the studied cores were affected by sea-level changes, the LC region was predominantly influenced by Pacific-origin waters flowing into the Indian Ocean from the northern and southern Pacific Ocean through the Indonesian Through Flow even during the last glacial period.

Keywords: Neodymium isotope composition, Leeuwin Current, Benthic foraminifera, Glacial-interglacial, Paleoenvironment, IODP

©2021. Japan Geoscience Union. All Right Reserved.

Changes in carbonate dissolution and preservation in Southern Ocean sediment off Chilean margin during the last 140 kyrs based on fragmentation and size-normalized weight of planktic foraminiferal tests.

*Takuto Kasuya[1], Yusuke Okazaki[2], Shinya Iwasaki[3], IODP Expedition 383 Scientific Party

1. Department of Earth and Planetary Sciences, School of Science, Kyushu University , 2. Department of Earth and Planetary Sciences, Faculty of Science, Kyushu University, 3. MARUM Center for Marine Environmental Sciences and Department of Geosciences, University of Bremen

The Southern Ocean plays an important role in global climate change as a reservoir of heat and carbon. Glacial atmospheric carbon dioxide concentrations were 80-100 ppm lower than the interglacial level. Changes in $CaCO_3$ dissolution and preservation in the deep-sea particularly for the Southern Ocean is thought to be a key factor for glacial carbon reservoir. In this study, we investigated change in dissolution and carbonate preservation in Southern Ocean sediment for the last 140 kyrs based on two proxies, fragmentation index and size-normalized weight of planktic foraminiferal tests. Fragmentation index represents a ratio of the number of fragments to the intact planktic foraminiferal tests. Two planktic foraminiferal species, *Neogloboquadrina pachyderma* and *Globigerina bulloides* were employed. For size-normalized weight of planktic foraminiferal tests, *Globigerina bulloides* tests were picked up from the 212-250 μm, 250-300 μm, and 300-355 μm sieve fractions. Sediment core samples used in this study were obtained at Site U1543 (54°35.06’ S; 76°40.58’ W; 3864 m water depth) in the eastern South Pacific west of the Chile Trench during the International Ocean Discovery Program (IODP) Expedition 383 in 2019. At U1543, foraminiferal tests in the sediment have been preserved only during glacial terminations to early interglacials during the last 140 kyrs, which is consistent with expected deep-sea carbonate ion response to atmospheric CO_2 elevations during the glacial terminations. During the last interglacial period (marine isotope stage 5e), both fragmentation ratio and size-normalized weight of planktic foraminiferal tests suggested two carbonate dissolution events at millennial time-scale.

Keywords: Carbonate preservation / dissolution, Southern Ocean, MIS 5, Planktonic foraminifera

©2021. Japan Geoscience Union. All Right Reserved.

Examining MIS 5e Sea-Levels around Japan: 60+ Years of Sea-Level Proxy Analysis and Applied Dating Techniques

*Evan Tam[1,2], Yusuke Yokoyama[1,2]

1. University of Tokyo, Atmosphere and Ocean Research Institute, 2. University of Tokyo, Graduate Program on Environmental Science

Sea-level proxies chronicling Marine Isotope Stage 5e (MIS 5e, ca. 124 ka) have been examined in Japanese geologic literature for over at least the last 60 years. Formed during sea-level highstands and preserved predominantly by tectonic uplift processes, sea-level proxies in Japan are commonly identified as marine terraces and are chronologically constrained by their relation to identified tephra layers or other dated strata. Stratigraphic correlations are used in conjunction to numerous dating techniques such as paleontological analysis, tectonic uplift rates, tephra (volcanic ash), Uranium-Thorium (U/Th), Carbon 14 (^{14}C), and Optically Stimulated Luminesce (OSL) dating techniques, linking these landforms to MIS 5e and a broader global history. Commissioned by the World Atlas of Last Interglacial Shorelines (WALIS), this study standardized data from over 70 studies, assembling data points for over 300 locations to create an updated overview of MIS 5e proxy sea-levels throughout Japan.

Keywords: Paleosea-level, MIS 5e, Last Interglacial

©2021. Japan Geoscience Union. All Right Reserved.

Integrated stratigraphy of the sediment core retrieved from the Manihiki Plateau in the central Pacific and the paleotemperature change for the last 800 kyr

*MISAKI URAKAMI[1], Takuya Sagawa[2], Yoshimi Kubota[3]

1. College of Science and Engineering, Kanazawa University, 2. Institute of Science and Engineering, Kanazawa University, 3. National Museum of Nature and Science

East-west sea surface temperature (SST) difference in the tropical Pacific like today developed after about 1.7 million years ago. Although many previous studies have investigated the evolution of the tropical Pacific SST using sediment cores in the east and west tropical Pacific, the central tropical Pacific SST is not well understood mainly due to the lack of long and continuous Pliocene/Pleistocene proxy record. The Manihiki Plateau is located at the southeastern edge of WPWP and is ideally situated to discuss the central tropical Pacific temperature changes. Here, we constructed an age model of the piston cores collected from the Manihiki Plateau (KR99-12 PC05) based on the magnetostratigraphy, the planktonic foraminiferal biostratigraphy, and the oxygen isotope stratigraphy. We obtained a total of 11 age constraints including four planktonic foraminiferal biohorizons and seven oxygen isotopic stratigraphic horizons in addition to five paleomagnetic polarity reversals reported by previous research. The results indicate that the core PC05 is continuously accumulated for the last 2.2 Ma with sedimentation rate of ~0.8 cm/kyr. We will also discuss the central Pacific SST change for the last 800 kyr reconstructed by Mg/Ca-paleothermometry of planktonic foraminifera.

©2021. Japan Geoscience Union. All Right Reserved.

Preliminary results of oxygen isotopic, paleomagnetic, and pollen analyses from a mid-Piacenzian marine succession in the Boso Peninsula, central Japan.

*Yuki Haneda[1]

1. Geological Survey of Japan, AIST

The Pliocene climate is one of the best analogs for the climate of a globally warmer future. In this presentation I show preliminary results of oxygen isotopic, paleomagnetic, and pollen analyses from the uppermost part of the Anno Formation, which is a forearc basin-fill deposit distributing in the Boso Peninsula. Lithological observations were conducted along the Minato River and its branch stream in Futtsu city, Chiba. The examined interval consists of silty stone, and pumice, scoria, and fine volcanic ash beds. Fifty-five samples for oxygen isotopic, paleomagnetic, and pollen analyses were collected from silty beds.
Progressive alternating field and thermal demagnetizations were conducted for each specimen to remove secondary remanence. Paleomagnetic results show a directional change from a reversed polarity to a normal polarity with transitional directions in the uppermost part of the examined interval. Oxygen isotope analyses were conducted for benthic foraminifera *Melonis pompiloides*, and *Bolivinita quadrilatera*. Resultant oxygen isotope record shows a glacial period in the lowermost part of the examined interval ($\delta^{18}O$ = ca. 3.70 ‰), and subsequent warm periods with a minor fluctuation of $\delta^{18}O$ between 3.07 ‰and 3.24 ‰in the upper interval. When comparing the oxygen isotope and paleomagnetic records of this study to the chronostratigraphy of the Anno Formation (Haneda & Okada, 2019), the examined interval ranges from Marine Isotope Stage (MIS) M2 to KM5 in the Mammoth Reversed Polarity Subchron.
A preliminary analysis of pollen fossil was conducted for 6 samples. All samples well preserve pollen fossils, and predominantly yield Taxodiaceae with *Cathaya* and *Quercus* (subgen. *Cyclobalanopsis*) as minor components. This flora indicates a warmer climate than present. Two samples from the MIS M2 interval yield genus *Picea*, *Tsuga*, and *Alnus*, likely indicating cooler climate condition relative to other 4 samples, consistent with the benthic oxygen isotope record. The oxygen isotope, paleomagnetic, and pollen records in this study indicate that the uppermost part of the Anno Formation is a potentially remarkable archive, recording paleoclimatic–paleoceanographic variations in the East Asian margin during the mid-Piacenzian warm period.

Keywords: oxygen isotope stratigraphy, magnetostratigraphy, pollen fossil, mid-Piacenzian Warm Period, Boso Peninsula, Anno Formation

©2021. Japan Geoscience Union. All Right Reserved.

The mid-Pliocene Warm Period: climate sensitivity to atmospheric CO_2 levels and inclusion of dynamic vegetation in the MIROC4m model

*Wing-Le Chan[1], Ayako Abe-Ouchi[1,2]

1. Atmosphere and Ocean Research Institute, The University of Tokyo, 2. National Institute of Polar Research

The mid-Pliocene Warm Period (mPWP), 3.3-3 million years ago, was a period of sustained warmth before global cooling occurred and a shift to glacial cycles. It was also the most recent time in the history of Earth when atmospheric CO_2 levels were similar to those of present day. The study of this period is thus of much importance, given the growing concerns over future climate change associated with anthropogenic emissions of greenhouse gases. A number of climate models have been used to investigate the mPWP climate, contributing to the Pliocene Model Intercomparison Project (PlioMIP), while a large collection of proxy data from both terrestrial and marine sources have become available. Reconciling model results and proxy data remains an important issue.

In our study, we use the mid-resolution MIROC4m coupled atmosphere-ocean general circulation model and apply ice sheet configuration, land-sea mask, orography and biome distribution based on PRISM data sets, as specified in the second phase of PlioMIP, one of the working groups of PMIP4. We conduct a series of experiments which include a range of atmospheric CO_2 levels given the spread in values suggested by different sources of proxy data and show how various aspects of the climate respond. While sea surface temperatures (SST) for all CO_2 levels show much less warming in the northern high latitudes as suggested by previous proxy data, there is improved agreement with more recent data in the tropical Pacific for 400ppm CO_2. We will show these and other results. Additional experiments were carried out with MIROC4m coupled to a dynamic global vegetation model. Compared to the prescribed Pliocene vegetation, temperate forests expand at mid-latitudes across Asia and North America. Across North Africa, shrubs and bare ground expand, replacing regions of savanna. Global surface temperatures are slightly lower with the inclusion of dynamic vegetation.

Keywords: Pliocene, climate modeling, dynamic vegetation, data-model comparison

©2021. Japan Geoscience Union. All Right Reserved.

Chemical weathering feedback during the early Paleogene hyperthermals based on osmium isotope analysis

*Kakeru Ikegami[1], Kazutaka Yasukawa[1,2], Erika Tanaka[1], Junichiro Ohta[1,2], Yusuke Kuwahara[1], Moei Yano[2,1], Koichiro Fujinaga[2,1], Yasuhiro Kato[1,2]

1. School of Engineering, The University of Tokyo, 2. ORCeNG, Chiba Institute of Technology

During the early Paleogene, multiple rapid global warming events called ‘hyperthermals’ occurred in a geologically short time scale (10^4–10^5 yr) [1]. These events coincided with distinct negative carbon isotope ($\delta^{13}C$) excursions, which indicates that the cause of hyperthermals was massive injection of ^{13}C-depleted greenhouse gases [2].

Chemical weathering of continental silicate rocks is known as one of the recovery processes from such warming events. Some previous studies have shown an intensification of the chemical weathering during the Paleocene-Eocene Thermal Maximum (PETM), using an osmium isotope ratio ($^{187}Os/^{188}Os$) in the ocean, which can constrain the changes in chemical weathering associated with short-term warming [3,4]. However, the marine Os isotope record during the early Eocene hyperthermals, including the PETM, has not been reported from the pelagic area of the Pacific Ocean.

In the presentation, we will report the results of $^{187}Os/^{188}Os$ measurement of deep-sea sediment samples collected from Ocean Drilling Program Site 1215 Hole A in the central North Pacific Ocean, which record multiple hyperthermal events including the PETM, Eocene Thermal Maximum (ETM) 2 and ETM3 [5]. Based on the analytical results, we will discuss the changes in the intensity of chemical weathering of continental silicate rocks during each hyperthermal event.

[1] Zachos et al. (2008) *Nature* **451**, 279-283. [2] Lunt et al. (2011) *Nature Geoscience* **4**, 775-778. [3] Ravizza et al. (2001) *Paleoceanography* **16**, 155-163. [4] Dickson et al. (2015) *Palaeogeography, Palaeoclimatology, Palaeoecology* **438**, 300-307. [5] Leon-Rodriquez and Dickens (2010) *Palaeogeography, Palaeoclimatology, Palaeoecology* **298**, 409-420.

Keywords: osmium isotopes, Paleogene, hyperthermals, chemical weathering, Earth system feedback

©2021. Japan Geoscience Union. All Right Reserved.

High latitude paleoenvironments in Southern Hemisphere during mid-Cretaceous

*Hiromichi Komiya[1], Takashi Hasegawa[1]

1. Kanazawa University

Cretaceous is known as a period of warm climate with higher sea levels and higher carbon dioxide concentrations than the present, as well as with active oceanic crust formation and volcanic activity. They were especially prominent during Mid-Cretaceous Cenomanian (100.5-93.9 Ma). Paleoenvironmental studies of the mid-Cretaceous have been conducted mainly in Europe and North America. In those areas, where global environmental changes such as oceanic anoxic events (OAEs) associated with isotope events and cyclic environmental changes derived from orbital forcing of Milankovitch cycle were recognized. In contrast, few studies have been reported in the high latitudes in the southern hemisphere. In high latitudes environmental changes more sensitive to global warming could be recorded. Can they be recognized actually? If yes, how can they be recorded, and can the magnitude and cyclicity be deciphered? This study analyzed the Cenomanian samples from the high latitudes in the Southern Hemisphere. It is a stage that typical Cretaceous greenhouse paleoenvironment developed, under ice-free condition.

This study used core samples from IODP Exp,369 Site U1516C Cores 34R and 35R, which are estimated to be deposited during mid-Cenomanian based on biostratigraphy. For high-resolution analysis, organic carbon isotope ratio (d13Corg), total organic carbon (TOC), total nitrogen (TN) and C/N ratio were obtained and discussed. Biomarker analysis, focused on specific markers such as alkenones that were interpreted to be related to surface productivity. The following were discussed and concluded.

(1) The d18O variations in sea surface temperature as large as 4˚C found by previous study did not have concordant fluctuation with the terrestrial and seafloor environmental changes shown by TOC and d13Corg variations. Land and seafloor were controlled by separate factors.

(2) The variations in d13Corg can be interpreted to be partly related to the redox conditions of the seafloor, rather than being controlled by the mixing ratio of terrestrial and marine in origin.

(3) C37 alkenones derived from haptophytes were recognized. The detection of C37 alkenone with two-unsaturation sites and the absence of that with three-unsaturation sites. These facts suggest that the sea surface temperature at that time may have been higher than the current equatorial water temperature (>28˚C) even in the high latitude. Negative correlation of C40 alkenones with d18O of carbonate indicates its potential significance for paleothermometry.

©2021. Japan Geoscience Union. All Right Reserved.

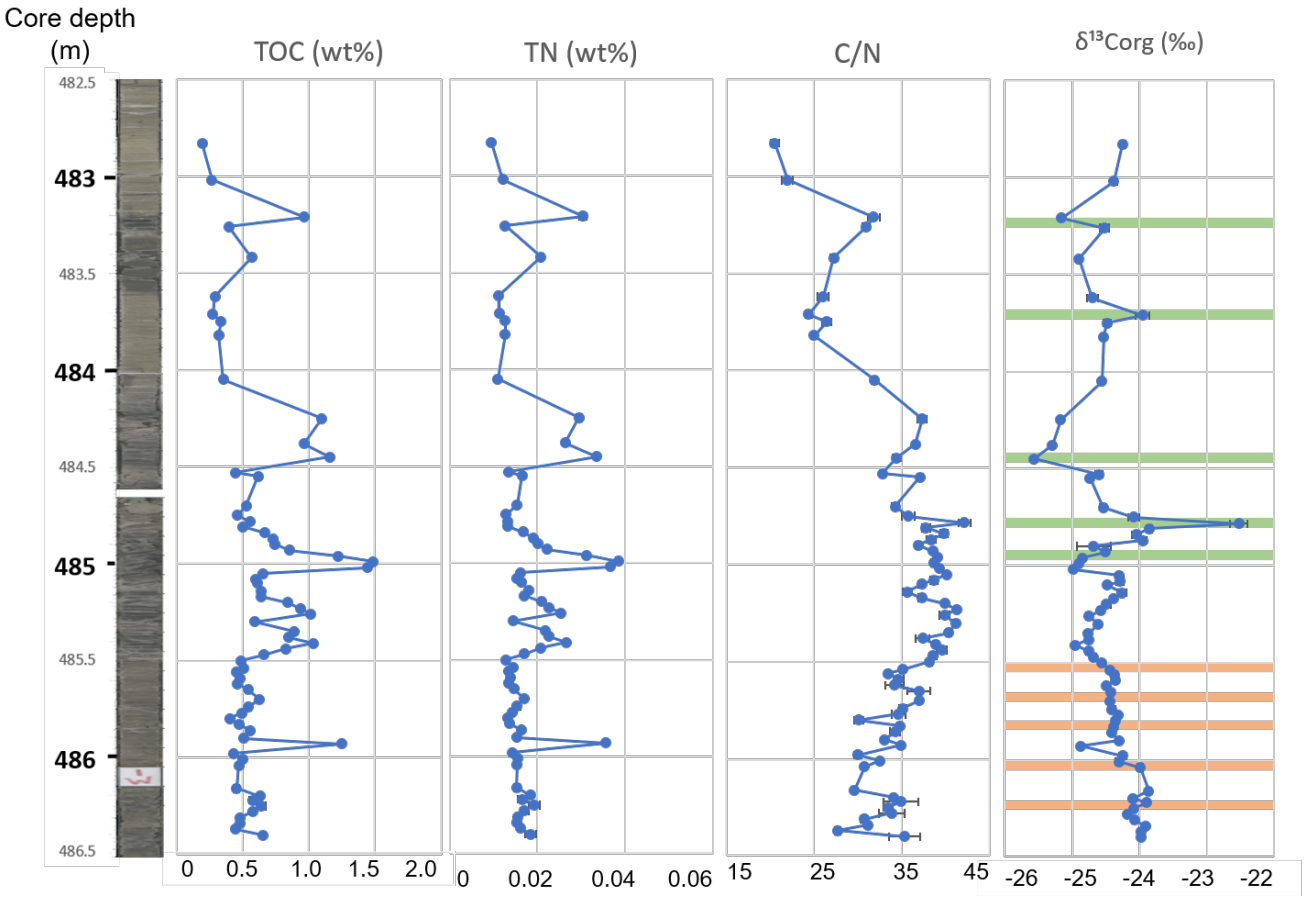

©2021. Japan Geoscience Union. All Right Reserved.

A study on the responses of the climate field in the Cretaceous to orbital parameter changes

*Taro Higuchi[1], Ayako Abe-Ouchi[1], Wing-Le Chan[1]

1. Atmospheric and Ocean Research Institute, the University of Tokyo

Insolation changes to the orbital parameters, such as the eccentricity, obliquity, and precession, have a great impact on the climate. In particular, it is well-known that there have been periodic changes in ice sheets and climatic fields in the past hundreds of thousands of years, related to changes in orbital parameters. The physical mechanism of these changes has been investigated by using numerical simulations. The Cretaceous is known as one of the warmest periods in the Phanerozoic due to increased levels of greenhouse gases, and the proxies indicate the striking temperature amplifications in the high-latitude and polar regions, resulting in a smaller equator-to-pole temperature difference. Also, the Cretaceous cyclic sediments recording signals related to changes in the orbital parameters have been found in many parts of the world. In this study, we investigated the response of the Cretaceous climate field to changes in the orbital parameters using an atmospheric-ocean vegetation coupling model, MIROC4m-LPJ and also compared it with the proxy data and orbital parameter sensitivity experiments using the present-day configuration.
In the high latitude regions, the change in temperature with respect to the change in the orbital parameters is noticeable in the Cretaceous experiment. In particular, in conditions where the northern hemisphere summer is at perihelion and the obliquity is higher than the present-day value, polar amplification as shown by Cretaceous proxy data is obtained. By comparing the hydrological cycle responses in the present day and the Cretaceous, it was found that the fluctuation of the precipitation in East Asia due to orbital parameter changes is larger in the Cretaceous. This is attributed to the major structural changes in the East Asian summer monsoon in the Cretaceous. Furthermore, as a result, the variety of vegetation across East Asia in the Cretaceous has increased.

Keywords: Cretaceous, Orbital parameters, Polar amplification, Asian monsoon

©2021. Japan Geoscience Union. All Right Reserved.

Eccentricity paced increase in the continental weathering in the latest Hauterivian, Early Cretaceous

*Hironao Matsumoto[1], Rodolfo Coccioni[2], Fabrizio Frontalini[2], Kotaro Shirai[1], Junichiro Kuroda[1]

1. Atmosphere and Ocean Research Institute, the University of Tokyo, 2. University of Urbino

The 405-kyr eccentricity is a constant orbital parameter throughout the Phanerozoic and is commonly associated with long-term variations in the global continental weathering mechanism. However, the lack of reliable geological evidence has hampered the understanding of the role of the orbital-parameter on continental weathering during the Cretaceous. Os isotopic ratio ($^{187}Os/^{188}Os$) of sedimentary record reflects the balance between the radiogenic Os derived from continental weathering and unradiogenic Os derived from the unradiogenic sources (e.g., hydrothermal activity, the weathering of mafic rocks, and extraterrestrial sources), and can be therefore regarded as the best proxy for estimation of the global continental weathering. To trace the orbital-paced continental weathering, this study reconstructs the marine Os isotopic records across the Upper Hauterivian to the Lower Barremian (Lower Cretaceous) where previous studies already reported that variation in the clay-mineral composition is paced by the 405-kyr cycle. Our new Os isotopic record shows periodic oscillation of $^{187}Os/^{188}Os$ between 0.7 and 0.9, which corresponds to the 405-kyr Earth’ s eccentricity cycle. Since the sedimentary interval with the radiogenic $^{187}Os/^{188}Os$ values (~0.9) corresponds to an interval characterized by intensive humidity in areas surrounding the Tethys, a variation of $^{187}Os/^{188}O$ likely reflects the cyclic changes in the continental weathering caused by the eccentricity-paced intensification of monsoonal activity at low latitude. This variation could have been further amplified by the increase in the radiogenic Os input from higher latitude Paleozoic shale and Pre-Cambrian crust that was caused by the latitudinal shift of the intertropical convergence zone.

Keywords: osmium, Cretaceous

©2021. Japan Geoscience Union. All Right Reserved.

Millennial-scale cyclicities recorded in the Cretaceous lacustrine core using Monte Carlo approach

*Hitoshi Hasegawa[1], Hirofumi Asahi[2]

1. Faculty of Science and Technology, Kochi University, 2. Center for Advanced Marine Core Research, Kochi University

Detail paleoclimatic records under exceptionally warm “hothouse” condition provide crucial insights toward future climate predictions. However, climatic variations in millennial-scale at such deep-time archives commonly faces difficulties owing to the large uncertainties of absolute age at more than hundred kyr-scale. Annually laminated lacustrine deposits of Early Aptian (ca. 123–119 Ma) in southeast Mongolia firstly enable to obtain millennial- and shorter time-scale climate variability at such immemorial period. By combining μm-scale analysis of fluorescence microscopy images (seasonal resolution) and ultra-high-resolution elemental XRF scanning techniques (~1–5 year resolution), we were able to generate a continental climate record of unrivalled temporal resolution. Age model of the subject core was established at annual- to decadal time-scale, taking account a casual relation of ITRAX elemental composition and (annually formed) varve thickness. FFT power spectrum of high temporal resolution and long duration ITRAX record, with consideration of maximum age uncertainties (Monte-Carlo approach), exhibit partial presences of millennial-scale extreme drought events during the mid-Cretaceous ‘hothouse’ periods.

Keywords: Varve, Millennial-scale cyclicity, Age uncertainty, Monte Carlo approach

©2021. Japan Geoscience Union. All Right Reserved.

[J] Poster | M (Multidisciplinary and Interdisciplinary)：M-IS Intersection

Sat. Jun 5, 2021 5:15 PM - 6:30 PM JST | Sat. Jun 5, 2021 8:15 AM - 9:30 AM UTC | Ch.21_4

[M-IS17] Interface- and nano-phenomena on crystal growth and dissolution

convener:Yuki Kimura(Institute of Low Temperature Science, Hokkaido University), Hitoshi Miura(Graduate School of Science, Department of Information and Basic Science, Nagoya City University), Hisao Satoh(Low-Level Radioactive Waste Disposal Center, Japan Nuclear Fuel Limited)

Recent developments of observations in nano-scale opened a detail discussion concerning mechanisms of crystal growth and dissolution based on interface phenomena including dynamics. In this session, growth and dissolution mechanisms of crystals will be discussed focusing on interface phenomena of minerals in the fields of biological origin, global environment, planets and space in addition to general minerals.

[MIS17-P01] Toward for the developing the thermal storage materials utilizing the Electrostatic Levitation Furnace in "Kibo" in space

*Hidekazu Kobatake[1], Kazuki Tonooka[2], Shumpei Ozawa[2], Ken'ichi Sugioka[3], Suguru Shiratori[4], Ken Nagashima[5], Hirohisa Oda[6], Hideki Saruwatari [6], Chihiro Koyama[6], Takehiko Ishikawa[6] (1.Hirosaki University, 2.Chiba Institute of Technology, 3.Toyama Prefectural University, 4.Tokyo City University, 5.Hokkaido University, 6.JAXA)

[MIS17-P02] Heteroepitaxial growth mechanism in colloidal crystallization

*Jun Nozawa[1], Hiromasa Niinomi[1], Junpei Okada[1], Satoshi uda[1] (1.Tohoku University)

[MIS17-P03] Fabrication of evaluation model for adgesion mechanism between bone mineral and soft tissue

*Yuki Sugiura[1], Masahiro Okada[2], Ken Hirano[1], Takuya Matsumoto[2] (1.National Institute of Advanced Industrial Science and Technology, 2.Okayama University)

[MIS17-P04] Conversion from a stable crystal to a metastable crystal by grinding

*Hiroyasu Katsuno[1], Makio Uwaha[2] (1.Institute of Low Temperature Science, Hokkaido University, 2.Center for General Education, Aichi Institute of Technology)

[MIS17-P05] Improvement of transmission electron microscope images by neural network model

*Hiroyasu Katsuno[1], Shizuka Hirakawa[1], Tomoya Yamazaki[1], Ichigaku Takigawa[2], Yuki Kimura[1] (1.Institute of Low Temperature Science, Hokkaido University, 2.RIKEN, Center for Advanced Intelligence Project)

[MIS17-P06] Development of an early detection method of nucleation in in-situ liquid-cell TEM observation

*Yuki Kimura[1], Hiroyasu Katsuno[1], Tomoya Yamazaki[1], Ichigaku Takigawa[2,3] (1.Institute of Low Temperature Science, Hokkaido University, 2.AIP, RIKEN, 3.ICReDD, Hokkaido University)

[MIS17-P07] In-situ observation at the moments of bubble nucleation using a liquid-cell transmission electron microscope

*Yuki Kimura[1], Tomoya Yamazaki[1], Hiroyasu Katsuno[1], Shizuka Hirakawa[1] (1.Institute of Low Temperature Science, Hokkaido University)

Toward for the developing the thermal storage materials utilizing the Electrostatic Levitation Furnace in "Kibo" in space

*Hidekazu Kobatake[1], Kazuki Tonooka[2], Shumpei Ozawa[2], Ken'ichi Sugioka[3], Suguru Shiratori[4], Ken Nagashima[5], Hirohisa Oda[6], Hideki Saruwatari [6], Chihiro Koyama[6], Takehiko Ishikawa[6]

1. Hirosaki University, 2. Chiba Institute of Technology, 3. Toyama Prefectural University, 4. Tokyo City University, 5. Hokkaido University, 6. JAXA

Thermal storage has attracted attention for stabilizing the supply of renewable energy or for the utilization of the heat, which is emitted from the industry. Thermal storage technology has the potential to efficiently store and stabilize thermal energy in relatively compact equipment, but it is necessary to increase the heat exchange efficiency and durability. A phase-separated alloy has predictably effective for that purpose as thermal storage materials. Thermophysical properties of the phase-separated alloy of molten state are required to control the microstructure of the alloys. Despite the importance, it is difficult to measure the thermophysical properties of molten alloys on the ground.
In this project, we focus on phase-separated alloys such as Fe-Cu, Al-Si, and Cu-Si, measure their thermophysical properties and nucleation rate in outer space, and aim to design highly efficient energy storage materials.

Keywords: Thermophysical property, Electro Static Levitation

©2021. Japan Geoscience Union. All Right Reserved.

Heteroepitaxial growth mechanism in colloidal crystallization

*Jun Nozawa[1], Hiromasa Niinomi[1], Junpei Okada[1], Satoshi uda[1]

1. Tohoku University

Colloidal crystals, periodic arrays of colloidal particles, have been attracting great attention due to their versatile applications such as novel optical devices. Besides, the colloidal crystals have been regarded as a useful model of various phenomena as it displays similar phase transition to the atomic system. Among variable methods to control growth and structure of the colloidal crystals, a colloidal epitaxy that utilizes a patterned substrate is an effective technique. However, the technique has been limited to homoepitaxial growth, where structure and lattice spacing of the substrate and epitaxial phase are similar. In this thesis, colloidal crystals are fabricated with the heteroepitaxial growth, where lattice constant of the substrate and epitaxial layer is different. The mechanism is discussed for the heteroepitaxial growth in colloidal crystallization.

Polystyrene particles of 700 nm was used to grow the epitaxial layers. The particle size of the substrates is ranged from 400 to 1300 nm. The sodium polyacrylate is added to induce depletion attractive interaction, by which colloidal crystallization is achieved. The lattice misfit ratio is defined as the $(d_{eq} - d_{subst})/ d_{eq}$, where d_{eq} is equilibrium particle distance as the particle distance of colloidal crystals formed without the substrate (on cover glass), and d_{subst} is lattice spacing of the substrate. The heteroepitaxial growth was performed in various lattice misfit ratios.

Three growth modes are recognized in the experiment: Layer-by layer, Layer-plus-island, and Island, which is denoted as FM, SK, and VW mode, respectively, as is the heteroepitaxial growth of atomic system. This has been firstly recognized in the growth of the colloidal crystals. Importantly, SK mode in some growth conditions is transitioned into VW by decomposition of the formed layers, the process of which is uncovered by the in-situ observation.

Contrary to the expectation, growth modes do not show clear correlation with the lattice misfit ratio. We inferred that interaction between epitaxial layer and the substrate influences the epaxial growth. Relative particle interaction between substrate and the epitaxial layer is estimated by the strength of the depletion interaction. Consequently, three growth modes are suitably categorized by using two parameters; the interaction between substrate and epitaxial layers as well as the lattice misfit ratio. The findings in the study will well contribute to rational control of the structure and phase of the colloidal crystals.

Keywords: Colloidal crystals, Epitaxial growth

©2021. Japan Geoscience Union. All Right Reserved.

Fabrication of evaluation model for adgesion mechanism between bone mineral and soft tissue

*Yuki Sugiura[1], Masahiro Okada[2], Ken Hirano[1], Takuya Matsumoto[2]

1. National Institute of Advanced Industrial Science and Technology, 2. Okayama University

The disadvantages of surgical sutures, such as secondary tissue damage, surgical site infection, and liquid leaking, can be reduced by biological softtissue adhesives. Although non-bioresorbable bone substitute materials sufficiently adhere to soft tissues, enabling immobilization of implantable devices, their non-bioresorbable property limits their clinical use. This study reports the excellent adhesion properties of octacalcium phosphate (OCP), a bioresorbable mineral analogue of immature bone. Blocks of OCP strongly adhere to mouse dermal tissues, enhancing their protein adsorption capacity as demonstrated in ex vivo shear adhesion tests. When soaked in antibacterial solution, the OCP blocks easily adsorb the antibacterial agents in their internal nano-pores and on their surfaces, imbuing them with antibacterial ability. Therefore, the OCP blocks are a solid-state material with strong adherence to biological soft tissues and, are especially promising for detachable body-implantable and/or external devices.

Keywords: bone mineral, calcium phosphate, bone formation, biological adhesive

©2021. Japan Geoscience Union. All Right Reserved.

Conversion from a stable crystal to a metastable crystal by grinding

*Hiroyasu Katsuno[1], Makio Uwaha[2]

1. Institute of Low Temperature Science, Hokkaido University, 2. Center for General Education, Aichi Institute of Technology

Materials have some crystal structures. In general cases, the crystal structure of the ground state is unique. Other structures with higher free energy are thermodynamically metastable. When stable and metastable crystals coexist in a system, the stable crystal grows and the metastable one shrinks. Although temporal appearance of metastable crystal is well known as the Ostwald’ s step rule, eventually large stable crystals form in the system in equilibrium.

In the case of a chiral crystal, the chiral pair of crystal structures are realized with the same probability since the pair of structures are energetically equal. In 2005, Viedma discovered the conversion from racemic mixture of chiral sodium chlorate crystals to crystals with single chirality in a saturated solution by stirring with glass beads. In this system, the racemic mixture of crystals is the equilibrium state, and the single chirality state is the one of metastable states. This phenomenon is distinguished from the ordinary Ostwald ripening and called Viedma ripening. One of the hypotheses, which explain Viedma ripening, is the acceleration of crystal growth by the cluster incorporation. If the mechanism of Viedma ripening works effectively, it might be possible to convert from crystals of a stable structure to crystals of a metastable structure.

We demonstrate the conversion from crystals of a stable structure to crystals of a metastable structure using the theoretical idea of Viedma ripening. We introduce the generalized Becker-Döring model, which includes the cluster incorporation to the crystal of the same structure. When the amount of metastable crystals is large enough for that of stable crystals, metastable crystals grow and stable ones disappear at the steady state. If the cluster incorporation mechanism does not work, the amount of the metastable crystal is not amplified from any initial state. The system only reaches the equilibrium as well as the case without crystal grinding. Grinding effectively breaks crystals, and supplies small clusters, and then, the metastable crystals completely consumes the stable crystals by the acceleration of crystal growth due to the small cluster incorporation.

Keywords: phase conversion, cluster incoporation, crystal grinding

©2021. Japan Geoscience Union. All Right Reserved.

Improvement of transmission electron microscope images by neural network model

*Hiroyasu Katsuno[1], Shizuka Hirakawa[1], Tomoya Yamazaki[1], Ichigaku Takigawa[2], Yuki Kimura[1]

1. Institute of Low Temperature Science, Hokkaido University, 2. RIKEN, Center for Advanced Intelligence Project

Transmission electron microscopy (TEM) is a powerful tool in the field of material science and provides structural information by visualizing at the atomic level. In order to obtain a clear image, improvements of hardware and software are proceeded. Despite of its benefits, the application is limited due to the electron beam damage and the time resolution. One of the important techniques in the high resolution TEM imaging is dictionary learning method, which is called sparse coding [A. Stevens *et al.*, Microscopy **63**, 41 (2014)]. This method provides a denoised image from a noisy image by using a linear combination of basic elements. Sparse coding is succeeded in the field of scanning TEM imaging and electron holography [S. Anda *et al.*, Ultramicroscopy **206** 112818 (2019)].

Recently, the image improvement by machine learning is evolved remarkably. To support the improvement for low-light image processing, a dataset, including short-exposure low-light images and corresponding long-exposure reference images, are introduced [C. Chen *et al.*, arXiv:1805.091934 (2018)]. In this paper, we apply this idea to the TEM imaging and demonstrate the improvement of TEM image by a convolutional neural network (CNN) model.
For the training of CNN, we prepare the training dataset of TEM images, which is a pair of low-exposure images and corresponding long-exposure reference images. The exposure time is about 1—10 ms and 1 s for low-exposure and long-exposure images, respectively. The images were observed using a CMOS camera (Flash, EM-Z15327TCMOS; JEOL Ltd.). Before the training, the dataset is preprocessed: adjusting the position and equalizing/rescaling the brightness of each image. The network architecture of our model is UNet with ResNet encoder. During training, we minimize the L_1 loss between the image predicted from low-exposure image and the long-exposure image. Using about 100 images for training, the noise is removed, and the edges become clear on the verification images. We will show the condition of our model in detail and examples for some materials.

Keywords: Machine learning, Transmission electron microscopy, Convolutional neural network

©2021. Japan Geoscience Union. All Right Reserved.

Development of an early detection method of nucleation in in-situ liquid-cell TEM observation

*Yuki Kimura[1], Hiroyasu Katsuno[1], Tomoya Yamazaki[1], Ichigaku Takigawa[2,3]

1. Institute of Low Temperature Science, Hokkaido University, 2. AIP, RIKEN, 3. ICReDD, Hokkaido University

One of our goal is direct observation at the moments of nucleation in atomic scale. Nucleation process seems easy: Growth units agglomerate and form a particle by overcoming a nucleation barrier, which depends on a difference of the chemical potentials of two phases. However, recent investigations using a liquid-cell transmission electron microscope (LC-TEM) have reported more complex processes in the actual case. For instance, oriented-attachment growth of nano-crystallites [1] and the two-step nucleation of calcium carbonate [2] are reported. We found that two types of amorphous particles with different roles and properties promote protein crystallization [3]. It is easy to observe a nucleation by our naked eye or under optical microscope because of lower magnifications, i.e., large solution volume. However, it is not easy to observe a nucleation process in atomic scale under TEM, because even if the nucleation rate is controlled to be very high, the solution volume in the field of view is much smaller and, therefore, expected number of nuclei becomes much lower. In addition, it is also difficult to increase nucleation rate dramatically after starting the observation. Recent achievements have been based on great efforts such as a bunch of experimental runs and long-term observations. Therefore, to observe whole a process of nucleation with higher magnification, we are trying to develop an early detection method of a nucleation event in a stochastic nature using a neural network model.

Acknowledgement

This work was supported by Grant-in-Aid for Scientific Research (S) of JSPS KAKENHI Grant Number 20H05657.

References

[1] D. Li et al., Science 336 1014 (2012).
[2] M. H. Nielsen et al., Science 345 1158 (2014).
[3] T. Yamazaki et al. PNAS 114 2154 (2017).

Keywords: Nucleation, Machine learning, Transmission electron microscopy

©2021. Japan Geoscience Union. All Right Reserved.

In-situ observation at the moments of bubble nucleation using a liquid-cell transmission electron microscope

*Yuki Kimura[1], Tomoya Yamazaki[1], Hiroyasu Katsuno[1], Shizuka Hirakawa[1]

1. Institute of Low Temperature Science, Hokkaido University

Recently, the development of solution cells sandwiched between graphene or silicon plates has made it possible to overcome the high vacuum environment unless the spatial limitation of a TEM sample chamber. As a result, the "in-situ" observation of phenomena in solution using TEM is being actively conducted [e.g., Nielsen et al. *Science* 345 (2014) 1158]. We have been working on this method since its early days and have succeeded in directly observing nucleation processes. For instance, we found multistep nucleation in the crystallization process of lysozyme protein crystal, which crystallized via dense liquid [Yamazaki, Kimura et al. *PNAS* 114 (2017) 2154]. Since dehydration is a largest barrier for crystallization in an aqueous solution, it seems that lysozyme molecules agglomerate together with their hydrated layers at first and then gradually dehydrate to be a crystal. In addition, the crystallinity gradually becomes higher due to mobile defects and occasionally undergoes a phase transition to a more stable crystal [Yamazaki, Van Driessche, Kimura *Soft Matter*, 16 (2020) 1955]. In these in-situ TEM observations, the effects of the electron beam are largest concern and must be considered to discuss an observed process.

When observing an aqueous solution by TEM, water radiolysis due to electron beam irradiation is inevitable. Electrons generate protons, ions, and radicals in the aqueous solution. Then, solution environment varies and, therefore, it makes difficult to discuss crystal growth and conduct experiments that simulate environments such as living organisms. Furthermore, bubbles may be generated depending on the conditions and, in case, the experimental run cannot be continuing anymore. Therefore, estimation of the solution environment, such as temperature, pH, and concentrations of ion, hydrogen, and oxygen, has been attempted in response to electron beam intensity by solving many equations of possible chemical reactions [Schneider et al, *J. Phys. Chem. C*. 118 (2014) 22373; Ambrožič et al. *Chem. Sci.* 10 (2019) 8735]. Generally, electron beam irradiates only on an area of the window on a liquid cell, and there are abundant aqueous solutions around it that are not directly irradiated by the electron beam. Even if we predict the relationship between the amount of generated hydrogen and oxygen and their equilibrium concentrations, we cannot expect a bubble formation, because bubbles are generated through a nucleation after supersaturation. Therefore, observed conditions such as the magnification and the brightness (electron dose rate) of the field of view are adjusted based on experience. To overcome these difficulties, in this study, we conducted an experiment to observe the moments of nucleation of bubbles in situ while accurately measuring the electron dose rate using a Faraday cup. We will show the detail experimental results and imprecations on the bubble formation for future in-situ observation.

Keywords: nucleation, liquid-cell TEM, TEM, water, radiolysis

©2021. Japan Geoscience Union. All Right Reserved.

[J] Poster | M (Multidisciplinary and Interdisciplinary)：M-IS Intersection

Sat. Jun 5, 2021 5:15 PM - 6:30 PM JST | Sat. Jun 5, 2021 8:15 AM - 9:30 AM UTC | Ch.20_3

[M-IS20] Ocean Plastics, an earth science perspective

convener:Atsuhiko Isobe(Research Institute for Applied Mechanics, Kyushu University), Kiichiro Kawamura(Yamaguchi University), Yusuke Okazaki(Department of Earth and Planetary Sciences, Graduate School of Science, Kyushu University), Masashi Tsuchiya(Research Institute for Global Change, Japan Agency for Marine-Earth Science and Technology)

Mismanaged plastic wastes accounting for 70% of marine debris remain persistently in the marine environment, even if they are degraded and fragmentized to tiny microplastics. To date, it has been unknown how this anthropogenic, buoyant, and persistent matter which was first appeared in the earth history, contaminates (or is incorporated into) the earth system. The ocean plastic study requires the insight and methodology of a variety of earth sciences such as the oceanography, geology, and palaeontology. Studies on the plastic circulation loaded from the land/atmosphere to upper oceans and bottom sediments, studies on microplastics as a proxy of the 'Anthropocene', and studies to establish procedures in monitoring and analyzing macro/microplastics are welcomed.

[MIS20-P01] Automatic detection for Nile Red-stained microplastic particles

*Masashi Tsuchiya[1], Tomo Kitahashi[1], Yosuke Taira[2], Hitoshi Saito[2], Kazumasa Oguri[1,3], Ryota Nakajima[1], Dhugal J. Lindsay[4], Katsunori FUJIKURA[1], Tomohiko Fukushima[1,5] (1.Research Institute for Global Change, Japan Agency for Marine-Earth Science and Technology, 2.NEC Corporation, 3.Danish Center for Hadal Research, University of Southern Denmark, 4.Institute for Extra-cutting-edge Science and Technology Avant-garde Research, Japan Agency for Marine-Earth Science and Technology, 5.Deep Ocean Resources Development Co., Ltd.)

[MIS20-P02] Deep sea Macro plastics in the Northwestern Pacific Ocean

*Tomoaki Kitayama[1], Takashi Hosono[1], Hideaki Saito[1] (1.Japan Agency for Marine-Earth Science and Technology)

Automatic detection for Nile Red-stained microplastic particles

*Masashi Tsuchiya[1], Tomo Kitahashi[1], Yosuke Taira[2], Hitoshi Saito[2], Kazumasa Oguri[1,3], Ryota Nakajima[1], Dhugal J. Lindsay[4], Katsunori FUJIKURA[1], Tomohiko Fukushima[1,5]

1. Research Institute for Global Change, Japan Agency for Marine-Earth Science and Technology, 2. NEC Corporation, 3. Danish Center for Hadal Research, University of Southern Denmark, 4. Institute for Extra-cutting-edge Science and Technology Avant-garde Research, Japan Agency for Marine-Earth Science and Technology, 5. Deep Ocean Resources Development Co., Ltd.

Marine microplastics (MPs) pollution has become a major social problem. MPs have been found to be widespread not only in coastal areas but also in the open ocean, including in the polar regions and in the Mariana Trench. Due to the effects of waves, UV and physical weathering, plastics become finer during and after discharged into the ocean. However, transporting processes into the deep sea have not yet been clarified. Although seafloor is considered to be one of the sinks of MP, there is less information about them than about the floating MPs at the surface of the ocean. In this study, we developed a flow system (flow cell) in which NR-stained MPs were continuously monitored, and the fluorescent particles that passed through the flow cell were visualized under a fluorescent stereomicroscope. In addition, we constructed an automatic detection system, with machine learning, to measure the shape and number of MPs from the captured images. As a result of image acquisition and automatic discrimination using this system, we were able to discriminate MPs consisting of particles and fibers smaller than 330 μm. This system enables discrimination at more than 60 MPs per minute.

Keywords: Microplastics, Nile-Red staining, machine learning, automatic detection

©2021. Japan Geoscience Union. All Right Reserved.

Deep sea Macro plastics in the Northwestern Pacific Ocean

*Tomoaki Kitayama[1], Takashi Hosono[1], Hideaki Saito[1]

1. Japan Agency for Marine-Earth Science and Technology

Enhancement of marine litter knowledge is essential to address the challenges of SDG14 such as marine pollution and conservation of sea and marine resources including biodiversity. However, information on seafloor litter is limited in marine litter studies. This is because it is not easy to approach the seafloor, and in order to clarify the life cycle of marine litter and the so-called Missing Plastics (99% out of all plastics that has entered into the ocean are missing), it is necessary to accumulate knowledge and information on seafloor litter. The Global Oceanographic Data Center (GODAC) of the Japan Agency for Marine-Earth Science and Technology (JAMSTEC) has published a “deep-sea debris dataset” using videos and photos taken during deep sea research in 2017, which data on categories, condition (accumulation point and drifting, etc.), and environments (sea bottom sediments and activities of organisms near the litters) of deep sea litter. A scientific paper based on this dataset has reported on distribution of plastic waste in the deep sea over 6000-m deep (Chiba et al., 2018). We also have been accumulating knowledge and information on seafloor litter of the northwestern Pacific Ocean, which has one of the most complex topographical characteristics in the world, with the triple junction and the world’s deepest seafloor, the Mariana Trench.
In this presentation, we will present a re-analysis of the spatial distribution and characteristics of seafloor litter of the northwestern Pacific Ocean using the “deep-sea debris dataset” with additional data from 2017 to 2021. Moreover, we will discuss how these data should be accumulated and provided to contribute to marine litter researches.

S. Chiba, H. Saito, R. Fletcher, T. Yogi, M. Kayo, S. Miyagi, M. Ogido, K. Fujikura,
Human footprint in the abyss: 30 year records of deep-sea plastic debris
Marine Policy (2018), 10.1016/j.marpol.2018.03.022

Keywords: Deep-sea debris, Marine litter, Seafloor litter, Macro plastics, Northwestern Pacific Ocean

©2021. Japan Geoscience Union. All Right Reserved.